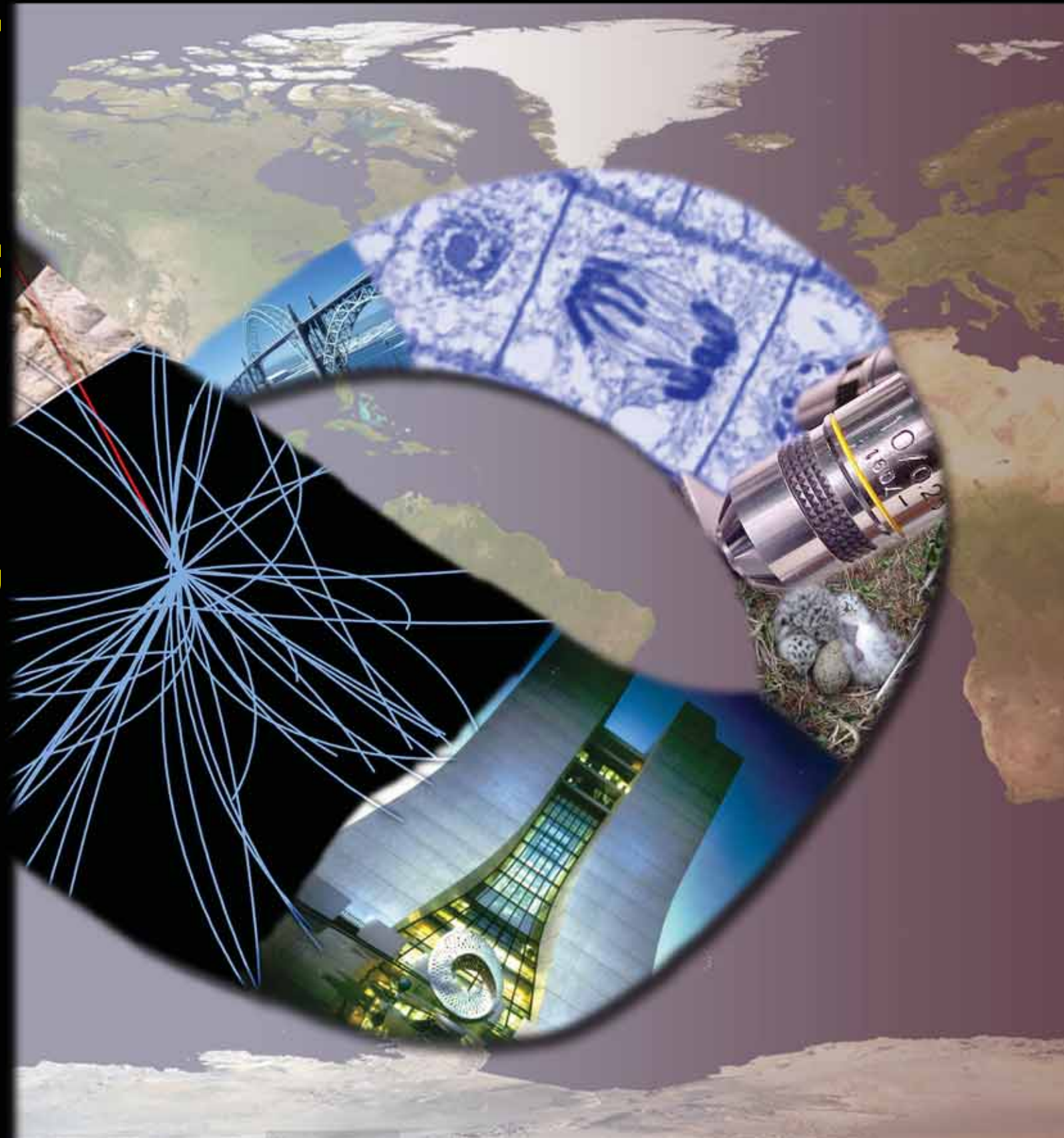


U.S. Department of Energy • Office of Science

JOURNAL OF UNDERGRADUATE RESEARCH

Volume VII, 2007



A Message from the Under Secretary for Science

The publication of this, the 7th Volume of the *Journal of Undergraduate Research*, is continuing evidence of the Department of Energy's support of the next generation of scientists and engineers. The body of knowledge contained in this volume of the *Journal* is striking evidence of the creativity and commitment of these young minds. We hope the excitement of discovery they have experienced will keep them in science. Our Nation needs them if we are to remain at the forefront of science and technology, a condition for our continued economic vitality and energy security.

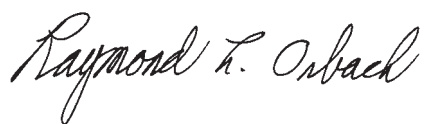
The articles and abstracts contained in this *Journal* are impressive. The disciplines cover science from high energy physics to genomics to nanoscience, and many other leading areas of modern scientific inquiry. The contents display the breadth of support the Department of Energy's Office of Science provides to basic research. The quality of the papers attests to the importance of Office of Science contributions to scientific discovery.

Office of Science supported research enables the U.S. to maintain its competitive edge. It transforms our energy future, supports our national security, and elucidates the fundamentals of matter and energy. The Department of Energy's 17 national laboratories, where all of the research contained in this *Journal* was produced, provide a special and critical resource for our Nation's needs.

For the Department to continue to serve our Nation, extraordinary scientific and technical talent must be nurtured and recruited. This 7th Volume of the *Journal of Undergraduate Research* reflects but one of the Department's ongoing efforts to develop this critical resource.

During 2006, more than 650 undergraduate women and men were awarded research internships at the Department of Energy's national laboratories. This volume of the *Journal* summarizes their achievements, and makes them available to the scientific and lay communities. These contributions demonstrate the skills and accomplishments of these young scientists. They will become the nucleus of our Department's and Nation's scientific and technical workforce of the future.

As Under Secretary for Science, I express my pride in the achievements, contained in this *Journal*, of these extraordinary young minds. I thank them for their dedication to science, and their accomplishments. I wish them well for an exciting future.



Raymond L. Orbach
Under Secretary for Science
U.S. Department of Energy



JOURNAL EDITORS

JEFFERY DILKS	EDITOR
KEVIN HARTMANN	EDITOR
DEBBIE MAYER	PRODUCTION EDITOR

TECHNICAL REVIEW BOARD

GRANT BROWHAL	JEFFREY HOLMES	LAXMIKANT SARAF
JAMES CHERRY	ERIC HOPPE	VAITHIYALINGAM SHUTTHANANDAN
ALICE CIALLELA	KIRK LABOBY	MICHAEL SIVERTZ
JESS TODD CLARK	LUKE LAURIE	S.K. SUNDARAM
JEFFERY DILKS	DON LINCOLN	BRUCE TOMKINS
AMY ELVERUM	ERIK RAMBERG	LEROY WENSTROM
BRADLEY FRITZ	EZEQUIEL RIVERA	WENDY WILLIAMS
DAVID GINLEY	LU RUAN	JOHNNY WONG
KEVIN HARTMANN	JOSEMARI SANSIÑENA	BRENDA WRIGHT

DISCLAIMER

The views and opinions of authors expressed in this *Journal* do not necessarily state or reflect those of the United States Government or any agency thereof and shall not be used for advertising or product endorsement purposes. Reference herein to any specific commercial product, process, or service by its trade name, trademark, manufacturer, or otherwise, does not necessarily constitute or imply its endorsement, recommendation, or favoring by the United States Government or any agency thereof. This document was prepared as an account of work sponsored by the United States Government and, while it is believed to contain correct information, neither the United States Government nor any of its agencies or employees makes any warranty, expressed or implied, or assumes any legal liability or responsibility for the accuracy, completeness, or usefulness of any information, apparatus, product, or process disclosed, or represents that its use would not infringe privately owned rights.

SCIENCE: CHANGE, GROWTH, OR PROGRESS?

During the 17th century, a new approach to understanding the nature of the world developed in Europe. Individuals such as Galileo began to describe the motion of objects in mathematical terms. Others, including Newton, began to emphasize the importance of comparing theoretical descriptions of phenomena to careful, quantitative observations of experimental results. Organizations were formed throughout the Continent to criticize, fund, and direct the activities encouraged by this new approach. Although this activity is the first clear expression of what we think of as “modern” science, it is equally clear that science has changed dramatically over the last four hundred years. As we take this opportunity to recognize the efforts of some of our young scientists, perhaps we can reflect on the nature of this change.

One view of scientific change has been described as “progress” so often that it is often accepted uncritically as the only view. Progress implies a directed change, a change that is evaluated with regard to some final goal or standard. The mathematical nature of much modern science creates an obvious goal for the creator of a scientific theory. The description of nature inherent in the theory should produce a description of phenomena that results in precise, quantitative agreement with the outcomes of experiments. Throughout the last four centuries, the success of many a scientific theory has been evaluated largely with regard to its ability to provide accurate numerical predictions. If quantitative accuracy is the standard, then closer agreement between theory and experiment is understandably described as “progress.”

However, progress toward accurate numerical descriptions of Nature does not necessarily imply movement toward a “better understanding” of the universe. At the same time that science has quantified the universe, it has also functioned as an attempt to “understand” the fundamental processes of Nature. One can imagine scientific theories that produce very accurate numerical predictions, but do not provide insights into the operations of the universe. Many would argue that such scientific theories are not understandable in the everyday sense of the word. Indeed, Richard Feynman is famously quoted as having said, “I think it is safe to say that no one understands Quantum Mechanics.” Quantum mechanics has repeatedly generated the most precise numerical predictions science has ever produced, but physicists have struggled for over 80 years to create a common interpretation, or “understanding,” of the theory. This is due, at least in part, to the subjective nature of understanding. This makes it difficult to define progress, for there may be no agreement on a “best” level of understanding. This is particularly apparent if we consider how society as a whole understands scientific theories. It is certainly arguable that the current understanding of the “nature of the universe” by the general public is no better than it was 400 years ago. According to this view of science, theories may “change,” but they do not (necessarily) progress.

If quantitative accuracy is the standard, then closer agreement between theory and experiment is understandably described as “progress.”

So, are scientific theories nothing more than algorithms to predict the future? Consider a third alternative, the development of “scientific knowledge” imagined as a process analogous to the growth of a living organism. Scientific theories take root in particular social and scientific environments that encourage the investigation of particular types of problems. As scientists interpret the results of their investigations, new theories are born. Many of these do not survive, cut down by unfavorable experimental results. However some live for a long time, posing new questions for investigation, generating new connections among old facts, and finding new environments in which to proliferate. One of the finest examples of this vision of science would be Darwin’s theory of evolution. In 19th century Europe, the environment was right for the “birth” of a theory of evolution. Indeed, Lamarck, Wallace, and Darwin independently developed theories of evolutionary change. Darwin’s conception is the version that has survived the pruning process. As this theory matured, it raised many questions in biology and allowed biologists to apply a single explanatory principle to areas as divergent as genetics, paleontology, and medicine. In addition, the theory has borne fruit in other fields such as artificial intelligence, economics, and psychology. Scientific theories flourish, in other words, insofar as they are able to bear copious intellectual fruit.

Scientific theories flourish, in other words, insofar as they are able to bear copious intellectual fruit.

Each of these three views of scientific change has its proponents and detractors, but whether you adhere to a vision of science as a process of change, growth, or progress, the future of science depends on the continued education of young scientists. This 7th volume of the *Journal of Undergraduate Research* documents the process by which the Department of Energy’s National Laboratories participate in the education of our new generation of scientists. Laboratory scientists and engineers have mentored these students just as many past generations mentored students. The work presented here illustrates how these young people changed during their internships. They have grown as scientists by developing new skills and abilities. They have progressed toward a particular, perhaps unspoken, image of an “ideal” scientist. We thank each mentor for the important role they have played in this process and congratulate the students for a job well done.



Jeffery Dilks
Albert Einstein Distinguished Educator Fellow
Office of Science

NATIONAL LABORATORIES: AGENTS OF CHANGE

Adapting to change is one of the great human attributes. From the very moment we are born, we begin to observe, see opportunity, and strive to reach new places in our lives. Realizing the potential to crawl, walk, talk, and reach new goals, we continuously assess our capabilities, recall our experiences, and synthesize ways to accomplish our mission, progressing toward some new state of being. Achieving change and progress is not always easy. We persevere through trials and tribulations, overcoming frustrations, making advances, sometimes suffering setbacks, but constantly driving forward. This is true of us as individuals, as communities, and as a Nation.

As a Nation, we are assessing our capabilities in terms of energy independence and national security. Realizing that great change may be necessary, we are identifying ways to utilize our existing infrastructure and new technologies to overcome these challenges. At the same time, as members of a global community, we are working to integrate new energy sources into climate-friendly production models. The solutions to these problems will come from many sources and will bring many other benefits. Our ability to work at the nanoscale with a new collection of tools will certainly serve the energy mission well. Nanoscience will become a revolutionary force with an impact akin to that of the automobile and airplane, and more recently, computing and the internet.

Nanoscience will become a revolutionary force with an impact akin to that of the automobile and airplane, and more recently, computing and the internet.

Over the past eighteen years, I have had the opportunity to be part of an agency that is at the forefront of national and, indeed, global change. Little did I know that contributing to the U.S. Department of Energy's mission was going to be such an addictive occupation. My military service made me proud of my contribution to our national security, my stint in corporate America was educational, but my work supporting science at the DOE's Brookhaven National Laboratory has been exciting. It is exhilarating to help shape the future of society through science, supporting facilities and staff that are tearing apart molecular and atomic structures, rearranging them in new ways, and developing

the underlying basis for scientific, medical, and life-changing technological advances. Nowhere is this done better than at our world-renowned Department of Energy National Laboratories, seventeen in all, ten of which are run by the Office of Science.

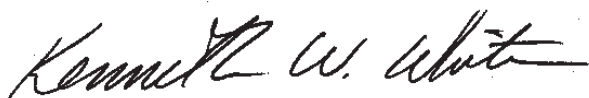
As we embrace the challenges of finite fuels, national security, and climate change, as we seek to advance medical capabilities, combat viruses and diseases, and improve food and water sources, it is the DOE's facilities, researchers, and support staff that will bring solutions forward. Recently the Center for Functional Nanomaterials at Brookhaven was placed in operation. This is the fifth of five such facilities within the DOE. These facilities, along with others in high energy physics, synchrotron light, and other priority areas, provide an infrastructure for science that continues to be unparalleled in the world, even as other countries seek to emulate our passion for

discovery and its resulting economic rewards. These laboratories are the places where basic science discoveries will be made that facilitate renewable and clean energy sources, develop detection systems for national security, and advance our understanding of the universe, dark matter, and dark energy.

Leading such change is complicated by challenges facing our educational systems, the desire of other countries to build scientific infrastructures to retain their domestic talent, and the added challenges of bringing foreign researchers into the United States. Once again, the DOE's role is clear. The National Laboratories

are a place where scientists of all ages — and those who teach them — can come to experience the excitement of science. A renewed focus has been placed on developing increasing numbers of our own technicians, engineers, and scientists, both through direct involvement, and by engaging teachers and professors.

This is an exciting time to be leading educational programs at one of the DOE's National Laboratories. Building the science and technology workforce of the future, the people who will use these extraordinary facilities and make these discoveries, is quite a satisfying way to spend a career. From my vantage point, the future is indeed bright. Our facilities are prepared to nurture the intelligent and inquisitive minds of youth who are anxious to address our Nation's challenges. As I write this, we have a new crop of 140 talented and curious undergraduate interns who arrived today to share our passion for discovery. I guess for now, the addiction to my work — helping our nation meet the challenges of change — will continue.



Ken White
Manager, Office of Educational Programs
Brookhaven National Laboratory

The National Laboratories are a place where scientists of all ages — and those who teach them — can come to experience the excitement of science.

TABLE OF CONTENTS

A Message from the Under Secretary for Science	1
Journal Editors	3
Technical Review Board	3
A Note from the Editor	
<i>Science: Change, Growth, or Progress?</i>	4
Jeffery Dilks	
<i>National Laboratories: Agents of Change</i>	6
Ken White	

About the Cover

The cover illustration provides examples of the many different scales at which science has changed our understanding of nature. The development of increasingly sophisticated tools has provided us with new ways to see the world around us. Our front and rear covers illustrate how modern technologies have allowed scientists to create images of the ocean floor, penetrating the veil of the overlying ocean water.

The Möbius strip demonstrates the interconnectedness of all things in the universe. Images depict objects and phenomena that range in scale from sub-atomic particles to galaxies. Living and non-living examples are juxtaposed, as are natural and man-made. The scientific instruments used to study these phenomena and examples of technologies which have resulted from our changing understanding of nature complete the montage.

Most prominently featured are images of the collision of subatomic particles and of a spiral galaxy. The Department of Energy's research programs investigate phenomena at all scales in the universe, from the very, very small to the very large. Images from the Department's Fermi National Accelerator Laboratory and Laser Interferometer Gravitational Wave Observatory serve to represent the breadth of the Department's scientific programs.

Microscope image courtesy of Tennessee Technological University; herring nest courtesy of Cornell University; particle physics image and Wilson Hall image courtesy of Fermilab; whirlpool universe and earth images courtesy of NASA; LIGO mirror telescope courtesy of LIGO Hanford Observatory; earth without water courtesy of Celestia Motherlode

Selected Student Papers

Suitability of a New Calorimeter for Exotic Meson Searches	10
Craig Bookwalter, Alexander Ostrovidov, and Paul Eugenio	
The Effects of Surface Chemistry on the Properties of Proteins Confined in Nano-porous Materials	15
Latasha M. Garrett and Hugh O'Neill	
Comparison of the Populations of Common Wood-Nymph Butterflies in Burned Prairie, Unburned Prairie and Old Field Grasses	22
Marlene Hahn and Rod Walton	
Analysis of the Water-Splitting Capabilities of Gallium Indium Phosphide Nitride (GaInPN)	26
Jeff Head and John Turner	
Study of Beam Spin Asymmetry in Exclusive π^0 Production	32
Ian Howley and Harut Avagyan	
Thermophoresis and its Thermal Parameters for Aerosol Collection	37
Zhuo Huang, Michael Apte, and Lara Gundel	
Solvent Purification and Fluor Selection for Gadolinium-loaded Liquid Scintillators	43
Tigisti Kesete, Amanda Storm, Richard L. Hahn, Minfang Yeh, and Suzanne Seleem	
Adaptively Improving Long Distance Network Transfers with Logistics	48
David LaBissoniere and Kenneth Roche	
Examination of Dislocations in Lattice-Mismatched GaInAs/Buffer Layer/GaAs for III-V Photovoltaics	55
Alejandro Levander and John Geisz	
Characterizing the Role of the <i>Nell1</i> Gene in Cardiovascular Development	63
Leah Y. Liu and Cymbeline Culiati	
A New GUI for Global Orbit Correction at the ALS Using MATLAB	71
Jacob Pachikara and Gregory Portmann	

Selected Student Papers, Continued

Development of Emittance Analysis Software for Ion Beam Characterization	77
Mariano J. Padilla and Yuan Liu	
Novel Coarsening of Pb Nanostructures on Si(111) 7 X 7	82
Charles J. Pye, Michael Yakes, Myron Hupalo, and Michael Tringides	
Power Grid Dynamics: Enhancing Power System Operation through Prony Analysis	87
Cody Ray and Zhenyu Huang	
Synthesis of Novel Crown Ethers Bearing the <i>exo-cis</i>-2,3-Norbornyl Group as Potential Na⁺ and K⁺ Extractants	91
Rachel M. Robeson and Peter Bonnesen	
Host Galaxies of X-shaped Radio Sources	97
Alessandra Springmann and Chi Cheung	
Calculation of Particle Bounce and Transit Times on General Geometry Flux Surfaces	103
Douglas Swanson and Jonathan Menard	
Climate Change Effects on Species Composition Mediates Decomposition in an Old-field Ecosystem	110
Marlene L. Tyner and Aimée T. Classen	
Lipid Production by <i>Dunaliella Salina</i> in Batch Culture: Effects of Nitrogen Limitation and Light Intensity	115
Chad Share Weldy and Michael Huesemann	
GEANT Simulations of Preshower Calorimeter for CLAS12 Upgrade of the Forward Electromagnetic Calorimeter	123
Kristin Whitlow and Stepan Stepanyan	
A Comparison of DNA Damage Probes in Two HMEC Lines with X-Irradiation	130
Christy L. Wisnewski, Kathleen A. Bjornstad, Christopher J. Rosen, Polly Y. Chang, and Eleanor A. Blakely	

Student Abstracts..... 135

Biology	136
Chemistry	148
Computer Science	158
Engineering	166
Environmental Science	183
General Sciences	197
Materials Sciences	199
Medical and Health Sciences	206
Nuclear Sciences	209
Physics	212
Science Policy	227

Participating National Laboratories

Ames Laboratory	228
Argonne National Laboratory	229
Brookhaven National Laboratory	230
Fermi Accelerator Laboratory	231
Idaho National Laboratory	232
Lawrence Berkeley National Laboratory ...	233
Lawrence Livermore National Laboratory	234
Los Alamos National Laboratory	235
National Renewable Energy Laboratory	236
Oak Ridge National Laboratory	237
Pacific Northwest National Laboratory	238
Princeton Plasma Physics Laboratory	239
Stanford Linear Accelerator Center	240
Thomas Jefferson National Accelerator Facility	241

Index of Authors 242

Index of Schools 251

DOE Office of Science Programs

Craig Bookwalter is studying Nuclear Physics at Florida State University in Tallahassee. His research for "Suitability of a New Calorimeter for Identifying Exotic Meson Candidates" was done at Thomas Jefferson National Acceleration Facility through the Science Undergraduate Laboratory Internship Program. He completed his undergraduate degree in applied physics and computer science at Christopher Newport University in Newport News, Virginia. Craig's hometown is Warrenton, Virginia. He is a member of the American Physical Society, and he enjoys surfing, soccer, martial arts, and music.

Paul Eugenio is a professor at Florida State University. He is conducting research in the Physics Division on a joint appointment between Jefferson Lab and Florida State University.

SUITABILITY OF A NEW CALORIMETER FOR EXOTIC MESON SEARCHES

CRAIG BOOKWALTER, ALEXANDER OSTROVIDOV, AND PAUL EUGENIO

ABSTRACT

Exotic mesons, particles that have quantum numbers that are inaccessible to conventional quark-model mesons, are predicted by quantum chromodynamics (QCD), but past experiments seeking to identify exotic candidates have produced controversial results. The HyCLAS experiment (E04005) at Thomas Jefferson National Accelerator Facility (TJNAF) proposes the use of the Continuous Electron Beam Accelerator Facility (CEBAF) Large Acceptance Spectrometer (CLAS) in Hall B to study the photoproduction of exotic mesons. However, the base detector package at CLAS is not ideal for observing and measuring neutral particles, particularly at forward angles. The Deeply Virtual Compton Scattering (DVCS) experiment at TJNAF has commissioned a new calorimeter for detecting small-angle photons, but studies must be performed to determine its suitability for a meson spectroscopy experiment. The $\eta\pi$ system has been under especial scrutiny in the community as a source for potential exotics, so the new calorimeter's ability at reconstructing these resonances must be evaluated. To achieve this, the invariant mass of showers in the calorimeter are reconstructed. Also, two electroproduction reaction channels analogous to photoproduction channels of interest to HyCLAS are examined in DVCS data. It is found that, while not ideal, the new calorimeter will allow access to additional reaction channels, and its inclusion in HyCLAS is warranted. Results in basic shower reconstruction show that the calorimeter has good efficiency in resolving π^0 decays, but its η reconstruction is not as strong. When examining $ep \rightarrow ep\pi^0\eta$, preliminary reconstruction of the $\eta\pi^0$ system shows faint signals in the $a_0(980)$ region. In the $ep \rightarrow e n \pi^+ \eta$ channel, preliminary reconstruction of the $\eta\pi^+$ system gave good signals in the $a_0(980)$ and $a_2(1320)$ regions, but statistics were poor. While more analyses are necessary to improve statistics and remove background, these preliminary results support the claim that the DVCS calorimeter will be a valuable addition to CLAS for upcoming exotic meson searches in photoproduction.

INTRODUCTION

Theory

In the early 1960s, the search for the elementary constituents of matter was at an impasse. Physicists, expecting to find a small number of tiny elemental particles making up protons and neutrons, were in fact finding an extraordinary number of unique particles in their scattering experiments. In response to this, Murray Gell-Mann and George Zweig independently formulated the quark model, an organization of the "particle zoo", by postulating that most of the particles were composed of different configurations of two or three elementary particles called quarks. Gell-Mann's Eightfold Way

organized the mesons (two-quark particles) and baryons (three-quark particles) into two octets and one decuplet. Using these organizing principles, Gell-Mann predicted the existence of an as yet unseen particle, the Ω^- , which was later detected by a group at Brookhaven National Laboratory. The quark model was a great success and it reinvigorated the fields of nuclear and elementary particle physics [1].

Soon, a theory governing the behavior of quarks was produced. Quarks were described by an additional quantum number, known as color charge. The color charge itself was mediated by particles known as gluons which possessed their own color charge. These interactions would be observed as the strong force. This theory of colored quarks and gluons was called quantum chromodynamics

(QCD). Development of QCD continues today. One of its predictions is that new hadronic matter should exist outside the predictions of the quark model of Gell-Mann and Zweig. These new particles would be identified by their quantum numbers, or J^{PC} , where J is the total angular momentum, P is the parity, and C is the charge conjugation. For an ordinary meson composed of a quark and an antiquark, with orbital angular momentum L and total spin S , J^{PC} is calculated as follows:

$$J = S + L$$

$$P = (-1)^{L+1}$$

$$C = (-1)^{L+S}$$

Given this prescription, the following $qq\bar{q}$ states are allowed:

$$J^{PC} = 0^{++}, 0^{+-}, 1^{--}, 1^{+-}, 1^{-+}, 2^{--}, 2^{-+}, 2^{++}, \dots$$

Any states with J^{PC} different from those allowed by the quark model are manifestly exotic and if experimentalists can identify them they will have validated a prediction of QCD. One should note that other exotic states exist with ordinary J^{PC} , but experimentalists have focused on those with exotic J^{PC} since those will be the easiest to identify [2].

The Experiment

Unfortunately, searches for exotic mesons have resulted in controversy within the nuclear physics community. The E852 collaboration at Brookhaven National Laboratory, studying reactions like $\pi\pi \rightarrow \eta\pi\pi$, $\pi\pi \rightarrow \eta'\pi\pi$, and $\pi\pi \rightarrow \pi^+\pi^-\pi^+\pi^-$, published the first claims of exotic measurements in 1998 with two candidates, the $\pi_1(1400)$ (masses in MeV in parentheses) and the $\pi_1(1600)$ [2]. While theoretical predictions for the mass of the glueball place it within this range, the $\eta\pi$ system has isospin 1 and thus excludes glueballs from being produced [2,3]. With that in mind, both model-based and lattice QCD calculations put the lightest quark-based exotics at around 1.9 GeV [4,5], significantly higher than the $\pi_1(1400)$. The $\pi_1(1600)$ is closer to the predicted mass, but the theory does not predict its observed decay to $\rho\pi$ [6].

At Thomas Jefferson National Accelerator Facility (JLab), an experimental program is underway to exhaustively study the lightest of the exotic meson candidates. In the long term, the GlueX experiment seeks to map the spectrum of light exotics in detail, but its commissioning will come only after a planned accelerator upgrade is complete [7]. In the near term, the Hy-CLAS experiment

(Jefferson Lab experiment E04005) searches for light exotics using the Continuous Electron Beam Accelerator Facility (CEBAF) Large Acceptance Spectrometer (CLAS) in Hall B [8].

Unlike E852, which used a pion beam on a hydrogen target, HyCLAS (as well as GlueX) will use photon beams on hydrogen. Several theorists [9,10] predict that photoproduction will provide an ideal environment to search for exotics. In addition, the world photo production data in exotic-rich reaction channels is thin at best [11]. HyCLAS seeks to increase world data for a number of exotic-rich photoproduction reaction channels. However, the experiment is limited in the number of channels it can study by the detector configuration of CLAS.

CLAS and the Inner Calorimeter

CLAS is a spectrometer made up of six identical segments, arranged in a spherical shape around a toroidal magnet. It contains several layers of drift chambers for charged particle tracking, scintillator paddles for time-of-flight measurement, gas Čerenkov counters for particle identification, and sampling calorimeters for energy measurement [12]. Unfortunately, the design of CLAS leaves a large hole in the forward area around the beamline so peripheral production experiments such as HyCLAS lose a lot of events in the forward angles. CLAS also does not reconstruct neutral particles well at any angle, consequently, reaction channels with two or more neutrals are unobservable for the base detector package.

Fortunately, the Deeply Virtual Compton Scattering experiment at CLAS, measuring $ep \rightarrow ep\gamma$, also required small-angle detection for photons [12] and a new calorimeter was built to suit the purpose. The inner calorimeter (IC) is built from 424 lead-tungstate crystals arranged in an octagonal shape with a square hole in the center for the beam to pass. It is placed downstream of the target, directly in front of the forward hole in CLAS. Upon commissioning, it was demonstrated to have a 7 MeV mass resolution at 1 GeV [13].

The inclusion of this calorimeter in HyCLAS could open a significant number of new reaction channels for study, particularly the $\eta\pi$ system, notorious from its study in E852[2]. So, it is necessary

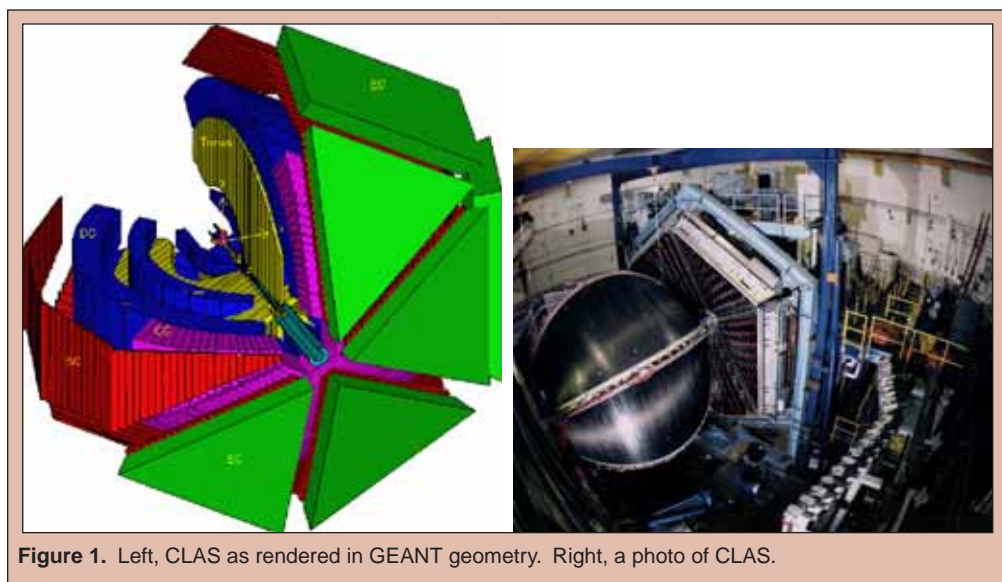


Figure 1. Left, CLAS as rendered in GEANT geometry. Right, a photo of CLAS.

that the IC be able to reconstruct showers originating from both π^0 and η decays. If it can be shown that the IC can accurately reconstruct neutral pions, then one may examine the data from the DVCS experiment and look for exotics and their companions in the $\eta\pi$ reaction channels. However, any observed resonances will be from electroproduction data, since DVCS examined $ep \rightarrow ep\gamma$. Thus, HyCLAS will provide the first opportunity to examine photoproduction data with improved CLAS acceptance.

METHODS OF ANALYSIS

Analysis Overview

The analyses below examined two channels similar to the systems studied in E852 and searched for exotic candidates in invariant mass spectra. The data, having already been reconstructed for the DVCS experiment, merely required the use of some in-house JLab libraries for event selection. Since the final analyses were performed using the ROOT software package [14], interesting events were transplanted into ROOT TTree format for easy access within ROOT scripts.

Reconstruction of π^0 and η

Evaluating the impact of the IC on the meson spectroscopy planned by HyCLAS requires examining the reconstruction of neutral pions and η mesons. Both of these particles decay primarily to 2γ , so events must have at least two showers in the IC, and the invariant mass can be reconstructed and the result plotted. An array of energy cuts on the showers in the IC are applied to determine the best cut to reduce background in further analyses. In the resulting plots, one expects to see a peak for the π^0 and a smaller peak for the η .

Examination of $ep \rightarrow ep\eta\pi^0$

After establishing the baseline characteristics of the calorimeter with the previous analysis, the first of two reaction channels is examined. Events are selected for this channel based on the following criteria:

1. an identified proton,
2. an identified electron, confirmed by examining the ratio of the energy calculated by the particle identification system and the energy reconstructed by the primary CLAS electromagnetic calorimeter,
3. two showers in the IC, each of at least 300MeV,
4. the invariant mass of the two showers is within 50MeV/ c^2 of the π^0 mass,
5. the missing mass of the event is within 50MeV/ c^2 of the η mass, and

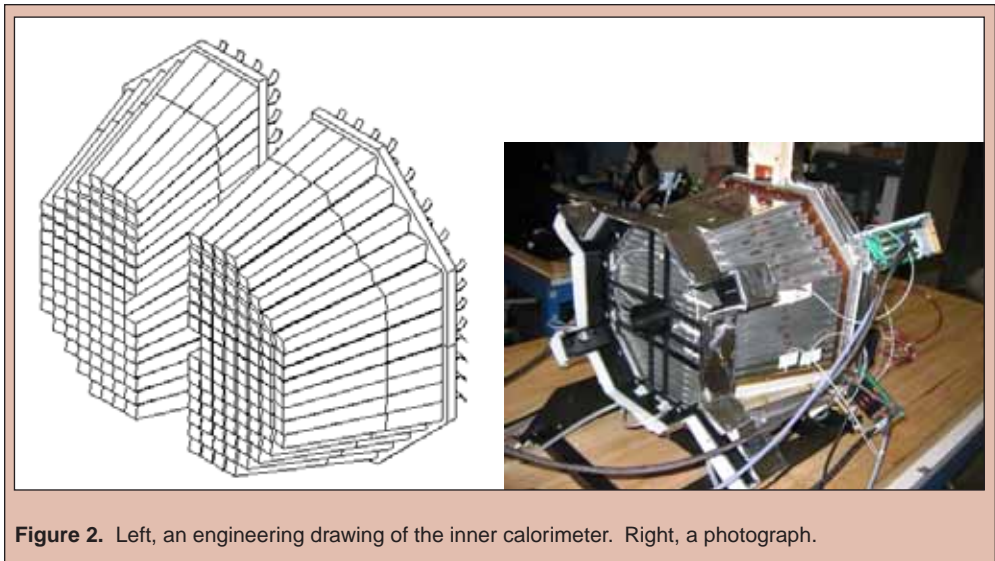


Figure 2. Left, an engineering drawing of the inner calorimeter. Right, a photograph.

6. the missing momentum is at least 400MeV/ c .

Examining the invariant mass of the $\eta\pi^0$ systems of the remaining events can provide information about the masses of particles that decay to $\eta\pi^0$.

Examination of $ep \rightarrow e\eta\pi^+$

Another variation of the $\eta\pi$ system is the $ep \rightarrow e\eta\pi^+$ channel. Events are selected by the following criteria:

1. an identified π^+ ,
2. an identified electron,
3. two showers of at least 300MeV in the IC,
4. the invariant of those two showers is within 100MeV/ c^2 of the mass of the η ,
5. the missing mass of the event is within 50MeV/ c^2 of the neutron mass, and
6. the missing momentum is at least 400MeV/ c .

From the surviving events the invariant mass of the $\pi^+\eta$ system is calculated and examined.

RESULTS

Reconstruction of π^0 and η

Basic shower reconstruction in the inner calorimeter produced excellent results for the π^0 and poor results for the η . Fig. 3 shows the reduction of background with energy cuts in 100MeV increments. The π^0 peak emerges early from the background, but even at a cut of 1GeV (when two showers each of at least 1GeV in energy are required) the η signal is not sufficient to show above background. This could be due to the small angular acceptance of the IC or, perhaps, to a large background of hadronic showers. Based on these data, a global cut of 300MeV was selected to reduce background on subsequent analyses.

$$ep \rightarrow ep\eta\pi^0$$

One might expect the best-quality results to come from this channel, due to the high efficiency of the inner calorimeter in its detection of π^0 . However, the effect of the background has been difficult to overcome, as Fig. 4 demonstrates. The $\eta\pi$ invariant mass plot displays some recognition of the $\alpha_0(980)$ in the appropriate place, but more studies will be required to be certain of its presence. Judgment should be withheld on the identity of the obvious peak at $800\text{MeV}/c^2$ until background is reduced. In addition, if one looks at the missing mass in Figure 4, there is no obvious η feature and a large portion of events are simply $ep \rightarrow ep\pi^0$ (zero missing mass). There are a large number of these events so they are removed during analysis to allow an appropriate scale to plot the desired physics.

$$ep \rightarrow e\eta\pi^+$$

The $ep \rightarrow e\eta\pi^+$ channel was expected to be more difficult, since events were required to have a reconstructed η in the IC. Despite suffering from low statistics, preliminary results show cleaner signals for relevant mesons than for the $ep \rightarrow ep\eta\pi^0$ channel. Examining

the $\eta\pi$ effective mass plot in Figure 5, the two peaks in question are seen, one near the $\alpha_0(980)$, and the other near the $\alpha_2(1320)$. Those results come with a caveat, as demonstrated by the other plot in Fig. 5, which shows the missing mass. One may notice the lack of a neutron peak in these data background is still high at this stage, therefore these results are still preliminary. However, the peaks in the $\eta\pi$ invariant mass still seem to imply that there is a neutron under that background.

CONCLUSIONS

The lack of robust η reconstruction is disappointing, but the added acceptance of π^0 is welcome. The sighting of the $\alpha_0(980)$ and $\alpha_2(1320)$ mesons, while tentative, gives cause for excitement, since in photoproduction the π^1 exotic and the α_2 should be produced in similar numbers [10]. Additional studies are being conducted to remove the substantial background, but hardware solutions have also been proposed. A charged-particle hodoscope to identify charged particles entering the calorimeter and masquerading as photons will further reduce background. Even though these results are preliminary, it seems clear that the IC will provide a decided benefit to the HyCLAS effort to study exotic meson spectroscopy.

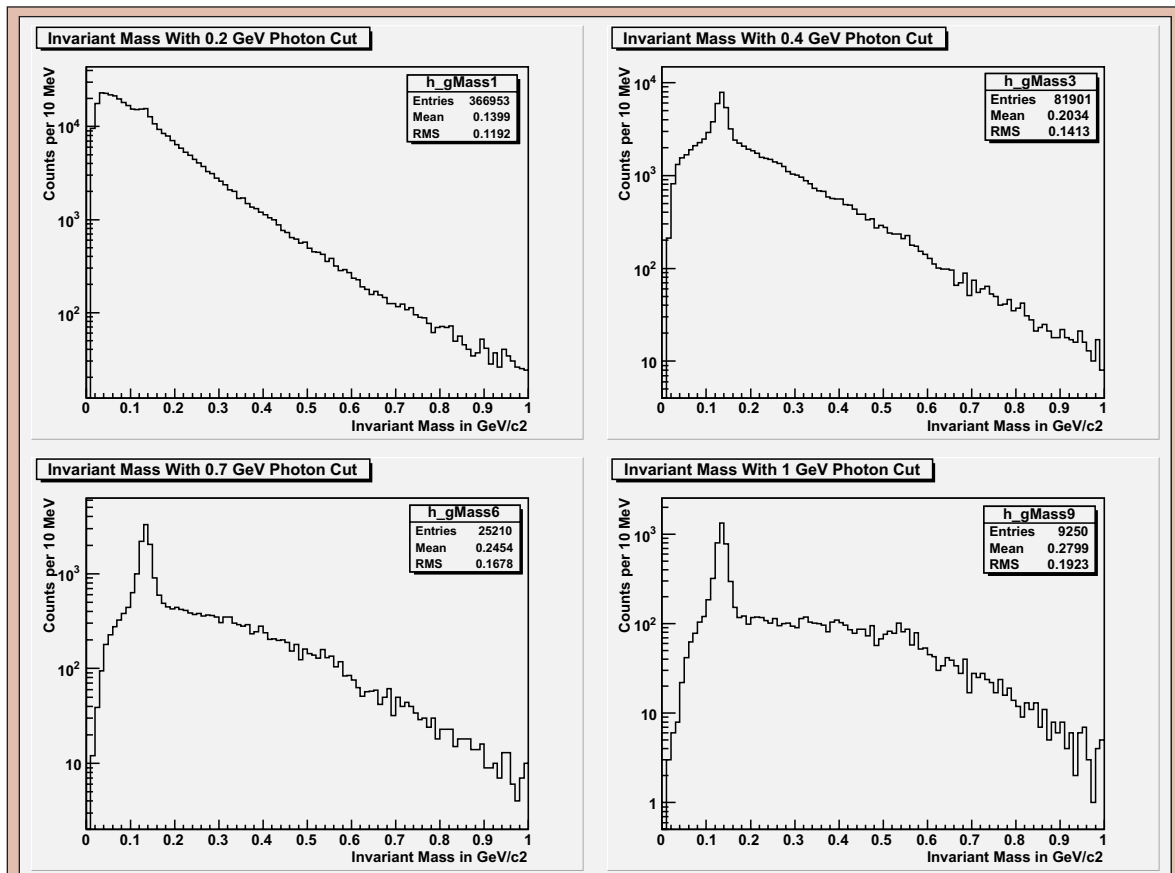
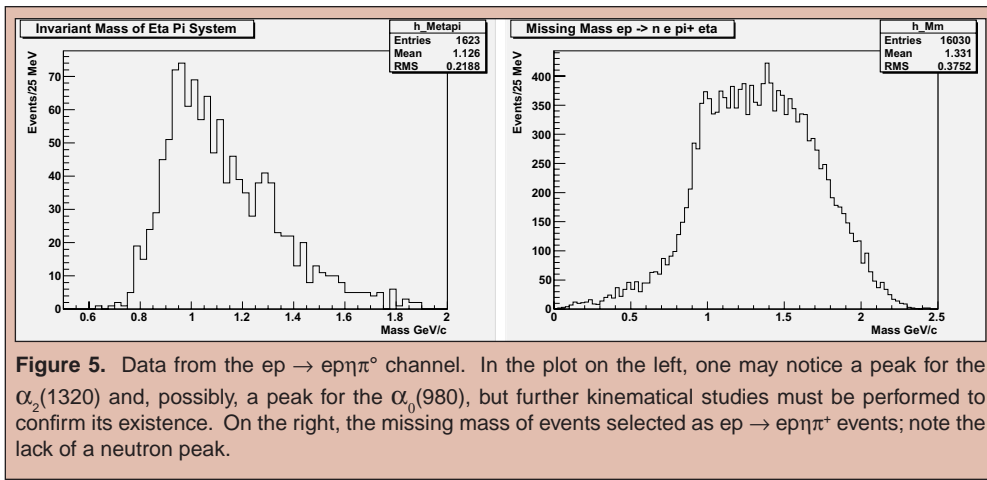
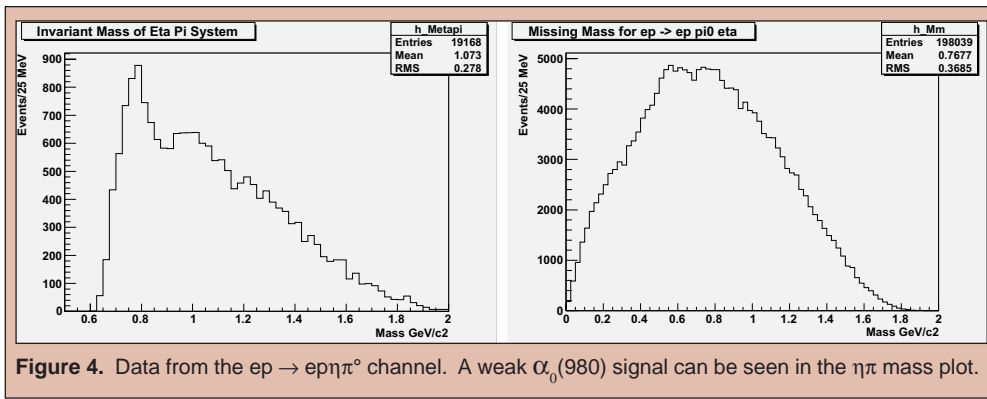


Figure 3. Effective mass of two-plus photon showers in the inner calorimeter subjected to cuts from 200MeV to 1GeV. Note the π^+ peak at $140\text{MeV}/c^2$ and the lack of an η peak at $550\text{MeV}/c^2$.



REFERENCES

- [1] L. Hoddeson, "The Rise of the Standard Model: Particle Physics in the 1960s and 1970s." *Cambridge University Press*, New York, 1997.
- [2] S.U. Chung, et al., "Phys. Rev. D" 60, 9, 1999.
- [3] Y. Chen, et al., "Phys. Rev. D" 73, 1, 2006.
- [4] N. Isgur, R. Kokoski, and J. Paton, "Phys. Lett." 54, 869, 1985.
- [5] P. Lacock, et al. (UKQCD Collaboration), "Phys. Lett." B401, 308 (1997).
- [6] G.S. Adams, et al., "Phys. Lett." 81, 5760, 1998.
- [7] GlueX/Hall D Collaboration. *The Hall D Project Design Report*, 2000.
- [8] P. Eugenio, et al., research proposal to Jefferson Lab PAC 25, "Search for New Forms of Hadronic Matter in Photoproduction." 2003.
- [9] F. Close and P. Page, "Phys. Rev. D" 52, 1706, 1995.
- [10] A. Szczepaniak and M. Swat, "Phys. Lett." B516, 72, 2001.
- [11] B.A. Mecking, et al., "Nuclear Instruments and Methods" 503, 3, 2003.
- [12] H. Avakian, et al., research proposal to Jefferson Lab PAC29, "Deeply Virtual Compton Scattering with CLAS at 6 GeV." 2006.
- [13] P. Rosier, R & D Detection Note IPN Orsay, "Thermal design for the CLAS-DVCS calorimeter." RDD2004-02 2004.
- [14] R. Brun and F. Rademakers, "ROOT User's Guide." <http://root.cern.ch/root/doc/RootDoc.html>, 2006.

Latasha Garrett is currently a graduate student in chemistry at the University of Tennessee at Knoxville. She is pursuing research with Dr. George Schweitzer with a focus on inorganic chemistry and lanthanide chemistry. Ms. Garrett graduated from the University of Tennessee at Knoxville with a B.S. in Chemistry and a minor in psychology in 2005. At Oak Ridge National Laboratory, she participated in the SULI program for two appointments. She worked in the chemical sciences division under the supervision of Dr. Hugh O'Neill. Her research project was to study the surface chemistry of encapsulating proteins in silica gels.

Hugh O'Neill is a staff scientist at Oak Ridge National Laboratory (ORNL), Tennessee. He received his Ph.D. in 1998 from University College Dublin, Ireland. He was a post-doctoral researcher at ORNL and a research assistant professor at University of Tennessee, Knoxville prior to joining the Chemical Sciences Division at ORNL. His research interests are focused on both solar hydrogen and fermentative hydrogen renewable energy production. He is also interested in the investigation of the structure, function, and interactions of bio-molecules at the biotic/abiotic interface.

THE EFFECTS OF SURFACE CHEMISTRY ON THE PROPERTIES OF PROTEINS CONFINED IN NANO-POROUS MATERIALS

LATASHA M. GARRETT AND HUGH O'NEILL

ABSTRACT

The entrapment of proteins using the sol-gel route provides a means to retain its native properties and artificially reproduce the molecular crowding and confinement experienced by proteins in the cell allowing investigation of the physico-chemical and structural properties of biomolecules at the biotic/abiotic interface. The biomolecules are spatially separated and 'caged' in the gel structure but solutes can freely permeate the matrix. Thus, properties such as the folding of ensembles of individual molecules can be examined in the absence of aggregation effects that can occur in solution studies. Green fluorescent protein from *Aequorea coerulea* was used as a model protein to examine the unfolding/re-folding properties of protein in silica gels. The recombinant protein was isolated and purified from *Escherichia coli* extracts by cell lysis, three-phase partitioning, dialysis, and anion exchange chromatography. The purity of the protein was greater than 90% as judged by SDS PAGE gel analysis. Sol-gels were synthesized using tetramethylorthosilicate (TMOS) in combination with, methyltrimethoxyorthosilane (MTMOS), ethyltrimethoxyorthosilane (ETMOS), 3-aminopropyltriethoxysilane (APTES), and 3-glycidoxypropyltrimethoxysilane (GPTMS). The acid induced denaturation and renaturation of GFP was analyzed by UV-visible, fluorescence, and circular dichroism (CD) spectroscopies. No renaturation was observed in gels that were made with TMOS only, and in the presence of APTES, MTMOS, and ETMOS. However, in gels that were made with GPTMS, the CD and UV-visible spectra indicated that the protein had refolded. The fluorescence emission spectrum indicated that approximately 20% of fluorescence had returned. This study highlights the importance of the surface chemistry of the silica gels for the refolding properties of the entrapped GFP. Future studies will investigate the effect of surface chemistry on the thermal and solvent stability of the entrapped protein.

INTRODUCTION

Cells can be described as crowded environments because they are composed of many different types of macromolecules, none of which are present at high concentration, but which collectively occupy a large fraction of the total volume of the fluid [1]. The complex mixture of nucleic acid, polysaccharide, protein and lipid comprises approximately 30–40% of the cell [2]. In this scenario, it is expected that non-specific interactions are individually weak but cumulatively quite strong. An important subset of these are excluded volume interactions that arise from steric repulsion between different macromolecules. They are always present and increase both the free energy of a solution and the chemical potential of each type of solute. Therefore, many proteins fold into their

native states in an environment that geometrically restricts their conformational space. This can dramatically affect protein stability, dynamics and function because of volume constraints, viscosity, and solvent and solute activity [1]. Conversely, the majority of protein characterization studies are carried out in dilute solution to mitigate against aggregation effects that can occur at higher concentrations. This approach fails to take into account physiological conditions where the excluded volume can influence the structure, function, and interactions of proteins.

Although sol-gel chemistry has been widely used for immobilization and stabilization of a range of different biomolecules [3] a recent and intriguing development is using sol-gel entrapment to mimic the crowded cellular environment [4]. The entrapment of proteins using the sol-gel route provides a means to retain their native

properties and artificially reproduce the molecular crowding and confinement experienced by proteins in the cell. The biomolecules are spatially separated and caged in interconnected nanopores such that solutes can freely permeate the matrix. The optically transparent matrix can be analyzed by a variety of spectroscopic techniques used to monitor the structure of macromolecules in dilute solutions. An important development in this area was the demonstration that circular dichroism spectropolarimetry could be used to directly measure the structural properties of proteins entrapped in sol-gels [4].

The unfolding equilibrium and kinetics of a mutated green fluorescent protein (GFPmut2) from *Aequorea victoria* in silica gels were investigated to gain insight into the effects of caging and crowding on protein structure and large scale dynamics [5]. The guanidium-HCl induced unfolding of GFP was a biphasic process in the sol-gel environment as opposed to monophasic in solution. This suggested the presence of a significant fraction of encapsulated molecules with a different conformation to the dominant species in solution. A further extension this work was to investigate unfolding and refolding of single GFP molecules entrapped in wet silica gels using two-photon fluorescence spectroscopy [6]. Several periodic oscillations among the chemical substates of the protein fluorophore immediately before unfolding could be resolved. This study highlights the effectiveness of protein encapsulation in silica gels to characterize the dynamic properties of individual molecules. The water-rich matrices offer a good simulation of the natural cellular environment: the proteins under investigation are spatially separated preventing interprotein interactions.

In the present study, a green fluorescent protein (GFP) from *Aequorea coerulea* was used to investigate the effect of the surface chemistry of sol-gel on the properties of the encapsulated protein [7]. The wild-type *A. coerulea* GFP homologue shares 92% sequence identity with *A. victoria* GFP, the most widely studied variant of this protein. The fluorophore forming residues, Ser⁶⁵, Tyr⁶⁶, and Gly⁶⁷ are conserved as are the evolutionary invariant Arg⁹⁶, Glu²²², His¹⁴⁸, Phe¹⁶⁵, Ile¹⁶⁷, and Thr²⁰³, all of which are very spatially very close to the chromophore. The *A. coerulea* mutated variant used in this study underwent five amino acid substitutions, V11I, F64L, K101E, T206A, and E222G, in comparison to its wild-type non-fluorescent parent protein. The E222G mutation is the key event that confers the fluorescent properties on the protein. The other mutations are suggested to improve the folding properties of the protein. It has an excitation maximum at 480nm and emission at 505nm.

The effect of surface chemistry on the refolding of acid-denatured GFP was investigated in sol-gels whose surface chemistry was altered by introduction of charged polar, uncharged polar and hydrophobic functional groups. Various spectrophotometric techniques were employed to determine how the microenvironment of the sol-gel pores affected the folding properties of the protein.

MATERIALS AND METHODS

Over-Expression of GFP in Escherichia coli

All recombinant DNA techniques and *E. coli* maintenance and propagation procedures were carried out as previously described [9]. *E. coli* JM109 cells were transformed with pAcGFP1 (BD Biosciences, USA) that encodes the gene for *A. coerulea* GFP. The transformed *E. coli* was grown in Luria Bertani medium at 37°C supplemented with ampicillin at a final concentration of 50µg/ml. For production of recombinant GFP, protein expression was induced at an optical density of 0.5 recorded at 600nm by addition of isopropyl-B-d-thiogalactopyranoside (IPTG) at a final concentration of 1.0mM. Growth was continued at 37°C for approximately 18h.

Protein extraction and purification

The bacterial cells were harvested by centrifugation at 10,000 x g for 10 min at 4°C. The cells were resuspended in sonication buffer (20mM Tris HCl, 10mM NaCl, 5mM EDTA, pH 7.5) that contained 1.0 mg/ml lysozyme. Sonication was performed using a Branson Sonicator equipped with a microtip for a total of 6 min with 20 sec sonication intervals followed by 1 min of cooling on ice/NaCl. The broken cells were centrifuged at 15,000 x g for 15 min and the pellet was resuspended and sonicated for a further 2 min with 30 sec bursts. The supernatants, containing the GFP were then pooled.

The combined crude extracts were subjected to the three-phase partitioning technique as previously described [9]. The protein preparation was further purified by anion-exchange chromatography (AEC) on Hi-Trap Q Sepharose (Amersham Biosciences). The equilibration buffer was 50mM Tris-HCl pH 8.0 (buffer A) and the limit buffer was 50mM Tris-HCl pH 8.0, 1M NaCl (buffer B). The protein was dialyzed into 50mM Tris-HCl pH 7.5 and filter-sterilized before applying it to the column. The column was washed with 6 volumes of buffer A to remove unbound protein, followed by application of a gradient from 0 to 100% of buffer B (15 column volumes) to elute GFP. The absorbance of the eluant was monitored at 490nm and 280nm.

Sol-gel synthesis

For sol-solutions made with tetramethylorthosilicate (TMOS), methyltrimethoxysilane (MTMOS), aminopropyltriethoxysilane (APTES) or 3-glycidoxypropyltrimethoxysilane (GPTMS) as precursors, the sol gel precursor (0.01 mol) was mixed with 0.338g H₂O and 0.02g 40mM HCl, and then sonicated (Laboratory Supply Sonicator, Model G112SPIT) at 4°C until a homogeneous solution was formed. Sol-solutions made with ethyltrimethoxysilane (ETMOS) were formed as described above except that the mixture was stirred at 4°C for several hours. Entrapment of GFP was achieved by initiation of the condensation reaction by mixing the protein solution, dissolved in 10mM Na phosphate, pH 7.0, with the hydrolyzed sol solution in a ratio of 2:3. The mol ratio of TMOS

hydrolyzed sol to ORMSIL hydrolyzed sol is shown in Fig 2B. After condensation occurred, the gels were allowed to age for at least 24h while immersed in 50mM Na phosphate, pH 7.0 before carrying out experiments. There were two types of gels made: gels (60–80 μ L) that were formed on quartz slides (9 \times 25mm) to form a thick film that was ~0.5mm and gels that were formed in plastic cassettes that were 8cm \times 8cm \times 0.1cm. The protein unfolding/refolding reactions were performed at 25°C.

Analysis Methods

Circular dichroism spectra were recorded on a Jasco 810 CD spectropolarimeter from 190–600nm at 25°C. UV-visible spectra were recorded between 190–800nm using a Cary 50 spectrophotometer. Protein content was estimated using the modified Lowry assay method (Pierce Biochemicals) with Bovine Serum Albumin as the standard protein. Sodium dodecyl sulfate (SDS) polyacrylamide gel electrophoresis (PAGE) and native PAGE were carried out as previously described [10].

RESULTS AND DISCUSSION

Purification of GFP

Over-expression of GFP in *E. coli* was carried out as described in Materials and Methods. The first step in the purification procedure was by three-phase partitioning [9]. Briefly, ammonium sulfate was added to the crude extract to a final concentration of 20% followed by addition of an equal volume of tert-butanol. After an incubation period the reaction was centrifuged to separate three phases. The aqueous phase containing the GFP fraction was removed and the ammonium sulfate concentration was adjusted to 60% and 2 volumes of tert butanol were then added. The incubation and centrifugation steps were repeated and this time GFP was present as a precipitate at the interface of the aqueous and organic phases. The protein was dissolved in 0.5ml of 10mM Tris-HCl pH 7.5.

Jain et al. [9] reported the purification of GFP to homogeneity using this approach. In our hands we were only able to achieve approximately 80% purification by this method, as judged by SDS PAGE analysis. One difference was that in the present study *E. coli* JM109 replaced *E. coli* DH5 α which is known to produce less carbohydrate and extracellular protein than the JM109 strain. The presence of extracellular carbohydrate and protein have been shown to effect the purity of biomacromolecules purified from *E. coli* by organic extraction [8]. The other major difference was that the ratio of cell mass to solvent was increased 10-fold in this study compared to the published procedure which may impact the isolation procedure. A thick interfacial phase was observed during the first round of three phase partitioning and to reduce the amount of GFP trapped in that phase, DNAase was added for 1 hour before starting the extraction. The addition of DNAase did not improve in the yield of GFP and hence this step could be removed in the future.

GFP purified by three-phase extraction was subjected to anion exchange chromatography on a HiTrapQ column. The chromatogram is shown in Figure 1a. GFP eluted from the column between 25-35% Buffer B as indicated by the 475nm absorbance

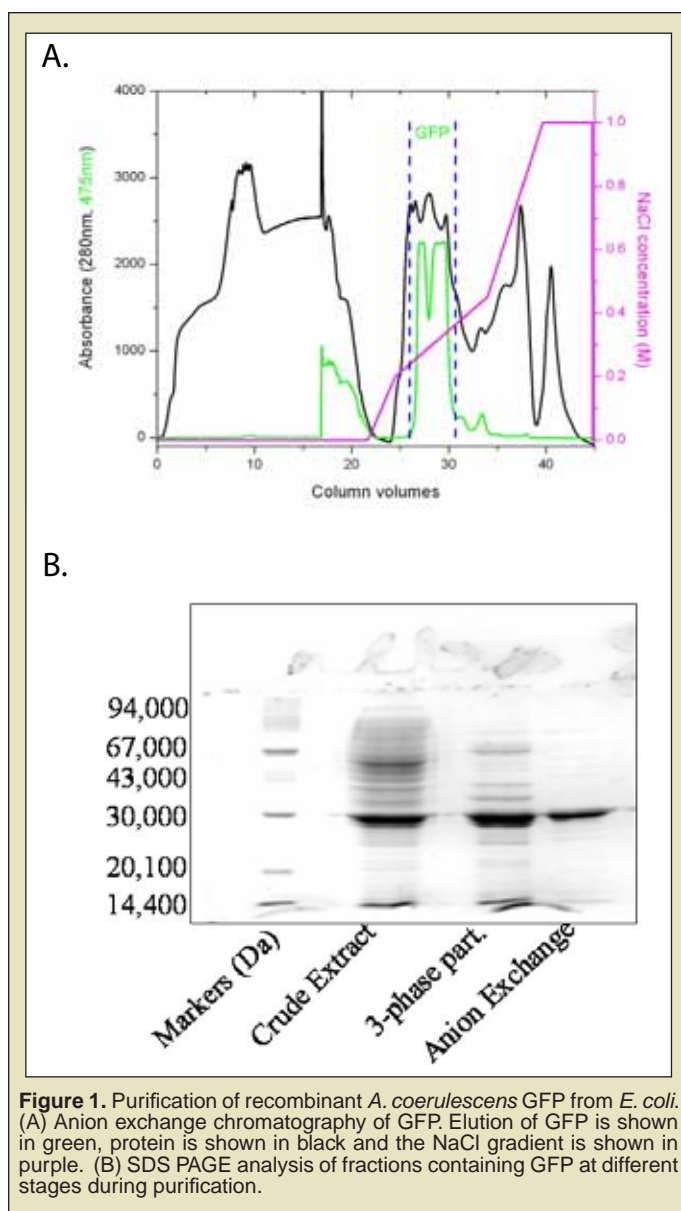


Figure 1. Purification of recombinant *A. coerulescens* GFP from *E. coli*. (A) Anion exchange chromatography of GFP. Elution of GFP is shown in green, protein is shown in black and the NaCl gradient is shown in purple. (B) SDS PAGE analysis of fractions containing GFP at different stages during purification.

profile. There were two peaks corresponding to GFP activity. These fractions were analyzed using spectrophotometry and fluorescence emission spectroscopy. The second peak contained the purest GFP. The SDS-PAGE analysis (Figure 1b) showed a single band at 27kDa after anion exchange chromatography which agreed with the known molecular mass of GFP. It was estimated that the purity of GFP was greater than 90%.

Entrapment of GFP in sol-gels

The procedure for entrapment of GFP in sol-gels was carried out using a previously described procedure [11] as described in Materials and Methods. An overview of the process is described in Figure 2A. Wet gels that were aged for 24–48 hours were used in this study. Two different approaches for casting the sol-gels were tested. The first approach was to layer the sol solution on a clean quartz slide and following gelation to immerse it in 10mM Na phosphate buffer pH 7.0. The second approach involved casting the gels in plastic gel

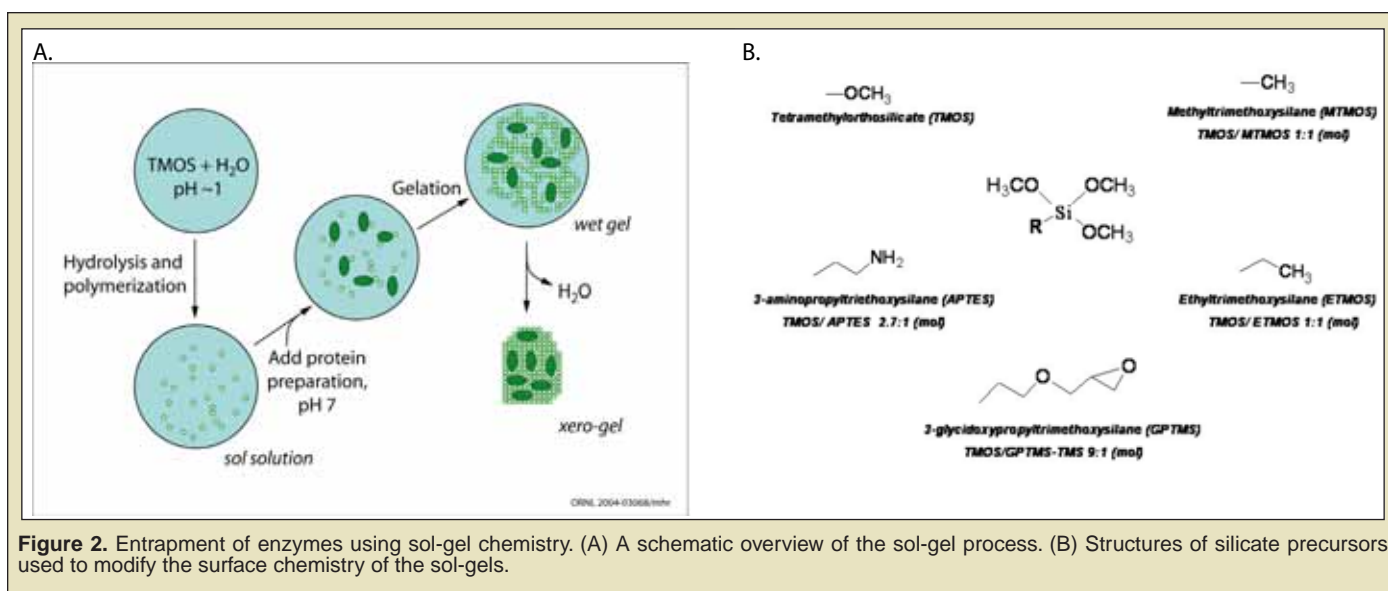


Figure 2. Entrapment of enzymes using sol-gel chemistry. (A) A schematic overview of the sol-gel process. (B) Structures of silicate precursors used to modify the surface chemistry of the sol-gels.

cassettes usually employed for PAGE applications. After gelation, the gels were overlaid with 10mM Na phosphate buffer pH 7 and aged at 4°C. The latter approach had the advantage that the gels were of uniform thickness (1mm) and not as prone to cracking due to changes in surface tension during the gelation process.

A series of gels were synthesized using TMOS singly and in combination with the ORMSILs (organically modified silicates) MTMOS, ETMOS, APTES and GPTMS. The structures of the precursors are shown in Figure 2B. The main criterion for the synthesis of the hybrid gels was to add the maximum amount of ORMSIL that would allow the entrapment of GFP in its native form and preserve the optical properties of the gels. The synthesis conditions are described in Materials and Methods. The absorbance, fluorescence emission spectra and CD spectra of the entrapped GFP in all gel types were identical to the solution spectra Figure 3A. No leakage of GFP was detected from the gels during the time frame the experiments were carried out.

The aim of the project was to investigate how the microenvironment of the entrapped protein affected the refolding of GFP entrapped in the gels. After aging for 24h in 10mM Na-phosphate pH 7.0 the protein sol-gel was immersed in 10mM HCl for at least 15 min or until all fluorescence had disappeared. This took less than 5 min for all types of gel except the APTES gels which required longer incubation times (~30 min). The gels were then placed in 50mM Na-phosphate buffer, pH7.0. The visible absorption, fluorescence emission and circular dichroism spectra of the native, denatured and renatured protein were recorded. A comparison of the acid denaturation-renaturation of GFP in solution and entrapped in silica gels is shown in Figure 3. The chromophore peak at 490nm shifted to 295nm when the protein was exposed to acid due to the protonation of the tyrosyl OH group on the chromophore (Figure 3B) [12]. It is usually in the anionic form in its native fluorescent state. The loss in fluorescence was accompanied by a change in the CD spectrum also. Re-equilibration of the protein at pH 7.0 resulted in partial recovery of fluorescence for GFP in solution (Figure 3C). This was accompanied by a recovery in the native CD spectrum of the protein. Conversely, no recovery of

fluorescence was observed for the protein entrapped in the silica gel. A similar result was obtained for gels functionalized with methyl, ethyl and aminopropyl groups. There was no recovery of fluorescence or evidence for the recovery of the native structure of the protein. A summary of the fluorescence emission data is shown in Figure 4.

In contrast, gels made with GPTMS produced a microenvironment that was favorable for refolding GFP. Gels were made in which the mol ratio of TMOS/GPTMS was varied from 9 to 3. A TMOS/GPTMS mol ratio of 6.7 appeared optimal, with approximately 20% recovery of native fluorescence of GFP (Figure 4). Figure 5 shows the absorption, fluorescence emission and CD spectra of the GFP entrapped in a TMOS/GPTMS gel (6.7 mol ratio). The spectra of the denatured protein was identical to other sol-gel formulations. However, after replacement of the protein in 50mM Na-phosphate buffer pH 7.0 a recovery in fluorescence at 509nm was observed. In addition, the CD spectrum partially regained its native shape. A deconvolution algorithm [13] was used to quantitatively estimate the fraction of each type of secondary structure present in GFP in its three different states (Table 1). There was a decrease in the amount of unordered polypeptide and a concomitant increase in the amount of β -sheet and α -helix present compared to the denatured protein, confirming that the protein refolded after replacement in phosphate buffer after denaturation.

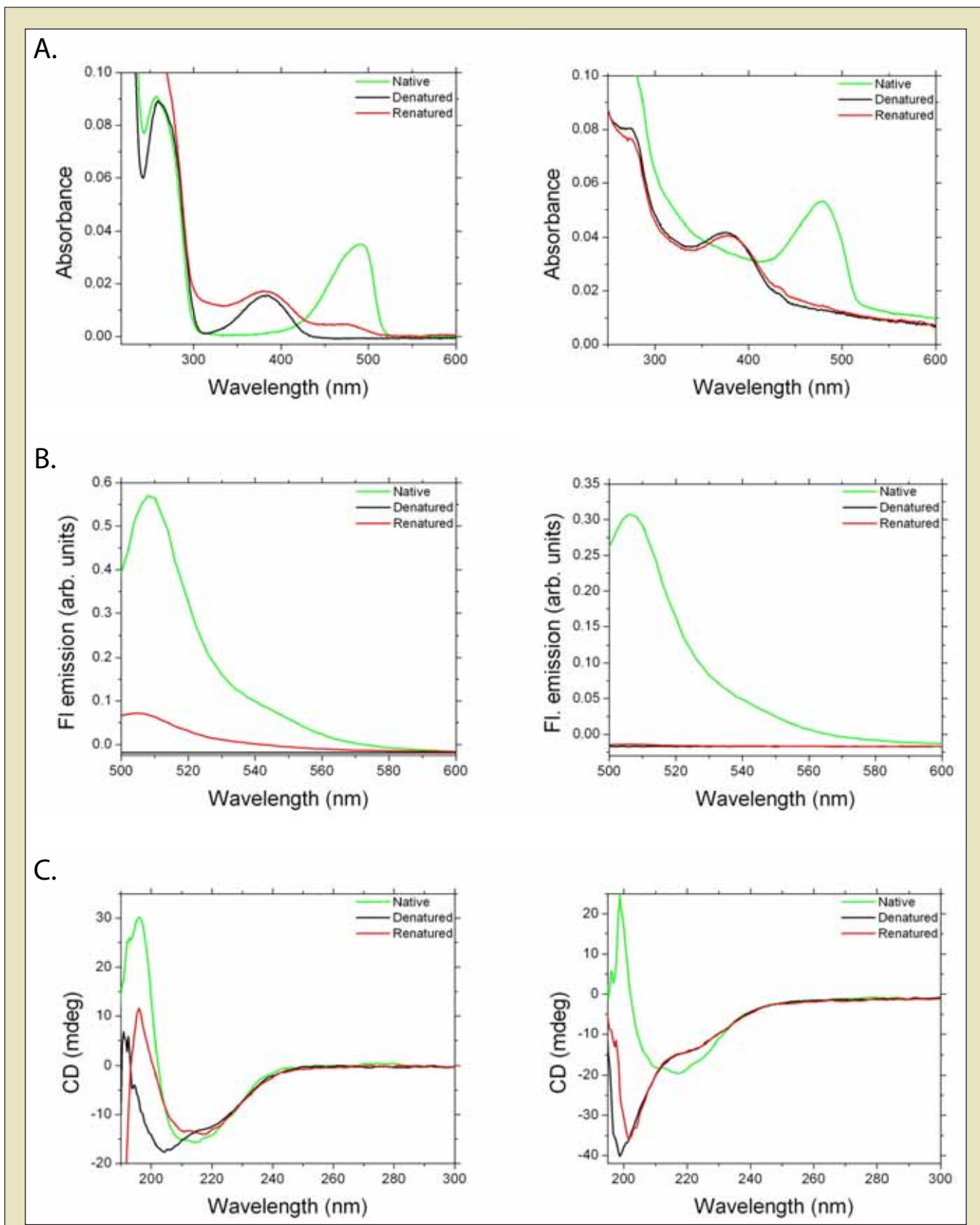


Figure 3. The properties of GFP in solution and entrapped in sol-gels. Spectrophotometric (A), fluorescence emission (B) and circular dichroism spectra (C) were recorded. The left panels correspond to GFP in solution and the right panels are GFP in TMOS gels. Spectra were recorded for native GFP in 10mM Na-phosphate buffer pH 7.0 (green), GFP in 10mM HCl (black) and renatured GFP in 10mM Na-phosphate pH 7.0 (red).

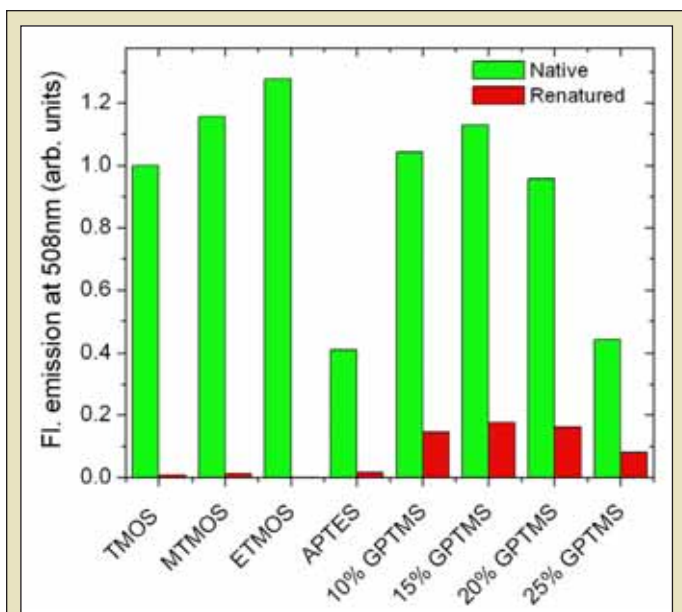


Figure 4. Comparison of fluorescence emission at 508nm of native GFP and the enzyme after renaturation in 10mM Na-phosphate buffer pH 7.0 in different formulations of sol-gels.

DISCUSSION

The aim of the study was to investigate the unfolding properties of GFP entrapped in sol-gels. There were three important aspects to the design of the experimental set-up used. First, the entrapment process resulted in the protein molecules being caged in nanopores creating conditions similar to the crowded environment of the cell. Furthermore, the proteins were spatially separated in the gel matrix allowing ensembles of individual molecules be investigated without interfering effects such as protein-protein interactions. Finally, the surface properties of the pores were altered by incorporation of organic groups into the sol-gel backbone influencing excluded-volume interactions in the pores.

Three different types of environment were created to investigate the refolding properties of GFP in this study. A polar charged environment was formed by negatively charged native sol-gel matrix and by the introduction of amino (NH_3^+) groups did not support the refolding of acid denatured GFP. Similarly, the hydrophobic groups such as methyl and ethyl groups also didn't support refolding of acid denatured GFP. GPTMS has a highly reactive epoxy functional group and under the conditions used for the hydrolysis of the sol precursors it is highly probable that the epoxy functional group was converted to a mixture of 1,2 diol and methoxy alcohol resulting in a hydrophilic uncharged polymer. These uncharged hydrophilic molecules formed by GPTMS precursor did support refolding of GFP. Inert polyethylene glycol like molecules have previously been shown to stabilize the compact native state relative to the less compact unfolded or partially unfolded state of polypeptides [14]. This study supports the view that under crowded conditions excluded volume interactions promoted by inert PEG-like molecules aid the folding properties of biomolecules.

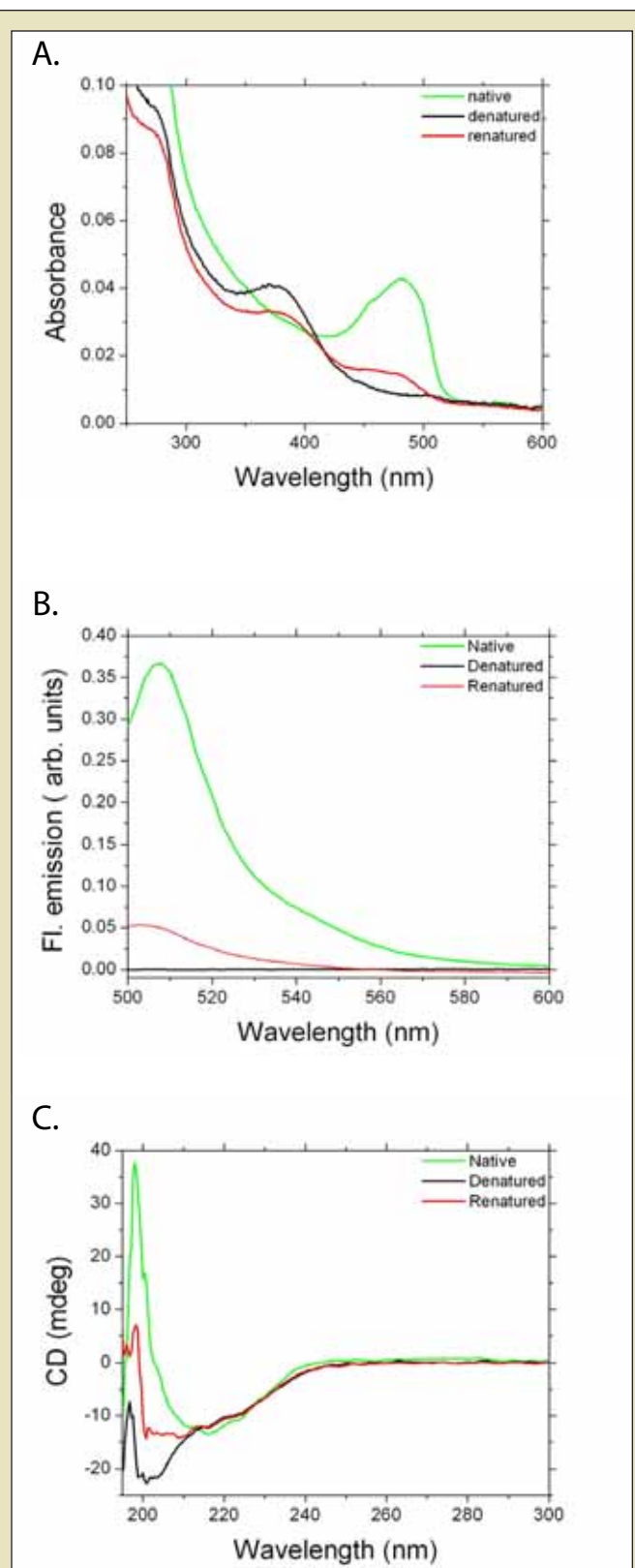


Figure 5. Properties of GFP entrapped in TMOS/GPTMS sol-gels. The spectrophotometric (A), fluorescence emission (B) and circular dichroism spectra (C) were recorded. Spectra were recorded for native GFP (green), GFP in 10mM HCl (black) and renatured GFP in 10mM Na-phosphate pH 7.0 (red).

Structure	H(r)	H(d)	S(r)	S(d)	Trn	Unrd
Native	0.091	0.088	0.228	0.109	0.194	0.289
Denatured	0.030	0.045	0.137	0.075	0.147	0.565
Renatured	0.036	0.045	0.164	0.092	0.170	0.493

Abbreviations: H(r), regular α -helix; H(d), distorted α -helix; S(r), regular β -sheet; S(d), distorted β -sheet; Trn, turn; Unrd, unordered

Table 1. Fractions of each type of secondary structure in GFP entrapped in TMOS/GPTMS sol-gels.

REFERENCES

- [1] Minton, A. P., Implications of macromolecular crowding for protein assembly. *Current Opinion in Structural Biology* **2000**, 10, (1), 34-39.
- [2] Zimmerman, S. B.; Trach, S. O., Estimation of Macromolecule Concentrations and Excluded Volume Effects for the Cytoplasm of Escherichia-Coli. *Journal of Molecular Biology* **1991**, 222, (3), 599-620.
- [3] Avnir, D.; Coradin, T.; Lev, O.; Livage, J., Recent bio-applications of sol-gel materials. *Journal of Materials Chemistry* **2006**, 16, (11), 1013-1030.
- [4] Eggers, D. K.; Valentine, J. S., Molecular confinement influences protein structure and enhances thermal protein stability. *Protein Science* **2001**, 10, (2), 250-261.
- [5] Campanini, B.; Bologna, S.; Cannone, F.; Chirico, G.; Mozzarelli, A.; Bettati, S., Unfolding of Green Fluorescent Protein mut2 in wet nanoporous silica gels. *Protein Science* **2005**, 14, (5), 1125-1133.
- [6] Cannone, F.; Bologna, S.; Campanini, B.; Diaspro, A.; Bettati, S.; Mozzarelli, A.; Chirico, G., Tracking unfolding and refolding of single GFPmut2 molecules. *Biophysical Journal* **2005**, 89, (3), 2033-2045.
- [7] Gurskaya, N. G.; Fradkov, A. F.; Pounkova, N. I.; Staroverov, D. B.; Bulina, M. E.; Yanushevich, Y. G.; Labas, Y. A.; Lukyanov, S.; Lukyanov, K. A., Colourless green fluorescent protein homologue from the non-fluorescent hydromedusa *Aequorea coerulea* and its fluorescent mutants. *Biochemical Journal* **2003**, 373, 403-408.
- [8] Sambrook, J., Fritsch, E.F. & Maniatis, T (1989). *Molecular cloning: a laboratory manual*. Cold Spring Harbor Press. Cold Spring Harbor..
- [9] Jain, S.; Singh, R.; Gupta, M. N., Purification of recombinant green fluorescent protein by three-phase partitioning. *Journal of Chromatography A* **2004**, 1035, (1), 83-86.
- [10] Laemmli, U. K., Cleavage of Structural Proteins during Assembly of Head of Bacteriophage-T4. *Nature* **1970**, 227, (5259), 680-&.
- [11] Ellerby, L. M.; Nishida, C. R.; Nishida, F.; Yamanaka, S. A.; Dunn, B.; Valentine, J. S.; Zink, J. I., Encapsulation of Proteins in Transparent Porous Silicate-Glasses Prepared by the Sol-Gel Method. *Science* **1992**, 255, (5048), 1113-1115.
- [12] Wiehler, J.; Jung, G.; Seebacher, C.; Zumbusch, Z.; Steipe, B., Mutagenic stabilization of the photocycle intermediate of green fluorescent protein (GFP). *ChemBiochem* **2003**, 4, (11), 1164-1171.
- [13] Sreerama, N.; Woody, R. W., Analysis of protein CD spectra: Comparison of CONTIN, SELCON3, and CDSSTR methods in CDPro software. *Biophysical Journal* **2000**, 78, (1), 334A-334A.
- [14] Tellam, R. L.; Sculley, M. J.; Nichol, L. W.; Wills, P. R., The Influence of Poly(Ethylene Glycol) 6000 on the Properties of Skeletal-Muscle Actin. *Biochemical Journal* **1983**, 213, (3), 651-659.

Marlene Hahn is currently a graduate student at Loyola University Chicago, pursuing an M.S. in Education — Curriculum and Instruction. She participated in the Pre-Service Teacher Internship Program at Fermilab, researching the comparison of the common wood-nymph population in differently treated habitats, resulting in the following paper. Ms. Hahn grew up in Wheaton, Illinois. She received an undergraduate degree on microbiology, from the University of Illinois (Champaign-Urbana).

Rod Walton is the coordinator for the DOE National Environmental Research Park (NERP) at Fermi National Accelerator Laboratory in Batavia, Illinois. While there he has worked on a wide variety of research projects, including plant-insect interactions, applications of game theory in animal behavior, and restoration ecology. He received his Ph.D. in Ecology and Evolutionary Biology in 1986 from Indiana University.

COMPARISON OF THE POPULATIONS OF COMMON WOOD-NYMPH BUTTERFLIES IN BURNED PRAIRIE, UNBURNED PRAIRIE AND OLD FIELD GRASSES

MARLENE HAHN AND ROD WALTON

ABSTRACT

Common wood-nymph butterflies are found throughout the United States and Canada. However, not much is known about how they overwinter or their preferences for particular grasses and habitats. In this study, the impact of prairie management plans on the abundance of the wood-nymph population was assessed, as well as the preference of these butterflies for areas with native or non-native grasses. The abundance of common wood-nymph butterflies was determined using Pollard walks; more common wood-nymph butterflies were found in the European grasses than were found in the burned and unburned prairie sites. The majority of the vegetation at each of the three sites was identified and documented. Using a 1 X 3 ANOVA analysis, it was determined there were significantly more butterflies in the European grasses than in the burned and unburned prairie sites ($p < 0.0005$). There was no significant difference between the burned and unburned treatments of the prairie on the common wood-nymph population. A multiple variable linear regression model described the effect of temperature and wind speed on the number of observed common wood-nymph butterflies per hour ($p = 0.026$). These preliminary results need to be supplemented with future studies. Quadrat analysis of the vegetation from all three sites should be done to search for a correlation between common wood-nymph butterfly abundance per hour and the specific types or quantity of vegetation at each site. The effect of vegetation height and density on the observer's visual field should also be assessed.

INTRODUCTION

In 1975, Fermi National Accelerator Laboratory (Fermilab) started prairie restoration [1]. Since then, this restoration project has continued to grow and now includes various ecosystems. To aid this endeavor, the Ecological Land Management (ELM) Committee meets and makes recommendations for land management and prairie restoration [2]. Understanding how different animals, including insects, utilize the landscape at Fermilab is critical in managing this restoration project. Furthermore, certain insects can be used as indicators to monitor the success of the restoration process.

One of the inhabitants of the Fermilab prairie is a butterfly called the common wood-nymph. Common wood-nymph butterflies (*Cercyonis pegala*) are medium-sized butterflies (2 to 3cm in length), which live in fields, prairies, woodlands, meadows, marshes, thickets, and roadsides [3]. Unlike other types of butterflies, the common wood-nymph is found throughout the United States and Canada. These opportunistic wood-nymphs can live even in ruderal habitats [4]. Physically, common wood-nymph butterflies are brown with eyespots; however, this species of butterfly shows quite a degree of

variation in appearance. Over the course of their lifespan, these butterflies lighten in color. Females are generally larger and lighter in color with larger eyespots than their male counterparts [3]. The caterpillars feed on various grasses including *Tridens flavus* (purpletop), *Andropogon gerardii* (big bluestem), *Elymus glaucus* (blue wildrye), *Festuca californica* (California fescue), and *Bromus carinatu* (California brome) [5, 6, 7]. The butterflies overwinter as caterpillars and generate one brood during the summer. The adult common wood-nymph feeds on rotting fruit and flower nectar from such plants as *Echinacea purpurea* (purple coneflower), *Liatrix spicata* (blazing star), *Aster novae-angliae* (aster), and *Asclepias syriaca* (common milkweed) [8, 9].

At Fermilab, land management and treatment is based upon the vegetation; mowing and burning cycles are used to control invasive, non-native plants. However, it is also important to study the impact of these different treatments on the insects and other animals inhabiting these areas. Since the common wood-nymph is not remnant-dependent and is seen in various environments, this butterfly was used as an indicator of the effects of using burning and mowing as management techniques on the prairie habitat at

Fermilab. In this study, burned prairie, unburned prairie, and old-field habitats were used to study the effects of habitat treatments on the abundance of the common wood-nymph butterfly.

MATERIALS AND METHODS

Relative Abundance of Butterflies

During the summer of 2006, three sites with different land management treatments at Fermilab were observed during this study. Site 1 is in an area called the Interpretive Trail in ELM-25 (Figure 1). This area consists of prairie habitat that is burned every two to three years. This site was last burned in the fall of 2005. Site 2 is southeast of the Main Injector in ELM-4. This site also consists of a prairie habitat that is managed by burning every two

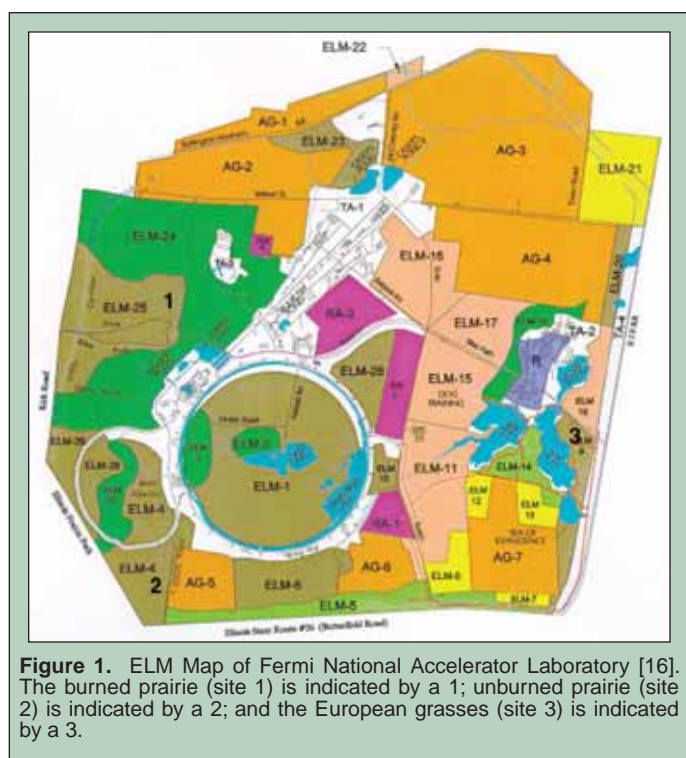


Figure 1. ELM Map of Fermi National Accelerator Laboratory [16]. The burned prairie (site 1) is indicated by a 1; unburned prairie (site 2) is indicated by a 2; and the European grasses (site 3) is indicated by a 3.

to three years. The last burn was in fall 2003, it has been defined as unburned prairie. Site 3 is along the eastern border of Fermilab in ELM-9 [10]. This site of European grasses is mowed every other season, leaving approximately 15 centimeters of growth after the mow. It was last mowed in the summer of 2005.

The number of butterflies was estimated using a Pollard walk. Each walk took approximately fourteen to fifteen minutes, covering approximately 550, 450, and 400 meters respectively for sites 1, 2 and 3. The Pollard walk consisted of walking five to seven minutes in one direction, a one- to five-minute walk perpendicular to the first walk, followed by a five- to seven-minute walk opposite the first direction, depending on the site [11, 12]. Walks were done between the hours of 10 AM and 3 PM on days with temperatures above 21°C with light to moderate winds [11, 13]. Meteorological data was obtained from a station maintained by Fermilab within 2 km of the

study sites [13]. Butterflies were counted using a hand counter to document observations of common wood-nymph butterflies within six meters of the Pollard walk [11, 12]. A walk-through of each site was performed to characterize the major plant compositions of each area [14, 15].

Statistical Analysis

A 1 X 3 Analysis of Variance (ANOVA) was used to compare the butterfly abundances at the three different sites. In this study, the independent variable was the treatment of the sites (burned prairie, unburned prairie, and old field); the dependent variable was the number of wood-nymph butterflies per hour found at each site.

Multiple variable linear regression analysis with a backward selection of variables was performed to determine which weather variables (relative humidity, temperature, and wind speed) affected the abundance of butterflies during the study.

RESULTS

Quantitative Analysis of Butterflies

Figure 2 shows the daily abundance of common wood-nymph butterflies per hour found at each site during the study. Over the course of the study, the average number of butterflies observed was 3.7 in the burned prairie, 4.1 in the unburned prairie, and 10.7

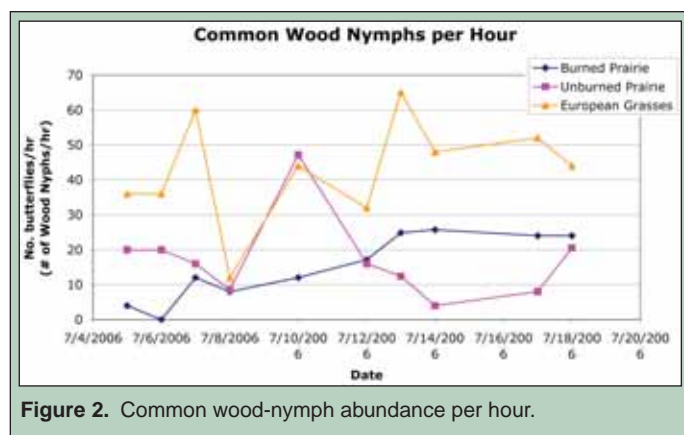


Figure 2. Common wood-nymph abundance per hour.

in the European grasses. To correct for slight timing differences, the average number of butterflies per hour was calculated. Figure 3 shows the average number of butterflies per hour found at each site during the course of the study. ANOVA results showed that there was a significant difference between the observed butterflies per hour at the three sites ($F_{2,27} = 15.569, p < 0.0005$). Results of the ANOVA were significant at 0.05. A Tukey HSD post-hoc test showed that the European grass habitat supported significantly more butterflies than either of the prairie sites ($p < 0.0005$); however, there was not a statistically significant difference between the prairie sites with different treatments.

Multiple linear regression analysis with backward selection of variables showed temperature and wind speed significantly affected the abundance of the common wood-nymph at any given site on

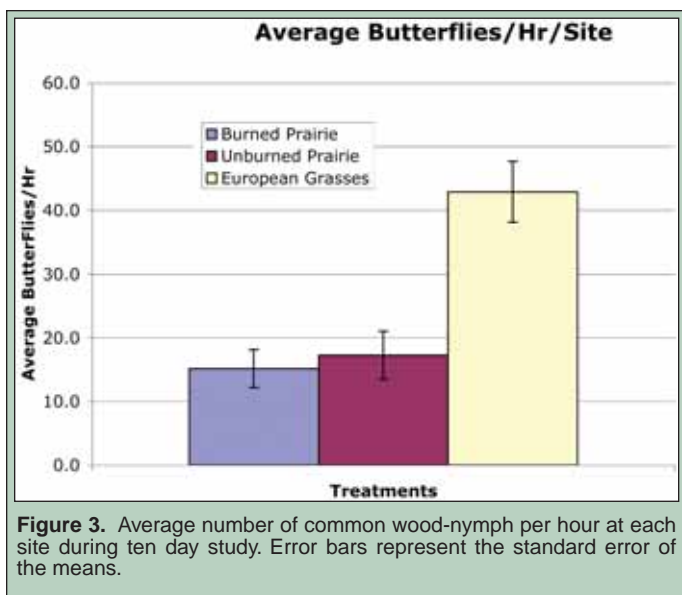


Figure 3. Average number of common wood-nymph per hour at each site during ten day study. Error bars represent the standard error of the means.

a given day ($F_{2,27} = 4.205, p = 0.026$). Wind speed had a negative effect on the number of butterflies observed per hour ($t = -2.240, p = 0.033$), while temperature had a positive effect on the number of butterflies observed per hour ($t = 2.339, p = 0.027$).

Description of Study Area

Site 1, the burned prairie, had the most diverse vegetation of the three sites (Table 1). The dominant species within this site was big bluestem (*A. gerardii*), although not overwhelmingly so. Site 2, the unburned prairie, had fewer species of vegetation than the burned prairie site. Again, the dominant species was big bluestem (*A. gerardii*); however, the distribution of vegetation within these two sites was very different. Based upon observation during the Pollard walks, the burned prairie's vegetation was more evenly distributed throughout the site, while the unburned prairie had two distinct areas with different distributions of vegetation. The northeastern area of the unburned prairie consisted mainly of forbs, while the rest of this site consisted mainly of grasses. Most of the butterflies seen in the unburned prairie were found within a small area of grasses just south of the forbs area. In contrast to both prairie sites, site 3 consisted of mainly non-native grasses; this European grassland area lacked the variation in vegetation species found in both prairie sites. The dominant vegetation at this site was Hungarian brome (*Bromus inermis*).

DISCUSSION AND CONCLUSIONS

The ANOVA and Tukey HSD post-hoc test results indicate a statistically significant difference in the abundance of common wood-nymph butterflies in the European grasses compared to both prairie sites. The fact that more common wood-nymph butterflies were found in the European grasses than in the two prairie sites was somewhat unexpected, in that common wood-nymphs are a native butterfly and might be expected to prefer native grasses. Nonetheless, this preliminary study on land management treatments of grasslands showed a native butterfly species preferentially living in non-native

Site 1: Burned Prairie	Site 2: Unburned Prairie	Site 3: European Grasses
big bluestem grass	big bluestem grass	Canadian thistle
black-eyed Susan	compass plant	chicory
compass plant	crown vetch	crown vetch
Culver's root	Culver's root	daisy fleabane
daisy fleabane	curled dock plant	dogwood
foxglove beard tongue	daisy fleabane	field clover
golden Alexander	dogwood	goat's beard
grey-headed coneflowers	foxglove beard tongue	Hungarian brome
Hungarian brome	Indian hemp	jimson weed
Indian hemp	mountain mint	multiflora rose
Indian milkweed	Queen Anne's lace	plantain
indigo	rattlesnake master	quack grass
mountain mint	rosin weed	Queen Anne's lace
obedient plant	sedge carex	ragweed
prairie dock	smart weed	reed canary grass
purple coneflowers	sweet black-eyed Susan	Timothy grass
Queen Anne's lace	tall coreopsis	wild grape vines
reed canary grass	tall goldenrod	yellow sweet clover
rattlesnake master	white sweet clover	
rosin weed	whorled milkweed	
sawtooth sunflowers	wild bergamot	
spiderwort	wild grape	
stiff goldenrod		
switch grass		
tall coreopsis		
tick trefoil		
white sweet clover		
wild bergamot		
wild quinine		
wild raspberry		
yellow sweet clover		

Table 1. Vegetation found at each site [14].

grasses. There was no significant difference in observed butterfly numbers between the two treatments of the prairie. These data suggest the types of vegetation within the area, or other unknown variables within a site, might be more significant than whether the land is burned, unburned, or mowed. It has been previously documented that various grasses are the host plant for the common wood-nymph larvae. All three sites contained various grasses, but, qualitatively, there were more grasses in the European site than in the prairie sites, which were more diverse in the number of vegetation species. This suggests that the common wood-nymph is a generalist species which does not discriminate between types of grasses.

The multiple regression analysis created a model in which temperature and wind speed affected the number of butterflies observed per hour. This result is not surprising. As it has been noted previously, butterflies should be observed on days with low wind and temperatures above 21°C [11]. Interestingly, the interaction between wind speed and temperature does seem to be more important than either wind speed or temperature alone.

This preliminary study provides guidance for future studies. Future research on land management treatments using the common wood-nymph as an indicator species should include a quadrat analysis of the existing vegetation in order to quantify differences between sites. Informal observations noted several common wood-nymphs on disrupted grasslands or edges of grasslands. This observation suggests future studies in which a path is mowed at each site to use as a comparison to the unmowed path. A caveat of this study is that the Pollard walk data is dependent on seeing the butterflies six meters on either side of a pathway. These data and analysis did not take into account the density of the vegetation and the visual field of the observer to see the butterflies.

ACKNOWLEDGMENTS

This research was done at Fermi National Accelerator Laboratory as part of the Department of Energy's Pre-Service Teacher internship program. I would like to thank the Department of Energy's Office of Science for giving me the opportunity to participate in the PST program, Spencer Pasero for helping me with statistical analysis, Rod Walton for help with the experimental design and the statistical analysis, and Tom Peterson for taking the time to share his knowledge of butterflies. I would also like to thank Anna Zuccarini for all her encouragement, aid, and knowledge throughout this PST program. I would also like to acknowledge everyone at the Lederman Science Center for their support and friendship throughout my internship, especially Mary Jo Murphy for her expert help in identifying vegetation at the three sites.

REFERENCES

- [1] "An Atlas of Biodiversity," Chicago Wilderness: A Regional Nature Reserve (2003)
- [2] Ecology/Nature – Prairie – Bringing back the prairie (2006, June 29), <http://www.fnal.gov/pub/about/campus/ecology/prairie/back.html>
- [3] R. M. Pyle, National Audubon Society Field Guide to North American Butterflies, New York: Chanticleer Press, 1994, pp. 560 and 614.
- [4] R. Panzer, D. Stillwaugh, R. Gnaedinger, and G. Derkovitz, "Prevalence of remnant dependence among the prairie- and savanna-inhabiting insects of the Chicago region." In Natural Areas Journal, Vol. 15, 1995, pp. 101-116.
- [5] "Butterflies of North America," USGS Northern Prairie Wildlife Research Center (2006, June 12), <http://www.npwr.usgs.gov/resource/distr/lepid/bflyusa/usa/98.htm>
- [6] "Host Plants by Common Name" (2006, July 26), <http://www.dallasbutterflies.com/Butterfly%20Gardening/Host%20Plants%20by%20Common%20Name.htm>
- [7] B. Newhouse, "Willamette Valley Butterflies and Native Host Plants" (2006, July 26), <http://www.naba.org/chapters/nabaes/btrfly-gdng2.html>
- [8] "Butterfly Gardening" (2006, July 26), <http://butterflywebsite.com/butterflygardening.cfm>
- [9] "Wildtype, where will these plants grow?" (2006, July 26), <http://www.wildtypeplants.com/butterflyplants.htm>
- [10] "Current ELM Track Summaries," Fermi National Accelerator Laboratory (2006, June 19), <http://www.fnal.gov/cgi-bin/ecology/frame?TYPE=TRACT&YEAR=NOW>
- [11] R. Panzer, D. Stillwaugh, D. Taron, and M. Manner, "Illinois Butterfly Monitoring Network Guidelines: Website Edition" (2006, June 19), <http://www.bfly.org/>
- [12] D. A. Wyrzykowski, "Analysis of the Vegetation in the Meadow Fritillary Butterfly Habitat," 2005 (unpublished)
- [13] "Weather at Fermilab," Fermi National Accelerator Laboratory (2006, June 18), http://www-esh.fnal.gov/pls/public/weather.year?this_year=2006
- [14] D. Young, Kane County Wild Plants Natural Areas, Batavia, Illinois: Kane County Forest Preserve District, 1994.
- [15] Mary Jo Murphy, private conversations, July 2006
- [16] "ELM Map" (2006, August 3), http://www-esh.fnal.gov/ELM/Map2000/elm_map.jpg

Jeff Head received his B.S. in chemistry from Colorado State University in the spring of 2006. As an undergraduate Jeff worked with Dr. Bruce Parkinson on a combinatorial analysis of metal oxides capable of driving the water-splitting reaction for hydrogen production. Before and after his senior year at CSU Jeff completed two Science Undergraduate Laboratory Internships (SULI) at the National Renewable Energy Laboratory (NREL). While at NREL the focus of his studies was to carry out the photoelectrochemical characterization of various nitride compounds. Specifically, the goal of the research was to determine the water-splitting capabilities of the compounds with light as the only energy input. Advising him on the project was Dr. John Turner (NREL). Jeff is currently pursuing graduate studies in analytical chemistry at the University of Arizona for his Ph.D. under the direction of Dr. Neal R. Armstrong.

John A. Turner, Ph.D., is a Principal Scientist at NREL. He received his B.S. degree from Idaho State University, his Ph.D. from Colorado State University, and completed a postdoctoral appointment at the California

Institute of Technology before joining the Laboratory. His research is primarily concerned with enabling technologies for the implementation of hydrogen systems into the energy infrastructure. This includes direct conversion (photoelectrolysis) systems for hydrogen production from sunlight and water, advanced materials for high temperature fuel cell membranes, and corrosion protection for fuel cell metal bipolar plates. Other work involves the study of electrode materials for high energy density lithium batteries and fundamental processes of charge transfer at semiconductor electrodes. He has twice received the Midwestern Research Institute President's Award for Exceptional Performance in Research. In addition, he has received the Hydrogen Technical Advisory Panel award for Research Excellence, an Idaho State University Outstanding Achievement Award (2006), and two Outstanding Mentor Awards from the U.S. Department of Energy for his work with undergraduate students. He is the author or co-author of over 90 peer-reviewed publications in the areas of photoelectrochemistry, fuel cells, batteries, general electrochemistry and analytical chemistry.

ANALYSIS OF THE WATER-SPLITTING CAPABILITIES OF GALLIUM INDIUM PHOSPHIDE NITRIDE (GaInPN)

JEFF HEAD AND JOHN TURNER

ABSTRACT

With increasing demand for oil, the fossil fuels used to power society's vehicles and homes are becoming harder to obtain, creating pollution problems and posing hazard's to people's health. Hydrogen, a clean and efficient energy carrier, is one alternative to fossil fuels. Certain semiconductors are able to harness the energy of solar photons and direct it into water electrolysis in a process known as photoelectrochemical water-splitting. P-type gallium indium phosphide (p-GaInP₂) in tandem with GaAs is a semiconductor system that exhibits water-splitting capabilities with a solar-to-hydrogen efficiency of 12.4%. Although this material is efficient at producing hydrogen through photoelectrolysis it has been shown to be unstable in solution. By introducing nitrogen into this material, there is great potential for enhanced stability. In this study, gallium indium phosphide nitride Ga_{1-y}In_yP_{1-x}N_x samples were grown using metal-organic chemical vapor deposition in an atmospheric-pressure vertical reactor. Photocurrent spectroscopy determined these materials to have a direct band gap around 2.0eV. Mott-Schottky analysis indicated p-type behavior with variation in flatband potentials with varied frequencies and pH's of solutions. Photocurrent onset and illuminated open circuit potential measurements correlated to flatband potentials determined from previous studies. Durability analysis suggested improved stability over the GaInP₂ system.

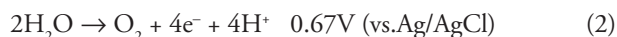
INTRODUCTION

Today humans collectively consume the equivalent of approximately 13 terawatts of energy; 85% of that comes from fossil fuels that release carbon dioxide, the primary greenhouse gas, into the atmosphere [1]. Moreover, pollution from fossil fuels used in society today creates many environmental and health problems. In addition, global warming is thought to be directly linked to the exponentially increasing anthropogenic carbon dioxide concentrations in the atmosphere that has been taking place over the past 200 years [2]. Several renewable energy sources exist that are capable of providing a cleaner form of energy from sun and wind power. For example, hydrogen is a clean and efficient energy carrier and has great potential when coupled to renewable energy resources. Various renewable

technologies, such as biomass and geothermal power, can produce hydrogen fuel for use when it is not sunny or windy.

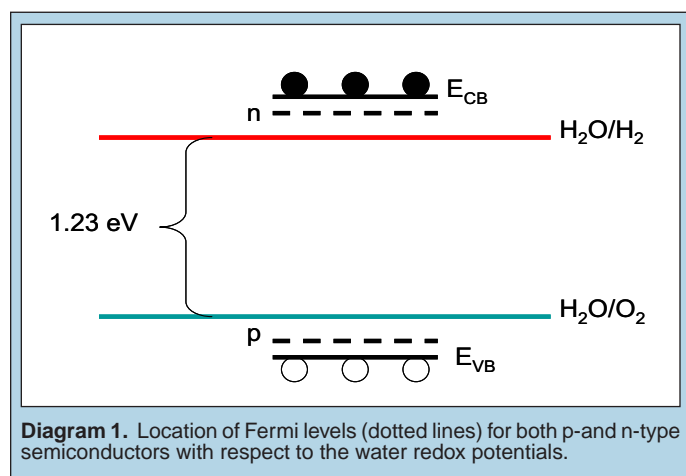
One of the most efficient ways of producing hydrogen is using sunlight to directly split water into hydrogen and oxygen on semiconductor surfaces [3]. An electric potential difference of at least 1.23V is required to split water into hydrogen and oxygen. Typically, a cathodic overpotential of 100mV and an anodic overpotential of 200mV are also required, so a band gap of at least 1.53eV is necessary for splitting water. It is important to take note that as band gap increases the portion of the solar spectrum the semiconductor can absorb diminishes [4]. In addition to having an adequate band gap, the semiconductor should exhibit stability in solution. Another key requirement relates to the energetic positions of the valence and conduction band edges at the solution interface.

Specifically, the energy bands must encompass the potentials at which the following half reactions occur:



The potentials associated with (1) and (2) will vary according to the Nernstian dependence on solution pH. The values given above are for a pH 6 electrolyte.

Semiconductors are classified as either n-type or p-type. Semiconductors in which the majority charge carriers are electrons are n-type whereas those in which the majority charge carriers are holes are p-type [5]. Oxygen evolution takes place on the surface of n-type materials and hydrogen evolution takes place on the surface of p-type materials. Preliminary characterization of semiconductors is carried out using open circuit potential measurements, photocurrent measurements, and Mott-Schottky analysis [6]. In estimating the location of the band edges one must factor in the Fermi level of the material, which for n-type materials lies just below the conduction band, and for p-type materials lies slightly above the valence band, as seen in Diagram 1.



The flatband potential, E_{fb} , the potential at which there is no net transfer of charge, and hence no band bending, or the energy of the Fermi level, which is the level at which the electrons are located, when the bands are flat, can be estimated from Mott-Schottky plots [5], based on the following equation:

$$\frac{1}{C^2} = \frac{1.41 \times 10^{32}}{\epsilon N_D} \left[E - (V_{fb}) \frac{kT}{e} \right] \quad (3)$$

where C is the capacity of the space charge layer, ϵ is the static dielectric of the semiconductor (assumed to be 10), e is the electronic charge, N_D is the doping density, and E is the electrode potential [5]. Plotting the inverse square of capacitance versus voltage will give a linear plot with x-intercept equal to the flatband potential and a slope inversely proportional to the doping density. Similarly, measuring the illuminated open circuit potential can give the location of the Fermi level at flatband conditions.

Current studies show that when p-GaInP₂ is grown in tandem on a p/n GaAs substrate, water-splitting is successful with 12.4% solar-to-hydrogen efficiency [8]. Although this system exhibits efficient photoelectrolysis, studies show that it is susceptible to photoinduced corrosion, rendering it useless after several hours of irradiation [7]. A possible solution to the instability of these materials in solution is the introduction of nitrogen into the system.

Through metal-organic chemical vapor deposition (MOCVD), various ratios of gallium indium phosphide to nitride can be achieved when grown on a gallium phosphide substrate. The goal of this research is to isolate a stable epilayer material capable offering protection to a water splitting photoelectrode.

METHODS

Preparation of Samples

Gallium indium phosphide nitride samples were grown by metal-organic chemical vapor deposition (MOCVD) in an atmospheric-pressure vertical reactor. Zinc-doped gallium phosphide substrates were used as the growth template at 650°C. Triethylgallium, nitrogen trifluoride, trimethylindium, and phosphine sources were used, with hydrogen as the carrier gas (Triethylgallium and trimethylindium were OptoGrade from Rohm and Hass Electronics, the phosphine was 99.9999% from Air Products and nitrogen trifluoride was 99.99% from Air Products). X-ray diffraction (XRD) measurements of the samples were taken to determine the lattice parameters used to estimate compositions. The XRD pattern was measured by means of a four-circle Scintag X-1 diffractometer (Thermolab) with a copper K α anode source. Once grown, electrodes of the samples were constructed using copper wire and epoxy. Samples were cleaved using a diamond scribe and lens paper and were mounted to coiled copper wire pieces within glass tubing using silver paint. The colloidal silver liquid was obtained from Ted Pella, Inc. Samples were then dried at 80°C for approximately 20 minutes. Edges of the semiconductor and exposed copper wire were then covered with HYSOL 9462 epoxy and left to dry overnight. After 24 hours the electrodes were again placed in the oven at 80°C for 2 hours. The 9462 epoxy was then covered with HYSOL E-120 epoxy, which was left to dry at room temperature for 3 hours, followed by being placed in the oven at 80°C for 2 hours. Surface areas of the electrodes were determined with a photocopy technique which compared the ratio of the photocopy area mass to that of a standard 1 cm² cutout [9].

Photocurrent Spectroscopy

A Stanford Research Systems chopper model SR540 along with a Stanford Research Systems Lock-in amplifier model SR830 DSP, and a PAR Potentiostat/Galvanostat Model 263A was used for photocurrent spectroscopy, along with Tungsten light source model LPS-220 at 75 Watts from Photon Technology International PTI. The experiments were performed in a glass cell with a borosilicate front face. The working electrodes were submerged in hexaammineruthenium (III) chloride in pH 2 buffer with a platinum counter electrode, and silver/silver chloride reference electrode, and

scanned from 350 to 700nm using a 345nm filter to block second order diffraction.

Various electrochemical measurements were taken using GaInPN as the working electrode, along with a platinum counter electrode, and a silver/silver chloride reference electrode. This configuration was in a three port glass cell containing separate solutions of 3M H₂SO₄ (J.T. Baker), pH 2-pH 12 buffer (Hydriion Buffer Kenvelopes 280-7.00), and 1M KOH (J.T. Baker).

Cyclic Voltammetry

Using a potentiostat and frequency response analyzer (Solartron 1286 electrochemical interface/SI 1260 Impedance/Gain-Phase Analyzer), cyclic voltammetry scans were taken in the dark and light (100mW/cm²), to see if the material passed anodic or cathodic photocurrent. Mott-Schottky analysis was carried out to determine flatband potentials as well as doping densities. Intensely illuminated open circuit potential measurements were taken using a DC power supply with a tungsten bulb at 10A (Oriel Corporation Model 66183 OSRAM Tungsten Bulb) for determining flatband positions.

Platinum Catalyst Surface Treatments

Platinum catalyst surface treatments were carried out using a two electrode technique of shorting the counter electrode, CE, and reference electrode, REF, leads connected to a platinum counter electrode, where samples were etched with concentrated sulfuric acid for approximately 20 seconds. Samples were then electroplated using a current relative to their surface areas in yellow chloroplatinic acid solution. These scans allowed for measurement of the photocurrent onset, another technique used to determine flatband potentials.

Durability Analysis of the Electrodes

Durability analysis of the electrodes was carried out using platinized electrodes and a DC powered lamp with a neutral density filter to attenuate the light intensity. After all the electrochemical data was collected the electrodes were disassembled for profilometry analysis to determine the amount of etching of the sample. Durability solutions were saved for future inductively coupled proton mass spectrometry, ICP-MS, analysis.

Software

Cyclic voltammetry, open circuit potential measurements, platinization, and durability measurement analyses were carried out using CorrWare2 software, and Mott-Schottky analysis was carried out using Zplot software from the vendor Scribner Associates International.

RESULTS

Samples were grown using metal organic chemical vapor deposition at 608 torr for 1 hour which resulted in 1μm thick materials of approximately 4cm². The substrate was p-type zinc doped gallium phosphide which served as the template for single

crystal epilayer growth. X-ray diffraction measurements of atomic spacing resulted in estimated compositions of Ga_{0.95}In_{0.05}N_{0.025}P_{0.975} (MF933) and Ga_{0.96}In_{0.04}N_{0.024}P_{0.976} (MF932).

Once the samples were manufactured into electrodes, photocurrent spectra of the materials were taken and the tungsten lamp spectra was divided out [11] giving a normalized photocurrent. The direct band gap of the sample was estimated using a plot of the photocurrent squared vs. photon energy, as shown in Figure 1. The x-axis intercept of the linear portion of this curve gives the figure of merit. Out of thirteen electrodes tested, the band gap varied only slightly, from 1.99 to 2.01eV (Table 1).

In a solution of 3M H₂SO₄ with a working, counter, and reference electrode, potential as a function of current resulted in a wide shift in cathodic current when illuminated, as seen in Figure 2. For both sample compositions the current shifted an order of magnitude upon illumination. Minimal shifts occurred when tests took place in pH's ranging from 2-12, and 1M KOH.

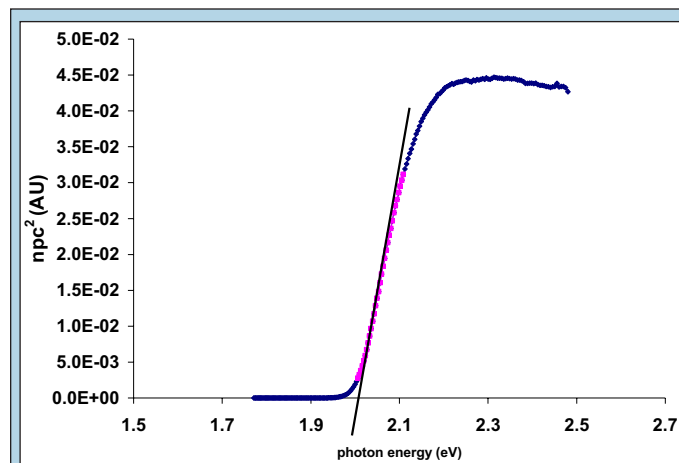


Figure 1. Band gap plot of Ga.96In.04N.024P.976 from 500 to 700nm in Hexaammineruthenium (III) Chloride with a 495nm filter with extrapolated intercept from normalized photocurrent squared versus photon energy (eV).

Material	Direct Band Gap (eV)
Ga.96In.04N.024P.936	
1	2.00
2	2.00
3	2.00
4	2.00
5	2.00
6	2.01
7	2.01
Ga.95In.05N.025P.975	
1	2.00
2	2.00
3	1.99
4	1.99
5	1.99
6	2.00

Table 1. Summary of band gap values for each respective composition with numbered electrodes tested with an error of ± 0.01eV.

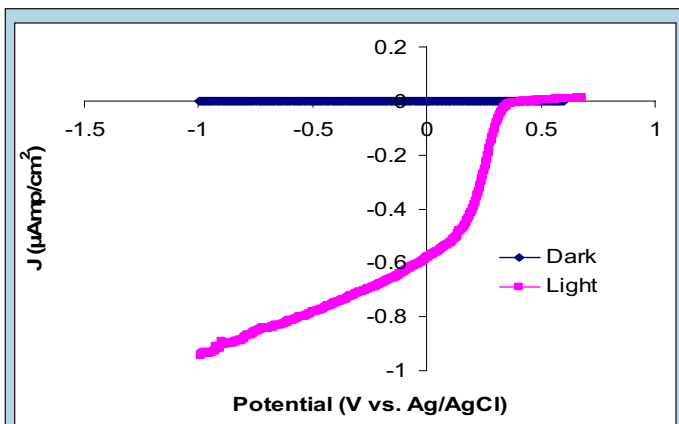


Figure 2. I-V plot in 3M H₂SO₄ of Ga_{0.86}In_{0.04}N_{0.24}P_{0.976} in dark and light conditions with a fiber optic lamp at 0.100W/cm².

Mott-Schottky analysis was performed on each sample in 3M H₂SO₄ while varying the frequency between 1000 and 20,000Hz in the dark and light. All plots obtained from analysis revealed doping densities on the order of 10¹³ to 10¹⁶/cm³, with varied aphysical x-intercepts, and all negative slopes, indicative of p-type behavior.

Illuminated open circuit potential, OCP, measurements were taken in a range of solution pH's and the values are assumed to be close to the flatband potential (Figure 3). Photocurrent onset measurements on platinized electrodes were also used to estimate the flatband potential (Figure 3). The difference between the two measurements is attributed to the overpotential of hydrogen evolution from the photocathode. Both techniques demonstrated

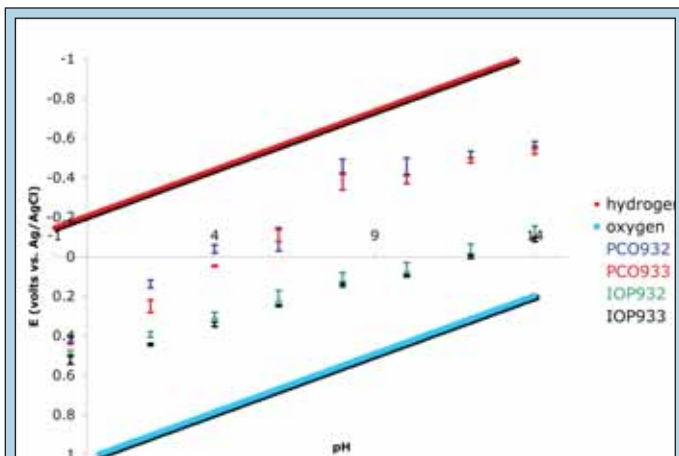


Figure 3. Illuminated open circuit potential (OCP) and photocurrent onset (PCO) measurements in pH values ranging from -0.5 to 14.

a steady increase in (flatband) potential with an increase in pH, as is typically observed in semiconductors.

Durability analysis was performed in 3M sulfuric acid with Triton X-100 in a two-electrode cell with a platinum black counter electrode. A DC lamp was used with a water filter and neutral density filter to attenuate light to AM1.5 [10] intensity. Samples passed a cathodic current of 5mA/cm² for 24 hours using the solarton as a galvanostat. Electrodes were disassembled and etching was probed

with a profilometer with an average depth of .13µm. Solutions were saved for future ICP-MS elemental analysis.

DISCUSSION AND CONCLUSIONS

The linear portion in the plot of normalized photocurrent squared vs. photon energy indicates a direct transition is present in these materials. The extrapolated intercept from this line results in a direct band gap of 2.00 ± 0.01eV (Figure 1). The results are tabulated in Table 1. GaInPN exhibits an appropriate band gap to drive the water-splitting reaction.

The sign of photocurrent observed in I-V scans can indicate whether a semiconductor is p-type or n-type (Figure 2). For p-type semiconductors, cathodic photocurrent arises at potentials negative of the flatband potential because of the orientation of the electric field in the space charge region. This behavior was observed inferring that these GaInPN materials are p-type despite being grown without the intentional introduction of dopants. In Figure 2 photocurrent onset can be observed near a positive potential of -0.4V, where during the scan bubble evolution took place on the surface of the working electrode suggesting hydrogen evolution.

Mott-Schottky analysis is another good indicator of p- and n-type semiconductor characteristics. The slope of an M-S plot (1/C² vs. applied potential) can reveal whether the material is p-type (negative slope) or n-type (positive slope) [5]. All electrodes tested displayed the suggested p-type negative slope (Figure 5). However, x-intercept values varied from 40 to 0.4V, casting doubt on the ability of this technique for flatband potential measurements. For example, looking at Figure 5, an x-intercept of 0.33V suggests a valence flatband potential of 0.33V.

Illuminated open circuit potential measurements give a good approximation of the location of the Fermi level of the material. Photocurrent onset, which looks at photocurrent squared vs. potential of platinized electrodes, also gives a good idea of the valence flat band potential in addition to the overpotential of hydrogen evolution. The illuminated open circuit potential measurements lie more positive than the photocurrent onset measurements but the Fermi level is too negative to allow water-splitting. Even though the band gap of this material is sufficient for water-splitting and the conduction band lies more negative of the reduction potential, the valence band does not lie more positive than the oxidation potential. This suggests that GaInPN is not capable of splitting water when grown on a GaP substrate.

Durability analysis was carried out as described above. In this study a (cathodic) current of -0.408 to -0.577µA was applied resulting in a current density of 5mA/cm². The solution was collected for future ICPMS and semiconductor materials were profiled for depth analysis, as seen in Figure 4. The average depth for all material compositions was .13µm, suggesting a corrosion rate of .13µm/24hrs. This is a significant improvement over p-GaInP₂, which has a corrosion rate of 1-2µm/24hrs. This result suggests that the addition of nitrogen enhances the stability of GaInP₂.

In conclusion, gallium indium phosphide nitride was studied for its water-splitting and corrosion-resistance capabilities. The results of this study suggest that GaInPN grown undoped on a Zn doped GaP substrate, exhibits p-type semiconductor characteristics

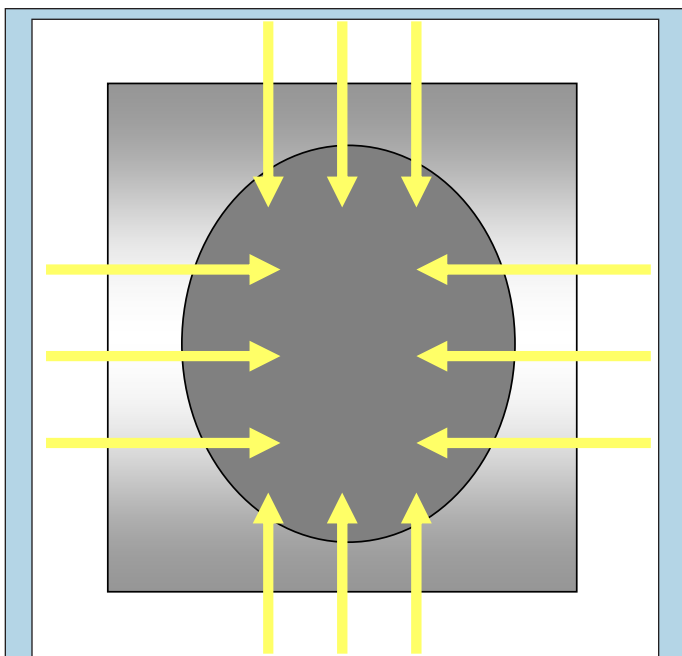


Figure 4. Profilometry scans of typical electrode material for depth analysis with stylus scanning in various locations of the semiconductor material after durability analysis.

with a band gap sufficient to split water, but unfortunately has band edges which lie too negative of the redox potentials for water-splitting to occur. Durability analysis suggests that the addition of nitrogen enhances the stability of the GaInP₂ epilayer. Other work currently in progress is looking at GaInPN silicon substrates in a tandem configuration. Future research might involve varying the compositional ratios of each element present. These novel materials may result in a semiconductor that meets the requirements for a photocathode.

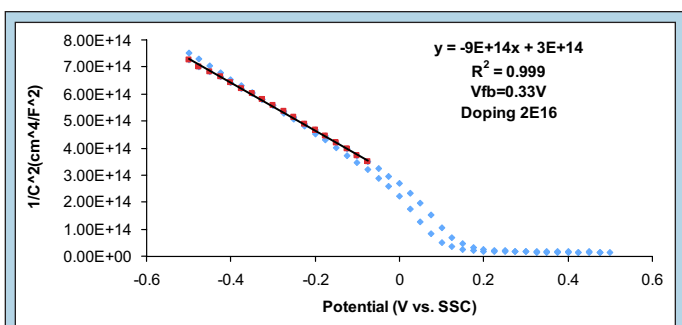


Figure 5. Mott-Schottky scan of GaInPN under illumination in 3M Sulfuric Acid at an applied potential of 20KHz.

ACKNOWLEDGMENTS

This research was conducted at the National Renewable Energy Laboratory in Golden, Colorado. I would like to thank the U.S. Department of Energy, Office of Science for the opportunity to participate in the SULI program for a second term in order to further my knowledge and appreciation of photoelectrochemistry and its applications in renewable energies. I would like to thank Dr. John Turner for inviting me back for a second summer to work in the Turner lab and carry out various photoelectrolysis experiments. I would also like to thank Dr. Todd Deutsch for his expertise in this area of research and for taking the time to further instruct me on the concepts applied in this study. I would also like to thank Dr. John Geisz for growing my samples, and finally I would like to thank my other coworkers in the Hydrogen, Fuel Cells, and Infrastructure Technologies program at NREL.

REFERENCES

- [1] Fischer, H. "Ice Core Records of atmospheric CO₂ around the last three Glacial Terminations". *Science*. Vol. 283. pp 1712-1714. Intergovernmental Panel on Climate Change. IPCC Third Assessment Report. 2003.
- [2] Turner, J. "Photoelectrochemical Water Splitting". 2004 DOE Hydrogen, Fuel Cells & Infrastructure Thechnologies Program Review. 2004.
- [3] Kocha, S., Turner, J. "Study of the Schottky barrier and determination of the energetic positions of band edges at the n- and p-type gallium indium phosphide electrode /electrolyte interface". *Journal of Electroanalytical Chemistry*. Vol. 367, 1994 pp. 27-30.
- [4] Bott, A. "Electrochemistry of Semiconductors". *Current Separations*. Vol. 17, 1998. pp. 87-91.
- [5] Turner, J. Energetics of the Semiconductor-Electrolyte Interface". *Journal of Chemical Education*. Vol. 60, 1983 pp.327-329.
- [6] Varner, K. "Evaluation of Amorphous Silicon as a Direct Water Splitting System". 2002 National Renewable Energy Laboratory Internal Report.
- [7] Hirota, Y. "Properties of silicon nitride films prepared by magnetron sputtering". *Thin Solid Films*. Vol. 253, 1994. pp. 425-429.
- [8] Khaselev, Turner. "A Monolithic Photovoltaic-Photoelectrochemical Device for Hydrogen Production via Water Splitting". *Science*. Vol. 280. No. 5362. 1998, pp. 425-427.
- [9] The photocopy technique involves using a copying machine as a magnifier. The copy machine is set at a specific

magnification and a copy is made of a piece of graph paper. The electrode whose area is to be measured is then copied at the same magnification. A 1 cm² piece of the copied and magnified graph paper cut from the page and the outline of the sample area is cut from the photocopied sample page. Weighing both and taking the ratio then provides an accurate measurement of the sample area.

[10] AM1.5 is Air Mass 1.5 and comes from the ASTM G173 spectra standard and represents the terrestrial solar spectral irradiance incident on an inclined plane at 37° tilt toward the equator, facing the sun (i.e., the surface normal points to the sun, at an elevation 48.81° above the horizon). These conditions are considered to be a reasonable average for the 48 contiguous states. The tilt angle selected is approximately the average latitude for the contiguous U.S.

[11] The intensity of the light coming from the lamp/ monochromator combination is not constant throughout the spectral range of interest. To correct the photocurrent for these intensity variations incident on the sample as a function of wavelength, the output spectrum from the monochromator (as measured with a thermopile with a flat response) is divided into the response of the sample. This of course assumes that the response of the sample is linear with light intensity, which over this intensity range is expected to be true for all samples. Note this is not a background correction, but rather an intensity correction.

Ian J. Howley is currently studying at The College of William and Mary, in Williamsburg, Virginia, and spent the spring of 2007 at St Andrews University in Scotland. He is studying physics and music, and will graduate in the spring of 2008. Ian will pursue a Ph.D. in either particle physics or astrophysics. He enjoys hiking, soccer, and golf.

Harut Avagyan is a staff scientist at the Thomas Jefferson National Accelerator Facility (JLab). He received his Ph.D. from Yerevan Physics Institute (Yerevan, Armenia) in 1986, for the research of radiation energy loss by relativistic electrons and positrons in crystals. As a member of INFN-Frascati

group (1993–2000) in HERMES collaboration (Hamburg, Germany), he introduced the subject of single-spin asymmetries to Hermes analysis and was responsible for coordinating the analysis of single-spin asymmetries (SSAs) in azimuthal distributions of pions produced in the semi-inclusive deep inelastic scattering (DIS). This study led to the first observation of SSAs in hadron electroproduction in DIS. At JLab (since 2001) his research activities have focused on studies of SSAs in semi-inclusive and exclusive electroproduction of pions and photons with polarized beam or target. Since 2004, he has been co-convenor of the JLab semi-inclusive working group involved in preparation of proposals for future measurements at upgraded to 12 GeV JLab.

STUDY OF BEAM SPIN ASYMMETRY IN EXCLUSIVE π^0 PRODUCTION

IAN HOWLEY AND HARUT AVAGYAN

ABSTRACT

Describing and understanding atomic nuclei is a puzzle that has intrigued scientists for decades. Approximately ten years ago, a description of nucleon structure, referred to as Generalized Parton Distribution (GPD), was introduced. GPDs are a way of describing scattering and production processes in a single framework. Deeply Virtual Compton Scattering (DVCS) is a process that scatters a photon from a proton and detects a scattered electron, a proton, and one photon in the final state. From DVCS, GPDs can be extracted in order to lead us to a more complete picture of nucleon structure. The focus of this study is to understand the beam spin asymmetry (BSA) of the neutral π^0 meson, a main source of background during the DVCS process. To calculate the BSA, the number of π^0 events with positive helicity (spin) and negative helicity were counted by integrating histograms with Gaussians fits. It is shown that there is a significant non-zero BSA in production of exclusive π^0 , namely 0.0655 ± 0.0022 . In the analysis of previous experiments, the BSA of π^0 was assumed to be zero and therefore ignored. Now, future analyses of DVCS data may incorporate this evidence of BSA. A deeper understanding of background processes (π^0) in the DVCS will allow precision measurements of GPDs, providing new insight concerning the structure of nucleons.

INTRODUCTION

Since the discovery of quarks in the 1960s, research in nuclear physics has been focused on understanding the role quarks play in nucleon structure. Early theories simplified the momentum distribution of quarks to a one-dimensional model. By limiting quark distributions to the longitudinal momentum (in the infinite momentum frame), theorists made relatively accurate predictions about the complex structure of the proton. Each quark carries a fraction of the total momentum of the proton, represented by x (Figure 1a). Many studies were conducted concerning form factors, which are descriptions of the charge distribution inside a proton (Figure 1b). Combining these methods allow for a three dimensional model of nucleon structure (Figure 1c) [1].

Deeply virtual Compton scattering (DVCS) is the cleanest process available to study general parton distributions (GPDs). The DVCS processes follow the pattern $ep \rightarrow e'p'\gamma$. However, other processes such as the Bethe-Heitler process yield the same result, except that the photon is emitted by the incoming or outgoing electron, rather than as a result of proton excitation (Figure 2). The decay of π^0 ($ep \rightarrow e'p'\gamma\gamma$) is another process which creates extraneous events that must be separated from desirable events when observing

the DVCS process. An understanding of background processes in the exclusive photon production allows measurement of DVCS asymmetry with a high degree of accuracy. Therefore, an asymmetry in the background must be taken into account in order to ensure the quality of the results.

The Asymmetry

The number of photons in the exclusive photon sample from π^0 and their asymmetry are the two most important factors in DVCS asymmetry measurement. Also, wide acceptance detectors, such as the Continuous Electron Beam Accelerator Facility (CEBAF) Large Acceptance Spectrometer (CLAS) at Jefferson Laboratory (JLab), require a wide range of kinematics to study the asymmetry, A_{LU} , where the beam is polarized (subscript L) and the target is unpolarized (subscript U). Cross section dependency on the azimuthal angle ϕ , defined as the angle between the scattering and production planes (Figure 3), gives rise to observable asymmetries. In order to understand the asymmetries' dependence on this angle ϕ , the general form of a cross section is used:

$$\sigma = \sigma_0 + \lambda \sigma_1 \sin \phi. \quad (1)$$

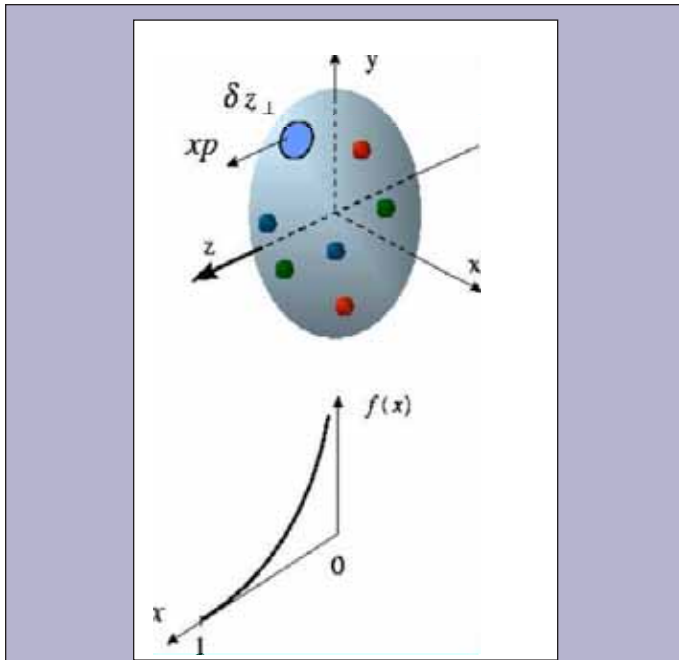


Figure 1a. Longitudinal Momentum Distribution; at large x , the probability is small since it is unlikely that one quark will carry all the momentum for the proton.

Here, σ is the probability of a π^0 being produced, λ is the helicity and ϕ is the azimuthal angle. σ_0 and σ_1 define the spin independent and spin dependent portions of the cross section, respectively, and are the primary parameters to be determined. Helicity is the projection of the spin of a particle with respect to the direction it's traveling. Electrons, including those at CEBAF, can have helicity '+' corresponding to positive beam polarization or helicity '-' corresponding to negative polarization. The beam polarization changes every 33ms and allows for more degrees of freedom while measuring the kinematic distribution inside the proton. Equation 1 then becomes:

$$\sigma^+ = \sigma_0 + \sigma_1 \sin\phi \quad \text{and} \quad \sigma^- = \sigma_0 - \sigma_1 \sin\phi, \quad (2) (3)$$

for positive and negative beam polarizations respectively. The asymmetry is defined as:

$$A = \frac{\sigma^+ - \sigma^-}{\sigma^+ + \sigma^-}, \quad (4)$$

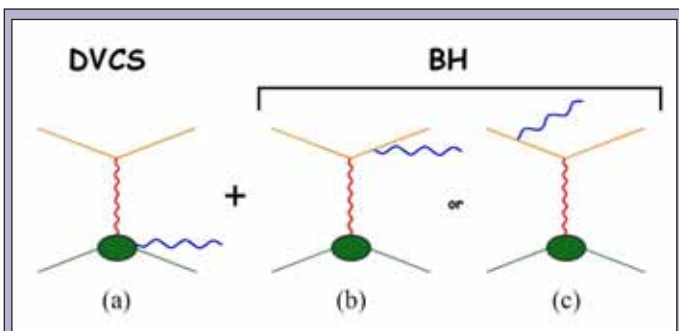


Figure 2. This figure shows how the three detected particle are the same (scattered electron, photon, and proton), but are not the result of the same process.

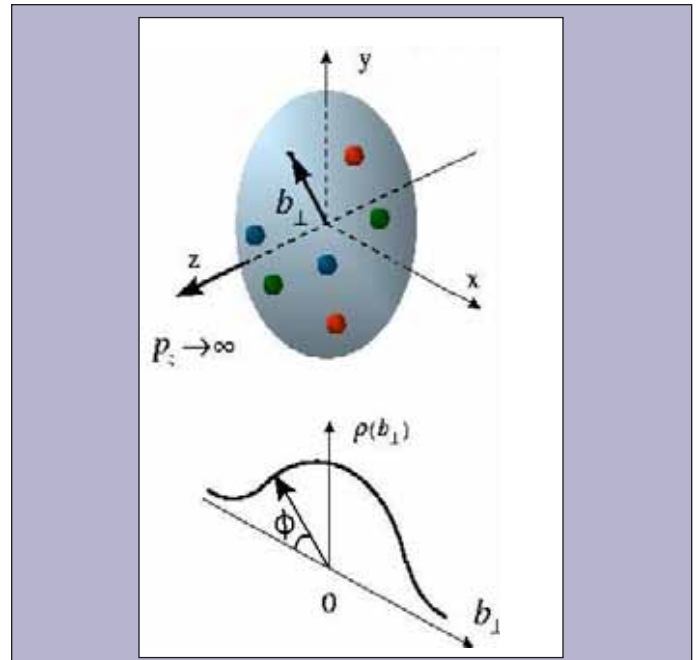


Figure 1b. Form factors showing the charge distribution inside the proton.

which, when equations 2 and 3 are substituted in, yields:

$$A = \frac{\sigma_1}{\sigma_0} \sin\phi. \quad (5)$$

From equation 5 it is clear that the ratio $\frac{\sigma_1}{\sigma_0}$ is the amplitude

of $\sin\phi$ and the most important quantity of this experiment. Since the detector detects particles within a certain acceptance (and efficiency), the number of events, $N^{+/-}$, can be written as the product of the detectors acceptance, a , and the cross section:

$$N^{+/-} = a^{+/-} \sigma^{+/-}. \quad (6)$$

The acceptance of the detector accounts for its ability to detect particles. Factors that limit the acceptance of the detector include areas where there is no detector (to allow room for superconducting magnets), very small angles, or even dead spots in the equipment itself. The factor a should be the same for both positive and negative

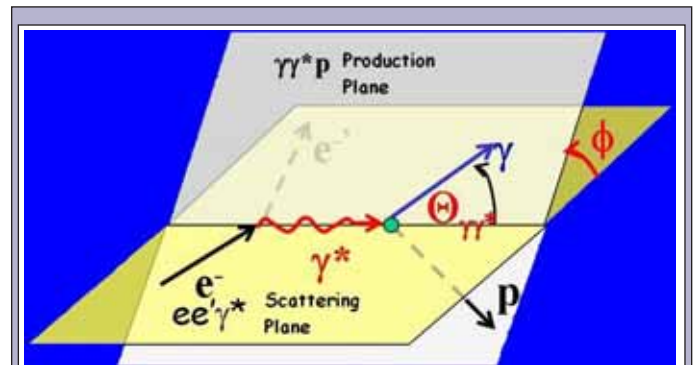


Figure 3. The Scattering and Production Planes.

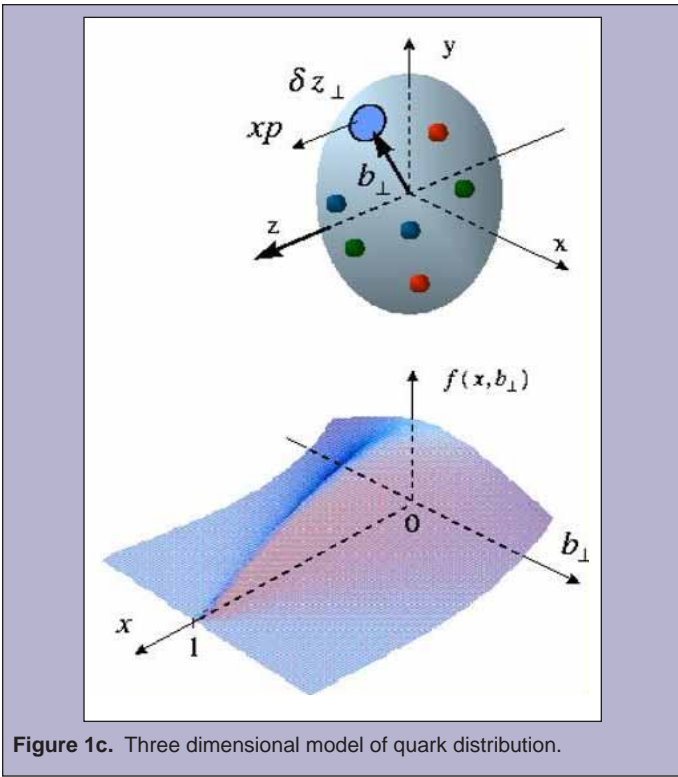


Figure 1c. Three dimensional model of quark distribution.

helicities so when equation 6 is substituted into equation 4 the form used for the calculation of asymmetry is found:

$$A_{LU} = \frac{N^+ - N^-}{N^+ + N^-}. \quad (7)$$

Previous experiments have attempted to measure the ratio $\frac{\sigma_1}{\sigma_0}$ but

have failed to produce a result with a reasonable degree of accuracy. In order for the accuracy of an experiment to increase to the point where the asymmetry is observed, a large number of π^0 events must be detected. More recent DVCS experiments [2] [3] have relied on estimates of π^0 background. Thanks to a new CLAS experiment, the π^0 background can finally be measured.

The Experiment

The 5.776GeV CEBAF electron beam was aimed at a 2.5cm long liquid hydrogen target placed 66cm upstream from the CLAS center. The experiment, e1-DVCS gathered data during the period from March to May 2005. It operated with 80% beam polarization. Developed and installed in CLAS for the purpose of studying DVCS, the Inner Calorimeter's (IC) main goal is to detect particles produced at very small angles, 4° - 15° . The 1.3cm x 1.3cm x 16cm IC consists of 424 crystals with Avalanche Photo Diodes (APDs) attached to the back of each crystal to record the light readout. The IC is placed inside CLAS very near the target which is surrounded by the superconducting magnet to protect from Møller background (Figure 4). When the π^0 decays into two photons, they are detected by the IC and organized into events which are then able to be analyzed.

METHODS

Paw++, a data analysis software, was used to organize data and to create and fit all plots. The first major step to determine the π^0 asymmetry is to calculate the number of detected events with positive

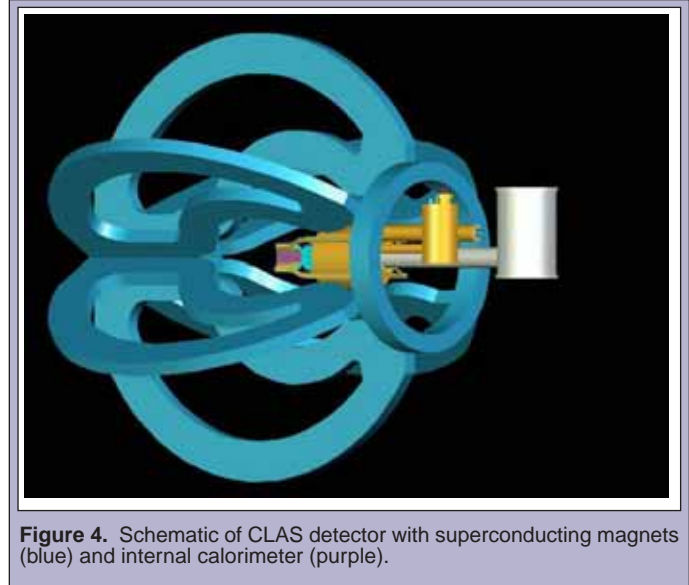


Figure 4. Schematic of CLAS detector with superconducting magnets (blue) and internal calorimeter (purple).

helicity and the number of events with negative helicity. To ensure the data quality, cuts were made to the approximately 250,000 events in the data set. In addition to fiducial cuts, three particle identification cuts were made to (1) the invariant mass, $M_{\gamma\gamma}$, (2) the missing mass of $e'p'X$, M_X , and (3) the scattering angle, θ' .

$$0.005 < |M_{\gamma\gamma}^2| < 0.03 \quad (8a)$$

$$|M_X^2 - M_\pi^2| < 0.1 \quad (8b)$$

$$|\theta' - \theta_\pi| < 1.5^\circ \quad (8c)$$

In equations 8b and 8c the subscript π represents the known or expected value. Also another cut was made on the measured energy

inside the calorimeter, E_π^m .

$$|E_\pi^c - E_\pi^m| < 0.5\text{GeV} \quad (8d)$$

$$E_\pi^c = E_{BEAM} + M - E_p - E_e \quad (8e)$$

In order to calculate the number of events; the variables t , the momentum transfer to the proton, and ϕ were fixed and divided into bins four bins in t ($.05 < t < .85\text{GeV}^2$) were created, each containing twelve bins in ϕ ($0 < \phi < 2\pi$). For each of these 48 bins, the graph of $M_{\gamma\gamma}$ was plotted. A minimum of 125 events were required for each bin to assure the quality of the fit. Just as the π^0 is a background to DVCS, there is background during π^0 production. While this effect is much less than that of π^0 on DVCS, it must be accounted

for. A combination of Gaussian and linear functions was used for the graphs because a Gaussian curve fits the decay of π^0 properly and the linear terms accounts for the background (Figure 5). The parameters listed in Figure 5 are used to calculate the events.

$$N_S = \int_{0.005}^{0.03} P_1 e^{-\frac{1}{2} \left(\frac{x-P_2}{P_3} \right)^2} dx, \quad (9)$$

is the integral of the Gaussian curve, and:

$$N_B = \int_{0.005}^{0.03} P_4 + P_5(x-P_3) dx \quad (10)$$

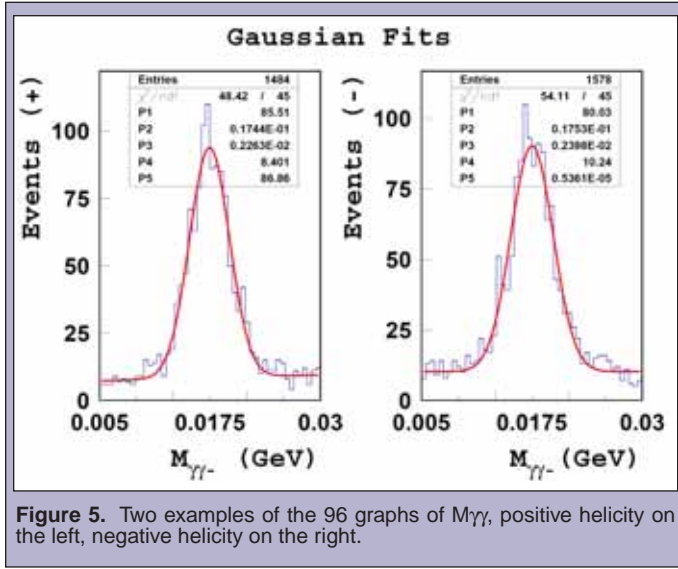


Figure 5. Two examples of the 96 graphs of $M_{\gamma\gamma}$, positive helicity on the left, negative helicity on the right.

are the linear terms used for the background events. After performing the integral, in order to get the appropriate number of events, it was necessary to divide by the width of each bin, defined as:

$$\Delta d = \frac{(x_{\max} - x_{\min})}{n}, \quad (11)$$

where x_{\max} and x_{\min} define the boundaries of the graph, 0.03 and 0.005 respectively, and n represents the number of histogram bins under the curve, in this case 50. Also listed in Figure 5 is the number of events. This number of events cannot be used to calculate the BSA because they include the background. Rather, this number is used to check the accuracy of the integration. The background (equation 10) and signal (equation 9) events calculated from the integral are added together and compared to the total number of known events. In all 96 bins the difference between the known events and the calculated events was within 10%. This magnitude of error is acceptable because the calculation of the background, which is quite small and difficult to measure accurately, accounts for most of this discrepancy. However, an accurate measurement of the BSA can still be made. The final equations to calculate the events were:

$$N_S^{+/-} = \frac{\sqrt{2}P_1P_3}{\Delta d} \left(\text{erf} \left(\frac{x-P_2}{\sqrt{2}P_3} \right) \right) \Big|_{0.005}^{0.03} \quad (12)$$

where $\text{erf}(x)$ is the error function defined as:

$$\text{erf}(x) = \frac{2}{\sqrt{\pi}} \int_0^x e^{-y^2} dy, \quad (13)$$

and:

$$N_B = \frac{P_4}{\Delta d} x \Big|_{0.005}^{0.03} + \frac{P_5}{\Delta d} \left(\frac{x-P_3}{2} \right)^2 \Big|_{0.005}^{0.03}. \quad (14)$$

Once all of the events were known from the fit function (equation 12), the events in the four bins for each helicity were added together and the asymmetry was calculated from equation 7. Naturally, because of equation 5, a sine function was used to fit the asymmetry graph. Also, a standard calculation to find the error:

$$\Delta A_{LU} = \sqrt{\frac{2}{N^+ + N^-}}, \quad (15)$$

was used. The asymmetry is also plotted against the individual bins of t but must first be divided by the average polarization, 0.79 to account for the beam polarization not being 100%.

RESULTS

The key to unlocking the BSA was to measure the amplitude of the $\sin\phi$ term in equation 5. Figure 6 shows the amplitude of the asymmetry, which is 0.0655 ± 0.0022 , plotted against degrees. This is the first time this amplitude has been measured to be significantly non-zero. Also, for the first time, the t dependence of the BSA for π^0 was measured (Figure 7). No significant variation with t was observed within the error bars. The error no longer eclipses the size of the measured asymmetry as it has in previous experiments; instead the BSA of exclusive π^0 production is observed to within 3%.

CONCLUSIONS

For the first time, a non-zero BSA for exclusive π^0 production has been measured. With more than 250,000 events in the data set, this experiment well exceeded the results and accuracy of any previous experiment. The χ^2 values are reasonable, and the error in the asymmetry fit is small, 3%. The success of this experiment was due almost entirely to the detection of more π^0 events than ever before.

This result will be used for precision GPD measurements from the CLAS DVCS data. DVCS asymmetries will no longer include an estimated π^0 subtraction. With this result accurately measured, DVCS processes will be better understood, and in turn they will ultimately shed light on the structure of the proton.

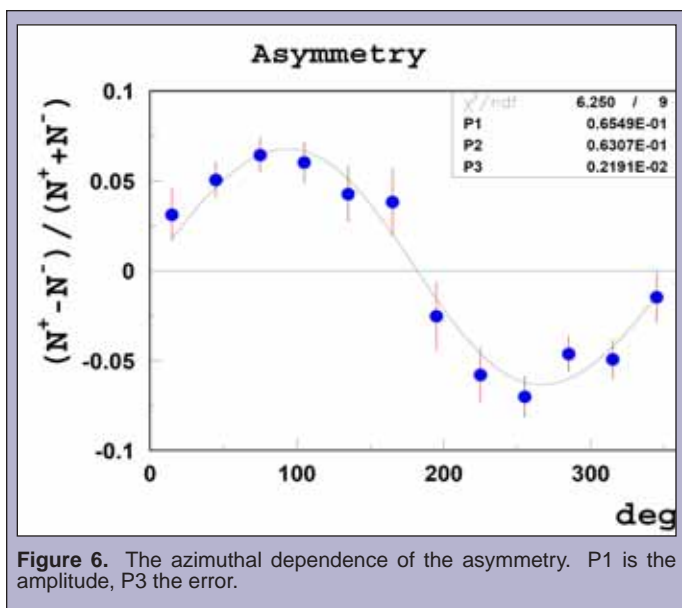


Figure 6. The azimuthal dependence of the asymmetry. P1 is the amplitude, P3 the error.

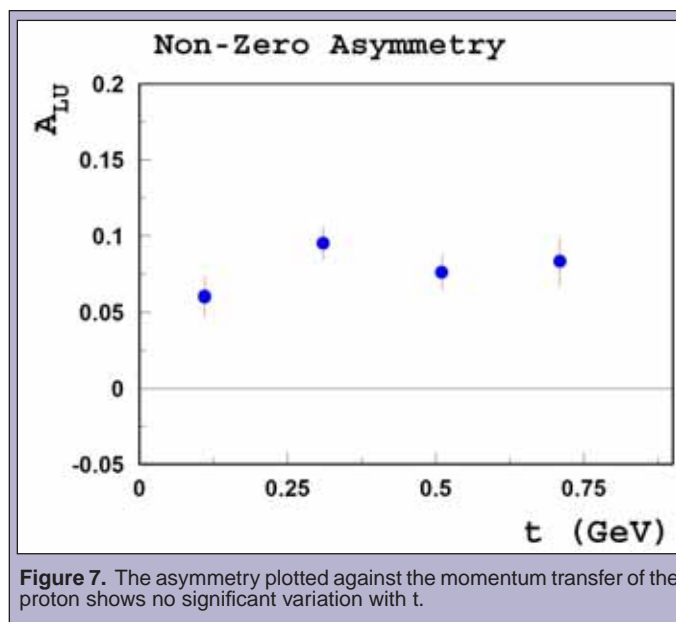


Figure 7. The asymmetry plotted against the momentum transfer of the proton shows no significant variation with t .

ACKNOWLEDGMENTS

I would like to thank first and foremost my mentor Dr. Harut Avakian. Without his endless patience and unbridled enthusiasm, I most certainly would not have had this kind of success. Second, I would like to thank the Thomas Jefferson National Accelerator Facility, in conjunction with the US Department of Energy, Office of Science for providing all the necessary resources to complete this project. A note of thanks also goes out to Dr. Keith Griffieon, Jan Tyler, and Dave Abbott for their support and companionship.

REFERENCES

- [1] X.-D Ji, Phys. Rev. D55, 7114 (1997), hep-ph/9609381.; A. V. Radyushkin, Physics. Letters. B380, 417 (1996), hep-ph/9604317.
- [2] M. Airapetian et. al, Phys. Rev. Lett. 87 (2001).
- [3] S. Stepanyan et al, CLAS Collaboration Phys. Rev. Lett. 87 (2001).

Zhuo Huang is majoring in Physics at California State University, Sacramento (CSUS), and attended a summer internship at Lawrence Berkeley National Laboratory (LBNL). He studied the collection mechanism of an LBNL environmental airborne particle sampler under the guidance of Dr. Michael Apte and Dr. Lara Gundel. After graduating from CSUS in May 2007, Zhuo will begin his graduate study in the Applied Sciences department at the University of California, Davis.

Lara Gundel is a staff scientist at Lawrence Berkeley National Laboratory, where she investigates fine airborne particles that have harmful impacts on human health and the environment. Her research involves chemical and physical characterization of aerosols, including optical, thermal and chromatographic methods development and miniature instrumentation for low-cost human exposure assessment and climate research. She holds a Ph.D. in physical chemistry from the University of California Berkeley.

THERMOPHORESIS AND ITS THERMAL PARAMETERS FOR AEROSOL COLLECTION

ZHUO HUANG, MICHAEL APTE, AND LARA GUNDEL

ABSTRACT

The particle collection efficiency of a prototype environmental tobacco smoke (ETS) sampler based on the use of thermophoresis is determined by optimizing the operational voltage that determines its thermal gradient. This sampler's heating element was made of three sets of thermophoretic (TP) wires 25 μ m in diameter suspended across a channel cut in a printed circuit board and mounted with collection surfaces on both sides. The separation between the heating element and the room temperature collection surface was determined in a numerical simulation based on the Brock-Talbot model. Other thermal parameters of this TP ETS sampler were predicted by the Brock-Talbot model for TP deposition. From the normalized results the optimal collection ratio was expressed in terms of operational voltage and filter mass. Prior to the Brock-Talbot model simulation for this sampler, 1.0V was used arbitrarily. The operational voltage was raised to 3.0V, and the collection efficiency was increased by a factor of five for both theory and experiment.

INTRODUCTION

Particulate matter (PM) is comprised of both solid and liquid particles that are suspended by gas molecules in the air. The composite mix of PM and the air in which it is suspended is defined as an aerosol. According to the U.S. Environmental Protection Agency (EPA), PM-2.5 and PM-10, which are particles with aerodynamic diameters less than 2.5 and 10 μ m, respectively, can cause adverse health effects with even short-term exposure. Environmental tobacco smoke (ETS) exposure increases the risk for respiratory diseases and lung cancer. The involuntary exposure for children (through secondhand smoke) causes lower respiratory illness in their infancy and early childhood and adverse effects on lung function across childhood [1]. Given the important public health implications of PM exposure, a continued need exists for development of cost effective, accurate, and practical measurement devices [2]. Various prototype instruments are being developed to measure the mass, size, and chemical composition of PM. Development of these devices is motivated by the desire to obtain a better exposure assessment tool to remedy misclassification of ETS exposure in epidemiological studies (see [1] Chapter 1 for details). The device under investigation measures particle phase (ETS) and gas phase (nicotine and 3ethenyl pyridine) ETS exposure. This portion of the project was focused on the ETS deposition mechanism of the particle phase sampling device.

The use of van der Waals induced dipole-dipole attraction is sufficient for surface retention of micron and sub-micron sized particles. Thermophoresis, the normal force on a particle created

by the momentum transfer along the decreasing direction of a thermal gradient [3], is an effective method for particle collection in validating traditional methods [4]. When an aerosol is flowing in a narrow channel, the thermal gradient strength determines the strength of thermophoretic (TP) forces on the particles.

Experiments were conducted with a new device developed to sample airborne particles in indoor air with support from the California Tobacco Related Disease Research Program (TRDRP). Seeking a better understanding of thermophoresis to improve the collection efficiency became a motivation for exploring the theories dealing with TP particle deposition in laminar flow regimes in ducts (~500 μ m high). In a series of particle phase experiments using a TP ETS sampler, the TP voltage that controls the thermal gradient in the sampler was increased until the optimal (maximal) ETS deposition was determined.

The Brock-Talbot model for TP deposition [5] was previously used for proof of concept. In this project, this model was extended over a larger particle size range. A second purpose was to compare theoretical predictions with the experimental performance of the TP ETS sampler. The sampler used TP wires (California Fine Wire Co., Grover Beach, CA, Nickel Alloy 120) 25 μ m in diameter to heat up the surrounding air by applying a voltage across the wires. An arbitrary operational voltage of 1.0V was selected for powering the TP wire prior to computer simulation and chamber experiments. Since the temperature of the wires was proportional to the applied voltage, establishing the temperature-voltage relationship was necessary to obtain optimal collection.

MATERIALS AND METHODS

Theoretical Model

In the presence of a thermal gradient, the phenomenon of thermophoresis becomes significant in influencing particle motion [6]. TP deposition is based on a temperature difference between two close surfaces; given the appropriate gradient and particle size range, the collection can be 100% efficient [3]. The TP force is very effective for depositing tiny particles flowing through a channel onto its cooler surface. Other than the temperature gradient, many other parameters such as thermal conductivity, dimension of the flow channel, and viscosity associated with the particle stream play important roles.

The Brock-Talbot TP force model given by He and Ahmadi [5] is:

$$F_{th} = 2 C_s C_c \frac{1}{\tau} \nu H \frac{\nabla T}{T} m, \quad (1)$$

where C_s is the thermal slip coefficient, and C_c is the Stokes-Cunningham slip correction:

$$C_c = 1 + \frac{2\lambda}{d} \left(1.257 + 0.4 \text{Exp} \left[-1.1 \frac{d}{2\lambda} \right] \right), \quad (2)$$

and τ is the relaxation time in equation (1) given by:

$$\tau = \frac{S d^2 C_c}{18 \nu}. \quad (3)$$

S is the ratio of particle density to fluid density [7]. T and ∇T are the room temperature and thermal gradient; m is the unit mass and ν is the kinematic viscosity of the molecules. H is the molecular accommodation coefficient given by:

$$H = \left(\frac{1}{1 + 3 C_m \text{Kn}} \right) \left(\frac{\frac{k_a}{k_p} + C_t \text{Kn}}{1 + 2 \frac{k_a}{k_p} + 2 C_t \text{Kn}} \right). \quad (4)$$

This equation indicates the relationship between particle diameter and thermal conductivity. Talbot found the values of the coefficients $C_s=1.17$, $C_t=2.18$, and $C_m=1.14$. C_t is a number of order unity which relates to temperature jump [5], and C_m is the momentum exchange coefficient that depends on the particle-gas configuration, and [5, 7]. $\text{Kn}=2\lambda/d$ is the Knudsen number, where λ is the mean free path of air and d is particle diameter; k_a and k_p are the thermal conductivity of gas (air) and particle respectively.

The TP collection ratio:

$$\eta = \frac{UL}{2h u_m} \quad (5)$$

is the ratio of the TP velocity and the mean air velocity u_m of the channel. Here, L and h are the length and the height of the channel. They are chosen to be 71.0mm and 0.5mm for the simulation, reflecting the dimensions of the TP ETS sampler. U is the TP velocity:

$$U = \frac{F_{th}}{m} \tau \quad (6)$$

which, in effect, determines the TP collection ratio. Substituting τ and H into Equation (1) and expanding in terms of its dependent parameters, the equation becomes:

$$F_{th} = 36 C_s \frac{\nu^2}{S d^2} \left(\frac{1}{1 + 3 C_m \text{Kn}} \right) \left(\frac{\frac{k_a}{k_p} + C_t \text{Kn}}{1 + 2 \frac{k_a}{k_p} + 2 C_t \text{Kn}} \right) \frac{\nabla T}{T} m \quad (7)$$

The C 's are collectively referred to as the drag forces. One can see that the TP force strength is inversely dependent on particle diameter and the temperature of forming the thermal gradient, where ν and k_a/k_p dependence are accounted for by the type of particles. This equation is simulated with the molecular diameter of air chosen to be 5.7nm, and the aerosol particles consist of NaCl (for consistency with the reported work in [5]) with thermal conductivity $k_p=6.69 \text{ W m}^{-1} \text{ K}^{-1}$.

Apparatus

The collection apparatus consists of a loom-like frame machined from a copper clad printed circuit board that holds a set of TP wires and acts as a flow channel, and a mounting surface for fin-cooled aluminum particle collection surfaces. When assembled, the device becomes an air-tight flow-through channel with three sets of TP collection areas; a small pump of flow rate 0.01L/min was used to draw a PM-laden air sample through the device. Four fine TP wires in diameter about 5mm in length were soldered, physically in parallel, and electrically in series to form a coplanar resistive heater about 5mm on a side on the collector frame. Three of these heaters were assembled on a single sampler to create three separate TP collection regions (see Figure 1). When the TP ETS sampler was assembled and a voltage was applied across one of the three wire

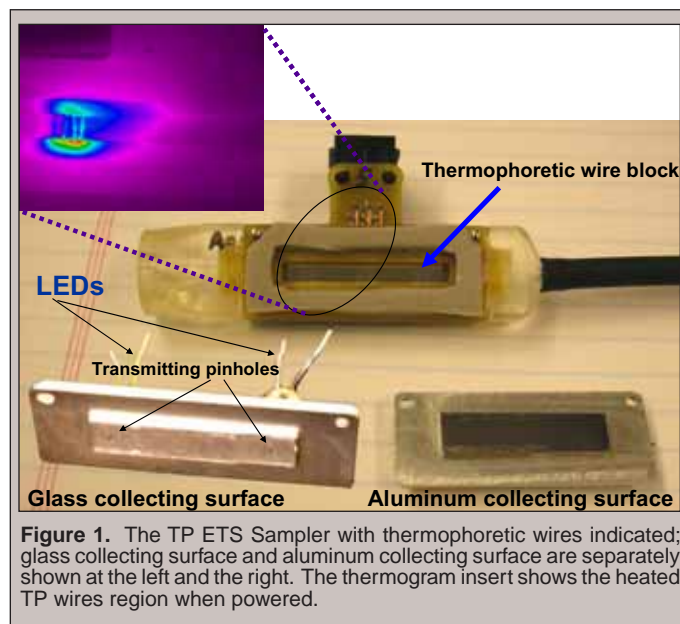


Figure 1. The TP ETS Sampler with thermophoretic wires indicated; glass collecting surface and aluminum collecting surface are separately shown at the left and the right. The thermogram insert shows the heated TP wires region when powered.

circuits, a thermal gradient was formed between the wires and the fin-cooled aluminum collection surface (Figure 1).

Two collecting surface configurations were used on the two sides of the TP wire blocks for particle collection. An aluminum collection surface (Figure 1) was fabricated with a polished thin aluminum surface attached to an aluminum body with double-sided heat conducting tape. A glass collection surface (opposite) was assembled with a thin glass cover slide and another aluminum body. The glass cover slide was glued at its edges to allow light transmission through two circular pinholes of diameter ~ 1mm that were each centered on a TP particle deposition area on the surface. LEDs (Roithner Lasertechnik, Vienna, Austria, UV-LED 380D30 and ELD-810-525) of peak wavelength of 380 nm (UV) and 810 nm (IR) were inserted into the back of the aluminum body allowing a light beam to be transmitted through the pinholes and to emerge normal to the glass surface. The LED pinholes were located in the center of the TP deposition surfaces for two of the three collection areas on the glass-covered collection body.

Thermophoretic Wire Temperature

In Figure 1, the thermogram insert shows the heated TP wires. Due to the low emissivity of the wires, the thermogram merely indicates the wires were hotter than their surroundings when powered, yet does not accurately indicate the *exact* temperature. Using an alternate approach to thermography, the approximate temperature of the TP wire could be calculated in terms of resistance with the known temperature coefficient of resistance of the TP wire provided by the manufacturer. A 50 x 50 x 80cm convection oven was used to measure the temperature-resistance relationship of the TP wires. A differential temperature controller gradually raised the temperature while two small 12V fans were used for air mixing inside the oven. A sampler was placed inside the oven and two blocks of TP wires' resistance were measured for comparison. The resultant voltage vs. temperature relationship could be obtained for determining the associated temperature with experimental voltage and current using Ohm's law.

Experiment Setup and ETS Generation

A 24m³ environmental chamber was built with a wooden frame, wallboard walls and ceiling, and magnetic refrigerator door seals. Low volatile organic compound emitting paints and sealants were applied inside the chamber to minimize unwanted room-ambient particles and volatile organic compounds [8]. The chamber was bolted in place in a one-story building, no ventilation equipment was used, and the room temperature stayed approximately steady during the sampling periods. The TP ETS sampler was hung from a stand 0.5 meters above the floor, side by side with the a Personal Environmental Monitor (PEM) PM-2.5 sampler (SKC Inc., Eighty Four, PA, 761-203). The PEM, assembled with a Teflon-coated fiberglass filter (SKC Inc., Eighty Four, PA, SKC Filter 761-203) and sampling at a rate of 2.0L/min, provided the integrated PM mass concentration in the chamber during the sampling period. Using the proportionality of the integrated PM mass concentration and

TP ETS sampler flow rates, the total particle mass that traversed the TP ETS sampler during operation was calculated.

ETS was generated by concurrently and completely smoldering 8 cigarettes for each run. ETS is a complex mixture of solid and vapor phase particles produced primarily from the burning of cigarettes and is dependent on the puff rate [8]. The TP ETS sampler validation was focused on the deposition mechanism, thus smoldering cigarette smoke was effective and appropriate for these experiments. The TP ETS sampler controller microprocessor was programmed to switch amongst the 3 sampler TP wire regions in a reversing sequence fashion (i.e., 1-2-3, 3-2-1, 1-2-3,...) every 5 minutes. The purpose of this was to avoid collection bias during decay of the aerosol concentration in the chamber, and therefore this non-random sampling pattern distributed near-equal particle mass collection on each of the three regions of the sampler's collection surfaces. A series of experiments were conducted at increasing wire voltage settings from the pre-set voltage of 1.0V to the optimal voltage of 3.0 volts where a maximum particle collection value (see Table 1) was reached. The voltage and current inputs of each wire were recorded for analysis. Each experiment was allowed to collect for at least 17 hours in order to obtain significant amount of ETS.

Spectrometry and Related Statistics

Thermal Conductivity Ratio (k_p/k_a) of Several Materials			
TP Voltage (V)	Resistance (Ω)	T [$^{\circ}$ C]	∇T [K/cm]
1.0	13.6	107	1740
1.5	15.4	179	5190
2.0	18.3	252	4640
2.5	19.5	325	6090
3.0	25.2	397	7540

Table 1. The corresponding thermal parameters for the TP voltages used.

The samples on the glass slide collection surface were then examined by using fiber optic probes connected to a UV-NIR spectrometer (Ocean Optics, Dunedin, FL, S2000 UV-VIS 250800nm). Figure 2 shows the schematic of the operation when the UV LED was powered. The LEDs were placed on a light-tight housing and connected to an external power supply. With the LEDs turned on, UV or NIR light was transmitted through the cover slide. Fiber optic probes were attached to the bottom of the housing cavity and connected via a channel selector to the spectrometer. After ETS was collected on the glass cover slide the sample spectrum was recorded. Next, the ETS sample was removed by cleaning off the glass collection surface to obtain the baseline spectrum. The absorbance was calculated with Beer's Law, $A = -\log(I/I_0)$, where I and I_0 were the calculated peak intensities of the spectrum taken by a spectrometer.

To account for small differences between ETS concentrations in each experiment, the calculated ETS absorbance was normalized by the integrated ETS concentration from the PEM during the sampling period in order to determine collection efficiency in

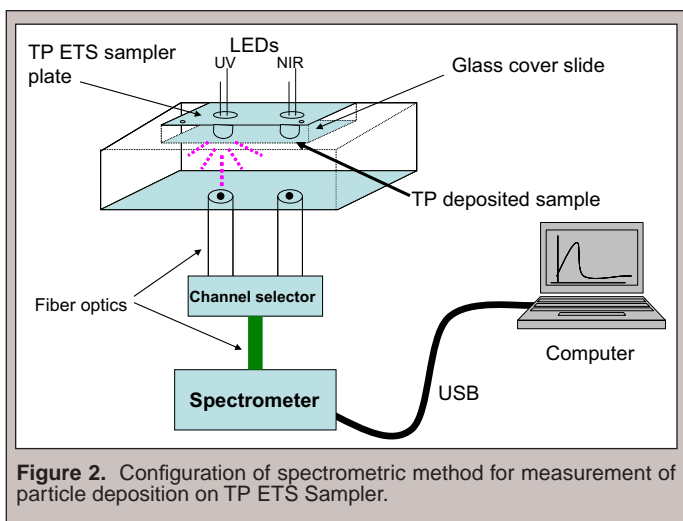


Figure 2. Configuration of spectrometric method for measurement of particle deposition on TP ETS Sampler.

terms of mass. The UV absorbance results were much more robust than those from the NIR LED since ETS has strongly enhanced UV absorbance. The NIR absorbance measurements in the case of these ETS samples were typically below the limit of quantitation for the method, making them of little use in this investigation. The filter mass collected by PEM Teflon-coated fiberglass filter was first measured with an electronic microbalance, and then the air PM concentration was calculated based on the sampling flow rate and duration. The ETS mass that entered the TP ETS sampler during each experiment was computed by multiplying the PEM-based PM concentration by the experiment sampling time and sampler flow rate. The TP ETS sampler UV absorbance was normalized to that of a 10 μ g mass sampling based on the above calculation.

RESULTS

Collection Ratio

The Brock-Talbot deposition ratio was plotted as a function of aerosol diameter for NaCl in Figure 3a. Figure 3b depicts the

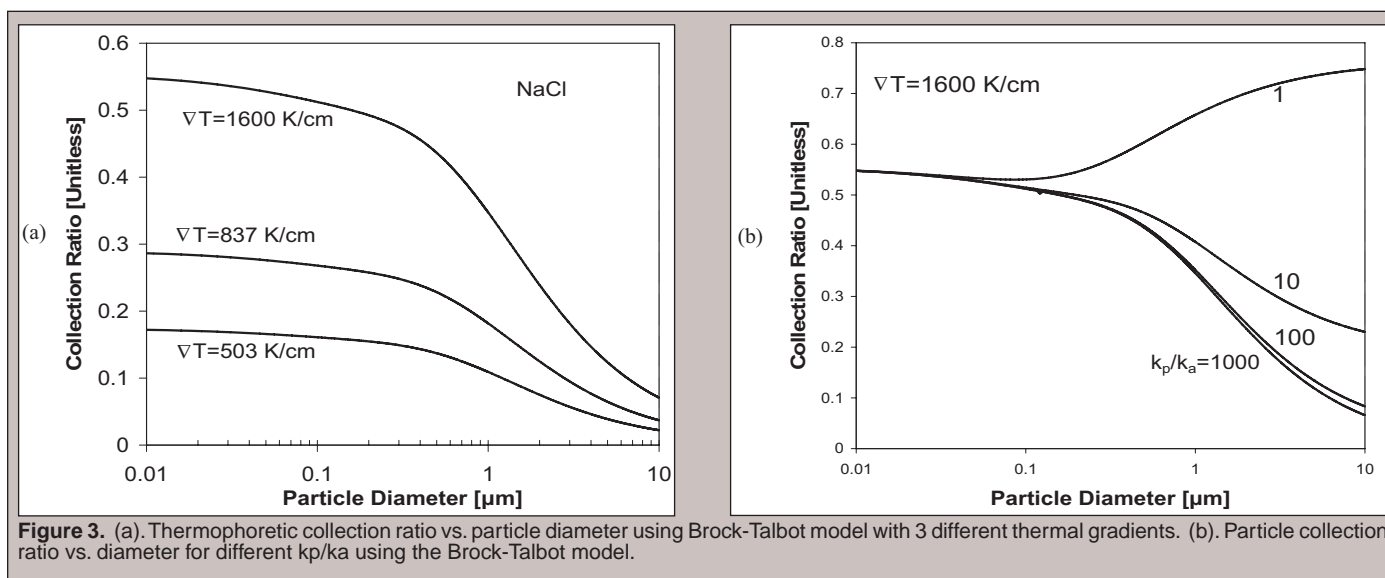


Figure 3. (a). Thermophoretic collection ratio vs. particle diameter using Brock-Talbot model with 3 different thermal gradients. (b). Particle collection ratio vs. diameter for different k_p/k_a using the Brock-Talbot model.

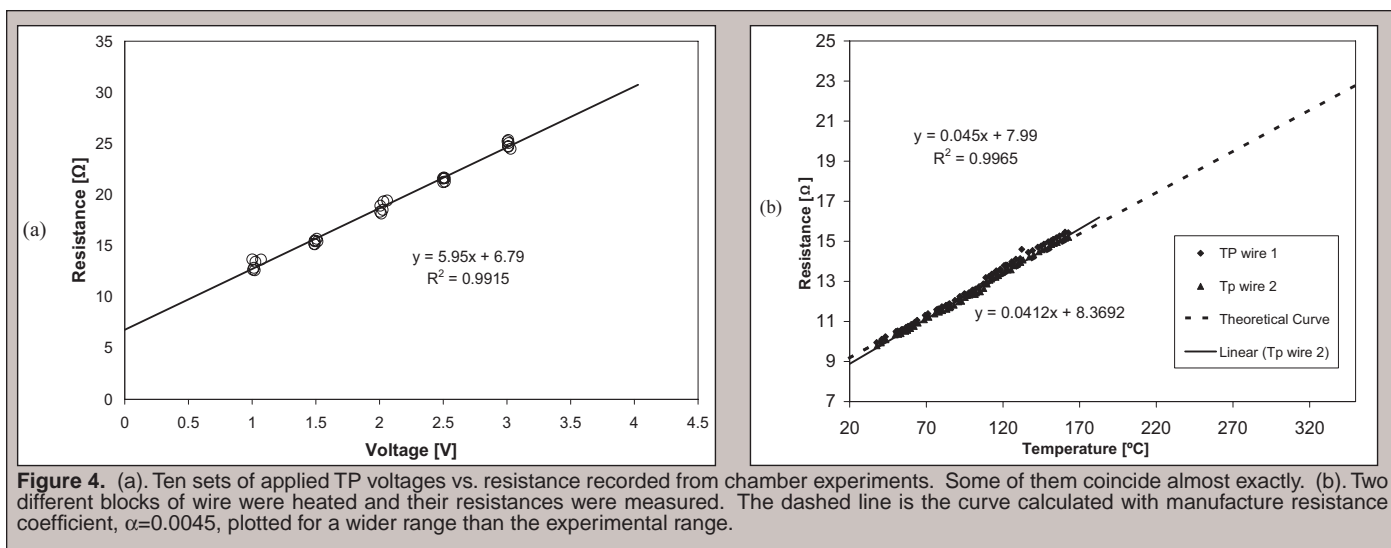
Thermal Conductivity Ratio (k_p/k_a) of Several Materials	
Materials	Unitless k_p/k_a
Air at 20°C	1
Asbestos	3
Paraffin oil	5
Magnesium oxide	5
Stearic acid	5
Castor oil	7
Water	23
Clay	27
Glass	32
Fused silica	38
Granite	81
Carbon	169
Sodium chloride	254
Mercury	323
Quartz	369
Iron	2573

Table 2. Ratio of thermal conductivity of several materials to air. k_p and k_a values were adopted from Ref. 3.

influence of the thermal conductivity of different materials on thermophoretic deposition. Table 2 lists the thermal conductivity ratio (k_p/k_a) of several possible material types that can be found in PM. These results taken together show how the different types of PM could have different thermal properties that affect the TP collection ratio. Figure 3a shows that the thermophoretic particle deposition ratio is about 0.6 and gradually decreases to 0.1 for the pre-set thermal gradient ($\nabla T = 1600$ K/cm), from 10 nm to about 1 micrometer.

Temperature Correlation

Heating the TP wires inside the oven generated resistance vs. temperature data that matched well with the wire manufacturer's temperature coefficient of resistance (see the dashed line in Figure 4a). The voltage applied to the TP wire during sampling was recorded each time and the correlation to resistance was plotted (Figure 4b).



Thus, by comparing Figure 4a to the former graph one can obtain the temperature as a function of applied voltage. Combining the fitted equation from Figure 4b and the theoretical curve from 4a, a relationship could be simply described as $T = 145.1V - 28.5$, where T is the TP wire temperature ($^{\circ}\text{C}$) forming the thermal gradient and V is the applied voltage. Table 1 summarizes the experimental applied voltages and their thermal parameters.

Normalized Absorbance and Optimal Collection

The chamber experiment data show increased particle collection in terms of absorbance with increasing wire voltage. ETS absorbance measurements from the TP ETS sampler normalized to a $10\mu\text{g}$ sample was plotted against TP wire voltage and fitted with a 2nd order polynomial (see Figure 5). Each data point was obtained

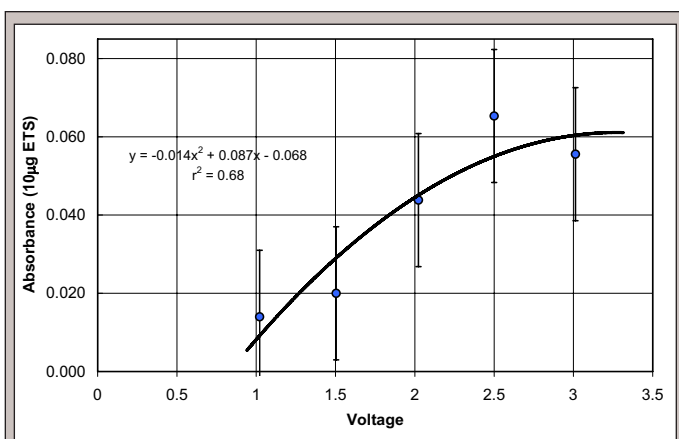


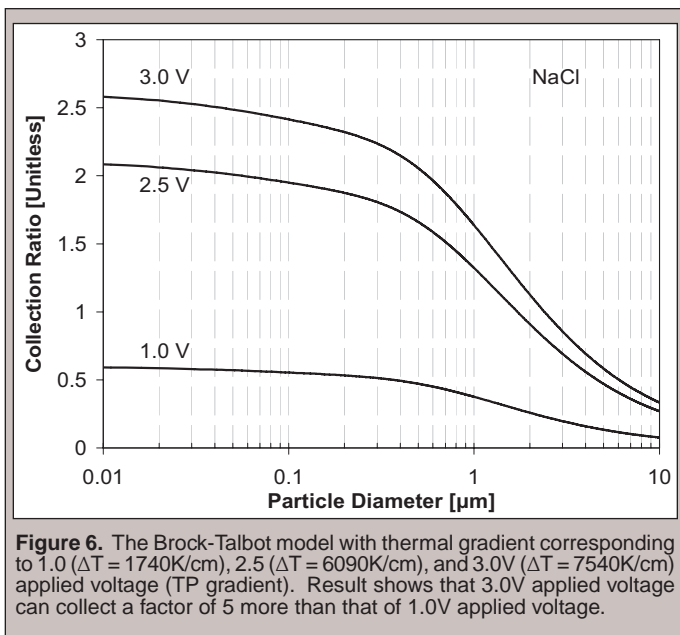
Figure 5. Particle phase titration result shows the optimal collection of the TP ETS sampler is with the input voltage of about 2.5V; the scattered absorbance data are averaged with two filter mass (PEM) normalized data. An enhancement by a factor of 5 is suggested. The error bars represent the greatest deviation from the experimental average based on two experiments for each voltage.

by averaging two experiments. Error bars in Figure 5 represent the greater deviation from the experimental average. The optimal voltage for this ETS sampler was identified to be between 2.5 and 3.0V based on this fit.

DISCUSSION AND CONCLUSIONS

Thermophoretic modeling (Figure 3a) shows an effective collection ratio for sub-micron particles. The collection ratio is defined as the ratio of TP velocity to the mean air velocity in the channel and the collection efficiency is the ratio of aerosol being collected to the amount that flows in the channel. Figure 3a also shows that the particle collection ratio quickly decreased in the micron region. As the diameter increases further ($Kn < 2$), the collection ratio decreases drastically to 0.1. The Brock-Talbot simulation predicts that particle deposition will increase substantially as the thermal gradient is raised above $T=1600\text{K}/\text{cm}$, a value that was previously set for this device. If the ratio kp/ka is small, the diameter of the particle determines the value of Equation (3) as the $Ct Kn$ term dominates; on the other hand, with kp/ka increasing the collection ratio decreases drastically as seen in Figure 3b. This result is consistent with the presentation by Hinds on the subject of thermophoretic velocity as a function of kp/ka [3].

Based on the Brock-Talbot theoretical prediction, we should expect higher particle deposition for sub-micron sized particles. The calculated thermal gradient for 2.5V is about $\nabla T=6090\text{K}/\text{cm}$, and the Brock-Talbot model collection ratio for this thermal gradient is well above 1.0. The original selection for TP voltage of this low-cost particle sampler took into account the power consumption; 1.0V TP voltage was believed to be above 80% efficient for PM-2.5 collection according He and Ahmadi's results [5, Figure 6]. This study has shown, both numerically and experimentally, the optimal deposition ratio occurs between 2.5 and 3.0V for this TP ETS sampler. The absorbance at 2.5V TP collection shows a signal five times stronger than that of 1.0V (Figure 5). It is obvious that the optimal collection efficiency in term of normalized ETS mass is at least a factor of 5 higher than the 1V thermal gradient. Figure 6 also shows the dependence of deposition ratio on voltage, verifying the Brock-Talbot model. This also shows an enhancement by a factor



of 5 (from about 0.5 to 2.5 for a 100nm particle diameter). This result may provide a useful calibration mechanism for developing the TP ETS sampler.

Future Work

This project investigated several major issues dealing with the TP ETS sampler particle collection efficiency and identified some important thermal parameters that influence aerosol collection by thermophoresis. This result raised a concern that the oven-treated TP wire temperature may not correctly describe the thermal gradient of the TP ETS Sampler's in-situ performance. Calibrating the sampler's thermal gradient will be helpful because the configuration of TP wires relative to a cool flat collection surface differs from the two-parallel plate configuration used in the Brock-Talbot model [7, 9]. We have shown that the applied voltage for the TP wires should be higher. Moreover, how the TP wire temperature affects the thermal gradient is unsolved for the configuration of this sampler. This question can be answered with future investigation.

ACKNOWLEDGMENTS

This work was supported by the Center for Science and Engineering Education at Lawrence Berkeley National Laboratory, Department of Energy, Office of Science, the California Tobacco Related Disease Research Program and the California Air Resources Board Innovative Clean Air Technologies Program. I would like to thank my mentors Michael Apte and Lara Gundel. I would also like to thank Matt McHugh, David Liederman, Rachelle Majeske, and Howdy Goudey for their assistance.

REFERENCES

- [1] U.S. Department of Health and Human Services. The Health Consequences of Involuntary Exposure to Tobacco Smoke: A Report of the Surgeon General. Atlanta, GA: U.S. Department of Health and Human Services, Centers for Disease Control and Prevention, Coordinating Center for Health Promotion, National Center for Chronic Disease Prevention and Health Promotion, Office on Smoking and Health, 2006.
- [2] Chung, A., Chang, D. P. Y., Kleeman, M. J., et al., Comparison of real-time instruments used to monitor airborne particulate matter, *Journal of Air and Waste Management Association*, 51, page 109-120, 2001.
- [3] Hinds, W., *Aerosol Technology: Properties, Behavior, and Measurement of Airborne Particles*, John Wiley & Sons, New York, 1982.
- [4] Tsai, C. J., Lin, J., et al., Thermophoretic deposition of particles in laminar and turbulent tube flows, *Aerosol Science and Technology*, 38, Page 131-139, 2004.
- [5] He, C., and Ahmadi, G., Particle deposition with thermophoresis in laminar and turbulent duct flows, *Aerosol Science and Technology*, 29, Page 525-546, 1998.
- [6] Talbot, L., Cheng, R.K., Schefer, R., W., and Willis, D. R., Thermophoresis of particles in a heated boundary layer, *Journal of Fluid Mechanics*, 101, Page 737-758, 1980.
- [7] Brock, J. R., On the theory of thermal forces acting on aerosol particles, *Journal of Colloid Science*, 17, page 768-780, 1962.
- [8] Apte, M. G., Gundel, L. A., et al., Indoor measurements of environmental tobacco smoke, Final Report to the Tobacco Related Disease Research Program, LBNL-49148, Lawrence Berkeley National Laboratory, University of California, Berkeley, CA 94720. 2004.
- [9] Tsai, C. J. and Lu, H. C., Design and evaluation of a plate-to-plate thermophoretic precipitator, *Aerosol Science and Technology*, 22, Page 172-180, 1995.

Tigisti Kesete is a graduate of Central State University, Wilberforce, Ohio, with a Bachelor of Science in Chemistry. During her four years at Central State University, Tigisti has tutored freshman chemistry and math at the Center for Student Academic Success. Over the years she has pursued many research opportunities. In the summer of 2005, she undertook research on Nanoscale Science for Affordable Nanoengineering for Undergraduates at Ohio State University. In the summer of 2006 she pursued summer research at Brookhaven National Laboratory on solar neutrinos, with the chemistry department; and still is planning to do research at Brookhaven National Laboratory this coming summer.

Amanda Storm is an intern in the FaST Program at Brookhaven National Lab, where she wrote a paper on "Solvent Purification and Fluor Selection for Gadolinium-loaded Liquid Scintillator." She completed her undergraduate degree in chemistry from Central State University, in Wilberforce, Ohio. Ms Storm is from Zanesfield, Ohio. Her interests include playing the piano, hiking, and church activities.

Richard L. Hahn is a Senior Scientist in the Chemistry Department at Brookhaven National Laboratory, and Leader of the Solar-Neutrino/Nuclear-Chemistry group there. For the past twenty years, he and his group have worked in two landmark solar neutrino experiments, in the GALLEX experiment in Italy and the SNO experiment in Canada. At present, the group is focusing on developing metal-loaded liquid scintillators for a variety of new neutrino experiments. Hahn was the recipient in 2000 of the American Chemical Society's National Award in Nuclear Chemistry.

Minfang Yeh is an Associate Scientist in the chemistry department at Brookhaven National Laboratory. He received his Ph.D. from the University of Kentucky in 1997 for the study of inelastic neutron scattering reactions in double-magic nuclides, and was the main author of the first observing two-phonon octupole-excitation state in ^{208}Pb . Yeh joined the solar neutrino group in 2000, and is a member of several international collaborations, including SNO, LENS and Daya Bay. Yeh is currently working on the design and development of large-scale, metal-loaded liquid scintillators for neutrino, antineutrino and double-beta-decay experiments.

SOLVENT PURIFICATION AND FLUOR SELECTION FOR GADOLINIUM-LOADED LIQUID SCINTILLATORS

TIGISTI KESETE, AMANDA STORM, RICHARD L. HAHN, MINFANG YEH, AND SUZANNE SELEEM

ABSTRACT

The last decade has seen huge progress in the study of neutrinos, elementary sub-atomic particles. Continued growth in the field of neutrino research depends strongly on the calculation of the neutrino mixing angle θ_{13} , a fundamental neutrino parameter that is needed as an indicative guideline for proposed next-generation neutrino experiments. Experiments involving reactor antineutrinos are favored for the calculation of θ_{13} because their derivation equation for θ_{13} is relatively simple and unambiguous. A Gd-loaded liquid scintillator (Gd-LS) is the centerpiece of the $\overline{\nu}$ detector and it consists of ~99% aromatic solvent, ~0.1% Gd, and < 1% fluors. Key required characteristics of the Gd-LS are long-term chemical stability, high optical transparency, and high photon production by the scintillator. This summer's research focused on two important aspects of the $\overline{\nu}$ detector: (1) purification of two selected scintillation solvents, 1, 2, 4-trimethylbenzene (PC) and linear alkyl benzene (LAB), to improve the optical transparency and long-term chemical stability of the Gd-LS, and (2) investigation of the added fluors to optimize the photon production. Vacuum distillation and column separation were used to purify PC and LAB, respectively. Purification was monitored using UV-visible absorption spectra and verified in terms of decreased solvent absorption at 430nm. Absorption in PC at 430nm decreased by a factor slightly >10 while the absorption in LAB was lowered by a factor of ~5. Photon production for every possible combination of two solvents, four primary shifters, and two secondary shifters was determined by measuring the Compton-Scattering excitation induced by an external Cs-137 gamma source ($E_{\gamma} \sim 662\text{-keV}$). The ideal shifter concentration was identified by measuring the photon production as a function of shifter quantity in a series of samples. Results indicate that 6g/L p-terphenyl with 150mg/L 1,4-Bis(2-methylstyryl)-benzene (bis-MSB) produces the maximum light yield for PC and 6g/L 2-(4-biphenyl)-5-(4-tert-butyl-phenyl)-1,3,4-oxadiazole with 50mg/L bis-MSB optimizes the light yield for LAB. Future work should focus on obtaining the fluorescence spectra for each of the shifters and studying the optical transparency of the LS as a function of shifter quantity.

INTRODUCTION

Neutrinos (ν) are neutral, nearly massless, subatomic particles. They pass through the surface of the Earth and all of its inhabitants at a rate of 65 billion particles per second per square centimeter. They exist as one of three flavors, electron, muon, and tau, but are capable of converting, or oscillating, between flavors [1]. Both neutrinos and

antineutrinos ($\overline{\nu}$) are produced by beta-decay reactions; however, neutrinos are emitted from proton rich nuclei while antineutrinos come from neutron rich nuclei ($p \rightarrow \beta^+ + \nu + n$; $n \rightarrow \beta^- + \overline{\nu} + p$). The major sources of neutrinos include the Sun, nuclear reactors, and particle accelerators. The Sun produces electron neutrinos as a by-product of the overall fusion process ($4\ ^1\text{H} \rightarrow\ ^4\text{He} + 2\ e^+ + 2\ \nu_e$

+ 26MeV of energy), while nuclear reactors emit antineutrinos as part of the beta-decay of the fission products.

The last decade has seen huge progress in the study of neutrinos and their properties. Some major advancements include the confirmation of the theory of neutrino oscillation [3] and the experimental determination of two of the three neutrino mixing angles, θ_{12} and θ_{23} . Continued growth in this field of research depends heavily on the measurement of the third mixing angle, θ_{13} . As one of the fundamental neutrino parameters, θ_{13} is needed for future research, including experiments utilizing very long base-line accelerators to determine the mass of each of the neutrino flavors [1]. This knowledge could indicate whether neutrinos are part of the solution to the mystery of dark matter that is assumed to be holding the universe together.

Theta-13, θ_{13} , can be calculated from experiments carried out at nuclear reactors or particle accelerator facilities. The nuclear reactor-based experiments, which measure the disappearance of antineutrinos, are favored because of their simpler derivation equation for θ_{13} .

Metal-loaded liquid scintillators (M-LS), specifically those loaded with gadolinium (Gd), have been chosen as detectors for the reactor antineutrino experiment because of their high sensitivity [2]. In addition, the antineutrino interaction is detected via two coupled signals that produce a delayed coincidence in the LS. This suppresses a large number of uncorrelated background events. Due to the weakness of neutrino interaction, each of the several detectors will contain approximately 20 tons of Gd-LS scintillator, and have a total mass of around 100 tons.

The M-LS will consist of an aromatic solvent, both a primary and a secondary chemical shifter, and an organo-gadolinium complex. Antineutrino detection begins when an antineutrino collides with a proton, supplied by the organic solvent, releasing a positron and a neutron ($\bar{\nu}_e + p \rightarrow e^+ + n$). The positron instantaneously produces photons whose energies are indicative of the neutrino energy; in addition, two gamma rays of 511keV each are produced when the positron annihilates with a nearby electron. After a delay of $\sim 30\mu\text{s}$, a second emission of gamma-ray photons occurs from the thermalization of the neutron, which can occur by one of two mechanisms, $n + p \rightarrow D + \gamma(2.2\text{MeV})$ or $n + Gd \rightarrow Gd^* \rightarrow Gd + \gamma(8\text{MeV})$ [2]. The scintillation solvent molecules absorb the gamma photons, shift to their excited molecular states, and then re-emit the energy as ultraviolet light ($\sim 280\text{nm}$). This energy is absorbed by the primary wavelength shifter or "fluor", which becomes excited and then re-emits the energy as photons with wavelengths in the 360nm region. Finally, the secondary wavelength shifter, which absorbs light in the 360nm range, will convert the energy to the visible blue light region (410nm-450nm) that is detected by the surrounding photomultiplier tubes (PMT). The signals from the PMT can then be amplified, converted to digital data by a multiple channel analyzer (MCA), and graphed. Collection of these data produces a Compton-scattering plot since the photons that reach the PMT have only a portion of the energy of the original gamma photon.

For the experiment to have the greatest effectiveness, the Gd-LS must have high photon yield, high optical transparency, and long-term chemical stability [2]. Detection of an antineutrino interaction depends on the scintillation efficiency of the detector

in converting the produced gamma photons into detectable light in the blue region, thus a scintillator with a high light yield is vital for a sensitive detector.

High optical transparency is necessary because the detector vessels will be very large, several meters in diameter, and photons must reach the PMT's on the outside of the detector. The scintillation solution should interfere as little as possible with light passage so the solvents must be exceptionally pure. The other motivation for extensive purification is to eliminate impurities that could react within the liquid scintillator and cause it to degrade. At a minimum, the reactor antineutrino experiment must run for 3 years. Radioactive contaminants also present an additional problem since some can mimic the neutron-capture signal of an antineutrino interaction, giving false results.

The research presented here focused on optimizing two of the key LS characteristics, solvent purity and high photon yield. Two selected scintillation solvents, 1, 2, 4-trimethylbenzene (pseudocumene - PC) and linear alkyl benzene (LAB), were purified to improve the optical transparency and long-term chemical stability of the Gd-LS. Photon yields were measured and compared for scintillation solutions that varied in the combinations and concentrations of the added wavelength shifters to find which solution had the maximum photon production. Four primary shifters, p-terphenyl (p-TP), 2-(4-Biphenyl)-5-(4-tert-butyl-phenyl)-1,3,4-oxadiazole (butyl-PBD), 2,5-diphenyloxazole (PPO), and 2-(4-Biphenyl)-5-phenyl-1,3,4-oxadiazole (PBD), and two secondary shifters, 1,4-bis(2-methylstyryl)-benzene (bis-MSB) and 1,4-bis(4-methyl-5phenyloxazol-2-phenyl)benzene (POPOP), were used.

MATERIALS AND METHODS

All chemical shifters were used as received and, with the exception of PPO (Fluka), were made by Sigma-Aldrich. The two scintillation solvents, PC (Aldrich) and LAB (Petresa), were further purified using vacuum distillation and dry column separation, respectively. With the vacuum distillation, both the first $\sim 20\text{mL}$ of distillate and the last $\sim 30\text{mL}$ of residue were discarded as waste. The extent of the purification was monitored by the comparison of UV-visible absorbance spectra taken before and after purification. Spectral data were collected and analyzed with a Shimadzu UV-1601 UV-Visible Spectrophotometer using air as the reference material. In the case of PC purification, a UV-visible spectrum of the final residue was also obtained. When analyzing the UV spectra, a significant decrease in solvent absorption within the wavelength region of 430nm was used to indicate an increase in purity level.

A list of all the scintillation solutions tested is given in Table 1. For the initial photon yield measurements, all the LS solutions were made using 10.0g of solvent, 0.030g of primary shifter, and 0.0015g of secondary shifter. A series of samples were then made to measure the photon yield (S%) of two specific shifter combinations, LAB + butyl-PBD + bis-MSB and PC + p-TP + bis-MSB, at different shifter concentrations in order to find the lowest concentration that produced the greatest amount of light. The primary shifter concentration was set at 6g/L for both butyl-PBD and p-TP while the secondary shifter, bis-MSB, was added at concentrations of 10, 20, 50, 100, 150, and 500mg/L.

Fluors	s%	Δ s%
LAB+PPO	1862.50	40.31
LAB+BU	1935.50	55.86
PC+PPO	2115.60	57.12
PC+PBD	2172.00	66.30
PC+BU	1911.50	62.04
PC+pTP	1317.67	44.16
LAB+PPO+MSB	2332.00	59.43
LAB+PPO+POPOP	2155.00	91.65
LAB+BU+POPOP	2388.00	73.98
LAB+BU+MSB	2287.50	6.36
PC+PPO+MSB	2475.57	66.54
PC+PPO+POPOP	2208.00	79.27
PC+pTP+MSB	2921.25	50.76
PC+pTP+POPOP	2753.67	46.05
PC+PBD+MSB	2597.00	2.83
PC+PBD+POPOP	2693.50	6.36
PC+BU+MSB	2378.50	79.90

Table 1. Average LS Light Yields.

The setup for the LS light yield measurement consisted of a 10 μ Ci, sealed Cs-137 gamma source, a Hamamatsu R2154-02 Photomultiplier tube, and a EG&G ORTEC 572 amplifier. Each sample was placed on top of the PMT and externally radiated with the Cs-137 source. Signals produced by the PMT were amplified to 5V and then digitally converted and collected by a multiple channel analyzer (MCA) and Genie2000 software. The data were reconstructed as Compton-scattering curves using Microsoft Excel and analyzed by the Full Width Half Maximum (FWHM) method to obtain the photon production value.

RESULTS

Figure 1 compares the UV-visible absorbance spectra of LAB before and after purification. The same comparison is shown for PC in Figure 2 along with the spectrum of the residual distillation fraction. In both Figures there is a notable decrease in absorbance, especially in the 350-450nm region. As a result of purification, the absorbance at 430nm decreases by a factor of \sim 5 for LAB and \sim 10 for PC. LAB's improvement factor is smaller because it arrives from the company in a purer state.

Table 2 describes the solubility of the six shifters in each of the solvents. Ease of solubility for primary shifters in PC is PPO>butyl-PBD>PBD>p-TP and for secondary shifters is bis-MSB>POPOP. Because LAB is a less effective solvent, the shifters either take longer to dissolve or are unable to dissolve completely. The order of solubility for primary shifters in LAB is PPO>butyl-PBD and for secondary shifters is bis-MSB>POPOP. Both PBD and p-TP were insoluble in LAB.

Light yield measurements were taken three times or more for each solvent-shifter combination. The average light yield values along with their respective standard deviations are given in Table 1. The addition of a secondary shifter increased the light yield in all

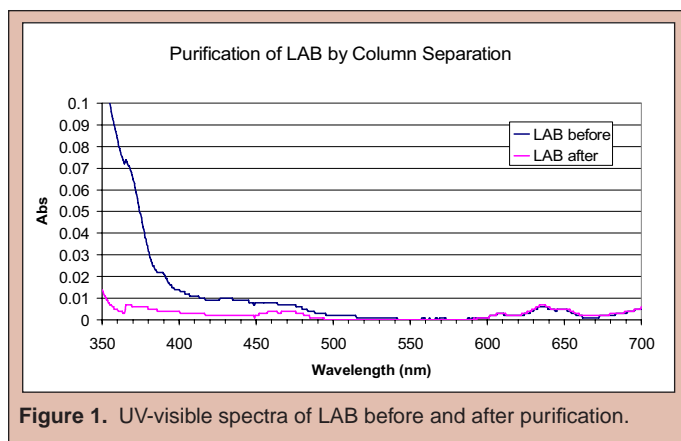


Figure 1. UV-visible spectra of LAB before and after purification.

Shifters	In PC	In LAB	Comments
butyl-PBD (Primary)	Soluble	Soluble	Dissolved quickly in PC, Overnight in LAB
PPO (Primary)	Soluble	Soluble	Dissolved quickly in PC, Overnight in LAB
PBD (Primary)	Soluble	Insoluble	Dissolved in PC after a period of shaking
p-TP (Primary)	Soluble	Insoluble	Dissolved in PC after a period of shaking
bis-MSB (Secondary)	Soluble	Soluble	Dissolved more quickly in PC than LAB; both required shaking
POPOP (Secondary)	Soluble	Soluble	Slower to dissolve than MSB, required vigorous shaking for PC and LAB

Table 2. Wavelength-Shifter Solubility Data.

the scintillator samples by at least \sim 10% with the largest increase resulting from the addition of bis-MSB to PC and p-TP (from 1317 to 2921 S%). The LS with the highest photon production for each solvent was PC + p-TP + bis-MSB and LAB + butyl-PBD + POPOP.

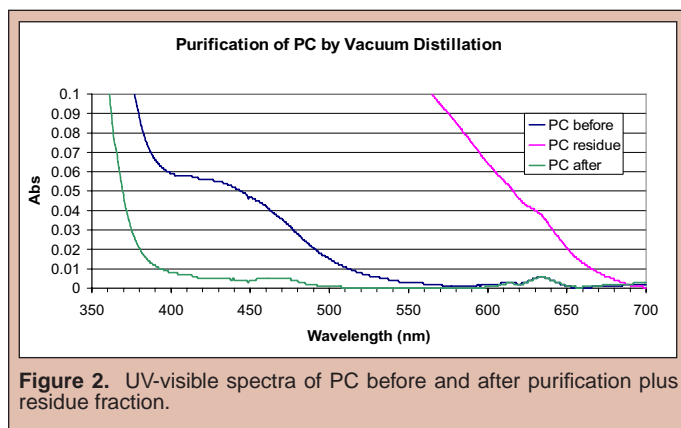


Figure 2. UV-visible spectra of PC before and after purification plus residue fraction.

Figure 3 shows the Compton-Scattering spectra of selected LS. These spectra were used to derive the scintillators' light yields. The x-axis in these Figures is directly proportional to photon production so the longer the data plot the greater the light yield.

DISCUSSION AND CONCLUSIONS

Results from the purification of PC and LAB show that their respective purification techniques, vacuum distillation and dry column separation, were effective at eliminating many impurities that were absorbing visible light. The evidence for this is that the visible light absorption in both solvents decreased by a factor of 5 or more after purification. Reducing the level of these contaminants not only rids the solution of foreign chemicals that could cause the LS to degrade but it also increases the scintillator's attenuation length by reducing the re-absorption of the scintillation light.

From the data gathered it has been determined that 6g/L p-TP with 150mg/L bis-MSB is the best shifter combination for PC while 6g/L butyl-PBD with 50mg/L bis-MSB is the best combination for LAB. The primary consideration for these choices was optimization of light yield but shifter solubility and cost were also taken into account.

Shifter solubility is an important consideration because the final Gd-LS for anti-neutrino experiment must be carried out on a very large scale (~200 tons of LS). Using a shifter that is difficult to dissolve would not be an economical use of time or of money.

In an experiment that is estimated to cost over 60 million dollars, it is important to save money wherever practically possible. One of the greatest expenses for the reactor antineutrino experiment is expected to be the purchase of fluors. As a result, the ideal shifter quantity should show a reasonable increase in light yield for every increase in concentration.

The LS containing p-TP and bis-MSB in PC had the highest average photon production out of all the samples tested. Since PC is such an effective solvent, consideration of shifter solubility does not come into play. There is also no contesting the ideal bis-MSB concentration since there is a large difference (>20%) in light yield between the samples with 100mg/L and 150mg/L bis-MSB.

Including experimental uncertainties, LAB had three shifter combinations with very similar light yields. Out of the three, butyl-PBD with bis-MSB was chosen because its average had the greatest precision and bis-MSB is easier to dissolve than POPOP. The concentration of 50mg/L bis-MSB is considered the optimal quantity for the LAB. Although 150mg/L produces more photons, its light yield is only 3% greater than the 50mg/L sample and requires three times more shifter.

Future work should focus on determining why these two solvent-shifter combinations produce more light than others. This can be accomplished by measuring the fluorescence spectra for each of the shifters and both LS. A scintillator's photon production, in addition to its quantum efficiency, depends on the extent to which the solvent's emission spectrum overlaps the primary shifter's absorbance spectrum and likewise on the overlap of the primary shifter's emission spectrum with the secondary shifter's absorbance spectrum. Greater overlap increases light transfer efficiency and the photon yield.

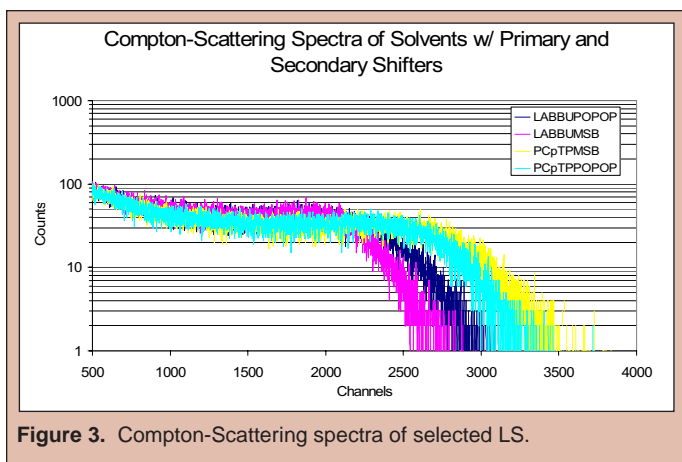


Figure 3. Compton-Scattering spectra of selected LS.

Figures 4 and 5 display light yield as a function of bis-MSB concentration for two LS, PC + p-TP + bis-MSB and LAB + butyl-PBD + bis-MSB, respectively. Light yield roughly increases with concentration up to a point and then levels off. Both tested LS begin leveling off in light yield at a concentration of ~150mg/L bis-MSB.

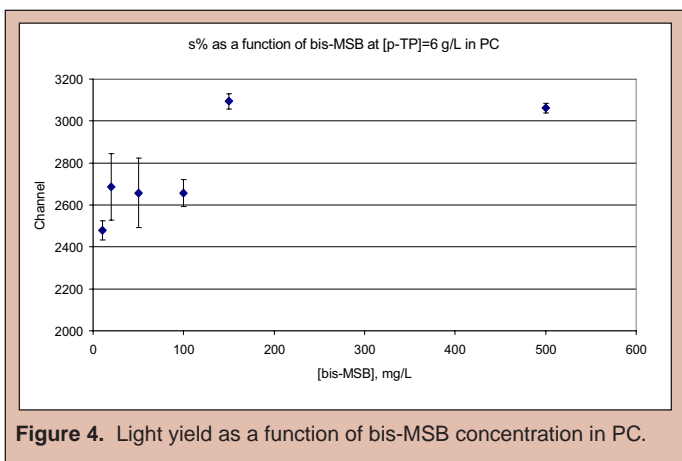


Figure 4. Light yield as a function of bis-MSB concentration in PC.

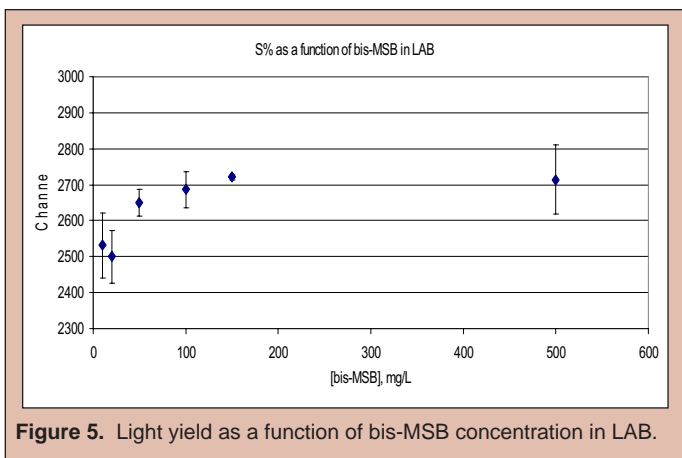


Figure 5. Light yield as a function of bis-MSB concentration in LAB.

ACKNOWLEDGMENTS

We would like to thank our mentors, Dr. Richard Hahn and Dr. Minfang Yeh for all the time they invested in introducing us to this field of study as well as guiding us through our research. Our thanks go to the U.S. Department of Energy, Office of Science for making this program available. We are thankful to Dr. Sri and Central State University for funding our research through the NSF-sponsored Quest program. We appreciate the hospitality of Brookhaven National Laboratory, especially the Chemistry Department, for providing the facilities needed for this internship. Finally, we are thankful to the Office of Educational Programs for managing and maintaining this wonderful undergraduate research program.

REFERENCES

- [1] R. L. Hahn, "Two proposals to measure antineutrinos: At the Braidwood (USA) and the Daya Bay (PRC) reactors," *Progress in Particle and Nuclear Physics*, vol. 57, pp.134-143, 2006.
- [2] M. Yeh, R.L. Hahn, A. Garnov, and Z. Chang, "Studies of Doped Scintillator at BNL: A Generic Method for Neutrino Measurement," *AIP Conf. Proc.*, vol. 785, p. 209, 2005.
- [3] The SNO Collaboration, "Measurement of charged current interactions produced by ^8B solar neutrinos at the Sudbury Neutrino Observatory," *Phys. Rev. Lett.*, 87, 071301, 2001.

David LaBissoniere is currently an intern at the Oak Ridge National Laboratory, in the Cyber Security and Information Infrastructure group. His work explores applications of textual content analysis techniques. In previous work at the laboratory, he developed algorithms which employ network logistics to improve long distance data transfer performance. Mr. LaBissoniere recently graduated from East Tennessee State University with a B.S. degree in computer science. He plans to continue on to graduate school in 2008.

Kenneth Roche is a staff scientist in the Future Technologies Group of the Computer Science and Mathematics Division of the Oak Ridge National Laboratory.

ADAPTIVELY IMPROVING LONG DISTANCE NETWORK TRANSFERS WITH LOGISTICS

DAVID LABISSONIERE AND KENNETH ROCHE

ABSTRACT

Long distance data movement is an essential activity of modern computing. However, the congestion control mechanisms in the Internet's Transmission Control Protocol (TCP) severely limit the bandwidth achieved by long distance data transfers. The throughput of such transfers can be improved by applying the logistical technique of breaking a single long distance transfer into multiple shorter transfers. This technique can result in significantly improved throughput while still respecting the shared nature of the Internet by not attempting to circumvent the TCP congestion controls. This technique has been incorporated into an algorithm which attempts to dynamically schedule transfers for optimal throughput. The algorithm couples graph techniques with real-time latency and bandwidth measurements to discover the best path and adaptively respond to network dynamics. The algorithm shows improvements in speed and flexibility over standard data transfer methods such as FTP. Specific transfers tests performed between Oak Ridge National Laboratory and a destination in Sunnyvale, CA show throughput increases by a factor of two.

INTRODUCTION

Tremendous increases in computational and storage capacity have made it possible to create, process, and store massive datasets. Scientific, commercial, and personal computing applications have all scaled to take advantage of these abilities. However, one important aspect of computing that has failed to improve proportionally is the performance of network data movement. Despite significant bandwidth improvements on commercial and academic Internet links, the throughput actually achieved during data transfers employing the standard Transmission Control Protocol (TCP) stack is often a small fraction of the capacity available on the link. Primarily because of the design of the TCP congestion controls, this disparity between available and achieved bandwidth is especially apparent in long distance transfers. The congestion controls cause such transfers to very slowly reach their maximum throughput and in fact may altogether prevent them from doing so.

Many network researchers have proposed schemes for improving throughput by circumventing [1] or replacing [2] the TCP congestion controls or the protocol itself [3]. These approaches have shown significant improvements but have been slow to be adopted, in part because of the extent of the existing TCP infrastructure as well as concerns that such approaches will exacerbate congestion on the Internet.

This paper describes a method that improves long distance transfer throughput by inserting intermediary buffers into the transfer path. This method works within the framework of the TCP congestion controls without attempting to circumvent them. Additionally, an algorithm which automatically and adaptively applies this method is presented. Finally, an implementation of this algorithm is described, accompanied by empirical data regarding its performance. The data demonstrates that the throughput of long distance TCP transfers can be significantly improved by applying this technique — in this case by nearly a factor of two.

Logistical Transfer Improvements

Long distance transfers are characterized by a large round-trip time (RTT), the total time required to send a packet from source to destination and receive an acknowledgment at the source. The maximal throughput achieved by such a transfer is determined in large part by the size of the TCP congestion window, the amount of data allowed to be sent without being acknowledged by the recipient. TCP employs a policy of additive increase and multiplicative decrease for the window size [4]: the window starts out small and slowly increases as the transfer proceeds, up to a system-defined maximum size. If any error occurs, however, the window size is dramatically decreased. In this way, TCP attempts to determine the maximum available throughput while avoiding

congestion. The optimal congestion window size is large for transfers on high-bandwidth network paths with large RTTs. As a result, TCP takes a significant amount of time to reach this optimal window size and, in fact, may never do so if errors occur.

These performance limitations can be reduced by employing the methodologies of *logistical networking* [5]. By breaking long distance transfers into a pipelined series of shorter transfers, each with a RTT smaller than that of the direct source-to-destination transfer, throughput can be improved. This pipelining is accomplished by using intermediate application-layer storage *depots* [6] located between the source and destination to buffer data for the transfer. Data is moved in small blocks from source to destination, through each depot. This technique is somewhat counterintuitive due to the additional overhead introduced by the intermediate depots. Additionally, the sum of the RTTs between all intermediary points will generally be larger than the direct RTT. Despite these detriments, breaking up long distance transfers into multiple segments can yield significant performance improvement.

The throughput improvements obtained by this method are due to several factors. First, because the RTT on any edge along the transfer path is smaller than the end-to-end RTT, the TCP congestion control mechanisms will more quickly discover the maximum available bandwidth along each edge. Second, when errors do occur in the transfer and TCP reactively reduces the window size, the optimal window size will be recovered more quickly because it does not have as far to grow. Additionally, when an error requires a packet retransmission, the packet can be retransmitted from the nearest depot instead of the source, reducing bandwidth consumption and retransmission time. Finally, the congestion window size is often ultimately limited by hard system thresholds which are significantly smaller than the optimal window size for long distance transfers. These maximum window sizes are imposed by the system to prevent TCP buffers from consuming too much memory. Breaking long transfers into several shorter transfers yields closer-to-optimal window sizes, even if they are still limited by the system maximum. Further discussion of the improvements garnered by this method can be found in [7].

While other techniques for throughput improvement involve circumventing [1] or even replacing [2] the TCP congestion controls, this technique works within the TCP framework to produce a benefit. However, though not addressed in this paper, preliminary work done by the authors has shown that coupling the logistical technique with other strategies such as employing parallel TCP streams or alternate congestion control mechanisms will often achieve even further throughput increases.

Adaptive Path Scheduling

In order for this pipelining technique to yield a throughput benefit, the throughput achieved on each section of the total transfer must exceed the throughput on the direct end-to-end transfer. This limitation requires that prior knowledge of the network be available for useful application of the method: the throughput available between the source, destination, and each possible intermediary depot must be known. This stipulation is unrealistic and limits the

usefulness of this technique alone, especially due to the dynamic nature of networks.

To generalize the use of the method, an algorithm was developed that attempts to dynamically determine critical information about the network and to use it to schedule the optimal path from source to destination, through as many intermediaries as needed to maximize throughput. When no information about the state of the network is available, the algorithm performs a *cold start* in which it explores the network and determines the throughput available on each link. Otherwise, the algorithm performs a *warm start* and is able to determine the optimal path more quickly.

The algorithm models the network as a weighted, directed graph and uses graph analysis techniques to determine the best path from source to destination. In the graph, the source, destination, and each possible intermediate depot are represented as vertices and are connected to each other by edges. Each edge is weighted by the throughput available between these two points in the network. A valid path in the algorithm is a cycle-free sequence of connected vertices starting from the source and ending at the destination. The predicted throughput for a valid path is the minimum value of all the edge weights in the path. Thus, the optimal path is the one which has the largest minimum weight.

The algorithm employs a path construction routine which determines the best path from source to destination, based on currently available information. This routine is a derivative of Dijkstra's shortest-path algorithm [8], differing primarily in that it seeks the path with the largest minimum weight instead of the smallest aggregate weight. This routine has a computational complexity of $O(V^2)$, where V is the total number of vertices. Pseudocode for this routine is included in the appendix.

Because the state of the network is dynamic, the algorithm frequently re-evaluates its knowledge and adjusts the transfer path if necessary. This process enables the algorithm to handle failures of intermediary depots and networking equipment as well as reductions of throughput due to increased traffic or congestion. The algorithm loops until the transfer completes, monitoring the throughput and maintaining the edge weights on the graph. Frequently, the algorithm calls the shortest-path routine and compares the result to the current path. If they differ, the current path is stopped and data flow is moved to the new path.

When an edge weight is unknown, the algorithm treats that value as infinity, thereby encouraging the shortest-path routine to produce a path containing that edge. In this way, measurements of throughput on edges are only done in the process of the actual transfer. In a cold start, nothing is known about the network and thus all edges have infinite weights. As a result, the algorithm will frequently change the path early in the lifetime of the transfer, but will quickly discover all relevant edge weights and settle on the best path across the network.

The algorithm's computational complexity depends on the extent of the transfer. The algorithm loops throughout the life of the transfer and repeatedly calls the path construction routine. Each iteration of the loop has a complexity of $O(V^2)$, where V is the number of depots (vertices) in the network. The number of times this routine is called varies based on the size of the transfer and the achieved transfer rate. In a small transfer, the loop may only

be executed once. In a theoretical infinite stream of data, the loop would be executed infinitely. As a result, the best general complexity analysis of the algorithm that can be provided is $O(kV^2)$ where k is the number of times the loop is executed.

It is perhaps more useful to consider the number of path attempts necessary for the algorithm to settle onto the best available path and how this complexity scales with the number of available depots. In a completely cold start, between V and V^2 path attempts must be made in order to find the best path through the vertices. Because each path attempt corresponds with one iteration of the main algorithm loop described above, the complexity for finding the best path in a cold start is $O(V^2 * V^2) = O(V^4)$. In a warm start, the algorithm uses prior information about the network to determine the best path in fewer attempts. If this information is accurate, the best path can be found in only one attempt. However, if this information is entirely inaccurate, the algorithm will behave like a cold start and can require as many as V^2 attempts to determine the best path. As a result, the worst-case complexity of a warm start is the same as that of a cold start: $O(V^4)$.

Because of the transient nature of networks, the throughput on an edge may not be accurately measured and thus may not be considered in a path when it could provide a benefit. To reduce this problem, the algorithm employs a policy of aging edge weights. Each edge weight is aware of the time at which its measurement was taken. When this time passes a threshold, the weight is scaled up by a predefined percentage and its timestamp is updated. In this way, mis-measured edges are given another chance. To prevent sudden dramatic path changes from being introduced by the aging mechanisms, only a fixed maximum number of weights are aged per iteration of the algorithm.

IMPLEMENTATION AND RESULTS

The algorithm implementation is multi-threaded and utilizes a third-party package, the Internet Backplane Protocol (IBP) [6][9]. IBP uses a client/server architecture to provide anonymous, time-limited, storage allocations in memory or on the disk of remote servers. The algorithm uses these allocations as buffers for data in the network. The logistical transfer improvement is achieved by moving small blocks of data from the source to the first intermediary depot in the path while other threads of transfer simultaneously move data between depots along every other edge of the path. This process effectively forms a pipeline.

To facilitate testing of the algorithm and methodologies, IBP depots were deployed directly on the Abilene Internet2 backbone [10]. Data transfers were performed from a system at the Oak Ridge National Laboratory to a depot located at the Sunnyvale, CA Abilene site. The network route over Abilene between these two hosts passes near by to several of the intermediary depots. A pool of six possible intermediary depots was employed, four of which are located, topologically speaking, between ORNL and Sunnyvale (in Atlanta, Indianapolis, Kansas City, and Denver) and are thus poised to provide a throughput benefit. The other two depots (in New York City and Washington D.C.) are located in the opposite direction and serve to demonstrate the algorithm's ability to reject intermediary points which do not provide a throughput benefit. Three types of

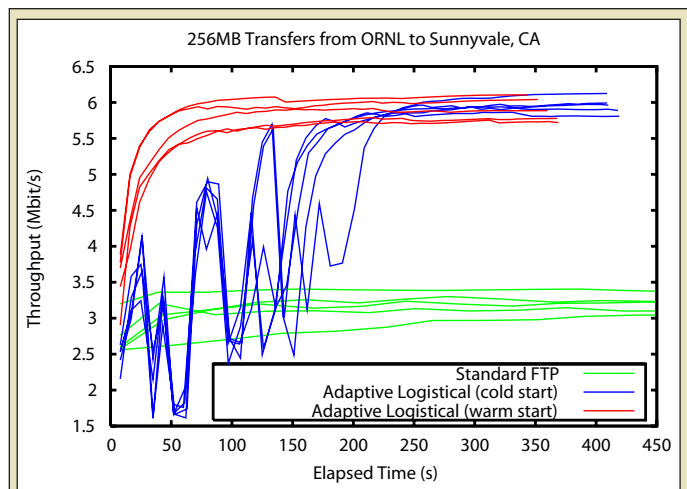


Figure 1. Repeated transfers from ORNL to Sunnyvale show that though initially the cold start transfer has significant fluctuation as it searches for the best path, it is ultimately able to achieve nearly double the performance of standard FTP. The warm start is able to achieve this improvement almost immediately.

transfers were repeatedly performed: standard FTP, logistical transfers with no prior network knowledge (cold start), and logistical transfers with prior knowledge of the network (warm start). The change in throughput over time for these transfers is plotted in Figure 1. The cold start transfers waver as the algorithm tries different paths across the network while attempting to determine the best one. Table 1 lists these paths for a single execution instance of the algorithm. These transfers even dip below the FTP throughput line at several points, when a path is being attempted which includes intermediaries not topologically between the source and destination—in our tests, New York and Washington D.C. The algorithm, however, quickly builds an accurate representation of the network and determines the best path across it.

Path	Throughput (Mbit/s)
ORNL → Sunnyvale	2.63
ORNL → Indianapolis → Sunnyvale	3.58
ORNL → Denver → Sunnyvale	3.75
ORNL → Atlanta → Sunnyvale	2.55
ORNL → Kansas City → Sunnyvale	3.23
ORNL → Washington → Sunnyvale	1.66
ORNL → New York City → Sunnyvale	1.74
ORNL → Atlanta → Denver → Sunnyvale	4.30
ORNL → Atlanta → Indianapolis → Denver → Sunnyvale	4.94
ORNL → Atlanta → Kansas City → Denver → Sunnyvale	4.40
ORNL → Atlanta → Washington → Denver → Sunnyvale	2.72
ORNL → Atlanta → New York City → Denver → Sunnyvale	2.44
ORNL → Atlanta → Indianapolis → Kansas City → Denver → Sunnyvale	5.99

Table 1. Order of path attempts in cold start transfer from ORNL to Sunnyvale, CA.

In the example, the best path from ORNL to Sunnyvale includes four sequential intermediary depots, located in Atlanta, Indianapolis, Kansas City, and Denver. The throughputs achieved on each edge of the path are listed in Table 2. Over time, transfers over this path achieve a throughput very close to the smallest edge value, in this case the 5.99Mbit/s edge between Denver and Sunnyvale. Note, however, that the best path for a particular source and destination may vary from transfer to transfer and even within the lifetime of a single transfer. If a depot or network link fails or experiences heavy load, the algorithm may choose a different path which at that time offers better throughput.

When information about the network is already known, the algorithm's warm start mode immediately achieves and maintains a throughput that is, at worst, the same as a direct transfer such as FTP. In our example (Figure 1), the warm start transfers quickly reach nearly double the throughput achieved by FTP. However, this improvement is contingent on the accuracy of the initial network information. Considerable incorrect information may result in a warm start taking as long as a cold start to determine the best path.

Edge	Throughput (Mbit/s)
ORNL → Atlanta	17.44
Atlanta → Indianapolis	11.76
Indianapolis → Kansas City	11.52
Kansas City → Denver	11.01
Denver → Sunnyvale	5.99

Table 2. Throughputs on each edge of the best path from ORNL to Sunnyvale over the Abilene network. In the long run, this path is able to achieve the minimum of these values, or 5.99Mbit/s.

CONCLUSIONS AND FUTURE WORK

This work demonstrates that a significant transfer performance benefit can be achieved by employing logistical techniques. These techniques work with the TCP congestion control mechanisms and do not attempt to circumvent them. As a result, the techniques respect the shared nature of the Internet while still improving throughput. Additionally, even without prior knowledge of the network, the adaptive algorithm determines and maintains the best logistical path to a destination.

Although significant throughput improvements were demonstrated, the actual bandwidth rates achieved were much lower than the theoretical maximum bandwidth available on the network links. This difference is believed to be a result of limited hardware availability and control. Specifically, many of the systems used were highly loaded and had restrictively low maximum TCP window sizes. Despite these setbacks, this work has shown notable performance improvements which demonstrate the utility of the logistical technique. Furthermore, related work [11] has shown that the technique still yields a benefit when employed in higher-bandwidth scenarios.

The algorithm also has limitations that this work did not address. First, the algorithm could conceivably starve a transfer on a highly irregular network through which an optimal path cannot be found. This issue can be easily addressed in the algorithm's implementation and must be addressed for any production application. Additionally, there is some question as to how the algorithm would behave if many instantiations of it were executed simultaneously on the same network of depots. Although this scenario has not been adequately tested, preliminary results suggest that the algorithm will scale as the number of processes grows, up to the point at which the depots are completely congested.

As well as addressing the above issues, further work on this project could involve algorithmic improvements to better predict and model network bandwidths. Additionally, a generalized library could be built that abstracts the logistical techniques further away from the user. Finally, these techniques could be demonstrated on higher-bandwidth links and as the data transfer mechanism for a large-scale grid application.

ACKNOWLEDGMENTS

This research was primarily conducted at the Oak Ridge National Laboratory in the Future Technologies group of the Computer Science and Mathematics division. Foremost thanks go to Kenneth Roche who supported and supervised the project and devoted countless hours of his time. Also, Micah Beck provided invaluable insight and resources. Additional thanks go to Christopher Wallace, Phillip Pfeiffer, Philip Roth, Jeffrey Vetter, the DOE Office of Science, and the SULI program.

REFERENCES

- [1] H. Sivakumar, S. Bailey, R. Grossman. "PSockets: the case for application-level network striping for data intensive applications using high speed wide area networks," in Proc. of the 2000 ACM/IEEE Conference on Supercomputing, 2000.
- [2] S. Floyd. "High-Speed TCP," IETF RFC3649, 2003.
- [3] Q. Wu, N. Rao. "Protocol for high-speed data transport over dedicated channels," Proc. of Third International Workshop on Protocols for Long-Distance Networks, 2005.
- [4] M. Allman, V. Paxson, W. Stevens. "TCP Congestion Control," IETF RFC 2581, 1999.
- [5] M. Beck, T. Moore, J. Plank, and M. Swany. "Logistical Networking: Sharing More Than the Wires," in Proc. of 2nd Annual Workshop on Active Middleware Services, 2001.
- [6] J. Plank, A. Bassi, M. Beck, T. Moore, M. Swany, and R. Wolski. "Managing Data Storage in the Network," in IEEE Internet Computing, 2001.
- [7] M. Swany and R. Wolski. "Data Logistics in Networking Computing: The Logistical Session Layer," in IEEE Network Computing and Applications, 2001.
- [8] E. Dijkstra. "A Note on Two Problems in Connexion with Graphs," Numerische Mathematik1, 1959.
- [9] Internet Backplane Protocol. <http://loci.cs.utk.edu/ibp/>.
- [10] Abilene. <http://abilene.internet2.edu/>.
- [11] M. Swany. "Improving Throughput for Grid Applications with Network Logistics," in Proc. of the 2004 ACM/IEEE Conference on Supercomputing, 2004.

Appendix – Algorithms

A. Path construction routine

This routine is a derivative of Dijkstra's shortest path algorithm. It determines the shortest path across the network, based on current information.

```
get_best_path(Vertex src, Vertex dest)
{
    /* Declarations */
    known[num_vertices];
    bandwidth[num_vertices];
    previous[num_vertices];

    /* Initializations */
    For each vertex {
        known[vertex] = False;
        bandwidth[vertex] = 0;
        previous[vertex] = -1;
    }
    bandwidth[src] = Infinity;

    while ( (vertex = largest unknown bandwidth vertex) != -1) {
        known[vertex] = True;

        For each unknown adjacent vertex {
            bw = minimum(bandwidth[vertex], Edge[vertex][adjacent]);
            if (bw > bandwidth[adjacent]) {
                bandwidth[adjacent] = bw;
                previous[adjacent] = vertex;
            }
        }
    }
    /* the best path is now stored in the previous[] array and can be
       read recursively starting at previous[dest]
    */
}
```

B. Main algorithm routine

This routine manages the transfer threads and edge weights.

```
perform_transfer(Vertex src, Vertex dest)
{
    Path cur_path = NULL;
    Path new_path;

    /* Loop until transfer is completed. */
    while (transfer is not complete)
    {
        /* Get the best path based on current information
           Complexity:  $O(V^2)$ 
        */
        new_path = get_best_path(src, dest);

        if (new_path != cur_path)
        {
            /* Stop transfer threads on current path, if any
               Complexity:  $O(1)$ 
            */
            stop_transfer(cur_path);

            /* Begin transfer threads on new path
               Complexity:  $O(1)$ 
            */
            start_transfer(new_path);

            cur_path = new_path;
        }

        /* Wait a predefined time to allow transfer to ramp up */
        sleep(t);

        /* Update graph weights with current bandwidth measurements
           Complexity:  $O(V)$ 
        */
        update_weights();

        /* Age a fixed maximum number of old weights to give mis-measured
           edges another chance
           Complexity:  $O(1)$ 
        */
        age_weights();
    }
}
```

Alejandro Levander is an intern in the Science Undergraduate Laboratory Internship program at the National Renewable Energy Laboratory, where he is analysing high efficiency multi-junction photovoltaics. He received his undergraduate degree in materials science and engineering from Pennsylvania State University. Mr. Levander is a member of Materials Advantage. He grew up in Silver Spring, Maryland, and he enjoys backpacking, mountain biking, and traveling.

John Geisz is a senior scientist at the National Renewable Energy Laboratory (NREL). He received his Ph.D. from the University of Wisconsin in 1995, studying the application of III-V semiconductor heterostructures to optical chemical sensing. At NREL, he has specialized in epitaxial growth of III-V semiconductors by metal-organic chemical vapor deposition (MOCVD) for photovoltaic applications. He has conducted pioneering research into the growth of novel III-V semiconductor alloys containing boron or nitrogen that are lattice-matched to GaAs and silicon. Recently, he has focused more on lattice-mismatched III-V growth for the development of new high-efficiency multijunction solar cell designs.

EXAMINATION OF DISLOCATIONS IN LATTICE-MISMATCHED GaInAs/BUFFER LAYER/GaAs FOR III-V PHOTOVOLTAICS

ALEJANDRO LEVANDER AND JOHN GEISZ

ABSTRACT

Dislocations act as sites for nonradiative electron/hole pair recombination, which reduces the efficiency of photovoltaics. Lattice-matched materials can be grown on top of one another without forming a high density of dislocations. However, when the growth of lattice-mismatched (LMM) materials is attempted, many dislocations result from the relaxation of strain in the crystal structure. In an attempt to reduce the number of dislocations that propagate into a solar device when using LMM materials, a compositionally step-graded buffer is placed between the two LMM materials. In order to confine the dislocations to the buffer layer and therefore increase material quality and device efficiency, the growth temperature and thickness of the buffer layer were varied. A GaInP compositionally graded buffer and GaInAs p-n junction were grown on a GaAs substrate in a metal-organic chemical vapor deposition (MOCVD) system. A multi-beam optical stress sensor (MOSS) and X-ray diffraction (XRD) were used to characterize the strain in the epilayers. Electrical and optoelectronic properties were measured using a probe station and multimeter setup, solar simulator, and a quantum efficiency instrument. It was determined that device functionality was highly dependent on the growth temperature of the graded buffer. As growth temperature increased, so did the dislocation density in the device despite an increase in the dislocation velocity, which should have increased the dislocation annihilation rate and the diffusion of dislocations to the edge of the crystal. The thickness of the graded buffer also affected device efficiency with thinner samples performing poorly. The thinner graded buffer layers had high internal resistances from reduced carrier concentrations. In terms of efficiency, the empirically derived recipe developed by the scientists at the National Renewable Energy Laboratory (NREL) produced the highest quality cells.

INTRODUCTION

Solar power is currently used in a multitude of applications including the supplementing of household electricity, the powering of remote systems, and the generation of electricity for satellites. The development of the photovoltaic (PV) industry is critical to keeping U.S. energy dollars at home and reducing greenhouse gas emissions from coal burning power plants.

Solar cells can be made from several different materials: organic, amorphous silicon, polycrystalline II-VI, and single crystal III-V semiconductors, which are typically multi-junction. The latter is currently the most expensive to produce, but also the most efficient. The cost comes from the need for high purity chemicals and complex manufacturing processes. In space applications, where quality is the

prime concern over cost, III-V multi-junction cells produced by Spectrolab and Emcore are already in use. To make multi-junction cells practical for terrestrial applications, concentrator systems are often used to focus the sunlight on a small cell, therefore reducing the cost of the cell relative to the entire system.

In general, photovoltaics made from single crystals are more efficient than those made from polycrystalline or amorphous materials. Amorphous semiconductors have a large density of dangling bonds and polycrystalline semiconductors contain grain boundaries [1]. Nonradiative electron/hole pair recombination occurs at these bulk defects, reducing the efficiency of photovoltaics made from the aforementioned materials. The superior efficiency of single crystals is caused in part by their lower density of bulk

defects. Reducing the defect density by increasing the material quality is a key method used to increase efficiency.

Single crystals of both silicon and various III-V semiconductors have been successfully produced as photovoltaics, but III-V semiconductors have certain advantageous characteristics that will make them the focus of this report. Many III-V semiconductors have a direct bandgap, high absorption coefficient, and can be produced with high-volume growth techniques, resulting in high crystalline and optoelectronic quality [2]. Depositing multiple layers of III-V semiconducting materials of differing band gap on top of each other can produce high-efficiency solar cells. Varying the band gap of the materials allows for greater absorption of the solar spectrum while minimizing thermalization of the minority carriers. Single crystal layers are epitaxially grown on top of each other using metal-organic chemical vapor deposition (MOCVD). Lattice-matched (LM) materials, materials with equal lattice spacing, can be grown on top of one another without the formation of many dislocations relatively easily. However, since lattice constant and band gap are related for III-V semiconductors, according to Figure 1, growing only LM materials limits the freedom of device design, therefore limiting theoretical efficiencies.

Having the ability to grow high quality lattice-mismatched (LMM) materials would allow the development of higher efficiency cells. Mismatch greater than 0.2% in a layer 1 μm in thickness, the “critical thickness” required to absorb most light, will result in significant dislocations and is therefore considered LMM [3]. The problem with LMM growth is that strain in the crystal results in the formation of dislocations.

Dislocations act as sites of nonradiative electron/hole pair recombination that reduce the efficiency of photovoltaics [1]. In an attempt to reduce the number of threading dislocations that propagate into the cell, a compositionally step-graded buffer is placed between the two LMM materials. Varying the chemical composition of III-V materials affects their lattice constant so simply changing the

flow rates of source materials into the reactor in a stepwise fashion can generate a buffer layer between two LMM materials. LMM materials have been successfully grown at NREL with properties similar to LM materials [4]. When photovoltaic design possibilities are expanded to include LMM materials, cells with higher theoretical efficiencies can be conceived.

In an attempt to grow a cell with a 1eV bandgap component, NREL has begun working on LMM growth of $\text{Ga}_{.75}\text{In}_{.25}\text{As}$ on GaAs. The two materials are LMM so a compositionally step-graded buffer must be grown between the two. GaInP was selected as the buffer layer material since it is transparent to the lower energies of light absorbed by the GaInAs bottom cell. The single-junction device examined is part of a triple junction cell composed of GaInAs ($E_g = 1.0\text{eV}$), a GaInP buffer layer, GaAs ($E_g = 1.4\text{eV}$), and GaInP ($E_g = 1.8\text{eV}$). This cell has the potential to reach an efficiency of more than 40% [4]. By gaining the ability to confine the dislocations formed in the buffer layer, the number of dislocations that propagate into the epilayer can be reduced. In an attempt to reduce the number of dislocations in the cell, and therefore increase material quality and device efficiency, the growth temperature and thickness of the buffer layer was examined.

MATERIALS AND METHODS

All of the cells were grown using an in-house built MOVCD reactor at atmospheric pressure with t-butylarsine, phosphine (PH_3), and triethylgallium serving as the III-V semiconductor precursors and hydrogen selenide and diethylzinc serving as dopant gases. A Zn-doped GaAs wafer with an intentional 2° miscut was used for a substrate. Before growth, the wafer was washed with an ammonia/hydrogen peroxide solution, followed by a deionized water rinse and spin-dry. The reactor was purged with arsine at 700°C prior to the growth of a $0.2\mu\text{m}$ nucleation layer of GaAs. $\text{Ga}_{.51}\text{In}_{.49}\text{P}$ was then grown LM onto GaAs as shown in Figure 2.

Eight compositionally graded LMM steps were grown as part of the Zn-doped buffer, using precisely controlled flow rates, until $\text{Ga}_{.26}\text{In}_{.74}\text{P}$ was reached. Eight steps were used in order to ensure that the mismatch between any two steps was small enough to maintain a relatively flat growth surface and a low number of dislocations. The compositional change of each step was consistent for each sample, but the step thickness varied from $0.0625 - 0.5\mu\text{m}$ to investigate the effect of that variable. In past experiments, the buffer layer thickness has been $0.25\mu\text{m}$, but in an effort to reduce the costs associated with materials and time, the use of a thinner buffer layer was examined. In a separate experimental set, the growth temperature of the buffer was varied from $600^\circ\text{C} - 650^\circ\text{C}$. Previous studies revealed efficiency has strong dependence on temperature, so relatively small changes from the baseline were necessary. The GaInAs cell was a $2\mu\text{m}$ thick layer of Zn-doped $\text{Ga}_{.75}\text{In}_{.25}\text{As}$, lattice-matched with $\text{Ga}_{.26}\text{In}_{.74}\text{P}$, and a $0.1\mu\text{m}$ thick layer of Se-doped $\text{Ga}_{.75}\text{In}_{.25}\text{As}$, forming a p-n junction. The active part of the device was grown at 650°C in all samples. A selenium doped window layer composed of $\text{Ga}_{.26}\text{In}_{.74}\text{P}$ and a $\text{Ga}_{.75}\text{In}_{.25}\text{As}$ contact layer were grown on top at 650°C so that photoelectrical properties could be measured.

A k-Space Associates Multi-beam Optical Stress Sensor (MOSS) mounted on the reactor recorded *in-situ* curvature measurements of

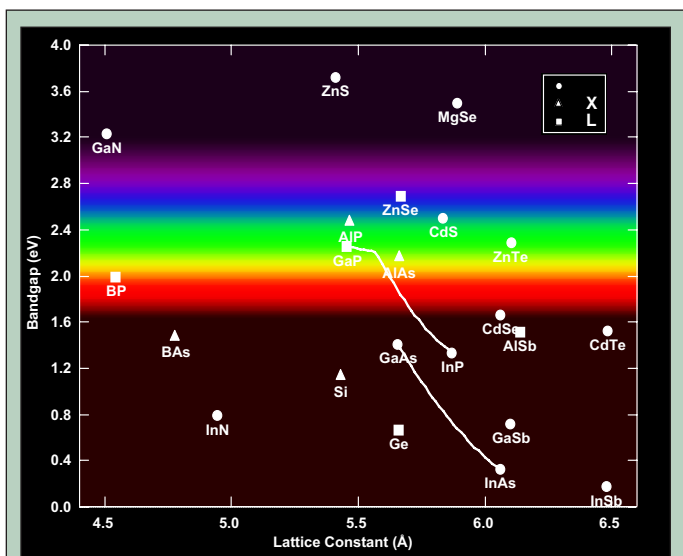


Figure 1. The relationship between chemical composition, lattice constant, and band gap for III-V semiconductors and other materials. Tie lines for the relevant materials, GaInP and GaInAs, are shown (J.F. Geisz and D.J. Friedman, “III-N-V semiconductors for solar photovoltaic applications”, *Semicond. Sci. Technol.* v. 17, p. 769-777, (2002)).

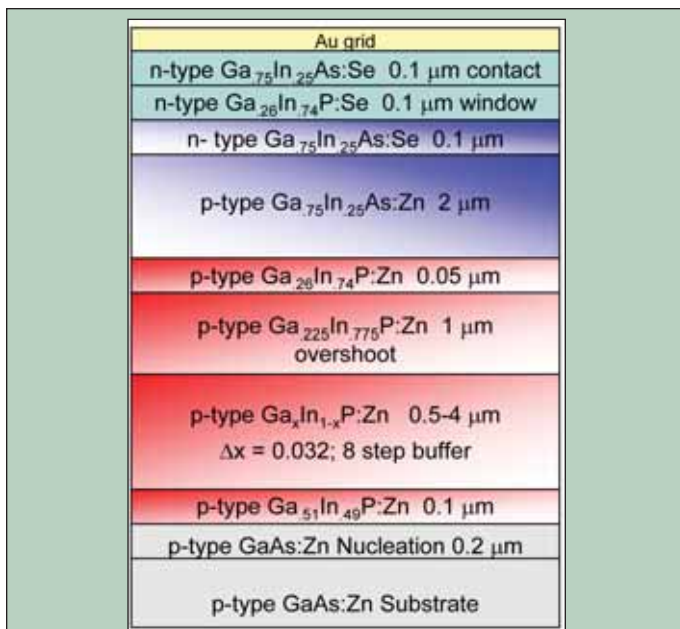


Figure 2. Schematic diagram of single-junction device grown. The temperature at which GaInP was grown and the thickness of the graded buffer were independent variables.

the growing crystal. The MOSS collects data using a single laser, split by an etalon into an array of nine parallel beams, which is incident on the sample. Any change in the curvature of the sample surface will result in a displacement change of the reflected lasers. This displacement change is detected by a charge-coupled device (CCD) camera, which digitizes the image and transmits the information to a data acquisition computer. The camera also detects the intensity of the laser allowing for the analysis of growth oscillations caused by wave interference.

The curvature change, Δk , is derived from the laser displacement change and is directly and quantitatively related to the strain in the sample [5]. The use of MOSS allows for the *in-situ* measurement of curvature during stress development versus an *ex-situ* measurement of the final strain in the multilayer crystal. However, the *ex-situ* technique of X-ray diffraction (XRD) is still useful for obtaining data on the tilt of the epilayer and quantitatively analyzing the strain and chemical composition of each layer. A Bede D¹ X-ray Diffractometer was used to characterize the tilt, strain, and composition of each sample. To calculate strain and composition of the epilayers, (224) grazing incidence XRD reciprocal space maps (RSM) were collected [6]. An example of a (224) RSM can be seen in Figure 3. The tilt of the epilayer was characterized by taking four (004) symmetric XRD RSMs.

Several other data sets were collected to fully characterize the quality of the cells produced. A probe station connected to a multimeter was used to measure the resistivity of the contact and window layer as well as ensure that the gold/semiconductor connection was ohmic. A modified XT-10 solar simulator from Spectrolab was used to measure I-V curves. From this data, the open circuit voltage (V_{oc}), short-circuit current (J_{sc}), fill factor (FF), and the device efficiency were derived, as well as a qualitative analysis of the internal resistance inside the cell. Quantum efficiency (QE) readings were taken using an in-house built QE instrument. QE is defined

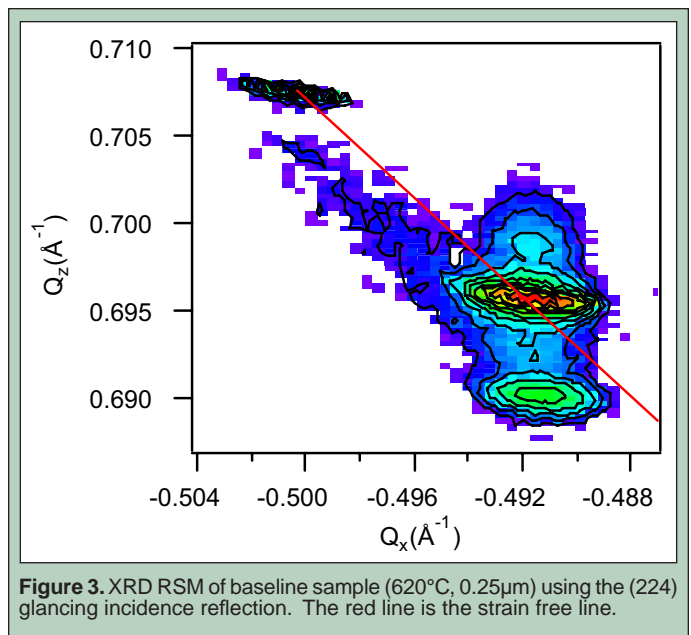


Figure 3. XRD RSM of baseline sample (620°C, 0.25μm) using the (224) glancing incidence reflection. The red line is the strain free line.

as the percentage of incident photons of a specific wavelength that generate an electron/hole pair. A scanning electron microscope was used to characterize dislocation density via electron-beam induced current (EBIC). On the EBIC image in Figure 4, the dark lines and spots represent dislocations.

RESULTS

The data is separated into two experimental groups with different independent variables: growth temperature of the graded buffer and thickness of the steps in the graded buffer. Tables 1 and 2 summarize the characterization data for the three samples including compositional and strain data gleaned from XRD as well as optoelectronic data gathered using the solar simulator.

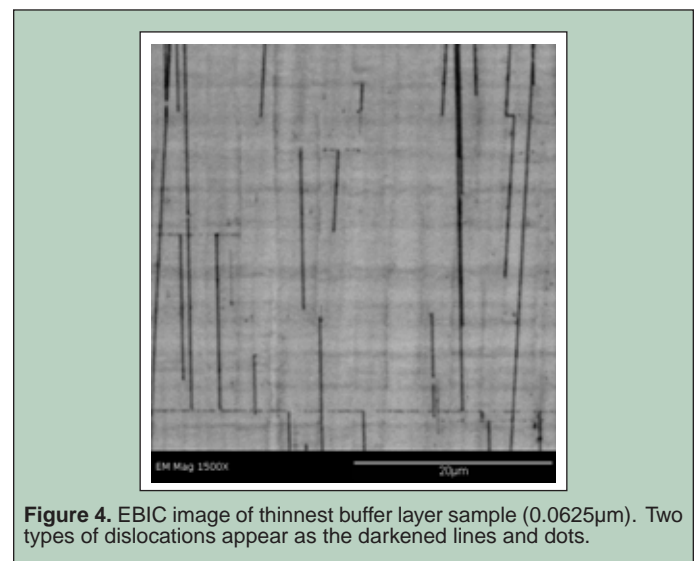


Figure 4. EBIC image of thinnest buffer layer sample (0.0625μm). Two types of dislocations appear as the darkened lines and dots.

Trends in this data are displayed in Figure 5, which includes an analysis of device efficiency, B tilt, and strain versus temperature.

The *in-situ* curvature measurements of the three growth temperatures, 600°C, 620°C, and 650°C, are shown in the same graph in Figure 6 for ease of comparison.

The cooler the growth temperature, the more compressive strain there was present in the compositionally graded buffer. The I-V and QE curves for the samples are in Figures 7 and 8 respectively.

Temp (°C)	Ga _x In _{1-x} P				Ga _{1-x} In _x As		Defect Density (#x10 ⁹ /cm ²)	
	A tilt	B tilt	X	Strain (%)	X	Strain (%)	Point	Line
600	0.042°	0.49°	0.220	-0.34	0.246	0.06	2.18	3.87
620	0.02°	1.2°	0.220	-0.27	0.244	0.09	4.97	3.23
650	0.032°	1.63°	0.221	-0.23	0.246	0.13%	3.33	6.45

Table 1. Tilt, composition, and strain data for the growth temperature experiment calculated using XRD RSMs.

Temp (°C)	V _{oc} (V)	J _{sc} (mA/cm ²)	FF (%)	Eff. (%)
600	0.556	16.12	77.50	6.95
620	0.547	15.00	75.70	6.21
650	0.537	13.45	26.94	1.95

Table 2. Optoelectronic data on growth temperature experiment collected using solar simulator.

Fig. 5.B) B Tilt (°) vs. Temperature (°C)

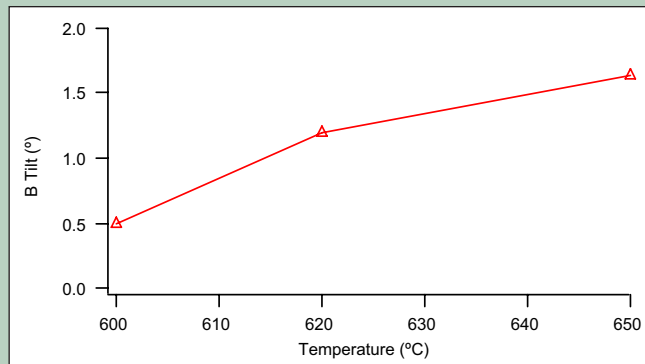


Fig. 5.C) Strain in GaInP and GaInAs (%) vs. Temperature (°C)

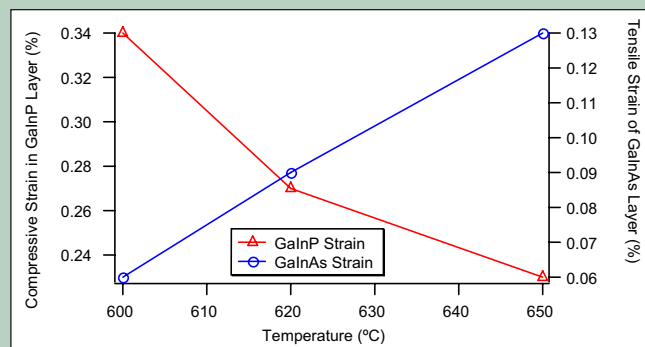


Figure 5.A-C. Several graphs showing the affect of temperature on efficiency and dislocation density (A), B tilt (B), and strain (C).

The characterization data for the thickness samples is summarized in Tables 3 and 4 with key trends highlighted in Figure 9.

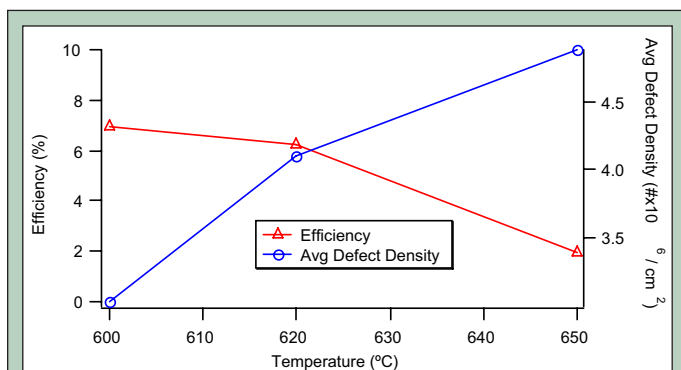


Fig. 5.A) Efficiency (%) and Avg Defect Density (#x10⁹/cm²) vs. Temperature (°C).

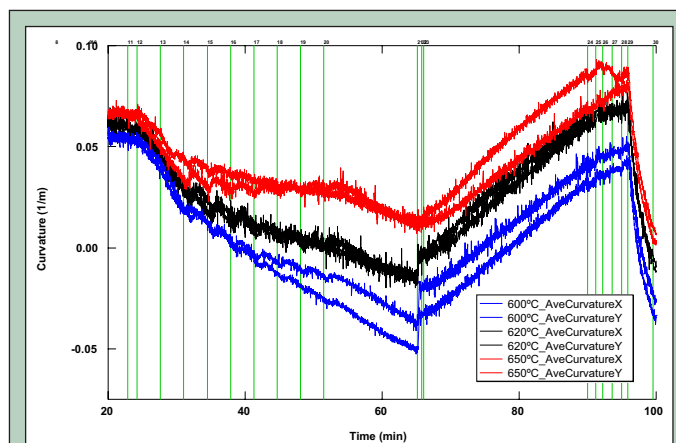


Figure 6. *In-situ* curvature measurements for the three samples in the growth temperature experiment.

The *in-situ* curvature measurements for the variable graded buffer thickness experiments are graphed separately, in Figure 10,

in order to cleanly observe the strain relaxation steps in the thicker samples.

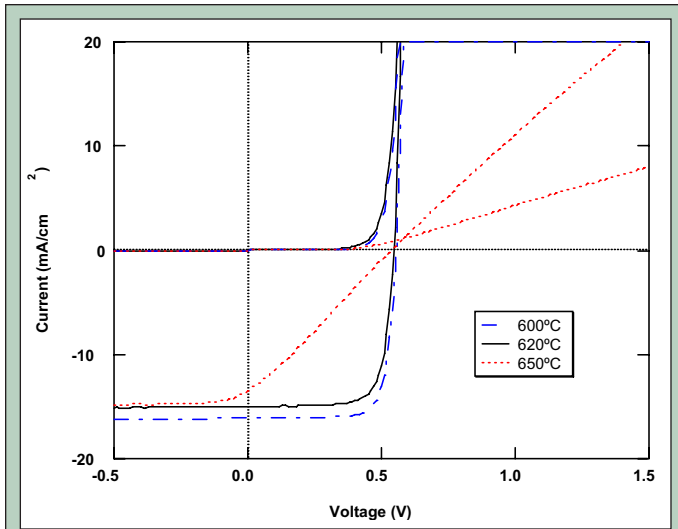


Figure 7. I-V curves of growth temperature experiment devices collected using a solar simulator.

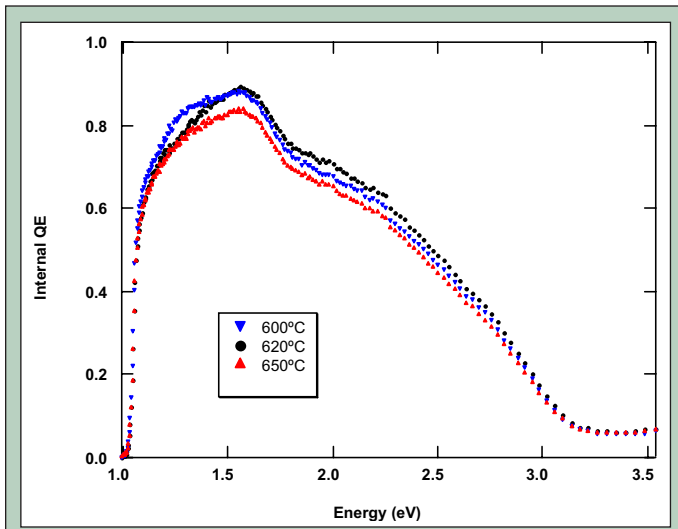


Figure 8. QE curves of the growth temperature experiment devices.

Step Thickness (μm)	$\text{Ga}_x\text{In}_{1-x}\text{P}$				$\text{Ga}_{1-x}\text{In}_x\text{As}$		Defect Density ($\#\times 10^6/\text{cm}^2$)	
	A tilt	B tilt	X	Strain (%)	X	Strain (%)	Point	Line
0.0625	0.016°	1.66°	0.220	-0.24	0.247	0.12	3.64	1.61
0.125	0.012°	1.53°	0.220	-0.25	0.244	0.12	5.27	4.84
0.25	0.02°	1.2°	0.220	-0.27	0.244	0.09	4.97	3.23
0.5	0.006°	1.14°	0.218	-0.23	0.247	0.12	5.33	5.81

Table 3. Tilt, composition, and strain data for the graded buffer thickness experiment calculated using XRD RSMs.

Step Thickness (μm)	V_{oc} (V)	J_{sc} (mA/cm^2)	FF (%)	Eff. (%)
0.0625	0.529	11.98	24.24	1.54
0.125	0.538	14.78	31.19	2.48
0.25	0.547	15.00	75.70	6.21
0.5	0.534	14.63	75.49	5.90

Table 4. Optoelectronic data on graded buffer thickness experiment collected using solar simulator.

Fig. 9.A) Efficiency (%) and Avg Defect Density ($\#\times 10^6/\text{cm}^2$) vs. Step Thickness (μm)

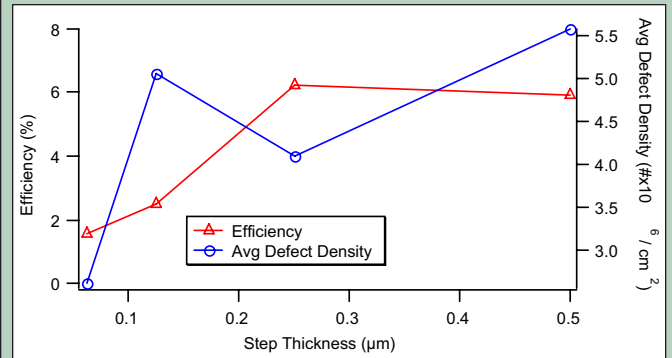


Fig. 9.B) B Tilt (°) vs. Step Thickness (μm)

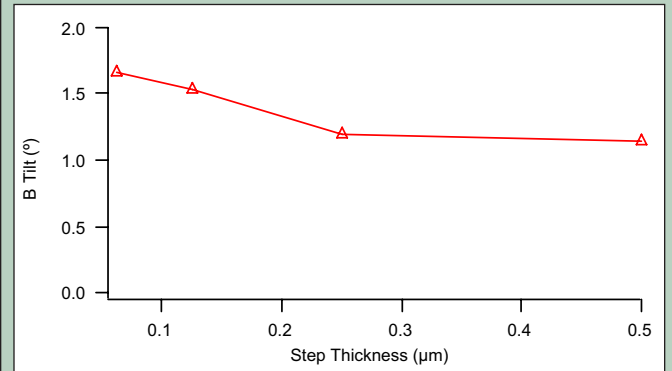


Fig. 9.C) Strain in GaInP and GaInAs (%) vs. Step Thickness (μm)

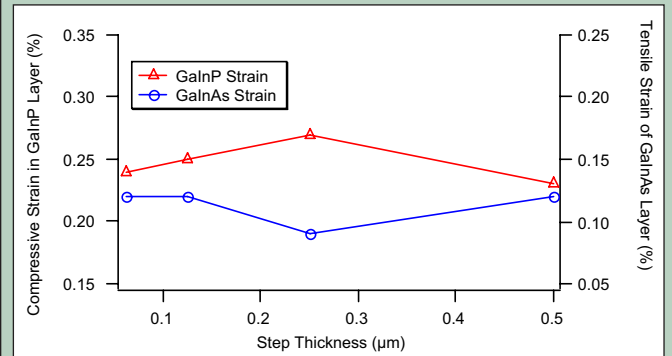


Figure 9. Several graphs showing the affect of the step thickness in the compositionally graded buffer on efficiency and dislocation density (A), B tilt (B), and strain (C).

The graphs are ordered in increasing buffer step thickness: 0.0625 μm , 0.125 μm , 0.25 μm , and 0.5 μm . Figures 11 and 12 have the I-V and QE curves for the variable buffer thickness experimental set.

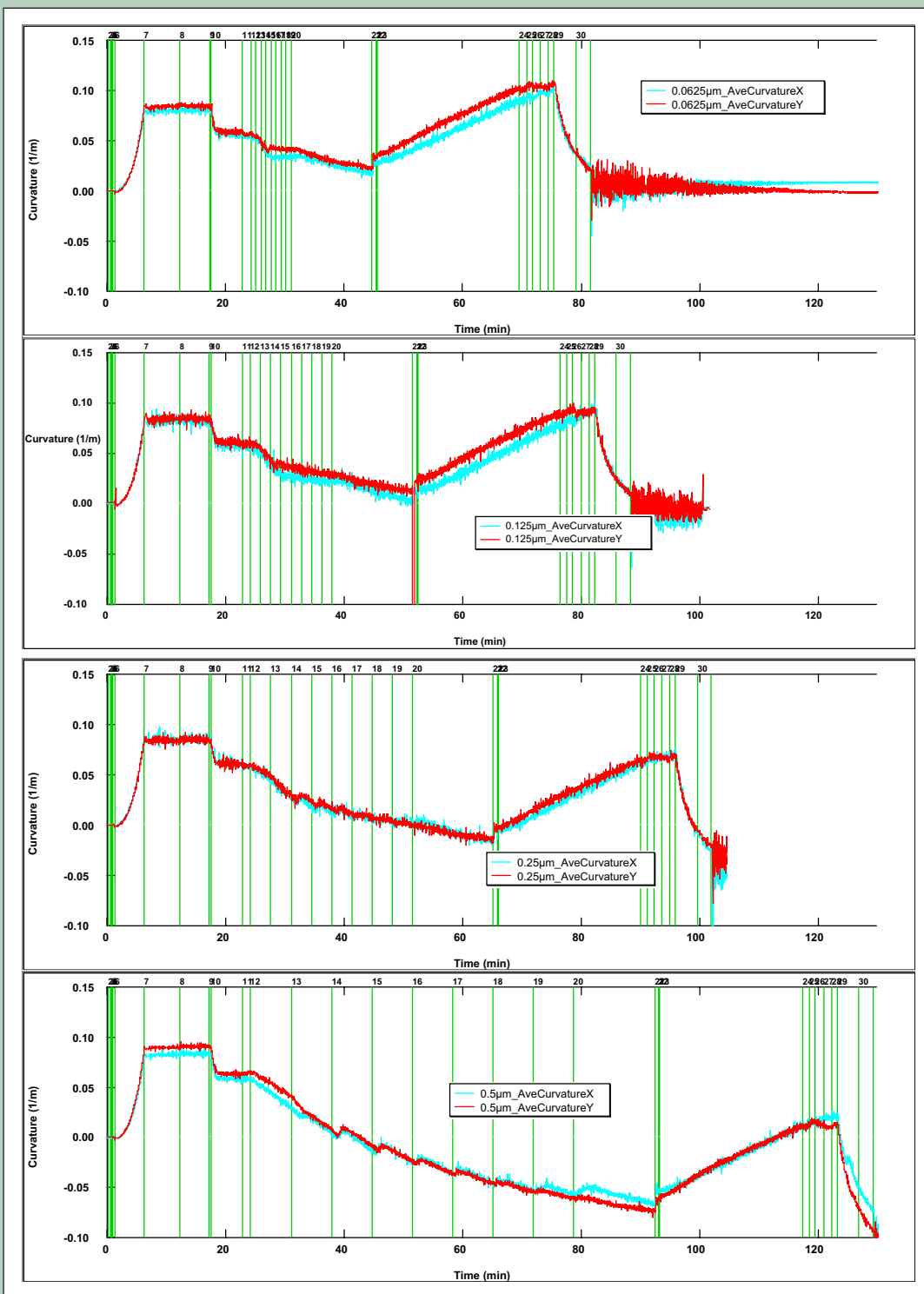


Figure 10. *In-situ* curvature measurements of the graded buffer thickness experiment samples. All of the graphs have the same scale to make qualitative examination more straightforward. The vertical lines indicate the beginning of a new stage in the growth process. The graphs are arranged in the order of thinnest buffer layer to thickest buffer layer. Deviation from the first horizontal segment is indicative of curvature in the surface. The buffer layer is grown during the segment starting near 25 min. and ends when the curvature begins to increase.

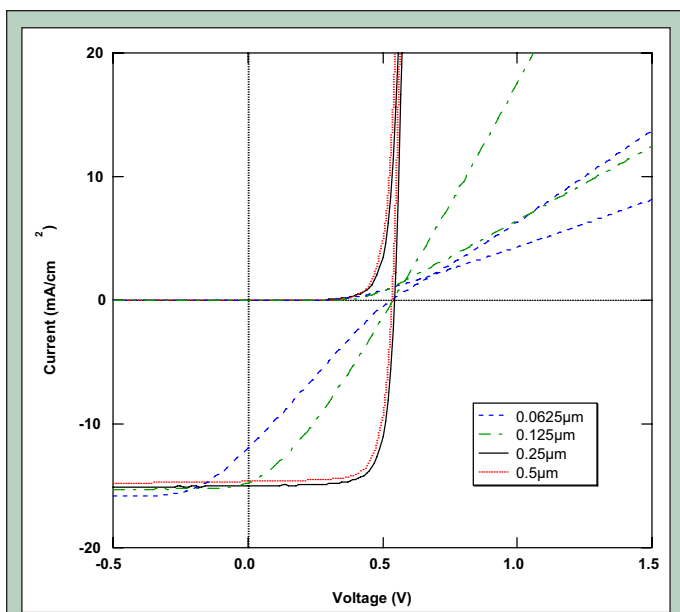


Figure 11. I-V curves of graded buffer thickness experiment devices collected using a solar simulator.

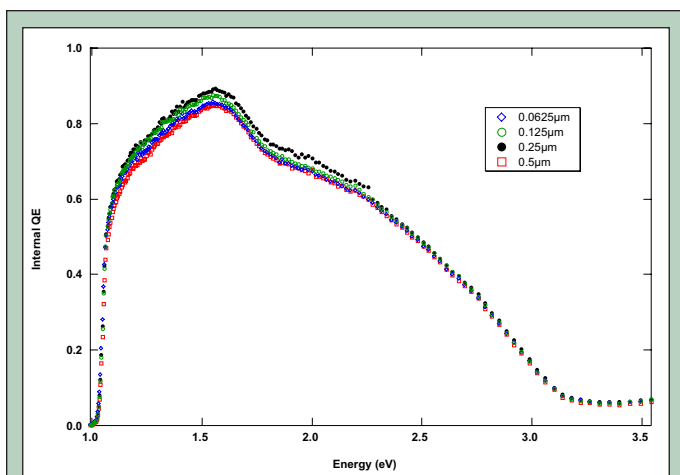


Figure 12. QE curves of the graded buffer thickness experiment devices.

DISCUSSION AND CONCLUSIONS

Temperature

Dislocations diffuse more rapidly at higher temperatures. When dislocations equal in magnitude but opposite in direction meet, they annihilate. With an increase in temperature, it was predicted that the dislocations formed during LMM growth would diffuse into each other and annihilate or diffuse to the edge of the crystal [7]. However, with higher temperatures, the formation rate of dislocations also evidently increased. This is shown in Figure 6, where the steps seen in the curvature are indicative of strain relaxation via dislocation formation. The device grown at 650°C has steps that are larger in magnitude than the steps in the 620°C and 600°C growth runs. The dislocation density increased with temperature as a result of an increased rate of formation. The predicted increase

in dislocation velocity was not enough to cancel out the increased formation rate.

Other trends that exist are that B tilt increased with temperature and that as the compressive strain in the GaInP layer decreased, the tensile strain in the GaInAs layer increased. This difference in the strain is determined by the composition of the two layers, which was constant, so it was expected that if one were to decrease, the other would increase. Any increase in the compressive strain of the GaInP buffer layer was offset by less tensile strain in the GaInAs cell. Based on the efficiency data, less strain in the GaInAs cell results in higher efficiencies. The tilt of the epilayer may cause a shear stress within the crystal structure, which is another way the dislocation velocity can be increased. Again, this was not sufficient to decrease dislocation density via annihilation or diffusion to the edge of the crystal.

The I-V curves reveal that the low efficiency of the 650°C sample was partially a result of a high internal resistance. Since the ability to dope GaInP with zinc falls off sharply at a certain temperature, the resistance may be a result of insufficient doping. This occurs because zinc has a relatively high vapor pressure and is not incorporated into the lattice as easily at elevated substrate temperatures. All of the QE data for the temperature experiment was statistically similar.

Thickness

With an increase in the thickness of the buffer layer, dislocations would have more time and space to diffuse out of the crystal or annihilate. There is also an economic consideration for this variable due to the high cost of high purity III-V precursors and dopant gases. The thinnest possible buffer layer with the highest efficiency is the optimum solution. Based on the trends of the thickness experiment, there appears to be an optimum thickness for the step size near 0.25µm. At a 0.25µm step size thickness, the efficiency was highest and plateaus at greater step sizes. The B tilt remained constant. The strain in both the GaInP and GaInAs layers was unchanging with variable thickness. The MOSS data in Figure 10 reveals that the thicker buffer layer samples have more pronounced relaxation steps. These steps decrease in magnitude during growth. This may be caused by dislocations piling up and becoming pinned, preventing the formation of new dislocations. Very little curvature developed in the thinnest sample during the growth of the buffer layer. The fact that the thinnest sample had the lowest dislocation density appears anomalous since the efficiency was also the lowest. This might be caused by a factor other than defect density.

Upon examination of the I-V data, it can be concluded that thinning the buffer layer results in higher internal resistances. The high resistance could be caused by a reduction in the carrier concentration. Similar to the temperature experiment, there were no statistically significant variations in the QE data.

Based upon the presented data, several conclusions and postulates can be made. During LMM growth, strain in the crystal structure is relaxed by the formation of dislocations. As growth continues, the dislocations pile up, preventing the development of more dislocations. Higher growth temperatures allow for more strain relaxation resulting in higher dislocation densities. The added benefit of increased dislocation velocities due to a higher growth

temperature and, possibly, a larger shear stress caused by increased B tilt did not increase the rate of dislocation annihilation or diffusion to the crystal edge enough to reduce the dislocation density in the device. Growing thinner buffer layers resulted in high internal resistances, possibly caused by the buffer layer having lower carrier concentration.

Several avenues should be explored when considering the future of this project. The anomalous dislocation density of the thinnest sample should be examined using EBIC again or transmission electron microscopy. The data is sparse due to the large time commitment and high cost required for each sample. More trials should be run to increase the statistical significance of the conclusions made. Growing the graded buffer with a higher flow rate of zinc dopant may reduce the resistance at higher temperatures. The dopant type is known to have an affect on the QE of this device. Investigating the growth of a selenium doped graded buffer may prove beneficial. Selenium acts as a surfactant, tending to flatten the surface during growth. Using selenium yields poor results, but examining the curvature of a cell doped with selenium *in-situ* with the MOSS might yield relevant information relating curvature changes during growth to cell performance. Also, slightly cooler growth temperatures should be explored for the possibility of growing high quality devices with slightly higher efficiencies.

ACKNOWLEDGMENTS

This research was conducted at the National Renewable Energy Laboratory during the summer of 2006 as a part of the Summer Undergraduate Laboratory Internship (SULI). I acknowledge the United States Department of Energy, Office of Science, and NREL for creating, organizing, and funding the SULI program. I especially thank my mentor, John Geisz, for his patience, instruction, and guidance. I also acknowledge Charlene Kramer for growing my samples, Michelle Young for processing my samples, Manuel Romero for performing EBIC, and the entire III-V group at NREL.

REFERENCES

- [1] Hans Joachim Möller, Semiconductors for Solar Cells, Boston: Artech House, 1993.
- [2] J. M. Olson, D. J. Friedman, and S. Kurtz, "High-Efficiency III-V Multijunction Solar Cells." in Handbook of Photovoltaic Science and Engineering, Ed. A. Luque and S. Hegedus, New York City: John Wiley & Sons Ltd, 2003, pp. 359-411.
- [3] J.W. Matthews and A.E. Blakeslee, "Defects in epitaxial multilayers. I. Misfit dislocations", Journal of Crystal Growth, v.27, n.1, 1974, pp.118-25.
- [4] M. W. Wanlass, S. P. Ahrenkiel, et. al., "Lattice-Mismatched Approaches for High-Performance, III-V Photovoltaic Energy Converters." in Proceedings of the 31st IEEE Photovoltaic Specialists Conference, 2005, pp. 530-535.
- [5] C. Lynch, R. Beresford, E. Chason, "Real-time Stress Evolution During Growth of $\text{In}_x\text{Al}_{1-x}\text{As}/\text{GaAs}$ Metamorphic Buffer Layers." in Journal of Vacuum Science Technology B, Vol. 22(3), May/June 2004, pp. 1539-1543.
- [6] P. van der Sluis, "Determination of Strain in Epitaxial Semiconductor Layers by High-Resolution X-Ray Diffraction." in Journal of Applied Physics, Vol. 26, 1993, pp. A188-A191.
- [7] D. Hull, "Introduction to Dislocations", 2nd ed., Pergamon Press, 1975.

Leah Liu is an intern in the Science Undergraduate Laboratory Internship Program at Oak Ridge National Lab. Her paper is titled "Characterizing the Role of the *Nell1* Gene in Cardiovascular Development." Ms. Liu's undergraduate studies were in biochemistry and molecular biology — developmental biology at Pennsylvania State University (University Park, PA). Her hometown is Silver Spring, Maryland.

Cymbeline Culiati is a senior staff scientist at the Biological Sciences Division of Oak Ridge National Laboratory (ORNL). She obtained her Ph.D. in biomedical sciences from the ORNL-University of Tennessee at Knoxville School for Biomedical Sciences [currently the Genome Science and Technology program], where she demonstrated that deletions in the mouse 3 subunit of the type-A -aminobutyric acid receptor (*Gabrb3*) gene generates severe cleft palate.

Her work suggested that a perturbation in *Gabrb3* function is a strong genetic basis for this common human birth defect. Other geneticists later established the association between human *GABRB3* and cleft palate. Dr. Culiati completed her post-doctoral training at ORNL as a recipient of the Department of Energy Alexander Hollaender Distinguished Postdoctoral Fellowship (1995-1999), before accepting her current position at ORNL. Dr. Culiati's research is focused on investigating the complex molecular pathways regulated by the cell signaling protein *Nell1* during early bone, cartilage and cardiovascular development. Moreover, her lab also conducts high-throughput and large-scale DNA and RNA analyses to identify and characterize the phenotypic consequences of induced mutations and natural DNA sequence variations in the mouse genome that control hereditary traits and disorders.

CHARACTERIZING THE ROLE OF THE *NELL1* GENE IN CARDIOVASCULAR DEVELOPMENT

LEAH Y. LIU AND CYMBELINE CULIAT

ABSTRACT

Nell1^{6R} is a chemically-induced point mutation in a novel cell-signaling gene, *Nell1*, which results in truncation of the protein and degradation of the *Nell1*^{6R} transcript. Earlier studies revealed that loss of *Nell1* function reduces expression of numerous extracellular matrix (ECM) proteins required for differentiation of bone and cartilage precursor cells, thereby causing severe skull and spinal defects. Since skeletal and cardiovascular development are closely linked biological processes, this research focused on: a) examining *Nell1*^{6R} mutant mice for cardiovascular defects, b) determining *Nell1* expression in fetal and adult hearts, and c) establishing how ECM genes affected by *Nell1* influence heart development. Structural heart defects in *Nell1*^{6R} mutant fetuses were analyzed by heart length and width measurements and standard histological methods (haematoxylin and eosin staining). *Nell1* expression was assayed in fetal and adult hearts using reverse transcription polymerase chain reaction (RT-PCR). A comprehensive bioinformatics analysis using public databases (Stanford SOURCE Search, Integrated Cartilage Gene Database, Mouse Genome Informatics, and NCBI UniGene) was undertaken to investigate the relationship between cardiovascular development and each of twenty-eight genes affected by *Nell1*. *Nell1*-deficient mice have significantly enlarged hearts (particularly the heart width), dramatically reduced blood flow out of the heart and unexpanded lungs. Isolation of total RNAs from hearts of adult (control and heterozygote) and fetal (control and homozygous mutant) mice have been completed and RT-PCR assays are in progress. The bioinformatics analysis showed that the majority of genes with reduced expression in *Nell1*-deficient mice are normally expressed in the heart (79%; 22/28), blood vessels (71%; 20/28) and bone marrow (61%; 17/28). Moreover, mouse mutations in seven of these genes (*Col15a1*, *Osf-2*, *Bmpr1a*, *Pkd1*, *Mfge8*, *Ptger4*, *Col5a1*) manifest abnormalities in cardiovascular development. These data demonstrate for the first time that *Nell1* has a role in early mammalian cardiovascular development, mediated by its regulation of ECM proteins necessary for normal cell growth and differentiation. In addition, understanding the mechanisms by which *Nell1* and its associated ECM genes affect the cardiovascular system can provide future strategies for the treatment of heart and blood vessel defects.

INTRODUCTION

Nell1 is a gene that encodes a mammalian cell-signaling protein necessary for cell growth and differentiation. The *Nell1* protein is secreted in the cytoplasm and contains six epidermal growth factor-like (EGF-like) domains. These domains are segments of polypeptide common to more than 100 proteins with roles in cell proliferation and differentiation. In cell signaling pathways, *Nell1* is phosphorylated by protein kinase C- β 1 (PKC- β 1) is

an enzyme that interacts with many different binding proteins in pathways that affect cell growth, differentiation, oncogenesis, and apoptosis. Because *Nell1* binds to PKC- β 1 via its EGF-like domains, *Nell1* seems to belong to a new class of cell-signaling ligand molecules with roles in cellular growth and development pathways [1]. *Nell1*'s over-expression in humans and mice causes craniosynostosis, the premature fusion of growing cranial sutures, which subsequently constrains growth in the brain [2,3]. This disorder is present in 1

of 3000 births in humans, and at the molecular level, seems to be caused by abnormalities in intramembranous ossification [4].

Nell1^{GR} is a point mutation induced by the common mutagen *N*-ethyl-*N*-nitrosurea, leading to a single base change in *Nell1*'s coding region (T→A) that results in the conversion of a cysteine codon to a premature stop codon (TGT→TGA). This mutation truncates the 810 amino acid polypeptide at amino acid residue #502 [4]. Consequently, the *Nell1* transcript is degraded and there is dramatically reduced expression of *Nell1* in mutant mice. Earlier studies revealed that loss of *Nell1* function reduces expression of numerous extracellular matrix (ECM) proteins required for the differentiation of bone and cartilage precursor cells. The reduced expression of ECM proteins leads to neonatal lethality and skeletal defects in the skull, ribcage and vertebral column in *Nell1*-deficient mice (Figure 1). Homozygote mutants (*Nell1*^{GR}/*Nell1*^{GR}) develop to late gestation (E18-19), but fetuses do not survive birth and those recovered by caesarean rescue are unable to breathe and nurse. There are no readily detectable phenotypic differences between heterozygote and wild-type mice [4].

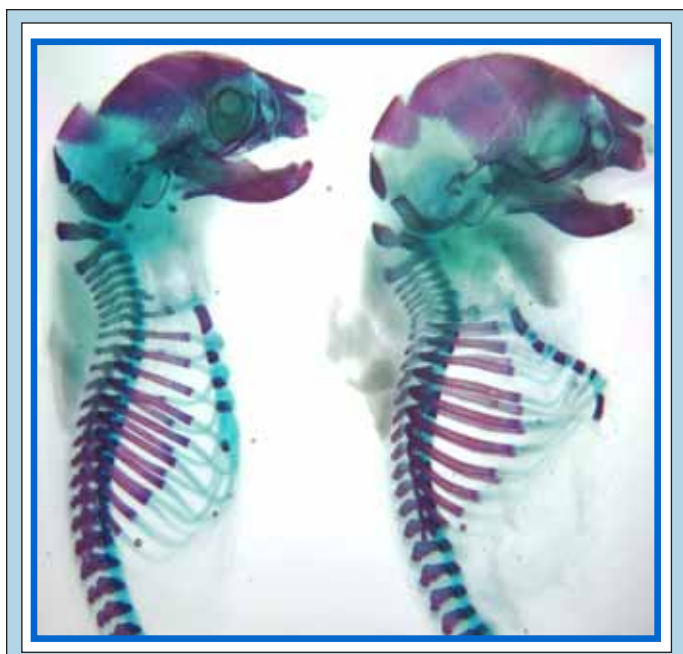


Figure 1. Compared to wild-type mice (left), *Nell1*^{GR} mutants (right) display craniofacial and spinal curvature defects.

Skeletal and cardiovascular development are closely linked biological processes because the two systems share many common genes and molecular pathways. For example, in the human genetic disease Marfan syndrome, a single mutation in chromosome 15 reduces expression of the connective tissue protein fibrillin-1 and causes gross skeletal and cardiovascular abnormalities such as bone elongation, scoliosis, mitral valve abnormalities, and aortic dilation [5]. Prominent pathways in the bone such as matrix deposition and calcification have been identified in arterial calcification. In addition, the protein collagen I and certain phosphatases are common to both bone formation processes and atherosclerotic lesions [6]. Studies of diseased heart valves have revealed expression of bone proteins

such as osteopontin [7] and even the presence of bone itself in the valves. Endochondral ossification, lamellar bone formation, and active bone remodeling have also been discovered in diseased heart valves, further verifying the molecular link between the skeletal and cardiovascular systems [8].

This research expanded upon earlier findings on the role of *Nell1* in the skeletal system and explored, for the first time, its impact on the cardiovascular system. During previous studies in *Nell1*^{GR}-deficient mice, the homozygote mutant hearts were observed to be noticeably larger than wild-type and heterozygote mutant hearts. However, this enlargement had never been quantified or verified to be statistically significant. In addition, it was unknown whether the suspected enlargement was caused by abnormal spine curvature and compression of intervertebral disc materials in mutants, which dramatically decreases the volume of the thoracic cavity and physically exerts pressure on the developing heart. Alternatively, the putative heart defect could be a direct effect of abnormal gene expression changes resulting from the loss of function of *Nell1*. This project was undertaken to accomplish the following specific objectives:

- a) Examine *Nell1*^{GR} mutant mice for cardiovascular defects,
- b) Determine *Nell1* expression in fetal and adult hearts, and
- c) Establish whether genes with reduced expression in *Nell1*^{GR} mutant fetal bodies are known to influence cardiovascular development.

Previous studies on the role of the *Nell1* gene during skeletal development revealed new insights into the mechanisms behind osteoblast and chondrocyte differentiation and identified novel molecular targets for the treatment of cranial and spinal defects in humans [2, 3, 4]. Analyzing how the *Nell1* pathway influences the cardiovascular system provides an opportunity to elucidate the role of *Nell1* in heart and blood vessel development. This research is also of significant medical interest because certain structural and morphological abnormalities such as left ventricle thickening, mitral valve abnormalities, and outflow obstructions in the heart are associated with heart enlargement in humans [9].

METHODS OF ANALYSIS

The mice used in these experiments were maintained and bred at the Mammalian Genetics Research Facility at Oak Ridge National Laboratory (ORNL), using protocols approved under the ORNL Institutional Care and Use Committee.

Characterization of Cardiovascular Defects. To determine if structural heart defects in *Nell1*^{GR} mutant fetuses were significant enough to warrant further study, hearts were dissected from formalin-fixed specimens and were analyzed by heart length and width measurements. These measurements were completed on 14 wild-type (+/+), 11 heterozygous (+/*Nell1*^{GR}), and 17 homozygous mutant (*Nell1*^{GR}/*Nell1*^{GR}) fetuses at 18.5 days of gestation, using the Wild Heerbrugg M8 Stereozoom microscope grid ruler. Statistical analysis was completed using a two-tailed T-test and a p-value cutoff of 0.05.

Histological observations were made on haematoxylin and eosin stained mouse sagittal sections. These sections were cut from mice that were fixed in formalin and embedded in paraffin. Observations

were made at 8X on the Zeiss Stemi SV11 stereomicroscope microscope, and at higher magnification (up to 400X) on the Zeiss AxioSkop microscope. Haematoxylin and eosin staining shows general cell morphology, such as cell shape, presence of nuclei, and extracellular components. The fixation, staining, and sectioning were conducted by a commercial histology service (Ridge Microtome).

Gene Expression Assays. *Nell1* expression was assayed in adult (wild-type and hemizygous mutants) and fetal (wild type, heterozygous, and homozygous mutants) hearts and brains using reverse transcription polymerase chain reaction (RT-PCR). RNA was extracted from animals using standard phenol-chloroform techniques and Phase Lock Gel (Eppendorf) tubes for purification. To generate the cDNA product, the reverse transcription reaction was performed on samples using the RETROscript® Kit manufactured by Ambion. The cDNA was amplified by PCR using three primer sets for the *Nell1* gene (Desai et al., unpublished). The three primer sets necessary to cover the length of *Nell1* are as follows: 1) CTC138 and Jaya 3R covered approximately 30 bases of the untranslated region and exon 1 to exon 8, total length: 840 bases, 2) Jaya 3F and Jaya 5R covered half of exon 4 up to the first 40 bases of exon 13, total length: 850 bases, 3) Jaya 8F and Jaya 10R covered exon 16 to exon 20 and into the untranslated region, total size: 800 bases. The primer sequences are as follows:

CTC 138: 5'-CTGAAGCATTGGTTTCTTGC-3'

Jaya 3R: 5'-AGTTGACCAAGTCTCGTCTC-3'

Jaya 3F: 5'-GCCGATGGACAGTGGCACAA-3'

Jaya 5R: 5'-GTGTTGGCATGACAATAGTG-3'

Jaya 8F: 5'-ACCACTGTGAGTGCAGAAGC-3'

Jaya10R: 5'-CAACCCAAACGCCTTCCTC-3'

Comprehensive Bioinformatics Analysis. To investigate the relationship between cardiovascular development and each of twenty eight genes affected by *Nell1*, a comprehensive bioinformatics analysis using publicly accessible databases was undertaken. These genes were previously identified as those that showed reduced expression in mutant mouse bodies (E18) [4]. Stanford SOURCE, Integrated Cartilage Gene Database, and NCBI UniGene were used to search for the expression of ECM genes in tissues related to the cardiovascular system: heart, blood vessels, bone marrow, and blood [10, 11, 12]. In addition to expression data, disorders and abnormalities in humans that have previously been associated with the genes were noted. The Mouse Genome Informatics database was used to search for known mouse mutations in these genes and to investigate if these mutations resulted in cardiovascular defects [13].

RESULTS

Characterization of Cardiovascular Defects: *Nell1*-deficient mice had significantly enlarged hearts based on length and width measurements. As shown in Table 1, length measurements for all three genotypes did not differ significantly, however, based on the statistical T-Test, the width measurements for mutant mice (*Nell1^{6R}/Nell1^{6R}*) were significantly greater than the width measurements for wild type and heterozygote mutant mice, thus confirming the presence of an abnormal heart phenotype in *Nell1*-deficient mice.

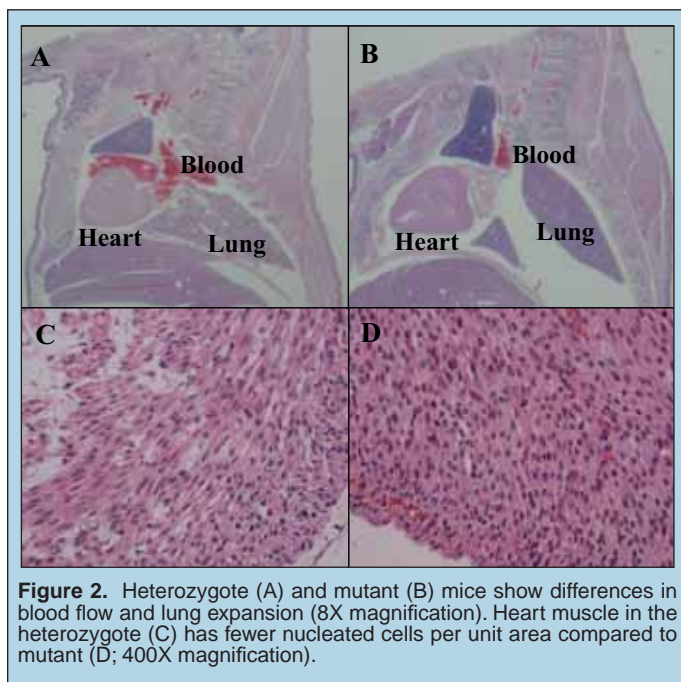
	Homozygote <i>Nell1^{6R}/Nell1^{6R}</i>	Heterozygote +/ <i>Nell1^{6R}</i>	Wild-type +/+
Width	3.3	2.8	2.7
	2.5	2.8	1.8
	2.8	2.3	2.8
	2.3	2.7	2.5
	2.8	2.8	2.7
	3.0	2.5	2.3
	3.2	2.5	2.2
	3.0	2.5	2.5
	2.8	2.2	2.8
	2.8	2.5	2.7
	3.3	2.2	2.7
	3.0	-	2.2
	3.0	-	2.5
	2.5	-	2.3
	2.5	-	-
3.0	-	-	
2.5	-	-	
No. of Fetuses	17	11	14
Average	2.853	2.530	2.476
Length	3.2	3.7	2.7
	2.8	3.2	2.7
	2.8	2.8	3.3
	2.7	3.2	3.0
	3.0	3.2	3.3
	3.2	3.0	3.0
	3.2	3.0	2.5
	3.3	3.3	3.0
	3.0	2.8	3.3
	2.8	3.0	3.2
	3.2	2.8	3.3
	3.2	-	2.7
	3.2	-	2.8
	2.8	-	3.0
	2.5	-	-
3.0	-	-	
2.8	-	-	
No. of Fetuses	17	11	14
Average	2.984	3.091	2.988
T-Test p-values			
	Mutant-Wildtype	Mutant-Heterozygote	Heterozygote-Wildtype
Width	0.0012442891	0.0046893426	0.6143698331
Length	0.9351530349	0.2470911230	0.3514701862

Table 1. Measurements (mm) of E18.5 fetal heart width and length of *Nell1^{6R}* heterozygote and homozygote mutant mice compared with wild-type littermates..

Observations on haematoxylin and eosin-stained, sectioned specimens showed additional morphological anomalies in the cardiovascular system at the organ and cellular level. At low magnification, dramatically reduced blood flow out of the heart was observed in mutant mice. Sections from wild-type and heterozygote mice distinctively showed bright red, blood-filled arteries whereas the sections from mutant mice showed a scant amount of blood.

Another prominent difference between normal and mutant mice was the variation in lung density and size. Wild-type and heterozygote mice had spongy lungs which occupied the entire thoracic cavity space while mutant mice have dark, compact, dense lungs (Figure 2A and 2B).

The slides were also observed at higher magnification to detect differences in cellular morphology. Images of the heart apex in heterozygote and mutant mice depicted differences in cell density. The cells were more closely packed in mutant hearts, revealing a higher density of cellular nuclei (Figure 2C and 2D), whereas there was more space between cells in the heterozygote. It was difficult to detect a marked heart width enlargement in mutant mice using just these histological observations because the orientation of the heart in the thoracic cavity differs with each animal, and only one plane of the mouse can be examined at one time. In addition, comparable sections were not available for all specimens because the sections were cut into the heart at different planes.



Gene Expression Assays. Isolation of total RNAs from the hearts and brains of adult (control and heterozygote) and fetal (wild-type, heterozygote, and homozygous mutant) mice have been completed and RT-PCR assays are in progress.

Comprehensive Bioinformatics Analysis. The comprehensive bioinformatics analysis showed that of twenty-eight genes studied, 79%, 71%, and 61% were normally expressed in heart, blood vessels and bone marrow, respectively. Table 2 summarizes the expression profile of these genes in the various tissues of the cardiovascular system. The database searches resulted in more specific expression data for 12 of the genes, such as expression at particular stages of development, increased or decreased expression in certain disease states, or localized expression in one particular tissue type such as cardiomyocytes (Table 3). Twenty genes (71%) had recorded mouse mutations according to the Mouse Genome Informatics database.

This database also referenced seven genes (*Col15a1*, *Osf-2*, *Bmpr1a*, *Pkd1*, *Mfge8*, *Ptger4*, *Col5a1*) that manifest certain abnormalities in cardiovascular development commonly associated with heart enlargement, as shown in the Table 4.

DISCUSSION

These data demonstrate for the first time that *Nell1* has a role in early mammalian cardiovascular development, mediated by its regulation of ECM proteins necessary for normal cardiovascular growth and differentiation. Observations of heart abnormalities are consistent with earlier studies on the skeletal effects of *Nell1*-deficiency. As in the skeletal system, the loss of *Nell1* function seems to disrupt the balance between cell proliferation and differentiation in the cardiovascular system.

The confirmation of a heart enlargement phenotype in *Nell1*-deficient mice, and the dramatic differences in blood flow and lung density between normal and mutant mice show clear cardiovascular defects associated with the reduced expression of *Nell1*. The lung phenotype is probably due to the inability of mutant mice to survive birth or open their mouths. As a consequence, mutant mice cannot breathe when they are born and therefore have unexpanded lungs compared to the spongy, air-filled lungs of the normal phenotype.

Histological analysis suggests that heart enlargement could be due to hypertrophy of the myocardium, indicated by the higher density of nucleated cells in the cardiac muscle of mutant mice. During development there is a delicate balance of cell differentiation and proliferation in the body. Since *Nell1* is necessary for cell differentiation, the absence of *Nell1* reduces cell differentiation and cell proliferation therefore becomes the predominant mechanism. This observation in the heart is consistent with observations in bone and cartilage tissue [4].

Heart enlargement is commonly caused by structural defects or disease states that force the heart to work harder. To compensate for this extra work, the cardiac muscle may increase in size. The detailed expression data in Table 3 shows expression in specific structures of the cardiovascular system, or specific stages of development when mutations may affect the ability of the heart to pump and direct blood efficiently. Many of the structures showing expression for the ECM proteins are some of the same ones affected by the disease phenotypes listed in Table 4, which are defects known to be associated with heart enlargement.

Because of the association between *Nell1* and the ECM proteins, the observed abnormalities are probably not caused by mere compression of the thoracic cavity as a result of vertebral column defects. The data from the bioinformatics analysis shows many possible cardiovascular defects associated with the reduced expression of *Nell1* and ECM proteins. Further work would involve verifying the expression of ECM genes in the cardiovascular system by staining mouse sections with antibodies specific to ECM proteins. Once RT-PCR experiments are completed and the resultant PCR products are sequenced, *Nell1* expression in fetal and/or adult hearts can be determined. In addition, *Nell1* and ECM genes can be researched with the goal of establishing a direct or indirect causal relationship with the heart defects mentioned in Table 3. Even if *Nell1* is not found to be expressed in the heart, it may still cause heart

Gene Symbol	Gene Name	Expression				# abnormal heart phenotype ¹³	# total mutants ¹³
		heart	vascular	blood	bone marrow		
Tnxb	tenascin	10	10	11	11		2
Prg4	proteoglycan 4	33	12	12			1
Thbs3	thrombospondin 3	10	10	12			2
Col5a3	collagen 5 alpha 3 subunit						
Neurog2	neurogenin 2						5
Col5a1	procollagen type V, alpha 1	10	10	10	10	1	1
Col6a1	procollagen Type VI, alpha 1	10	16	12	10		1
Col15a1	procollagen type XV, alpha 1	10	19	10	12	1	1
Pacsin3	PKC and casein kinase substrate in neurons 3	10			10		
Tnc	tenascin c	10	10	21	11		3
Col12a1	procollagen type XII, alpha 1	10	12		10		
Chad	chondroadherin	15	15				
Osf2-pending	osteoblast specific factor 2	10	10		10	1	2
Col17a1	procollagen type XVII alpha 1						
Prkcc	protein kinase C						2
Prkch	protein kinase C, eta symbol	10	10	10	10		1
Bk-pending	brain and kidney protein						
Ptk9l	PTK9L protein tyrosine kinase 9-like	10	10	10	10		
Npdc1	neural proliferation, differentiation and control gene	10	10				1
Bmpr1a	bone morphogenetic protein receptor type 1a	10	12		10	2	4
Pkd1	polycystic kidney disease I homolog	10	27	10	12	7	12
Tnfrsf11b	tumor necrosis factor (ligand)	10	34		12		3
Mfge8	milk fat globule-EGF factor 8 protein	10	12	10	10	1	5
Matn3	matrilin 3, cartilage matrix protein	28					1
Bmp7	bone morphogenetic protein type 7	10			10		8
Matn2	matrilin 2, cartilage matrix protein 2	10	10	10	10		2
Ptger4	prostaglandin E receptor 4		10	10	10	3	4
Notch3	notch gene homolog 3	10	30				4
	# of Genes	22	20	13	17	7	20
	Percentage	79%	71%	46%	61%	25%	71%

*Compiled from references 10, 11, 12, 13, 15, 16, 19, 21, 27, 28, 30, 33, 34. Superscripted numbers in table refer to specific references.

Table 2. Expression profile of genes in the *Nell1* pathway and association with mutant mouse phenotypes.

abnormalities by acting on the associated ECM genes from elsewhere in the body through paracrine mechanisms. The identification of the role of *Nell1*-mediated pathways in cardiovascular development can provide potential drug or cell-based strategies for treating heart and blood vessel defects.

ACKNOWLEDGMENTS

Lori Hughes and Jaya Desai provided invaluable instruction and advice in the handling of mouse fetuses, histology, RNA and RT-PCR protocols. Don Carpenter and Bob Olzewski conducted the mouse breeding and provided the mice used in this project.

This research was conducted at Oak Ridge National Laboratory. Funding was provided through the U.S. Department of Energy Office of Science (contract DE-AC05-00OR22725) and the Science Undergraduate Laboratory Internship program.

Gene	Detailed Expression	Expression in Cardiac Developmental Processes	Associated Disorders
Tnxb	cardiac muscle ¹¹		
Prg4			Jacobs Syndrome (pericarditis) ^{11,39}
Col6a1	mitral valve ⁴⁰ pericardium ⁴⁰		abdominal aortic aneurysm disease ¹⁶ congenital heart defects in Down Syndrome ¹⁷ dilated descending aorta ¹⁸
Col15a1			cardiac muscle degeneration ¹⁹ collapsed capillaries ¹⁹
Tnc	expression only in disease states ^{20,22}	neovascularization ²⁰ migrates in response to cardiac growth factors ²⁰ stromal cell dependent erythropoiesis ²¹	
Postn (Osf2)	vascular injury increases expression ³⁷ overexpression in myocardium in heart failure patients ³⁸	endocardial cushion development ³⁵ valve formation ³⁵ developing endothelium of ventricular trabeculae ³⁶ outflow tract development ³⁶ valve leaflet development ³⁶ chordae tendinae development ³⁶	
Prkch	expressed during ischemia (in myocardial infarction) ²³		
Bmpr1a	cardiomyocytes ¹⁴	signaling in cardiac organogenesis ²⁴ outflow tract development ²⁵ ventricular myocardium development ²⁵ annulus fibrosus development ²⁶	
Pkd1		myoelastic arterial organization ²⁷	
Tnfrs11b			calcification of aorta and renal arteries ³⁴
Bmp7	myocardium ¹⁴	atrioventricular cushion development ¹⁴ outflow tract development ¹⁴ endocardial cushion formation ¹⁴ septation ¹⁴	
Notch3	arteries (but not veins) ³⁰ arterial pericytes ³²		increased chance of myocardial infarction ²⁹ cerebral arteriopathy (CADASIL) ²⁹ degeneration of vascular smooth muscle cells ³¹

*Compiled from references 11, 14, 16, 17, 18, 19, 20, 21, 22, 23, 24, 25, 26, 27, 29, 30, 31, 32, 34, 35, 36, 37, 38, 39, 40. Superscripted numbers in table refer to specific references.

Table 3. Detailed expression of *Nell1*-pathway genes in the cardiovascular system.

Gene	Defect
Col15a1	Abnormal heart capillaries
Osf-2	Discontinuity in valve leaflets
Bmpr1a	Persistent truncus arteriosus Mitral valve prolapse Abnormal cardiomyocyte apoptosis
Pkd1	Vascular leaks/ruptures Endocardial cushion defects Abnormal atrial septum morphology Abnormal septation
Mfge8	Abnormal neovascularization
Ptger4	Dilated left ventricle Patent ductus arteriosus Congestive heart failure
Col5a1	Abnormal vasculature

*Compiled from reference 13.

Table 4. Mutations in genes of the *Nell1* pathway generate defects in mice associated with heart enlargement.

REFERENCES

- [1] S. Kuroda S. and K. Tanizawa, 1999. "Involvement of epidermal growth factor-like domain of NELL proteins in the novel protein-protein interaction with protein kinase C," Biochemical and Biophysical Research Communications 265, 752-757.
- [2] K. Ting, H. Vastardis, J.B. Mulliken, C. Soo, A. Tieu, H. Do, E. Kwong, C.N. Bertolami, H. Kawamoto, S. Kuroda, and M.T. Longaker, 1999. "Human NELL-1 expressed in unilateral coronal synostosis," Journal of Bone and Mineral Research 14, 80-89.
- [3] X. Zhang, S. Kuroda, D. Carpenter, I. Nishimura, C. Soo, R. Moats, K. Iida, E. Wisner, F.Y. Hu, S. Miao, S. Beanes, C. Dang, H. Vastardis, M. Longaker, K. Tanizawa, N. Kanayama, N. Saito, and K. Ting, 2002. "Craniosynostosis

- in transgenic mice overexpressing Nell-1," Journal of Clinical Investigation 110, 861-870.
- [4] J. Desai, M. E. Shannon, M.D. Johnson, D.W. Ruff, L.A. Hughes, M.K. Kerley, D.A. Carpenter, D.K. Johnson, E.M. Rinchik and C.T. Culiati, 2006. "Nell1-deficient mice have reduced expression of extracellular matrix proteins causing cranial and vertebral defects," Human Molecular Genetics 15, 1329-1341.
- [5] H.C. Dietz, G.R. Cutting, R.E. Pyeritz, C.L. Maslen, L.Y. Sakai, G.M. Corson, E.G. Puffenberger, A. Hamosh, E.J. Nanthakumar, S.M. Curristin, G. Stetten, D.A. Meyers, and C. A. Francomano, 1991. "Marfan syndrome caused by a recurrent *de novo* missense mutation in the fibrillin gene," Nature 352, 337-339.
- [6] L.A. Fitzpatrick, A. Severson, W.D. Edwards, and R.T. Ingram, 1994. "Diffuse calcification in human coronary arteries," Journal of Clinical Investigation 94, 1597-1604.
- [7] E.R. Mohler, L.P. Adam, P. McClelland, L. Graham, and D.R. Hathaway, 1997. "Detection of osteopontin in calcified human aortic valves," Arteriosclerosis, Thrombosis, and Vascular Biology 17, 547-552.
- [8] E.R. Mohler, F. Gannon, C. Reynolds, R. Zimmerman, M.G. Keane, and F.S. Kaplan, 2001. "Bone formation and inflammation in cardiac valves," Circulation 103, 1522-1528.
- [9] L.C. Poliac, M.E. Barron, and B.J. Maron, 2006. "Hypertrophic Cardiomyopathy," Anesthesiology 104, 183-192.
- [10] M. Diehn, G. Sherlock, G. Binkley, H. Jin, J.C. Matese, T. Hernandez-Boussard, C.A. Rees, J.M. Cherry, D. Botstein, P.O. Brown, and A.A. Alizadeh, 2003. "SOURCE: a unified genomic resource of functional annotations, ontologies, and gene expression data," Nucleic Acids Research 31, 219-223.
- [11] Y.Q. Song, D.K. Smith, B.C.W. Wong, M.Y. Yeung, and S.Y.M. Chan. The iCartiGD Database. The University of Hong Kong. Available at: <http://bioinfo.hku.hk/iCartiGD/>. Accessed July 2006.
- [12] J.U. Pontius, L. Wagner, and G.D. Schuler, 2003. "UniGene: a unified view of the transcriptome," The NCBI Handbook. Bethesda (MD): National Center for Biotechnology Information.
- [13] J.T. Eppig, C.J. Bult, J.A. Kadin, J.E. Richardson, J.A. Blake, et al., 2005. "The Mouse Genome Database (MGD): from genes to mice—a community resource for mouse biology," Nucleic Acids Research 33, 471-475.
- [14] J.V. Barnett and J.S. Desgrosellier, 2003. "Early Events in Valvulogenesis: A Signaling Perspective," Birth Defects Research 69, 58-72.
- [15] E.S. Tasheva, A. Ke, and G.W. Conrad, 2004. "Analysis of the expression of chondroadherin in mouse ocular and non ocular tissues," Molecular Vision 10, 544-554.
- [16] P.J. Armstrong, J.M. Johanning, W.C. Calton Jr., J.R. Delatore, D.P. Franklin, D.C. Han, D.J. Carey, and J.R. Elmore, 2002. "Differential gene expression in human abdominal aorta: aneurysmal versus occlusive disease," Journal of Vascular Surgery 35, 346-355.
- [17] G.E. Davies, C.M. Howard, M.J. Farrer, M.M. Coleman, L.B. Bennett, L.M. Cullen, R.K. Wyse, J. Burn, R. Williamson, and A.M. Kessling, 1995. "Genetic variation in the COL6A1 region is associated with congenital heart defects in trisomy 21 (Down's syndrome)," Annals of Human Genetics 59, 253-269.
- [18] A.F. Rope, R.B. Hinton, R.L. Spicer, R. Blough-Pfau, and H.M. Saal, 2004. "Dilated ascending aorta in a child with ring chromosome 21 syndrome," American Journal of Medical Genetics Part A 130, 191-195.
- [19] L. Eklund, J. Pihola, J. Komulainen, R. Sormunen, C. Ongvarrasopone, R. Fassler, A. Muona, M. Ilves, H. Ruskoaho, T.E. Takala, and T. Pihlajaniemi, 2001. "Lack of type XV collagen causes a skeletal myopathy and cardiovascular defects in mice," Proceedings of the National Academy of Sciences of the United States of America 98, 1194-1199.
- [20] V.L. Ballard, A. Sharma, I. Duignan, J.M. Holm, A. Chin, R. Choi, K.A. Hajjar, S.C. Wong, and J.M. Edelberg, 2006. "Vascular tenascin-C regulates cardiac endothelial phenotype and neovascularization," The Federation of American Societies for Experimental Biology Journal 20, 717-719.
- [21] M. Seki, J. Kameoka, S. Takahashi, H. Harigae, N. Yanai, M. Obinata, and T. Sasaki, 2006. "Identification of tenascin-C as a key molecule determining stromal cell-dependent erythropoiesis," Experimental Hematology 34, 519-527.
- [22] A. Sato, K. Aonuma, K. Imanaka-Yoshida, T. Yoshida, M. Isobe, D. Kawase, N. Kinoshita, Y. Yazaki, and M. Hiroe, 2006. "Serum tenascin-C might be a novel predictor of left ventricular remodeling and prognosis after acute myocardial infarction," Journal of the American College of Cardiology 47, 2319-2325.
- [23] C.J. Albert and D.A. Ford, 1998. "Identification of specific nuclear protein kinase C isozymes and accelerated protein

kinase C-dependent nuclear protein phosphorylation during myocardial ischemia," FEBS Letters 438, 32-36.

- [24] V. Gaussin, T. Van de Putte, Y. Mishina, M.C. Hanks, A. Zwijsen, D. Huylebroeck, R.R. Behringer, and M.D. Schneider, 2002. "Endocardial cushion and myocardial defects after cardiac myocyte-specific conditional deletion of the bone morphogenetic protein receptor ALK3," Proceedings of the National Academies of Science of the United States of America 99, 2878-2883.
- [25] R.W. Stottman, M. Choi, Y. Mishina, E.N. Meyers, and J. Klingensmith, 2004. "BMP receptor IA is required in mammalian neural crest cells for development of the cardiac outflow tract and ventricular myocardium," Development 131, 2205-2218.
- [26] V. Gaussin, G.E. Morley, L. Cox, A. Zwijsen, K.M. Vance, L. Emile, Y. Tian, J. Liu, C. Hong, D. Myers, S.J. Conway, C. Depre, Y. Mishina, R.R. Behringer, M.C. Hanks, M.D. Schneider, D. Huylebroeck, G.I. Fishman, J.B. Burch, and S.F. Vatner, 2005. "Alk3/Bmpr1a receptor is required for development of the atrioventricular canal into valves and annulus fibrosus," Circulation Research 97, 219-226.
- [27] Q. Qian, M. Li, Y. Cai, C.J. Ward, S. Somolo, P.C. Harris, and V.E. Torres, 2003. "Analysis of the polycystins in aortic vascular smooth muscle cells," Journal of the American Society of Nephrology 14, 2280-2287.
- [28] D. Segal, C. Frie, P.D. Nitsche, A.R. Klatt, D. Piecha, E. Korpos, F. Deak, R. Wagener, M. Paulsson, and N. Smyth, 2000. "Expression of matrilin-1, -2 and -3 in developing mouse limbs and heart," Matrix Biology 19, 649-655.
- [29] S.A. Lesnik Oberstein, J.W. Jukema, S.G. Van Duinen, P.W. Macfarlane, H.C. Houwelingen, M.H. Breuning, M.D. Ferrari, and J. Haan, 2003. "Myocardial infarction in cerebral autosomal dominant arteriopathy with subcortical infarcts and leukoencephalopathy (CADASIL)," Medicine (Baltimore) 82, 251-256.
- [30] N. Villa, L. Walker, C.E. Lindsell, J. Gasson, M.L. Iruela-Arispe, and G. Weinmaster, 2001. "Vascular expression of Notch pathway receptors and ligands is restricted to arterial vessels," Mechanisms of Development 108, 161-164.
- [31] M. Dichgans, 2002. "CADASIL: a monogenic condition causing stroke and subcortical vascular dementia," Cerebrovascular Diseases 13, 37-41.
- [32] S. Claxton and M. Fruttiger, 2004. "Periodic Delta-like 4 expression in developing retinal arteries," Gene Expression Patterns 5, 123-127.
- [33] S. Ikegawa, M. Sano, Y. Koshizuka, and Y. Nakamura, 2000. "Isolation, characterization and mapping of the mouse and human PRG4 (proteoglycan 4) genes," Cytogenetics and Cell Genetics 90, 291-297.
- [34] N. Bucay, I. Sarosi, C.R. Dunstan, S. Morony, J. Tarpley, C. Capparelli, S. Scully, H.L. Tan, W. Xu, D.L. Lacey, W.J. Boyle, and W.S. Simonet, 1998. "Osteoprotegerin-deficient mice develop early onset osteoporosis and arterial calcification," Genes and Development 12, 1260-1268.
- [35] A. Kruzynska-Frejtag, M. Machnicki, R. Rogers, R.R. Markwald, and S.J. Conway, 2001. "Periostin (an osteoblast-specific factor) is expressed within the embryonic mouse heart during valve formation," Mechanisms of Development 103, 183-188.
- [36] R.A. Norris, C.B. Kern, A. Wessels, E.I. Moralez, R.R. Markwald, and C.H. Mjaatvedt, 2004. "Identification and detection of the periostin gene in cardiac development," The Anatomical Record, Part A: Discoveries in Molecular, Cellular, and Evolutionary Biology 281, 1227-1233.
- [37] V. Lindner, Q. Wang, B.A. Conley, R.E. Friesel, and C.P. Vary, 2005. "Vascular injury induces expression of periostin: implications for vascular cell differentiation and migration," Arteriosclerosis, Thrombosis, and Vascular Biology 25, 77-83.
- [38] N. Katsuragi, R. Morishita, N. Nakamura, T. Ochiai, Y. Taniyama, Y. Hasegawa, K. Kawashima, Y. Kaneda, T. Ogihara, and K. Sugimura, 2004. "Periostin as a novel factor responsible for ventricular dilation," Circulation 110, 1806-1813.
- [39] A.M. Alazami, S.M. Al-Mayouf, C.A. Wyngaard, and B. Meyer, 2006. "Novel PRG4 mutations underlie CACP in Saudi families," Human Mutation 27, 213.
- [40] A. Reymond, V. Marigo, M.B. Yaylaoglu, A. Leoni, C. Ucla, N. Scamuffa, C. Caccioppoli, E.T. Dermitzakis, R. Lyle, S. Banfi, G. Eichele, S.E. Antonarakis, and A. Ballabio, 2002. "Human Chromosome 21 Gene Expression Atlas in the Mouse," Nature 420, 582-586.

Jacob Pachikara participated in the Science Undergraduate Laboratory Internship (SULI) program during the summer of 2006, completing an internship in the Engineering Division of Lawrence Berkeley National Laboratory, where he contributed to the development of a Graphical User Interface for the particle accelerator control room. He presented this work in February 2007 at the AAAS conference in San Francisco. He is currently pursuing an undergraduate degree in electrical engineering at The University of Texas at Arlington. In addition to his academic pursuits, he is active in numerous honor societies including Tau Beta Pi, Eta Kappa Nu, and National Society of Collegiate Scholars.

Greg Portmann has worked in particle physics for the past 15 years at Lawrence Berkeley National Laboratory (LBNL) and Stanford Linear Accelerator Center (SLAC). In general, he works on algorithms to optimize the performance of electron accelerators. Before that he worked at the Johns Hopkins University Applied Physics Laboratory, designing algorithms for radar target tracking and flight control applications. He also had a brief career in the bio-device sector, developing signal processing algorithms to analyze the electrical and mechanical activity of the stomach to determine optimal gastric pacing strategies. Greg has a B.S. in mathematics and M.S. in electrical engineering from Penn State University.

A NEW GUI FOR GLOBAL ORBIT CORRECTION AT THE ALS USING MATLAB

JACOB PACHIKARA AND GREGORY PORTMANN

ABSTRACT

Orbit correction is a vital procedure at particle accelerators around the world. The orbit correction routine currently used at the Advanced Light Source (ALS) is a bit cumbersome and a new Graphical User Interface (GUI) has been developed using MATLAB. The correction algorithm uses a singular value decomposition method for calculating the required corrector magnet changes for correcting the orbit. The application has been successfully tested at the ALS. The GUI display provided important information regarding the orbit including the orbit errors before and after correction, the amount of corrector magnet strength change, and the standard deviation of the orbit error with respect to the number of singular values used. The use of more singular values resulted in better correction of the orbit error but at the expense of enormous corrector magnet strength changes. The results showed an inverse relationship between the peak-to-peak values of the orbit error and the number of singular values used. The GUI interface helps the ALS physicists and operators understand the specific behavior of the orbit. The application is convenient to use and is a substantial improvement over the previous orbit correction routine in terms of user friendliness and compactness.

INTRODUCTION

The Advanced Light Source (ALS) is one of the world's brightest ultraviolet and soft x-ray producing facilities. These powerful beams of light are used for various scientific experiments including the investigation of the structure of atoms, molecules, polymers and chemical reaction dynamics. The ALS is a third generation synchrotron light source which produces light using bend magnets, undulators, and wigglers. Bend magnets are electromagnets used to bend the electron beam and make it travel in a circular ring. As the electron beam bends, light is emitted in the ultraviolet to x-ray region of the spectrum. Undulators and wigglers are composed of numerous magnetic poles. By combining the light created from each pole, they can create particularly bright sources of light.

The electron beams ideally travel through a predetermined orbit, but many times the electron beams are subject to orbital shifts in the transverse direction due to ground settlement, thermal drift in the magnets and vacuum chamber, ground vibrations, and power supply instability [1]. If left uncorrected, this will lead to degradation of the light produced, and will compromise the experiments at the ALS. A global orbit correction system developed in MATLAB, a high-level data manipulation software language, has been implemented to solve this problem. This system uses Beam

Position Monitors (BPMs) to measure the current position of the electron beam orbit and electron dipole magnets for orbit steering. The orbit correction algorithm uses a Singular Value Decomposition (SVD), a method of solving singular matrix equations, to analyze these data and to correct the orbit. The current orbit correction routine is cumbersome due to its menu driven system. It asks several questions one by one and based on the answers selected for each of them it narrows down to the type of correction. This report presents a new, user friendly, GUI for SVD global orbit correction developed using MATLAB.

SVD Orbit Correction

For orbit correction in accelerators it is usually enough to assume a linear relationship between the electron beam position and the corrector magnet strength. This can be expressed as:

$$\Delta X = A \times \Delta Y \quad (1)$$

where ΔX is a vector that contains all the desired changes to the BPM values, ΔY is a vector that contains all the necessary changes in corrector magnet strength to achieve that change and A is the corrector-to-BPM response matrix. A contains the ratios between

the various corrector strengths and their associated BPM values. Each corrector is represented by a single column in the response matrix [2]. Figure 1 shows a response matrix measured at the ALS. The response matrix can be calculated either by using beta function theory or measuring directly on the accelerator. The response matrix can be measured by varying the strength of a corrector magnet and recording all the BPM measurements and repeating the process for all the corrector magnets individually. For global orbit correction, the next step is to find the desired corrector magnet strength change; this can be done by inverting Eq. (1) as:

$$\Delta Y = A^{-1} \times \Delta X. \quad (1)$$

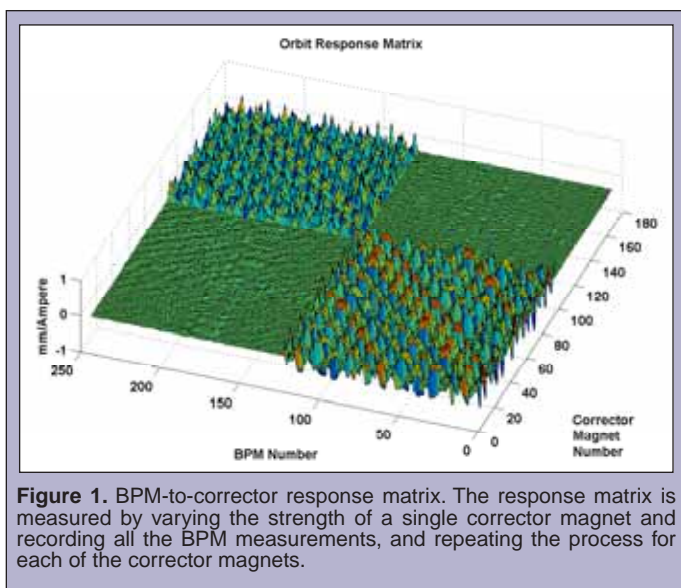


Figure 1. BPM-to-corrector response matrix. The response matrix is measured by varying the strength of a single corrector magnet and recording all the BPM measurements, and repeating the process for each of the corrector magnets.

To find the inverse of the response matrix, it has to be a square matrix and nonsingular. Most of the time, however, response matrices are non-square and are often close to singular and therefore do not have a well-defined inverse. One of the ways to tackle this problem is SVD. The SVD method is based on factorization of the matrix. Using SVD, any $M \times N$ response matrix A can be written as $A = U \cdot S \cdot V^T$, where U is an $M \times M$ orthogonal matrix, S is an $M \times N$ diagonal matrix and V is an $N \times N$ orthogonal matrix. Therefore, the pseudo-inverse of the response matrix can be expressed as:

$$A^{-1} = V \cdot S^{-1} \cdot U^T \quad (3)$$

where V is a set of orthonormal vectors with each axis corresponding to a corrector magnet, U is a set of orthonormal vectors with each axis corresponding to a BPM, and S is a set of vectors that contain singular values of the matrix A . This leads to a solution for Eq. 1 where the corrector magnet strength change, ΔY , is given by:

$$\Delta Y = V \cdot S^{-1} \cdot U^T \cdot \Delta X. \quad (4)$$

A typical orbit correction algorithm is as follows. The first step is to measure the response matrix. After acquiring the response matrix, calculate its pseudo-inverse. Next, measure the current orbit error. This is used to calculate the required corrector strength changes to correct the orbit. Once the corrector strength change is calculated and applied to the orbit, the orbit error is measured again to see how well the orbit was corrected. If the desired orbit is not obtained, the corrector strength change is calculated again. This procedure will be repeated until the user stops the process [3].

It is convenient to use a GUI to correct the electron beam orbit. Figure 2 shows the orbit correction GUI. All the primary features of the GUI are divided into five different panels. These are plane, goal orbit, miscellaneous tasks, correct orbit, and scale down correctors.

Plane

This panel provides the user with the ability to correct the electron orbit in either the horizontal direction, the vertical direction, or both. The ability to choose different predefined BPM sets as well as corrector sets is provided in the GUI. The user is also able to edit the list of BPM and corrector magnet sets to omit a possibly malfunctioning BPM or to disable a weak corrector magnet from strength changes so that the measurements will be more accurate. It is also useful for test and maintenance purposes.

Goal Orbit

An integral part of the GUI is a panel called the goal orbit which enables the user to correct the current orbit to the ideal or goal orbit. It also allows the user to save the current orbit or load a previously saved orbit. It can then be used as the goal orbit for orbit correction.

Miscellaneous Tasks

The GUI also allows the users to set the number of singular values to be used in calculating the corrector magnet strength change. Using more singular values results in higher corrector magnet strength changes and smaller orbit errors. This panel also allows the user to include the RF frequency. RF changes the energy of the electron beam, and changing the energy of a beam changes the electron orbit. Therefore, varying RF frequency provides another means of correcting the electron orbit.

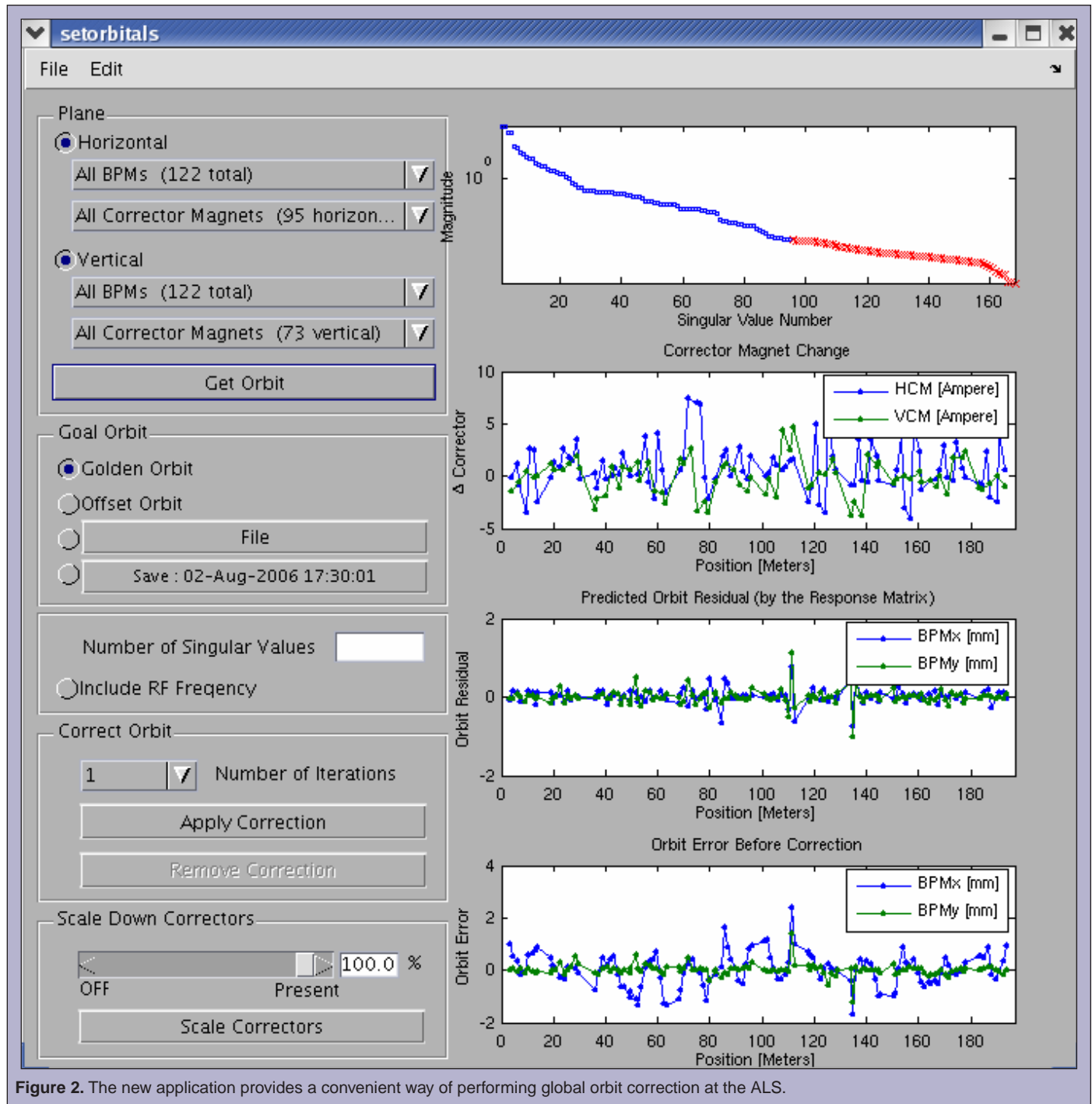
Correct Orbit

After selecting the BPMs, corrector magnets, and number of singular values to be used, the GUI display shows information on how the orbit will behave if those settings were to be applied. If those settings predict a reasonable correction to the current orbit, then the user can apply those settings to the actual orbit. The GUI display includes the magnitude of each of the singular values used in correction, the change in corrector magnet strength that will be applied, the predicted orbit residual (which is the difference

between the goal orbit and the predicted orbit after correction), and the current orbit error before correction. The GUI also has an option to display the sum of the corrector magnet strengths relative to the number of singular values and the standard deviation of the current orbit error relative to the number of singular values. The user will be able to choose between displaying just the four plots or all the plots.

Scale Down Correctors

It is often desirable to scale down the correctors before orbit correction. Some accelerators are able to zero all correctors. If the corrector magnets are never scaled down before starting orbit correction, then over time the total corrector strength may grow quite large. Therefore, users are inclined to turn the correctors down before orbit correction. One of the features of the GUI allows the users to scale the correctors down by percentages of the present corrector value.



RESULTS

The orbit correction GUI was tested in the ALS and data was collected regarding the orbit error before and after correction using three different singular values (1 to 47, 1 to 50 and 1 to 92). The application worked effectively. Results for the horizontal plane will be shown. All 122 BPMs and 95 horizontal corrector magnets in the ALS were used in the testing. The orbit correction was tested by saving an orbit, then scaling down the correctors to introduce a large horizontal error. After scaling, the orbit error was observed to be around 2mm. This is a large orbit distortion compared to the few micrometer level of error during normal ALS operations. The perturbed orbit was then corrected using the GUI. Figure 3(a) shows

the orbit error before and after the correction. After the correction, the error was only about $5.6\mu\text{m}$, showing that the algorithm worked quite well. The corrector magnet change and the number of singular values used are shown in figures 3(b) and 3(c) respectively.

DISCUSSION AND CONCLUSIONS

As discussed earlier, the use of more singular values results in better correction of the orbit. This can be seen in figure 4. The three lines in the plot represent the orbit after correction when different numbers of singular values were used. The plot shows an inverse relationship between the peak-to-peak values of the orbit error and the number of singular values used. For the set of singular values of

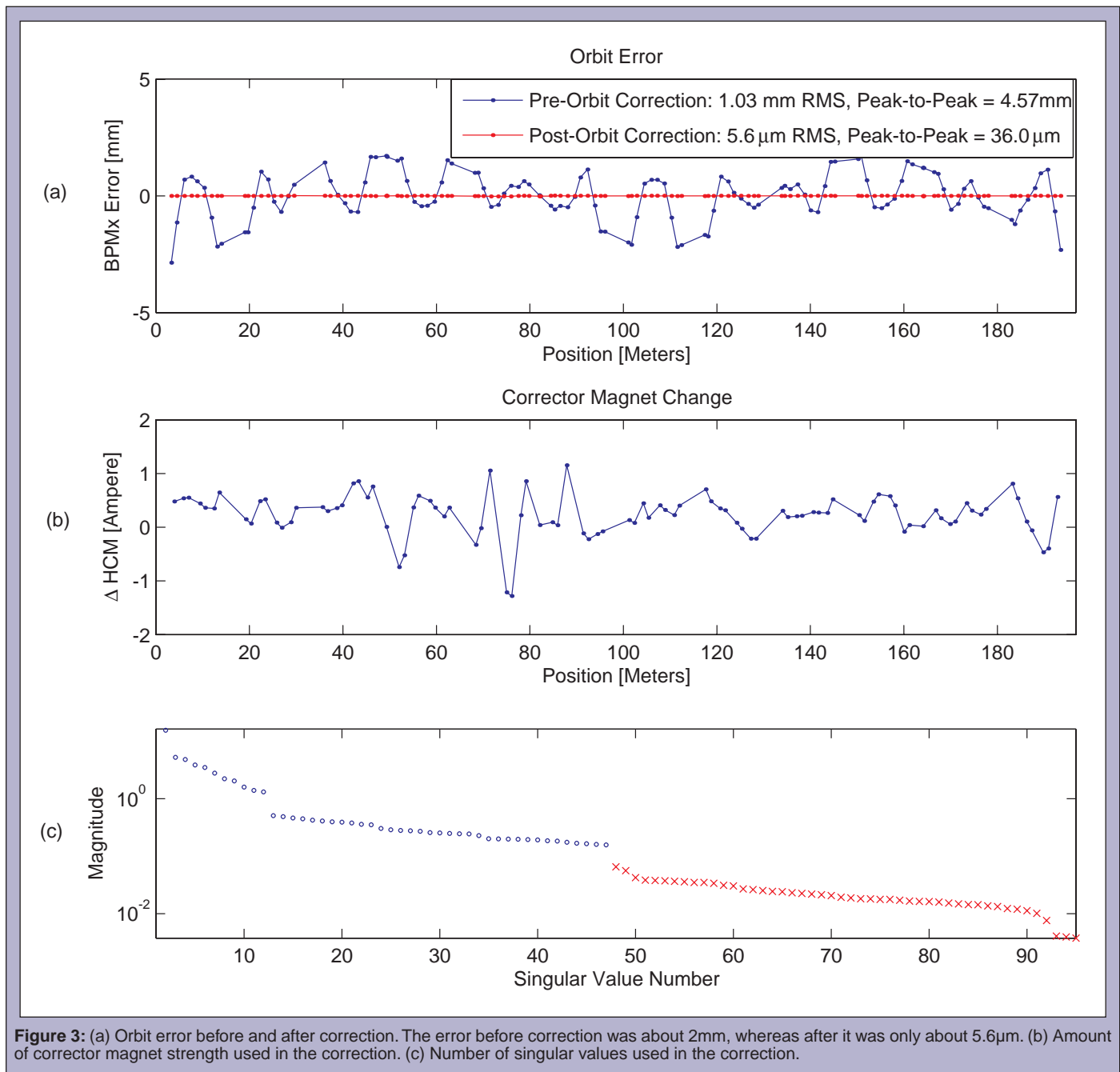


Figure 3: (a) Orbit error before and after correction. The error before correction was about 2mm, whereas after it was only about $5.6\mu\text{m}$. (b) Amount of corrector magnet strength used in the correction. (c) Number of singular values used in the correction.

47, 50, and 92, the peak-to-peak values were 36.0 μm , 21.8 μm and 18.7 μm respectively.

Another result obtained from testing the application is the data regarding the standard deviation of the orbit error and the

sum of the corrector strength compared to the number of singular values. Standard deviation of the orbit error is illustrated in figure 5(a). It can be seen that the standard deviation of the orbit error is dramatically decreased by using just the first few singular values.

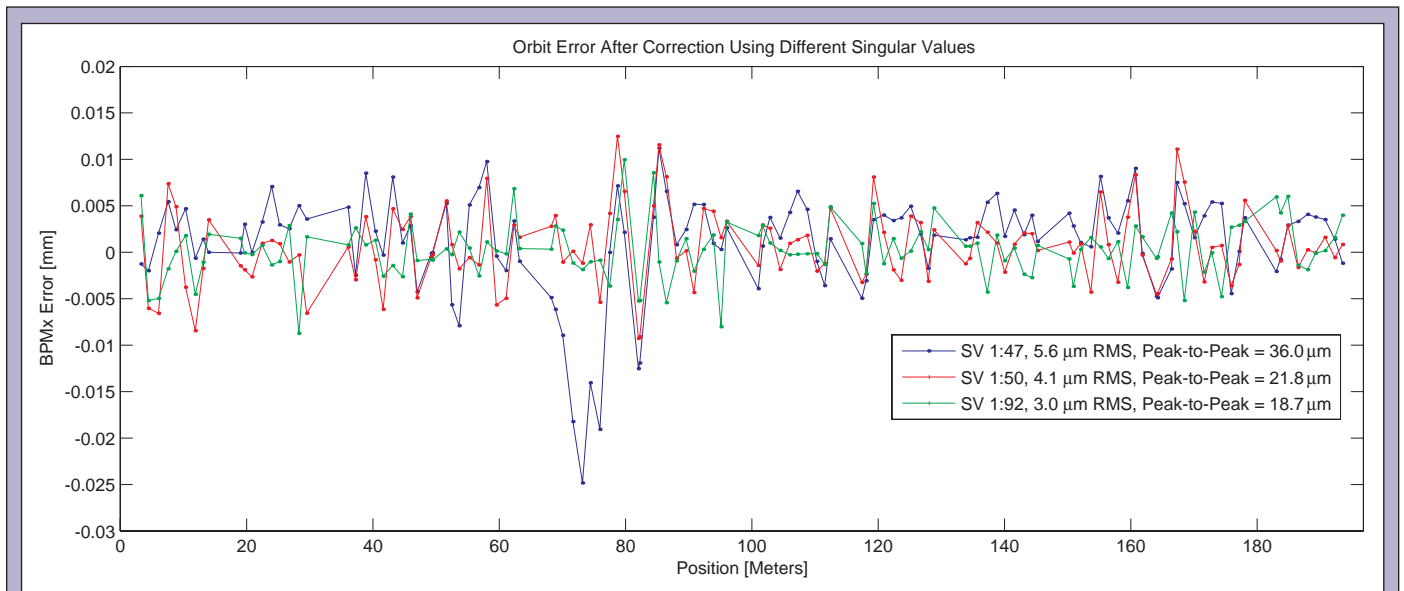


Figure 4. The three different plots represent the orbit after correction with each corresponding to a different set of singular values. The plots show that there is an inverse relationship between the RMS and peak-to-peak value of the orbit error and the number of singular values used.

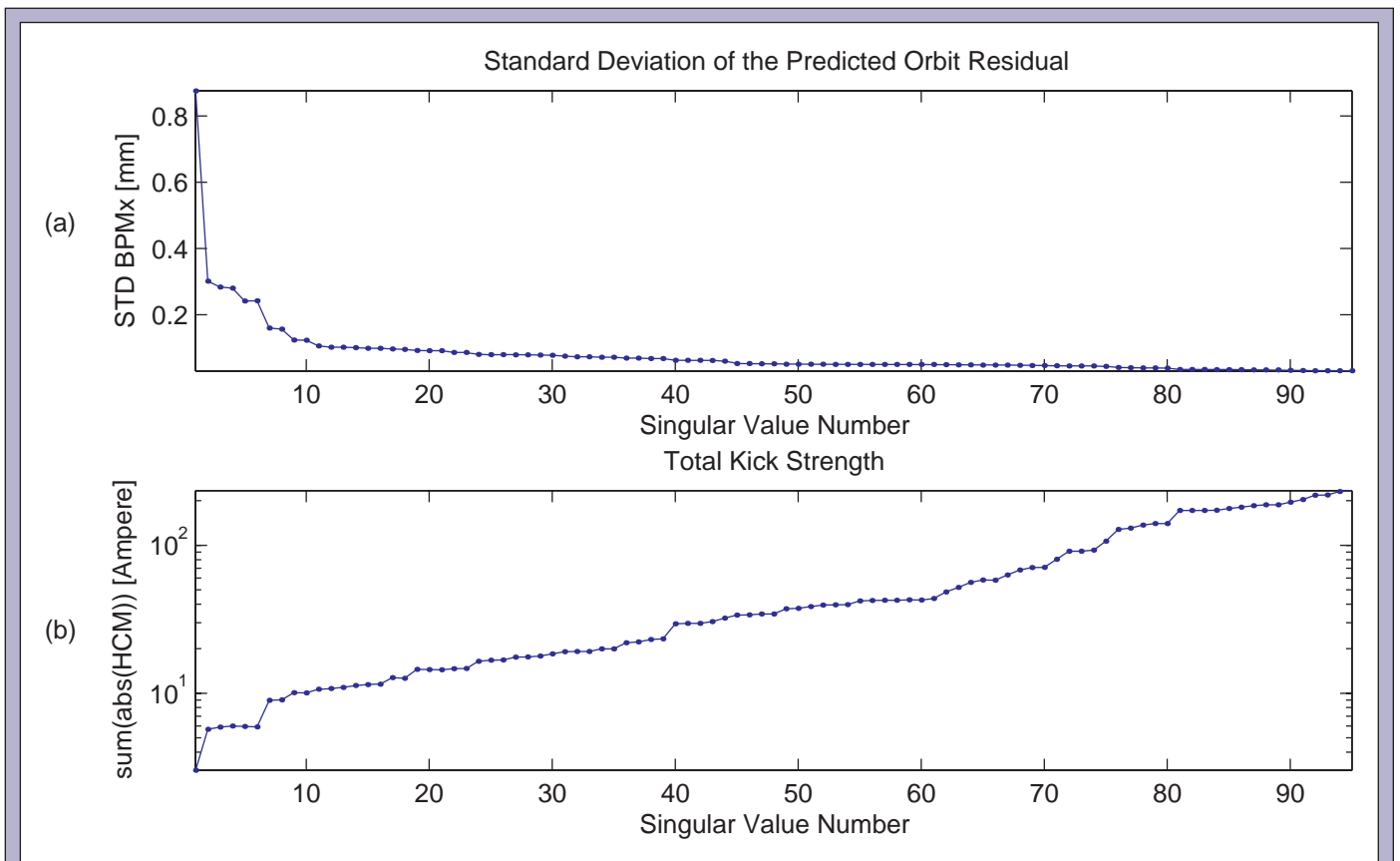


Figure 5: (a) Standard deviation of the orbit error is dramatically reduced by using just the first few singular values. Subsequently more and more singular values will only result in a very small reduction in the standard deviation and thus the orbit error. (b) As more and more singular values are included, it takes a huge amount of corrector strength to reduce the orbit error by a very small number.

Subsequently, more and more singular values will only result in a very small reduction in the standard deviation and thus the orbit error. However, as more and more singular values are included, it takes a huge amount of corrector strength to reduce the orbit error by a very small number. This is illustrated in figure 5(b). The figure shows the sum of all the absolute corrector strength changes for each number of singular values used. Higher strength changes could potentially cause damage to the corrector magnets. These plots are useful in seeing the relationship between the total corrector strength changes and the number of singular values used. SVD is useful because it allows the user to choose the number of singular values to be used for calculations. This would not be possible with a linear least squares method, the method that was used in many accelerators before SVD, because it uses all the singular values for calculation.

In conclusion, the global orbit correction application worked effectively when tested in the ALS. Its features are self-explanatory and are relatively easy to use. The plots displayed on the GUI help the ALS physicists and operators to understand the behavior of the orbit. It is a convenient application to use and is a substantial improvement over the previous orbit correction routine in terms of user friendliness and compactness.

ACKNOWLEDGMENTS

This research was conducted at the Lawrence Berkeley National Laboratory. I would like to thank the Department of Energy, the Office of Science, and the SULI Program for allowing me the opportunity to take part in this internship program. I would like to express my sincere gratitude to my mentor Gregory Portmann for being patient and responding to all my questions with valuable answers. I would also like to thank Hiroshi Nishimura, Tom Scarvie and Christoph Steier for all the support and guidance they have given me throughout the internship.

REFERENCES

- [1] J. Safranek, "Orbit Control at Synchrotron Light Sources," International Conference on Accelerator and Large Experimental Physics Control Systems, Trieste, Italy, 1999, p.241.
- [2] G. White, T. Himel, and H. Shoaee, "A Hybrid Numerical Method for Orbit Correction," PAC, Vancouver, Canada, p.2425.
- [3] Y. Chung, G. Decker, and K. Evans, "Global DC Closed Orbit Correction Experiment on the NSLS X-ray Ring," Advanced Photon Source, Argonne National Laboratory, LS Note No. LS-213, Sept. 14, 1992.

Mariano J. Padilla is a native of Guatemala, and has had a 15-year career in Computer Information, holding the position of Director of Information Systems for an international feature film subtitle and translation company. During his computer career, he designed fiber-optics networks with video servers and gigabit backbone infrastructure. His return to school marks a return to his original passions: engineering and applied physics. He participates in the Transfer Achievement Program (TAP), and the Mathematics, Engineering and Science Achievement program (MESA), and is a member of the Fullerton College Honors program. He is a facilitator at Fullerton College, where he conducts the supplemental instruction of Intermediate Algebra to students enrolled in the TAP program. He is a student member of the American Physical Society and the American Association for Advancement of Science. Dr. Kathleen Hodge, president of Fullerton College, appointed him to the Orange County Engineering Council, where he serves as a delegate to the council representing Fullerton College. He plans to pursue a doctorate degree in atomic theory, general theoretical involving M-Theory and string theory, particle physics or quantum gravity/relativistic physics.

Yuan Liu is a research scientist at the Holifield Radioactive Ion Beam Facility (HRIBF) at Oak Ridge National Laboratory. She received her Ph.D. in electrical engineering from Rice University in 1987. After postdoctoral research at University of Washington in Seattle and University of Tennessee in Knoxville, she went to Japan to join the Advanced Technology Laboratories of Hoechst Japan in 1991. There, she was the project leader for the development of optical chemical sensors for on-line detection of organic pollutants in air and water. She has been at HRIBF since 1997. Her current research interests include high efficiency ion sources that generate beams of short-lived, unstable nuclei for nuclear physics and nuclear astrophysics research, laser based beam purification techniques, and new techniques to improve ion beam quality. She runs two separate experimental stations for developing and testing ion sources.

DEVELOPMENT OF EMITTANCE ANALYSIS SOFTWARE FOR ION BEAM CHARACTERIZATION

MARIANO J. PADILLA AND YUAN LIU

ABSTRACT

Transverse beam emittance is a crucial property of charged particle beams that describes their angular and spatial spread. It is a figure of merit frequently used to determine the quality of ion beams, the compatibility of an ion beam with a given beam transport system, and the ability to suppress neighboring isotopes at on-line mass separator facilities. Generally a high quality beam is characterized by a small emittance. In order to determine and improve the quality of ion beams used at the Holifield Radioactive Ion beam Facility (HRIBF) for nuclear physics and nuclear astrophysics research, the emittances of the ion beams are measured at the off-line Ion Source Test Facilities. In this project, emittance analysis software was developed to perform various data processing tasks for noise reduction, to evaluate root-mean-square emittance, *Twiss* parameters, and area emittance of different beam fractions. The software also provides 2D and 3D graphical views of the emittance data, beam profiles, emittance contours, and RMS. Noise exclusion is essential for accurate determination of beam emittance values. A Self-Consistent, Unbiased Elliptical Exclusion (SCUBEE_x) method is employed. Numerical data analysis techniques such as interpolation and nonlinear fitting are also incorporated into the software. The software will provide a simplified, fast tool for comprehensive emittance analysis. The main functions of the software package have been completed. In preliminary tests with experimental emittance data, the analysis results using the software were shown to be accurate.

INTRODUCTION

Nuclear and particle physics experiments use charged particle beams [1, 2]. The ability to transport the beams over long distances and/or to focus them into small areas depends largely on the quality of the beams; hence to have a measure of beam quality is paramount. The quality of a particle beam is usually described by its emittance and brightness. Ion beam emittance influences charged particle accelerator design, operation, mass resolution, and neighboring isotope suppression at on-line mass separator facilities. In this paper, the method used for transverse emittance measurement is briefly described and the development of a software

program to assist with the data analysis is discussed in detail. Possible enhancements and additions to the software are also described.

Experimental Emittance Measurement

The Ion Source Test Facility-2 (ISTF-2) is one of two off-line facilities at the Holifield Radioactive Ion Beam Facility (HRIBF) at Oak Ridge National Laboratory (ORNL) available to test ion sources for on-line generation of Radioactive Ion Beams (RIBs). The ISTF-2 consists of a high voltage platform, ion source, motor generator, cooling system, Einzel lenses, 90° dipole magnet for mass separation, Faraday cups for measuring beam intensities, and

an emittance measurement apparatus. Figure 1 illustrates the setup at ISTF-2.

Different methods exist to measure emittance; at ISTF-2 emittance is measured using a slit-harp device, illustrated in Figure 2, which measures the ion beam spatial and angular distributions. The emittance device consists of a thin slit 0.1mm wide and a detector array, which is made up of 32 electrically isolated tungsten strips, located down-stream of the slit. The ion beam is sampled by the slit producing a sheet beamlet which is then allowed to drift freely towards the detector array located 400mm (15.75 inches) away from the slit. The slit-detector is stepped across the beam and angular distribution measurements at each step are recorded. Thus, the beam distribution as a function of position and angle is obtained. The recorded data is saved in text or Microsoft Excel format. The ISTF-2 emittance measurement apparatus consists of two such step-motor driven slit-detector units for determining the transverse emittance of an ion beam in the x and y directions, respectively.

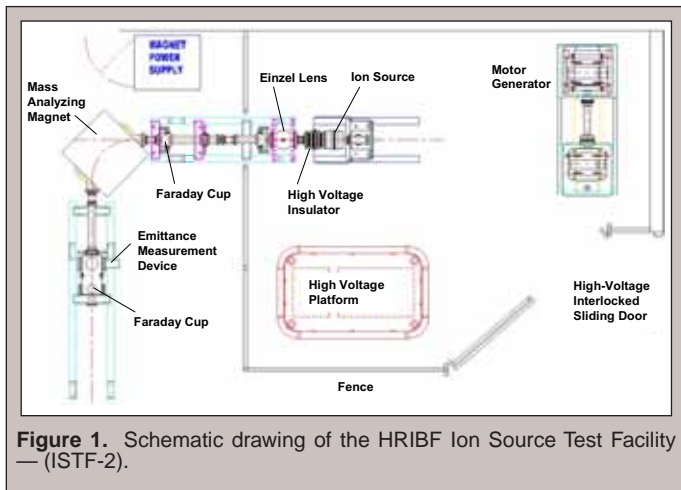


Figure 1. Schematic drawing of the HRIBF Ion Source Test Facility — (ISTF-2).

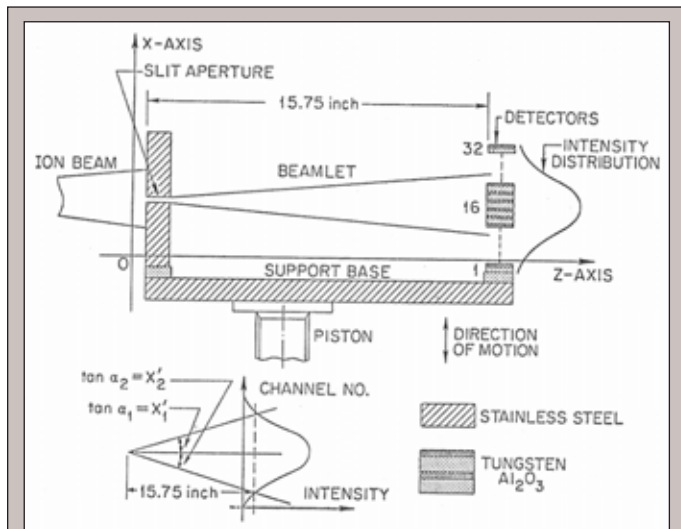


Figure 2. Schematic drawing of the "Slit-Harp" emittance measuring device.

Software Design

An emittance analysis program using the Mathematica language has been in use; however it is limited to users who have knowledge of Mathematica. In addition the processing time is relatively long and requires adjustments to scripts for every emittance data file. This study describes an Emittance Evaluation Program (EEP) developed in Microsoft Visual Basic .net (VB.NET) for general users. EEP is based on the previous Mathematica program and implements the external software gnuplot [3] for 3-dimensional plots and graphs. The software makes possible data import for text and Microsoft Excel formats, manual background exclusion, Self-Consistent Unbiased Elliptical Exclusion (SCUBEE_x) algorithms [4] for noise reduction, emittance calculation, visualization, and report generation. The algorithms used within the software are discussed in detail in the next section. EEP allows the analysis of emittance data without the need for manual programming. The beam profile, root-mean-square (RMS) emittance, Twiss parameters, and fractional emittances of an ion beam are calculated simultaneously. Figure 3 and Figure 4 illustrate the features and functions of the EEP software. The analysis results can be saved either as text or in Microsoft Word format. The Microsoft Word format includes RMS emittance and beam profile graphs.

Algorithms

The experimental emittance data are stored as an array of beam intensities $I(x_j, x'_j)$ measured from each detector strip at each motor position, where x_i is the i^{th} slit position ($i = 1$ to N , N being the total number of the selected slit positions), and x'_j corresponds to the divergence angle of the j^{th} ($j = 1$ to 32) detector. The data are displayed in a 3D graph, as shown in Figure 3, and in Excel style grids for manual inspection. Before emittance evaluation, the data are inspected manually and, if needed, subjected to background

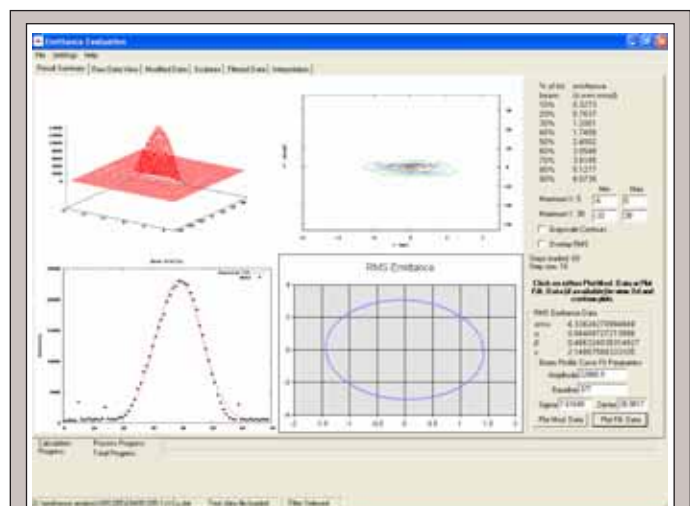


Figure 3. A screenshot of the Result Summary page of the emittance evaluation program. The graphs shown include a 3D plot of the raw or filtered emittance data (upper left), the beam profile plot with Gaussian fit (lower left), fractional emittance contours (upper right), and the RMS ellipse (lower right). Listed on the right are the calculated 90% fractional and RMS emittance values for the raw or filtered data and the Gaussian fit results.

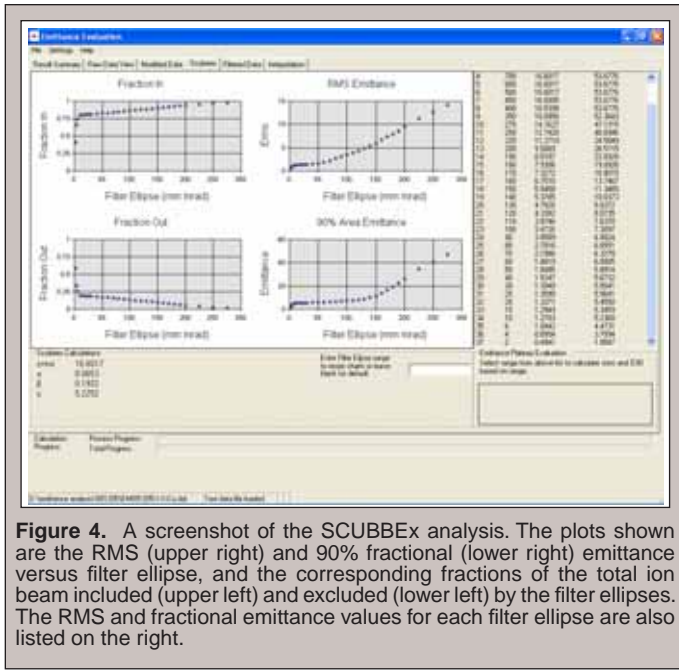


Figure 4. A screenshot of the SCUBBEx analysis. The plots shown are the RMS (upper right) and 90% fractional (lower right) emittance versus filter ellipse, and the corresponding fractions of the total ion beam included (upper left) and excluded (lower left) by the filter ellipses. The RMS and fractional emittance values for each filter ellipse are also listed on the right.

subtraction using data taken under the same conditions without the ion beam. In order to compensate for variations in beam intensity during a particular measurement, the data set can be normalized using the slit current obtained at each slit position. The slit-detector assembly is driven by a 1.8° stepping motor with a minimum linear step of 0.015mm per 0.9° . The angular step is the angle between two adjacent strips in the emittance detector array (2.285mrad). These constants are used in the algorithms throughout the software. The algorithms for evaluating beam emittances in the xx' -plane are described below. Similar algorithms hold for the yy' -plane.

The beam profile is calculated by summing, for each position x_i , the ion currents on all 32 strips and stored in an array of variables $I_{profile}(x_j)$:

$$I_{profile}(x_i) = \sum_{j=1}^{32} I(x_i, x'_j). \quad (1)$$

Gaussian fit can be performed on the resulting beam profile data using the following function:

$$a + be^{-\frac{(x-c)^2}{2\sigma^2}}, \quad (2)$$

where a is the baseline, b is the amplitude, c is the mean, and σ is the standard deviation. The full width at half maximum (FWHM) of the ion beam can then be calculated as

$$FWHM = 2\sqrt{2 \ln 2} \sigma. \quad (3)$$

The calculated beam profile is displayed together with the Gaussian fit in EEP, as shown in Figure 3.

The RMS emittance of an ion beam is defined as:

$$\mathcal{E}_{rms} = \sqrt{\langle x^2 \rangle \langle x'^2 \rangle - \langle xx' \rangle^2}, \quad (4)$$

where $\langle x^2 \rangle$, $\langle x'^2 \rangle$ and $\langle xx' \rangle$ are the second moments of the beam distribution in the xx' -plane:

$$\langle x^2 \rangle = \frac{\sum_{i=1}^N \sum_{j=1}^{32} (x_i - x_c)^2 I(x_i, x'_j)}{I_{total}}, \quad (5)$$

$$\langle x'^2 \rangle = \frac{\sum_{i=1}^N \sum_{j=1}^{32} (x'_j - x'_c)^2 I(x_i, x'_j)}{I_{total}}, \quad (6)$$

$$\langle xx' \rangle = \frac{\sum_{i=1}^N \sum_{j=1}^{32} (x_i - x_c)(x'_j - x'_c) I(x_i, x'_j)}{I_{total}}, \quad (7)$$

where I_{total} is the total ion beam current detected:

$$I_{total} = \sum_{i=1}^N \sum_{j=1}^{32} I(x_i, x'_j), \quad (8)$$

and (x_c, x'_c) is the centroid of beam distribution calculated using the following formulas:

$$x_c = \frac{\sum_{i=1}^N \sum_{j=1}^{32} x_i I(x_i, x'_j)}{I_{total}}, \quad (9)$$

$$x'_c = \frac{\sum_{i=1}^N \sum_{j=1}^{32} x'_j I(x_i, x'_j)}{I_{total}}. \quad (10)$$

The RMS distribution can be represented by an ellipse with an area equal to the RMS emittance multiplied by π :

$$\gamma_T x^2 + 2\alpha_T xx' + \beta_T x'^2 = \mathcal{E}_{rms}, \quad (11)$$

where the coefficients are the *Twiss* parameters given by:

$$\alpha_T = -\frac{\langle xx' \rangle}{\mathcal{E}_{rms}}, \quad \beta_T = \frac{\langle x^2 \rangle}{\mathcal{E}_{rms}}, \quad \gamma_T = \frac{\langle x'^2 \rangle}{\mathcal{E}_{rms}}. \quad (12)$$

Equal-intensity contour graphs depicting the emittances corresponding to given fractions of the total ion beam distribution are also calculated. The area within each contour divided by π is taken as the emittance for that particular beam fraction. The calculated RMS emittance, *Twiss* parameters, and fractional beam emittances for 10–90% of the total beam, together with the corresponding RMS ellipse and emittance contour plots, are summarized in the Result Summary page in EEP, as illustrated in Figure 3.

DISCUSSION AND CONCLUSIONS

Noise exclusion is essential for accurate determination of beam emittance values. Non-zero background noise in emittance data can have a large impact on the values of RMS-emittances derived from the data. The SCUBBEx method developed by Stockli et al. [4] is employed in EEP with slight modifications for unbiased noise reduction. This method applies successively smaller exclusion ellipses around the centroid of the emittance data. Any data points falling outside of an ellipse are assumed to be background noise. The RMS and fractional emittances are then calculated using the data within the ellipse. Figure 4 illustrates an example of the SCUBBEx process: the calculated RMS and 90% fractional emittances decrease with decreasing ellipse size as more noise is excluded, reaching a flat region where the emittance value stays relatively the same because most of the background is excluded. When the ellipse is further decreased the emittance values will decrease sharply as the ellipse begins to cut out the actual ion beam. It can be seen in Figure 4,

the 90% fractional emittance shows a clear plateau between ellipses of 10–120mm-mrad, while a plateau in the RMS emittance is reached between 10–60mm-mrad. Figure 5 presents a side-by-side comparison of a data set prior to and after the SCUBEEEx filtering. The left graph shows the raw data with background currents, which give a RMS emittance of 16.6π -mm-mrad. The right graph displays the data after excluding the background current with a filter ellipse of 120mm-mrad. It clearly shows that most of the background noise is removed while the real beam distribution is intact. The resulting RMS emittance is reduced to 4.3π -mm-mrad.

After SCUBEEEx analysis, the RMS and 90% fractional emittances of the ion beam are determined as the average emittance values in the corresponding plateau or flat regions of the SCUBEEEx results. EEP allows users to easily view and select the plateau region for final emittance evaluation. A user can examine the SCUBEEEx results shown in Figure 4 and select the emittance values in the

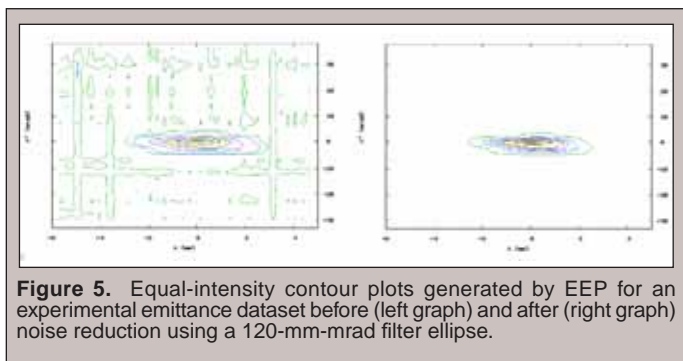


Figure 5. Equal-intensity contour plots generated by EEP for an experimental emittance dataset before (left graph) and after (right graph) noise reduction using a 120-mm-mrad filter ellipse.

plateau region using simple mouse clicks from the list supplied on the right; the average RMS and fractional emittances and their standard deviation are calculated from the selected values and the results are displayed immediately, as illustrated in Figure 6.

The main functions of the software package, including data input and visualization, data processing, SCUBEEEx, emittance evaluation, and results output, have been completed. The codes have been tested with experimental emittance data and shown to be accurate. During the RIA 2006 Summer School [5] held at HRIBF, EEP was used in the Hands-on-Program on Ion Source Beam Emittance for ion beam emittance evaluation and the analysis results from EEP were in excellent agreement with the Mathematica results. The installation of EEP is simple and in standard (MSI) Microsoft Installation Package format. The EEP software package requires the .net framework (which most computers running Microsoft XP software have) and Microsoft Office 2003 for report and graphic functionality.

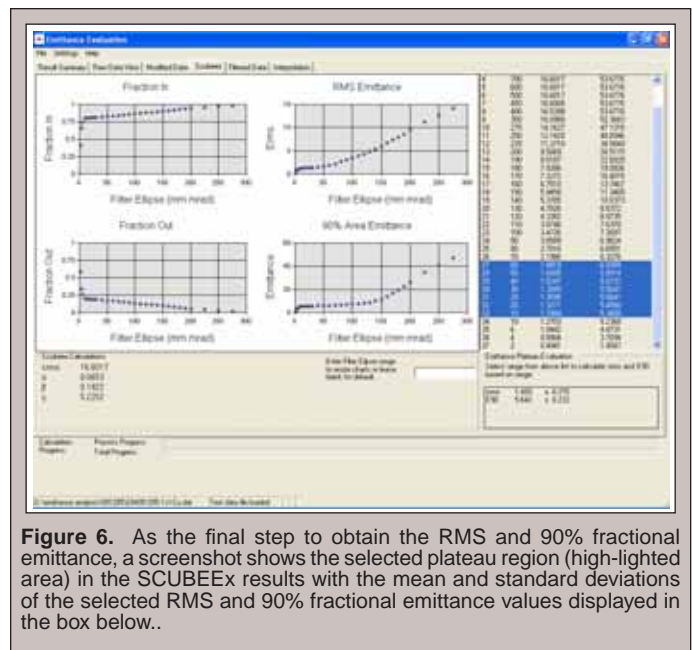


Figure 6. As the final step to obtain the RMS and 90% fractional emittance, a screenshot shows the selected plateau region (high-lighted area) in the SCUBEEEx results with the mean and standard deviations of the selected RMS and 90% fractional emittance values displayed in the box below.

EEP provides a simplified, fast tool for comprehensive emittance analysis. The interactive interface of the EEP software allows the user to easily perform emittance analysis without performing manual calculations and formula derivations. Future EEP software enhancements include polynomial and cubic spline interpolation of data points, interpolated data visualization, and multiple emittance data file capabilities for cross reference or comparison. Such enhancements would provide additional capabilities for accurate emittance evaluation and further simplify the emittance evaluation of ion beams.

ACKNOWLEDGMENTS

This research was conducted at Oak Ridge National Laboratory. I thank the U.S. Department of Energy Office of Science for allowing me to participate in the CCI program to further my studies, broaden my perspective on my science field, and to have a unique and highly productive learning experience. Special thanks to my mentor Yuan Liu for her patience, guidance, and teaching. I would also like to thank Daniel Stracener of the Physics Division, Paul Mueller also of the Physics Division for his advice and cordial support, and Kathy Ketner, Cheryl Terry, and Lee Vang of the Oak Ridge Institute for Science and Education for their organization and coordination.

REFERENCES

- [1] Stanley Humphries Jr., "Charged Particle Beams," John Wiley and Sons, 1990.
- [2] J. Nolen and M. Portillo, "Charged Particle Optics" in The Optics Encyclopedia – Basic Foundations and Practical Applications, Vol. 1, Thomas G. Brown, et al. (eds.), Wiley-VCH, Berlin, 2003.
- [3] gnuplot ver. 4.0, Peter Mikulík and Ethan Merritt, et al.
- [4] M.P. Stockli, R. F. Welton, R. Keller, A. P. Letchford, R. W. Thomae, and J. W. G. Thomason, AIP Conference Proceedings, Volume 639, pp. 135-159, 2002.
- [5] Oak Ridge Associated Universities, "Fifth RIA Summer School on Exotic Beam Physics", July 2006, "<http://www.ornl.gov/ria/ria06/program.htm>"

Charles Pye is studying Surface Nanostructure Analysis in the SULI Program at the Ames Laboratory, where he investigated "Novel Coarsening of Pb Nanostructures on Si(111) 7 X 7." As an undergraduate, he studied physics at the University of Kansas in Lawrence, Kansas, his hometown. Mr. Pye is a member of the American Physical Society, and he enjoys music and drawing.

Michael Yakes received his Ph.D. from Iowa State University in 2006. His thesis research was focused on the study of Pb nanostructures on Si substrates using high resolution electron diffraction. He is currently studying III/V semiconductor devices using cross-sectional scanning tunneling microscopy as a National Research Council postdoc at the Naval Research Laboratory in Washington, D.C.

Myron Hupalo received a Ph.D. in physics from Lviv State University in Ukraine, in 1982. He is currently Associate Scientist at Ames Laboratory

USA-DOE. His expertise is in surface physics, especially the construction and use of Scanning Tunneling Microscope. He is author or coauthor of more than 45 publications in the study of epitaxial growth in the 2-d physics of surface overlayers and self organization on surfaces. Currently he is interested in the study of Quantum Size Effects in metal nanostructures.

Michael C. Tringides is a Professor of Physics at Iowa State University, and Senior Scientist at Ames Laboratory USA-DOE. He received his PhD from University of Chicago in 1984 on surface physics. He is the organizer of two major conferences in surface diffusion, and coeditor of the proceedings books. He is author or coauthor of 120 publications and has given more than 125 invited talks at international conferences and institutions. His current interests involve the study of surface physics, epitaxial growth and nanostructure formation with the use of High Resolution Electron Diffraction and Scanning Tunneling Microscopy.

NOVEL COARSENING OF Pb NANOSTRUCTURES ON Si(111) 7 X 7

CHARLES J. PYE, MICHAEL YAKES, MYRON HUPALO, AND MICHAEL TRINGIDES

ABSTRACT

In order to study a possible means of controlling the growth of an epitaxially grown, self-assembled nanostructure, Pb/Si(111) was analyzed. An atomically clean Si(111) 7 X 7 crystal was prepared under Ultra High Vacuum (UHV) conditions followed by Pb deposition. The islands were monitored over time with a Scanning Tunneling Microscope (STM) to see how they coarsen (the process of smaller islands disappearing and larger islands growing even larger) and determine the applicability of the classical theory of Ostwald ripening. STM Images of the resulting Pb islands were taken as they evolved in time. Height measurements indicated that initially, the majority of islands (25 out of 33) were 4 or 5 layer islands, but by the end of the experiment 68 minutes later, the majority (18 out of 24 islands) were 7 or 9 layer islands. Additional measurements of the area indicate that the total area of all the islands was reduced by 10%, but the total coverage increased by ~40%, presumably coming from the wetting layer. Measurements of island area and height over time indicated that an increase in height was accompanied by a sudden (within 2-3 minutes) increase in volume and decrease in area. Interestingly, some islands grew by adding a ring of higher height around the edge before filling in the center. These rings, on average, would fill in less than 5 minutes. Generally, the islands started with a random shape, and gradually became more like a regular hexagon over time. These observations are very unusual because they do not fit the classical expectations based on Ostwald ripening and they show the role of Quantum Size Effects upon the coarsening process.

INTRODUCTION

One of the major goals of surface science has been the creation of self-assembled nanostructures of a controlled height, size, and shape. Many patterns have already been discovered in the formation of these nanostructures. The ability to control these nanostructures would be of great importance, both in practical applications such as computer miniaturization, and in basic understanding of how nature functions at the scale of 10^{-9} meters.

The particular goal of this experiment was to determine whether Pb on Si(111) 7 X 7 followed classical Ostwald Ripening. In Ostwald Ripening, atoms transfer from islands smaller than a certain radius to those larger than that radius so as to minimize the Gibbs free

energy of formation [1]. This causes a coarsening process which results in fewer islands of a larger size, which continuously change volume while the total volume of all the islands remains constant [2]. Pb on Si(111) 7 X 7 has shown several unusual behaviors in the past which are not explained by Ostwald Ripening, particularly its Quantum Size Effects (QSE) [3,4,5].

Some of the specific questions investigated during this experiment were: how did the height of the islands change over time? How did their size, volume and shape change over time? How did these change when the islands changed height? What were the sizes and durations of the rings that often accompanied a change in height? What was the growth mechanism of the islands?

MATERIALS AND METHODS

An atomically clean Si(111) 7 X 7 crystal was prepared at a pressure of 2×10^{-11} torr followed by Pb deposition at a flux of 0.05 monolayers (ML)/minute and a temperature of 242K. Images of the resulting lead islands were taken with a Scanning Tunneling Microscope (STM) using a constant voltage of 1.5V and a current of 1nA over an area of 500 x 500nm as they evolved in time. Commercial imaging software (Scala 4.2 and Scion Image 4.03) was used to take measurements of the islands on the resulting images.

RESULTS AND DISCUSSION

Figure 1(a) shows the average volume for an individual island in each image. The large increase shows that some sort of coarsening process is going on. Figure 1(b) shows that the number of islands is decreasing, from 33 islands at time 0 to only 24 after 68 minutes, which is further indication of a coarsening process. This decrease in the number of islands can be seen in the difference between figures 1(c) and 1(d). Both images show an area measuring 500 x 500nm, at a temperature of 242K and a voltage of 1.5V. Figure 1(c) was taken just after Pb deposition, but 1(d) was the last image taken, 68 minutes after the acquisition of 1(c). It is apparent in these images that the number of islands had decreased, and detailed measurements showed that their height had also grown. The islands with the smallest volumes had decayed completely. This is consistent with the coarsening process that occurs during Ostwald Ripening.

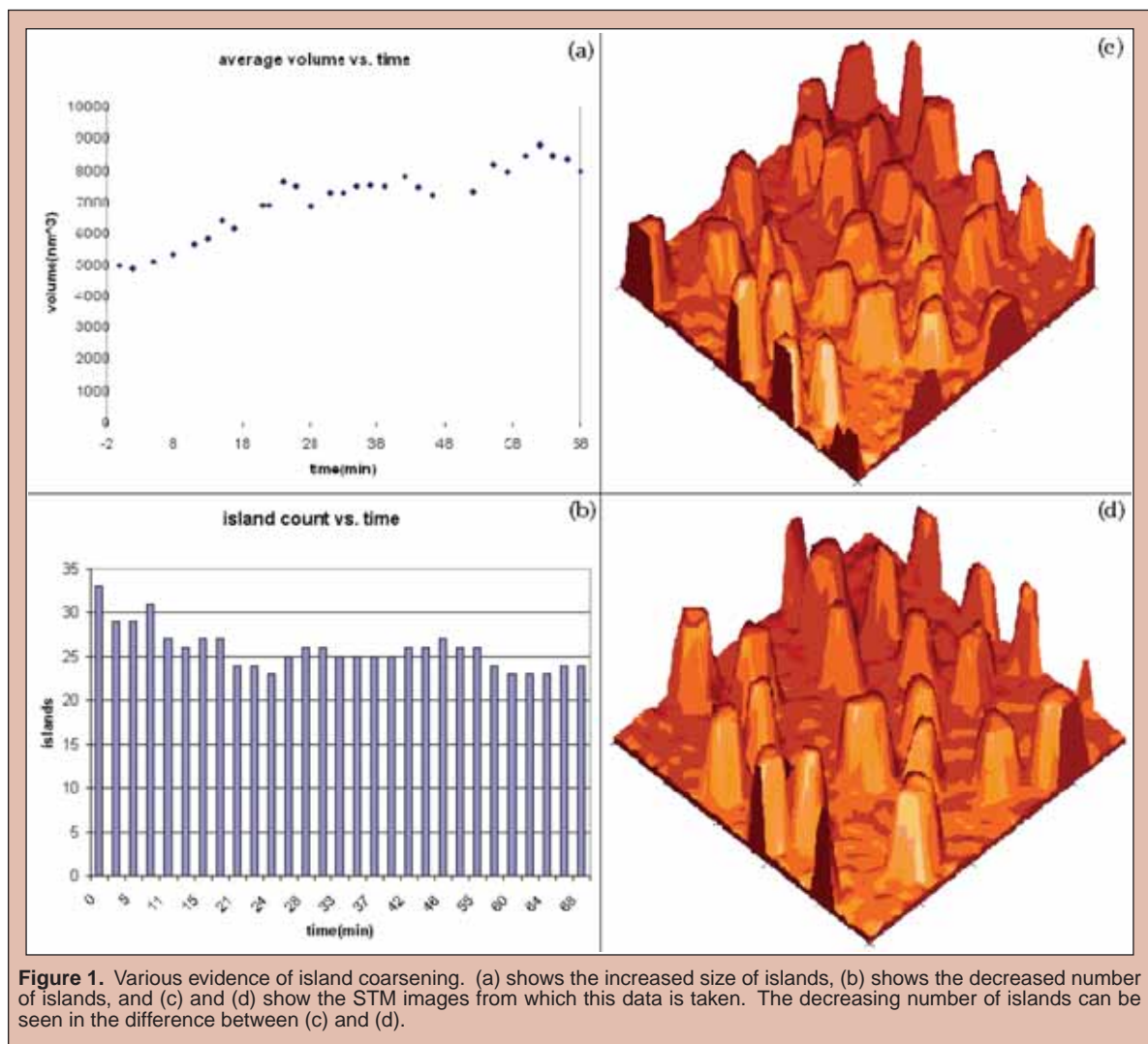


Figure 1. Various evidence of island coarsening. (a) shows the increased size of islands, (b) shows the decreased number of islands, and (c) and (d) show the STM images from which this data is taken. The decreasing number of islands can be seen in the difference between (c) and (d).

Figure 2 shows the total island volume increasing over time. In Ostwald Ripening, however, overall volume is conserved. The increase in total volume indicates that there is a transfer of atoms from the wetting layer to the islands throughout the experiment. Another important difference is that, in Ostwald Ripening, islands continuously change in volume depending on their size and the size

of their neighboring islands [3]. However, these observations show that islands grow suddenly in volume when they grow in height, but before or after the sudden increase their volume changes very little. The reason for this growth pattern is not yet understood. This increase in volume is also typically accompanied by a decrease in area.

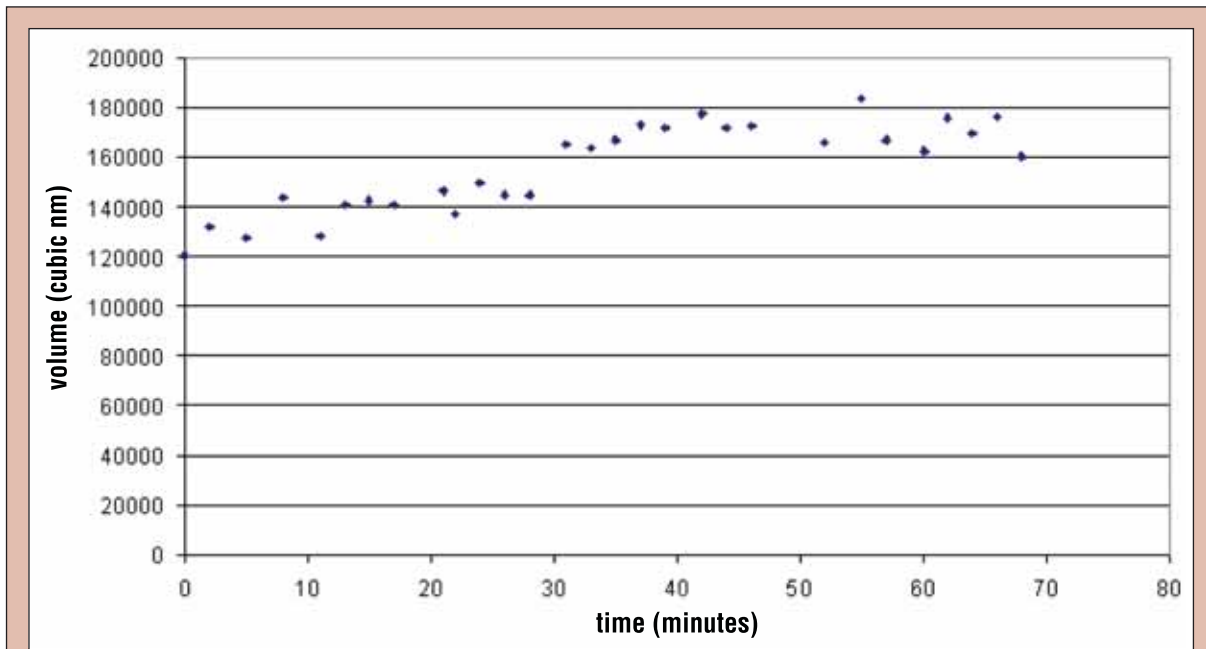


Figure 2. Total island volume vs. time. The relatively stable volume early on, followed by a dramatic jump after 30 minutes, and then another long stable period, shows that the island coarsening is not caused by Ostwald Ripening.

Figures 3(a) and 3(b) show this behavior. 3(a) shows the volume of one typical island over time: the blue represents the volume of the island when it is 5 layers tall, and the yellow represents the volume of the island when it is 7 layers tall. At 23 minutes it grew a ring, so some of it was 5 layers tall and some of it was 7 layers tall. There is a ~20% increase in volume from time 21 to 24, but

before and after the increase the volume remained constant. Figure 3(b) relates the percentage change in volume to the change in area for all islands that increased in height. All increases in height led to an increase in volume and 14 of the 17 changes in height were accompanied by a decrease in area.

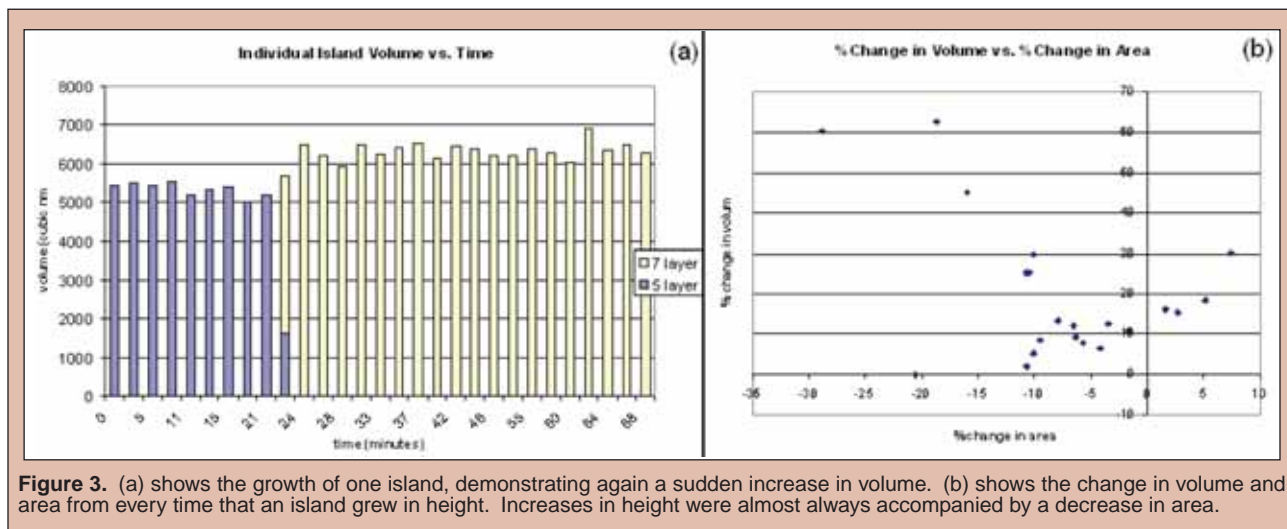


Figure 3. (a) shows the growth of one island, demonstrating again a sudden increase in volume. (b) shows the change in volume and area from every time that an island grew in height. Increases in height were almost always accompanied by a decrease in area.

Figure 4(a) shows the height of islands as they evolved over time. Initially, 24 of the 33 islands were either 4 or 5 layers tall. After 68 minutes, 18 of the 24 visible islands were 7 or 9 layers tall, and none of the islands were 4 or 5 layers tall. Figures 4(b) and 4(c) show this difference in the distribution of island heights between the first and last images taken. This is clear evidence of QSE,

because it shows that 7- and 9-layer heights are the most stable[3]. It should be noted that some of the small spikes in figure 4(a) are the result of islands which moved on or off the imaged area due to instrument drift (an unavoidable problem with the STM especially for experiments that take long times).

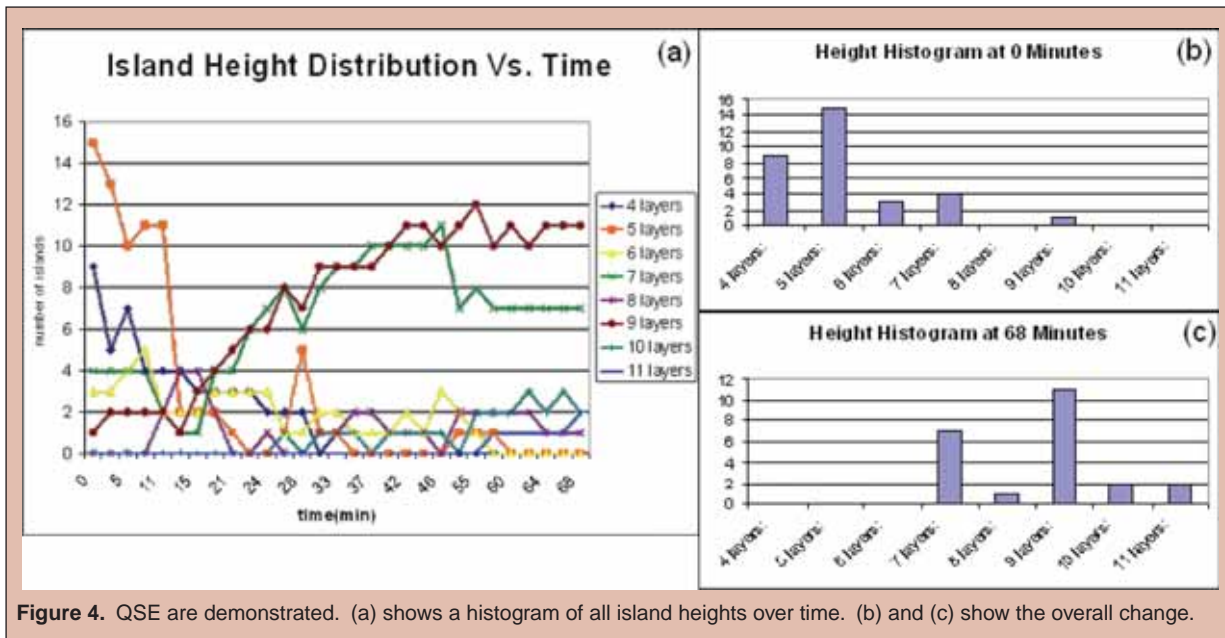


Figure 4. QSE are demonstrated. (a) shows a histogram of all island heights over time. (b) and (c) show the overall change.

Figure 5(a) is a 500nm x 500nm STM image showing numerous rings. These islands, instead of being atomically flat on top, have a section at least one level higher than the rest of the island. One of the rings in this image is still incomplete, and divides the island in half instead of stretching around the edge as complete rings do. Figure 5(b) shows a histogram of how long an island maintained a ring before becoming flat again. These rings appear to be unstable, and fill in to produce the next stable layer. 13 of the 23 rings lasted

less than five minutes, and it is possible that many more lasted less than two minutes, but were not detected due to the two minute gap between images. The temperature of 242K is high for this sort of experiment, and lowering this temperature would lead to longer lasting rings.

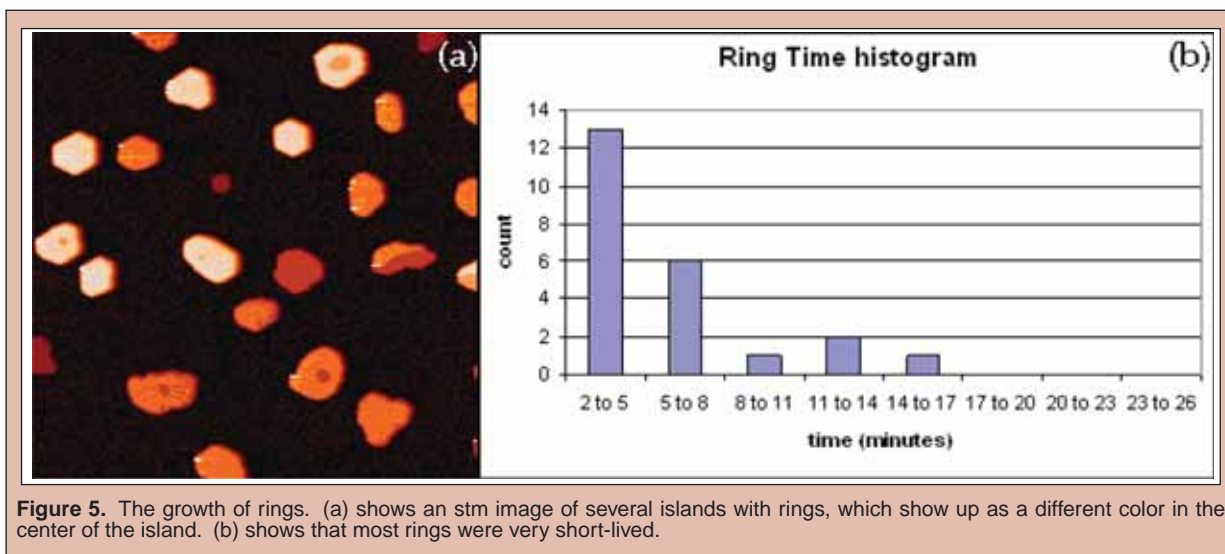


Figure 5. The growth of rings. (a) shows an stm image of several islands with rings, which show up as a different color in the center of the island. (b) shows that most rings were very short-lived.

DISCUSSION AND CONCLUSIONS

These results provide some insight into the behavior of Pb on a Si(111) 7 X 7 crystal, but much is still unknown about its behavior. It is clear that QSE play a strong role in its coarsening process, due to the very strong preference for heights of 7- and 9- layers. It also seems clear that the coarsening process is not classical Ostwald Ripening. Although the growth in average island volume and the decay of the islands with the smallest volume shows that a similar coarsening process is going on, the increase in total volume and the stepwise growth in island volume clearly differ from classical Ostwald Ripening. The question of what causes these differences remains: it could be the result of QSE, or it could be a different process entirely.

One of the most unusual characteristics of Pb/Si(111) is its ring growth. The rings in this experiment were frequently associated with an increase in height, suggesting that whatever process is causing the coarsening of these islands is also causing their ring growth. The instability of these rings implies that they might be even more frequent than what was observed here. Any ring which lasted less than 2 minutes might not have been observed (due to the gap between images) — it is possible that all increases in height began with a ring.

A key investigation which remains is to determine how the islands grow in height. The results of this experiment seem to indicate that there is a transfer of atoms from the wetting layer to the islands. This could be accomplished either by adding atoms from the wetting layer which push the atoms in the island higher, or by adding atoms from the wetting layer directly to the top of the island after diffusing on the facet planes. These two processes would be indistinguishable in this experiment, so further work must be done to establish the process by which the islands are growing in height. Understanding this process is crucial to understanding the overall coarsening process.

ACKNOWLEDGMENTS

I would like to thank the Department of Energy and the Office of Science, for funding my research. I would also like to thank Ames Laboratory and Iowa State University for hosting me. Finally, I would like to thank Jizhou Chen and Steven Binz for all of their help with this project.

REFERENCES

- [1] M. Zinke-Allmang, L.C. Feldman, and M.H. Grabow, "Clustering on Surfaces," Surface Science Reports, vol.16, issue 8, pp. 377-463, Dec. 1992.
- [2] L. Ratke and P.W. Voorhees, Growth and Coarsening. Berlin: Springer, 2002.
- [3] C.A. Jeffrey, E.H. Conrad, R. Feng, M. Hupalo, C. Kim, P.J. Ryan, P.F. Miceli, and M.C. Tringides, "Influence of Quantum Size Effects on Island Coarsening," Physical Review Letters, vol. 96, no. 106105, March 17 2006.
- [4] K. Budde, E. Abram, V. Yeh, M. C. Tringides, "Uniform, self-organized, seven-step height Pb/Si(111)-(7x7) islands at low temperatures," Physical Review B, vol. 61, R10602, April 15 2000.
- [5] Hiroshi Okamoto, Dongmin Chen, and Toshishige Yamada, "Competing Classical and Quantum Effects in Shape Relaxation of a Metallic Island," Physical Review Letters, vol 89, no. 25, Dec. 16 2002.

Cody Ray is studying mechanical engineering at Oregon State University, Corvallis, Oregon. He participated in the Science Undergraduate Laboratory Internship Program at Pacific Northwest National Laboratory, where he investigated "Power Grid Dynamics: Enhancing Power System Operation through Prony Analysis." As an undergraduate, he majored in applied mathematics at the University of Montana in Missoula. Mr. Ray is a member of the Society for Industrial and Applied Mathematics, the Mathematics Association of America, and PME. His hometown is Milton-Freewater, Oregon, and his interests include hiking, camping, and mathematical art.

Zhenyu Huang received his Ph.D. in electrical engineering from Tsinghua University, Beijing, China, in 1999. From 1998 to 2002, he conducted extensive research on power system analysis and control at McGill University (Canada), the University of Alberta (Canada), and the University of Hong Kong. He is currently a senior research engineer with the Energy Science and Technology Directorate, Pacific Northwest National Laboratory, Richland, Washington. His research interests include power system modeling and simulation, power system data analysis, and high performance computing applications. He is author of more than 40 peer-reviewed publications, and a Senior Member of the Institute of Electrical and Electronics Engineers (IEEE).

POWER GRID DYNAMICS: ENHANCING POWER SYSTEM OPERATION THROUGH PRONY ANALYSIS

CODY RAY AND ZHENYU HUANG

ABSTRACT

Prony Analysis is a technique used to decompose a signal into a series consisting of weighted complex exponentials and promises to be an efficient way of recognizing sensitive lines during faults in power systems such as the U.S. Power grid. Positive Sequence Load Flow (PSLF) was used to simulate the performance of a simple two-area-four-generator system and the reaction of the system during a line fault. The Dynamic System Identification (DSI) Toolbox was used to perform Prony analysis and use modal information to identify key transmission lines for power flow adjustment to improve system damping. The success of the application of Prony analysis methods to the data obtained from PSLF is reported, and the key transmission line for adjustment is identified. Future work will focus on larger systems and improving the current algorithms to deal with networks such as large portions of the Western Electricity Coordinating Council (WECC) power grid.

INTRODUCTION

Power system dynamics is highly complex. The number of interconnected nodes in the United States Power Grid exceeds any other man-made device on earth. It is the most complex system ever designed and is far from perfect. On August 10, 1996, the power grid had a massive blackout. A major system disturbance separated the Western Electricity Coordinating Council (WECC, formerly Western Systems Coordinating Council (WSCC)) system into four islands, interrupting service to 7.5 million customers for periods ranging from several minutes to about nine hours [1]. This very serious event led to an investigation of the reliability of the grid.

One of the outcomes from the investigation is the deployment of a Wide Area Measurement System (WAMS) across the WECC system. A WAMS network is a collection of Phasor Measurement Units (PMUs) and Phasor Data Concentrators (PDCs). WAMS provides high-speed GPS-time-synchronized phasor data, which can capture the dynamic behavior of a power grid.

One aspect of WAMS data analysis is to apply modal identification methods to identify major system oscillatory modes and damping information, which are excellent indicators of system stability status. PNNL (Pacific Northwest National Laboratory) has

been working with BPA (Bonneville Power Administration) for more than a decade developing algorithms and tools for WAMS data modal analysis. The Dynamic System Identification (DSI) Toolbox, jointly developed by PNNL and BPA, has been extensively used by many major power companies for WAMS data analysis, especially the Prony analysis function of this Toolbox.

With the modes and damping information, one would naturally ask what that information means to power system operators, in other words, how to use modal information to enhance power system operation.

This report summarizes initial results obtained working with power engineering researchers using modal information to identify key transmission lines for power flow adjustment to improve system damping. The results show that the method proposed and validated in this study is very promising.

This report is organized as follows: Basics of power system dynamics are first presented, followed by introductions to the methods and tools used in this study. The major part of the report is focused on the specific case studies and results, followed by a conclusion.

Power System Dynamics

Linearized form of power system dynamics can be described by a set of linear differential equations around an operation point:

$$\begin{aligned} \dot{x}(t) &= Ax(t) + Bu(t) \\ y(t) &= Cx(t) + Du(t) \end{aligned} \quad (1)$$

The homogeneous ($u(t) = 0$) solutions of the system are a series of exponential terms, written as the following:

$$y(t) = \sum_{i=1}^n c_i e^{\lambda_i t} = \sum_{i=1}^n c_i e^{(-\sigma_i \pm j\omega_i)t} = \sum_{i=1}^n A_i e^{-\sigma_i t} \cos(\omega_i t + \phi_i) \quad (2)$$

In equation (2), λ_i are the eigenvalues of the system, also known as the dynamic modes of the object system, with ω being the oscillatory angular frequency and σ being the damping factor.

The damping ratio is defined as:

$$\xi = \frac{\sigma}{\sqrt{\sigma^2 + \omega^2}} \cdot 100\% \quad (3)$$

Damping ratios are a key indicator of system dynamic stability as follows:

$$\begin{cases} \xi > \xi_0 \rightarrow \text{Stable System} \\ 0 < \xi < \xi_0 \rightarrow \text{Poorly Damped System} \\ \xi < 0 \rightarrow \text{Unstable System} \end{cases} \quad (4)$$

TOOLS AND METHODS

There are many methods for analyzing a signal, especially one generated from a system such as the power grid. One can analyze the frequency of the grid, and how it changes due to fluctuations in the supply and demand of power. One can also monitor the voltage across sections of the grid. All of these signals, however, demand that one's methods of analysis deal with noise effectively. Noise usually plagues such signals so that any direct application of mathematical techniques is stricken with error as output. Thus, it is common to pre-filter a signal with methods designed to reduce noise, smooth the signal, and yet retain important data. In reality, even the best filtering techniques fail to completely eliminate noise from the signal.

Two very important mathematical methods for understanding such a system are Fourier and Prony analysis (Figure 1). There are fundamental differences in how these methods are implemented and analyzed.

Fourier analysis, implemented with the fast Fourier transform (FFT), is a relatively fast operation. It can be used to dissect a signal into its constituent frequency components, approximating the phase, amplitude, and frequency of the components in the signal. Fourier analysis offers both a deep understanding of a signal and can be implemented in a powerful filtering algorithm.

Prony analysis also dissects a signal into many components, each consisting of an amplitude, phase and frequency, but goes further to estimate the damping coefficients of the signal. Thus Prony analysis is best suited to a system experiencing damping.

The DSI Toolbox is used to perform Prony analysis throughout this study. Positive Sequence Load Flow (PSLF), General Electric's

tool for power system dynamic simulation, was used to generate power system signals simulating a sample power grid stimulated by disturbances.

Prony Analysis

Prony analysis decomposes signals into damped sinusoidal waveforms, so the modes can be determined.

$$y(t) = \sum_{i=1}^q 2B_i e^{-\sigma_i t} \cos(\omega_i t + \phi_i) = \sum_{i=1}^q A_i e^{(-\sigma_i \pm j\omega_i)t} \quad (5)$$

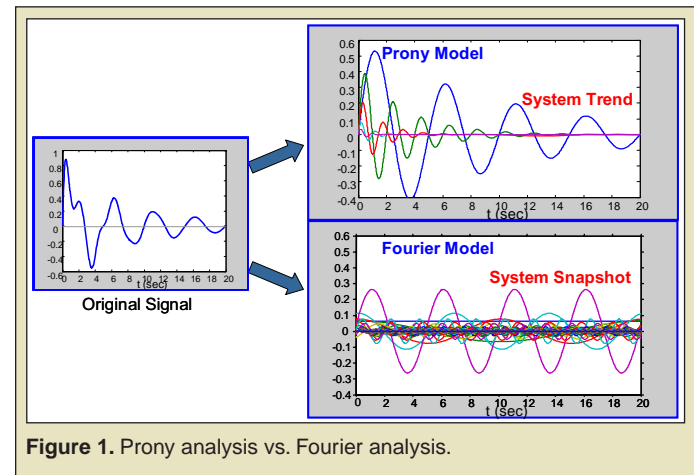


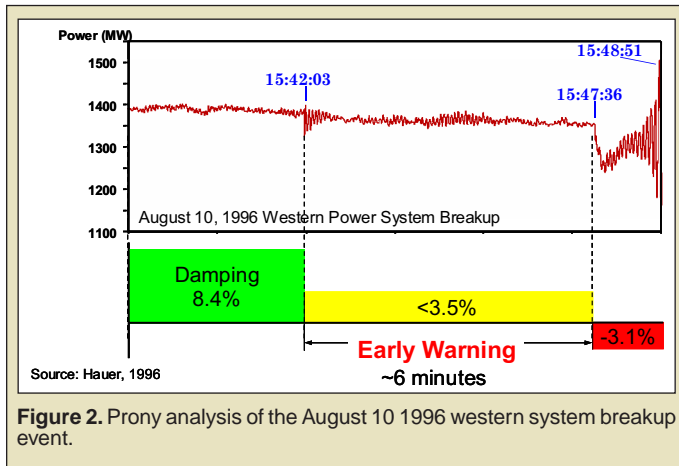
Figure 1. Prony analysis vs. Fourier analysis.

In comparison with Equation (2), Prony analysis results can be used to determine the key parameters of the system dynamics. With high-speed phasor measurement data, Prony analysis can be performed in a real-time manner, and system stability characteristics can be determined in real-time as well. This has been a monitoring function in industrial practice. Figure 2 shows an example of Prony analysis applied to the measured data of the 10 August 1996 western system blackout. One can see that after the first sign of system deterioration, there were about 6 minutes before the system broke up.

The Power System Monitoring (PSM) Toolset, or PSMtools, is a collection of processing utilities that is contained within the Dynamic System Identification (DSI) Toolbox developed by the Bonneville Power Administration (BPA) and the Pacific Northwest National Laboratory (PNNL). The DSI Toolbox is a Matlab version of BPA systems analysis tools that trace their origins to wide area control projects in the mid 1970's, and that have undergone extensive use and refinement since that time [1]. The DSI Toolbox contains Prony analysis tools, which are capable of importing data created by PSLF.

Research Plan

Can modal information be utilized for control and operation purposes? That is the fundamental question in this research. For the 10 August 1996 event, what should have been done during the 6 minutes shown in Figure 2? Using Prony analysis, the signal can be decomposed into a series of signals containing mode, damping, and amplitude information (see Figure 1). This study explores the capability of using the modal information to enhance power system operations.



Low damping is typically caused by long-distance heavy power transfer, which means a heavily stressed transmission system. Once low damping is detected/observed, one can re-dispatch generation or adjust load in certain areas to reduce system stress. Prony analysis provides residual information together with modal information. Residual information can serve as indicators of the sensitivity of the quantity with respect to the mode. This residual information can then be used to identify critical components where power transfer should be adjusted to improve damping.

Case Creation

A simple two-area-4-generator model [3] was obtained for use in PSLF. The model is shown in Figure 3. A baseline 1767MW load at bus 13 was used with output from each generator being about 700MW, as the model was stable at this point. Trial and error yielded an upper bound for oscillatory behavior, which was approximately +79MW change in generation and load. Each case was created by incrementing the generation of G1 by 15.8MW (= 79MW/5), and also increasing/decreasing the load on bus 13 by the same amount. So there are 11 resulting cases including the original base case. This new model was then allowed to run for one second. At one second, the system experienced a programmed line fault at bus 3 for 0.05 seconds. The fault was then cleared and the simulation was allowed to run for another 20 seconds. The resulting data was then exported, using a script, to a file that the DSI toolbox could import.

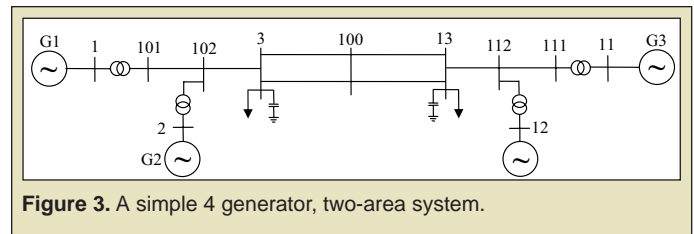


Figure 3. A simple 4 generator, two-area system.

RESULTS

The 11 cases are simulated using PSLF. Each case has a different loading level and exhibits different dynamic behavior. In this section, the time-domain dynamic simulation results and the frequency-domain Prony analysis results (modal information) are presented. These cases test the possibility of using modal information to improve power system operation.

The simulation yielded very different behavior for each case. As shown in Figure 4, the upper-limit increase of 79MW in load and generation resulted in an unstable system, with high frequency oscillations. This contrasts with the increase of only 15.8MW, in which a barely noticeable oscillation occurs immediately following the line fault, but is then damped out quickly, resulting in a stable system.

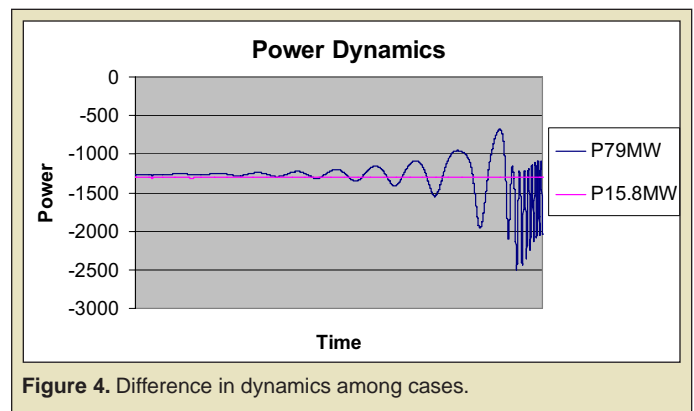


Figure 4. Difference in dynamics among cases.

The oscillatory behavior results from a system that is over stressed or has too much power being transferred between areas. A system that becomes unstable following an event like the line fault in our simulation, can lead to terribly damaging consequences. Power grids can also experience this behavior; in fact there are oscillations constantly occurring in real systems. Most of these are small with respect to the overall size of the grid and are quickly damped out. A very large scale event however, such as the tripping of an entire generator, can result in a situation similar to the 79MW case. Currently, one way to prevent the entire system from becoming unstable is to dispatch load or generation in key areas to lead to a high damping coefficient for the system. Prony analysis can add insight into what areas are most sensitive.

Damping ratios are correlated with changes in load/generation, with the overall damping ratio decreasing with more load and generation and hence greater system stress. Thus, as the power is increased in this system, the ability of the system to reach stability after a fault is compromised. This agrees with Figure 4; the system

becomes more unstable with heavier load and generation. The larger the event, the more unlikely the system will naturally damp out the dangerous oscillations that occur. This emphasizes the importance for finding a method of recognizing key lines/areas within a system that, when adjusted, can result in higher damping coefficients and thus a more stable system.

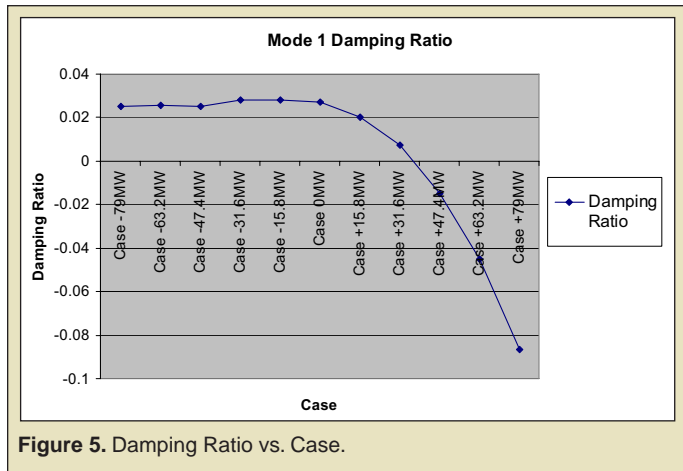


Figure 5. Damping Ratio vs. Case.

Prony analysis yields residue information that can be used to identify important lines that the overall modal information depends upon. Thus, these lines are the key lines to adjust to increase stability in the time of an event. Figure 6 shows a plot of the amplitude of the residue information for each line in each case. It readily becomes obvious that line 13-112 has the greatest amplitude, and thus must be of great importance.

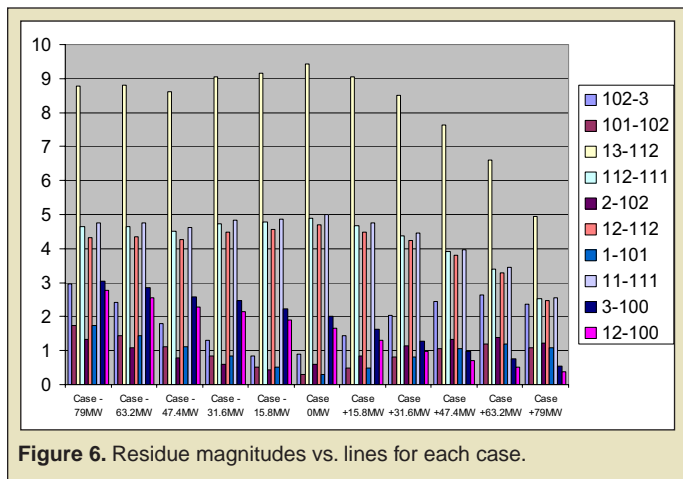


Figure 6. Residue magnitudes vs. lines for each case.

After this insight is obtained, another plot of the overall system damping ratio versus the key line loading further suggests this line is of the utmost importance in the stability of this system. Figure 7 displays a strongly correlated plot between system damping and key line loading. This is another strong indication that the damping ratio could be affected by adjustments on this line.

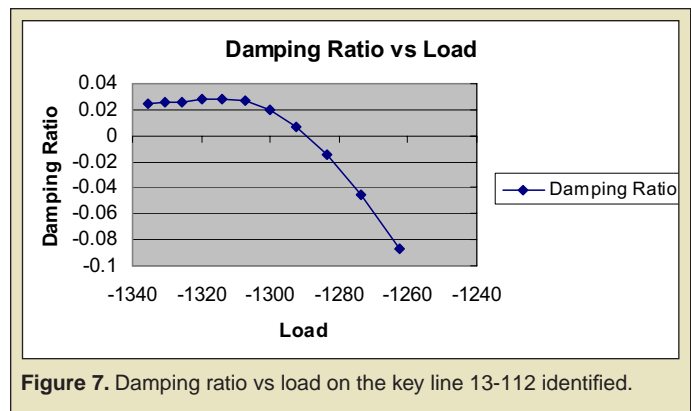


Figure 7. Damping ratio vs load on the key line 13-112 identified.

The data from each case strongly correlates the damping ratio to load levels. Using the residue information output from Prony analysis, every case yields the same result: the line most sensitive to changing load and generation is line 13-112 (see Figure 6). This line is therefore the most important as far as overall system stability. Adjusting the loading on this line would help to damp the inter-area oscillations between the two areas.

CONCLUSION

New tools such as Prony analysis, coupled with simulation models and already existing techniques, are enormously useful for interpreting data from systems such as the simple system used in this research. The next step is to apply the techniques used above to larger systems, with complexity great enough to preclude intuitive human responses (such as the IEEE 14 bus system and the WECC system). A system such as the WECC power grid is entirely too complex for crude adjustments based on intuition and past experience. Prony analysis and the resulting modal and residual information obtained could greatly increase the ability to decide what lines/areas to adjust to prevent a cascading failure of the system.

ACKNOWLEDGMENTS

This research was conducted at the Pacific Northwest National Laboratory. I thank the U.S. Department of Energy, Office of Science for giving me the opportunity to participate in the SULI program and to engage in this incredible learning experience. Special thanks go to my mentor Zhenyu Huang for his knowledge, patience, and humor. I thank Ning Zhou for his knowledge and assistance with the project. I also thank Karen Wieda for her excellent management of the SULI program at PNNL.

REFERENCES

- [1] J. F. Hauer, PSMtools: Matlab Utilities for Processing of Power System Response Records.
- [2] W.S.C.C. Disturbance Report for August 10th, 1996 15:48 PAST.
- [3] P. Kundur, "Power System Stability and Control", McGraw-Hill, 1994.

Rachel Robeson participated in the spring 2005 Science Undergraduate Laboratory Internship Program at Oak Ridge National Laboratory (ORNL). As an undergraduate, she attended Earlham College in Richmond, Indiana.

Peter V. Bonnesen is a research staff scientist in the Chemical Sciences Division and the Center for Nanophase Materials Sciences at the Oak Ridge National Laboratory (ORNL). He received a B.S. in chemistry from Lafayette College, a Ph.D. in inorganic chemistry from the University of California at Los Angeles, and completed a postdoctoral appointment at the

University of California at Berkeley before joining ORNL. He has been involved in the development of a number of processes relating to environmental restoration and the removal of contaminants, including the Caustic-Side Solvent Extraction (CSSX) process for separation of radioactive cesium from nuclear waste, and a process that utilizes a bifunctional anion-exchange resin for the removal of perchlorate and pertechnetate from groundwater. More recently, his research interests have included the design and synthesis of molecules for cation and anion sequestration, the preparation of novel materials for fuel cell applications, and the synthesis of deuterated materials for neutron studies.

SYNTHESIS OF NOVEL CROWN ETHERS BEARING THE *exo-cis*-2,3-NORBORNYL GROUP AS POTENTIAL Na⁺ AND K⁺ EXTRACTANTS

RACHEL M. ROBESON AND PETER BONNESEN

ABSTRACT

The synthesis of a series of novel dinorbornyl-16-crown-5 and dinorbornyl-18-crown-6 ethers that incorporate the *exo-cis*-2,3-norbornyl moiety within the macrocycle framework is described. The key starting material for the crown ethers, *exo-cis*-2,3-norbornanediol, was successfully prepared on a large (>30g) scale in 88% yield from norbornylene by osmium tetroxide-catalyzed hydroxylation. The *syn* and *anti* isomers of the dinorbornyl-16-crown-5 ether family were prepared using diethylene glycol with ring closure achieved using a methallyl linkage. The isomers *cis-syn-cis* and *cis-anti-cis* di-norbornano-15-methylene-16-crown-5 (**6A** and **6B**) could be separated using column chromatography, and a single crystal of the *syn* isomer **6A** suitable for X-ray crystal structure analysis was obtained, thereby confirming the *syn* orientation. The *syn* and *anti* isomers of the dinorbornyl-18-crown-6 ether family were successfully prepared employing a different synthetic strategy, involving the potassium-templated cyclization of two *bis*-hydroxyethoxy-substituted *exo-cis*-2,3-norbornyl groups under high dilution conditions. Attempts to fully separate *cis-syn-cis* di-norbornano-18-crown-6 (**10A**) and *cis-anti-cis* di-norbornano-18-crown-6 (**10B**) from one another using column chromatography were unsuccessful. All intermediates and products were checked for purity using either thin layer chromatography or gas chromatography, and characterized by proton and carbon NMR. Crown ethers **6AB** and **10AB** are to our knowledge the first crown ethers to incorporate the *exo-cis*-2,3-norbornyl moiety into the crown ring to be successfully synthesized and characterized.

INTRODUCTION

The ability to coordinate and mobilize sodium (Na⁺) and potassium (K⁺) ions is of great interest and importance in areas as diverse as medical applications, industrial processes, and even nuclear waste remediation. Ever since the discovery by Charles Pedersen in 1967 [1] that cyclic polyethers or “crown ethers” have the ability to effectively complex metal cations (see Figure 1 for examples) there have been tremendous research efforts aimed at understanding and controlling the factors that influence both the metal-ion binding strength and the selectivity. Among these factors are the basicity of the ether oxygens, the size and shape of the crown cavity, and the degree of “preorganization” of the cavity. As observed by Cram [2], preorganization can reduce conformational changes that occur

during metal ion complexation, thereby increasing metal ion binding strength.

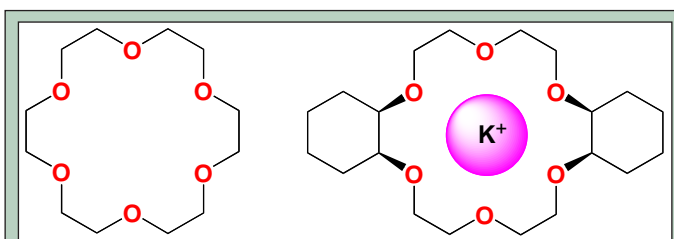
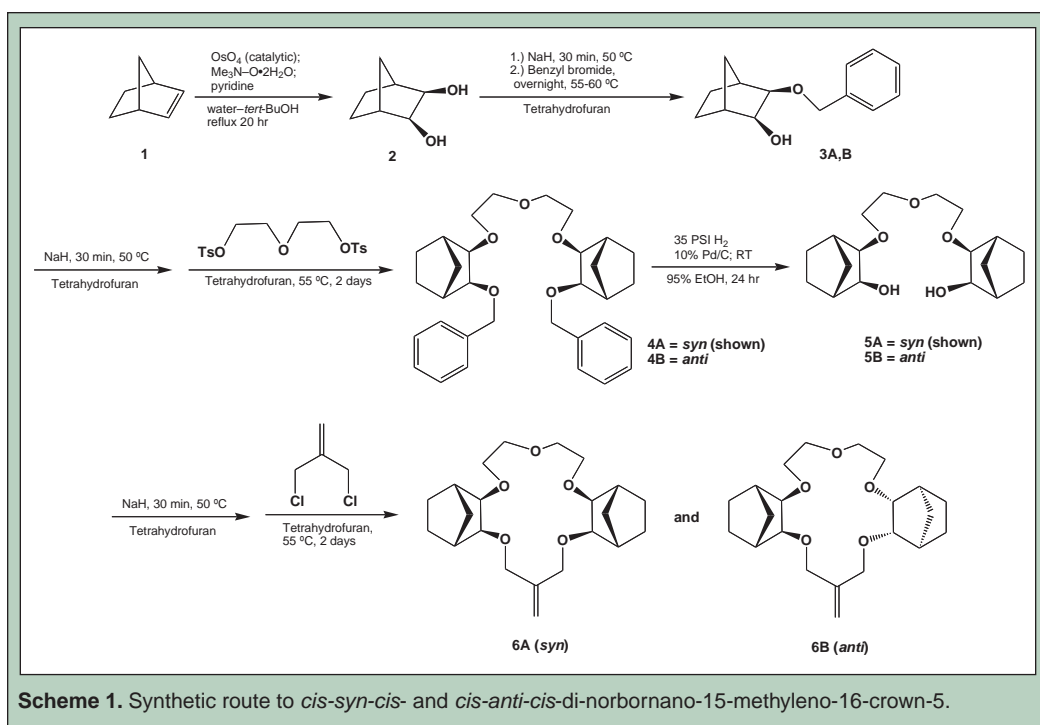


Figure 1. Two examples of crown ethers: on the left 18-crown-6, on the right, a representation of potassium complexed by *cis-syn-cis*-diclohexano-18-crown-6.



purified as described by Peletier [4]. Sodium hydride was used as a 57% dispersion in mineral oil. Diethyleneglycol ditosylate was previously prepared following the procedure described by Ouchi et al [5]. Ozonolysis was performed using an OZONOLOGY Ozone Generator. A Hewlett Packard 6850 gas chromatograph was used for all GC analyses. Proton and carbon (proton decoupled) NMR spectra were obtained in CDCl_3 , unless otherwise noted (acetone- d_6), on a Bruker Avance DRX 400MHz spectrometer. Proton chemical shifts (See Table 1) were referenced to internal tetramethylsilane, and carbon chemical shifts to the solvent peaks (77.0ppm for CDCl_3 , or 29.8ppm for acetone- d_6).

At ORNL there is interest in developing a novel class of crown ethers with enhanced binding strength for Na^+ (and to a lesser extent for K^+), for use in nuclear waste remediation applications, though it is anticipated such crown ethers would find many other important uses. In the nuclear waste application, the objective was to develop lipophilic crown ethers that could be used in solvent extraction processes for the removal of sodium and potassium hydroxide and nitrate, which could then be potentially recycled for use in other processes. Previous research demonstrated that the crown ether *cis-syn-cis*-dicyclohexano-18-crown-6 (DCH18C6), in combination with lipophilic phenols or fluorinated alcohols, could be used to enhance extraction of sodium hydroxide [3]. However, crown ethers that are more preorganized for sodium would be expected to possess higher binding strength for sodium, and accordingly could be far more effective than DCH18C6. One way preorganization might be enhanced is by rigidifying the ether oxygens, and molecular modeling has suggested that use of *exo-cis*-norbornanediol, in which both oxygens are *exo* to the bridgehead and are more rigidly directed toward the center of a binding cavity with a radius specific to that of the Na^+ ion, may confer higher binding strength than the more flexible *cis*-1,2-cyclohexanediol moiety that is present in DCH18C6. Accordingly, for the first time, a series of 16-crown-5 and 18-crown-6 ethers incorporating the *exo-cis*-norbornanediol moiety have been synthesized, and their preparation is described.

MATERIALS AND METHODS

General

All solvents and chemical reagents were used as received without further purification, with the exception of *p*-tosyl chloride, which was

Synthesis of *cis-syn-cis* and *cis-anti-cis* di-norbornano-15-methylene-16-crown-5 (6AB)

The synthesis was performed as outlined in Scheme 1 and as described below.

Exo-cis-2,3-norbornanediol (2)

Norbornylene (28.26g, 0.300mol), trimethylamine N-oxide dihydrate (45.01g, 0.405mol), pyridine (25.4g), *tert*-butanol (300mL), and water (200mL) were added to a 3-neck 1-L round bottom flask equipped with an addition funnel containing a solution of OsO_4 (0.23g, 0.90mmol) in *tert*-butanol [6]. The OsO_4 solution was slowly added to the reaction mixture at room temperature with constant stirring. The reaction mixture was then refluxed for ~19 hours at 100°C. The reaction was allowed to cool to room temperature whereupon 20% aqueous sodium bisulfite (160mL) solution was added with stirring followed by *in vacuo* removal of *tert*-butanol. A solution of saturated sodium chloride (200mL) was added to the reaction mixture, which was then extracted with diethyl ether (3 x 300mL). The combined ether extracts were dried over anhydrous Na_2SO_4 and the solution concentrated and placed in the refrigerator overnight, affording a first crop of 2 (15.5g) as highly pure white crystalline flakes ($\geq 99\%$ by GC) suitable for subsequent reaction. MP 139–140°C (lit [6] 139.5–140.5°C). An additional 18.4g of material of ~98% purity by GC with slightly lower melting point can be obtained from the filtrate, affording a combined yield of 33.9g (88%).

Bicyclo[2.2.1]-3-benzyloxy-2-heptanol (3AB)

Exo-cis-2,3-norbornanediol (10.0g, 78.0mmol) was dissolved in 200mL dry THF in a 1-L 3-neck round bottom flask under argon. Sodium hydride (3.61g, 85.8mmol) was added to the stirred contents using a Merlic-type solid addition funnel, and the solution warmed to 50°C and stirred for 30 minutes. A solution of benzylbromide (12.0g, 70.2mmol) in dry THF (200mL) was then added dropwise to the stirred contents under argon at 50°C. The progress of the reaction was followed by TLC using a mixture of ethyl acetate and hexanes (1:9) and GC. After 16 hours at 50°C the reaction was judged complete. After cooling, excess sodium hydride was hydrolyzed by slow addition of methanol. The solvents were then removed *in vacuo*, and the crude product oil purified by silica gel (70/230 mesh) chromatography to afford racemic **3** as a pale yellow oil (6.3g, 45%). ¹H NMR: δ 0.89–1.07 (m, 3H), 1.40–1.42 (m, 2H), 1.77 (d, 1H, *J* = 10 Hz), 2.14 (s, 1H), 2.24 (s, 1H), 3.38–3.41 (m, 2H), 3.67 (s, 1H), 4.51–4.60 (m, 2H), 7.26–7.30 (m, 5H). ¹³C NMR: δ 23.88, 24.40, 31.76, 39.32, 42.86, 72.19, 74.64, 81.79, 127.26, 127.43, 128.10, 137.59.

Di(ethylene glycol) di(exo-3-benzyloxy-exo-2-bicyclo [2.2.1] heptyl) ether (4AB)

To a solution of **3AB** (5.70g, 26.1mmol) in dry THF (50mL) was added sodium hydride (1.265g, 30.0mmol) under argon, and the reaction warmed to 50°C with stirring for 30 minutes. A solution of diethyleneglycol ditosylate (4.99g, 12.0mmol) in dry THF (50mL) was added dropwise under argon over 10 minutes to the stirred reaction mixture at 55–60°C, and heating continued at 55–60°C for two days, during which the reaction's progress was monitored by TLC using ethylacetate and hexanes (1:3). After 2 days the reaction was judged complete, and after cooling, the reaction mixture was treated with a few mL of 95% ethanol. Solvents were evaporated *in vacuo*, and the residue was extracted into 100mL of dichloromethane, washed with 0.1M HCl (50mL) and brine (50mL), and dried over anhydrous Na₂SO₄. The solvents were then removed *in vacuo*, and the crude product oil purified by silica gel (70/230 mesh) chromatography to afford **4AB** as a clear oil (3.594g, 59%). ¹H NMR: δ 0.94–1.06 (m, 6H), 1.40–1.44 (m, 4H), 1.89–1.92 (m, 2H), 2.25 (s, 4H), 3.36–3.43 (m, 4H), 3.59–3.65 (m, 8H), 4.51–4.63 (m, 4H), 7.23–7.37 (m, 10H). ¹³C NMR: δ 24.68, 24.80, 32.97, 40.26, 40.45, 69.89, 70.68, 72.13, 83.00, 84.66, 127.58, 17.92, 128.39, 139.10.

Diethylene glycol di(exo-3-hydroxy-exo-2-bicyclo [2.2.1] heptyl) ether (5AB)

To a solution of **4AB** (3.594g, 7.09mmol) in 95% ethanol (35mL) in an Ace-threaded hydrogenation vessel, 10% Pd/C catalyst (700mg) was added. The solution was placed on a Parr shaker and was hydrogenated under 35 PSI hydrogen for 6 hours, after which additional catalyst (110mg) was added before continuing with the hydrogenation for another 19 hours. The catalyst was removed by filtration through Celite, and the filtrate was diluted with dichloromethane (75mL), and washed with 0.1M HCl (75mL),

water (50mL), and dried over anhydrous Na₂SO₄. Removal of the solvents afforded 1.87g (81%) of **5AB** that was sufficiently pure as judged by NMR to use without further purification. ¹H NMR: δ 0.99–1.07 (m, 6H), 1.42–1.45 (m, 4H), 1.76–1.78 (m, 2H), 2.14–2.21 (m, 4H), 3.33–3.35 (m, 2H), 3.60–3.85 (m, 12H). ¹³C NMR: δ 24.00, 24.75, 31.98, 40.00, 40.14, 42.95, 42.97, 69.95, 70.03, 70.26, 70.29, 74.96, 75.02, 83.30, 83.39.

Cis-syn-cis- and cis-anti-cis-di-norbornano-15-methylene-16-crown-5 (6AB)

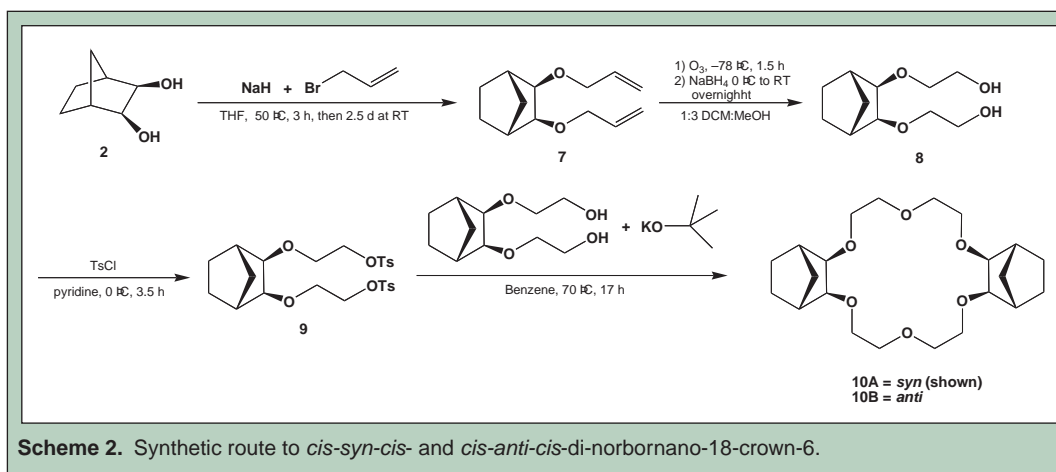
To a solution of **5AB** (1.87g, 5.7mmol) in dry THF (200mL) sodium hydride (0.607g, 14.3mmol) was added under argon at room temperature. The reaction mixture was warmed to ~50°C and stirred for 30 minutes, after which a solution of methallyl dichloride (0.82g, 6.6mmol) in dry THF (100mL) was slowly added dropwise over the course of an hour. The reaction mixture was heated at 55–60°C for two days, during which the reaction's progress was monitored by TLC using ethylacetate and hexanes (1:3), and GC. After 2 days the reaction was judged complete, and after cooling and treatment with a few mL of 95% ethanol, the mixture was diluted with dichloromethane (200mL), washed with 0.1M HCl (200mL), and water (200mL), and dried (anhydrous Na₂SO₄). Removal of the solvents *in vacuo* afforded the crude product mixture (2.171g). Chromatography on 40-micron silica gel with ethyl acetate and hexanes (1:2) allowed partial separation of the *cis-anti-cis* isomer (**6B**) as an oil, and the *cis-syn-cis* isomer (**6A**) as a low melting solid. The combined yield on **6AB** was 1.27g (59%). Slow evaporation of a 1:2 ethyl acetate/hexane solution of **6A** afforded a single crystal suitable for X-ray crystallographic analysis revealing **6A** to be the *cis-syn-cis* isomer. **6A** ¹H NMR: δ 0.96–1.06 (m, 6H), 1.42–1.45 (m, 4H), 1.84–1.87 (m, 2H), 2.23 (s, 4H), 3.40 (s, 4H), 3.51–3.76 (m, 8H), 4.07 (d, 2H, *J* = 12 Hz), 4.20 (d, 2H, *J* = 12 Hz), 5.12 (s, 2H). ¹³C NMR: δ 24.66, 24.92, 32.89, 39.45, 40.88, 69.73, 70.88, 71.58, 82.49, 84.74, 111.15, 144.19. **6B** ¹H NMR: δ 0.93–1.06 (m, 6H), 1.43–1.48 (m, 4H), 1.87–1.89 (m, 2H), 2.21–2.26 (m, 4H), 3.37 (d, 2H, *J* = 8 Hz), 3.42 (d, 2H, *J* = 4 Hz), 3.52–3.64 (m, 6H), 3.73–3.76 (m, 2H), 4.01 (d, 2H, *J* = 13 Hz), 4.29 (d, 2H, *J* = 13 Hz) 5.12 (s, 2H). ¹³C NMR: δ 24.55, 25.01, 33.00, 39.18, 41.27, 69.44, 70.17, 72.45, 83.44, 84.89, 110.22, 144.87.

Synthesis of cis-syn-cis and cis-anti-cis di-norbornano-18-crown-6 (10AB)

The synthesis was performed as outlined in Scheme 2 and as described below.

Exo-cis-2,3-bis allyloxy-bicyclo [2.2.1] heptane (7)

Allylbromide (18.9g, 156mmol) and **2** (6.43g, 50.0mmol) were dissolved in dry THF (100mL) under argon. Sodium hydride (6.30g, 150mmol) was slowly added, and the reaction mixture was allowed to stir for 1 hour at room temperature before being heated to 50°C for ~60 hours, with the progress of the reaction followed by GC. After cooling to room temperature, methanol (~2mL) was added, and the solvents evaporated *in vacuo*. The residue was



Exo-cis-2, 3-bis (2'-hydroxyethoxy)-bicyclo [2.2.1] heptane di-*p*-toluene sulfonate (9)

A solution of recrystallized tosyl chloride (4.7g, 25.0mmol) in pyridine (5mL) was cooled under argon to 0°C in an ice bath. A solution of 8 (2.17g, 10.0mmol) in pyridine (mL) was added dropwise to the reaction mixture, and stirring was continued for 3 hours at 0°C. Water (5mL) was added

extracted with dichloromethane (2 x 75mL), washed with water (75mL) and brine (75mL), dried over Na₂SO₄, and evaporated solvents to obtain 10.44g of crude 7. Chromatography on silica gel (70/230 mesh) using ethyl acetate/hexanes (1:9) as an eluent gave purified 7 (5.236g, 50%). ¹H NMR: δ 0.96–1.01 (m, 2H), 1.05–1.08 (m, 1H), 1.42–1.48 (m, 2H), 1.87–1.90 (m, 1H), 2.25 (m, 2H), 3.40 (d, 2H, *J*₁ = 1.5 Hz), 4.05 (d, 4H, *J* = 5.6 Hz), 5.14 (dd, 1H, *J*₁ = 1.2 Hz, *J*₂ = 10.4 Hz), 5.27 (dd, 1H, *J*₁ = 1.2 Hz, *J*₂ = 17.2 Hz), 5.89–5.99 (m, 1H). ¹³C NMR: δ 24.75, 32.92, 40.29, 71.45, 83.22, 116.34, 135.38.

Exo-cis-2,3-bis (2'-hydroxyethoxy)-bicyclo [2.2.1] heptane (8)

A solution of 7 (5.00g, 24.0mmol) in dichloromethane and methanol (1:3) was placed under argon in a 3-neck round bottom flask (300mL) equipped with a dry ice cold finger condenser with a CaCl₂ drying tube. An argon/ozone bubbler inlet was attached to one of the side arms of the flask. The reaction mixture was cooled to –78°C under argon with stirring; the argon inlet was replaced with an inlet from the ozone generator, and ozone (~5% O₃ in O₂) was bubbled through the solution, with stirring, until a blue color (signifying the presence of excess ozone) persisted for 15 minutes. The ozone inlet was then replaced with an argon inlet; argon was bubbled through the solution for 10 minutes during which the solution became clear. The –78°C bath was replaced with an ice water bath and NaBH₄ (5.02g, 133mmol) was slowly added to the reaction using a Merlic-type solid addition funnel. Once the NaBH₄ was added, the ice water bath was removed, and the reaction allowed to stir at room temperature for ~20 hours. The solvents were removed *in vacuo*, and the residue dissolved in dichloromethane (150mL) and water (75mL), with 1 M HCl (25mL) added. The layers were separated and the organic layer was washed with brine (100mL). The aqueous layer was back-extracted with dichloromethane (100mL), and the combined dichloromethane layers were dried over anhydrous Na₂SO₄. The solvent was evaporated to afford 8 (4.19g, 81%) of sufficient purity to use in the subsequent reaction without further purification. ¹H NMR: δ 1.0–1.02 (m, 2H), 1.09 (d, 1H, *J* = 10 Hz), 1.47–1.49 (m, 2H), 1.84 (d, 1H, *J* = 10 Hz), 2.25 (s, 2H), 3.44 (s, 2H), 3.49–3.76 (m, 8H), 3.99 (s, 2H). ¹³C NMR: δ 24.58, 32.81, 40.21, 61.71, 71.93, 83.85.

to stop the reaction, and the mixture was stirred for 15 minutes, and then transferred to a 1-L separatory funnel. Refrigerated water (100mL) and diethyl ether (100mL) were added to the funnel; the organic phase was separated and washed with cold 4M HCl (75mL) and water (50mL), and dried over anhydrous Na₂SO₄. The solvent was removed *in vacuo* and the product oil dried under high vacuum for ~1 hour to obtain 9 (3.8g, 92%) of sufficient purity for direct use in the subsequent reaction. ¹H NMR: δ 0.92–0.94 (m, 2H), 0.99 (d, 1H, *J* = 9.9 Hz), 1.40–1.42 (m, 2H), 1.67 (d, 1H, *J* = 9.9 Hz), 2.11 (s, 2H), 2.44 (s, 6H), 3.31 (s, 2H), 3.47–3.67 (m, 4H), 4.08–4.12 (m, 4H), 7.33 (d, 4H, *J* = 8.2 Hz), 7.78 (d, 4H, *J* = 8.2 Hz). ¹³C NMR: δ 21.62, 24.55, 32.72, 40.29, 67.96, 69.60, 84.54, 127.91, 129.82, 133.03, 144.74.

Cis-syn-cis- and cis-anti-cis-di-norbornano-18-crown-6 (10AB)

A solution of 8 (1.54g, 7.12mmol) and 9 (3.75g, 7.15mmol) dissolved in dry benzene (230mL) were combined in a 3-neck round bottom flask under argon. Potassium *tert*-butoxide (2.72g, 24.2mmol) contained in a Merlic-type solid addition funnel was slowly added under argon to the solution at room temperature with stirring. The solution was then heated to 60°–65°C under argon for ~17 hours and monitored for completion by TLC. Upon cooling, a precipitate formed and was removed by filtration. The filtrate was washed with water (2 x 150mL). The aqueous layers were back extracted with benzene (50mL); the benzene layers were then combined and dried over anhydrous Na₂SO₄. The solvent was removed *in vacuo*; the residue was further dried by oil pump vacuum to obtain crude 10AB (3.30g). Chromatography on silica gel (40 micron) using 95% ethanol as eluent gave 10AB as mixed isomers as a solid (0.786g, 28%). Earlier fractions were enriched in one isomer, and latter fractions enriched in the other, but separation was not achieved using these chromatographic conditions. ¹H NMR (acetone-d₆): δ 0.98–1.02 (m, 6H), 1.41–1.43 (m, 4H), 1.78–1.82 (m, 2H), 2.14 (s, 4H), 3.33–3.38 (m, 4H), 3.55–3.67 (m, 16H). ¹³C NMR (acetone-d₆): δ 25.22, 25.27, 33.35, 33.45, 41.05, 41.20, 70.67, 70.70, 70.93, 71.10, 84.94, 84.99.

RESULTS AND DISCUSSION

Synthesis of di-norbornano-15-methylene-16-crown-5 (6AB)

The synthesis of *exo-cis* diol **2** has been obtained in high yield (88%) and high purity ($\geq 98\%$ by GC) through the use of catalytic OsO_4 [6,8]. The course of this reaction is *syn* hydroxylation resulting in the expected *exo-cis* stereochemistry. The OsO_4 -catalyzed procedure affords diol **2** in a significantly higher yield compared to previous reactions employing stoichiometric KMnO_4 [7,9] (40–52%). The crown ethers **6AB** were prepared from **2**, as shown in Scheme 1, using diethylene glycol and methallyl linkages. Monobenzyl protection of **2** afforded enantiomeric pair **3AB**, which was separated from unreacted **2** and dibenzylated **2** by silica-gel column chromatography. Reaction of **3AB** with diethylene glycol ditosylate produced **4AB** in reasonable yield (59%) as an equimolar mixture of the *syn* and *anti* isomers revealed by carbon-13 NMR. Removal of the benzyl groups proceeded well using standard Pd/C hydrogenation conditions [10] to give diol **5AB**. The cyclization of **5AB** was initially attempted using 1,3-propanediol ditosylate, but was unsuccessful due to elimination. Methallyl dichloride, which does not possess any beta-hydrogens for elimination, was employed to successfully complete the cyclization; thereby, forming **6AB** in a combined 59% isolated yield. The *syn* and *anti* isomers were distinguishable by GC with some separation possible by column chromatography (40 micron silica gel) with ethylacetate/hexanes (1:3), affording a product distribution of ca. 35% pure **6A** as a solid, ca. 20% mixed **6A** and **6B** fractions, and ca. 45% pure **6B** as an oil. It was not possible to unambiguously determine which isomer was *syn* and *anti* by NMR; however, X-ray crystallography on a single crystal of **6A** revealed **6A** to be the *syn* isomer (Figure 2), indicating **6B** as the *anti* isomer.

Synthesis of cis-syn-cis and cis-anti-cis dinorbornano-18-crown-6 (10AB)

The synthesis of **10AB** from **2** was accomplished employing a technique similar to that reported by Whitman et al [11] for the synthesis of *trans-syn-trans*-dicyclohexyl-18-crown-6 from *trans*-cyclohexane-1,2-diol. Allylation of **2**, obtaining bis-allyl **7**, proceeded well, but the final yield of pure product was reduced a bit (to 50%)

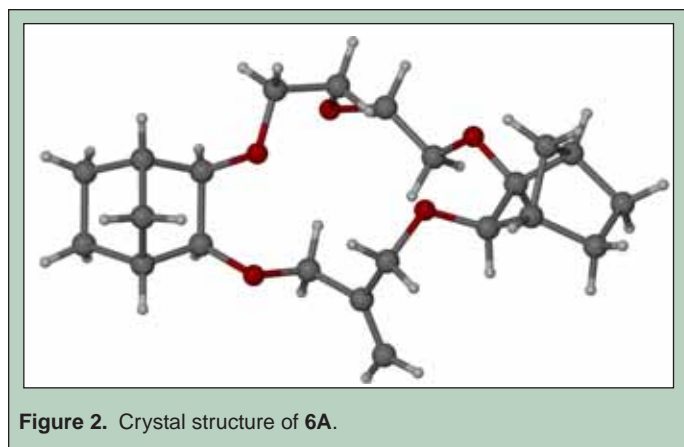
during isolation by column chromatography. Ozonolysis of **7**, followed by reduction of the ozonide using NaBH_4 to afford diol **8**, proceeded in good yield (81%). A portion of **8** was converted to ditosylate **9** in high yield (92%), and equimolar amounts of **8** and **9** were reacted together under high dilution conditions in benzene using potassium *tert*-butoxide to afford **10AB** in 28% isolated yield following chromatography as an isomeric mixture.

CONCLUSION

Crown ethers **6AB** and **10AB**, which to our knowledge are the first crown ethers to incorporate the *exo-cis*-2,3-norbornyl moiety into the crown ring, have been successfully synthesized. Purification and separation of **6AB** isomers was achieved; however, separation of **10A** from **10B** requires further investigation. Column chromatography provided purified mixed-isomer material, but yielded no distinct separation of the **10AB** isomers. Future work toward separating **10A** from **10B** may include separation methods utilizing differences in solubility properties between each isomer either as the free crown or as a complex with an ion pair. Future research will evaluate the sodium and potassium binding properties of **6A**, **6B**, and **10AB** and compare to the binding properties of crown ethers such as DCH18C6 and octamethyl-16-crown-5.

ACKNOWLEDGMENTS

This research was conducted under the project: "Ion Recognition Approach to Volume Reduction of Alkaline Tank Waste by Separation of Sodium Salts" sponsored by the U.S. Department of Energy, Environmental Management Sciences Program, Office of Science. A special thanks to Oak Ridge National Laboratory, SULLI, ORSS, and Peter V. Bonnesen, of the Chemical Separations Group in the Chemical Sciences Division.



REFERENCES

- [1] Pedersen, C.J. (1967) Cyclic Polyethers and Their Complexes with Metal Salts. *J. Am. Chem. Soc.* 89, 7017-7036.
- [2] Cram, D.J. (1983) Cavitands: Organic Hosts with Enforced Cavities. *Science*, 219, 1177-1183.
- [3] Levitskaia, T.G.; Bonnesen, P.V.; Chambliss, C.K.; Moyer, B.A. (2003) Synergistic Pseudo-Hydroxide Extraction: Synergism and Anion Selectivity in Sodium Extraction Using a Crown Ether and a Series of Weak Lipophilic Acids. *Anal. Chem.* 75, 405-412.
- [4] Pelletier, S.W. (1953) The Purification of p-Toluenesulfonyl Chloride. *Chem. Ind.* 1034.
- [5] Ouchi, M.; Inoue, Y.; Kanzaki, T.; Hakushi, T. (1984) Molecular Design of Crown Ethers. 1. Effects of Methylene Chain Length: 15- to 17-Crown-5 and 18- to 22-Crown-6. *J. Org. Chem.*, 49, 1408-1412.
- [6] Ray 1980: Ray, R.; Matteson, D.S. (1980) Osmium Tetroxide Catalyzed Hydroxylation of Hindered Olefins. *Tetrahedron Lett.*, 21, 449-450.
- [7] Wiberg 1957: Wiberg, K.B.; Saegbarth, K.A. (1957) The Mechanisms of Permanganate Oxidation. IV. Hydroxylation of Olefins and Related Reactions. *J. Am. Chem. Soc.* 79, 2822-2824.
- [8] Van Rheenen, V.; Cha, D.Y.; Hartley, W.M. (1978) Catalytic Osmium Tetroxide of Olefins: cis-1,2-cyclohexanediol. *Org. Syn.*, 58, 43-52.
- [9] Sauers, R.R.; Odorisio, P.A. (1979) Synthesis and Chemistry of Some Orthoesters of Bicyclo[2.2.1]heptanediols. *J. Org. Chem.*, 44, 2980-2983.
- [10] Heathcock, C.H.; Ratcliffe, R. (1971) A Stereoselective Total Synthesis of the Guaiazulenic Sesquiterpenoids α -Bulnesene and Bulnesol. *J. Am. Chem. Soc.* 93, 1746-1757.
- [11] Hayward, R.C.; Overton, C.H.; Whitman, G.H. (1976) Chiral Crown Ethers Derived from (+)-(1S,2S)-trans-Cyclohexane-1,2-diol. *J. C. S. Perkin. I*, 2413-2415.

Alessandra (Sondy) Springmann is an intern in the SULI Program at Stanford Linear Accelerator Center, where she researches host galaxy shapes of X-shaped radio sources. She studied astrophysics as an undergraduate at Wellesley College, Wellesley, Massachusetts. Ms. Springmann is a member of the American Astronomical Society, and the Society of Physics Students. She grew up in Point Reyes Station, California, and she enjoys photography, cooking, sailing, aikido, fire poi, frisbee, and hiking.

C.C. (Teddy) Cheung is a postdoc at the Kavli Institute for Particle Astrophysics and Cosmology at Stanford University. He received his Ph.D. from Brandeis University in 2004, for work on relativistic jets in active galactic nuclei, and continues research on cosmic radio sources. He came to Stanford as a Karl Jansky fellow of the National Radio Astronomy Observatory, after an initial year at the Massachusetts Institute of Technology on the same fellowship.

HOST GALAXIES OF X-SHAPED RADIO SOURCES

ALESSONDRA SPRINGMANN AND CHI CHEUNG

ABSTRACT

Most radiation from galaxies containing active galactic nuclei (AGNs) is emitted not by the stars composing the galaxy, but from an active source at the galactic center, most likely a supermassive black hole. Of particular interest are radio galaxies, active galaxies that emit much of their radiation at radio wavelengths. Within each radio galaxy, an AGN powers a pair of collimated jets of relativistic particles, forming a pair of giant lobes at the end of the jets and thus giving a characteristic double-lobed appearance. A particular class of radio galaxies has an "X"-or winged-shaped morphology: in these, two pairs of lobes appear to originate from the galactic center, producing a distinctive X-shape. Two main mechanisms have been proposed to explain the X-shape morphology: one being a realignment of the black hole within the AGN and the second positing that the radio jets are expanding into an asymmetric medium, causing backflow and producing secondary wings. By analyzing radio host galaxy shapes, the distribution of the stellar mass is compared to the differing model expectations regarding the distribution of the surrounding gas and stellar material about the AGN. Results show elliptical host galaxies with an orthogonal offset between the semi-major axis of the host galaxy and the secondary radio wings, which lends support to the hydrodynamical model. However, results also show circular host galaxies with radio wings, making the realignment scenario a more likely model to describe the formation of these X-shaped radio sources.

INTRODUCTION

Among the largest and most prevalent structures in the Universe are extragalactic radio sources, emitting strongly in the radio portion of the spectrum. Thousands of these objects exist, ranging in size from approximately 50 kiloparsecs across (approximately 150,000 light-years) to 100 kiloparsecs (300,000 light-years). These radio sources are composed of relativistic plasma jets traveling at high speeds and emitting synchrotron radiation (relativistic electrons moving through weak magnetic fields). Extragalactic radio sources contain a central host galaxy from which two jets are emitted. As the jets interact with the surrounding intergalactic medium, a pair of giant radio lobes forms. Figure 1 shows Cygnus A, a typical extragalactic radio source approximately 100 kiloparsecs across, which exhibits a central host galaxy (blue), collimated jets, and radio lobes (both red).

In addition to being large, coherent structures, extragalactic radio sources are also highly energetic. The energy output of

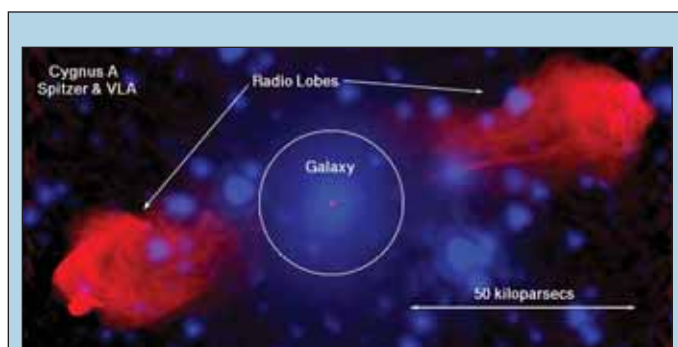


Figure 1. Extragalactic radio source Cygnus A. The host galaxy is imaged in the optical band shown in blue at the center, while the radio jets and lobes are shown in red. The total size of Cygnus A is 100 kiloparsecs across, approximately 300,000 light-years. The optical image of the host galaxy is courtesy of the Spitzer Space Telescope and the radio image was taken with the Very Large Array, courtesy of the National Radio Astronomy Observatory/Associated Universities, Inc..

typical extragalactic radio sources is 10^{44} ergs/second, with some sources having total energies up to 10^{59} ergs/second. (Our Sun, in comparison, has a luminosity of 10^{33} ergs/second, making it 11 orders of magnitude less energetic than Cygnus A.) The majority of radio galaxies emit most of their radiation not from the stars, gas, and dust composing the galaxy, but from the active source at the center, an active galactic nuclei (AGN), widely believed to be a supermassive black hole [1].

Thousands of these extragalactic radio sources resemble the canonical object, Cygnus A, in that they possess one pair of radio jets. Three decades ago approximately a dozen radio galaxies displaying two sets of jets emitting from the central supermassive black hole, forming a distinctive “X”-shape were known [2]. Over the past three decades, the number of known sources possessing the X-shaped morphology has grown to over a hundred candidates, allowing for more detailed studies of these objects, particularly regarding their shape and origin. Figure 2 shows double radio source 3C315, which displays a distinctive X-shaped morphology.

Astronomers propose that this distinct shape may be the result of a recent collision or merger between two supermassive black holes, which can produce the extra set of jets and lobes. Another explanation is that the main jets expanded into an asymmetric medium, generating an additional pair of radio lobes.

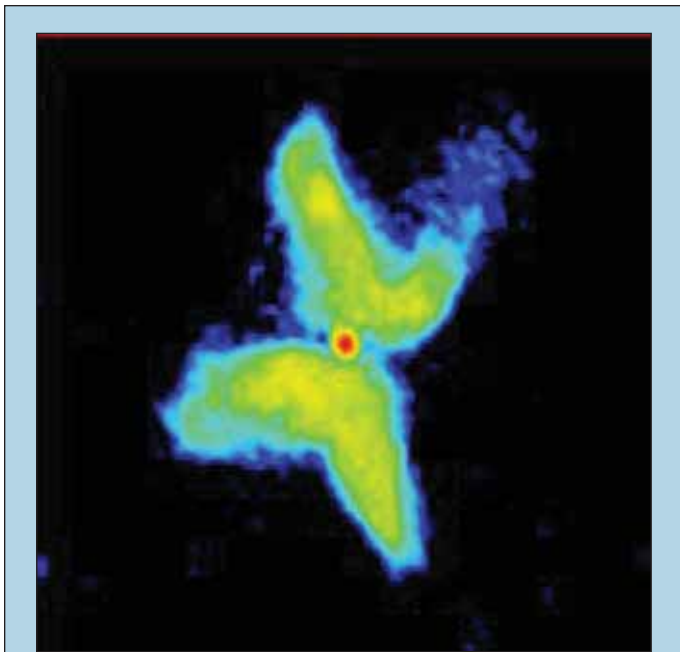


Figure 2. 3C 315, an extragalactic radio source with two pairs of jets, from Leahy and Williams [7].

Hydrodynamical simulations by Capetti et al. in Figure 3 show that as a jet, aligned parallel to the semi-major axis of an elliptical galaxy¹, propagates into the surrounding gas distribution, two major jets form, and smaller wings will form orthogonal to the major jets, producing X-shaped radio lobes [3].

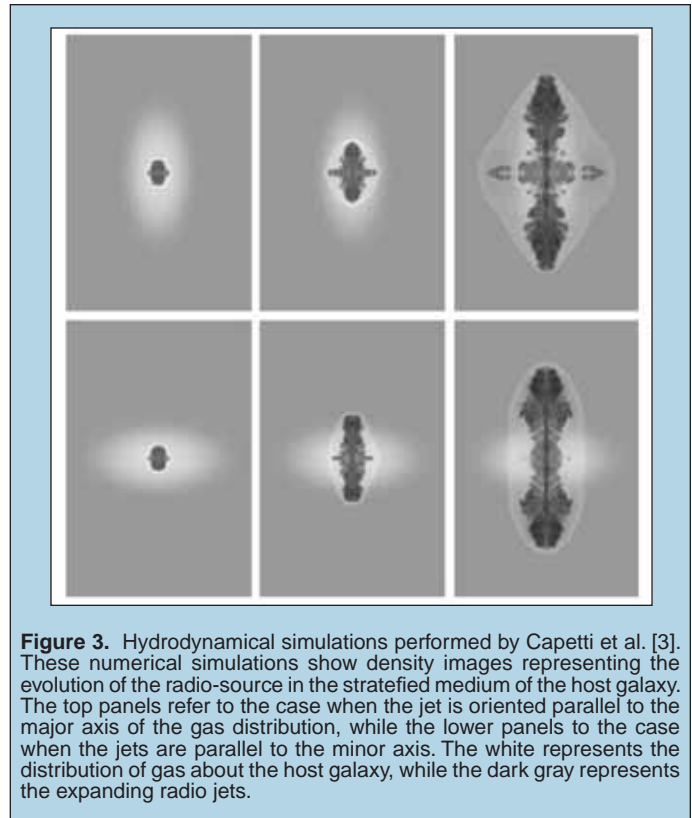


Figure 3. Hydrodynamical simulations performed by Capetti et al. [3]. These numerical simulations show density images representing the evolution of the radio-source in the stratified medium of the host galaxy. The top panels refer to the case when the jet is oriented parallel to the major axis of the gas distribution, while the lower panels to the case when the jets are parallel to the minor axis. The white represents the distribution of gas about the host galaxy, while the dark gray represents the expanding radio jets.

From the x-ray observations performed by Kraft et al. of the gas surrounding elliptical galaxies, it is known that stellar light is an efficient way of probing gas distribution, as the distribution of gas around a host galaxy follows the distribution of stars in the galaxy [4]. Thus, a galaxy with an elliptical distribution of stars will have an elliptical distribution of surrounding gas. Wing formation is most pronounced in elliptical galaxies, with the main set of jets forming parallel to the major axis of the galaxy. Studying a small set of host galaxies, Capetti et al. found that many elliptical galaxies have a small set of “wings”, which align orthogonal to the semi-major axis of the host galaxy, as shown in their simulations and in Figure 5 [3].

In this paper, the ellipticity of the galaxies that play host to the X-shaped jets, is investigated to determine if galaxies with more elliptical distributions of gas have X-shaped jets. Using the ellipse package for Image Reduction and Analysis Facility (IRAF)² to model the elliptically-shaped isophotes, or regions of equal brightness, of the galaxies, the ellipticity and extent of the host galaxies and

¹An elliptical galaxy is an ellipsoid, or a three-dimensional ellipse, as shown in Figure 4. Viewed from Earth, it appears as an ellipse in the sky.

²IRAF is distributed by the National Optical Astronomy Observatories, which are operated by the Association of Universities for Research in Astronomy, Inc., under cooperative agreement with the National Science Foundation.

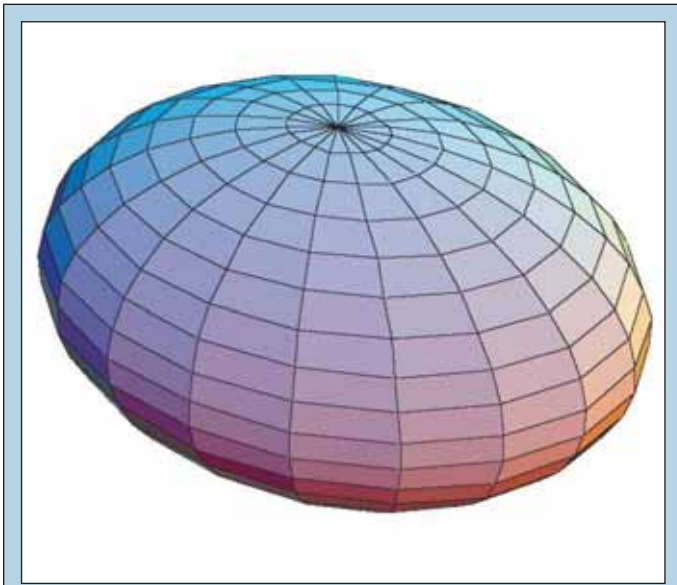


Figure 4. A model of an elliptical galaxy as a three-dimensional ellipsoid. When viewed from Earth it appears to be a flat ellipse .

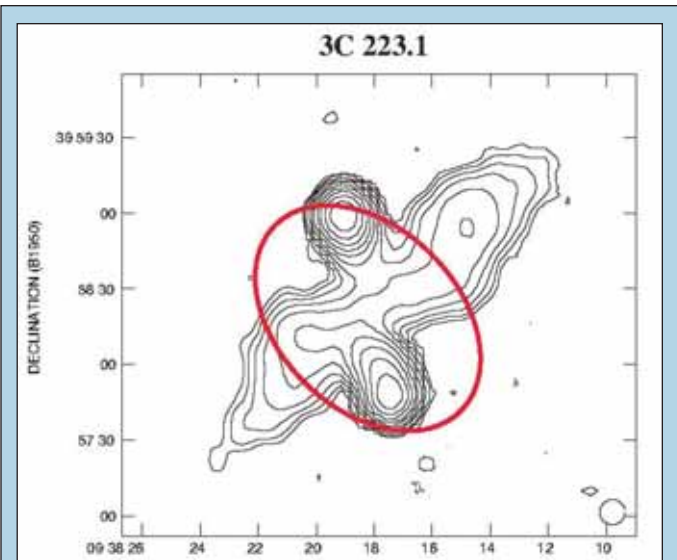


Figure 5. Superposition of the host galaxy shape (not to scale) onto the radio image maps for X-shaped source 3C 223-1. Superposition by Capetti et al. [3], with radio maps from Dennett-Thorpe et al. [8].

compared was determined to radio galaxy morphology. These results can be compared to the results of previous studies (such as those carried out by Capetti et al. [3]) with an expanded sample of X-shaped radio sources.

³The magnitude scale is a logarithmic scale that describes the relative brightness of stars, with the star Vega (α Lyrae) defined as having magnitude 0.

⁴STS-DAS is a product of the Space Telescope Science Institute, which is operated by the Association of Universities for Research in Astronomy, Inc. for the National Aeronautics and Space Administration.

⁵Ellipticity is defined as $f = 1 - a/b$, where a is the semi-major axis of the ellipse, and b is the semi-minor axis of the ellipse. An ellipse with $f = 0$ is a circle.

METHODS OF ANALYSIS

Images of the host galaxies of nine X-shaped extragalactic radio sources were collected by the Sloan Digitized Sky Survey. The images are 56-second exposures taken in the r-band filter, which has a central wavelength of 6,280 Ångstroms. All objects imaged are

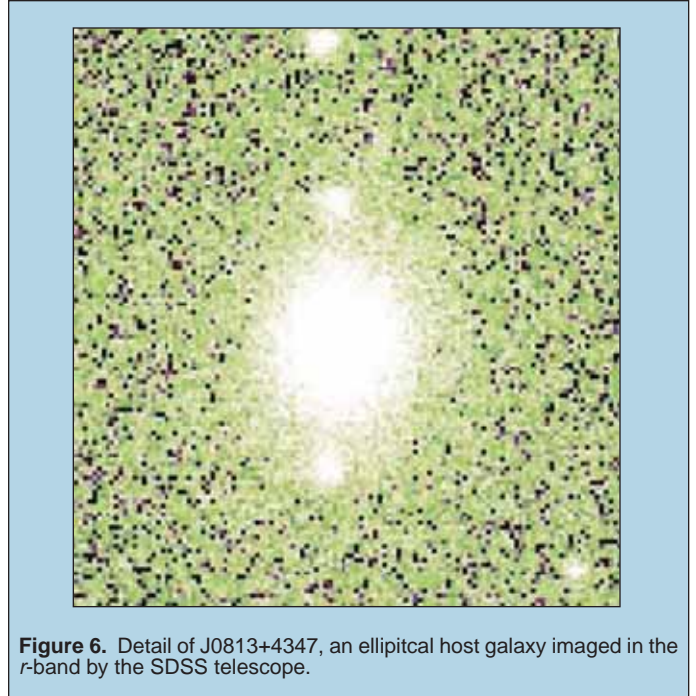


Figure 6. Detail of J0813+4347, an elliptical host galaxy imaged in the r-band by the SDSS telescope.

18th magnitude³, or brighter in the r-band, as dimmer objects would otherwise not be sufficiently resolved. The pixel scale of the CCD is 0.4 arcseconds and the seeing for each image is approximately one arcsecond. A sample source image, the host galaxy of source J0813+4347, is shown in Figure 6.

Elliptical isophotes, or regions of equal brightness, of these host galaxies were fitted by the ellipse routine of the Space Telescope Science Data Analysis System (STS-DAS)⁴ isophote package for IRAF. The isophote fitting methods are described in Jedrzejewski [5]. The center and length of the outermost elliptical isophote's semi-major axis are specified by the user, then the software plots successively smaller isophotes on the image, as seen in Figure 7. Information pertaining to the isophote plots, such as the semi-major axis of the isophote in pixels, ellipticity of the isophote⁵, and position angle of the isophote relative to north in the image are written to a table. A routine called bmodel then converts this table to a model of relative isophotal intensities and sizes, which can then be subtracted from the original image to judge the goodness

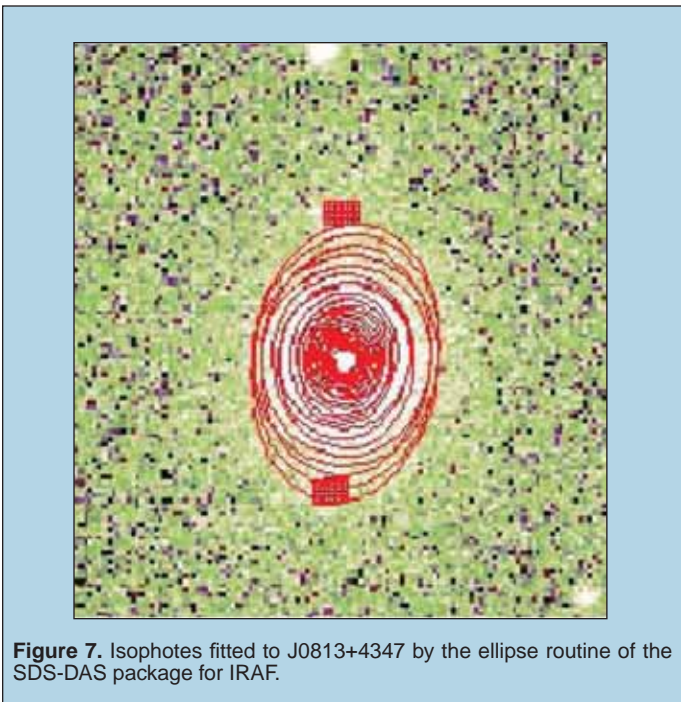


Figure 7. Isophotes fitted to J0813+4347 by the ellipse routine of the SDS-DAS package for IRAF.

of the isophote fits. Figure 8 shows the isophote model subtracted from the background image and indicates that the isophote model matches the intensity of the host galaxy, leaving minimal residual background on the image.

The position angles of the radio lobes and wings of the actual X-shaped sources were measured from data taken by the Very Large Array (VLA)⁶. The difference between the position angles of the

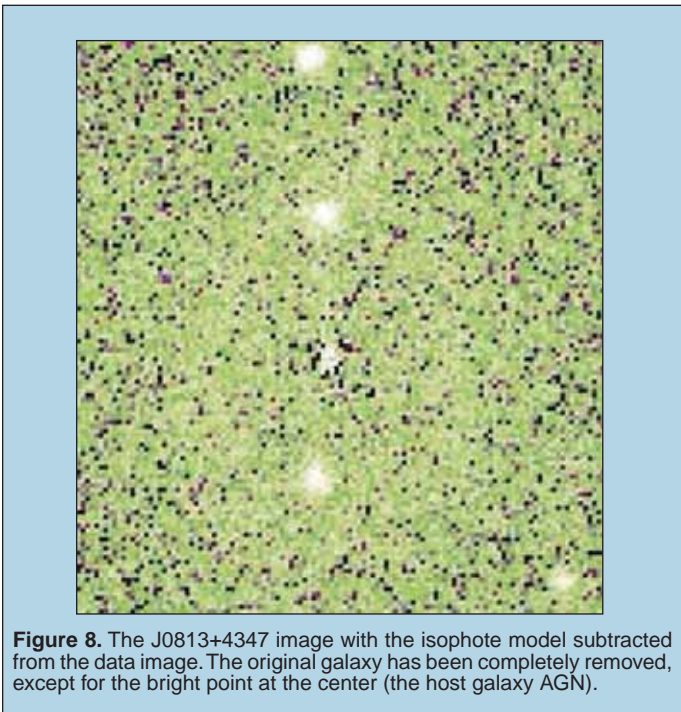


Figure 8. The J0813+4347 image with the isophote model subtracted from the data image. The original galaxy has been completely removed, except for the bright point at the center (the host galaxy AGN).

host galaxies' semi-major axes and the position angles of the radio wings of the X-shaped sources are shown in Table 1 with the values for the ellipticities of host galaxies calculated from the isophote fits calculated from the ellipse routine.

RESULTS

Galaxy parameters (position angle of the main set of radio jets, position angle of the radio wings, position angle of the host galaxy in the optical, ellipticity of the host galaxy, and offset between the radio wing position angle and the optical host galaxy position angle) were measured for four known X-shaped sources from the literature and five new objects with a distinct X-shape found by Cheung [2].

The distribution of host galaxy ellipticities for these nine sources (in blue) is compared to a sample of "normal" (not X-shaped) host galaxies of extragalactic radio sources analyzed by Capetti et al. (white) is shown in Figure 9 [3]. Some of these host galaxies are highly elliptical; however, approximately two thirds of these objects have ellipticities consistent with the host galaxy being circular. Capetti found that the host galaxies of X-shaped sources tended to be highly elliptical [3], which is contrary to this study's finding that the host galaxies of these X-shaped objects range from being circular to highly elliptical. It appears that the host galaxy need not be highly elliptical to cause wing formation in these cases.

Although the ellipticities of these host galaxies show no specific trend toward either high or low ellipticity, the offset between the host galaxy optical semi-major axis position and that of the radio wings tends to be approximately orthogonal for six out of nine objects for which exist VLA observations, as shown in Figure 10.

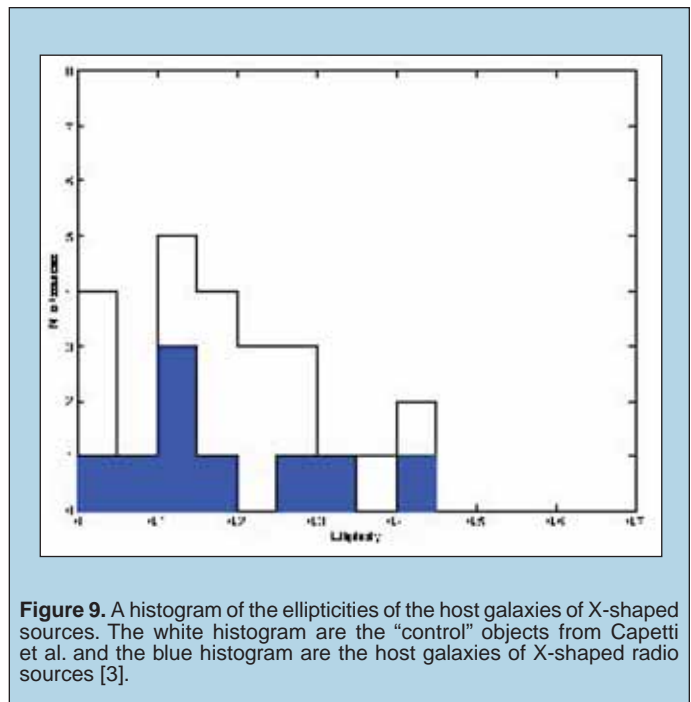


Figure 9. A histogram of the ellipticities of the host galaxies of X-shaped sources. The white histogram are the "control" objects from Capetti et al. and the blue histogram are the host galaxies of X-shaped radio sources [3].

⁶VLA data courtesy of the National Radio Astronomy Observatory/Associated Universities, Inc.

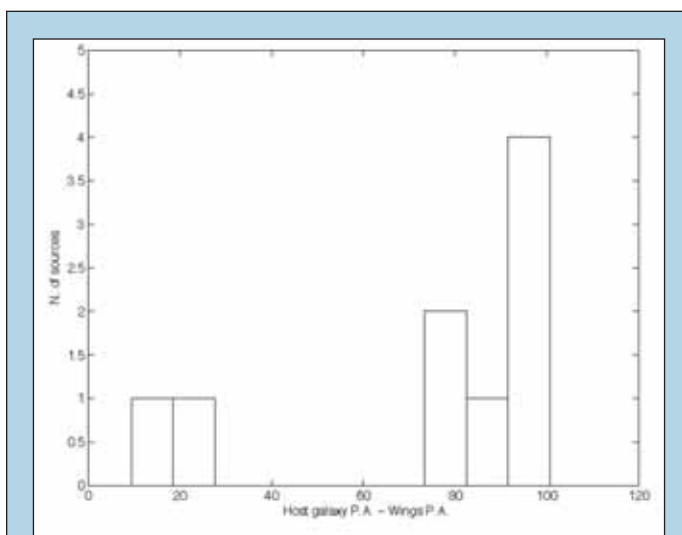


Figure 10. A histogram of the position angle offsets between the semi-major axis of the host galaxies and radio wings of the x-shaped radio sources. Approximately two thirds of the sources show an offset of 90 degrees.

With the position angles of the radio lobes and wings taken from the VLA data in Table 1, there appears to be little connection between the ellipticity of the host galaxy and the presence of radio wings orthogonal to the semi-major axis of the host galaxy. This is evidenced by objects with low ellipticities (less than 0.12) and an approximately orthogonal offset between the radio wings and optical semi-major axis of the host galaxy.

However, host galaxy position angles can only be measured if they are highly elliptical (for ellipticities greater than 0.12), which produces low-confidence measurements of the isophotal position angles of the semi-major axes of the host galaxies.

Comparing the host galaxy position angle to the wing position angle, the difference in these angles are clustered around 90°, i.e. the position angles are orthogonal, consistent with the findings of Capetti et al. However, unlike Capetti, galaxies with circular isophotes play host to X-shaped radio sources.

CONCLUSIONS

Host galaxy ellipticities from nine sources are plotted in Figure 9. Some of these host galaxies are highly elliptical, having ellipticity values of over 0.12; however, four of these objects have ellipticities consistent with being circular. The ellipticities are compared to a sample of normal radio galaxies from Capetti et al. and the distributions are indistinguishable (Figure 9), contrary to the findings of Capetti [3]. Simulations performed by Capetti show that an elliptical distribution of gas about a host galaxy produces the main lobes and auxiliary wings seen in X-shaped sources. The host galaxy need not be highly elliptical to for there to be secondary wings in extragalactic radio sources.

X-ray observations performed by Kraft et al. of 3C 403, an X-shaped source, found that the optical position angle of the host galaxy follows the X-ray gas distribution [4].

Therefore, in at least one X-shaped source, it is known that the gas follows the star distribution of the galaxy, and thus, if the

galaxy appears elliptical in the optical band, it is likely elliptical in its gas distribution. According to Capetti, if the stellar light follows the distribution of gas around the galaxy, is elliptical, and is on a scale much larger than that of the host, comparable to the size of the X-shaped lobes and wings, then the double morphology of the X-shaped radio galaxies will form as the main set of jets expand into the surrounding gas [3].

Several of the host galaxies sampled show circular isophotes, contrary to the findings of Capetti. This can be resolved if the orientation effects of the host galaxy are consistent. A galaxy with the form of an ellipsoid viewer from its most circular side will appear to have circular isophotes as a consequence of the observer's position. However, it is unlikely that a galaxy having the shape of a spheroid (an ellipsoid with two axes equal in length) would have a spherical side facing Earth. It is more likely that, although our results for J0831+3219 agree with deeper observations by Ulrich et al., the data from the Sloan Digital Sky Survey is "shallow", or that the objects were not sufficiently exposed to obtain a high enough signal to noise ratio in order to resolve the elliptical isophotal structure of these host galaxies [6].

We compared our measurements with much deeper data taken at longer exposures for one well-studied, low-ellipticity object, J0831+3219 [6]. As our values for ellipticity and position angle of the host galaxy are consistent with Ulrich's, this demonstrates that the Sloan Digital Sky Survey data is valid and comparable to "deeper", or longer-exposure observations.

The model proposed by Capetti might have difficulty explaining the circular hosts of these X-shaped sources, however, it should not be immediately discounted. There are a number of papers, including Capetti, which describe hydrodynamical situations that lead to X-shaped source formation supported by data and simulations.

Other models exist that propose that the formation of secondary wings in extragalactic radio sources due to the realignment of the central supermassive black hole of a host galaxy, due perhaps to galactic mergers, but they lack significant simulations or data to reinforce their predictions. In order to verify whether the Capetti or black hole realignment model most accurately describes the creation of X-shaped extragalactic radio sources and further understand the formation of these objects, more simulations of galactic mergers should be performed, in addition to additional observations of both the host galaxies and X-shaped sources.

ACKNOWLEDGMENTS

This research was conducted at the Kavli Institute for Particle Astrophysics and Cosmology at the Stanford Linear Accelerator Center. I thank the U.S. Department of Energy, Office of Science and Michael Woods for the opportunity to participate in the SULI program and for the tremendous learning and research experience. Immense thanks are due to my mentor Teddy Cheung for his knowledge of extragalactic radio astronomy, in addition to his patience, persistence, sense of humor, and skill at pool. I also thank Alexandra Rahlin for providing invaluable help with Matlab scripting and LATEX formatting. I am grateful to the faculty and staff of KIPAC, especially Stuart Marshall and Grzegorz Madejski, for hosting me this summer and generously providing us students with a wealth of resources and encouragement.

REFERENCES

- [1] D. S. De Young, *The Physics of Extragalactic Radio Sources*, 1st ed. Chicago, Illinois: The University of Chicago Press, 2002, vol. 1.
- [2] C. C. Cheung, "First 'Winged' and 'X'-shaped radio sources," *Astronomy Journal*, 2006 (submitted).
- [3] A. Capetti, S. Zamfir, P. Rossi, G. Bodo, C. Zanni, and S. Massaglia, "On the origin of X-shaped radio-sources: New insights from the properties of their host galaxies," *Astronomy & Astrophysics*, vol. 394, pp. 39–45, Oct. 2002.
- [4] R. P. Kraft, M. J. Hardcastle, D. M. Worrall, and S. S. Murray, "A Chandra Study of the Multicomponent X-Ray Emission from the X-shaped Radio Galaxy 3C 403," *The Astrophysical Journal*, vol. 622, pp. 149–159, Mar. 2005.
- [5] R. I. Jedrzejewski, "CCD surface photometry of elliptical galaxies. I -Observations, reduction and results," *Monthly Notices of the Royal Astronomical Society*, vol. 226, pp. 747–768, June 1987.
- [6] M.-H. Ulrich and J. Roennback, "The host of B2 0828+32, a radio galaxy with two sets of radio lobes," *Astronomy & Astrophysics*, vol. 313, pp. 750–754, Sept. 1996.
- [7] J. P. Leahy, G. G. Pooley, and J. M. Riley, "The polarization of classical double-radio sources," *Monthly Notices of the Royal Astronomical Society*, vol. 222, pp. 753–785, Oct. 1986.
- [8] J. Dennett-Thorpe, P. A. G. Scheuer, R. A. Laing, A. H. Bridle, G. G. Pooley, and W. Reich, "Jet reorientation in active galactic nuclei: two winged radio galaxies," *Monthly Notices of the Royal Astronomical Society*, vol. 330, pp. 609–620, Mar. 2002.

Douglas Swanson is a senior physics major at Yale University. In addition to plasma physics, he has conducted research in experimental nuclear physics and cosmology, and is a member of the nuclear structure group at Yale's Wright Nuclear Structure Laboratory. He is a 2007 National Science Foundation Graduate Research Fellow.

Jonathan Menard is Principal Research Physicist and lecturer at the Princeton Plasma Physics Laboratory (PPPL). He is an experimental plasma physicist

who works primarily on the National Spherical Torus Experiment (NSTX) at PPPL. Dr. Menard's research interests include the linear and non-linear magnetohydrodynamic (MHD) stability properties of spherical torus (ST) plasmas, advanced operating scenarios in the ST, plasma startup, and wave physics. Among his honors, Dr. Menard received the Presidential Early Career Award for Scientists and Engineers in 2004, and was a recipient of the Kaul Prize in 2006.

CALCULATION OF PARTICLE BOUNCE AND TRANSIT TIMES ON GENERAL GEOMETRY FLUX SURFACES

DOUGLAS SWANSON AND JONATHAN MENARD

ABSTRACT

A viable nuclear fusion reactor must confine energetic plasmas long enough so that the fusion energy produced exceeds the energy consumed to heat the plasma and maintain confinement. It is well-known that magnetohydrodynamic (MHD) or plasma fluid instabilities limit confinement. One such important instability is the resistive wall mode (RWM). Plasma rotation faster than a critical frequency has been observed to stabilize the RWM. Some theories predict that the critical frequency will vary inversely with the characteristic times particles take to orbit the plasma. Previous calculations of these orbit times have assumed high aspect ratio and circular plasma cross-section, approximations unsuitable for the National Spherical Torus Experiment (NSTX). Analytic solutions for the orbit times have been derived as functions of particle energy and magnetic moment for low aspect ratio and elliptical cross-sections. Numeric solutions for arbitrary aspect ratio and cross-sectional geometry were also computed using Mathematica and IDL and agree with the analytic forms. In typical parameter regimes for NSTX, the generalized orbit times can differ from the high aspect ratio, circular approximations by as much as 40%. This result might help to assess how accurately theory describes RWM stabilization in NSTX. If theory and experiment are found to agree, generalized orbit times can be used to predict RWM stabilization in low aspect ratio nuclear fusion reactors.

INTRODUCTION

In a nuclear fusion reactor, energy is released when plasma particles fuse. A viable reactor must confine energetic plasmas long enough so that the fusion energy produced exceeds the energy consumed to heat the plasma and maintain confinement. It is well-known that magnetohydrodynamic (MHD) or plasma fluid instabilities limit confinement. Instabilities arise from current or pressure gradients in the plasma, and result in turbulence and energy loss [1]. To maximize the efficiency and fusion power output from a toroidal fusion reactor (tokamak), it is essential to control MHD instabilities.

One such important instability is the resistive wall mode (RWM), which grows due to electrical resistivity in the walls surrounding the plasma [2]. Plasma rotation faster than a critical frequency has been observed to stabilize the RWM [3]. Some theories, including the kinetic damping theory of Bondeson and Chu, predict that the critical frequency will vary inversely with the characteristic times particles take to orbit the plasma [4]. These orbit times fall into two categories. Transit times are orbit times for particles with small magnetic moments that complete full orbits around the plasma. Bounce times are orbit times for particles with large magnetic moments that are trapped by the magnetic mirror effect and cannot complete full orbits around the plasma.

Previous calculations of these bounce and transit times have assumed high aspect ratio and circular plasma cross-section, approximations unsuitable for the National Spherical Torus Experiment (NSTX). NSTX maintains aspect ratios, A , of around 1.3 to 1.6, whereas previous calculations were for aspect ratios of 2.5 and above. NSTX also routinely achieves elongations (ellipticities) κ of 1.8 to 3, as compared with a purely circular cross-section ($\kappa=1$).

Experimentally-measured critical rotation frequencies in the DIII-D tokamak can differ by a factor of 2 from previously predicted values [5]. Although such comparisons have not been made for NSTX, a similar disparity is predicted. Since the critical rotation frequency depends strongly on bounce and transit times, it is hypothesized that generalizing these times to NSTX parameter regimes might improve predictions of critical frequencies and RWM stabilization; important for maximizing the efficiency of a spherical torus (low aspect ratio) fusion reactor. This also might test how accurately Bondeson and Chu's kinetic damping theory describes RWM stabilization in NSTX. Hence it is desirable to calculate bounce and transit times for arbitrary aspect ratios and cross-sections (flux surface geometry).

This paper will consider analytic and numeric solutions for bounce and transit times in the general geometry case.

MATERIALS AND METHODS

Analytic Solutions

Analytic solutions for bounce and transit times τ may be derived as functions of particle energy E and magnetic moment μ for arbitrary aspect ratio and flux surface geometry. Bounce and transit times are defined by:

$$\tau = \oint \frac{ds}{v_{\parallel}} \quad (1)$$

where v_{\parallel} is the component of particle velocity parallel to the magnetic field and ds is a differential of arc length along the magnetic field lines. For transit times τ_t the integral is taken along the magnetic field lines over a full cross-sectional circuit. For bounce times τ_b it is taken between adjacent bounce points.

Using conservation of energy and the adiabatic invariance of the magnetic moment, the parallel velocity v_{\parallel} may be written as:

$$v_{\parallel} = \sqrt{\frac{2}{m} (E - \mu B)} \quad (2)$$

where B is the magnitude of the magnetic field at every point in space and m is the particle mass. Then the bounce and transit times become:

$$\tau = \sqrt{\frac{m}{2}} \oint \frac{ds}{\sqrt{E - \mu B}} \quad (3)$$

For trapped particles, bounce points occur where $E = \mu B$. The problem of calculating bounce and transit times requires evaluating this integral for any B and ds .

Figure 1 illustrates the coordinates and parameters used in the derivations below. Two different coordinate systems will be employed: an (r, θ, ϕ) toroidal coordinate system and an (R, Z, ϕ) cylindrical coordinate system. The aspect ratio A is defined as $A = R_0 / a$.

In the high aspect ratio, circular flux surface limit considered previously, B may be taken to vary as $1/R$, where $R = R_0 + r \cos \theta$ is the standard cylindrical radial coordinate. This may be expanded to first order in the small parameter $\varepsilon = r/R_0 \ll 1$ to yield $B \cong B_0(1 - \varepsilon \cos \theta)$, with $B_0 = B(R = R_0)$. The same first order approximation gives $ds \approx (R_0 q) d\theta$, where the safety factor q represents the number of toroidal transits made by the magnetic field lines per poloidal transit. The integral above may then be evaluated analytically to obtain:

$$\begin{aligned} \tau &\cong \sqrt{\frac{m}{2}} \oint \frac{R_0 q}{\sqrt{E - \mu B_0 (1 - \varepsilon \cos \theta)}} d\theta \\ &= q R_0 \sqrt{\frac{2m}{E - \mu B_0 (1 - \varepsilon)}} F\left(\frac{\theta}{2} \middle| \frac{2\mu B_0 \varepsilon}{E - \mu B_0 (1 - \varepsilon)}\right) \end{aligned} \quad (4)$$

where F is the incomplete elliptic integral of the first kind. This result is due to Bondeson and Chu [4].

For the arbitrary aspect ratio and flux surface cases, the above approximations for B and ds must be generalized. Consider a generic equilibrium where the poloidal flux Ψ is given in terms of the radial coordinate r and minor radius a of the plasma by:

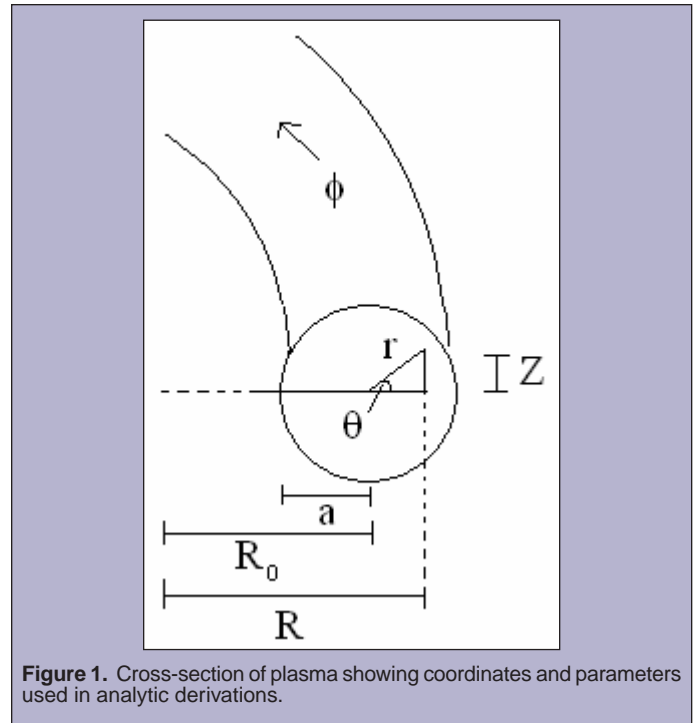


Figure 1. Cross-section of plasma showing coordinates and parameters used in analytic derivations.

$$\Psi = \Psi_0 \frac{r^2}{a^2} \quad (5)$$

Here the toroidal radial coordinate r is related to the cylindrical coordinates R, Z by: $R = R_0 + r \cos \theta$, $Z = \kappa r \sin \theta$, where $\kappa = Z/(R - R_0)$ is the elongation. Then the magnetic field strength may be written as:

$$\begin{aligned} B &= \sqrt{B_\theta^2 + B_R^2 + B_Z^2} = \sqrt{\frac{B_0^2 R_0^2}{R^2} + \left(-\frac{1}{R} \frac{\partial \Psi}{\partial Z}\right)^2 + \left(\frac{1}{R} \frac{\partial \Psi}{\partial R}\right)^2} \\ &= \frac{1}{R} \sqrt{B_0^2 R_0^2 + \frac{4\Psi_0^2 r^2}{a^4 \kappa^2} (\sin^2 \theta + \kappa^2 \cos^2 \theta)} \end{aligned} \quad (6)$$

The differential of arc length becomes:

$$\begin{aligned} ds &= \sqrt{R^2 d\phi^2 + r^2 d\theta^2} \\ &= d\theta \sqrt{\frac{B_0^2 R_0^2 a^4 \kappa^2}{4\Psi_0^2 (\sin^2 \theta + \kappa \cos^2 \theta)^2} + r^2 (\sin^2 \theta + \kappa^2 \cos^2 \theta)} \end{aligned} \quad (7)$$

The bounce and transit time integral in general cannot be evaluated analytically using these expressions. However, by specializing to low aspect ratio but circular flux surfaces (setting κ to 1), an analytically integrable form arises.

Similarly, by specializing to high aspect ratio but elliptical flux surfaces, an analytically integrable form arises. Taking Taylor expansions of the relevant expressions to first order in the small parameter $\varepsilon = r/R_0 \ll 1$ gives:

$$\frac{1}{\sqrt{E - \mu B}} = \frac{1}{\sqrt{E - \mu B_0}} - \frac{\mu B_0 \cos \theta}{2(E - \mu B_0)^{3/2}} \varepsilon + O(\varepsilon^2) \quad (8)$$

$$ds \cong \frac{B_0 R_0 a^2 \kappa}{2\Psi_0 (\sin^2 \theta + \kappa \cos^2 \theta)} d\theta \quad (9)$$

Then the bounce and transit times become:

$$\begin{aligned} \tau &= \frac{B_0 R_0 a^2 \kappa}{2\psi_0} \sqrt{\frac{m}{2}} \left[\frac{1}{\sqrt{E - \mu B_0}} \int \frac{d\theta}{\sin^2 \theta + \kappa \cos^2 \theta} - \frac{\mu B_0 \varepsilon}{2(E - \mu B_0)^{3/2}} \int \frac{\cos \theta}{\sin^2 \theta + \kappa \cos^2 \theta} d\theta + O(\varepsilon^2) \right] \\ &= \frac{B_0 R_0 a^2 \kappa}{2\psi_0} \sqrt{\frac{m}{2}} \left[\frac{1}{\sqrt{E - \mu B_0}} \frac{\tan^{-1}\left(\frac{\tan \theta}{\sqrt{\kappa}}\right)}{\sqrt{\kappa}} - \frac{\mu B_0 \varepsilon}{2(E - \mu B_0)^{3/2}} \frac{\tanh^{-1}\left(\sin \theta \sqrt{\frac{\kappa-1}{\kappa}}\right)}{\sqrt{\kappa(\kappa-1)}} + O(\varepsilon^2) \right] \\ &\propto \frac{B_0 R_0 a^2 \kappa}{2\psi_0} \sqrt{\frac{m}{2}} \frac{1}{\sqrt{\kappa}} \propto \sqrt{\kappa} \end{aligned} \quad (10)$$

Hence at high aspect ratio the bounce and transit times scale with elongation as $\sqrt{\kappa}$.

The Bondeson forms for bounce and transit times scale linearly with the safety factor q . The scaling of the safety factor with elongation may also be determined. The safety factor is defined as:

$$q = \frac{1}{2\pi} \int_0^{2\pi} \frac{d\varphi}{d\theta} d\theta = \frac{1}{2\pi} \int_0^{2\pi} \frac{r B_\varphi}{R B_\theta} d\theta \quad (11)$$

The toroidal magnetic field B_θ may again be taken to vary as $1/R$. Then using the expressions above for the components of B and projecting along the θ -direction gives:

$$\begin{aligned} B_\theta &= \frac{2\psi_0}{a^2} \frac{1}{R} \left(\frac{Z \sin \theta}{\kappa^2} + (R - R_0) \cos \theta \right) \\ &= \frac{2\psi_0}{a^2 \kappa} \frac{r}{R} (\sin^2 \theta + \kappa \cos^2 \theta) \end{aligned} \quad (12)$$

Substituting into the expression above for the safety factor gives:

$$\begin{aligned} q &= \frac{1}{2\pi} \int_0^{2\pi} \frac{r B_\varphi R_0 a^2 \kappa R}{R^2 2\psi_0 r (\sin^2 \theta + \kappa \cos^2 \theta)} d\theta \\ &= \frac{B_0 a^2 \kappa}{4\pi \psi_0} \int_0^{2\pi} \frac{1}{(1 + \varepsilon \cos \theta)(\sin^2 \theta + \kappa \cos^2 \theta)} d\theta \\ &\propto \frac{B_0 a^2 \kappa}{4\pi \psi_0} \frac{1}{\sqrt{\kappa}} \propto \sqrt{\kappa} \end{aligned} \quad (13)$$

At high aspect ratio the Bondeson forms for bounce and transit times also scale like $\sqrt{\kappa}$.

Numeric Solutions

Numeric solutions for arbitrary aspect ratio and flux surface geometry were also computed using Mathematica and IDL. Numerical singularities were handled by linearizing B and integrating analytically in the neighborhood of the singularity.

A series of generic plasma equilibria were generated spanning aspect ratios $A=1.3$ to 10 and elongations $\kappa=1$ to 2. The equilibria were used to test the numeric solutions in IDL.

Computations were performed in terms of a free parameter γ defined as the ratio of particle parallel velocity v_{\parallel} to total velocity v . As γ increases, μ decreases, and so the particle becomes less trapped in its orbit. The range of γ values from 0 to 1 captures the full range of variation in μ .

The numeric solutions were compared with Bondeson forms using two definitions of the parameter ε : first,

$$\varepsilon = \sqrt{\Psi} \frac{a}{R_0} \quad (14)$$

where Ψ is the normalized poloidal flux, and second,

$$\varepsilon = \frac{B_{\max}(\Psi) - B_{\min}(\Psi)}{B_{\max}(\Psi) + B_{\min}(\Psi)} \quad (15)$$

where B_{\max} and B_{\min} are the maximum and minimum values of B respectively on each flux surface. Similarly, a redefinition of R_0 in the Bondeson forms was also considered:

$$(R_0)_{\text{effective}} = \frac{R_{\max}(\Psi) + R_{\min}(\Psi)}{2} \quad (16)$$

where R_{\max} and R_{\min} are the maximum and minimum values of R respectively on each flux surface.

A simple regression model in the radial coordinate r and the parameter γ was also applied to transform the Bondeson results into the general geometry solutions for given aspect ratio and elongation.

RESULTS

Analytic results for bounce and transit times are in Equations 3, 4, and 10 above.

Numeric results are presented in Figures 2-5 below as functions of normalized radial coordinate (r/a) for equilibria of varying aspect ratio and elongation. On the left in each figure are plots of numerically-calculated bounce and transit times and corresponding Bondeson forms for four values of the parameter γ described above. The solid lines represent numerically-calculated results and Bondeson results are shown with asterisks. Spikes in the plots occur at the boundary between transit times toward the center of the plasma and bounce times toward the edge. The ratios of the numerically-calculated solutions to the Bondeson forms are plotted on the right in each figure.

Figure 2 shows agreement between numeric solutions and Bondeson forms for high aspect ratio ($A=10$) and circular flux surfaces, using the renormalized definitions

$$\varepsilon = \frac{B_{\max}(\Psi) - B_{\min}(\Psi)}{B_{\max}(\Psi) + B_{\min}(\Psi)} \quad \text{and} \quad (R_0)_{\text{effective}} = \frac{R_{\max}(\Psi) + R_{\min}(\Psi)}{2}.$$

These renormalized expressions for ε and R_0 will be used in all further plots and results below.

Figure 3 shows disagreements between numeric solutions and Bondeson forms, for lower aspect ratio ($A=3$) and elliptical flux surfaces ($\kappa=1.8$).

Figure 4 shows pronounced disagreements between numeric solutions and Bondeson forms, for low aspect ratio ($A=1.3$) and elliptical flux surfaces ($\kappa=2.0$).

Figure 5 shows improvements in agreement between numeric solutions and Bondeson forms corrected by simple regression in r and γ , for low aspect ratio ($A=1.3$) and elliptical flux surfaces ($\kappa=2.0$). On the left are plotted the ratios of the numerically-calculated solutions to the Bondeson forms for four values of γ . On the right

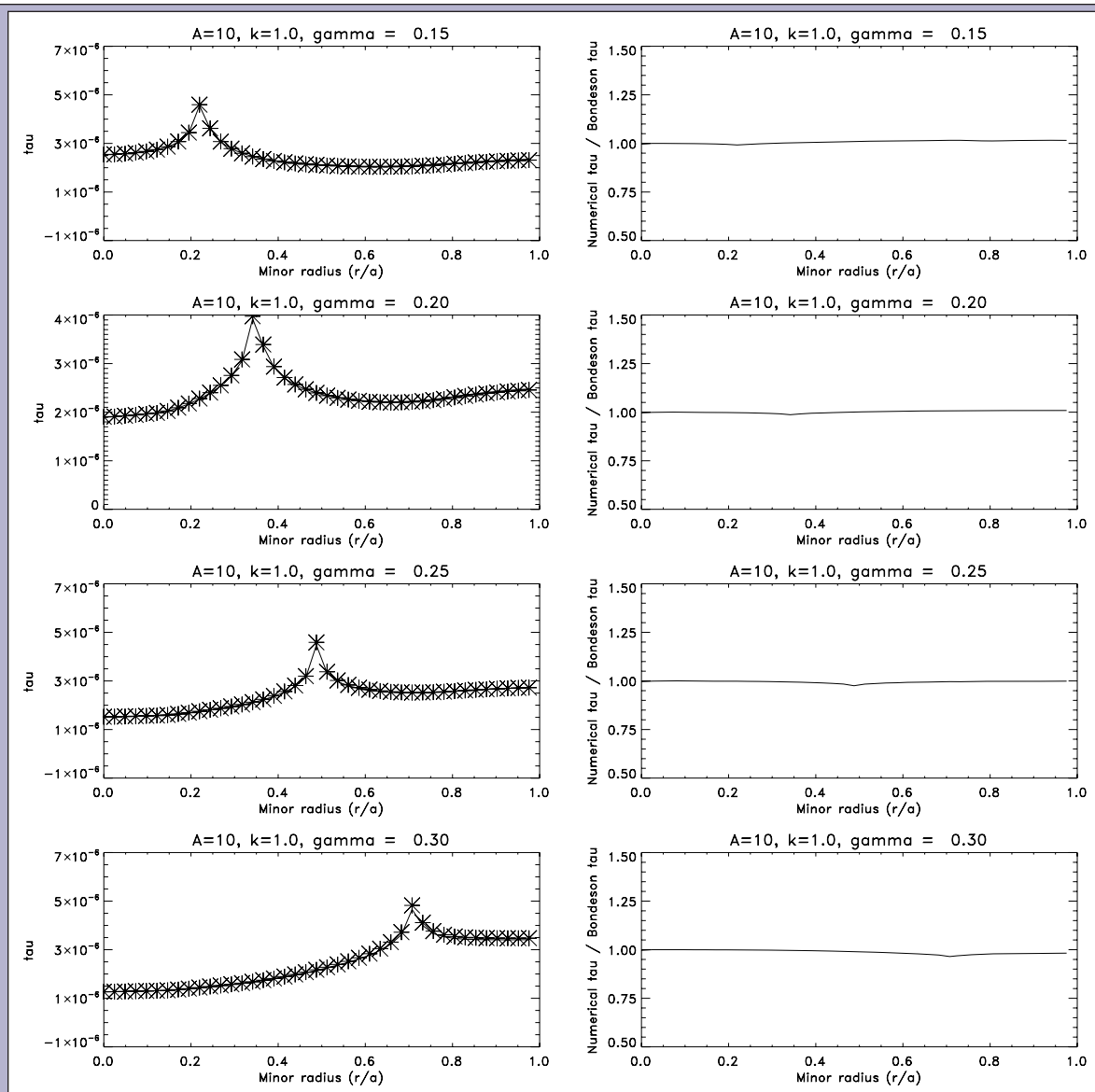


Figure 2. Comparison of numeric solutions and Bondeson forms for high aspect ratio ($A=10$) and circular flux surfaces, as functions of normalized minor radius.

are similar plots, but with the Bondeson solutions corrected by simple regression in r and γ .

DISCUSSION AND CONCLUSIONS

Analytic solutions for bounce and transit times have been derived as functions of particle energy and magnetic moment for low aspect ratio and elliptical flux surfaces. Numeric solutions for arbitrary aspect ratio and flux surface geometry have also been calculated using Mathematica and IDL and agree with the analytic forms. In typical parameter regimes for the National Spherical Torus Experiment (NSTX), aspect ratios A around 1.5 and elongations κ around 2 to 3, the deviation between the numeric solutions and the high aspect ratio, circular (Bondeson) approximations can be 40% or more near the edge of the plasma. This result might help assess how accurately kinetic damping theory describes RWM stabilization in NSTX, by experimentally measuring the critical

rotation frequency and comparing it against the value predicted by theory, using generalized orbit times. If theory and experiment are found to agree, generalized orbit times can be used to predict RWM stabilization in low aspect ratio tokamak fusion reactors.

Analytic transformations to map Bondeson solutions into general geometry solutions are currently being investigated. If such transformations can be found, they could be incorporated into stability codes such as MARS to refine predictions of RWM stabilization, with few modifications to the existing code. The regression shown in Figure 5 is a rudimentary attempt at such a transformation. Even using simplistic regression techniques for rescaling, the error in the Bondeson forms could be decreased by as much as 30%.

The aspect ratio dependence of the orbit times was found to be more significant than the elongation dependence. This is likely due to the orbit times scaling with elongation in the same way the safety factor q , as shown above. Since the Bondeson result is proportional

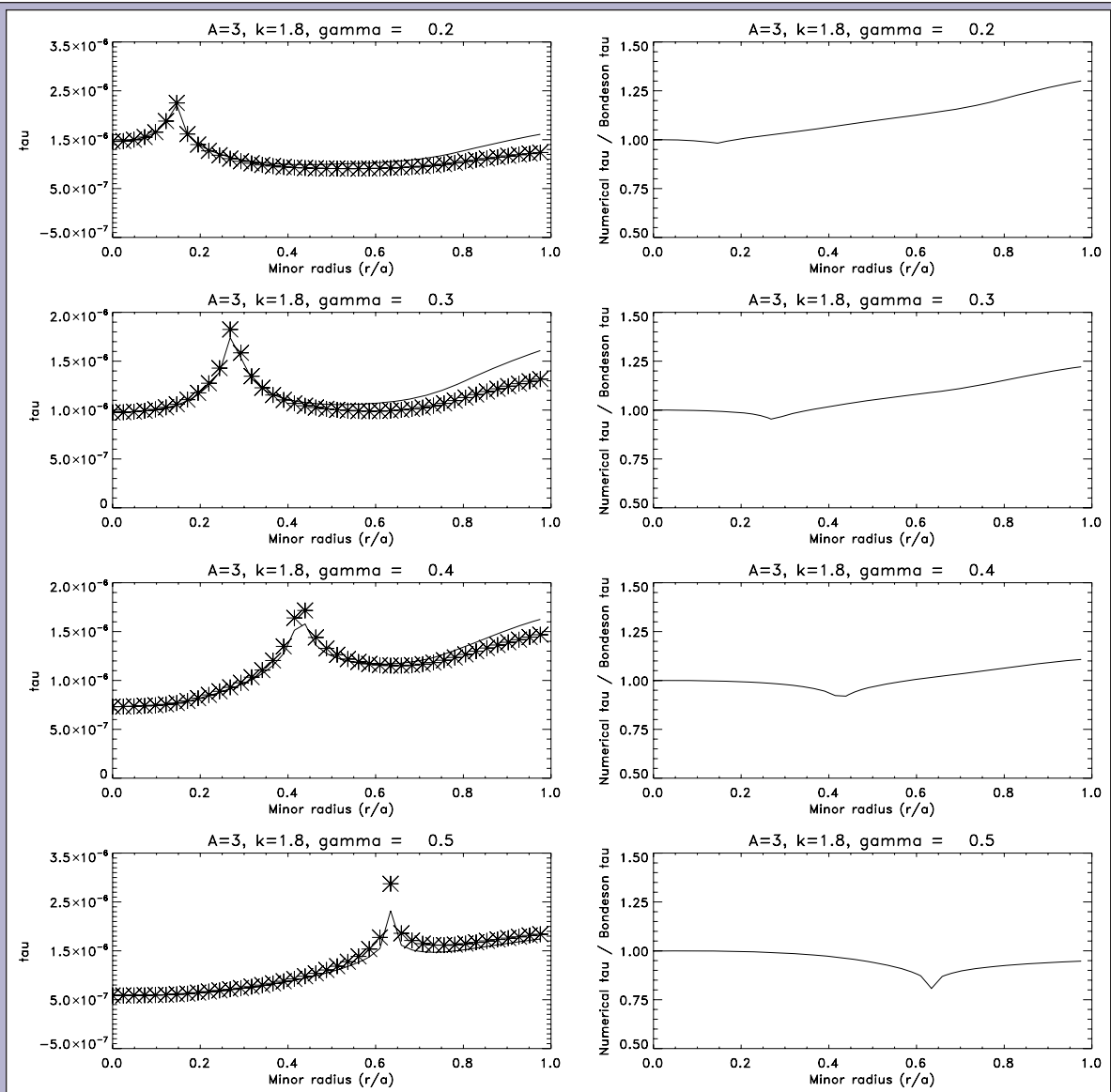


Figure 3. Comparison of numeric solutions and Bondeson forms for lower aspect ratio ($A=3$) and elliptical flux surfaces ($\kappa=1.8$), as functions of normalized minor radius..

to q , it likely captured much of the elongation dependence of the full numeric solution.

For small radial coordinate r the high aspect ratio approximation $r/R_0 < 1$ should provide reasonable accuracy, and so the numeric solutions and the Bondeson forms should agree. Indeed, for small r the ratio of numeric solutions to Bondeson solutions was found to be nearly 1 for all values of κ and γ . Hence the Bondeson approximations agree closely with the general geometry solutions in the center of the plasma but deviate from the general solutions at the edge.

Another possibility for future work would be to choose a θ -coordinate such that the magnetic field exactly satisfies $B = B_0(1 - \epsilon \cos \theta)$, and expand the arc length differential ds in a Fourier series in this coordinate. Each term of the series would be analytically integrable, and the series might converge quickly to the full numeric solution. This could also be easily incorporated into

stability codes since it would only require elliptic integrals already implemented.

ACKNOWLEDGMENTS

Thanks to Dr. Jonathan Menard for his time and patience as a mentor, the Science Undergraduate Laboratory Internships program at the U.S. Department of Energy for funding, and Mr. James Morgan for support and administration. This work supported by DOE contract DE-AC02-76CH03073.

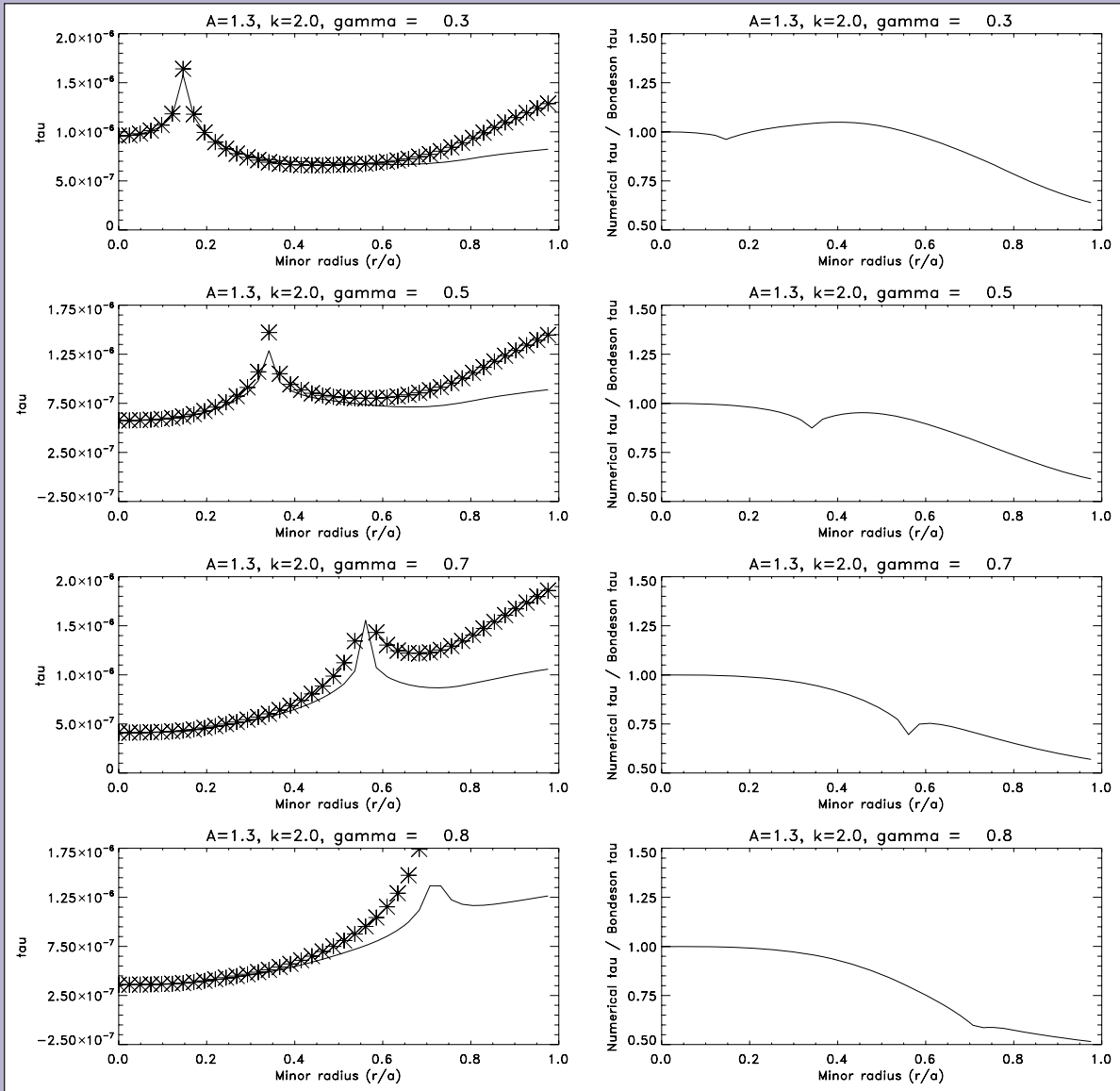


Figure 4. Comparison of numeric solutions and Bondeson forms for low aspect ratio ($A=1.3$) and elliptical flux surfaces ($\kappa=2.0$), as functions of normalized minor radius.

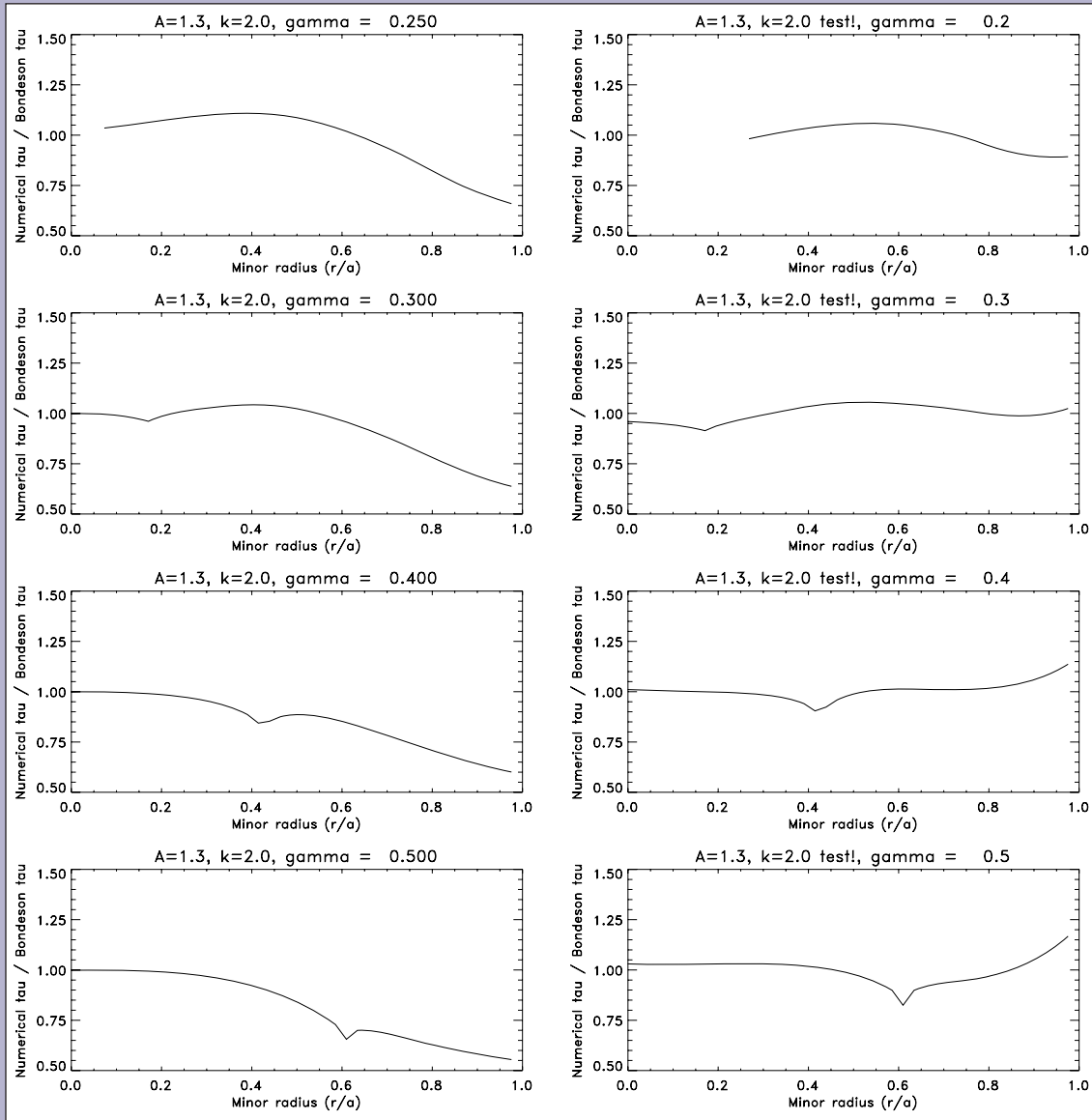


Figure 5. Comparison of numeric and Bondeson solutions for low aspect ratio ($A=1.3$) and elliptical flux surfaces ($\kappa=2.0$) with Bondeson solutions transformed by regression in r and γ .

REFERENCES

- [1] John Wesson, Tokamaks, Third Edition, Oxford University Press, 2004, pp. 304-342. Wesson's book is an excellent source of background on magnetohydrodynamics and fusion physics in general.
- [2] A. Bondeson and D. J. Ward, "Stabilization of external modes in tokamaks by resistive walls and plasma rotation," in Physical Review Letters, Vol. 72, April 25, 1994, pp. 2709-2712.
- [3] A. M. Garofalo, T. H. Jensen, L. C. Johnson, R. J. La Haye, G. A. Navratil, M. Okabayashi, J. T. Scoville, E. J. Strait, D. R. Baker, J. Bialek, M. S. Chu, J. R. Ferron, J. Jayakumar, L. L. Leo, M. A. Makowski, H. Reimerdes, T. S. Taylor, A. D. Turnbull, M. R. Wade, and S. K. Wong, "Sustained rotational stabilization of DIII-D plasmas above the no-wall beta limit," in Physics of Plasmas, Vol. 9, May 2002, pp. 1997-2005.
- [4] A. Bondeson and M. S. Chu, "Inertia and ion Landau damping of low-frequency magnetohydrodynamical modes in tokamaks," in Physics of Plasmas, Vol. 3, Aug. 1996, pp. 3013-3022.
- [5] R. J. La Haye, A. Bondeson, M. S. Chu, A. M. Garofalo, Y. Q. Liu, G. A. Navratil, M. Okabayashi, H. Reimerdes, and E. J. Strait, "Scaling of the critical plasma rotation for stabilization of the $n = 1$ resistive wall mode (ideal kink) in the DIII-D tokamak," in Nuclear Fusion, Vol. 44, Nov. 2004, pp. 1197-1203.

Marlene Tyner is an intern in the Science Undergraduate Laboratory Internship Program at Oak Ridge National Laboratory, researching how climate change effects on decomposition are mediated by species composition. Her paper entitled "Climate Change Effects on Species Composition Mediates Decomposition in an Old-Field Ecosystem" was based on this research. Ms. Tyner received her undergraduate degree in ecology and evolutionary biology at the University of Michigan in Ann Arbor, and she is a member of the Society of Biological Students. Her hometown is Royal Oak, Michigan, and she enjoys hiking, reading, music, movies, mushrooms, China, and shoes.

Aimée Classen is a staff scientist at Oak Ridge National Laboratory, in the Environmental Sciences Division, and an Assistant Research Professor in the Ecology and Evolutionary Biology Department at the University of Tennessee. She received a B.A. in biology from Smith College, and a Ph.D. in biological sciences from Northern Arizona University. Her research in the Classen lab focuses on the interactions and feedbacks among communities of plants, herbivores, and ecosystem processes with an emphasis on the impacts of global change. Recent projects include understanding: how multiple climate change stressors might alter ecosystem function in terrestrial and aquatic ecosystems; how genes may be linked to ecosystem function; and how arthropods may impact ecosystem structure and function.

CLIMATE CHANGE EFFECTS ON SPECIES COMPOSITION MEDIATES DECOMPOSITION IN AN OLD-FIELD ECOSYSTEM

MARLENE L. TYNER AND AIMÉE T. CLASSEN

ABSTRACT

Decomposition of leaf litter collected from an old-field community grown under a combination of elevated atmospheric CO₂ concentrations (+300ppm) and elevated surface temperature (+ 3.2°C) was examined in ambient conditions over 8 months in two separate experiments. In the first experiment, we examined the main effects and interactions of CO₂ and warming on litter quality and subsequent mass loss rates. Multi-species litter bags were constructed with litter collected from chambers with ambient CO₂ and ambient temperatures (ACAT), elevated CO₂ and elevated temperature (ECET), ambient CO₂ and elevated temperature (ACET), and elevated CO₂ and ambient temperature (ECAT). Litter collected from 6 species in each chamber was represented in decomposition bags in equal proportions. There were no differences in initial litter percent carbon (C) or nitrogen (N) among treatments. After 8 months, litter collected from ACET chambers lost over 20% more mass than litter collected from ECET or ACAT chambers, although biological differences were small. In the second experiment, we examined the indirect effect climate change may have on plant community composition, litter inputs, and subsequent mass loss rates. Litter bags were made from the same chambers mentioned above, but the amount of litter in the bag from each species was proportional to peak standing biomass of that species within the treatment. Initial litter in ECAT bags had up to 4% less C and 29% less N than ECET and ACET bags. Mass loss from ACET bags was 48% higher than mass loss from ECAT bags and 37% higher than mass loss from ACAT bags after 8 months of decomposition. These differences may have been driven by the higher proportion of litter from *Lespedeza*, a N-fixer, in the natural ACET bags. Taken together, these data suggest that climate change will have a larger effect on decomposition by causing shifts in plant communities than it will by altering litter quality.

INTRODUCTION

Global changes in atmospheric CO₂ concentration, temperature, and moisture will have important consequences for the functioning of ecosystems [1]. Climatic warming will occur in response to rising atmospheric greenhouse gas concentrations, and elevated CO₂ can alter or compensate for many of the responses of plants and ecosystems to temperature, thus the effects of warming and CO₂ on ecosystem responses should be studied together [2]. Previous research has focused on how single factors such as changes in CO₂ concentrations [e.g. 1] or changes in temperature [e.g. 3] may alter ecosystem functions such as decomposition, but the interactions of climate change drivers have been less studied [4-5]. Interactions among climate drivers may increase or decrease the effect single factors have on ecosystem function, thus understanding how they shape ecosystem responses is important if we are to make good

predictions about how ecosystems will respond to climatic change in the future.

Decomposition is the process that links decaying organic material to living organisms by transforming nutrients from organic to inorganic forms [6]. Decomposition is responsible for recycling nutrients, including carbon, in ecosystems and can be an important indicator of changes in plant available nutrients [6]. Ecosystem decomposition and nutrient release rates can be altered when the quality of litter inputs into ecosystem changes [7-8]. Litter quality inputs could be altered by changing the litter chemistry and inputs of existing plants or it can happen when the community of plants in an ecosystem changes [4]. Much research has focused on how increases in atmospheric CO₂ concentrations may alter initial litter quality and thus decomposition rates [e.g., 1] or how climate may alter decomposition rates [e.g., 9]. It is possible that changes in climate will also alter the community of species in an ecosystem and

the change in species litter inputs will be greater than the change in litter chemistry due to elevated CO₂. Additionally, until recently, research has focused on manipulating single climate change factors such as the effects of elevated CO₂ or elevated temperature on ecosystem processes [e.g., 1, 3]. These factors, however, will not occur independently and are likely to alter ecosystem processes differently, perhaps mediating some of the effects [10]. This project investigated how climate change drivers (elevated CO₂ and temperature) and their interactions effected decomposition rates either directly by altering litter quality or indirectly by altering the community of species present, which would then alter the quality of litter input to the ecosystem.

An open-top chamber experiment was utilized that contained a constructed old-field ecosystem with plant species that included C3 and C4 grasses, forbs, and legumes. Two experiments were constructed that investigated the direct (litter quality) and indirect (changes in species composition) effects of elevated CO₂ and temperature on decomposition rates in an adjacent old-field ecosystem. The first experiment examined the main effects and interactions of CO₂ and warming on litter quality and subsequent mass loss rates. The second experiment examined the indirect effect climate change may have on plant community composition, litter inputs, and subsequent mass loss rates. Changes in atmospheric CO₂ and temperature appear to have a greater effect on decomposition rates by changing the species composition in the chambers than by causing a change in litter chemistry.

MATERIALS AND METHODS

Site Description

This experiment was conducted on the Oak Ridge National Laboratory National Ecological Research Park (NERP) in Oak Ridge, Tennessee, USA. Agricultural use of the site was abandoned in 1943 and the soil at the site is classified as Captina silt loam [11]. The Oldfield Community Climate and Atmospheric Manipulation (OCCAM) project was established in 2002. Five research plots in three blocks (n = 3) were trenched to 75cm to create 4-m diameter plots. Plots were trenched down the center and all the trenches were lined 4 mil PVC film and backfilled with soil to provide a moisture and thermal barrier. Vegetation remaining in the plots was killed with herbicide and removed.

Seedlings of seven plant species, *Plantago lanceolata*, *Dactylis glomerata*, *Lespedeza cuneata*, *Trifolium pratense*, *Solidago canadensis*, *Andropogon virginicus*, and *Festuca pratense*, were grown in a green house and planted in each plot in July 2002 and April 2003. These plants include a C3, C4, and N-fixing grasses, forbs, and shrubs (Table 1).

Open-top chambers (OTCs) with rain-out shelters were constructed on three of the four treatments in each block, the fourth was left unchambered as a control. There was a significant chamber effect, thus unchambered plots were not sampled for this experiment. OTCs were 2.2m high and 4m in diameter, constructed of aluminum frames and covered with clear PVC panels. The bottom half of the PVC panel is a plenum with the inner wall perforated with 2.5cm holes. A fan pushed ambient air through an evaporative cooler and

Treatment (bag designation)	Plantago C3 dicot	Andropogon C4 bunchgrass	Solidago perennial forb	Dactylis C3 bunchgrass	Lespedeza N-fixing shrub
ECAT	0.03	0.44	0.07	0.98	0.48
ACAT	0.01	0.35	0.04	0.88	0.72
ECET	0.04	0.03	0.06	0.57	0.80
ACET	0.08	0.42	0.18	0.35	0.97
Standard	0.40	0.40	0.40	0.40	0.40

Table 1. Leaf litter mass (g) placed in decomposition bags in the field. Litter mass was determined from peak standing biomass of plants in the open-top chamber experiment. Treatments are designated as following: EC = Elevated CO₂, AC = Ambient CO₂, ET= Elevated Temperature, AC = Ambient Temperature, Standard = Standard Amount of litter in each bag.

in-line heating coils into the plenum distributing it around the plot. Heaters and coolers regulated chamber temperature while pure CO₂ was introduced into the plenum of elevated CO₂ plots to achieve daytime CO₂ enrichment of 300 ppm over ambient air. Treatments began in May 2003. Elevated [CO₂] treatments have averaged 338ppm above outside ambient [CO₂], and elevated temperatures averaged 3.2°C above outside ambient temperatures. These values are consistent with IPCC projections of climate change in the southeastern US within the next 100 years. Treatments are designated as: ECAT, ACAT, ECET, ACET, where EC = Elevated CO₂, AC = Ambient CO₂, ET= Elevated Temperature, AC = Ambient Temperature.

Irrigation treatments began in June 2003 and mimicked long-term mean weekly precipitation records from a local weather station in Oak Ridge, TN. Rainwater was collected and added weekly to dry (2mm) and wet (25mm) plots.

Experimental Design

At the end of the growing season in 2005, leaf litter material was collected from species in each plot. Litter was brought back to the laboratory, air-dried, and each species was homogenized within each plot. Insufficient leaf material was available to use litter from wet and dry treatments, so wet and dry treatments were combined. Also, *Trifolium* was not present in significant amounts in 2005 and thus was not included in the experiment. Using peak biomass data from each species in each of the plots in 2005 (Engle et al. unpublished data), decomposition bags were constructed that reflected the proportion of plant material entering the ecosystem in each of the treatments (hereafter 'natural' bags). Decomposition bags were also constructed that contained a standard amount of leaf material collected in each plot (hereafter 'standard' bags). These bag types represent the different possible effects treatments (elevated temperature and CO₂) may have on decomposition; direct via tissue quality changes, indirect via species composition changes. Each decomposition bag contained approximately 2g of leaf material (Table 1).

Leaf litter decomposition bags (15.5cm x 15.5cm) were constructed of a double layer of 3-mm nylon mesh on the side facing up and a single layer of 1.3mm plastic window screening on the side in contact with the soil surface. The larger mesh size on top enabled litter microarthropods to access the bags, while the smaller mesh

on the bottom reduced litter loss due to fractionation. Bags were stitched together on three sides with polyester thread and closed with stainless steel staples. For each chamber, two replicates of natural and standard bags were constructed with three removal dates. In total, 144 bags were placed in an oldfield adjacent to the experimental plots (12 plots x 2 bag types x 2 replicates x 3 removal dates = 144). The adjacent old-field contained species that were similar to those found within the experimental plots. The experimental chambers were not used for this experiment, as insufficient space in the plots for the decomposition bags and their placement would have compromised the experiment.

Decomposition bags were deployed in May of 2005 and collected in July 2005, September 2005, and January 2006. Litter bags were secured to the soil surface using metal stakes and their locations flagged for easy collection. Upon collection, decomposition bags were brought back to the laboratory in individual paper bags, air dried, and sorted to remove debris that might have entered the bag after deployment. Air-dried samples were oven dried at 70°C, weighed, and ground using a Pica ball-mill grinder (Cianflone Scientific Instruments Corporation, Pittsburg, PA) to a fine powder. Subsamples were analyzed for total C and N using a Costech CHN analyzer (Milan, Italy). Samples were ashed in a muffle furnace at 550°C for 6 hours and data are presented on an ash-free oven-dry mass basis.

Data Analysis

All statistical analyses were conducted using JMP 4 statistical software with significance defined as $P \leq 0.05$ (SAS Institute, 2001, Pacific Grove, CA). Natural and standard decomposition bag data were analyzed separately. Initial litter chemistry data were analyzed using ANOVA with the independent variable chamber type (ECAT, ACAT, ECET, ACET). For decomposition data, full factorial, fixed effects ANOVAs were conducted to test the independent variables of chamber type (ECAT, ACAT, ECET, ACET) and sample removal date (July, September, January) with interactions on mass loss. A student-t test was used to test for differences among treatment means. Proportional data were transformed using the arcsine square root transformation. All data are shown as non-transformed means in figures and tables. Where appropriate, data are shown on an ash-free, oven-dry mass basis.

RESULTS

Initial litter %C, %N, and C:N values were not different among treatments in standard decomposition bags (Table 2). Initial litter chemistry in natural decomposition bags differed significantly among treatments (Table 2). % C values were 4.5% higher ($F_{3,11} = 5.48$, $P = 0.02$) and %N were 41% higher ($F_{3,11} = 4.19$, $P < 0.05$) in ACET and ECET chambers than the ECAT chambers (Table 2). C:N ($F_{3,11} = 4.87$, $P = 0.03$) values were significantly lower in ACET and ECET chambers relative to ECAT chambers (Table 2).

Chamber type ($F_{11,3} = 3.53$, $P = 0.03$) and removal date ($F_{11,2} = 301.41$, $P < 0.001$) each had a significant effect on standard decomposition bag mass loss, but there were no interactions (Table 3,

Bag Type	Standard			Natural		
	%C	%N	C:N	%C	%N	C:N
ECAT	44.01	1.05	41.91	44.27 ^a	0.99 ^a	44.72 ^a
ACAT	44.72	1.10	40.65	45.10 ^{ab}	1.22 ^{ab}	36.97 ^{ab}
ECET	45.00	1.05	42.86	45.77 ^b	1.40 ^b	32.69 ^b
ACET	45.08	1.19	37.88	45.95 ^b	1.40 ^b	32.82 ^b

Table 2. Initial litter chemistry for decomposition bags in each treatment (n=3). Litter was placed in decomposition bags in the percentages found in open-top chambers. Natural bags reflect natural percentages of plants found in the field, while standard bags have a standard amount of each species. Treatments are designated as following: EC = Elevated CO₂, AC = Ambient CO₂, ET = Elevated Temperature, AC = Ambient Temperature. Letters denote significant differences ($P \leq 0.05$) within columns.

Model	Standard			Natural		
	df	P-value	F-value	df	P-value	F-value
Model	11	< 0.001*	55.94	11	< 0.001*	33.30
Effect						
Chamber	3	< 0.03*	3.54	3	< 0.004*	5.92
Removal date	2	< 0.001*	301.41	2	< 0.001*	170.15
Chamber x Removal date	6	0.92	0.32	6	0.27	1.38

Table 3. Probability values and F statistics generated using ANOVA of leaf litter % mass remaining over three collection dates for standard and natural decomposition bags. Chamber refers to the source of the litter. Stars (*) indicate significant differences ($P \leq 0.05$).

Figure 1). ACET showed the highest rates of mass loss followed by ECAT, ECET, and ACAT. ACET mass loss rates were significantly higher than ECET and ACAT rates ($P < 0.05$, Table 3, Figure 1). ECET bags contained 26% more mass than ACAT bags after 8 months of decomposition (Figure 1).

Chamber type ($F_{11,3} = 5.92$, $P < 0.004$) and removal date ($F_{11,2} = 170.15$, $P < 0.001$) also had a significant effect on natural decomposition bag mass loss, and again there were no interactions (Table 3, Figure 1). Once again, ACET lost more mass than the other treatments followed by ECET, ACAT, and ECAT. ECET showed significantly higher mass loss rates than ECAT and ACAT. ECAT showed significantly slower mass loss rates than ACET and ACET (Figure 1). After 8 months of decomposition, 94% more mass remained in ECAT bags than ACET bags (Figure 1).

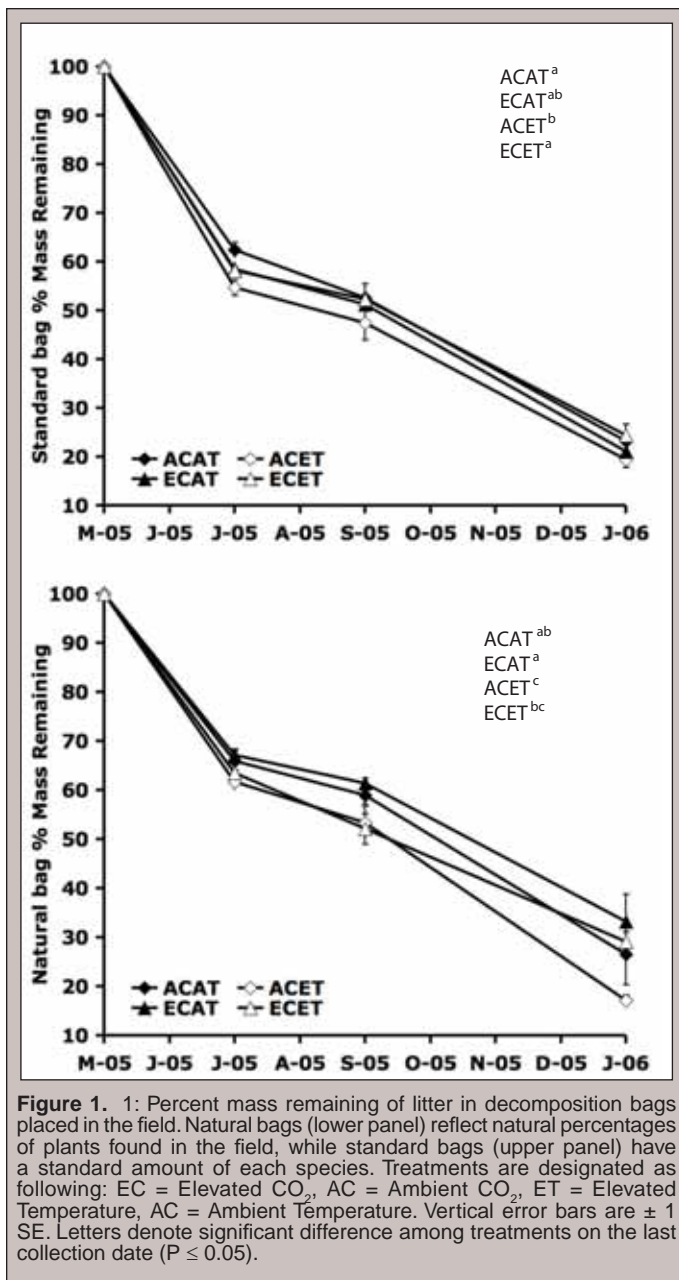


Figure 1. 1: Percent mass remaining of litter in decomposition bags placed in the field. Natural bags (lower panel) reflect natural percentages of plants found in the field, while standard bags (upper panel) have a standard amount of each species. Treatments are designated as following: EC = Elevated CO₂, AC = Ambient CO₂, ET = Elevated Temperature, AC = Ambient Temperature. Vertical error bars are ± 1 SE. Letters denote significant difference among treatments on the last collection date (P ≤ 0.05).

DISCUSSION

This project resulted in two significant findings: 1) Although initial litter %C and %N did not differ among treatments in standard decomposition bags, litter from ACET chambers lost over 20% more mass than litter collected from ECET or ACAT chambers. This result, while statistically significant, is likely to have little biological significance. 2) Differences in plant communities under different climate treatments resulted in changes in initial litter quality. Initial litter in ECAT bags had up to 4% less C and 29% less N than ECET and ACET bags. Mass loss from ACET bags was 48% higher than mass loss from ECAT bags. *Lespedeza*, a N-fixing shrub, was found in a higher proportion in ACET and ECET chambers and, therefore made up the largest proportion of ACET and ECET decomposition bags. The increase in nitrogen in these bags may be

driving their increase in mass loss over time. These results will be discussed in turn below.

Elevated CO₂ and temperature have a limited direct effect on litter chemistry and decomposition

Elevated CO₂ and temperature have limited direct effects on litter chemical quality and mass loss in this experiment. Initial litter %N and %C did not differ among treatments. Although ACET lost more mass than litter collected from other chambers, the biological difference is small and unlikely to change nutrient cycling rates, at least during the first 8 months of the decomposition process. These results support other studies showing minimal effects of elevated CO₂ on litter chemistry [12-13] and decomposition [1]. These studies suggest that other impacts of global change on decomposition, such as changes in species composition, may have a larger impact on litter mass loss and litter nutrient dynamics in ecosystems than small changes in litter chemistry [1].

Elevated CO₂ and temperature mediate decomposition via their impacts on plant community composition

Previous research has documented that changes in plant species composition in communities will occur with rising atmospheric CO₂ concentrations and temperature [4]. This shift in plant community composition may lead to changes in mass loss and nutrient cycling if nutrient rich or nutrient poor species become more abundant in the community. For example, if changes in climate lead to an increase in N-fixers in an N-limited ecosystem, then decomposition and nutrient availability may increase with an increase in N-rich plant material [8]. Alternatively, N-fixers could become less abundant, leading to a decrease in the quality of litter inputs at a community-level and an overall decrease in community litter decomposition and nutrient cycling rates [7]. The current study found that treatments that resulted in a greater abundance of N-fixers also had higher rates of decomposition after 8 months (Figure 1). *Lespedeza*, a N-fixing shrub, was found in higher proportion in the ACET and ECET chambers compared to ACAT and ECAT. It is possible that elevated temperature created a more favorable climate for *Lespedeza* to establish in, thus leading to an increase in N inputs and decomposition rates of litter in these plots.

CONCLUSION

The results of this study corroborate those of other studies demonstrating that the indirect effect of climate change on species composition has a larger impact on decomposition than the direct effect of climate on initial litter chemical quality [9]. However, it is important to remember that resource availability, such as site nitrogen availability, and the large amount of variation found within natural ecosystems substantially broadens the range and timing of climate effects on nutrient processes [7]. When establishing experiments and developing hypotheses about climate impacts on ecosystems, researchers should be as cognizant of how the existing community may shift as they are about how the existing plants will respond to a single climate change factor.

ACKNOWLEDGMENTS

I would like to thank ORNL for an invaluable research opportunity. Many thanks to Aimée Classen and Richard Norby for their guidance, leadership, endless support, and dedication throughout the project. I would also like to thank Rebecca Roha, Emily Mitchell, Colleen Iversen, Joanne Ledford, Luke Zachmann, Katherine Sides, Emmi Felker-Quinn, Joey Roberts, and Kerri Crawford for their assistance. Suggestions by two DOE reviewers greatly improved this manuscript. This project was funded by the U.S. Department of Energy, Office of Science, Biological and Environmental Research Program and completed as part of its Student Undergraduate Laboratory Internship (SULI) program. ORNL is managed by UT-Battelle, LLC, for the U.S. Department of Energy under contract DE-AC05-00OR22725.

REFERENCES

- [1] Norby, R.J., et al., Elevated CO₂, litter chemistry, and decomposition: a synthesis. *Oecologia*, 2001. 127: p. 153-165.
- [2] Houghton, J.J., et al., eds. *Climate change 2001: The scientific basis, contribution of working group I to the third assessment report of the intergovernmental panel on climate change*. 2002, Cambridge University Press: Cambridge, U.K.
- [3] Rustad, L.E., et al., A meta-analysis of the response of soil respiration, net nitrogen mineralization, and aboveground plant growth to experimental ecosystem warming. *Oecologia*, 2001. 126(4): p. 543-562.
- [4] Dukes, J.S. and B.A. Hungate, Elevated carbon dioxide and litter decomposition in California annual grasslands: Which mechanisms matter? *Ecosystems*, 2002. 5(2): p. 171-183.
- [5] Henry, H.A.L., et al., Interactive effects of elevated CO₂, N deposition and climate change on plant litter quality in a California annual grassland. *Oecologia*, 2005. 142(3): p. 465-473.
- [6] Brady, N.C. and R.R. Weil, *The nature and properties of soils*. Twelfth ed. 1999, New York: Macmillan Publishing Company. 1-881.
- [7] Joel, G., et al., Species-specific responses of plant communities to altered carbon and nutrient availability. *Global Change Biology*, 2001. 7(4): p. 435-450.
- [8] Allard, V., et al., Elevated CO₂ effects on decomposition processes in a grazed grassland. *Global Change Biology*, 2004. 10: p. 1553-1564.
- [9] Shaw, M.R. and J. Harte, Control of litter decomposition in a subalpine meadow-sagebrush steppe ecotone under climate change. *Ecological Applications*, 2001. 11(4): p. 1206-1223.
- [10] Dukes, J.S., et al., Responses of grassland production to single and multiple global environmental changes. *Plos Biology*, 2005. 3(10): p. 1829-1837.
- [11] Edwards, N.T. and R.J. Norby, Below-ground respiratory responses of sugar maple and red maple saplings to atmospheric CO₂ enrichment and elevated air temperature. *Plant and Soil*, 1998. 206(1): p. 85-97.
- [12] Finzi, A.C., et al., Forest litter production, chemistry, and decomposition following two years of free-air CO₂ enrichment. *Ecology*, 2001. 82(2): p. 470-484.
- [13] Hall, M.C., et al., Elevated CO₂ increases the long-term decomposition rate of *Quercus myrtifolia* leaf litter. *Global Change Biology*, 2006. 12(3): p. 568-577.

Chad Weldy participated as an intern in the Science Undergraduate Laboratory Internship Program at Pacific Northwest National Lab, where he researched lipid production by microalgae for the purpose of biodiesel fuel. His paper is titled "Lipid Production by *Dunaliella salina* in Batch Culture: Effects of Nitrogen Limitation and Light Intensity." Mr. Weldy's undergraduate major was environmental sciences — environmental toxicology, at Western Washington University (Bellingham, Washington). He is a member of the Air and Waste Management Association, and the Society of Environmental Toxicology and Chemistry. His interests include competitive ultimate frisbee, backcountry hiking, climbing, and snowboarding, and his hometown is Bainbridge Island, Washington.

Michael Huesemann is a Staff Research Engineer at PNNL Marine Sciences Laboratory, Sequim, Washington. He has conducted both experimental and theoretical research in environmental and marine biotechnology for more than fifteen years. Dr. Huesemann is the principal investigator on numerous major U.S. Department of Energy-funded research projects. The projects have focused on diverse areas such as photosynthetic hydrogen production, biofixation of carbon dioxide from flue gases by marine microalgae, the effects of ocean carbon sequestration on nitrogen cycling, and hydrocarbon bioavailability in aged petroleum contaminated soils undergoing bioremediation treatment. He is also the principal investigator on a project on in-situ phytoremediation of PAH and PCB contaminated marine sediments with sea-grasses. In addition, Dr. Huesemann has published many journal articles, and serves as a program manager for DOE's Small Business Innovation Research (SBIR) program. He received his M.S. and Ph.D. in 1989 in biochemical engineering from Rice University, Houston, Texas.

LIPID PRODUCTION BY DUNALIELLA SALINA IN BATCH CULTURE: EFFECTS OF NITROGEN LIMITATION AND LIGHT INTENSITY

CHAD SHARE WELDY AND MICHAEL HUESEMANN

ABSTRACT

Atmospheric carbon dioxide (CO₂) concentrations are increasing and may cause unknown deleterious environmental effects if left unchecked. The Intergovernmental Panel on Climate Change (IPCC) has predicted in its latest report a 2°C to 4°C increase in global temperatures even with the strictest CO₂ mitigation practices. Global warming can be attributed in large part to the burning of carbon-based fossil fuels, as the concentration of atmospheric CO₂ is directly related to the burning of fossil fuels. Biofuels which do not add CO₂ to the atmosphere are presently generated primarily from terrestrial plants, i.e., ethanol from corn grain and biodiesel from soybean oil. The production of biofuels from terrestrial plants is severely limited by the availability of fertile land. Lipid production from microalgae and its corresponding biodiesel production have been studied since the late 1970s but large scale production has remained economically infeasible due to the large costs of sterile growing conditions required for many algal species. This study focuses on the potential of the halophilic microalgae species *Dunaliella salina* as a source of lipids and subsequent biodiesel production. The lipid production rates under high light and low light as well as nitrogen sufficient and nitrogen deficient culture conditions were compared for *D. salina* cultured in replicate photobioreactors. The results show (a) cellular lipid content ranging from 16 to 44% (wt), (b) a maximum culture lipid concentration of 450mg lipid/L, and (c) a maximum integrated lipid production rate of 46mg lipid/L culture*day. The high amount of lipids produced suggests that *D. salina*, which can be mass-cultured in non-sterile outdoor ponds, has strong potential to be an economically valuable source for renewable oil and biodiesel production.

INTRODUCTION

An increase in atmospheric carbon dioxide (CO₂) concentration may be causing a dramatic change to our climate and deleterious effects to the environment [1, 2, 3]. The Intergovernmental Panel on Climate Change (IPCC) has stated in its latest assessment that atmospheric CO₂ concentrations between 550ppm and 1,000 ppm will be reached by 2,100. Even with the most aggressive CO₂ mitigation practices, these concentrations would result in 2°C and 4°C rises in temperature, respectively [2,3]. The increase in atmospheric CO₂ is in large part the result of fossil fuel combustion as the rise in fossil fuel combustion is directly proportional to the rise in atmospheric CO₂ [2, 3]. Although prices for fossil fuels are increasing due to more expensive extraction practices as oil becomes more scarce, demand for fuel has increased. It has been previously

reported that energy demand for transport world wide will nearly double by 2020 [4]. Demand for energy and fuel will not disappear, but the optimal mitigation scenario is to completely shift from fossil fuel use to renewable fuels that do not add CO₂ to the atmosphere. If CO₂ emission rates are not reduced or eliminated, unknown environmental damage will result [5]. The potential worldwide effects from global warming, the observed increase in average atmospheric and oceanic temperatures, has led to an increase in efforts to develop reliable, economically feasible, and sustainable alternative energy sources to replace coal and petroleum [6, 7].

Studies that strategize the complete phase out of fossil fuel use by 2100 include the extensive use of biofuels as one source of energy [7]. The IPCC has concluded that biofuel production can offset fossil fuel emissions by 10–20% by 2050 [7]. Currently, biofuel production has focused on terrestrial plants and ethanol

production from starches. Terrestrial plants have been popular for biofuel production because of the low price for cultivation and production [7]. Terrestrial plants are severely limited by land availability which inherently limits the amount of fuel which can be produced and utilized by humans. If biomass were to supply all primary energy currently used, the production of biomass would have to increase by a factor of seven. Currently, 30-40% of worldwide primary terrestrial productivity is appropriated for food, fiber, and energy [5]. It is simply infeasible to dramatically increase biomass production of terrestrial plants without causing a detrimental impact on the environment.

The production of microalgal lipids that can be synthesized into biodiesel has been of interest to the U.S. Department of Energy (DOE) since the energy shortage in the mid-1970s. The possibility for renewable biofuels led the DOE to establish a program to develop microalgae technology in the late 1970s [8]. The major areas of interest in microalgae research were to determine which strains of algae are capable of producing high amounts of lipids, and what environmental conditions lead to highest lipid yields.

While many microalgae species were found to be capable of producing high amounts of lipids, it was also determined that higher lipid concentrations can be obtained in nitrogen limiting culture conditions [9]. For example *Monallantus salina* was reported to produce as much as 72% lipids in nitrogen-deficient conditions [10]. The relationship between nutrient availability and algal lipid concentration has been understood for more than fifty years. Spoehr and Milner [16] were the first to report that lipid concentration of algal cells can be increased when cultured in nitrogen-deficient medium.

Although biofuels produced by photosynthetic microbes received interest and funding for research, it is currently believed to be infeasible due to the inefficiency and large costs of fuel production [7]. The Aquatic Species Program (ASP) of the U.S. National Renewable Energy Laboratory (NREL) invested US \$25 million into renewable fuels produced by photosynthetic microbes over a period of 20 years, only to terminate funding in the late 1990s due to concerns over economic feasibility [11].

Algal biodiesel production was determined to be economically infeasible because large scale sterile bioreactors are very expensive and difficult to develop [7]. Sterile bioreactors are required for many species that are known to produce high amounts of lipids (e.g., *Cyclotella cryptica*, *Tetraselmis suecica*, and *Monoraphidium minutum*). Relatively inexpensive, large outdoor algal ponds are critical to economically worthwhile production from photosynthetic species. Outdoor culture ponds have been studied over the last four decades and ponds which lead to maximum growth have been developed. Feasible, non-sterile open pond production has been found for only three taxa: *Spirulina platensis*, *Dunaliella salina*, and *Chlorella* [12]. This is due to the extreme environments that they live in, e.g. *S. platensis* can grow in highly alkaline medium with a pH up to 10, *D. salina* can grow in salinity levels greater than 200g NaCl L⁻¹. Because these species grow in extreme conditions, parasitic contamination is avoided and maximum productivity can be achieved [7].

Very little research has been done on the effects of nitrogen limitation and light intensity on lipid content of one of these taxa, *D. salina*, which can be industrially cultured in outdoor growing

ponds. The lipid content of *Dunaliella salina* has been previously published to be between 45% and 55% of its total weight [13], but few tests have been done regarding N-limitation or light intensity. There has been some effort to look at photosynthetic hydrocarbon production by *D. salina* in Korea [6, 11, 12, 14, 15], but all papers published were poorly written and the data were inconsistent. The results reported range in lipid content from 0.22 to 52.12 to 350mg hydrocarbons L⁻¹.

Recently, the Pacific Northwest National Laboratory has submitted *Dunaliella salina* for genome sequencing at the Joint Genome Institute (JGI). This will open possibilities for metabolic regulation research and the potential to better understand metabolic regulation and lipid production with the goal to optimize certain products.

This study has three objectives: First, to determine if *Dunaliella salina* can produce high amounts of lipids, second, to determine if nitrogen limitation increases the cell lipid content, and third, to determine if a higher light intensity that is more representative of an outdoor culture pond increases lipid production. It is the hypothesis of this study that *D. salina* produces lipids at rates that could make large scale biodiesel production economically feasible, and that lipid production rates will increase with higher light intensity and with decreased nitrogen available in solution.

The results of this research can have great importance. If *D. salina* is capable of producing significant quantities of biodiesel, the microalgae biodiesel could become a large factor in reducing CO₂ emissions by replacing limited oil based fuel sources and thereby reducing the potential deleterious effects of global warming.

MATERIALS AND METHODS

The green algae, *Dunaliella salina*, strain CCAP1918, from the Culture Collection of Algae and Protozoa (CCAP), was cultured in four 1L Roux bottles. Two bottles were under a 24 hour high light exposure (800µmol/m²*sec) and two bottles were under a 24 hour low light exposure (200µmol/m²*sec). The medium of one bottle at each light intensity had a high starting nitrogen concentration (20mM NO₃) and the other bottle at each light intensity had a low starting nitrogen concentration (2mM NO₃), Table 1. Bottles were sparged with CO₂ enriched air (0.5% v/v CO₂) at 30mL/min for the duration of the experiment by a Pasteur pipette inserted into the culture medium. During the entire experiment, temperature and pH were maintained at 28°C and 8.1 respectively. Over-heating was avoided by the use of cooling bottles placed between the light source and the culture bottles. The culture medium within the Roux bottles was mixed constantly by shaker table at 60rpm. The experiment was continued for roughly 13 days and was conducted in replicate at the same time. The culture medium contained a NaCl

	Low Light	High Light
Low Nitrogen	2 mM NO ₃ , 200µmol/m ² *sec	2 mM NO ₃ , 800µmol/m ² *sec
High Nitrogen	20 mM NO ₃ , 200µmol/m ² *sec	20 mM NO ₃ , 800µmol/m ² *sec

Table 1. Table of experimental conditions.

concentration of 1M. The culture medium composition is described in detail in Table 2.

D. salina cell growth was measured by ash free dry weight (AFDW) and optical density at a wavelength of 590nm (OD590). AFDW was determined by vacuum filtering a selected volume (V) of culture through a Whatman, 55mm, GF/F glass microfibre filter. The difference in weight between the filter after drying overnight in a 105°C oven (M_1) and after combusting the cells on the filter in a 550°C furnace for 30 minutes (M_2) was then divided by the volume of culture that was vacuum filtered, i.e., $AFDW = (M_1 - M_2)/V$. All AFDW measurements were conducted in replicate and expressed in mg/L. Filters were pre-vacuum rinsed with 25ml of de-ionized water and then pre-ashed in a 550°C furnace for 15 minutes. Two culture medium blanks were used to correct any blank error in AFDW determination. All weight measurements were made with a Mettler Toledo AG135 four place analytical balance. Optical density (OD590) was measured by using a UNICO 1100

Spectrophotometer. All samples were diluted with blank medium to the model's linear range (<0.5 A) if needed.

Nitrate concentration was measured by conductivity using an Orion Model 420A along with an Orion 93 series electrode body. The instrument was calibrated using the same culture medium as in the experiment with varying known nitrate concentrations. Due to a high salt concentration in the medium, the sensitivity of the instrument was low and the data are used as reference only since it is not entirely reliable.

Lipid measurements were made using a method adapted from Bligh and Dyer [16]. This method extracts the lipids from the algal cells by using a mixture of methanol, chloroform, and water. A culture sample is collected at three points during the experiments for lipid analysis. The culture sample is centrifuged at 3,500rpm for 10 minutes in a large (200ml) plastic centrifuge tube, the pelleted cells along with 35ml of supernatant are then transferred to a glass centrifuge tube (50ml) to be re-centrifuged again at 3,500rpm for 10 minutes. The supernatant is removed by pipette. The pellet is

RECIPE FOR THE GROWTH MEDIUM OF <i>DUNALIELLA SALINA</i> (MODIFIED FROM THE ORIGINAL MEDIUM RECIPE FROM DR. POLLE, 6/26/06)	
(A) CONCENTRATED NUTRIENT MIX	Per 1 L
Distilled H ₂ O	500 ml
2 M Tris-HCl (FW:=57.6 g/mol; 315.2 g/L) Adjust to pH 7.5	200 ml
1 M MgSO ₄ (FW=120.4 g/mol; 60.2g/0.5L)	50 ml
60 mM CaCl ₂ (FW=111.1 g/mol; 3.33g/0.5L)	50 ml
20 mM KH ₂ PO ₄ (FW=136.1 g/mol; 2.72g/L)	100 ml
0.4 mM FeCl ₃ (FW=162.3 g/mol; 0.065 g/L)	
in 4 mM EDTA (FW=292.2 g/mol; 1.17 g/L) Adjust to pH 7.5	100 ml
(B) MICRONUTRIENT MIX	Per 1 L
3M H ₃ BO ₃ (FW of anhydrous form=61.83g/mol; 9.27g/50ml)	50 ml
200 mM MnCl ₂ (FW of tetrahydrate form=197.9 g/mol; 1.98g/50ml)	50 ml
16 mM ZnSO ₄ (FW of heptahydrate form=237.5 g/mol; 0.19g/50ml)	50 ml
6 mM CuCl ₂ (FW of dihydrate form=170.5 g/mol; 0.051g/50ml)	50 ml
40 mM Na ₂ MoO ₄ (FW=241.95 g/mol; 0.484g/50ml)	50 ml
40 mM NaVO ₃ (FW=121.9 g/mol; 0.244g/50ml) ORDERED	50 ml
4 mM CoCl ₂ (FW of hexahydrate form=237.9 g/mol; 0.048g/50ml)	50 ml
Distilled water	650ml
Dissolve each ingredient separately before mixing. Heat NaVO ₃ and H ₃ BO ₃ to dissolve. Add individual solution one by one (from the list above, top to bottom) slowly in distilled water (650 ml).	
(C) BICARBONATE SOLUTION (1.0 M)	
Dissolve 84 g of NaHCO ₃ (sodium bicarbonate, FW=84 g/L) in about 900 ml of distilled water. Then titrate to pH of 7.4 and afterwards fill with distilled water up to 1,000 ml.	
(D) SODIUM CHLORIDE SOLUTION (4M)	
Dissolve 233.6 g of NaCl in 1 L of warm distilled water to obtain a 4 M solution.	
(E) POTASSIUM NITRATE (KNO₃) SOLUTION (0.4 M)	
Dissolve 40.48 g KNO ₃ in 1 L distilled water to obtain a 0.4 M solution.	
GROWTH MEDIUM (1.0 M NaCl)	Per 1 L
H ₂ O	550 ml
SODIUM CHLORIDE SOLUTION (D)	250 ml
CONCENTRATED NUTRIENT MIX (A)	100 ml
MICRONUTRIENT MIX (B)	1 ml
NITRATE SOLUTION (E)	50 ml
1.0 M NaHCO ₃ (C)	50 ml
STERILE FILTER MEDIUM, AUTOCLAVE ROUX BOTTLES	

Table 2. Growth Medium for *Dunaliella salina*.

then resuspended with 4ml of DIH₂O, then 10ml of methanol and 5ml of chloroform is added, resulting in a 10:5:4 ratio of methanol:chloroform:water. At this ratio, all solvents are miscible and form one layer. After overnight extraction on a shaker table, 5ml of water and 5ml of chloroform are added which results in a 10:10:9 ratio of methanol:chloroform:water. Tubes are centrifuged for 10 minutes at 3,500rpm. At this solvent ratio, two layers are formed, a water-methanol upper layer and a chloroform lower layer. The chloroform lower layer which contains the extracted lipids is then removed by Pasteur pipette and placed into a pre-weighed vial. After the first extraction, 10ml of additional chloroform is added to conduct a second extraction. The additional 10ml of chloroform again results in a 10:10:9 methanol:chloroform:water ratio and two layers are formed. The tube is centrifuged at 3,500rpm for 10 minutes, and the lower chloroform layer is removed by Pasteur pipette and placed into another pre-weighed vial. The chloroform is evaporated by heating in a 55°C water bath under a constant stream of nitrogen gas. After 1 hour in a 105°C oven, vials are weighed again. The weight difference represents weight of lipids extracted from the culture sample. Percentage of lipid content can be determined by measuring the AFDW of the culture sample at the same time as the lipid analysis. The mass of cells used for the lipid analysis can be determined by multiplying the AFDW by the volume of culture used for the lipid sample. The weight of lipids extracted can then be divided by the mass of cells extracted to determine the % lipid content.

Fifty milliliters of culture were collected daily for AFDW, OD590 and nitrate determination. Lipid analysis was performed for the inoculum culture to derive a lipid concentration value at time “zero”, and at three points during growth, at the early exponential phase, the late exponential phase, and the late stationary phase (end of experiment). All data were analyzed using Microsoft Excel 2003.

RESULTS

Growth

Biomass growth in both high and low light 2mM NO₃ cultures slowed when an AFDW of 400 (mg/L) was reached (Figures 1 and 2). The 20mM NO₃ cultures continued to grow but the high light 20mM culture grew to a much higher AFDW than the low light 20mM culture (Figures 1 and 2). The highest AFDW was measured in Replicate 1 at over 1,500mg/L.

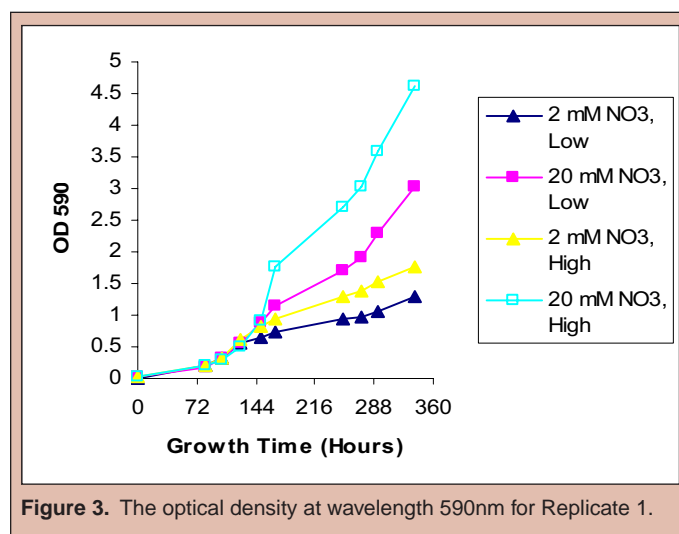
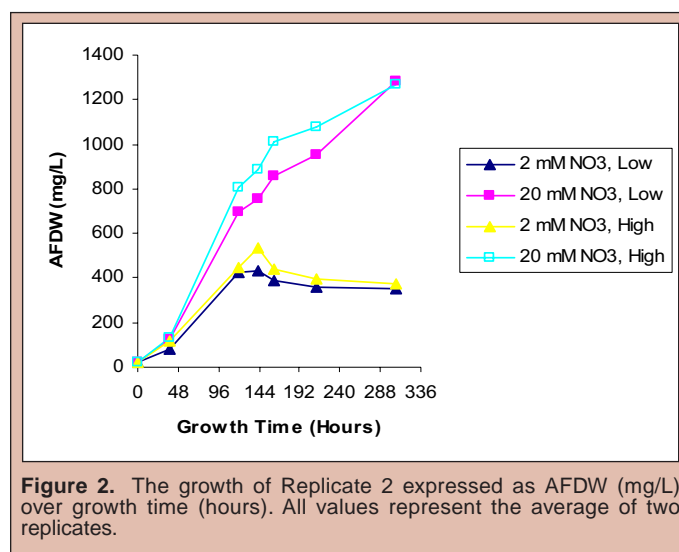
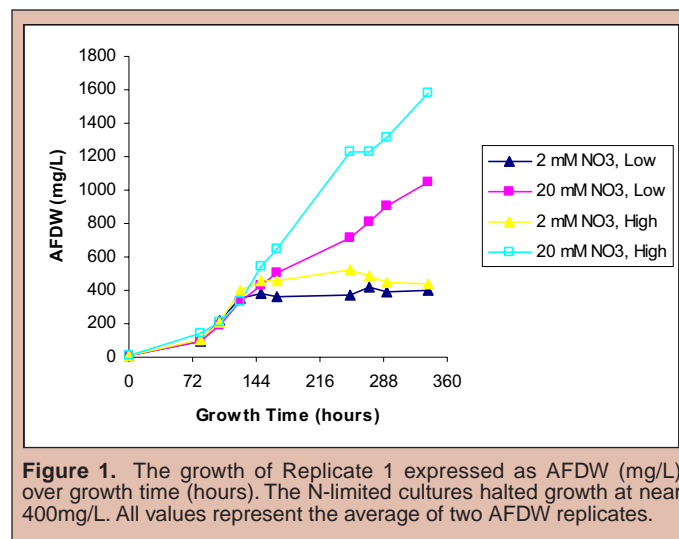
Nitrate

The results show that there is a general decline in N concentration and that there is a large difference in N concentration between the N-sufficient cultures and the N-deficient cultures (Figures 5 and 6). The results also indicate that the high N cultures did not reach N-limitation, while the low N-cultures did.

Lipid Content

The % lipid content for *D. salina* ranged from 16–44% when in early exponential phase to early stationary phase, respectively.

(Figures 7 and 8). In Replicate 2, the maximum lipid content was measured at 44% for N-deficient under high light while only 38% for N-sufficient under high light. In Replicate 1, lipid content was



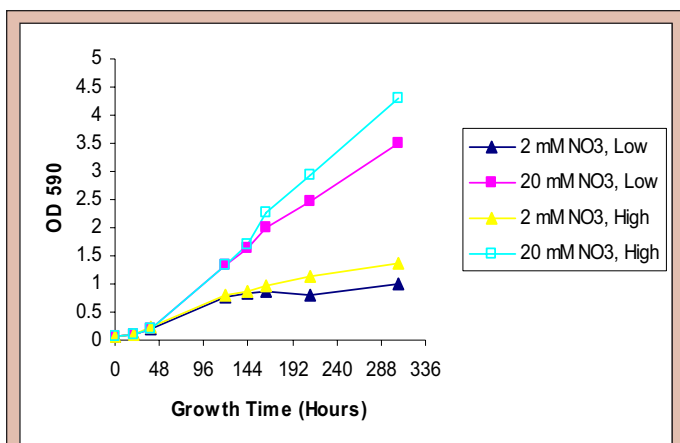


Figure 4. The optical density at wavelength 590nm for Replicate 2.

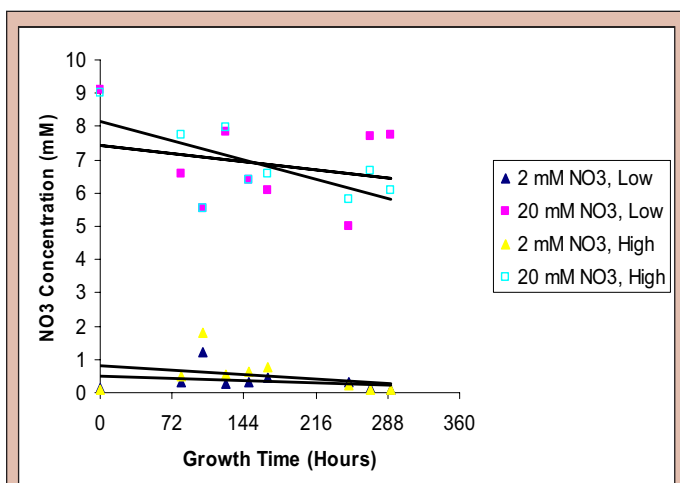


Figure 5. Nitrate concentration as a function of time for Replicate 1.

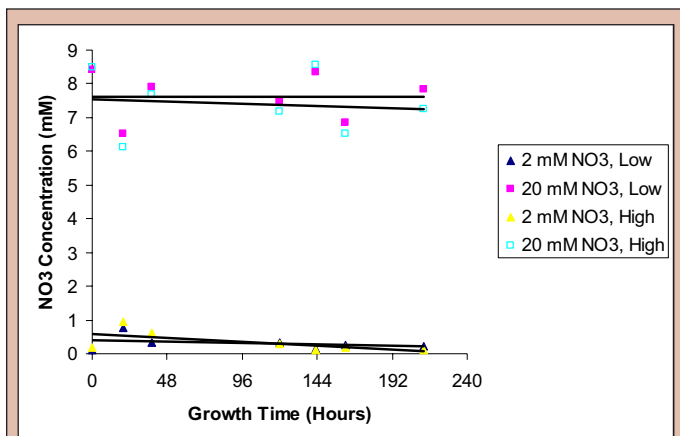


Figure 6. Nitrate concentration as a function of time for Replicate 2.

23% for the low light, N-sufficient culture while it was 30% for the high light, N-sufficient culture.

As shown in Figures 9 and 10, the highest lipid concentration is reached in N-sufficient medium under high light (Figures 9 and 10). Replicates 1 and 2 reached a maximum of 450 and 440mg lipid/liter culture respectively. This was reached in the high light 20mM NO₃ cultures. The highest lipid concentration for the low light cultures in N-deficient medium was recorded to be 110 and 135mg lipid/liter culture for Replicates 1 and 2 respectively (Figures 9 and 10).

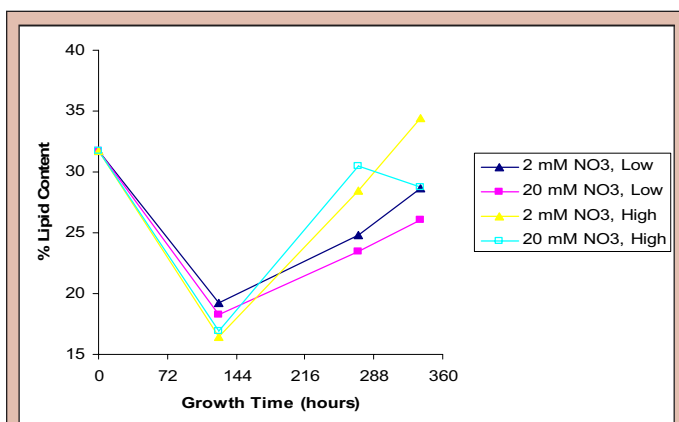


Figure 7. Percent lipid content as a function of growth time (hours) for Replicate 1. The minimum lipid content is 16% and the maximum is 34%.

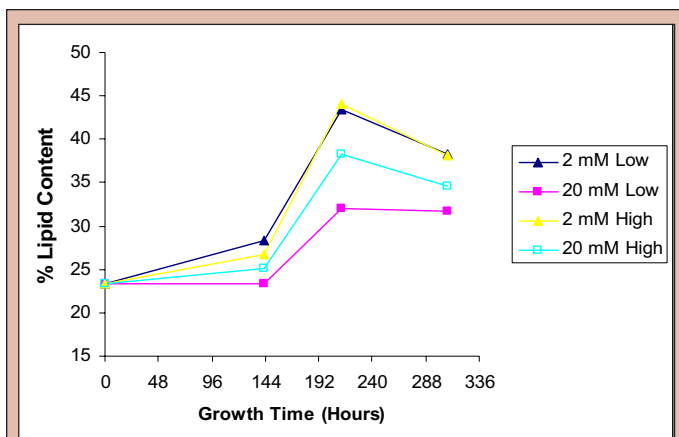


Figure 8. Percent lipid content as a function of growth time (hours) for Replicate 2. The minimum lipid content is 23% at inoculation and the maximum is 44%.

Lipid Production Rates

The rate of lipid production is expressed in mg lipid/ L*day. It is reported either as integrated lipid production rate over the number of total elapsed days (Figures 11 and 12) or lipid production rate between the (sampling) times of lipid analysis (Figures 13 and 14). The highest integrated rate of lipid production over total elapsed days was reached in Replicate 2 for the N-sufficient culture under high light. Lipid production was 46mg/L*day after about 9 days of growth. The highest lipid production rate found for Replicate 1 was

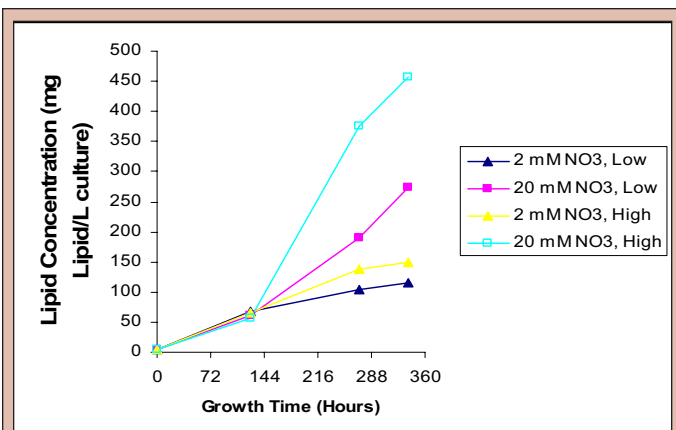


Figure 9. Lipid concentration in the culture medium over time (mg lipid/L culture) for Replicate 1. The highest lipid concentration was recorded for the N-sufficient, high light culture.

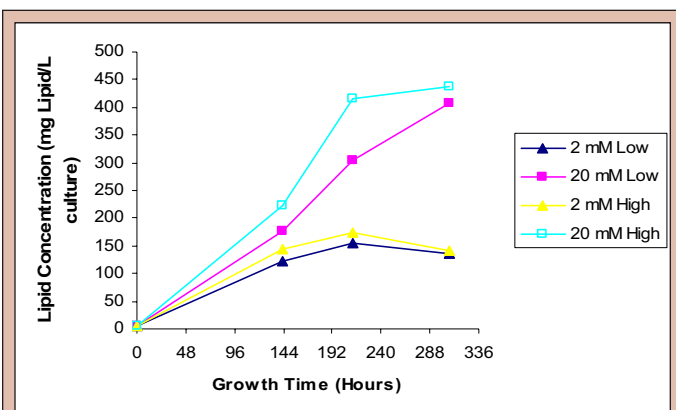


Figure 10. Lipid concentration in the culture medium over time for Replicate 2. Replicate 2 supports Replicate 1, i.e., the highest lipid concentration was recorded in high light and N-sufficient culture.

also in the N-sufficient culture under high light at 33mg lipid/L*day after 11 days (Figures 11 and 12).

Lipid production rates between the times of lipid analysis are also recorded in mg lipid/L culture*day. The rates are calculated for each time interval to determine when highest lipid production rates are achieved. Lipid production rates are greatest during high

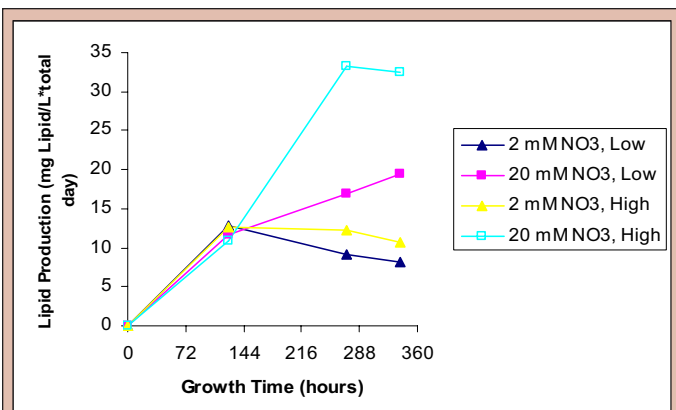


Figure 11. Integrated lipid production rate over total elapsed days for Replicate 1. The highest integrated production rate was recorded after 11 days for the N-sufficient, high light, culture at 36mg lipid/L*day.

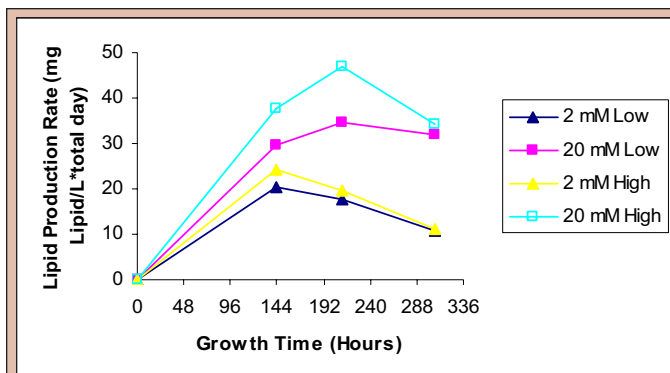


Figure 12. Integrated lipid production rate over total days for Replicate 2. The highest integrated lipid production rate was recorded after 9 days for the N-sufficient, high light, culture at 46mg lipid/L*day.

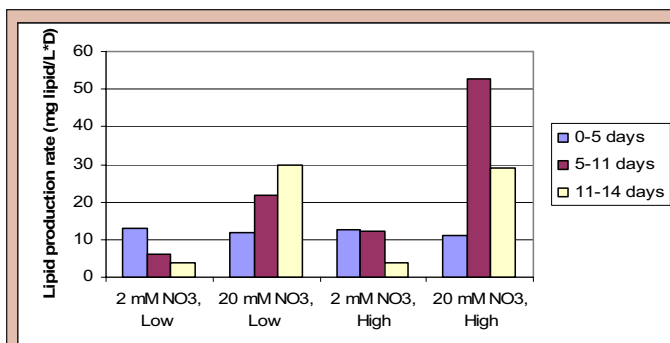


Figure 13. Lipid production rates between the times of lipid analysis for Replicate 1. The highest lipid production rate was achieved between days 5 and 11 at 52mg lipid/L*day.

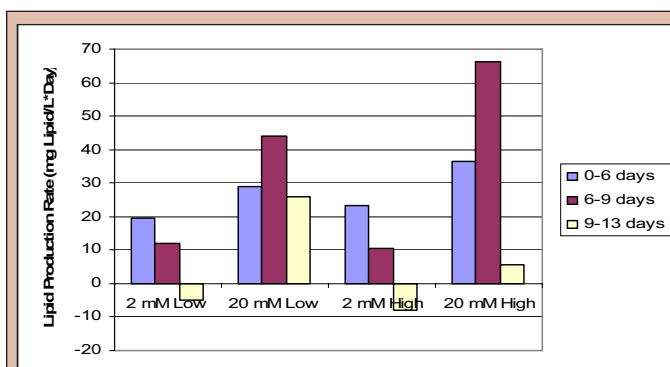


Figure 14. Lipid production rates between the times of lipid analysis for Replicate 2. The highest lipid production rate was for the N-sufficient, high light culture at 66mg lipid/L*day.

rates of biomass growth (Figures 13 and 14). The highest lipid production rate was recorded for Replicate 2 between day 6 and 9 of growth at 66mg lipid/Liter culture*day (Figure 14). As the algal culture reaches the late stationary phase and the death phase, the lipid production rate dramatically decreases (Figures 13 and 14). The highest lipid production for N-deficient cultures was recorded at 12mg lipid/L culture*day.

DISCUSSION

There are four conclusions that can be made from the results. First, the experimental results indicate that N-deficient cultures will develop higher % lipid content than N-sufficient cultures. Second, cultures under high light will develop higher % lipid content than cultures under low light. Third, culture lipid concentration and lipid production rates indicate that higher amounts of lipids are produced under N-sufficient conditions and high light due to higher biomass growth. Fourth, the % lipid content is less important than maximizing growth with respect to lipid production.

The results from this research suggest that actual lipid content of *D. salina* ranges from 15–45% depending on growing conditions and growth phase. This is less than the previously published 45–55% lipids by Tornabene et al. [13]. Lipid content data indicate that N-deficiency will increase lipid content for *D. salina*. There has been no published literature on this relationship with *D. salina*. Although the replicate tests differed in percent lipid content, they were very similar in general lipid trends and on lipid concentration of the culture, reaching a maximum of approximately 450mg lipid/liter culture for both replicates.

Currently, it is the general belief that large scale production of biodiesel from photosynthetic microalgae is economically infeasible due to the tremendous costs of sterile growing conditions [11]. But there has been little research on species which can grow in non-sterile conditions and their respective lipid production rates. Current microalgae biofuel research is focused on the species *Botryococcus braunii* due to its high lipid content [17], but little thought has been devoted to the fact that *B. braunii* requires sterile growing conditions and thus will not be economically feasible for large scale biofuel production. Not only does this species require sterile growing conditions, as this paper indicates, percent lipid content is not as important as actual biomass growth when considering total lipid production rates.

Future research for biodiesel production from microalgae must focus on species which can grow in non-sterile outdoor culture ponds. When considering the large scale production of biodiesel from microalgae, outdoor aquacultures are relatively inexpensive and efficient at maximizing the biomass growth of the species. Currently there are only three taxa which are known to be cultured in outdoor ponds, including *D. salina*. *D. salina* is currently mass cultured for beta-carotene production and results from this research suggest that *D. salina* can be cultured to produce high amounts of lipids (46mg lipid/L*day). Future research should examine the large scale production of lipids for biodiesel with *D. salina*, including an in depth economic analysis considering beta-carotene as a high value co-product.

Huntley and Redalje [7] mass-cultured *H. pluvialis* to determine lipid production rates and to perform an economic analysis on the large scale culturing of microalgae for biofuel production. Their results with *H. pluvialis* show lipid production rates equal to or less than those observed with *D. salina* in this study. Their average lipid production was 3.78g m⁻²d⁻¹ grown in 12cm deep outdoor ponds, which is equivalent to 31.5mg lipid/L*day. Although Huntley and Redalje [7] cultured their species outside under natural diurnal (light/

dark) lighting conditions, the light intensity outdoors can be twice as high as the high light intensity used in this study. The conclusion of the economic analysis of Huntley and Redalje [7] suggested that biodiesel mass production is economically feasible. They came to this conclusion by analyzing the lipid production rates and costs of culturing for their species with their method. They determined that the price of oil derived from microalgae would be \$84/bbl. To mass culture *H. pluvialis*, Huntley and Redalje [7] used both sterile and non-sterile growing conditions, where they cultured the species under sterile conditions until inoculation of a large outdoor pond where the single species was being maintained.

Although *H. pluvialis* can potentially produce an economically feasible amount of biofuel, there are at least four reasons why *Dunaliella salina* would be better suited for large scale production of biofuel. First, *D. salina* produces higher amounts of lipids. The lipid production rate of *H. pluvialis* of 31.5mg lipid/L*day is nearly 30% lower than *D. salina* which was found to be near 45mg lipid/L*day. Not only does *H. pluvialis* have a lower lipid production rate, it has much lower percent lipid content than *D. salina* (25% compared to about 40%). Second, *D. salina* does not require sterile growing conditions. The cost of growing *H. pluvialis* under sterile conditions in the initial phase dramatically increases the cost of culturing compared to *D. salina* and its ability to be cultured in outdoor ponds. Third, *D. salina* is already currently mass produced in Australia, India, Israel, and USA for beta-carotene production. Finally, *D. salina* can synthesize beta-carotene as a high value co-product. The ability to increase sales by producing beta-carotene along with oil adds to the potential economic feasibility of mass culturing *D. salina*.

It is the opinion of the author that the halophilic marine microalgae *Dunaliella salina* has great potential to provide large quantities of hydrocarbons that can be converted into biodiesel. The need for renewable biofuels will continue to grow as fossil fuel reserves decline. Continued research leading to an economically viable process that produces biofuel and beta-carotene co-product from *Dunaliella salina* is suggested.

REFERENCES

- [1] Intergovernmental Panel on Climate Change (IPCC): 1995, 'Climate change 1995: Impacts, adaptations and mitigation of climate change: Scientific-technical analyses. Contribution of working group II to the second assessment report of the intergovernmental panel on climate change', in R.T. Watson, M.C. Zinyowera and R.H. Moss (eds.), Cambridge, UK, Cambridge University Press.
- [2] Intergovernmental Panel on Climate Change (IPCC): 2001a, *Third Assessment Report-Climate Change 2001: The Scientific Basis, A Report of Working Group I-Summary for Policymakers*, www.ippcc.ch.
- [3] Intergovernmental Panel on Climate Change (IPCC): 2001b, *Third Assessment Report-Climate Change 2001: The Scientific Basis, Technical Summary of Working Group I*, www.ippcc.ch.

- [4] EIA: 1999, *International Energy Outlook*, Washington, DC, US Department of Energy, Energy Information Administration, DOE/EIA-0484 (1999).
- [5] Huesemann, M.H.: 2006, 'Can Advances in Science and Technology Prevent Global Warming?', *Mitigation and Adaption Strategies for Global Change* **11**, 539-577.
- [6] Pak, J.H., S.-Y. Lee, W.C. Shin, and H.Y. Lee.: 1991, 'Optimization of Producing Liquid Fuel from Photosynthetic Algal Growth', *Journal of Microbiology and Biotechnology*, **1(2)**: 111-115.
- [7] Huntley, M.E., Redalje, D.G.: 2006, 'CO₂ Mitigation and Renewable Oil from Photosynthetic Microbes: A New Appraisal', *Mitigation and Adaption Strategies for Global Change*, Available Online First, May 22, 2006.
- [8] Benemann, J.R. and Tillett, D.M.: 1987, 'Effects of Fluctuating Environments on the Selection of High Yielding Microalgae', *Final Report to the Solar Energy Research Institute*.
- [9] Roessler, P.G.: 1990, 'Environmental Control of Glycerolipid Metabolism in Microalgae: Commercial Implications and Future Research Directions', *Journal of Phycology*, **26**: 393-399.
- [10] Shifrin, N.G. and Chisholm, S.W.: 1981, 'Phytoplankton Lipids: Interspecific Differences and Effects of Nitrate, Silicate and Light-Dark Cycles', *Journal of Phycology*, **17**: 374-384.
- [11] Sheehan, J., Dunahay, T., Benemann, J. and Roessler, P.: 1998, 'A Look Back at the U.S. Department of Energy's Aquatic Species Program-Biodiesel from Algae', Golden, CO, National Renewable Energy Institute, NREL/TP-580-24190, 328 pp.
- [12] Jimenez, C., Cossio, B.R. and Niell, F.X.: 2003, 'Relationship Between Physiochemical variables and productivity in open ponds for the production of *Spirulina*: A predictive model of algal yield', *Aquaculture* **221** (1-4), 331-345.
- [13] Tornabene, T.G., Holzer, G. and Peterson, S.L.: 1980, 'Lipid Profile of the Halophilic Alga, *Dunaliella salina*', *Biochemical and Biophysical Research Communications* **96(3)**: 1349-1356. [16] Bligh, E.G. and Dyer, W.J.: 1959, 'A Rapid Method of Total Lipid Extraction and Purification'. *Canadian Journal of Biochemistry and Physiology* **37 (8)** 911-917.
- [14] Pak, J.H., S.-Y. Lee, Y.-N. Kim, and H.-Y. Lee.: 1993, 'The Production of Algal Hydrocarbons in Outdoor Cultivations of *Dunaliella salina* 1650', *Journal of Microbiology and Biotechnology*, **3(1)**: 46-50.
- [15] Park, D.-H., H.-W. Ruy, K.-Y. Lee, C.-H. Kang, T.-H. Kim, and H.-Y. Lee.: 1998 'The Production of Hydrocarbons from Photoautotrophic Growth of *Dunaliella salina* 1650', *Applied Biochemistry and Biotechnology*, **70-72**: 739-746.
- [16] Spoehr, H.A. and Milner, H.S.: 1949, 'The Chemical Composition of *Chlorella*: Effect of environmental conditions', *Plant Physiology* **24**: 120-149.
- [17] Metzger, P. and Largeau, C.: 2005, '*Botryococcus braunii*: a rich source for hydrocarbons and related ether lipids', *Applied Microbiology and Biotechnology* **66**: 486-496.

Kristin Whitlow participated as an intern in the Science Undergraduate Laboratory Internship Program at the Thomas Jefferson National Accelerator Facility, where she undertook the research presented here. As an undergraduate, she studied Nuclear Engineering at the University of Florida in Gainesville. Ms. Whitlow is a member of the American Nuclear Society, and the Society of Women Engineers. She grew up in Fort Walton Beach, Florida, and she enjoys traveling, soccer, and reading.

Stepan Stepanyan is a staff scientist at the Department of Energy's Thomas Jefferson National Accelerator Facility (Jefferson Lab) in Newport News, Virginia. He received his Ph.D. from Yerevan Physics Institute, Yerevan (Armenia), for a study of deeply bound nucleon states in nuclei using high energy electron-nucleus interactions. He leads several projects for hadron spectroscopy and nucleon structure studies using electron and photon beams and the CEBAF Large Acceptance Spectrometer (CLAS) in Jefferson Lab's Experimental Hall B. He is also working on detector development for the Jefferson Lab 12 GeV Upgrade project.

GEANT SIMULATIONS OF PRESHOWER CALORIMETER FOR CLAS12 UPGRADE OF THE FORWARD ELECTROMAGNETIC CALORIMETER

KRISTIN WHITLOW AND STEPAN STEPANYAN

ABSTRACT

Hall B at the Thomas Jefferson National Accelerator Facility uses the CEBAF (Continuous Electron Beam Accelerator Facility) Large Acceptance Spectrometer (CLAS) to study the structure of the nucleon. An upgrade from a 6 GeV beam to a 12 GeV beam is currently planned. With the beam energy upgrade, more high-energy pions will be created from the interaction of the beam and the target. Above 6 GeV, the angle between the two-decay photons of high-energy pions becomes too small for the current electromagnetic calorimeter (EC) of CLAS to differentiate between two photon clusters and single photon events. Thus, a preshower calorimeter will be added in front of the EC to enable finer granularity and ensure better cluster separation for all CLAS experiments at higher energies. In order to optimize cost without compromising the calorimeter's performance, three versions of the preshower, varying in number of scintillator and lead layers, were compared by their resolution and efficiency. Using GSIM, a GEANT detector simulation program for CLAS, the passage of neutral pions and single photons through CLAS and the new preshower calorimeter (CLAS12 EC) was studied. The resolution of the CLAS12 EC was calculated from the Gaussian fit of the sampling fraction, the energy CLAS12 EC detected over the Monte Carlo simulated energy. The single photon detection efficiency was determined from the energy and position of the photon hits. The fractional energy resolution measured was $\Delta E/E = 0.0972$ in the five-module version, 0.111 in the four-module version, and 0.149 in the three-module version. Both the five- and four-module versions had 99% single photon detection efficiency above 0.5 GeV while the 3 module version had 99% efficiency above 1.5 GeV. Based on these results, the suggested preshower configuration is the four-module version containing twelve layers of scintillator and fifteen layers of lead. This version provides a reasonable balance of resolution, efficiency, and cost. Additional GSIM simulations will be undertaken to verify that the four-module version has acceptable π^0 mass reconstruction and to continue Research and Development (R&D) analysis on the preshower calorimeter.

INTRODUCTION

The Thomas Jefferson National Accelerator Facility (Jefferson Lab) in Newport News, Virginia currently uses the Continuous Beam Electron Accelerator Facility (CEBAF) to send a 6 GeV beam of electrons to three experimental halls. Hall B uses the CEBAF Large Acceptance Spectrometer (CLAS) to study nucleon structure in multi-particle reactions. CLAS detects and measures almost all final-state particles created in collisions using multi-wire drift chambers (DC), time-of-flight scintillation counters (SC), a gas-filled threshold Cherenkov counter (CC), and an electromagnetic calorimeter (EC) [1]. A beam upgrade from 6 GeV to 12 GeV is currently in the planning stages for CEBAF. With the doubling of the beam energy, each of the three halls must also upgrade its

detectors. While the upgraded CLAS detector (CLAS12) will utilize many of the existing detector components, major new components include superconducting torus coils, a new gas Cherenkov counter, a new vertex detector, a new DC, an upgraded SC, and a preshower calorimeter [2, 3].

The main purposes of the electromagnetic calorimeter are to measure the energy of high-energy showering particles [4], to differentiate between electrons and π^0 , and between photons and neutrons [1]. Detection of photons is primarily used for π^0 and η reconstruction via their two photon decays. Background pions are a recurrent problem for the analysis of single photon reactions (DVCS) and must be accurately detected so that the appropriate cuts can be made to exclude them [3]. Since pions themselves cannot be detected due to their short lifetimes, their two-photon decay is used

to determine their presence [3]. With the beam energy upgrade, more high-energy pions will be created from the interaction of the beam and the target. Above 6GeV, the angle between the two photons from a π^0 decay becomes too small for the existing electromagnetic calorimeter to distinguish between two photon clusters and single photon events (Figure 1). Thus, an additional preshower calorimeter with finer granularity to resolve photon clusters from high-energy

The preshower calorimeter will be positioned in front of the existing electromagnetic calorimeter, creating the CLAS12 electromagnetic calorimeter. It will have a geometry similar to the current EC: a lead-scintillator sandwich in a truncated triangular pyramid utilizing a three stereo readout system [1] (Figure 2). Each scintillator layer is sliced into a number of strips which are rotated by 120° in each successive layer [1]. The pattern is repeated every three scintillator layers, creating a module [1].

After evaluating π^0 mass reconstruction and fiducial acceptance, the five-module version with fifteen layers of lead and scintillator and 108 scintillator strips per layer (Figure 3) was taken as a standard for comparison since it showed the best detection efficiency and resolution. The focus of this project was to optimize cost without compromising the calorimeter's performance by comparing the energy resolution and single photon detection efficiency of three different versions of the preshower varying in the number of scintillator and lead layers. The three-module version contained fifteen layers of lead and nine layers of scintillators with the first six layers having double lead thickness (Figure 4). The four-module version contained fifteen layers of lead and twelve layers of scintillators but with the first three layers having double lead thickness (Figure 5).

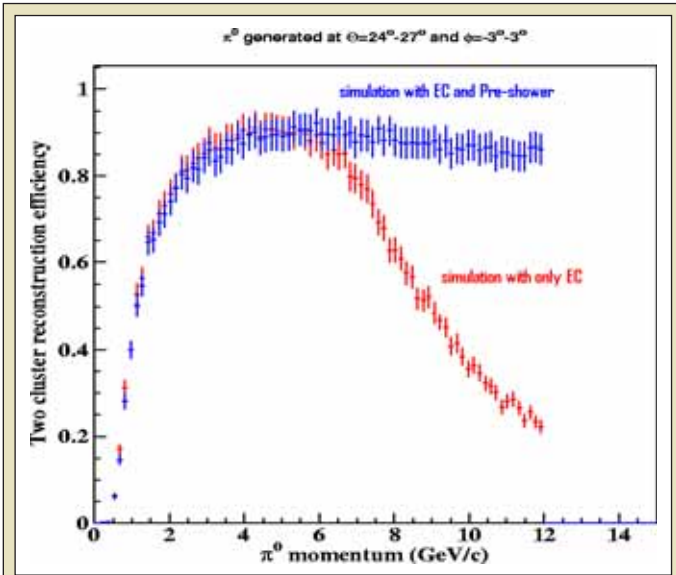


Figure 1. Two cluster reconstruction efficiency of EC with and without preshower for $\pi^0 \rightarrow \gamma\gamma$ for momentum up to 12GeV.

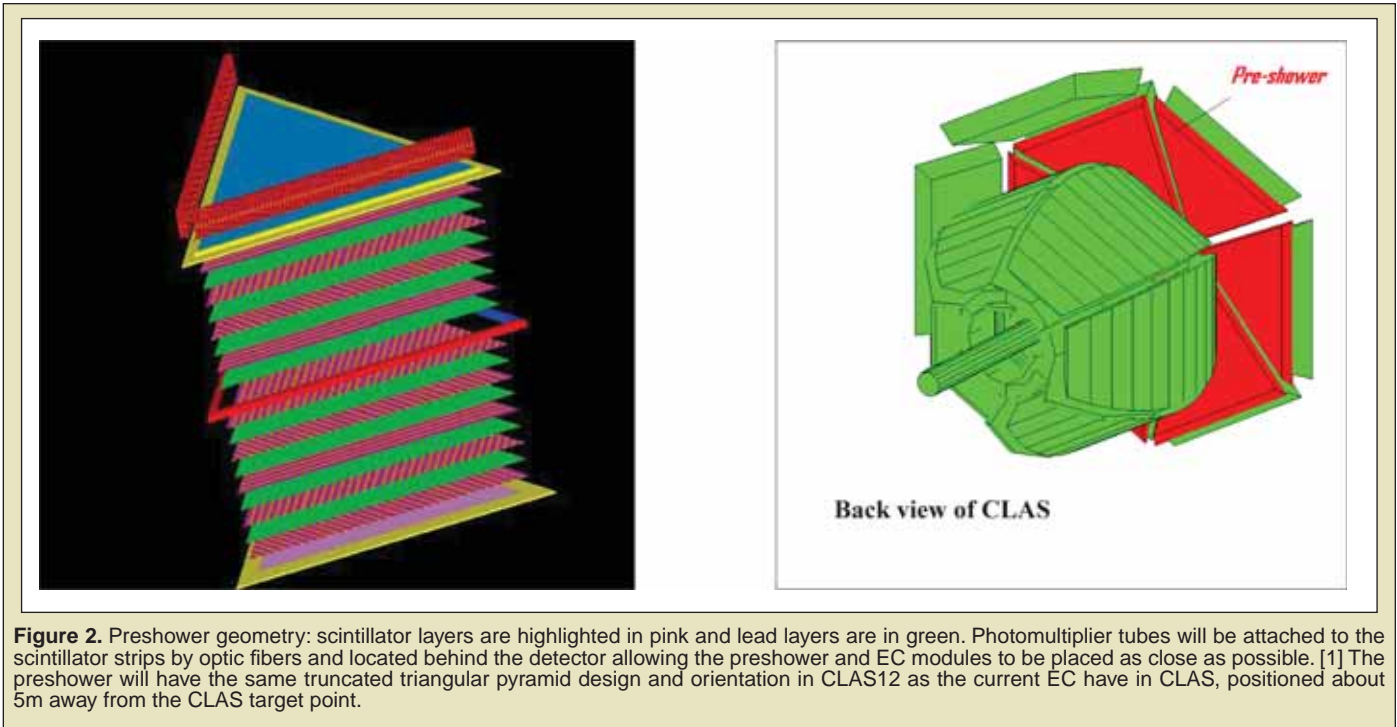
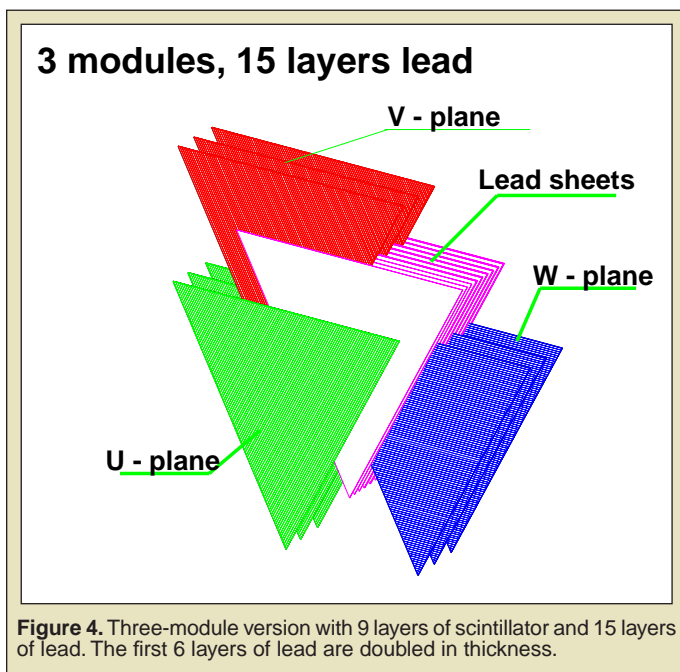
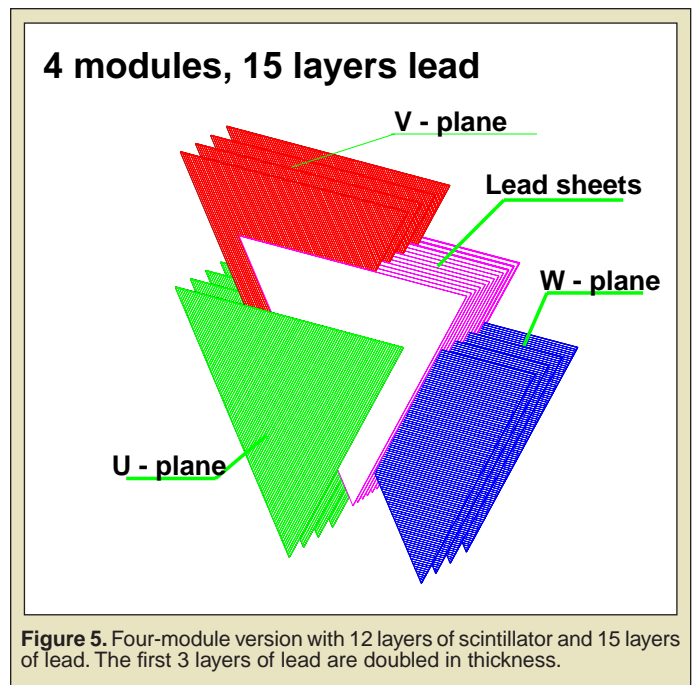
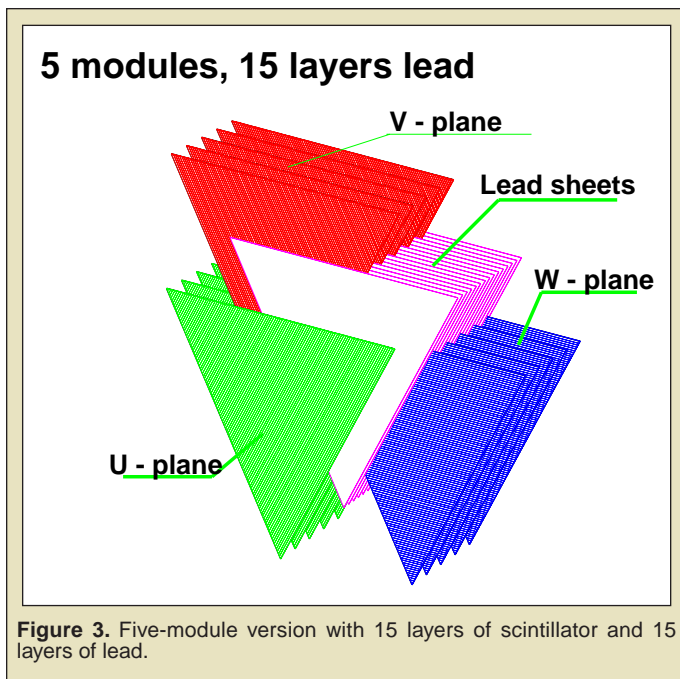


Figure 2. Preshower geometry: scintillator layers are highlighted in pink and lead layers are in green. Photomultiplier tubes will be attached to the scintillator strips by optic fibers and located behind the detector allowing the preshower and EC modules to be placed as close as possible. [1] The preshower will have the same truncated triangular pyramid design and orientation in CLAS12 as the current EC have in CLAS, positioned about 5m away from the CLAS target point.

π^0 -decay is needed.



METHODS AND MATERIALS

The first task was to simulate the single gammas and π^0 s using a single particle generator, SPGEN. Two sets of photon events were generated, one for evaluating the fiducial acceptance and the other for efficiency and energy resolution. The single photons used to calculate the detection efficiency and resolution had a momentum range from 0 to 9GeV, a distribution azimuthal angle (ϕ) of 0° , and a polar angle (θ) of 25° . The single gammas generated for the fiducial acceptance had the same momentum range but ϕ angles from 0° to 360° and θ angles 5° to 48° . The generated π^0 s had a momentum range from 0 to 9GeV, ϕ range of -3° to 3° and θ angle range of 24° – 27° .

GSIM code was modified to simulate the particles' passage through the CLAS detector. The files were then processed through the CLAS event reconstruction program, RECSIS, and the resulting ntuples were used to analyze the different models. Data analysis was performed using the physics analysis workstation, PAW++, FORTRAN functions, and kumac files. The same histograms were filled for each model, so comparisons between the various versions could be made easily.

π^0 Mass Reconstruction

The π^0 mass was calculated only on the five-module version because it was necessary to verify that the photon energy calibrations were correct. This was critical for comparing the energy resolutions of various models, the focus of this study. In order to determine the ability of the five-module version to reconstruct π^0 masses accurately, the π^0 mass had to be evaluated and compared with its known value. The mass was calculated from the following equation:

$$M_{\pi^0} = 2E_{\gamma_1}E_{\gamma_2}(1 - \cos\theta_{\gamma_1\gamma_2})$$

Where E_{γ_1} and E_{γ_2} are energies of decay photons and $\theta_{\gamma_1\gamma_2}$ is the angle between the photons' momentum vectors. The only events used to reconstruct the π^0 mass in this study were those that contained two cluster hits that have energy in both the preshower and EC. The energies of the photons were found by adding the hit energies of each photon in the preshower and the EC and then correcting with the sampling fraction. The sampling fraction was determined from the average ratio of the detected energy and the Monte Carlo simulated energy of a photon. In principle, the sampling fraction has some energy dependence but within this study's energy range and calorimeter resolution that dependence can be ignored [3]. It is important to stress that the sampling fraction only has meaning for a single showering particle like a photon or electron. Therefore with correctly calibrated photon readings, such as an accurate sampling fraction and correctly reconstructed angles, the π^0 mass should be correct. The positions of the photon events were then used to calculate the angle of separation between the decay photons. From the Gaussian fit to the mass distribution, the mean was compared with the known value and checked for accuracy.

While both the angular and energy resolution of the preshower are critical in evaluating the reconstructed π^0 mass, the focus of this project was to evaluate the energy resolution of different models. This study is one of many that are responsible for deciding the final geometry of the preshower calorimeter and primarily focuses on comparing the energy resolution and single photon detection efficiency of different calorimeter models.

Fiducial Acceptance

The maximum acceptance range of the preshower was determined by using the five-module version and turning off the geometry of all other detectors in CLAS. The θ and ϕ angles of the photons were calculated using the positions of the hits in the lab coordinate system. Plotting the θ vs. ϕ graph revealed the range at which the photons had been detected. Then, a function that followed the edge of the distribution was found so it could be used as a fiducial cut in later analysis programs.

Energy Resolution

The energy resolution of a calorimeter is a measure of how accurately it determines the energy of a particle. Experimentally, resolution reflects fluctuations in the amount of energy the scintillators absorb. The EC used in CLAS is a sampling calorimeter; it detects or "samples" a fraction of the energy of the showering particles that pass through it [4]. The sampling fraction is the intrinsic fraction of energy the calorimeter samples. Due to the effects of electromagnetic showering, the resolution of a sampling calorimeter obeys the following equation [3]:

$$\frac{\Delta E}{E} = \frac{Const}{\sqrt{E}} \oplus \frac{a}{E} \oplus b$$

Term a is important at low energies, term b is important at high energies. In the range of energies we are interested, 1 to 10GeV, the resolution can be approximated with the following expression:

$$\frac{\Delta E}{E} \approx \frac{Const}{\sqrt{E}}$$

The energy of the photon was calculated by adding the energy of the clusters in both the preshower and the EC. Then the sampling fraction was calculated by dividing the total energy of the photon by its Monte Carlo simulated momentum. CLAS12 calorimeter's resolution was obtained by fitting a Gaussian curve to the sampling fraction distribution over several energy bins and using the corresponding sigma (peak width) and mean values according to the following equations:

$$\frac{\Delta E}{E} = \frac{\sigma}{Mean} \Rightarrow Const = \frac{\sigma}{Mean} \sqrt{E}$$

Single Photon Detection Efficiency

The single photon detection efficiency of the preshower and electromagnetic calorimeter specifies the percentage of photons the calorimeters detect at the appropriate energy deposition. For each model, this efficiency was determined by comparing the Monte Carlo momentum distribution after a cut was performed on the sampling fraction to that of the Monte Carlo momentum distribution without any cuts. The sampling fraction cut was determined by plotting the sampling fraction vs. the number of events and placing a cut at the beginning of the sampling fraction distribution.

RESULTS

π^0 Mass Reconstruction

In Figure 6, the reconstructed π^0 mass, M_{π^0} , of the five-module version is shown. The Gaussian fit to the distribution had a mean of 0.131GeV and a width of 0.01340GeV.

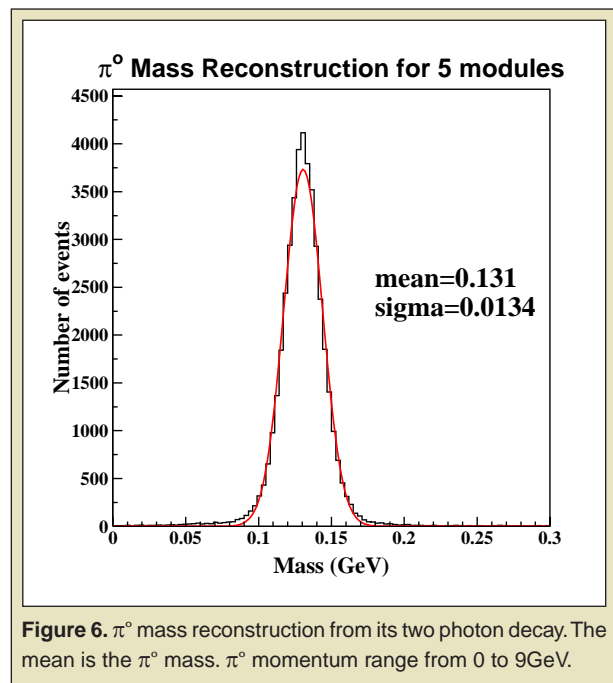
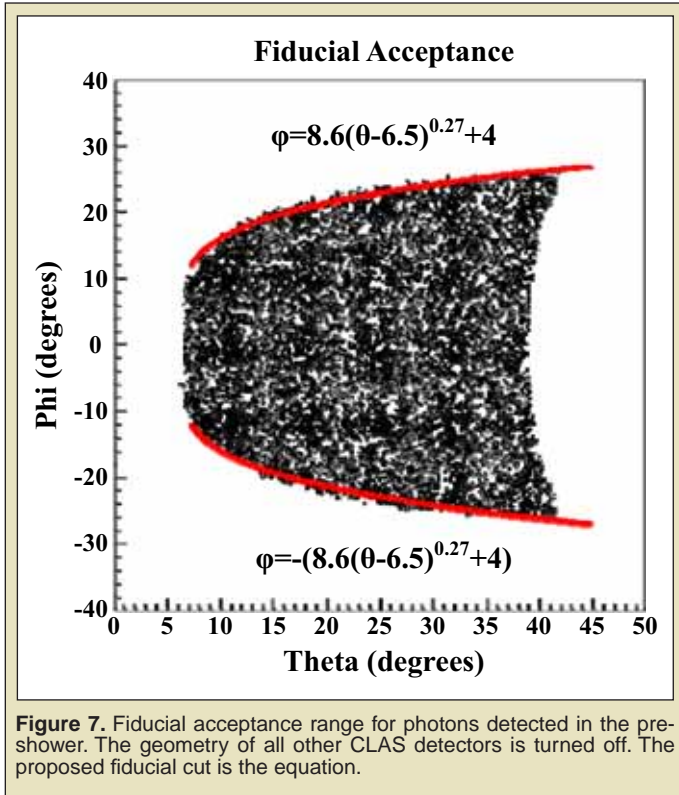


Figure 6. π^0 mass reconstruction from its two photon decay. The mean is the π^0 mass. π^0 momentum range from 0 to 9GeV.

Fiducial Acceptance

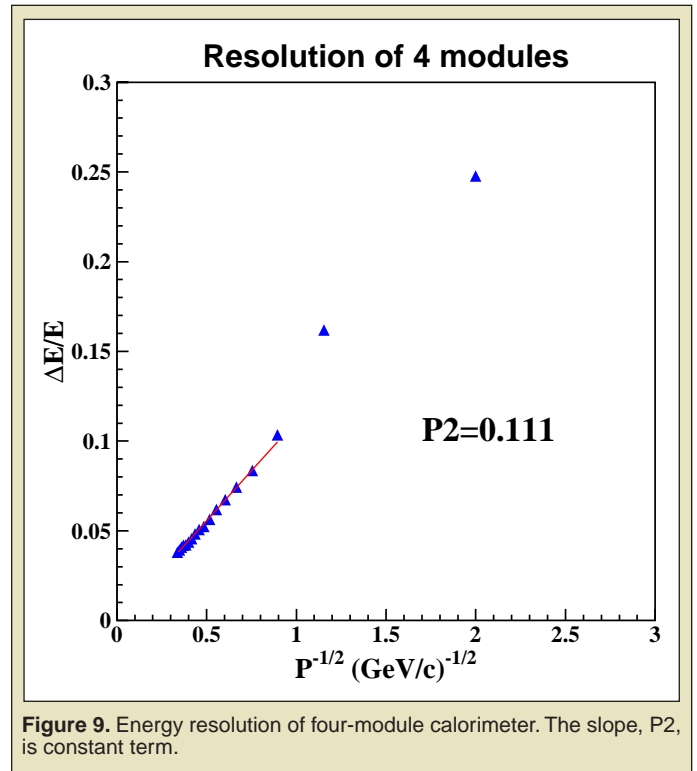
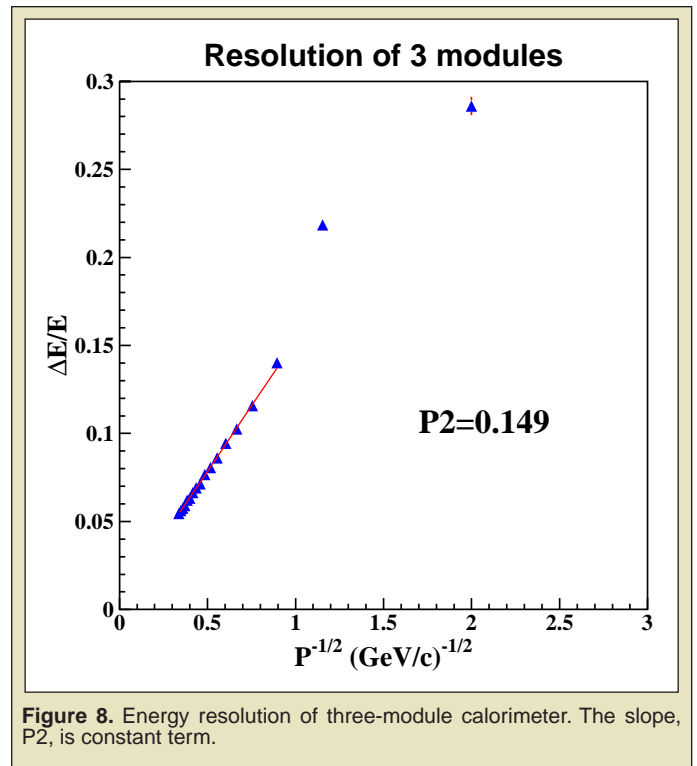
In Figure 7, the distribution azimuthal angle (ϕ) vs. polar angle (θ) of detected photons is shown. The proposed equation for a fiducial cut of the acceptance range is:

$$\phi = 8.6(\theta - 6.5)^{0.27} + 4$$



Energy Resolution

The graphs were created by plotting $\frac{\sigma}{Mean}$ vs $\frac{1}{\sqrt{E}}$ and the slope of the linear fit was taken as the energy resolution constant. As shown in Figure 8, the resolution measured in the five-module version was $0.972E-01 \pm 0.108E-02$. As shown in Figure 9, the resolution of four-module was $0.111 \pm 0.117E-02$. The resolution of the three-module was $0.149 \pm 0.152E-02$, Figure 10.



DISCUSSION

π^0 Mass Reconstruction

The reconstructed π^0 mass was found to be 4MeV from the accepted π^0 mass. This can be attributed to error in the sampling fraction correction. The acceptable mean and sigma values verified that the five-module version has appropriate π^0 mass reconstruction and is a good model for comparison.

Fiducial Acceptance

Higher beam energies will require the CLAS12 detector upgrade to increase its detection and particle identification capabilities. This will be done many ways, including increasing the acceptance of photons and electrons to 5° – 40° [2]. As seen from Figure 7, the additional surface area (5° per side) of the preshower widens the acceptance of the CLAS12 calorimeter to the specifications of the upgrade. This demonstrates that the five-module version is an acceptable standard model and that the geometry of the preshower has acceptable photon cluster acceptance.

Energy Resolution

The larger the constant term, the worse the energy resolution and the less accurate the calorimeter is at reconstructing the hit energy. The four-module version differed from the five-module version by only by 1.4% in resolution. The three-module version, however, showed a marked difference of 5% in resolution. The three-module version is not adequate because the decrease in resolution does not outweigh the saved financial cost of constructing the preshower with fewer scintillators.

Single Photon Detection Efficiency

It is believed that the depletion of low energy photons in the three-module version occurs because most of the low-energy photons lose all their energy in the first six layers of lead. In order to be reconstructed, a particle must hit all three stereo readout planes. Since the first six layers of lead have double thickness in the three-module version, many photons cannot be properly reconstructed because they do not have enough energy to reach the third stereo readout panel. In addition, fewer photons are able to hit the second set of readout panels. As a consequence, due to readout threshold, such photons will not be properly reconstructed. Failure to traverse the second set of readout panels results in a depletion of low-energy photons. In addition, the sampling fraction of the three-module version is considerably wider than either the four- or five-module version. Thus, more photons below the 0.15 sampling fraction cutoff lead to a possible depletion in low-energy photons. Although the four- and five-modules versions are almost indistinguishable, the three-module does not appear to be a good choice for the preshower geometry.

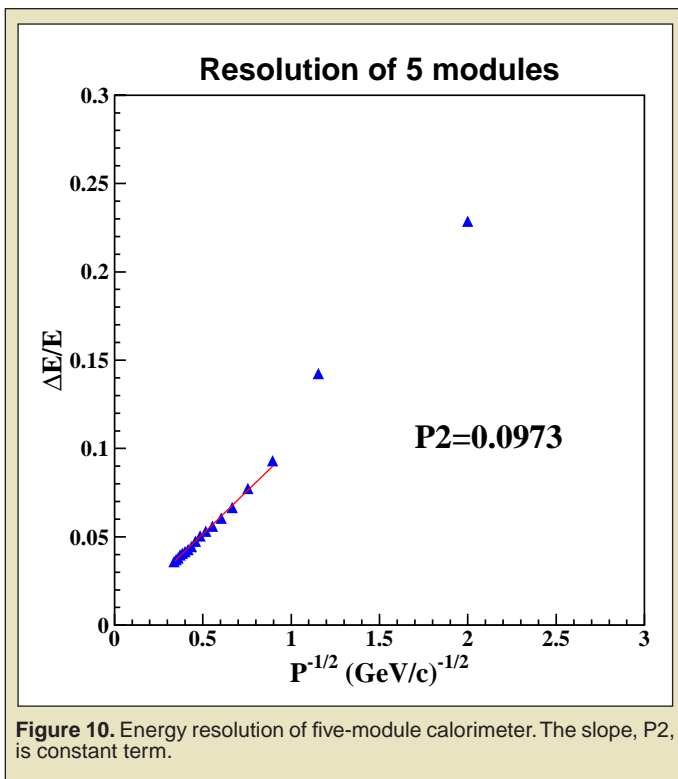


Figure 10. Energy resolution of five-module calorimeter. The slope, P2, is constant term.

Single Photon Detection Efficiency

The same sampling fraction cut, above 0.15, was applied to all versions. Both the five- and four-module versions had 99% efficiency above 0.5GeV while the three-module version had 99% efficiency above 1.5GeV (Figure 11).

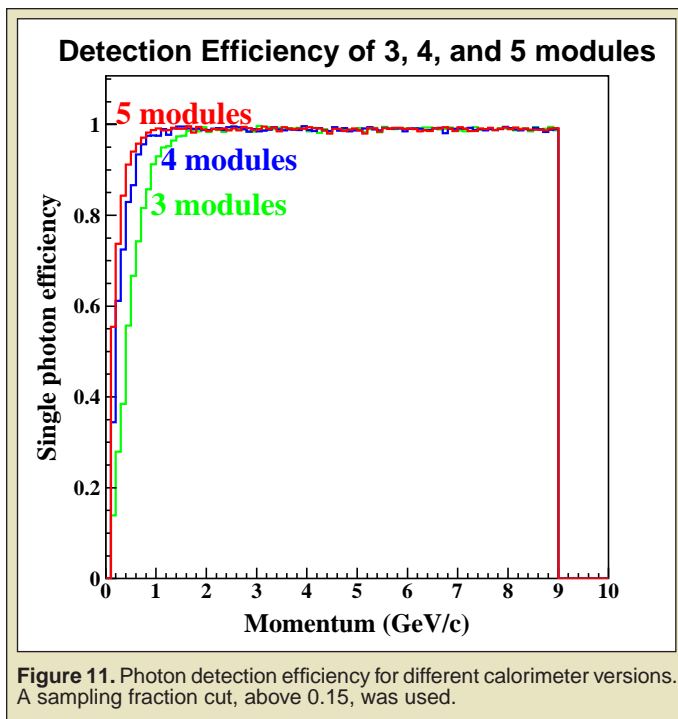


Figure 11. Photon detection efficiency for different calorimeter versions. A sampling fraction cut, above 0.15, was used.

CONCLUSION

Considering there is a difference of only 1.4% in the energy resolution, and a negligible difference in single photon detection efficiency between the five- and four-module preshower calorimeters, the four-module preshower with twelve layers of scintillators and fifteen layers of lead is the best combination in resolution, efficiency, and cost. Additional GSIM simulations to verify that the four-module version has acceptable π^0 mass reconstruction will be undertaken, and Research and Development (R&D) analysis will continue.

ACKNOWLEDGMENTS

Thank you to the Department of Energy for giving me the opportunity to work in a great summer internship program. I would also like to thank Jefferson Lab and all of its people who made this summer an invaluable experience. Special thanks to my mentor, Stepan Stepanyan, and Natasha Dashyan for their guidance and patience.

REFERENCES

- [1] M. Amarian et al, "The CLAS forward electromagnetic calorimeter," Nuclear Instruments and Methods in Physics Research A 460 (2001) 239-265 August 2000.
- [2] "The JLab CLAS12 Detector", Thomas Jefferson National Accelerator Facility, Newport News, Virginia.
- [3] S. Stepanyan (private communication), 2006.
- [4] B. Surrow, "Calorimetry in High-Energy Nuclear and Particle Physics Experiments", [Online document], 2004 August 23, [cited 2006 July 27], Available HTTP: <http://www.hepl.harvard.edu/~NEPPSR04/Talks/Calorimetry-Surrow.pdf>.

Christy Wisniewski received her B.S. in biological sciences with an emphasis in neurobiology, physiology, and behavior, at the University of California, Davis in June 2007. In the summer of 2005, she was awarded an internship at Lawrence Berkeley National Laboratory (LBNL) through the Department of Energy, Office of Science. She accepted another internship at LBNL the following summer, which the work here represents. Under the mentorship of Dr. Eleanor Blakely and Kathleen Bjornstad, Christy researched the effects of immortalization in DNA damage marker expression using two human mammary epithelial cell lines. This research was presented at the 2007 American Association for the Advancement of Science (AAAS) Annual Conference. She is planning on attending graduate school in a program concerning reproduction and developmental cell biology.

Kathleen A. Bjornstad is a Principal Research Associate at LBNL. She received a B.S. in microbiology, immunology, and biochemistry from the University of Washington, and has worked in radiation studies with Dr. Eleanor Blakely for 22 of her 26 years at LBNL.

Chris J. Rosen is a Research Associate at LBNL and has worked in the Blakely group for the last 7 years. He received a B.S. in molecular and cellular biology at the University of California, Berkeley, with an emphasis in neurobiology.

Polly Y. Chang is a Senior Molecular Toxicologist who is Director of the Molecular and Genetic Toxicology Department at SRI International, and has worked in radiation biophysics with Eleanor Blakely at LBNL for the last 31 years, but only part-time since assuming her duties at SRI in 1997. She received her Ph.D. in biophysics from the University of California, Berkeley, and before joining LBNL, completed a 2-year NIH/Fogarty Fellowship at the University of Tokyo in Japan.

Eleanor A. Blakely is a Senior Staff Biophysicist at LBNL, with more than 32 years of professional experience in cellular and molecular radiobiology research directed at studying the basic mechanisms of radiation responses, funded by DOE, NIH and NASA. She serves as consultant in support of clinical radiotherapy trials, and in issues pertinent to radiation protection. Her current research involves investigating mechanisms of radiation-induced molecular signaling after low dose exposures to human lens and mammary epithelial cells.

A COMPARISON OF DNA DAMAGE PROBES IN TWO HMEC LINES WITH X-IRRADIATION

CHRISTY L. WISNEWSKI, KATHLEEN A. BJORNSTAD, CHRISTOPHER J. ROSEN,
POLLY Y. CHANG, AND ELEANOR A. BLAKELY

ABSTRACT

In this study, we investigated γ H2AX^{ser139} and 53BP1^{ser25}, DNA damage pathway markers, to observe responses to radiation insult. Two Human Mammary Epithelial Cell (HMEC) lines were utilized to research the role of immortalization in DNA damage marker expression, HMEC HMT-3522 (S1) with an infinite lifespan, and a subtype of HMEC 184 (184V) with a finite lifespan. Cells were irradiated with 50cGy X-rays, fixed with 4% paraformaldehyde after 1 hour repair at 37°C, and processed through immunofluorescence. Cells were visualized with a fluorescent microscope and images were digitally captured using Image-Pro Plus software. The 184V irradiated cells exhibited a more positive punctate response within the nucleus for both DNA damage markers compared to the S1 irradiated cells. The dose and time course will be expanded in future studies to augment the preliminary data from this research. It is important to understand whether the process of transformation to immortalization compromises the DNA damage sensor and repair process proteins of HMECs in order to understand what is "normal" and to evaluate the usefulness of cell lines as experimental models.

INTRODUCTION

DNA damage from ionizing radiation triggers the mobilization of damage sensor proteins to damage sites resulting in a temporary delay of cell cycle progression and activation of repair machinery [1]. ATM (Ataxia Telangiectasia Mutated) and ATR (Ataxia Telangiectasia and Rad-3-related) proteins are two related kinases central to signaling DNA damage, and recent evidence indicates ATM activation occurs prior to ATR activation following radiation

damage [2]. The published literature of these phenomena has been obtained primarily with human and other mammalian fibroblasts.

A major focus for breast cancer research is to understand the key mechanisms responsible for initiating carcinogenesis. It is the epithelial cell that becomes a cancer cell. Normal epithelial cells have a finite life span and then senesce, and thus are more difficult to study in the laboratory. Evidence exists from studies of human and murine normal mammary glands that multiple epithelial cell-

subtypes exist with distinct patterns of susceptibility to different subtypes of breast cancer [3, 4, 5]. Malignant transformation is a multi-step process in which genetic changes in these different cell subtypes can occur due to exposure to a number of environmental factors, such as viruses, carcinogens, dietary factors, and radiation. Mutations of the TP53 gene are the most frequent genetic lesion in breast cancer and its loss as a result of mutation is thought to be an early step in breast tumorigenesis [6].

Numerous cell culture models derived from Human Mammary Epithelial Cells (HMEC) are available [4, 7, 8]. The role of tumor suppressor proteins, inhibitors of cyclin-dependent kinases, telomerase, and small G proteins have been defined in normal and various stages in the progression to immortalization of HMECs. This paper investigates whether DNA damage foci recruitment after exposure of HMECs to a relatively low dose of X-rays (50cGy) to determine its dependence on immortalization. We have selected two non-malignant HMECs: the 184V non-immortalized HMEC with a finite life span, and the immortalized HMEC HMT-3522 (S1) [9, 10, 11, 12]. Differences in gene expression between these two cell types during normal differentiation into polarized acini have recently been compared to test correlation of marker genes with poor and good prognosis groups among breast cancer patients [13].

Two markers in the ATM DNA damage pathway for radiation-induced effects are compared, histone family 2A member X (γ H2AX), and tumor protein TP53 binding protein 1 (53BP1) [14, 15]. Both proteins are phosphorylated in response to DNA damage [16, 17, 18]. It is possible that the transformation process that immortalizes cells for unlimited growth in culture may affect the DNA damage response pathway. Biological cell models cultured *in vitro* in the laboratory are used to investigate many unknown mechanisms of action underlying molecular responses to stressors in normal human tissues. It is important to understand biological characteristics common to a cell type, as well as differences that may exist in various cell models.

MATERIALS AND METHODS

Cells and Cell Culture Conditions

HMEC HMT-3522 (S1) immortalized cells are non-malignant early passage human cells that were made available by Drs. Mina Bissell and Mary Helen Barcellos-Hoff (LBNL). The cells originated from a reduction mammoplasty of a woman with a non-malignant breast lesion and were derived through continuous cell passaging in defined medium [20, 21]. Cells from passages #40-60 were used. These cells were grown at 37°C in a humidified incubator at 5% CO₂ in a chemically-defined medium (DMEM / F12 - H14) composed of DMEM (Dulbecco's Modified Eagle's Medium) plus Ham's F12 (1:1, Invitrogen), 2mM glutamine, 250ng/ml insulin, 5mg/ml sheep prolactin, 10mg/ml transferrin, 10¹⁰ M estradiol (all from Sigma, St. Louis, MO), 10ng/ml EGF, 2.6ng/ml sodium selenite, and 1 μ M hydrocortisone (from Collaborative Research, MA). Cells were set up in plastic four well LabTek slides or 60mm plastic Falcon petri dishes at 4 x 10⁴ cells/well or 1 x 10⁵ cells/petri dish, respectively, five days prior to the experiment and were fed every other day.

HMEC 184V is a subtype of the 184 HMEC line that is mortal and non-malignant. These cells were kindly provided by Dr. Martha Stampfer (LBNL), who developed this cell line from a human non-tumorigenic reduction mammoplasty [10, 19]. Cells were grown as described by Stampfer [19] in serum-free MCDB 170+IP Growth Media containing MEBM, (Mammary Epithelial Basal Medium, Clonetics Corporation, San Diego, CA) in a 37°C humidified incubator at 0.2% CO₂. 184V cells were fed every Monday, Wednesday, and Friday, and transferred at 80% confluency. Cell transfer consisted of 3X rinses of 0.05% trypsin w/EDTA (Invitrogen/GIBCO) of 3, 2, and 1ml, respectively, in 100mm petri dishes. The 184V cells required a 30 second wait between trypsin rinses, with the final trypsinization for 5 minutes at 37°C. Following the final trypsinization, cells were neutralized (with 10ml 1X PBS without Ca or Mg) and spun down in a centrifuge at 1,000 RPM for 5 minutes. Cells were resuspended in growth media, counted, and plated. Cells were plated at 2-4 x 10⁴ cells/ml per well into plastic four well LabTek slides three days prior to the experiment.

Irradiation

Four well LabTek slides and 60mm petri dishes were irradiated one at a time, on a rotating platform, in a 160kVp Pantak X-ray machine, running at 150kVp, 20mA, for a dose of radiation of 50cGy. Dose calibration was done with a NIST-based calibrated Victoreen probe 154. Following irradiation, slides or dishes containing S1 or 184V HMECs were incubated at 37°C at 5.0% and 0.2% CO₂, respectively, until fixation.

Fixation

Cells were fixed following irradiation, at 1 hour. Cells were rinsed 2X with PBS and then incubated with Nucleoplasmic Extraction Solution (NES): 0.5% Triton-X, 20mM HEPES (pH 7.9), 50mM NaCl, 3mM MgCl₂, and 200mM sucrose at RT for 10 minutes. The cells were rinsed 1X with PBS and fixed with 4% paraformaldehyde for 10 mins at RT in a time course after radiation exposure. Cells were rinsed 2X with PBS, and, finally, PBS was added to each area of the slide/dish containing cells, and placed at 4°C overnight.

Immunofluorescence

Cells fixed with 4% paraformaldehyde were permeabilized in 0.1% NP-40 in PBS for 30 minutes. Cells were blocked with 0.5% casein in PBS for 1 hour, followed by 10% goat serum in PBS for 1 hour. The primary antibodies for γ H2AX^{ser139} monoclonal mouse (1:1000 Upstate) or 53BP1^{ser25} polyclonal rabbit (1:200 Bethyl Labs) were applied overnight at 4°C in a humidified chamber.

Cells were rinsed 3X20 minutes in PBS, and secondary antibody was applied. Alexa 488 goat anti-mouse (1:300 Invitrogen) or Alexa 594 goat anti-mouse (1:300 Invitrogen) was applied for 1 hour for the S1 or 184V cells, respectively, for γ H2AX^{ser139}. Alexa 488 goat anti-rabbit (1:300 Invitrogen) or Alexa 594 goat anti-rabbit (1:300 Invitrogen) was applied for 1 hour for the 184V or S1 cells,

respectively, for 53BP1^{ser25}. Alexa 488 produces a green fluorescent signal and Alexa 594 produces a red fluorescent signal.

Cells were rinsed 3 x 15 minutes in PBS, followed by nuclear staining in DAPI (0.25µg/ml) for 5 minutes (nucleus stains blue) covered with vectashield, cover-slipped, and sealed with nail polish.

Image Acquisition

A Zeiss Axiovert 200M microscope was used to view fluorescent cell signals that were digitally captured with a 40XAPO objective and a QImaging Retiga EX digital CCD camera. Image-Pro Plus software was used to acquire individual 40x images. A minimum of five images from each experimental condition were taken.

Fluorescence Analysis

The number of fluorescent cells was manually counted for each image field. The fraction of responders in the field was obtained by dividing the number of positive fluorescent nuclei divided by the total number of cells indicated by the blue DAPI stained nuclei. A minimum of 5 images from each sample were analyzed and the data is summarized in Table 1.

HMEC Line	Antibody	Cells Counted					
		Control			1 hr post 50 cGy X-ray		
		+	Total	%	+	Total	%
S1	γ H2AX ^{ser139}	56	257	22.0 ± 8.1%	405	490	83.4 ± 15.8%
	53BP1 ^{ser25}	2	323	0.7 ± 0.1%	353	524	69.2 ± 12.5%
184V	γ H2AX ^{ser139}	78	329	24.1 ± 7.2%	336	368	91.6 ± 9.7%
	53BP1 ^{ser25}	230	298	77.9 ± 15.8%	359	368	97.8 ± 2.7%

Table 1. Number percent of responders for each cell type and marker.

RESULTS

A representative fluorescent image from the 5 fields acquired from each 50cGy irradiated sample after 1 hour of incubation at 37°C, and its respective control for each of the two DNA damage marker proteins with each cell type is depicted in Figure 1A for the γ H2AX^{ser139} response, and in Figure 2A for the 53BP1^{ser25} response. A histogram representing the quantitative analysis of the fraction of the fluorescence positive cells for the γ H2AX^{ser139} response is presented in Figure 1B and for the 53BP1^{ser25} in Figure 2B. About 20% of the nonirradiated control samples for the exponentially-growing S1 cells or 184V cells were measured to be γ H2AX^{ser139} positive. Although a comparable number of background positive cells were seen for each of the cell types, the nature of the fluorescence was quite different. Most of the signals from the S1 control samples were punctate in nature while some 184V cells showed a distribution of both overall nuclear staining as well as punctate signals. Both cell lines showed increased fluorescent signals one hour after an X-ray dose of 50cGy,

but the fluorescent signals had a different appearance. Most of the positive S1 cells showed global nuclear staining while signals from the 184V cells appeared to contain a distribution of both punctate and overall nuclear staining. Quantitative comparison of the number of positive cells in the DAPI merged H2AX images showed that 91.6 ± 9.7% of the 184V cell nuclei were positive compared to the 83.4 ± 15.8% positive S1 cells. This is illustrated in the histograms in Figure 1B. Error bars show the standard deviation between image fields for the same probe and treatment condition.

In Figure 2A, the nonirradiated S1 cells showed a very small background signal for 53BP1^{ser25} fluorescence. In stark contrast, the 184V cells showed a high background signal of small punctate dots. Both cell types showed increased 53BP1^{ser25} fluorescence 1 hour after exposure to 50cGy. Quantitation of the fluorescence signal indicated that 97.8 ± 2.7% of the 184V cells were fluorescence positive, but only 69.2 ± 12.5% of the S1 cells were positive. Results from a student t-test show that the radiation-induced increase in fluorescence in the 184V cells are significantly different (p<0.01) than the S1 cells.

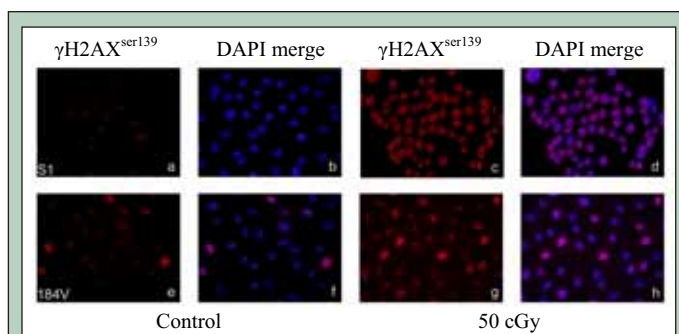


Figure 1A. γ H2AX^{ser139} response in control (a, b, e, f) and 50cGy (c, d, g, h) images for HMEC S1 (a-d) and HMEC 184V (e-h). Panels a, c, e, g consist solely of the red signal from γ H2AX^{ser139} and panels b, d, f, h are color composite images derived from merging the blue DAPI nuclear and the red γ H2AX^{ser139} images.

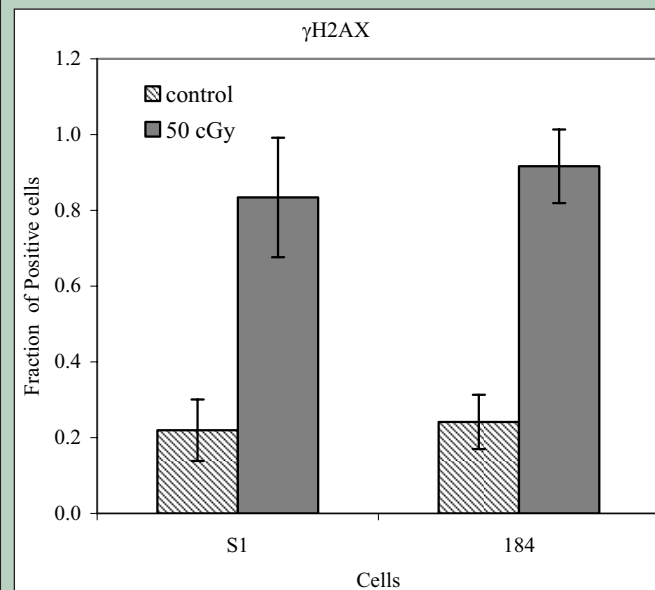


Figure 1B. Comparison of the level of positive γ H2AX^{ser139} in control or irradiated cell populations, in HMECs S1 or 184V.

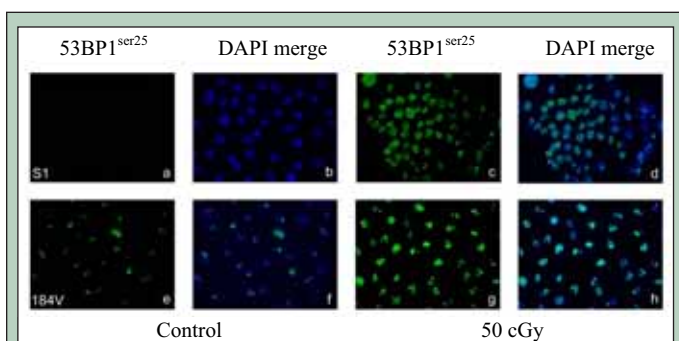


Figure 2A. 53BP1^{ser25} response in control (a, b, e, f) and 50cGy (c, d, g, h) images for HMEC S1 (a-d) and HMEC 184V. Panels a, c, e, g consist solely of the green signal from 53BP1^{ser25} and panels b, d, f, h are color composite images derived from merging the blue DAPI nuclear and the green 53BP1^{ser25} images.

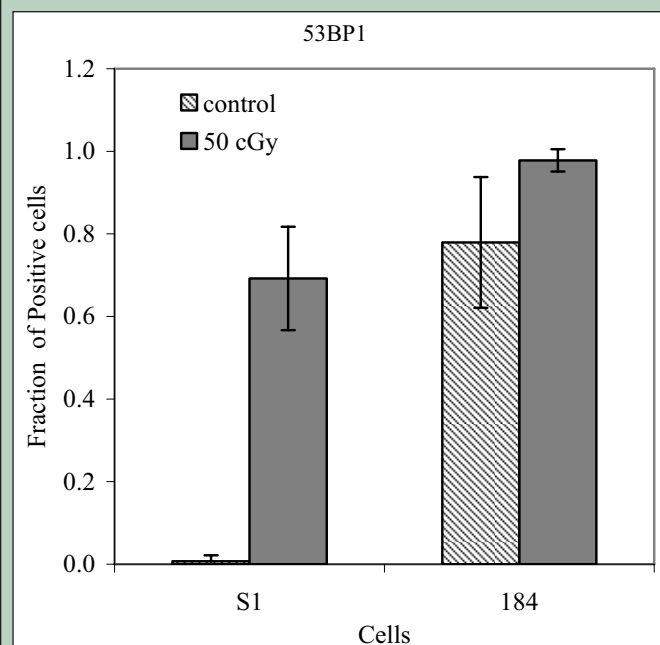


Figure 2B. Comparison of the level of positive 53BP1^{ser25} in control or irradiated cell populations of HMECs S1 or 184V.

DISCUSSION AND CONCLUSIONS

The major observation from the work presented here is that the control background fluorescent signals for the two molecular markers used as indicators for radiation damage are different for the two non-malignant HMECs studied. Furthermore, although it appears that radiation exposure produced a similar level of enhanced γ H2AX^{ser139} fluorescent signals in both cell lines, significant differences were observed in both the level and in the pattern of radiation-induced 53BP1^{ser25} fluorescence signal. The non-immortalized 184V HMECs showed almost 100% response 1 hour after exposure to 50cGy with each of the two probes, γ H2AX^{ser139} and 53BP1^{ser25}. The immortalized HMT-3522 S1 HMECs showed approximately 70% 53BP1 response 1 hour after exposure to 50cGy. To our knowledge, this work represents the first documentation of differences in DNA repair markers between two non-malignant HMECs.

Both cell types were exponentially dividing cultures at the time of radiation exposure. One explanation for the observed differences could be due to variable distributions of cells in the cell cycle for each cell type. However, the magnitude of the difference seems unlikely to account for this possibility, but this needs to be ruled out in future studies by examining the cell cycle distribution. The data presented are for a single radiation dose and time point after exposure. It is therefore possible that the time course of the expression of these DNA damage markers is different for each of these cell lines. This would be an interesting observation and future work with a more complete dose response and time course is planned. It is known that multiple genetic changes are required for efficient immortalization of different subtypes of normal human mammary epithelial cells leading to carcinogenesis [4] and that some of these genetic changes can alter the radiation resistance of carcinoma of the breast (22). There are indications that DNA damage markers like γ H2AX^{ser139} can be used as therapeutic targets for improving the efficacy of radiation therapy for breast cancer [23] by blocking γ H2AX foci formation or by inhibiting DNA damage repair processes in breast tumor cells. It is important to understand whether the process of transformation to immortalization compromises the DNA damage sensor and repair process proteins of HMECs in order to understand what is “normal” and to evaluate the usefulness of cell lines as experimental models.

ACKNOWLEDGMENTS

I would like to thank the U.S. Department of Energy, Office of Science for allowing me to participate in this magnificent undergraduate internship research experience within the SULI program. I want to thank the CSEE staff and coordinator Laurel Egenberger. Special thanks go to my mentors Eleanor Blakely, Kathleen Bjornstad, Polly Chang and Chris Rosen for their guidance and patience with my research project and for their immeasurable assistance with the research presented here. I would also like to thank Martha Stampfer, Al Thompson, Jim Garbe, Sylvain Costes, and Ekaterina Bassett for their knowledge regarding different aspects of this research. This work was supported by the Director, Office of Science, Office of Science Education and Workforce Development, of the U.S. Department of Energy under Contract No. DE-AC02-05CH11231. In addition, this work was supported by the U.S. DOE’s Low Dose Radiation Research Program under Contract No. DE-AC03-76SF00098 and the Center for Science and Engineering Education.

REFERENCES

- [1] Kurz, EU and Lees-Miller, SP, “DNA damage-induced activation of ATM and ATM-dependent signaling pathways,” *DNA Repair (Amst)*, vol. 3, pp. 889-900, 2004.
- [2] Adams, KE, Medhurst, AL, Dart, DA, and Lakin, ND, “Recruitment of ATR to sites of ionising radiation-induced DNA damage requires ATM and components of the MRN protein complex,” *Oncogene*, vol. 25, pp. 3894-904, 2006.

- [3] Band, V, "Preneoplastic transformation of human mammary epithelial cells," *Semin Cancer Biol*, vol. 6, pp. 185-92, 1995.
- [4] Ratsch, SB, Gao, Q, Srinivasan, S, Wazer, DE, and Band, V, "Multiple genetic changes are required for efficient immortalization of different subtypes of normal human mammary epithelial cells," *Radiat Res*, vol. 155, pp. 143-150, 2001.
- [5] Dimri, G, Band, H, and Band, V, "Mammary epithelial cell transformation: insights from cell culture and mouse models," *Breast Cancer Res*, vol. 7, pp. 171-9, 2005.
- [6] Liu, FS, Yang, HY, and Sui, GJ, "The metastatic pattern of malignant tumors," *Zhonghua Yi Xue Za Zhi*, vol. 74, pp. 406-9, 454, 1994.
- [7] Taylor-Papadimitriou, J, D'Souza, B, Berdichevsky, F, Shearer, M, Martignone, S, and Alford, D, "Human models for studying malignant progression in breast cancer," *Eur J Cancer Prev*, vol. 2 Suppl 3, pp. 77-83, 1993.
- [8] Stampfer, MR and Yaswen, P, "Culture models of human mammary epithelial cell transformation," *J Mammary Gland Biol Neoplasia*, vol. 5, pp. 365-78, 2000.
- [9] Hammond, SL, Ham, RG, and Stampfer, MR, "Serum-free growth of human mammary epithelial cells: rapid clonal growth in defined medium and extended serial passage with pituitary extract," *Proc Natl Acad Sci U S A*, vol. 81, pp. 5435-9, 1984.
- [10] Stampfer, MR and Bartley, JC, "Induction of transformation and continuous cell lines from normal human mammary epithelial cells after exposure to benzo[a]pyrene," *Proc Natl Acad Sci U S A*, vol. 82, pp. 2394-8, 1985.
- [11] Petersen, OW, Ronnov-Jessen, L, Howlett, AR, and Bissell, MJ, "Interaction with basement membrane serves to rapidly distinguish growth and differentiation pattern of normal and malignant human breast epithelial cells," *Proc Natl Acad Sci U S A*, vol. 89, pp. 9064-8, 1992.
- [12] Weaver, VM, Petersen, OW, Wang, F, Larabell, CA, Briand, P, Damsky, C, and Bissell, MJ, "Reversion of the malignant phenotype of human breast cells in three-dimensional culture and in vivo by integrin blocking antibodies," *J Cell Biol*, vol. 137, pp. 231-45, 1997.
- [13] Fournier, MV, Martin, KJ, Kenny, PA, Khaja, K, Bosch, I, Yaswen, P, and Bissell, MJ, "Gene expression signature in organized and growth-arrested mammary acini predicts good outcome in breast cancer," *Cancer Res*, vol. 66, pp. 7095-102, 2006.
- [14] Fillingham, J, Keogh, MC, and Krogan, NJ, "γ-H2AX and its role in DNA double-strand break repair," *Biochem Cell Biol*, vol. 84, pp. 568-577, 2006.
- [15] Iwabuchi, K, Hashimoto, M, Matsui, T, Kurihara, T, Shimizu, H, Adachi, N, Ishiai, M, Yamamoto, K, Tauchi, H, Takata, M, Koyama, H, and Date, T, "53BP1 contributes to survival of cells irradiated with X-ray during G1 without Ku70 or Artemis," *Genes Cells*, vol. 11, pp. 935-48, 2006.
- [16] Crawford, LV, Pim, DC, Gurney, EG, Goodfellow, P, and Taylor-Papadimitriou, J, "Detection of a common feature in several human tumor cell lines--a 53,000-dalton protein," *Proc Natl Acad Sci U S A*, vol. 78, pp. 41-5, 1981.
- [17] Rogakou, EP, Pilch, DR, Orr, AH, Ivanova, VS, and Bonner, WM, "DNA double-stranded breaks induce histone H2AX phosphorylation on serine 139," *J Biol Chem*, vol. 273, pp. 5858-68, 1998.
- [18] Mochan, TA, Venere, M, DiTullio, RA, Jr., and Halazonetis, TD, "53BP1 and NFB1/MDC1-Nbs1 function in parallel interacting pathways activating ataxia-telangiectasia mutated (ATM) in response to DNA damage," *Cancer Res*, vol. 63, pp. 8586-91, 2003.
- [19] Stampfer, MR, "Isolation and growth of human epithelial cells," *Journal of Tissue Culture Methods*, vol. 9, pp. 107-115, 1985.
- [20] Briand, P, Nielsen, KV, Madsen, MW, and Petersen, OW, "Trisomy 7p and malignant transformation of human breast epithelial cells following epidermal growth factor withdrawal," *Cancer Res*, vol. 56, pp. 2039-44, 1996.
- [21] Briand, P, Petersen, OW, and Van Deurs, B, "A new diploid nontumorigenic human breast epithelial cell line isolated and propagated in chemically defined medium," *In Vitro Cell Dev Biol*, vol. 23, pp. 181-8, 1987.
- [22] Jameel, JKA, Rao, VSR, Cawkwell, L, Drew, "Radioresistance in carcinoma of the breast" *The Breast*, vol 13, pp 452-460, 2004.
- [23] Kao, J, Milano, MT, Javaheri, A, Garofalo, MC, Chmura, SJ, Weichselbaum, RR, Kron, SJ, "γ-H2AX as a therapeutic target for improving the efficacy of radiation therapy" *Current Cancer Drug Targets*, vol 6, pp. 197-205 2006.

ABSTRACTS

TABLE OF CONTENTS

BIOLOGY	136
CHEMISTRY	148
COMPUTER SCIENCE	158
ENGINEERING	166
ENVIRONMENTAL SCIENCE	183
GENERAL SCIENCES	197
MATERIAL SCIENCES	199
MEDICAL AND HEALTH SCIENCES	206
NUCLEAR SCIENCES	209
PHYSICS	212
SCIENCE POLICY	227

Many participants in the DOE's undergraduate research programs are supported by grants from the National Science Foundation. These participants are designated with an "*" preceding the title of their abstract.

Biology

A Comparative Study of the Age Class Structures of *Quercus alba*, *Quercus coccinea*. KATHRYN GUTLEBER (Connecticut College, New London, CT 06320) TIM GREEN (Brookhaven National Laboratory, Upton, NY 11973). Investigation of the age class structure of *Quercus* species and *Pinus rigida* within the Long Island Pine Barrens core area is an important aspect of monitoring the health of the Pine Barrens. The age class structures of *Quercus alba*, *Quercus coccinea*, *Quercus velutina*, and *Pinus rigida* are primary indicators of successful reproduction and the possibility of the successional change between community types. By comparing the numbers of seedlings, saplings and mature trees, the success of reproduction for these three *Quercus* species and *Pinus rigida* was analyzed. The numbers of seedlings and saplings were recorded through the use of four two-meter wide belt transects within 16 by 25 meter plots. These plots were located within the Pine Barrens subtargets of Pitch Pine, Pine-Oak, Oak-Pine, Coastal Oak, Scrub Oak and Dwarf Pine forests. This study found the success of reproduction for all the study tree species within the six community types to be varied. *Q. alba*, *Q. coccinea* and *Q. velutina* all displayed a low number of saplings in all community types surveyed, indicating that current reproduction is not very successful. In Coastal Oak and Oak-Pine communities, *Q. alba* was the most successful in reproduction. The reproduction of *P. rigida* was dominant within Pine-Oak, Pitch Pine and Pitch Pine-Scrub Oak Woodland communities. However, the low average number of *P. rigida* saplings found could possibly indicate the succession from pine-dominated forest to oak dominated forest. There are several factors that may influence these trends in reproduction, including exposure to light, levels of litter and duff, and deer browse. Although the current levels of reproduction for *Quercus* species and *P. rigida* are varied and range across the different community types, they are still an important indicator of forest succession within the Long Island Pine Barrens core area. Forest succession is an important factor in this ten-year longitudinal study of the Long Island Pine Barrens core area, as forest succession and species competition are primary indicators of forest health.

A Comparison of DNA Damage Probes in Human Mammary Epithelial Cells with 150 kVp X-Rays. CHRISTY WISNEWSKI (University of California-Davis, Davis, CA 95616) ELEANOR BLAKELY, KATHLEEN BJORNSTAD (Lawrence Berkeley National Laboratory, Berkeley, CA 94720). In this study we investigated 53BP1 and γ H2AX, DNA damage markers, to look at genetic mechanisms underlying responses to radiation insult. Two human mammary epithelial cell (HMEC) lines, one subtype of HMEC 184 with a finite lifespan and S1 with an infinite lifespan were investigated to research the role of immortalization in DNA marker expression. Cells were irradiated with 50 cGy, fixed after 1 hour with 4% paraformaldehyde, and processed through immunofluorescence. Cells were imaged using an immunofluorescent microscope and digitally captured using Image Pro Plus software. 8-bit images were analyzed using Image J and counted. The 184 cells showed more positive response within the irradiated samples than the S1 samples. It was observed that the S1 had a previous peak time of 30 minutes with an alternative DNA damage probe; this could explain the decrease in signal for S1 for both probes used in this research. We also noted that the γ H2AX response was more punctate in the 184 cells, whereas the 53BP1 response was punctate in both cell lines. We hope to expand the dose and time course studied in the hope that this will broaden the knowledge obtained from the preliminary data of this research. It is important to understand whether the process of transformation to immortalization compromises the DNA damage sensor and repair process.

A New Method for Protein Sequence Characterization Using Hidden Markov Models. HARSH SHAH (University of Illinois at Chicago, Chicago, IL 60607) GYORGY BABNIGG (Argonne National Laboratory, Argonne, IL 60439). Predicted protein sequences of newly sequenced species are normally analyzed for similarity to existing protein sequences using BLAST. The sequences are also characterized by searching with Hidden Markov Models (HMMs) of existing protein families in order to assist function assignment. While the BLAST searches are performed quickly, the more accurate searches using HMMs are computation intensive and might take a long time. Once new sequences are identified that belong to a certain protein family,

these sequences should be incorporated into family profile (HMM) in order to represent these new members. The new HMM in return should be used to search the protein space again for inclusion of potential new members not found previously or simply rebuilding statistical data for the existing family members. While HMMs are very powerful for the detection of protein family members, the dynamic construction of them is computationally prohibitive. We have explored the possibility of constraining the protein space and therefore speeding up searches with HMMs using two methods: 1) using a regular expression (REGEX) obtained from the HMM or 2) using PSI-BLAST with a position-specific scoring matrix generated from the HMM to select candidate sequences from the protein space (about 3.5 million sequences). The smaller proteins sequence database was used for the more accurate search by the HMM. We have compared execution times and the accuracy using a direct HMM search approach with the two-step techniques. We have determined that while the current implementation of the REGEX-based approach was resulting in fast execution times, its accuracy was greatly affected by the type of HMM and was only applicable for a small subset of cases. The second, PSI-BLAST-based approach resulted in fast execution times and high accuracy when compared to the HMMSearch standard. Using the combination of PSI-BLAST and HMMSearch programs (PSI-HMMER) improved accuracy even further with small impact on execution times. The software developed during this project (PSI-HMMER) enables the searches of protein sequences databases about 200 times faster than traditional tools with negligible impact on search accuracy. This tool will be incorporated into the currently used bioinformatics pipelines.

A Simplified Approach to Stereoscopic Imaging of Tomographic Reconstructions in Transmission Electron Microscopy. SALIM RAHIMI (Nassau Community College, Garden City, NY 11530) ROBERT BENNETT (Brookhaven National Laboratory, Upton, NY 11973). In biological applications, transmission electron microscopy (TEM) enables an investigator to view a specimen at the molecular level, offering a resolving power of ~ 0.2 nm. The two-dimensional (2-D) micrographs captured using the TEM are grayscale images in which contrast is typically achieved using heavy metal stains that limit electron transmission with respect to specimen density. In order to ascertain an adequate understanding of the structure and function of biological systems, it is important to view these structures in three dimensions (3-D), as they appear in life. Currently, there is a myriad of protocols that use various software applications for creating tomographic volumes. Moreover, the lack of a uniform approach often makes the process difficult to replicate for those with limited resources. A simple, consistent method for generating tomographic volumes of TEM micrographs to be viewed stereoscopically was investigated. Sections ranging from ~ 60 -100nm in thickness were collected on formvar-coated copper grids. Samples were viewed using a Philips EM300 TEM with a side-mounted goniometer stage, and images were captured with an integrated Gatan ES500W CCD camera. Common to many laboratories working with limited budgets, various challenges are faced during data acquisition and processing. Physical limitations of the goniometer have restricted datasets to a 45 degree maximum rotation in either direction about the horizontal axis. A tilt image series was digitally captured from -45 to $+45$ degrees in 1 or 2 degree increments and reconstructed into tomograms and rendered using Stanford University's EM3D software. Finally, stereoscopic visualizations of the rendered three-dimensional volumes were generated through the creation of movies that were viewed using the software application StereoMovie Maker.

Acetyltransferase Activity of the 11-Amino Acid Peptide Cofactor of the Adenovirus Proteinase. YUE LIANG (University of California-Berkeley, Berkeley, CA 94704) WALTER F. MANGEL (Brookhaven National Laboratory, Upton, NY 11973). The 11-amino acid peptide pVIc (GVQSLKRRRCF) from the C-terminus of the precursor to adenovirus protein VI has a transacetylase activity. Acetylation is an important physiological process in eukaryotic cells. For example, it is involved in DNA replication, transcription and repair. pVIc was incubated with acetyl coenzyme-A (Ac-CoA) at pH 7.0 for 15 minutes and the reaction was fractionated by high performance liquid chromatography (HPLC). A new peak appeared whose mass corresponded to mono-acetylated pVIc as determined by Matrix-Assisted Laser Desorption Ionization (MALDI) Mass Spectrometry. The kinetics of acetylation were linear for at least 21 minutes. The equilibrium dissociation constant (Kd) for the

interaction of Ac-CoA with pVlc was 1.1 mM. When purified mono-acetylated pVlc obtained at pH 7.7 was incubated at pH 10.3 for 15 minutes, multiple peaks were observed upon HPLC. MALDI analysis of each peak indicated one peak contained pVlc, another the original mono-acetylated pVlc, two other peaks contained mono-acetylated pVlc, three peaks contained di-acetylated pVlc and one peak contained tri-acetylated pVlc. The reaction at pH 10.3 was repeated but in the presence of the C-to-A mutant of pVlc. The mutant pVlc did not become acetylated. Thus, the new acetylations at pH 10.3 occurred in cis, except for the trans-acetylation between cysteine residues on different pVlc. A long-term goal is to find out the effects of acetylation on pVlc and, therefore, on virion assembly, and further discover anti-viral agents that can interfere with viral assembly.

Amplification and Tagging of *Sulfolobus solfataricus* Genes for Recombinant Expression. STEPHANIE PETERSON (*Del Mar College, Corpus Christi, TX 78404*) STEVEN M. YANNONE (*Lawrence Berkeley National Laboratory, Berkeley, CA 94720*). In organisms that thrive at moderate temperatures, many biological processes such as DNA repair occur through transient protein interactions. Understanding these interactions and the temporary protein complexes that they form is vital to understanding how cells function especially in how they repair damaged DNA. Protein interactions within hyperthermophiles like *Sulfolobus solfataricus* may be stabilized at moderate temperatures. The work presented in this study provides the initial steps towards thermally trapping otherwise short-lived protein complexes. Genes associated with DNA repair were selected from the *S. solfataricus* P2 genome and were modified with a directional tag on the N-terminus and a six-histidine tag (6x-hist) on the C-terminus using gene specific primers. Genes were amplified, cloned into entry vectors, and transformed into *E. coli* cells. Colonies were then selected and grown in liquid culture. Plasmid DNA was isolated using alkaline-lysis extraction method and constructs were confirmed with restriction digestion. Sixteen out of twenty-nine constructs were successfully confirmed by restriction digestion and fragment pattern on 1% agarose gels. These constructs will be further studied through two different expression systems: *E. coli* expression and *S. solfataricus* expression. *E. coli* expression should provide insight into independent protein structure and function. Native expression will not only provide information about the structure and function but will also identify obligate protein partners in their native organism. In addition, this approach will identify the root causes of difficulties that arise from recombinant expression.

Analysis of Cell Wall Mutations in Maize Using Pyrolysis Molecular Beam Mass Spectrometry. BRIANNA HARP (*Metropolitan State College of Denver, Denver, CO 80217-3362*) MARK DAVIS (*National Renewable Energy Laboratory, Golden, CO 89401*). This study applies Pyrolysis Molecular Beam Mass Spectrometry (PyMBMS) as a high throughput screen of cell wall substrates to characterize cell wall mutations. We had 3 goals in our study: improve PyMBMS technique, confirm cell wall mutations, and characterize differences between mutant lines and controls. We tested two methods of extraction: the Accelerated Solvent Extraction (ASE) and a simplified, rapid ethanol/acetone extraction using PyMBMS and multivariate statistical analysis to determine which method is most effective for removing extraneous cell wall material. This investigation found the ASE extraction to be most effective. A second study was performed using a combination of ASE extracted and untreated whole mutant 33_00FL-041-39 and 34_02S-1030-22 samples and controls to identify mutant lines and characterize differences among the samples, while analyzing benefits of the ASE extraction technique. The results of this study showed no significant differences in cell wall chemistry or advantage in using the ASE extraction technique. Our third investigation sampled six different mutants using only whole samples. We found that the mutant line 27_02s-1137-40 had a significant increase in C5 and C6 sugars. The results of our analysis of mutant line 39_00FL-042-20 (387, 388, 393, 395, 396, 399) is inconclusive.

Analyzing the Structure and Function of Novel Cytochromes from a Natural Microbial Community. ANNA SIEBERS (*University of California—San Diego, La Jolla, CA 92093*) MICHAEL P. THELEN (*Lawrence Livermore National Laboratory, Livermore, CA 94550*). The Richmond mine in Iron Mountain, California, provides an unusual ecosystem suitable for the growth of microbial biofilms which produce many unique proteins. Through iron oxidation, these proteins facilitate acid mine drainage (AMD). Because this habitat is extremely acidic, survival is an extraordinary feat and the process of environmental selection is rare. In order to understand the mechanisms by which these organisms oxidize iron and gain electrons for energy, biochemical studies were applied. More specifically, column chromatography, spectrophotometry, and gel electrophoresis were used to determine

the proteins present in different biofilms. Two specific locations of the mine researched were the AB drift and Ultraback C (UBC), which were both found to contain at least five different types of protein and a large amount of heme-bound cytochromes. Another application of these methods was to investigate cytochromes playing a major role within the community; one protein selected was cytochrome 579 (Cyt579) due to its abundance in the biofilm, iron oxidizing potential, and signature absorbance of 579nm. The structure and function of Cyt579 could be characterized by the isolation of its heme, which was completed using column chromatography; however, one of the challenges has been liberating the heme from the column. Further research, including acid-base and temperature profiling of Cyt579 should help elucidate its structural changes within alternate environments and metabolism within the community.

Characteristic Colonization of Poplar Trees with GFP Expressing Bacterial Endophytes. ERIKA FREIMUTH (*Cornell University, Ithaca, NY 14850*) DANIEL VAN DER LELIE (*Brookhaven National Laboratory, Upton, NY 11973*). Endophytic bacteria that colonize the internal systems and spaces of plants contribute valuable functions and services to the plant both individually and as a community. The enhancement of plant growth and metabolic processes by endophytic bacteria offers the opportunity to mediate both increased production of plant material and the sequestration of toxins within its tissues. Cuttings of poplar trees were inoculated with selected strains of endophytic bacteria (*Pseudomonas putida* W619 and *Enterobacter* sp. 638) genetically modified to stably express a green fluorescent protein and resistance to kanamycin. The colonization behavior and effects of these bacteria on the plant were monitored biweekly using fluorescent microscopy as well as by grinding and plating different sections of plant tissue (including sections of the rhizosphere, roots, shoots, and leaves). By thus tracking select endophytic bacterial strains marked with gfp through the plant's development, the colonization efficiency and patterns of these endophytes in poplar can be utilized in various applications. Poplar biomass production and chemical sequestration efficiency can be maximized via endophytic bacteria for use in biofuels, carbon management and recycling, and the phytoremediation of environmental pollutants.

Characterizing the Role of the Nell1 Gene in Cardiovascular Development. LEAH LIU (*Pennsylvania State University, University Park, PA 16802*) CYMBELINE CULIAT (*Oak Ridge National Laboratory, Oak Ridge, TN 37831*). Nell16R is a chemically-induced point mutation in a novel cell-signaling gene, Nell1, which results in truncation of the protein and degradation of the Nell16R transcript. Earlier studies revealed that loss of Nell1 function reduces expression of numerous extracellular matrix (ECM) proteins required for differentiation of bone and cartilage precursor cells, thereby causing severe skull and spinal defects. Since skeletal and cardiovascular development are closely linked biological processes, this research focused on: a) examining Nell1 mutant mice for cardiovascular defects, b) determining Nell1 expression in fetal and adult hearts, and c) establishing how ECM genes affected by Nell1 influence heart development. Structural heart defects in Nell16R mutant fetuses were analyzed by heart length and width measurements on formalin-fixed specimens and standard histological methods (haematoxylin and eosin staining). Nell1 expression was assayed in fetal and adult hearts using reverse transcription polymerase chain reaction (RT-PCR). A comprehensive bioinformatics analysis using public databases (UCSC Genome Browser, Mouse Genome Informatics, Integrated Cartilage Gene Database, PUBMED) was undertaken to investigate the relationship between cardiovascular development and each of the 28 ECM genes affected by Nell1. Nell1-deficient mice have significantly enlarged hearts (particularly the heart width), dramatically reduced blood flow out of the heart and unexpanded lungs. Isolation of total RNAs from hearts of adult (control and heterozygote) and fetal (control and homozygous mutant) mice have been completed and RT-PCR assays are in progress. The bioinformatics analysis showed that the majority of ECM genes with reduced expression in Nell1-deficient mice are normally expressed in the heart (80%; 22/28), blood vessels (71%; 20/28) and bone marrow (61%; 17/28). Moreover, mouse mutations in seven of these genes (Col15a1, Osf-2, Bmpr1a, Pkd1, Mfge8, Ptger4, Notch3) manifest abnormalities in cardiovascular development. These data demonstrate for the first time that Nell1 has a role in early mammalian cardiovascular development, mediated by its regulation of ECM proteins necessary for normal cardiovascular growth and differentiation. In addition, the identification of Nell1 and its associated ECM genes can provide future targets for treatment of heart and blood vessel defects.

***Cloning of DNA Repair Genes from a Hydrothermal Vent Worm.** ANABEY CORNEJO (*Contra Costa College, San Pablo, CA 94806*) JILL O. FUSS (*Lawrence Berkeley National Laboratory, Berkeley, CA 94720*). Abstract The primary structure of DNA is highly reactive with molecular by-products of metabolism as well as UV radiation from the sun, and these reactions alter and damage the human genome. Alterations to the DNA structure and chemistry result not only from natural physical agents but also from man made chemicals, although to a lesser extent. If these alterations are not detected and either corrected or removed, a mutation can be fixed in the genome potentially leading to cancer and aging. Through evolutionary adaptation, cells have developed a series of mechanisms which allow them to remove the damage and restore the normal nucleotide sequence and DNA structure. One such mechanism is Nucleotide Excision Repair (NER) which removes oligonucleotides, which are short nucleotide segments that contain damaged bases. NER is further categorized based on the location of the repair. GG-NER or global genome repair refers to NER taking place in DNA not undergoing transcription. TC-NER or transcription-coupled repair refers to NER occurring in the transcribed strand of active genes. If the NER pathway is compromised, a number of human genetic diseases such as Xeroderma pigmentosum (XP), Cockayne syndrome (CS) and Trichothiodystrophy (TTD) may result. These diseases are characterized by causing premature aging or a predisposition for cancer. To investigate the human DNA mechanisms of repair, we are studying an organism highly genetically homologous to humans, in this case *Alvinella pompejana* or Pompeii worm. The effectiveness behind using the Pompeii worm as a model for studying the process of DNA repair is due to the fact that most of its protein activity occurs at temperatures as high as 80°C. The Pompeii worm inhabits geysers found along underwater volcanic mountain ranges known as hydrothermal vents. These underwater formations release jets of water reaching temperatures as high as 300°C. Not only does it serve as a great organism for comparative studies due to its genetic similarity to the human genome but also because of its extreme heat tolerance. This would imply that its proteins will be fairly stable at room temperature which will allow for extensive in vitro study. More specifically to investigate DNA repair genes involved in NER, through the cloning of these genes from *Alvinella pompejana* as well as constructing plasmid vectors for recombinant protein expression, protein purification, protein to protein interaction studies, transfection of cultured human cells with expression vectors followed by assays for reporter gene expression, and analyzing particular proteins as a function of the cell cycle in mammalian cells.

Comparison of Fragmentation-Directing Properties of Amino Acids. DANNY TAASEVIGEN (*Montana State University, Bozeman, MT 59715*) WILLIAM R. CANNON (*Pacific Northwest National Laboratory, Richland, WA 99352*). Proteomics is the study of proteins and their function by the use of high, throughput methods such as mass spectrometry. With the use of molecular theory and computation, our group helps to develop more accurate peptide identification methods. Taking into account the potential energy of the system and the forces that affect peptide formation, simulations can be run to determine the probability of obtaining a configuration conducive to proton transfer to the respective carbonyl oxygen along the side chain. These simulations are run in the gas phase with a total time of 5 nanoseconds. Once complete, radial distribution functions provide us with the probability of proton donation along the chain. This data will be compared to predicted spectra in hopes of identification. The peptides are composed of various proportions of 20 naturally occurring amino acids and were derived from polyalanine, which proves to be the basis of analysis. However, these peptides have to have specific charges and the simulations have certain specifications that must be set to properly match the spectra. If detection of peptides is successful in this manner, it is likely to be scaled up to the genome-wide scale.

Creating Information System of Oncological Methylated DNA Data. REGINALD GABRIEL (*Cheyney University of Pennsylvania, Cheyney, PA 19319*) DR. SEAN R. MCCORKLE (*Brookhaven National Laboratory, Upton, NY 11973*). DNA methylation is the addition of a methyl group to the cytosine ring of the CpG dinucleotide, forming methyl-cytosine and is catalysed by DNA methyltransferases. An information system is needed for biologists to retrieve empirical data and relate it to DNA methylation sequences experimentally identified in human cancer cells. This project is intended to create such information system available for biologists. Information was collected from biomedical article reviews and existing Internet database, such as RefSeq (NCBI), the UCSC Genome database. PostgreSQL database server running on MAC OS X (DARWIN – BSD) system was established. The tool NetBeans Integrated Development Environment

(IDE) was used to create the Graphical User Interface (GUI), the client application with the Java programming language. The Java client can run virtually on any computer because of the benefits of Java; "write once and run anywhere". Communication between the Java client and PostgreSQL database server was established through the Java Data-Base Connectivity (JDBC) package. Object Oriented Techniques (OOT) is ideal for connecting various sub-components of the system: network connections and GUI application. A class PostJDBC was implemented to connect to the database, issue queries, and retrieve resultant data. UserGui, the user interface, relies heavily on inheritance and polymorphism techniques to achieve dynamic data manipulation and graphical display of the output. The client application presents the user with a list of gene symbols which are contained in the database, and allows the user to browse for more detailed information by mouse selection. This project can be easily expanded by including information about different types of features in DNA sequences and their relation to human cancer cells.

Crystal Structure of Mn²⁺ Bound *Escherichia coli* L-arabinose Isomerase Complex: Its Implications in Protein Catalytic Mechanism and Thermo-Stability. WEISHA ZHU (*Cornell University, Ithaca, NY 14853*) BABU MANJASETTY (*Brookhaven National Laboratory, Upton, NY 11973*). *Escherichia coli* L-arabinose isomerase (ECAI) is responsible for the initial stage of L-arabinose catabolism, converting arabinose into ribulose in vivo. This enzyme also plays a crucial role in catalyzing the conversion of galactose into tagatose (low calorie natural sugar) in vitro. The crystal structure of its native form has been recently solved. This project aims to determine the crystal structure of enzyme in complex with co-factor metal ions and candidate substrates/inhibitors to further study structure-function relationships important for the enzyme's biological mechanism. High-throughput techniques were adopted for protein structure analysis. Crystals of different complexes were grown using hanging drop vapor diffusion method. Diffraction datasets were collected at X4C, X6A and X29 beamlines, National Synchrotron Light Source, Brookhaven National Laboratory. The method of molecular replacement was utilized in structure solving using the native structure as the initial model. A series of crystallographic software packages were used to build and refine the structural model. The analysis of the structure of Mn²⁺ bound ECAI protein complex completed to 2.8 Å resolution with the R-factor of 23% and the structure was deposited to Protein Data Bank (PDB ID 2HXG). The overall fold and biological arrangement of the complex are conserved. Active site of ECAI is located at the subunit interface and forms deep cleft. Mn²⁺ ion is identified at the active site surrounding with an octahedral coordination. Comparison between apo and holo structures reveals variations in the metal coordination sphere, conformational changes associated with the active site residues and increased number of interactions between subunits. The available biochemical and structural data provides the structural basis for efficient protein catalytic mechanism and increase in thermo-stability of the enzyme induced by the presence of Mn²⁺. This study will benefit optimization of low-calorie sugar production. The target of this project is one of the many selected under investigation by New York Structural Genomics Research Consortium (NYSGXRC ID T2031).

Deletion of a Chitin Synthase Gene in a Citric Acid Producing Strain of *Aspergillus niger*. TORRI RINKER (*Oregon State University, Corvallis, OR 97331*) SCOTT BAKER (*Pacific Northwest National Laboratory, Richland, WA 99352*). Fungi have the potential to convert biomass into high-value chemical products. Filamentous fungi produce organic acids, such as citric, lactic, and fumaric acid. Citric acid production by the filamentous fungus *Aspergillus niger* is carried out in a process that causes the organism to drastically alter its morphology. This altered morphology includes hyphal swelling and highly limited polar growth resulting in clumps of swollen cells that eventually aggregate into pellets of approximately 100 microns in diameter. In pelleted form, *A. niger* has increased citric acid production rates when compared to those in filamentous form. Production of citric acid by *A. niger* serves as a model in which a filamentous fungus can take on a particular morphology and increase product output. Chitin, a polysaccharide in fungal cell walls, plays a central role in the morphology of fungi. A gene coding for chitin synthase with a myosin-motor domain (*csmA*) was deleted from the genome of *A. niger* using a PCR-based gene deletion construct. The mutant was tested on minimal media with and without osmotic stabilization. In the absence of osmotic stabilization, the germlings of the deletion strain (*csmΔ*) were abnormally swollen and highly vacuolated. This suggests that chitin synthase is important for germination of spores, which in turn impacts morphology and may affect citric acid production rates. Genetic manipulation, such as gene deletion, can be used in the future in

other strains of filamentous fungi to obtain desired morphologies and optimized product output.

Detecting and Quantifying Heavy Metal Contamination in Water. MATTHEW LARSEN (*Brigham Young University–Idaho, Rexburg, ID 83460*) ANGELICA STORMBERG (*Idaho National Laboratory, Idaho Falls, ID 83415*). The DOE has a goal of remediating environmental contaminants. We must first know where the contaminants are, and in what concentration. For detection of heavy metals in aqueous media a transgenic nematode has been developed. *C. elegans* releases a Green Fluorescent Protein (GFP) upon contact with heavy metals. Our work was to calibrate the amount of fluorescence with the concentration of heavy metal contamination. Water samples can be analyzed in 24 hours, and cost less than 10 cents per sample. We were able to analyze five metals: Zinc, Lead, Mercury, Cadmium, and Nickel. Each was analyzed at 4 different concentrations. The calibration curves developed may be used to test a water sample and determine the concentration of the heavy metal contaminants.

Determination of a Role for Cellular XPG in Repair of Oxidative Damage to DNA. EMILY FOX (*City College of San Francisco, San Francisco, CA 94112*) HELEN BUDWORTH (*Lawrence Berkeley National Laboratory, Berkeley, CA 94720*). Mutation of XPG can cause the debilitating diseases Xeroderma Pigmentosum (XP) and Cockayne's Syndrome (CS), which result from a deficiency in DNA repair. XPG cuts 3' to DNA lesions during nucleotide excision repair (NER), as well performing the non-catalytic roles of recognizing stalled RNA polymerase II and binding transcription-sized bubbles in transcription coupled repair. Through *in vitro* tests with purified proteins, XPG has been found to stimulate hNth1, which removes oxidized pyrimidines in the base excision repair (BER) pathway. In this study, whole cell extracts from XPG-deficient cells obtained from patients with XP-G/CS were found to be defective in incision of 5,6-dihydrouracil (DHU). This defect was corrected by the addition of purified XPG, suggesting that the mutated XPG in XP-G/CS cells is unable to stimulate hNth1. In addition, cells from XP-G/CS patients were found to be slightly sensitive to X-rays and hydrogen peroxide, as determined by colony formation survival assays. shRNA against XPG was used to knockdown XPG in normal cells in order to provide another model for XPG deficiency in which the only variation from control cells is reduced levels of XPG.

Determining Cellular Localization of Candidate Cilia Proteins in Transgenic *Caenorhabditis Elegans*. SANDRA MCGILL (*Clayton State University, Morrow, GA 30281*) EDWARD J. MICHAUD (*Oak Ridge National Laboratory, Oak Ridge, TN 37831*). Primary cilia are small organelles that protrude from cell surfaces and are conserved in most eukaryotes, including nematodes, mice, and humans. In humans primary cilia have vital sensory functions; flaws in these organelles lead to many diseases. Based on comparative genomics and proteomics studies it has been estimated that the cilia proteome consists of 300-500 proteins, but the functions of most are unknown. Disruption of the homologous genes in mice is an effective approach for determining function. However, prior to performing lengthy and costly experiments in mice, it is desirable to verify that these candidate genes do indeed localize to primary cilia. An efficient method for determining the *in vivo* cellular localization of candidate cilia proteins is to perform translational GFP assays in transgenic nematodes. In a previous project, translational fusion vectors were constructed in which two nematode candidate cilia genes, E02H1.5 and R148.1, were cloned in-frame with the Green Fluorescence Protein (gfp) reporter gene in a plasmid vector, pPD95.81. In this project, the two vectors are being microinjected into the gonads of nematodes, where transcription and translation of the fusion vector results in the nematode protein being tagged with the GFP protein. Visualizing the GFP marker under a fluorescent microscope reveals the locations of the fusion proteins in nematodes. Three independent lines of transgenic nematodes were established for E02H1.5, but examination of the transgenic nematodes did not reveal any GFP expression. Based on this result, and on further examination of the genomic locus encompassing the E02H1.5 gene, it appears that E02H1.5 may be one gene in a four-gene operon. Approximately 10% of all worm genes exist in operons, where one promoter region directs the expression of all genes in the operon. The entire E02H1.5 operon is now being cloned into the pPD95.81 vector and will be used to generate new lines of transgenic nematodes. Microinjection of the R148.1 vector into nematodes is under way. Additionally, translational fusion vectors are being made for two other candidate cilia genes, K07G5.3 and C02H7.1, which will also be used to generate transgenic nematodes to determine protein localization. If these four proteins are shown to localize to cilia in nematodes, the stage will be set for analysis of the functions of the homologous proteins in mice and humans.

Developing EPIMODEL2: A Computer Program for Teaching Population Growth Modeling. DANIEL HEIDFELD (*Michigan Technological University, Houghton, MI 49931*) FORREST W. NUTTER JR. (*Ames Laboratory, Ames, IA 50011*). EPIMODEL is a computer teaching program that is currently being used in more than 40 universities worldwide to teach students biological concepts concerning population growth modeling. EPIMODEL has become outdated because it was originally created in Quick BASIC for MS-DOS. Therefore, the goal of this project was to rewrite EPIMODEL using a computer language that would support Windows™. The programming language Java was chosen to develop EPIMODEL2 because Java is capable of operating on many platforms, including Windows™. EPIMODEL2 was programmed with the aid of various online manuals to develop algorithms that implement features within the Java environment. EPIMODEL2 was designed to mimic all of the features of the old version of EPIMODEL, but the new program implements a Graphical User Interface (GUI). The new program, EPIMODEL2, is a valuable and more versatile replacement for the outdated version, and the development of a new version in Java successfully accomplished the goal of this internship.

Developing Software Within Gatan's Digital Micrograph in Order to Create Automated STEM Tomography. MICHAEL MYLENSKI (*State University of New York at Albany, Albany, NY 12222*) HUILIN LI (*Brookhaven National Laboratory, Upton, NY 11973*). Automated Scanning Transmission Electron Microscope (STEM) tomography follows the ideals of Jianglin Feng, a researcher in the Department of Molecular Physiology and Biological Physics at the University of Virginia. Feng's automated version of STEM tomography revolves around the ideas of auto-tracking and auto-focusing. An automated STEM tomography program will be the first of its kind at Brookhaven National Laboratory (BNL). The development of the automated STEM tomography program was based on scripts created using Digital Micrograph (DM), which is the program of choice for communication between the researchers at BNL and the JEOL 2010F microscope. When creating these scripts, JEOL's FasTEM Communication Kit (FTCOMM) and Digital Micrograph's Software Developers Kit (DMSDK) were essential in creating new functions to implement auto-tracking and auto-focusing. Feng's paper provided the basic algorithm for automated STEM tomography and also a gradient formula in order to implement auto-focusing. Overall, there were five scripts and a Dynamic Link Library (DLL) that were developed in order to implement automated STEM tomography. The DLL file was the means of communication between the microscope and DM using FTCOMM and DMSDK, and it was developed using Microsoft's Visual Studio .NET 2003. The Graphical User Interface (GUI) was created using functions within DM's scripting language in order to benefit the user. The arithmetic for the auto-tracking and auto-focusing is primarily based in the DM scripts. When they communicated with the microscope, there were functions created in the DLL file that used FTCOMM functions in order to link the microscope and the DM scripts. The program that was completed includes the basics of an automated STEM tomography system with simple implementations of auto-tracking and auto-focusing. This project must be continued in the future in order for this version of automated STEM tomography to fully benefit researchers at Brookhaven National Laboratory in their study of structural biology.

Development of a Biosensor for Measuring Antibody-Antigen Interactions. CASSANDRA ARMSTEAD-WILLIAMS (*Washington University School of Medicine, St. Louis, MO 63110*) KARA KRUSE (*Oak Ridge National Laboratory, Oak Ridge, TN 37831*). In recent years the Nanoscale Science and Devices group at Oak Ridge National Laboratory has developed and continues to study how microcantilever technology can be used to create high-throughput, label-free tests for biological macromolecules. The Vascular Research Laboratory at the University Of Tennessee Medical Center of Knoxville is studying the effects of certain drugs on the concentrations of Matrix Metalloproteases (MMP's) in the blood. The Vascular Research Laboratory and the Nanoscale Devices and Sciences group are working together to create a dependable, high-throughput, label-free system for quantitatively measuring concentrations of MMP's. Microcantilevers bend due to a change in the entropy and energy on one side of the cantilevers and not the other. This bending can be monitored optically by reflecting a laser beam off of the cantilevers and onto a position sensitive detector (PSD). The PSD translates the optical signal into an electronic signal for real-time monitoring of microcantilever bending. For this experiment, gold-coated silicon microcantilevers were immobilized with 3,3-Dithio bis(sulfosuccinimidylpropionate) (DTSSP)-a homobifunctional, amine reactive cross linking agent. Immobilizing the cantilevers with a DTSSP monolayer allows selective attachment of biochemical molecules onto

the gold and silicon/silicon nitride microcantilever substrate. MMP specific probe antibodies were then attached to the microcantilevers via a captavidin-biotin linkage system. Surface amine groups of captavidin were reacted with the succinimide terminals of DTSSP. The biotin-conjugated, MMP specific probe antibodies selectively adsorb onto the captavidin protein layer. After functionalization (immobilization), solutions containing unknown concentrations of MMP's are introduced to the microcantilevers while bending is being monitored. Using a model antibody system, Current tests indicate that DTSSP and antibodies can reliably be immobilizing on to the cantilevers surfaces. However, we have not been able to determine the antibodies' range of sensitivity for protein concentration detection. The reliability of the DTSSP and antibody immobilization shows that this detection system can work. We are currently modifying our detection system and probe immobilization procedures to find the optimal working range for this technology.

Dialysis or Column Exchange: Developing an Efficient and Quantifiable Protocol for Detergent Exchange Prior to Crystallization of Membrane Proteins. NICK IMPELLITTERI (*UW Stevens Point, Stevens Point, WI 54481*) PILIP D. LAIBLE (*Argonne National Laboratory, Argonne, IL 60439*). The goal of this study was to develop quantitative methods to replace detergents used for the solubilization and purification of a membrane protein with a diverse range of detergents that could potentially increase the success rate of the proteins characterization and crystallization. Previously it has been anecdotally perceived that detergent exchange could be accomplished either by dialysis or by extensively washing and eluting column bound membrane protein with an alternate buffer containing a different, yet desired, detergent. *Rhodobacter sphaeroides* reaction centers (RCs), as well as foreign affinity-tagged *Escherichia coli* membrane protein APC00809 (809) were solubilized, concentrated, and purified using the detergents N,N-Dimethyldodecylamine-N-Oxide (LDAO) and deriphat-160, respectively. These two membrane protein's detergents were exchange into the following detergents using both on column exchange and dialysis: LDAO, Triton X-100, n-Octyl-β-D-Glucopyranoside (OG), Tetraethylene Monoethyl Ether (C8E4), Deriphat-160, and CHAPS. Column-bound membrane proteins were eluted and analyzed after being washed with 1, 5, 10, and 20 column volumes of buffer containing the desired detergent, while membrane proteins were left in dialysis tubing with large reservoirs for 1, 2, 5, or 7 days. After concentrating all samples to ~10 mg/mL and analyzing them using thin layer chromatography (TLC), iodine staining and Image J software, the results of this experiment explicitly show the superiority of column exchange over dialysis in terms of accomplishing complete exchange of detergents with every combination attempted. For every trial, detergent exchange for RCs is more complete after 20 column volumes of detergent buffer than after 7 days of dialysis. Column exchange yielded a complete detergent exchange for all detergents except deriphat, which did not exchange well with LDAO in RCs in either column exchange or dialysis. Though all dialysis and most column exchange samples for 809 were lost in concentration, the column exchange samples that were concentrated and analyzed clearly showed that column exchange was fast and effective. In this experiment it clearly shows that column exchange is the most suitable means by which to exchange one detergent with many others of varying CMC. Dialysis, as this experiment shows, can only yield up to a 90% exchange after 7 days when exchanging with detergents of extremely low CMC. These results or this experiment will lead to more defined and reproducible protein-detergent complexes for input into structural and functional studies.

Effectiveness of Driving Surveys to Locate Burrowing Owls (*Athene cunicularia*). SARITA INCE (*Lane Community College, Eugene, OR 97401*) MICHAEL SACKSCHEWSKY (*Pacific Northwest National Laboratory, Richland, WA 99352*). The burrowing owl (*Athene cunicularia*) is classified as a Species of Concern in the Columbia Basin by the U.S. Fish and Wildlife Service, a candidate species by the Washington Department of Fish and Wildlife, and as Endangered in Canada. A standardized, reliable, and time-effective population survey method has yet to be developed for burrowing owls. Without a reliable survey method, long term population trends cannot be accurately estimated. Driving surveys were evaluated as a method to locate burrowing owls in shrub steppe habitat and estimate relative population density. Burrowing owls are tolerant of human activities and are often found near roadways, making them an ideal candidate for driving surveys. Surveys were conducted on pre-determined routes at a prescribed speed of 20 mph. Seven routes within the Department of Energy's Hanford Site near Richland, Washington, were chosen based on habitat type and previous burrowing owl sightings. The surveyed routes consist of shrub steppe habitat with short grass and sagebrush

cover ranging from dense to none. Surveys were undertaken for two to three hours during the owls' most active times of day, after sunrise and before sunset. Driving surveys require two people, a driver and an observer who carefully watched one side of the road for burrowing owls. At the end of the route, the driver turns around and the observer watches the other side of the road. When a burrowing owl was observed, the location from the road was recorded using a GPS (Global Positioning System). Burrowing owls were sighted on all but one of the seven routes. Burrows and owls were found very close to the road and over 100 meters off road. Proximity to human activities seemed to have little effect on burrowing owl sightings. Driving surveys are effective in locating burrowing owls on the Hanford Site and should be repeated in future years as part of an on-going population monitoring effort. Relatively few of the owl groups were seen during both surveys of each route, indicating that more than two surveys per route is required to assure that all of the owls along each route are found. Driving surveys also may prove useful for gathering population density data on other animals within the Hanford Site.

Effects of Low-Level Cadmium on Cyr61 Expression in Pre-Osteoclastic Cells. KATHRYN TORMOS (*Benedictine University, Lisle, IL 60532*) MARYKA H. BHATTACHARYYA (*Argonne National Laboratory, Argonne, IL 60439*). Cadmium is a heavy-metal element that is a major component of orange or red pigments and is naturally occurring in trace amounts in air, water, and soil. It is well known that high, unnatural exposures to cadmium can result in toxic effects in human beings, in particular in the kidneys, liver, and lungs. However, the discovery that cadmium is linked to the severe bone-breaking Itai-Itai disease has shed light on the potential impact of cadmium on bone systems as well. Previous microarray experimentation of cadmium's effects on genes expressed in bone cells in vivo in mice has shown the most up regulated gene early after cadmium treatment to be *cyr61*. The *Cyr61* protein has been linked to such molecular processes as angiogenesis, ossification, embryogenesis, and cell migration. Preliminary immunohistochemistry staining and RNA isolation in bone cell cultures have shown potential *Cyr61* protein expression in osteoclasts (bone resorbing cells); this expression appeared to be greater than in cultured osteoblasts (bone matrix secreting cells). This summer, we continue to test the hypothesis that cadmium triggers osteoclastic precursor cells to secrete *Cyr61*, increasing their migration, aggregation, and fusion into mature osteoclasts. Using the pre-osteoclastic RAW264.7 cell line, *Cyr61* protein expression is being analyzed using Western blotting and immunoprecipitation, and *cyr61* gene expression is being analyzed using RT-PCR technology. We aim to conclusively demonstrate whether the *Cyr61* protein is significantly up regulated in cadmium's presence in RAW 264.7 cells. Showing *Cyr61*'s role in osteoclastic precursors in the presence of cadmium will pinpoint a new, previously unresearched, role for the protein, and will also help our laboratory continue to construct a hypothetical pathway proving cadmium's central role in bone resorption.

Established an Information System Comprised of CpG Methylated DNA Data in Cancers. WENYI BI (*Cheyney University of Pennsylvania, Cheyney, PA 19319*) SEAN MCCORKLE (*Brookhaven National Laboratory, Upton, NY 11973*). Determining the global pattern of DNA methylation, or the methylome and its variation in cells has become an area of considerable interest primarily because of its potential use as an early diagnostic biomarker for cancers. For time being, the research papers, results and literatures on this subject have grown rapidly and scattered in different systems. However, because there is lack of a comprehensive information system available to gain all correlated information into one picture, it forces the researchers to manually search through scores of biomedical journals and related websites. To meet the requirements to acquire them automatically, we developed an information system consisting of database system (back-end), and web application (front-end) by querying from a gene level to the related to methylated genes, cancers and literatures to gain all information by one-short deal. Our research went through data source collection, database system establishment, and web application coding. In addition, we developed a novel algorithm to identify genes near the diTag found in the experiment data.

Expression and Purification of a Yeast Hypothetical Protein. TIFFANY JORDAN (*Elizabeth City State University, Elizabeth City, NC 27909*) S. SWAMINATHAN (*Brookhaven National Laboratory, Upton, NY 11973*). Solving protein crystal structures by X-ray diffraction or NMR is essential for doing protein chemistry and novel drug design. This project involves several aspects of macromolecular crystallography; for example expression and purification of proteins, optimization of crystallization conditions by use of robot, crystallization by sitting drop vapor diffusion method, observation and analysis of the

crystals under the microscope and lastly x-ray diffraction of the crystals. During our ten weeks stay at Brookhaven National Laboratory, we were successful in expressing and purifying a 29 kDa hypothetical Yeast protein by His-tag purification using nickel chelated columns and by the size exclusion method of protein purification by using a FPLC machine. We ran 1D SDS-protein gels for analyzing and confirming our results.

Expression of Cyr61 in Pre-Osteoclastic Cells as a Result of Cadmium Exposure. MARYN VALDEZ (University of Maryland, College Park, MD 20742) MARYKA BHATTACHARYYA (Argonne National Laboratory, Argonne, IL 60439). Cadmium (Cd) is a natural metal commonly present in paint, plastics, batteries, the protective coating of steel, fertilizers, and in cigarettes. Cd has been shown to start having adverse effects on bone organ and cell culture systems at levels ranging from 10nM-100nM. However, the mechanism by which Cd acts on the bone system to cause bone loss has yet to be deciphered and thus needs to be further studied. This is the ultimate goal of our research. Past experiments and the literature have led us to think that Cry61 plays a pivotal role in the pathway. Cyr61 is a ligand to the integrins $\alpha\text{V}\beta\text{3}$. We hypothesize that Cd provokes expression of Cry61 in Osteoblast(OB) or Osteoclast(OC) cells, which binds to $\alpha\text{V}\beta\text{3}$ located on the surface of OC precursors. The binding eventually leads to responses that lead to bone resorption. Specifically in this paper we are trying to determine whether Cd triggers OC precursor cells to secrete elevated levels of Cry61. Total Cell lysate(TL), extracellular matrix(ECM), and concentrated media(CM) samples collected after exposure to 100nM Cd for 2-48hrs, were analyzed for Cry61 expression using western blots. Most of our time was spent working out the proper protocol and we feel it has been developed to the best of our ability. We concluded that fetal calf serum (FCS) does indeed cause Cry61 expression, as reported by others. We tentatively concluded, that at 24 hours and possibly at 48 hours, Cd is causing an increase in Cry61 expression in the media, but we can not say Cd is inducing Cry61 expression in TL or ECM. Perhaps a different cell line needs to be used—one in which Cry61 is overexpressed to begin with, or perhaps we need to look at the pre-OB cell lines. More experiments that include more than 0.1% serum and more negative controls also need to be done. Immunohistochemical staining experiments may also be needed. Thus we made progress, but much more work needs to be done.

Expression of Type I Cohesin and Type I Dockerin Domains from *Clostridia thermocellum* for Nano Patterning. CATHERINE COFFMAN (University of Tennessee—Chattanooga, Chattanooga, TN 37403) JENNIFER MORRELL-FALVEY (Oak Ridge National Laboratory, Oak Ridge, TN 37831). Cellulosomes are multienzymatic complexes from bacteria that have been studied for their ability to break down the cellulose in plant walls yielding ethanol as a byproduct. The scaffoldin protein is a significant component of the cellulosome structure because it binds to both the cellulose and cellulose degrading enzymes in the most advantageous manner for hydrolysis. In the assemblage of scaffoldin, nine Cohesin domains, in the presence of Calcium, mediate binding to enzymes that contain a Dockerin domain. This investigation examines the specific binding of the Type I Cohesin (Cohl) and Type I Dockerin (DoCl) molecules, which are components of the scaffoldin in the cellulosome. The objective is to artificially generate and assemble Cohl and DoCl using their unique binding specificity as an affinity pair. A 6x Histidine (His) tag will be added to the Cohl so that it can bind to a nickel surface. Green fluorescent protein (GFP) and a strep tag are added to DoCl. The interaction between the Cohl and DoCl would be visible through the GFP, and the strep tag allows for purification of the DoCl fusion protein. Thus far, the Cohl and DoCl domains have been identified in the sequences of CipA and CelS respectively in *Clostridia thermocellum*. Using genomic material from *C. thermocellum*, the Cohl and DoCl domains were PCR amplified. Expression vectors were constructed with the Cohl and DoCl inserts. A GFP with no stop codon was also ligated into the vector containing DoCl so that, when expressed, the GFP forms a fusion protein with DoCl. The ligated plasmids were transformed into *E. coli* strain BL21(DE3) where the Cohl and DoCl-GFP can be expressed. After the cell produces the proteins, they can be purified using the attached His and strep tags. This affinity pair can potentially be useful in nano patterning as Cohl can be positioned using nickel beads and binding events can be mediated through the Cohesin-Dockerin specificity. Binding can also be controlled since the Cohl and DoCl do not bind unless calcium is present in the system.

Extracting Methylated DNA Using His-Strep Tagged Clones of McrB, MBD2b and MBD3L1 Proteins. DANNY KOHUT (New York University, New York, NY 10003) JESSICA POLICASTRO (University of Scranton, Scranton, PA 18510) DR. JOHN J. DUNN (Brookhaven National Laboratory, Upton, NY 11973). Epigenetic modification of DNA

by the addition of a methyl group to the 5 position of the cytosine ring, the methylome, is the only common covalent modification of mammalian DNA. This modification has been shown to control the expression of various genes. Changes in methylation patterns have been observed in both brain cells exposed to cocaine and in developing tumor cells. McrB, a GTP-powered protein, binds to sites containing methylated cytosines preceded by either guanine or adenine residues. This protein was cloned from *E. coli* into the pET28 vector between NdeI and BamHI sites, expressed and purified for use. In order to be effectively used in methylome pull-downs, McrB was cloned onto a His-Strep tag previously ligated onto the pET28 vector between the NcoI and NdeI restriction enzyme sites. The tag will aid in binding the streptavidin-coated beads used in pull-downs. MBD2b binds methylated cytosines followed by guanines, which are found in CpG islands, and does so even more tightly when in the presence of MBD3L1. These proteins were also bound to the His-Strep tag as part of this novel approach in extracting methylomes. The efficiency of the synthesized McrB protein will be compared with that of MBD2b and also with the MBD2b-MBD3L1 protein complex. Each protein may pull down varying or very similar sections of a genome, whether a mixture of two or more must be used for effective pull-downs will be decided. The cloning of McrB into pET28 was successful; sequencing of the clone revealed no mutations or transformations created during PCR. Ligating the Strep tag onto the digested pET28 vector has also been successful. With the construction of functioning methylome pull-down proteins, drug addiction studies and the early detection of cancer may be improved.

***EZ-Viz Version 2.0, Further Simplification and Increased Functionality of Pymol Made EZ.** BRETT HANSON, CHARLIE WESTIN (Rochester Institute of Technology, Rochester, NY 14623) PAUL CRAIG, LEN SLATEST (Brookhaven National Laboratory, Upton, NY 11973). PyMol, a powerful open source molecular modeling tool, has a notoriously difficult user interface. In order to decrease the steep learning curve associated with PyMol, Laura Grell and Chris Parkin developed PyMol made EZ, (EZ-Viz), a plug-in user interface, to simplify the use of PyMol. Despite the simplicity of the new plug-in, it lacked many of PyMol's powerful features, severely limiting its versatility. To alleviate these shortcomings, numerous functions were added, including: Enhanced movie making ability, multiple view modes, electron density map importing and controls, Ramachandran plot fetcher, ray trace options, amino acid reference guide, mouse modes, multiple perspective options, polar contacts, and roving functions. With the new user in mind, buttons, sliders, and various other widgets were implemented to provide greater ease of use and efficiency. Instead of entering multiple character commands, a mere push of a button now renders the same outcome with much less frustration and time. Beyond these implementations, over 20 known catalytic active site motifs have been defined in EZ-Viz and are shown differentiated from the rest of the enzyme. Once the motif has been selected and returned for a PDB file, the user can easily show surface contacts, polar contacts, residue labels, and bound substrates. The prediction algorithms are based on measurements between specific amino acid atoms in relation to the other catalytic residues. The predefined measurement range can be modified by the user to increase or decrease precision of motif return. It is also possible for a user to define their own motif and exert a great deal of selectivity in searching for their domain of interest. Further pursuits regarding EZ-Viz will entail the implementation of complex algorithms for the prediction of ligand and protein docking, easier sequence alignment, and inclusion of a functional hydrogen bonding scheme. Utilization of EZViz's abilities will allow researchers to easily investigate sites of interest within proteins, enabling quicker and more efficient research. It will also provide instructors with the tools to present more detailed and visually appealing overviews of protein structure and function.

Gene Cloning and Expression in the Hyperthermophile *Sulfolobus Solfataricus*. MEGAN HOCH (Del Mar College, Corpus Christi, TX 78404) STEVEN M. YANNONE (Lawrence Berkeley National Laboratory, Berkeley, CA 94720). *Sulfolobus solfataricus* is a hyperthermophile Archaeon that lives in a very extreme environment, and for this it is considered an extremophile. This organism lives in acidic hot springs of Yellowstone National Park. *S. solfataricus* has become a model system for studying human DNA repair. Protein interactions that are needed to study DNA repair are sometimes transient. Protein interactions that are transient in high temperatures where Archaea live might be more stable at room temperature. This would allow a better look at and understanding of the protein complexes involved. Also, it is accepted that Archaea are more closely related to humans than bacteria, and the DNA replication and translation of the two is very similar. A group of genes was selected for cloning, and

primers were designed for each gene. The genes were amplified using the polymerase chain reaction (PCR) method. The PCR products for the gene of interest, were cloned into a directional topoisomerase I (TOPO[®]) cloning vector. These vectors were transformed into *E. coli* cells from Invitrogen. The cells were then plated on Luria-Bertani (LB) agar plates using sterile techniques. Clones were picked from the plates and a culture was grown overnight. The plasmid DNA was separated from the cells using alkaline lysis. Restriction enzyme digests were set up to confirm that the correct gene was inserted into the vector. The digest was visualized on a 1% agarose gel. This study successfully cloned sixteen out of the original twenty-nine genes selected. Some of the clones that grew on the LB plates did not contain any gene at all; it was simply the vector alone. After several restriction enzyme digests, there were about eight genes whose digests were not clear enough to confirm the presence of the correct insert. These constructs will need to be further digested with different restriction enzymes to confirm the gene. Currently methods are being developed for expressing these genes in *E. coli* and *S. solfataricus*. In future studies, proteins expressed from *S. solfataricus* will be studied and characterized to understand the protein-to-protein interactions that are occurring.

Generation of Translational Fusion Vectors for Candidate Cilia Genes. SANDRA MCGILL (Clayton State University, Morrow, GA 30260) EDWARD J. MICHAUD, III (Oak Ridge National Laboratory, Oak Ridge, TN 37831). Cilia are small organelles that protrude from the surfaces of cells and are conserved in most eukaryotes, including nematode worms, laboratory mice, and humans. Cilia fall into two broad classes: motile cilia, which occur in clusters on mammalian cells and move fluids over cell surfaces; and primary cilia, which are found singly on virtually all cell types in mammals. It was recently discovered that primary cilia have vital sensory functions in many human tissues, and that flaws in these organelles lead to numerous human diseases. Comparative genomics and proteomics studies have determined that the cilia proteome consists of some 300-500 proteins. However, the functions of most of these candidate cilia proteins are unknown. The goal of this project was to select two of these candidate proteins identified by computational methods and to construct plasmid vectors in which the worm genes are cloned in-frame with the green fluorescence protein (gfp) reporter gene. Two candidate cilia genes in *C. elegans* nematodes, E02H1.5 and R148.1, were selected for cloning into the GFP reporter vector, pPD95.81. The DNA sequence of each gene was obtained from the University of California at Santa Cruz Genome Browser, and polymerase chain reaction (PCR) primers were chosen using the MacVector 6.5.3 sequence analysis program. These primers were used to amplify the promoter and coding regions of each gene from *C. elegans* DNA. Each gene was amplified by PCR and cloned in-frame with gfp in the pPD95.81 vector, resulting in two translational vectors, E02H1.5::GFP and R148.1::GFP. The E02H1.5::GFP and R148.1::GFP translational vectors were subjected to restriction enzyme digestions and DNA sequence analysis, which confirmed that the two *C. elegans* genes were cloned into the pPD95.81 vector in the correct orientation and in-frame with gfp. Future work will involve microinjection of these generated transgene vectors into the gonads of nematodes to produce transgenic worms, which will be used to determine experimentally if these proteins localize to primary cilia. These worms will be examined under a fluorescence microscope to determine if the E02H1.5::GFP and R148.1::GFP fusion proteins localize only to ciliated cells. If they do localize to ciliated cells exclusively, E02H1.5 and R148.1 will be confirmed as cilia proteins. This will set the stage for analysis of the functions of the homologous proteins in mice and humans.

Global Analysis of Iron Response and Fur Regulon in Shewanella Oneidensis MR-1. DANIEL HARRIS (Albion College, Albion, MI 49224) JIZHONG ZHOU (Oak Ridge National Laboratory, Oak Ridge, TN 37831). Iron is an essential micronutrient for both prokaryotic and eukaryotic organisms. In addition to structural roles in proteins, the iron redox potential makes it a useful cofactor for proteins functioning in respiration, electron transport, photosynthesis, nitrogen fixation, DNA biosynthesis and other important processes. However, accumulation of free Fe(II) will catalyze Fenton reactions, which produce highly reactive oxygen species that damage cellular components. Levels of intracellular iron must therefore be precisely regulated to meet metabolic needs while minimizing risk of iron toxicity. Most bacteria moderate iron through the use of the Ferric Uptake Regulator (Fur), an iron-responsive global transcriptional factor that represses transcription when iron is present. In this study, the iron response network was analyzed in *Shewanella oneidensis* MR-1, and in a fur deletion mutant derived from MR-1. Cells were harvested at various intervals after addition of iron chelator (2,2'-dipyridyl), and then after iron repletion with iron

sulfate (FeSO₄). Total RNA from extracted from each strain at 13 time intervals, reverse transcribed, fluorescently labeled, and hybridized to DNA microarray slides. Four biological replicates were collected for each mutant for a total of 102 microarray hybridizations. Our results indicate that transcription of proteins involved in iron uptake and storage are mediated by Fur, and that these proteins are highly sensitive to iron availability. Proteins involved in energy metabolism are also regulated by iron availability and Fur, though to a lesser extent. Interestingly, Fur not only acts globally as a repressor, but also activates certain genes in response to fluctuations in extracellular iron concentration. Most of these genes have unknown function. In addition, we also identified regulatory genes controlled by Fur. Further investigations into the interaction between regulatory genes and Fur would be interesting and significantly increase our understanding of transcriptional regulation in *S. oneidensis*, an important metal-reducing bacterium with potential in the bioremediation of contaminated sites.

***High-Throughput X-ray Protein Crystallography.** BINH NGUYEN (Contra Costa College, San Pablo, CA 94806) DR. MINMIN YU (Lawrence Berkeley National Laboratory, Berkeley, CA 94720). Proteins play an integral function in cells, hence understanding them is critical, especially in medical research. Structural analysis of proteins is particularly important to the field of Structural Genomics, which aims to study protein molecules in nature to provide a fundamental understanding in biology. Knowing the three dimensional structures of proteins will enable the grouping of fold patterns and family of proteins that can lead to clues of how the proteins work. High-throughput protein crystallography allows structural determination of the protein via x-ray diffraction. Proteins are crystallized and the resulting crystals are analyzed with X-ray to create diffraction patterns that can be determined into three dimensional structures. The first important step in this process is we subject our proteins to series of crystallization matrices to find the right crystallization condition. We utilized various crystal screens from Hampton Research and Emerald Biosystems. The initial crystal hits-crystal formation-leads to further optimization of the crystallization solution so as to obtain crystals that have reasonable diffraction quality. Our crystals are analyzed mostly with the synchrotron at the Advance Light Source (ALS) within the Lawrence Berkeley National Lab (LBNL). Through protein 3-D structures, the folding topologies and local conformations of the proteins can be analyzed. The Li-Wei Hung Lab is currently analyzing various proteins for the Integrated Center for Structure and Function Innovation (ISFI) and TB Structural Genomics Consortium (TBSGC). These proteins are derived from interesting targeted DNA sequences of various sources, mostly species causing human diseases. Solved protein structures are deposited on our ISFI/TBSGC database (www.tbgenomics.org, <http://techcenter.mbi.ucla.edu>) and the Protein Data Bank (<http://www.pdb.org>).

Human Adenovirus Precursor Protein VI and Mature Protein VI: Cloning, Expression and Characterization. MICHELLE LOUIE (The George Washington University, Washington, DC 20037) WALTER F. MANGEL (Brookhaven National Laboratory, Upton, NY 11973). More than 50 different serotypes of adenovirus are known to infect humans, causing upper respiratory tract, gastrointestinal, and eye infections. The adenovirus proteinase (AVP) becomes activated inside nascent virions and subsequently cleaves virion precursor proteins thereby rendering a virus particle infectious. AVP requires two viral cofactors for maximal activity—adenovirus DNA and an 11-amino-acid peptide known as pVIc derived from the C-terminus of the precursor to protein VI (pVI). The interaction of AVP and DNA with pVI and VI has not been characterized. In order to characterize these interactions, the genes for pVI and its mature form VI must be cloned, expressed in bacterial hosts, and the resultant recombinant proteins purified. Cloning of pVI and VI from genomic DNA and insertion of restriction sites into the genes were accomplished by polymerase chain reaction (PCR) using gene-specific primers. Purified pVI and VI PCR products and the pET13a expression vector were then digested with Nde-1 and BamHI enzymes. Ligation of the pVI and VI DNA into the expression vector is completed before the plasmid is transformed into bacterial hosts and expression of the protein is attempted. pVI and VI DNA were successfully cloned. pVI was ligated into the pET28a-HS vector and transformed into the bacterial host. VI has been successfully inserted into the pET13a plasmid and transformed into a bacterial host. Expression of the pVI and VI proteins was observed in BL21-codon plus(DE3)-RIPL cells. Currently, optimal conditions for recombinant protein purification of protein pVI and VI are being investigated. Experiments using purified recombinant pVI and VI will determine how AVP liberates the pVIc cofactor from pVI. This study will determine if the C-terminus of pVI binds to AVP to produce an activated complex that subsequently removes pVIc from pVI or if AVP binds to DNA forming an active complex that then liberates pVIc

from pVI. In addition, proteins derived from this investigation will help to reveal the crystal structures of pVI and VI and determine the equilibrium dissociation constants and stoichiometries of binding of pVI and VI to DNA. Finally, the products of this investigation will also be used to elucidate the sites of interaction of pVI and VI with AVP and with DNA to ultimately determine potential drug targets for anti-viral agents.

Identification of PSI Complexes in Mammalian Cell Membranes.

KUSHBOO GOEL (*Earlham College, Richmond, IN 47374*) **HUGH O'NEILL** (*Oak Ridge National Laboratory, Oak Ridge, TN 37831*). Macular degeneration is a disease wherein the eyes lack photoreceptor activity in spite of having intact neural wiring to the brain. This disease is the leading cause of blindness worldwide. Past research showed that retinal tissue can be electrically stimulated by implanting pinhead-sized electrodes in the eye. Photosystem I (PSI), a naturally occurring photovoltaic protein, generates a 1 volt potential after capturing the energy of incoming photons. It has been proposed that PSI could play a role analogous to the micro-electrode approach. The reaction centers are inserted into retinal cells via liposomes and shown to elicit an action potential as measured by calcium flux. In this investigation a method was developed to directly identify the presence of PSI complexes in mammalian cell membranes. Green Fluorescent Protein (GFP) was chosen as a potential marker as it is commonly used as a fluorescent probe in mammalian systems. Recombinant GFP from *Aequorea victoria* was over-expressed in *E. coli* cells. It was purified from a crude cell lysate by a three phase extraction procedure using tert-butanol and ammonium sulfate. This protein preparation was then dialyzed and further fractionated by anion exchange chromatography on a HiTrap Q column. The purified GFP was characterized by spectrophotometry, fluorimetry and SDS-PAGE analysis. It was estimated that the protein was greater than 90% pure. A three step procedure was developed to crosslink PSI complexes and GFP. In the first step GFP was reacted with either citraconic anhydride or sulfo-NHS-acetate to block the primary amines on its surface, followed by dialysis to remove excess reactants. The modified GFP was then reacted with 1-Ethyl-3-[3-dimethylaminopropyl] carbodiimide hydrochloride, and N-hydroxysuccinimide to activate the surface carboxyl groups. In the final step, the activated GFP was added to the PSI preparation and primary amines of PSI reacted with the activated carboxyl groups of GFP. A covalent crosslink between the proteins was formed in this manner. The success of the cross-linking procedure was analyzed by fluorimetry. The yields were typically 30-50%. Most fluorescence was lost after modification of the primary amines. In future work the GFP tagged PSI complexes will be incorporated into liposomes and fused with mammalian cells. Confocal microscopy will be used to image GFP fluorescence thus indicating the location of PSI in the cell membranes.

Isolation of Independent Spontaneous Thymidine Kinase-Deficient Mutants and an Estimation of the Mutation Rate at the Thymidine Kinase Locus in a Human B-Lymphoblast Clone.

LAWRENCE CHYALL (*University of California—Berkeley, Berkeley, CA 94720*) **AMY KRONENBERG** (*Lawrence Berkeley National Laboratory, Berkeley, CA 94720*). Programmed cell death, or apoptosis, is tightly regulated by signals originating from both within the cell and its surroundings. The BCL-2 family of proteins helps modulate the balance between the life and death of cells. BCL-XL (a BCL-2-like protein) assists in limiting apoptosis by titrating the concentration of pro-apoptotic proteins through the formation of a heterodimer. TK6-Bcl-xL gly-159-ala #38 is a TK6 human B-lymphoblast cell line that was engineered to express BCL-XL gly-159-ala, a mutated form of the BCL-XL protein that does not have anti-apoptotic activity. A fluctuation experiment was used to estimate the mutation rate of TK6-Bcl-xL gly-159-ala #38 cells. The mutation rate was found to be closer to the historical results for TK6-neo #1 cells than cells expressing the wild-type BCL-XL protein, TK6-Bcl-xL #4. The plating efficiency of TK6-Bcl-xL gly-159-ala #38 cells was found to be the same as historical results for TK6-neo #1 cells and TK6-Bcl-xL #4 cells. Thirty-four early-arising and sixty-three late-arising spontaneous TK1-deficient mutants of the TK6-Bcl-xL gly-159-ala #38 cell line were isolated. DNA from each of these mutants was extracted for future analysis.

Membranes, Surfactants, and Membrane Proteins: Successful Partnering to Facilitate Structure and Function Studies.

AARON BOWLING (*University of Illinois, Champaign, IL 61820*) **PHIL LAIBLE** (*Argonne National Laboratory, Argonne, IL 60439*). Despite recent revolutionary advances in science and medicine, the structures and intricate molecular workings of membrane proteins remain one of the least understood aspects of any cell. These specialized cellular machines, which comprise an estimated 70% of all pharmaceutical targets, are so dependent on the membrane which accommodates

them that their extraction into aqueous buffers for study, typically causes degradation. Previous investigations have yielded several methods leading to extraction of these proteins into detergent micelles, yet there is no rational method to partner a given protein to a surfactant that will work successfully. Herein, a method of analysis is outlined that suggests to researchers the most appropriate surfactant for use with membrane proteins under experimental consideration. This method classifies detergents based on their 'strength' using several complexes of varied susceptibility found in photosynthetic bacteria. This protocol was coupled with an ink-based spectroscopy approach designed to accurately determine the critical micelle concentration of a surfactant, information vital to the strength analysis. These techniques were applied to several libraries of commercially available surfactants never before considered for use in structural biology. It is hoped that with this system of surfactant classification, the ability to obtain the structural knowledge of membrane proteins will be greatly enhanced; which in turn, will support the foundation for substantial advances in pharmaceuticals.

***Multimodality Nanoparticle for Targeted in Vivo Imaging with Xe NMR and Fluorescence.** **LESLEY LARA** (*Contra Costa College, Richmond, CA 94805*) **FANQING FRANK CHEN** (*Lawrence Berkeley National Laboratory, Berkeley, CA 94720*). One of the major challenges for antibody-based therapeutics is the lack of sensitive and convenient methods for in vivo imaging that track the distribution, metabolism, movement of the drug delivery system, and provide an effective means to monitor the treatment efficacy of the drugs. The lack of sensitivity also made early detection of cancerous tumors unrealistic. Currently, radiolabels are the most sensitive labeling technology; however, radioactivity labels are undesirable for large-scale use due to the harmful effects of ionizing radiation to both the technicians and the patients. Current generation MRI contrasting reagents work in a very high concentration range of several millimolars, and there is a high false positive rate. To solve this problem, we have constructed a novel class of imaging reagent that uses near-infrared CdSe nanocrystals. The nanocrystals are clustered with Gd-based MRI contrasting reagents for regular MRI imaging, or with a novel zero- to low-field MRI agent. This dual modality nanoparticle composite would be detectable with both deep tissue near infrared in vivo imaging and MRI/zero-field MRI. To target this to breast cancer, the nanoparticle also uses single-chain antibody against ErbB2, which is a protein in the EGFR family over expressed in 15% to >50% of breast cancers, depending on the stage of the disease. The nanoparticle is highly fluorescent with a high quantum yield and the clustering of the Gd chelating compound or zero-field MRI agent is demonstrated to be at least 500 per nanoparticle. This new class of nanoparticle based imaging solution can be applied to diagnostic and monitoring imaging of other cancers, or even other diseases.

***Nanoplasmonic Molecular Ruler for DNA-Protein Interaction.** **YUVRAAJ KAPOOR** (*Contra Costa College, San Pablo, CA 94609*) **FANQING FRANK CHEN** (*Lawrence Berkeley National Laboratory, Berkeley, CA 94720*). One of the major challenges of quantitative biochemistry and molecular biology is to monitor enzymatic activity within a femtoliter volume in real time. We have constructed a novel nanoscale plasmonic probe-based molecular ruler, which can perform label-free, real-time, and sensitive monitoring of DNA length during nuclease enzymatic reactions. The bionanoplasmonic molecular ruler was fabricated by tethering specifically-designed double-stranded DNA to single Au nanoparticles. Nuclease enzymatic activity was tracked via the evolution of the plasmon signal of a single Au-DNA nanoconjugate, which reflects DNA size changes introduced through site-specific DNA digestion by endonuclease. The scattering spectra of individual Au-DNA nanoconjugates are measured continuously in real time during nuclease incubation. The scattering spectra of Au-DNA nanoconjugates show a blue-shift of the plasmon resonance wavelength, as well as decrease in intensity and a time-resolved dependence on the reaction dynamics. With a series of enzymes that generate DNA incisions at different sites, the shifts of the plasmon resonance wavelength are observed to correlate closely with the positioning of the nuclease-targeted sites on the DNA, demonstrating DNA axial resolution in nanometer precision (5 nm of wavelength shift per nm of DNA length change, or 1.4 nm wavelength shift per base pair difference). DNA length differences of as little as 2 nm (6 base pairs) after nuclease digestion are differentiated by the corresponding plasmon resonance shifts of the Au-DNA nanoconjugate. Based on the mapping relationship between the DNA length and the plasmon resonance wavelength of the nanoconjugate, we further develop the nanoparticles into a new DNase footprinting platform. This DNase footprint mapping is demonstrated through the binding of DNA repair enzyme XPG to DNA bubbles. This

work promises a novel molecular ruler that can monitor nuclease enzymatic reactions with single-particle sensitivity in real-time. It suggests the possibility of developing ultra-high density nanoarrays for parallel enzyme activity measurement in functional proteomic studies or biofunctional nanoprobe for intracellular enzymatic studies.

Nramp1 Activity Reduces the Protein Abundance of SodCl: A [Cu, Zn] Superoxide Dismutase of Salmonella enterica Serovar Typhimurium. SHIRABRANDY GARZA (*Washington State University, Pullman, WA 99301*) LIANG SHI (*Pacific Northwest National Laboratory, Richland, WA 99352*). Macrophages play an important role in the pathogenesis of Salmonella-mediated systemic infection in mice. Critical to the ability of macrophages to kill the Salmonella is the activity of the divalent metal ion transporter natural resistance-associated macrophage protein 1 (Nramp1), a major regulator of host resistance. However, it is still unclear how Nramp1 activity eliminates the Salmonella in macrophages. Previously, we have found by global proteomic analysis that Nramp1 activity may reduce the amount of SodCl, a [Cu, Zn] superoxide dismutase of Salmonella that protects Salmonella cells from the superoxide anions produced by host macrophages to kill Salmonella cells. In this report, we used Western blot analysis to confirm that Nramp1 activity indeed lowered the abundance of SodCl. Reduction of SodCl by Nramp1 may contribute to the killing of Salmonella by macrophages. Confirmation that Nramp1 activity reduces the abundance of SodCl helps to better understand the roles of Nramp1 in Salmonella-macrophage interaction.

Optimization of Extracting Intact Proteins for Top-down Proteomics. ANGELA ZHANG (*University of Washington, Seattle, WA 98195*) ERIC LIVESAY (*Pacific Northwest National Laboratory, Richland, WA 99352*). In recent proteomics studies, the top-down approach for identification of proteins via mass spectrometry has shown several advantages over the commonly used bottom-up approach. The top-down approach requires no prior digestion of proteins, enables the measurement of the molecular weight of intact proteins, and preserves protein sequence and post-translational modifications. In order to successfully utilize top-down approach, an optimization of protocol for extracting intact proteins is necessary. *Saccharomyces cerevisiae* (yeast) is a proteome typically used for examination of proteomic analysis developments. The cells need to be broken up before extraction of proteins. Several ways of breaking these cells and protein extractions are investigated in this study. *Saccharomyces cerevisiae* cells stored in glycerol were grown in Yeast Extract Peptone Glucose (YPD) broth to OD6000.47 and OD6000.53 and harvested during log phase of growth. Different alcohol buffers including 25% 1-propanol, 25% 2-propanol, 25% 2-butanol, and 5% 1-butanol 20% 1-propanol were coupled with bead beating to break the cells. Other cells were lysed with Y-PER Plus, Dialyzable Yeast Protein Extraction Reagent, Y-PER and bead beat, and Y-PER twice. Samples were then prepared with Laemmli Sample Buffer. All samples prepared were examined using 1D gel electrophoresis. This project is a portion of the research that is currently being conducted to improve procedures and results for top-down proteomics.

Overexpression of Human SOST in Transgenic Mice Results in Defective Patterning of Limb Cartilage Elements. LEILA BEACH (*Stanford University, Stanford, CA 94305*) GABRIELA G. LOOTS (*Lawrence Livermore National Laboratory, Livermore, CA 94550*). Sclerosteosis is a generalized progressive bone overgrowth disorder due to the loss of function of the SOST gene product sclerostin. Null mutations in SOST result in occasional polydactyly and syndactyly along with a substantial progressive increase in bone density. Accumulation of abnormal bone mass begins in late childhood and affected patients display increased bone formation, while bone resorption is undisturbed. SOST is expressed in osteocytes, the mature metabolic cells in ossified bone. To investigate the physiological function of the SOST protein, we have generated several lines of transgenic mice carrying a ~160kb human SOST bacterial artificial chromosome or BAC. Transgenic mice overexpressing SOST (hSOSTwt) exhibit a decrease in bone mineral density in the appendicular and axial skeleton when compared to non-transgenics from four to six months of age as evaluated by Dual Energy X-ray Absorptiometry (DEXA) and quantitative computed tomography pQCT. When bred to homozygosity (hSOSTwt/wt) these animals also show congenital limb defects. Hereditary hand malformations occur frequently in human populations, therefore these animals can serve as a model for understanding molecular perturbations that lead to improper limb patterning. The fore- and hind-limbs of these animals are severely deformed displaying a wide range of fused and missing digits as visualized by autoradiography and pQCT. Since limb development is initiated prior to ossification of the skeleton, we find SOST to be expressed in the developing embryo as early as

embryonic day 9 (E9), predominantly in the mesenchyme tissue of the developing limb bud. We have performed a detailed phenotypic analysis of these transgenic embryos using skeletal preparations and histology which revealed a defect in cartilage formation. To investigate whether the limb defect stems from defective chondrocyte differentiation, proliferation, or apoptosis we set out to examine limb sections by in situ hybridization. We identified cDNA clones to generate antisense RNA probes for Fgfr1 (expressed in distal proliferating chondrocytes), Bmp7 (columnar proliferating), Fst and Tgf β 2 (early hypertrophic), Bmp2, and Tgf β 3 (hypertrophic cells), and Spp1 (terminal hypertrophic). These markers represent distinct stages in the chondrocyte differentiation program, and misexpression of these markers revealed by in situ hybridization will indicate cell types that may show excessive proliferation or apoptosis.

Phenotypes Vary Among Recombinant Inbred Strains of BXD (C57BL/6JxDBA/2J) Mice. TERRI KAMINSKY (*Christopher Newport University, Newport News, VA 23606*) DR. DABNEY K. JOHNSON (*Oak Ridge National Laboratory, Oak Ridge, TN 37831*). Mammals normally respond to cold exposure by increasing thermogenesis, but this adaptive response can be altered by genetic factors affecting metabolic capacity and the hypothalamic-pituitary-thyroid axis. We used the response to cold stress as a means to screen a panel of recombinant inbred C57BL6 X DBA (BXD) mice for genetic variation in metabolism. Core body temperature, tail length, body and organ weights were also measured to determine if metabolic and morphometric traits were genetically correlated, or if they appeared to be controlled by separate loci. To study thermoregulation, male, age-matched mice (n=2-6 per strain) representing eighteen BXD strains were placed in transparent, individual plastic containers in a 4°C environment after an initial measure of baseline body temperature. Core body temperatures were measured at thirty-minute intervals for two hours. Following the cold stress test, mice were euthanized and the body weights were recorded. Tail length was measured and various organs and fat pads were dissected and weighed. Baseline core body temperature was similar across all BXD strains analyzed (average = 38.0° ± 0.3°). On average, body temperature dropped 1.5° after the cold exposure. However significant genetic variability in the response was apparent. For example, two strains (BXD 068 and BXD 039) deviated considerably from the average response. Strain BXD 068 had an average baseline temperature of 37.5° (±0.2°) and dropped to 35.4° (± 0.9°), a change of - 2.1°. Strain BXD 039 had a similar baseline temperature (37.7° ± 0.4°), but experienced little change after two hours of cold exposure (average change of - 0.3°). These results indicate a considerable amount of genetic variation in the ability to thermoregulate, likely reflective of core variation in metabolism and/or endocrine regulation. Organ weights also varied across strains, with spleen exhibiting the most variation, but the strain-specific patterns did not parallel those observed in body temperature. Our findings confirm that core physiological processes are impacted by naturally occurring genetic polymorphisms found in BXD strains of mice. Future efforts will determine the genetic relationships among metabolic and morphometric parameters and the genetic intervals linked to thermoregulation and other complex biochemical processes.

Polymeric Micelles as Fluorescent Probes for Stem Cell Imaging. MICHELLE ROSA, MELIXA RIVERA (*University of Puerto Rico at Mayaguez, Mayaguez, PR 00680*) LIAOHAI (LEO) CHEN (*Argonne National Laboratory, Argonne, IL 60439*). The goal of this research is to explore the feasibility of using polymeric micelles as the template to fabricate target specific imaging agent for molecular cellular imaging. Nano-particles based on polymeric micelles have drawn much attention recently and they have been successfully used as drug delivery vehicles in pharmaceuticals. Yet, little study exists for using polymeric micelles as imaging probes. Polymeric micelles are generally formed by the self-assembly of amphiphilic copolymers above their critical micelle concentration in aqueous medium. Upon micellization, the hydrophobic core regions can function as the reservoirs for the fluorescent molecules. The size of a typical polymer micelle is in the range of 30-50 nm, thus, a fluorescent molecule loaded polymeric micelle should form a core-shell fluorescent nanoparticle with diameter ~50 nm. So far, research demonstrates that the polymeric micelles can efficiently load the fluorescence dye to form core-shell fluorescent nanoparticles. The formed particles are very stable in different pH (ranging from pH2 to pH10). Temperature dependency studies indicated that the polymeric micelles have a phase transition temperature at ~ 70 C. In order to see the interaction between these polymeric micelles and cells, a study was carried out using stem cells. It was demonstrated that stem cells do not uptake polymeric micelles. It was also found that the dye is toxic for these cells, therefore polymeric micelles can reduce cell toxicity against

organic compounds. Currently, we are conjugating a stem cell specific antibody to the fluorescent polymeric micelles and the experiments of imaging stem cell in situ will be followed.

Protein Purification on Tuberculosis Protein. ASHLEY JONES (*Fisk University, Nashville, TN 37208*) DR. CHANG YUB KIM (*Los Alamos National Laboratory, Los Alamos, NM 87545*). Tuberculosis (TB), caused by *Mycobacterium tuberculosis* (*M. tb*), is an infectious disease known to affect the lungs in most cases. In 2004, there were about 14.6 million people with latent TB including nine million new cases. Over 2 million people die every year from this disease. Although different drugs have been developed to fight this disease, these drugs are no match for the spontaneous mutations of this deadly disease with new *M. tb* strains resisting multi-drugs. Thus scientists continue to look for new methods to combat this disease. After the completion of sequencing TB genome, TB Structural Genomics Consortium was established to determine the structure for over 400 proteins. Since 2000, the Los Alamos National Laboratory (LANL) has partaken in this Structural Genomics project by cloning and purifying target proteins. The purified proteins are to be used in determining the three dimensional structure of the protein and ultimately its function. Eventually, this will allow scientists to produce a pharmaceutical drug that will inhibit the protein, which will then stop TB. In this paper, we will discuss the developed protocol of protein purification and the role that I played in the purification process this summer.

Protein SDS-PAGE Characterization and Comparison of Soybean Cyst Nematodes. ALEXANDER PATANANAN (*University of California-Los Angeles, Westwood, CA 90095*) DR. STEVEN C. GOHEEN (*Pacific Northwest National Laboratory, Richland, WA 99352*). Soybean cyst nematodes (SCN, *Heterodera glycines* Ichinohe) represent one of the most serious threats to the stability of soybean crops in the United States. Initially discovered in North Carolina in the 1950s, it has spread rapidly through the Midwest generating an estimated \$1 billion in failed crops each year. In order to counteract this infection, numerous methods of pest management have been established, such as crop rotation and the development of SCN resistant soy plants. However, at least sixteen distinct populations of SCN have been differentiated based upon their relative rates of reproductive success on different strains of soybean, making it difficult to use only one sole technique. Although it is well accepted that these deviations in reproductive rates are not associated with any morphological differences in the various SCN populations, knowledge of biochemical differences is lacking. Therefore, the protein profiles of five different SCN populations were characterized using sodium dodecyl sulfate-polyacrylamide gel electrophoresis (SDS-PAGE) in order to identify similarities and differences in their most prominent proteins. SCN eggs obtained from the Tennessee Soybean Promotion Board were homogenized in SDS, diluted in sample buffer, and examined by SDS-PAGE. Out of 25 major proteins ranging in molecular weight from 40 to 200 kDa, no major biochemical differences were observed between any of the races. These results implicate that SCN populations are consistent with being biochemically similar, and that any real differences in protein composition or relative expression are small compared to the resolution of SDS-PAGE.

***Quantifying the Effect of Temperature on Chlorophyll Fluorescence.** JESSICA STONE (*California State University-Fresno, Fresno, CA 93630*) WILLIAM STRINGFELLOW (*Lawrence Berkeley National Laboratory, Berkeley, CA 94720*). A daily change in chlorophyll concentration was observed in the field (San Joaquin River) algae samples. A lab study of algae growth at various temperatures was needed to determine if the change in chlorophyll concentration was indeed due to temperature changes of the environment, or if this was not a true change in concentration, but just a temperature effect, instrument default, or some other factor on the algae. A Hydralab sonde was used measure the temperature (°C), and chlorophyll fluorescence (volts) every minute for 2 hours and 15 minutes. The algae culture, grown for 4-17 days in single source carbon (SSC) media was diluted to ~1 volt was cooled with an ice water bath, then heated with a hot water bath followed by another cool ice water cycle. The results showed an inverse relationship of chlorophyll fluorescence versus temperature. Cooler temperatures resulted higher the chlorophyll concentration. Thus, temperature is having an effect on chlorophyll fluorescence. Further experiments need to address any possible differences between using a young culture or an old culture. Also, the sonde (Hydrolab unit #41) that was used needs to be compared with data acquired from the Shmadzu spectrofluorophotometer and chlorophyll extraction methods.

Regiospecificity Changes in Ivy Mutants. KIRA SCHULTHEISS (*Stony Brook University, Stony Brook, NY 11794*) ED WHITTLE (*Brookhaven National Laboratory, Upton, NY 11973*). A delta(4)-16:0-

ACP desaturase enzyme from *Hedera helix* (English Ivy) introduces a double bond between the fourth and fifth carbons of its fatty acid substrate (16:0-ACP). A closely related desaturase from *Castor* directs its bond to the $\Delta 9$ position. Amino acid alignment of the two desaturases at the critical ACP binding domain indicates potential changes that contribute to the different regiospecificities. By creating mutations in the genetic code to make Ivy more similar to *Castor*, a single amino acid change was introduced into the ivy desaturase converting lysine (K) to an aspartic acid (D) at amino acid position 308. The mutant enzyme, Ivy K308D, was cloned into a pet24a expression vector and transformed into BL21 cells. These cells were induced to produce protein. The desaturase was purified, assayed, and the products of the assay were analyzed with the use of a GC-Mass Spectrometer. Products made with the Ivy K308D mutant were compared with those from the wild-type Ivy enzyme and any changes in activity from the usual $\Delta 4$ to the expected $\Delta 9$ position were noted. When analyzed, approximately 4% of products had a double bond in the $\Delta 9$ position. By comparison, the wild type Ivy produced no $\Delta 9$ product. This mutation indicates some involvement and change in regiospecificity, though the fact that only 4% of the product fatty acid was desaturated in the 9-position suggests that other amino acids are also involved in this process. Additional research is being performed to introduce mutations at other positions that potentially contribute to regiospecificity.

Sequenced Based Identification of Yeast. MARTHA JOHNSON (*Jackson State University, Jackson, MS 39217*) DR. TAMAS TOROK (*Lawrence Berkeley National Laboratory, Berkeley, CA 94720*). The study of microorganisms is important due to the rapid advances in microbiology and its substantial contribution to the commercial, scientific, and medical aspects of life. Fungi offer molecular biologists well-developed genetic systems to use as eukaryotic model organisms and have contributed to our understanding of human genetics. Fungi also have significant potential for bioremediation. The use of fungi to recycle nutrients through biodegradation is useful and will help with green chemistry and polluted soils. Yeasts are single cellular fungi that have either aerobic or anaerobic metabolic capabilities. Some of the most common uses of yeasts are in bread making, and in beer and wine fermentation. Researchers at Lawrence Berkeley National Laboratory (LBNL) are investigating the possibility of using specific biomarker DNA sequences to detect and identify yeasts. This technique applied in a high-throughput DNA microarray format will provide researchers with a novel cutting edge for rapid identification of yeast species. The current project focuses on the analysis of the D1/D2 domain sequences of the 26S ribosomal RNA genes of a large number of yeast species that were isolated from various environments. The yeasts were grown on potato dextrose agar (PDA). Following genomic DNA extraction, the D1/D2 domains of the 26S rRNA genes were amplified using the polymerase chain reaction (PCR). After amplicon cleanup and sequencing, the edited sequences were compared to sequences of known yeasts available in a public database hosted by the National Center of Biotechnology Information (NCBI). Ten of the 34 yeasts examined showed DNA sequence homology of less than 98% when compared to DNA sequences of known yeast species. Additional experiments will be performed to examine deletions, insertions, and differences in nucleotide sequence for any evolving alterations. These alterations could lead to greater knowledge of how yeast adjusts to the given habitat.

Spawning Interval Behavior of Fishes in Association with Parental Care and Migration Patterns. EMMANUEL ISANG (*East Tennessee State University, Johnson City, TN 37614*) HENRIETTE JAGER (*Oak Ridge National Laboratory, Oak Ridge, TN 37831*). Spawning interval is the time, measured in years, that it takes for species to undergo reproduction of offspring. Some species spawn several times a year while others spawn every couple of years. The species that spawn several times a year, known as batch spawners, released eggs in a series of batches over a period of time that can last from days to months. Other species, that don't spawn annually, are known as capital breeders. These species use stored energy to make large, fecundity-investment at each breeding opportunity. Factors that can affect the spawning interval values are whether these species go through long spawning migrations and/or whether there is any parental care provided to the offspring. In order to support ongoing research to determine the spawning interval of a variety of species, this project searches for three primary variables of interest: migration, spawning intervals, and parental care. The search primarily uses programs such as ISE Web of Knowledge, Google, and ORNL Library Catalog. After information was found about any of the three variables of interest, it was entered into an excel file. After creating as extensive a database as possible, the data will be analyzed to draw any conclusions about the

relationship between parental care and spawning migrations and the extent it affects spawning intervals of the fish species. Looking at the analyses, the overall values for the spawning intervals of the species as a whole seemed to favor the species that either had spawning migrations, parental care, or both. Overall the species that had any of the two characteristics had a higher amount of time between spawning opportunities than the species that didn't go through a spawning migration or provide parental care. However, further studies and research will be needed to increase knowledge of fish life history, and to fill in the gaps for the species that lack complete information and other species that have not been studied. This work is a very small portion of studies conducted on the relationship of spawning interval and how it is affected by spawning migrations or parental care.

Sporulation of *Clostridium thermocellum* in Media for Thermophilic Clostridia with Various Amounts of Nitrogen and Buffering Agent.

SARAH WHITAKER (Middle Tennessee State University, Murfreesboro, TN 37132) JONATHAN MIELENZ (Oak Ridge National Laboratory, Oak Ridge, TN 37831). *Clostridium thermocellum* are anaerobic, thermophilic, spore forming bacteria that hydrolyzes cellulose to cellobiose and cellobioses through the utilization of a membrane bound cellulase system called a cellulosome that attaches to cellulose fibers. Once cellobiose and cellobioses are formed, these products are internalized and utilized by the bacterium to produce energy in the form of ATP. By-products of this metabolism include hydrogen, carbon dioxide, lactic acid, acetic acid, and ethanol. The production of ethanol, which is rapidly becoming a widely accepted alternative to fossil fuel energy, and the world-wide abundance of cellulosic material, is what make *C. thermocellum* such an attractive organism to study. Culturing of *C. thermocellum* was done at various pH levels and nitrogen concentrations of media for thermophilic clostridia, MTC, to assess the ability of the modified medium to support sporulation of the bacterium. Understanding the conditions under which sporulation occurs, as well as the mechanisms of the process, will add to the full characterization of this organism. A complete characterization will help to answer questions and solve problems that may arise if ethanol production using this organism is to grow to industrial levels. A method commonly used to assess bacterial growth rate is optical density. Light absorbance at 600nm was measured through the use of a spectrophotometer during the growth of each culture and plotted vs. time to determine the exponential growth phase. Phase-contrast light microscopy was employed to visualize the *C. thermocellum* in order to assess the presence of spores. *C. thermocellum* spores are said to shimmer under phase-contrast. Culturing experiments and microscopy reveal an apparent lack of sporulation in all media recipes tested. Knowing that *C. thermocellum* will not sporulate, which could interrupt the production of ethanol in MTC media, can help define and enhance the process of making ethanol.

Structural Study of the DNA Repair Protein XPG Using Constructed Proteins with Individual Domains. JONATHAN ROYBAL (University of California–Berkeley, Berkeley, CA 94720) SUSAN TSUTAKAWA (Lawrence Berkeley National Laboratory, Berkeley, CA 94720).

Cockayne syndrome and xeroderma pigmentosum are two distinct genetic disorders, characterized by sun sensitivity and severe developmental disorders in the former, and by extreme sun sensitivity and skin carcinogenesis in the latter. Paradoxically, both are caused by different defects in many of the same DNA repair proteins. One such protein, XPG, is thought to be particularly important among these proteins. Structural analysis of XPG would greatly elucidate the mechanistic basis for the distinct functions of XPG. However, XPG has proven difficult to crystallize. Two proteins, XFX delta exon 15 and GST-M4, were created from parts of XPG and other proteins to perform structural studies of the two main catalytic regions of XPG, the "N" and "I" domains, and part of its regulatory region (the R domain). Purification was attempted for each protein via its own protocol using affinity and ion exchange chromatography. GST-M4 was purified to ~80% homogeneity, then split to give separated GST and M4 using Precision Protease. Conditions to produce homogeneous M4 alone are still being determined. We obtained 5 mg of purified XFX delta exon 15 which was shown to be monodisperse as dimers by dynamic light scattering, found to be active with DNA, and was analyzed via small angle X-ray scattering. Screens for crystallization conditions were then run on purified XFX delta exon 15 samples, yielding crystal showers; optimization of conditions to produce larger crystals will be done in the near future.

Structure Solved for the ywmB Protein from *Bacillus Subtilis*. KRISTIN MUSSAR (Knox College, Galesburg, IL 61401) ANDRZEJ JOACHIMIAK (Argonne National Laboratory, Argonne, IL 60439).

During my internship at Argonne National Laboratory I worked on

protein purification in Andrzej Joachimiak's biochemistry lab. The purification process is the second part of a larger three step procedure in which the goal is to determine the structure and function of specific proteins. Once clones producing significant amounts of the target protein have been selected they are passed on to the next lab. Here, the clones are incubated and grown in salt media for two days, and then harvested by centrifugation. Protease inhibitor is added and the protein must be kept on ice throughout the remaining steps of the process in order to prevent denaturing. The cells are then broken open by the addition of lysozyme and sonication (brief electric pulses). The protein is separated by centrifugation and filtered before loading onto the AKTA purification robot. This machine uses a nickel column and his-tag system to divide the protein of interest from the excess protein and collects the target protein for continuation. TEV is added to the protein to remove the his-tag and cleavage is confirmed by gel electrophoresis. In order to remove the cut his-tags and imidazole, the protein is filtered again through nickel agarose solution and brought to a higher concentration. The protein is then ready for crystallization. In this step the protein is placed in various chemical conditions and incubated for the promotion of crystal growth. Once a crystal has formed it is moved into the third step of the process during which it is x-rayed and the diffraction patterns are analyzed to determine the structure of the protein. The structure of the protein is directly related to the function of the protein. This can be added to a database and the combined information can be used in medical applications.

Synthesis of Polypyrrole Nanowires by Interfacial Polymerization.

XIAOHAI ZHANG (University of Washington, Seattle, WA 98195) JUN WANG (Pacific Northwest National Laboratory, Richland, WA 99352).

Polypyrrole (Ppy) is a type of conductive organic polymer composed from a number of interconnecting pyrrole monomer rings. Its conductive properties are highly valued in several areas of research, most notably as materials for sensitive biosensor applications. Therefore, in order to further this area of research, a facile and reliable method of producing such nanoscale Ppy polymers is highly sought for. The interfacial synthesis polymerization is a method of producing Ppy; it is a continuation of previous work for other conductive polymers. In this research, the use of interfacial polymerization as the synthesizing method for Ppy will be tested and analyzed. In this method, the Pyrrole monomers are dispersed into an organic solvent and an oxidant will be dissolved into an inorganic solvent. The two solvents are then placed together into a single container so that the pyrrole monomer will be oxidized at the surface of the aqueous/organic solution. Utilizing this approach, various concentrations of the monomer and oxidant were tested to determine the optimal condition for creating nanoscale Ppy wires. The synthesized polymer structures will then be analyzed by means of Scanning Electron Microscopy (SEM) for detection of its structure and size. Average Ppy diameter lengths between 100 nm to 500 nm were produced through these tests, indicating that the sizes of these nanostructures are subject to change depending on the concentration of the oxidant and monomer tested. The results of this experiment do not provide a clear characterization of specific qualities in the interfacial process because granular polymers were produced instead of intrinsically true nanoscale wires. However, data does show that various scales of nanoscale polymers could be created by treating the process with different concentrations of oxidant and monomer. Further research and experiments are still required in order to utilize this method for creating industrially exploitable Ppy nanowires.

Synthetic Biology: Widespread Use Is Closer Than You Think.

KEHINDE O'DUNIKAN (University of the Pacific, Stockton, CA 95211) DR. PETER LICHTY (Lawrence Berkeley National Laboratory, Berkeley, CA 94720). Synthetic biology is the synthetic redesign of biological systems. Synthetic biologists' goal is to make from scratch, programmable organisms that do not currently exist in nature. Possible applications include: development of bioengineered microorganisms that can produce medicine, identify harmful chemicals, disintegrate environmental pollutants, demolish cancerous cells and remedy flawed genes; hydrogen fuel; and development of bioengineered organisms to diagnose and treat certain illnesses. Synthetic biology consists of specifying the DNA that is entered into an organism and from there determining its function in a foreseeable way. With talks about this new science in the media the public has developed some concerns about it. People worry about dual use and terrorism, who will regulate research, the ethics of synthetic biology, it becoming privatized and monopolized and if something will go wrong in the current experiments. Also, some religions see synthetic biologist as trying to play God. Synthetic Biology is so controversial that national conferences were held. The second of its kind, The Synthetic Biology 2.0 (SB2) conference was held in Berkeley, California back in May. There, scientists meet to talk about the

latest advances and applications of the science and about the security concerns as well. After the three-day conference they developed a community declaration, which will serve as a form of scientific self-governance, outlining the way researchers and companies should act to warrant openness and security of synthetic biology research. A lot of the everyday products that we take for granted would not be here without the developments in the field of biotechnology and some day we could say the exact same thing about synthetic biology. Biotechnology is used to produce everyday food products such as yogurt, cheese, beer; produce vaccines; to produce laundry detergents and dishwashing liquids; to do DNA Fingerprinting techniques for forensic investigations and paternity tests; to genetically engineer crops and agriculture; and to create human therapeutics and proteins. The possible applications can potentially save millions of lives in the near future and tremendously improve the environment. With the current research of many universities, pharmaceutical companies and even laboratories in our own communities like the Lawrence Berkeley National Laboratory, widespread use of synthetic biology is closer than you think.

The Effects of Pressure Changes and Elevated Dissolved Gas Levels on Chinook Salmon (*Oncorhynchus Tshawytscha*) and Rainbow Trout (*Oncorhynchus Mykiss*). BROOKE SAKARA (*Gustavus Adolphus College, Saint Peter, MN 56082*) ABIGAIL CAPETILLO (*Pacific Northwest National Laboratory, Richland, WA 99352*). As juvenile salmon pass from their spawning ground to the ocean, they must cross through hydroelectric dams. The pressure changes and elevated dissolved gas levels that occur during turbine passage can cause injury and mortality to the fish especially when combined with high dissolved gas levels within the river. Using two hyperbaric chambers, the effects of pressure changes and water supersaturation were tested on run of the river and hatchery-reared Chinook salmon (*Oncorhynchus tshawytscha*) and hatchery-reared rainbow trout (*Oncorhynchus mykiss*) at McNary Dam. The chambers were used to subject the fish to rapid pressure changes which represented passage through turbines. Fish were acclimated at the pressure present at depths of 0, 5, 10, 20, and 40 feet and at dissolved gas levels of 100, 110 and 120% saturation. The fish were allowed to recover at varying pressures for two days, and were then euthanized and necropsied. It was found that as the pressure during acclimation increased, mortality also increased in all test groups. As the total change in pressure increased, appearance of emboli in the gills, hemorrhaging inside the pericardial sac and caudal veins, ruptured swim bladder and stomach eversion also increased. There was less overall mortality in the rainbow trout than in either group of Chinook salmon. There was more emphysema of the fins at higher dissolved oxygen levels when fish were allowed to recover in supersaturated water. These experiments will be expanded to also include the rate of pressure change during turbine passage. This work is part of a multi-year study funded by the U.S. Army Corps of Engineers designed to find a method of turbine passage that will result in lower juvenile salmonid mortality rates.

The Expression and Purification of Hypothetical Yeast Protein. JACQUELINE GIBBS (*Elizabeth City State University, Elizabeth City, NC 27909*) DR. S. SWAMINATHAN (*Brookhaven National Laboratory, Upton, NY 11973*). Solving protein crystal structures by X-ray diffraction or NMR is essential for doing protein chemistry and novel drug design. This project involves several aspects of macromolecular crystallography; for example expression and purification of proteins, optimization of crystallization conditions by use of robot, crystallization by sitting drop vapor diffusion method, observation and analysis of the crystals under the microscope and lastly x-ray diffraction of the crystals. During our ten weeks stay at Brookhaven National Laboratory, we were successful in expressing and purifying a 29 kDa hypothetical Yeast protein by His-tag purification using nickel chelated columns and by the size exclusion method of protein purification by using a FPLC machine. We ran 1D SDS-protein gels for analyzing and confirming our results.

Thermoregulation Abilities of the 8-Way-Cross Parental Lines: A Comparative Phenotype Project. SUSAN KENNEY (*Christopher Newport University, Newport News, VA 23606*) DABNEY K. JOHNSON (*Oak Ridge National Laboratory, Oak Ridge, TN 37831*). In the Life Sciences Division at Oak Ridge National Laboratory a new genetic reference population, more complicated and with more possibilities than a standard (two-line) recombinant inbred (RI) population, is being developed. Eight strains of inbred laboratory mice, chosen for their genetic and phenotypic diversity, were selected to be the progenitors for the 8-Way-Cross: Mus castaneus (CAST/EiJ), New Zealand Obese (NZO/HILtJ), Non-Obese Diabetic (NOD/LtJ), 129S1/SvImJ, C57BL6/J, PWK/PhJ, WSB/EiJ, and A/J. Although each strain has been studied individually and extensively, no studies have been done on all eight

strains under the same conditions. The purpose of this research is to compare these parental strains across a panel of morphometric and metabolic phenotypes and to measure the thermoregulation abilities of these mice. This is accomplished using a cold stress test, which assesses a mouse's ability to maintain its core body temperature when put into a 4°C environment. Core body temperatures were taken at the beginning of the experiment to determine a baseline temperature and then every 30 minutes for a total of 120 minutes during the test. After the test, mice were weighed and dissected and other phenotypes were measured such as spleen, liver, kidney, thymus, and heart weight. Results indicate that the NOD/LtJ males (n = 5) have different cold stress responses from the females of the same strain (NOD/LtJ males change = +0.6°C; females = -0.6°C). NOD/LtJ and PWK/PhJ females (n = 5; 6) were unable to respond to the cold, shown by a decrease in core temperature over the two hours. A/J females (n = 4) responded to the cold by quickly increasing their core temperature; however, they were unable to maintain the increase and their core temperature eventually fell lower than the baseline (change = -0.2°C). Wild-derived CAST/EiJ females maintain their core temperature during the test (change = +0.02°C). These results suggest that the leaner strains of mice, such as CAST/EiJ, can regulate their metabolism whereas NOD/LtJ females can not. These data will be contributed to MuTrack, a large scale mouse phenotype database (<http://www.tnmouse.org/mutrack>). Once the 8-way-cross RI strains have been established, each strain's response can be compared to the parental lines so that the genes affecting thermoregulation and other phenotypes can be identified.

Use of Indocyanine Green in Photodynamic Therapy of Melanoma. DYLAN RODEN (*Massachusetts Institute of Technology, Cambridge, MA 02139*) LISA MILLER (*Brookhaven National Laboratory, Upton, NY 11973*). Skin cancer accounts for over 50% of all human cancers and melanoma is the most deadly form. It is estimated that in the United States in 2006, over 62,000 people will be diagnosed with melanoma, resulting approximately 8,000 deaths. Photodynamic Therapy (PDT) is a new treatment method for many types of cancer and is a very practical therapy for treating melanoma. PDT involves a special dye, called a photosensitizer, which is absorbed by cancer cells. The dye is activated by a specific wavelength of laser light and releases oxygen radicals which kill the surrounding cells. In this study, indocyanine green (ICG), a chemical with many favorable properties for use as a PDT photosensitizer, was taken up by human melanoma cells in culture (at a concentration of 150 µM) and then these cells were irradiated with laser light (800 nm) for different exposure times (15, 30, 45, and 60 minutes). After exposure, the cells were stained with trypan blue and counted with a hemocytometer to determine the percentage of cell death. The cells were also examined using Fourier Transform Infrared Spectroscopy (FTIR) to examine chemical changes that occur as cells undergo apoptosis. Hierarchical cluster analysis was performed on the FTIR data to determine differences in treatment times. The 60 minute exposure time was most successful and corresponded with a 75% death rate in the cells. Cluster analysis showed that generally the longer exposure times clustered differently from the samples not receiving any laser in both the lipid (2600-3120 cm⁻¹), and protein and nucleic acid (800-1900 cm⁻¹) regions. This indicated a significant difference in chemical composition between the two groups suggesting death by apoptosis. In the future, we hope to determine a more efficient concentration of ICG to give to the melanoma cells and expose them to a more powerful pulsed laser for a longer period of time.

Using Microarray Technology to Compare Bacterial Diversity Within Different Horizons of Contrasting Soils. DHARSHINI VENKATESWARAN (*California State Polytechnic University-Pomona, Pomona, CA 91768*) GARY ANDERSEN (*Lawrence Berkeley National Laboratory, Berkeley, CA 94720*). There is emerging interest in understanding the linkages between above- and below ground microbial communities. As part of a large DOE funded climate change project, the Andersen lab is studying the microbiological responses of Californian grassland ecosystems. Various mesocosm conditions were set up to replicate the effects of climate change (modified temperatures and precipitation) on plant and microbial communities. Since climate change influences the function of these ecosystems, we compared bacterial diversity within different horizons of contrasting soils. Two soils compared were from Hopland, in Northern California, and Sedgwick, from Southern California. Since the pattern of growth in plant roots is directly dependent on water supply, climate change such as increased or decreased rainfall may indirectly affect the microbial communities found in different horizons depending on the growth of the roots in response to water. Generally there are different approaches to profile soil microbial diversity. One way is to use Phospholipid fatty acid analysis (PLFA), which analyzes membrane lipids; however, this

approach is not sensitive and will not effectively resolve microbial speciation. Another conventional method is cloning of the 16S rRNA gene, which requires transferring the amplified DNA fragments into a plasmid, and randomly sequencing a few hundred plasmids. In soil samples where one will expect to find at least 100,000 species then one would need to sequence 100,000 clones using this method, which is time consuming, expensive, and inefficient. Instead, a high-density photolithography microarray displaying 500,000 oligonucleotide probes complementary to diverse 16S rRNA sequences was used. This new technology, allowed us to identify species or groups of bacteria present in the soil sample more efficiently. The study showed the horizon B1 to have more microbial communities than horizon A. The observed microbial biomass also seems to increase at deeper horizons. Clostridia for example was found to be in higher microbial amounts in the 40-65 cm depth of the Hopland-B2 soil, where as Cellulomonas (Actinobacteria) and Phyllobacteriaceae (Alpha-proteobacteria) were predominately present at the top horizon (Hopland-A).

Chemistry

A Molten Salt Synthesis of Single Crystalline YBCO Nanorods.

DARYL WONG (University of California–Berkeley, Berkeley, CA 94720) **STANISLAUS S. WONG** (Brookhaven National Laboratory, Upton, NY 11973). $\text{YBa}_2\text{Cu}_3\text{O}_7$ (YBCO) is a high T_c superconductor that has potential applications in both high field magnets and superconductive circuitry. Although its utility as a high field magnet has been realized, bulk YBCO loses its high temperature superconducting ability due to low critical current densities deriving from the bulk's polycrystalline nature which lacks directionality. One potential remedy, aligning monocrystalline subunits through material texturing techniques, can be achieved with the production of uniform, monocrystalline one-dimensional YBCO nanorod structures. The molten salt synthesis method has been shown to be a procedurally simple technique to create metal oxide nanorods. Using a molten salt method, attempts to make YBCO have been conducted with a number of yttrium, barium, and copper containing precursors which are combined with a salt, usually sodium chloride and/or potassium chloride, in varying precursor and salt ratios. These precursors were finely ground with a mortar and pestle and baked in a furnace to temperatures above the melting point of the salt. Powder x-ray diffraction (XRD) analysis was conducted to determine whether the molten salt samples contained the orthorhombic crystal structure indicative of high temperature superconducting YBCO, while scanning electron microscopy (SEM) and atomic force microscopy (AFM) images were taken to determine if a rod morphology had been formed. XRD analysis of the numerous molten salt products has shown that the desired orthorhombic YBCO nanorods cannot readily be formed, while SEM and AFM images show aggregates of nanorods and nanoparticles which vary in size. Other analytical techniques, including SQUID (Superconducting Quantum Interference Device) measurements, will be useful to further ascertain and characterize the properties of as-prepared YBCO nanorods. Because the mechanism of molten salt nanorod formation is not fully understood, creation of these desired nanorods involves a lot of experimentation with variable parameters. A more comprehensive analysis of precursors, precursor ratios, and baking temperatures should be performed before concluding the inefficacy of the use of the molten salt technique in the generation of nanoscale motifs of these superconducting materials.

A Search for Cerium Doped Lanthanum Oxide Scintillators.

LATORIA WIGGINS (North Carolina A&T State University, Greensboro, NC 27411) **DR. YETTA PORTER-CHAPMAN** (Lawrence Berkeley National Laboratory, Berkeley, CA 94720). The need for new and improved radiation detectors, scintillators, is at an all time high due a progression in detection knowledge. Commonly used scintillators such as BGO and LSO have undesirable properties such as low luminosity, and slow decay times. Discovering new scintillators required literature searches, synthesizing and the characterization of compounds. The research at hand concentrated on cerium (III) doped lanthanum oxides. Compounds were synthesized using solid-state chemistry techniques such as ceramic and hydrothermal methods. Characterization consisted of x-ray diffraction, fluorescence spectroscopy and pulsed x-ray measurements. Several new inorganic scintillators were founded, however, findings concerning lanthanum oxide synthesis warrant further investigation of the compound.

Analysis of the Water-Splitting Capabilities of Gallium Indium Phosphide Nitride (GaInPN).

JEFF HEAD (University of Arizona, Tucson, AZ 85705) **JOHN TURNER** (National Renewable Energy Laboratory, Golden, CO 89401). With increasing demand for oil, the fossil fuels used to power society's vehicles and homes are becoming harder to obtain, creating pollution problems, and are posing hazard's

to people's health. Hydrogen, a clean and efficient energy carrier, is one alternative to fossil fuels. Certain semiconductors are able to harness the energy of solar photons and direct it into water electrolysis in a process known as photoelectrochemical water splitting. P-type gallium indium phosphide ($\text{p-Ga}_x\text{In}_{1-x}\text{P}_2$) in tandem with GaAs is a semiconductor system that exhibits water-splitting capabilities with 12.4% solar-to-hydrogen efficiency. Although this material is efficient at producing hydrogen through photoelectrolysis it has been shown to be unstable in solution. By introducing nitrogen into this material, there is great potential for enhanced stability. In this study, gallium indium phosphide nitride $\text{Ga}_{1-y}\text{In}_y\text{P}_{1-x}\text{N}_x$ samples were grown using metal-organic chemical vapor deposition in an atmospheric-pressure vertical reactor. Photocurrent spectroscopy determined these materials to have a direct band gap around 2.0 eV. Mott-Schottky analysis indicated p-type behavior with variation in flatband potentials with varied frequencies and pH's of solutions. Photocurrent onset and illuminated open circuit potential measurements correlated to flatband potentials determined from previous studies. Durability analysis suggested improved stability over the GaInP2 system.

Calibration for Methane Hydrate Research Unit. XIAE SHI (State University of New York at Stony Brook, Stony Brook, NY 11790)

DEVINDER MAHAJAN (Brookhaven National Laboratory, Upton, NY 11973). Methane hydrate, one of the most common gas hydrates, forms at low temperature and high pressure; conditions typically found below the seafloor and permafrost. Although the amount of methane hydrate trapped under the seafloor on Earth has been estimated to be enough to meet human needs for the next several hundred years, due to their dispersed nature it is very difficult to extract the hydrates¹. A customized unit, named Flexible Integrated Study of Hydrates (FISH) that BNL is using for methane hydrate research, mimics seafloor conditions. In a typical process, methane gas is charged to the vessel, which initially contains a water/sediment mixture under high pressure, cooled down to 4 degrees Celsius. The hydrate formation can be visualized in the vessel through a 12-inch glass window. The kinetics of methane hydrate formation and decomposition could be studied through temperature, pressure and flow/mass meters for the duration of the experiment. The goal of my project is to test the operation and dynamics of the system, such as calibration of all flow/mass meters and BPR (Back Pressure Regulator), as well as testing the system's cooling rate. Preliminary results show that the system is well suited for hydrate formation. Volumetric balances at the inlet and outlet reveal a discrepancy of approximately 4 ml, which is well within tolerances for experimental error. Heat transfer analyses revealed a maximum cooling rate of 0.293°C/hr using a tube-like heat exchanger with forced convection in conjunction with a thermally controlled water-ethylene glycol bath.

Characterization of GaInPN:Si Tandem Cells for Hydrogen Production from Photoelectrochemical Water Splitting.

PAUL VALLETT (University of Vermont, Burlington, VT 05405) **DR. JOHN TURNER** (National Renewable Energy Laboratory, Golden, CO 89401). In order for hydrogen to be part of a renewable energy infrastructure, it must be produced from a renewable energy resource. The direct photoelectrolysis of water using certain types of semiconductors have been known to split water using absorption of solar energy, but difficulties concerning efficiencies and corrosion have limited this technology. This research focused on the ability of GaInPN grown on a silicon substrate to efficiently split water. Photocurrent spectroscopy determined the band gap of the material to be 1.96 eV, which is above the necessary 1.7 eV required for water splitting. Mott-Schottky analysis, photocurrent onset, and open circuit potential were used to determine potential of the Fermi level of the system in relation to the redox potentials of hydrogen and oxygen formation. These techniques showed that the Fermi level lied just below the oxygen redox potential. The electrodes were platinized and short circuit current density measurements under air mass (AM) 1.5 illumination determined extent of water photolysis. Unbiased water splitting was achieved, at a maximum of 0.65% solar to hydrogen conversion efficiency (SHCE). Corrosion of the semiconductor in solution was determined by applying a standard current to the electrode while in solution and using profilometry to estimate the volume of semiconductor removed. On average a 0.1 μm deep well was etched into the material after 24 hours. Incident photon current efficiency (IPCE) measurements of 30% revealed that the growing process for nitrogen addition to the sample decreased the electronic properties of the material. While this system is able to produce hydrogen from water using solar power as the only energy input, and the addition of nitrogen to the material appears to have increased its durability, the material suffers a heavy loss in

electronic efficiency, limiting its use in potential solar water splitting devices.

Clay Synthesis and Platinum Loading for Catalytic Applications.

LEAH PRANGER (Rhodes College, Memphis, TN 38112) KATHLEEN CARRADO (Argonne National Laboratory, Argonne, IL 60439). Contributions to the Catalyst Design Group were made concerning the development of synthetic clays for eventual catalytic and materials applications in three different areas. One project provides clay supports for metal species activity in catalysis. The variety of clays prepared includes silica-lithium-hectorite and tetraethoxysilane-hectorite in various dilutions. In the past, the group has used such supports in an array of projects, including loading cobalt-molybdenum-sulfide species for hydrodesulfurization and Pt(0) metal nanoparticles for oxidation catalysis. All of the samples prepared within this project were determined to be suitable for further testing. Loading of Pt(II) salts and reduction in H₂/N₂ atmospheres was performed. It was found that only very slight temperatures (50°C) were needed to effect reduction to Pt(0). Another task explored clay synthesis under extreme dilutions in order to foster a phenomenon called "exfoliation". Such samples lose all their layer-to-layer registry and instead the silicate layers are randomly distributed, similar to a "house of cards" structure. These materials are useful for atomic layer deposition experiments of catalytic species commonly used within the research group. Finally, work on another layered porous material was initiated. This involved reproduction of a literature synthesis of a layered zeolite dubbed "ITQ-2". Synthesis of these materials was performed in an autoclave under controlled temperature conditions. All materials were characterized by x-ray powder diffraction to establish crystallinity and thermal gravimetric analysis to determine water and organic contents. The Pt-loaded samples and dilute hectorites were determined to be of value for future research, while the ITQ-2 project had only partial success in synthesis.

Comparing the Physical Properties of Ionic Liquids Bearing Chiral and Achiral Hydroxyl Units. *JASMINE HATCHER (Queensborough Community College, Bayside, NY 11364) JAMES WISHART (Brookhaven National Laboratory, Upton, NY 11973).*

Ionic liquids have generated much interest due to their potential green chemistry applications. They are considered to be environmentally friendlier solvent alternatives to traditional volatile (and hazardous) organic solvents because of their lack of vapor pressure. We report here on the synthesis and preliminary characterization of achiral and chiral ionic liquids. The chiral species were synthesized by taking a chiral auxiliary, 3-chloro-1,2-propanediol, and adding it to a tertiary amine. The achiral ionic liquids were synthesized by adding our achiral auxiliary 3-chloro-1-propanol, to a tertiary amine. Some of the tertiary amines used were DMAP (4-dimethylaminopyridine) N,N,N',N' tetramethyl hexadiazine. The halide salts were converted into potential ionic liquids by anion exchange. Anions studied include phosphate and bis(triflyl)imide. A large problem with many ionic liquids is that they are very viscous. Theoretically, the induction of a chiral center would reduce viscosity, however this has not been the case with the materials synthesized using 3-chloro-1,2-propanediol. Preliminary results suggest that these chiral ionic liquids are more viscous than the achiral ILS. This may be due to the presence of an extra hydroxyl group, which increases hydrogen bonding. Future work will focus on finding a new chiral auxiliary and comparing the properties of racemic vs. enantiopure ionic liquids.

Controlled Synthesis, Characterization, and Properties of Tin Oxide Nanoparticles. *JENNIFER CODDING (McMurry University, Abilene, TX 79697) WEI WANG (Oak Ridge National Laboratory, Oak Ridge, TN 37831).*

Tin oxide nanoparticle based materials have various applications as sensors, catalysts, pigments, and electrode materials. Physical and structural properties, along with crystallinity and particle size and morphology of the tin oxide nanoparticles, depend on the method of synthesis. In this research, tin oxide nanoparticles were synthesized by forced hydrolysis of Tin(IV) chloride in a hydrochloric acid-alcohol aqueous solution. The use of alcohols in the synthesis of tin oxide nanoparticles provided the ability to correlate procedures of experimental synthesis with the properties of the desired compound. A systematic study was performed to examine nanoparticle formation at different conditions by varying the type of alcohol, alcohol/water ratio, reaction temperature, and time. Dynamic Light Scattering was used to verify the size and distribution of the particles and a UV-visible spectrometer was used to measure absorption to determine the temperature at particle appearance. Experiment shows that tin oxide nanoparticles form in alcohol-water media with alcohol volume fractions below thirty percent, and that particle size increases with a decrease in alcohol percentage. In an ethanol-water mixture, particle formation initiates at 84°C in thirty percent alcohol, while particles develop at 86°C

in twenty-five percent alcohol in a methanol- or butanol-water mixture and at 85°C in twenty percent alcohol in an iso-propanol or n-propanol-water mixture. Particle size and concentration also increase with an increase of reaction time above the formation temperature. Under uniform conditions, the size of the nanoparticle is directly proportional to the size of the alcohol molecule. Additional experiments are needed to determine more precisely the required time versus temperature ratio for the controlled synthesis of nanoparticles. Ultimately, forced hydrolysis is a good method to control the size and shape of discrete tin oxide colloidal nanoparticles.

***Designing Cyclic Polyammonium Salts for Potential Uses as**

Anionic Receptors. *ALEJANDRA CASTANO (Queens College, Flushing, NY 11367) JAMES WISHART (Brookhaven National Laboratory, Upton, NY 11973).*

The goal of this project is to synthesize cyclic polyammonium compounds that will be able to accommodate an electron as a guest. There have been several reports of cyclic ammonium polycations used as receptors for anionic guests such as chloride. The newly synthesized anion receptors will be used to control the solvation environment for excess electrons generated by pulse radiolysis. Providing a well-defined environment for the electron will help us to understand (by comparison) how the electron is solvated in bulk liquids (ionic and molecular) where the environment is highly disordered. The cyclic cations were synthesized by reacting tertiary diamines such as diazabicyclo[2.2.2]octane (Dabco) and N,N,N',N'-tetramethylbutanediamine with dihaloalkanes to produce the polyammonium cyclic adducts. These polyammonium halide salts were then converted to bis(trifluoromethylsulfonyl)imide salts and were investigated as potential ionic liquids. Preliminary NMR and Mass Spectrometry results indicate that the target cyclic polyammonium compound was not isolated using current reaction conditions. There is evidence that the product isolated is an ionene polymer. Differential Scanning Calorimetry (DSC) and Mass Spectroscopy analysis of this polymer is reported. Future work will focus on synthesizing cyclic polyammonium salts using different reaction conditions and analyzing the products using NMR spectroscopy, elemental analysis, Mass Spectrometry and pulse radiolysis techniques.

Detection of Botulinum Toxin Using a Sandwich Assay with Quantum Dots as the Fluorophore. *ABBY TYLER (Utah State University, Logan, UT 84321) MARVIN WARNER (Pacific Northwest National Laboratory, Richland, WA 99352).*

Development of assays and technology for biological toxins is a priority in the world today. Botulinum toxin is a potential bioterrorism agent for which new detection technologies are being developed. Effective detection systems need to have high sensitivity, and be rapid, automated, and accurate. Automated fluidics systems using sandwich immunoassays for detection have been developed at PNNL to fulfill these requirements. In order to increase sensitivity of biotoxin detection, quantum dots are used as the fluorophore. Quantum dots, or semiconductor nanocrystals, are becoming widely used in bioimaging but their use in biodetection is relatively new. Some advantages of quantum dots are good photostability, and a broad excitation spectrum and narrow emission spectrum that is highly red-shifted compared to the excitation wavelength. A fragment of the botulinum neurotoxin was used in these studies as well as two antibodies that are specific for different epitopes on the toxin. One antibody was coupled to several types of beads and the other antibody was coupled to the quantum dot. Bench top sandwich assays were performed by mixing the antibody-labeled beads, a sample of the toxin fragment, and antibody-labeled quantum dots. After reacting and washing this mixture, the fluorescent response was recorded. Assays were also done by packing a column of antibody-labeled beads in a cell in the automated fluidics system, perfusing a sample of toxin over it, then perfusing the fluorophore over it. Detection of 10pM toxin in buffer was achieved using the bench top assay with Sepharose 4-B beads and 655nm quantum dots with a fifteen minute reaction time. Polyacrylimide beads were used for detection using the automated system. Detection limits were slightly higher and there was more variability in the on column assay. Quantum dots have been an effective reporting agent in the bead based sandwich immunoassay for botulinum toxin.

Determination of Binding Constants Between Thiourea Anion Receptors and Selected Monovalent Anions. *ALICIA POWERS (Georgia Institute of Technology, Atlanta, GA 30332) LAETITIA DELMAU (Oak Ridge National Laboratory, Oak Ridge, TN 37831).*

The selective extraction of anions, particularly those in nuclear waste, is desirable because some anions hinder waste processing. Anion receptors can increase anion extraction and can possibly exhibit selectivity when designed from ligand modeling calculations. In this project, three thioureas, chosen for their geometry and ability to develop hydrogen

bonds with anions, are compared as anion receptors for several monovalent anions—nitrate, chloride, bromide, iodide, bicarbonate, and perchlorate—by measuring the binding constants between each thiourea and anion. Radiotracer experiments are used to measure the distribution of cesium between the organic and aqueous phases at varying initial concentrations of cesium for systems with and without anion receptors. Data from these experiments is modeled using the Fortran modeling program SXLSQL. In this program the predicted species formed in the organic phase are entered and the binding constants are calculated. The stoichiometry of the predicted species is varied in order to determine which model best fits the obtained data. Electrospray mass spectrometry (ESMS) is used to provide further evidence that the species used in the model are the actual species formed. Results show that all of the thioureas increased cesium extraction for all anions except perchlorate, although the order of the amount by which the thioureas increased extraction varied by anion. Most of the systems were best modeled with one thiourea binding to each monovalent anion although some were best modeled by both one and two thioureas binding to each anion. ESMS results for the nitrate anion with one of the thioureas showed that nitrate did bind to one thiourea although some nitrate also bound to two thioureas. These results show that thioureas were successful both in increasing anion extraction and in selectively extracting certain anions.

Determination of Forcefield Parameters to Evaluate the Binding of Porphyrin Structures to c-type Cytochrome Architectures.

ADRIENNE EASTLAND (*Chicago State University, Chicago, IL 60628*) **DR. DAVID TIEDE** (*Argonne National Laboratory, Argonne, IL 60439*). The binding of porphyrin-like molecules to the surface of c-type cytochrome proteins allows the initiation of electron transport. In order to develop biomimetic photosynthetic devices, the initiation step must be tuned by the choice of substituents on the porphyrin molecules. Computational docking studies combined with experimental fluorescence studies allow the evaluation of the effects of substituent changes on electron transport rates. The aim of this work is to develop a scoring function that is fast enough to be successfully applied to the prediction of the binding energy of a c-type cytochrome to a porphyrin-like ligand. Docking studies depend heavily on the scoring function employed. By using ab initio calculations at the Hartree Fock//6-31G* level, bond, angle, and dihedral parameters for the CHARMM scoring function were developed for a series of small molecules, representative of functional groups found in organic and biochemical systems. Upon parameterization, the dihedral force constant, k_{ϕ} , for the CA-CC-OC-OC dihedral in carboxybenzene was determined to be 3.66 kcal/mol/degree with $n = 2$ (n is the multiplicity of the function). For naphthalene dicarboxylate $k_{\phi} = 1.16$ kcal/mol/degree with $n = 4$. The magnitudes of the k_{ϕ} values are in good agreement with existing CHARMM forcefield parameters. Furthermore, these values reproduce the quantum mechanical energy profiles as a function of angle with R2 values of 0.97 and 0.94 for the carboxybenzene and naphthalene dicarboxylate molecules, respectively. A successful method will bridge the gap between expensive free-energy simulations and empirical scoring functions that are currently used to predict binding energy.

Determination of the Efficiency of Mixed-Acid Digestions of Sediments. **ALEJANDRA HUERTA** (*Hartnell Community College, Salinas, CA 93901*) **GARY GILL** (*Pacific Northwest National Laboratory, Richland, WA 99352*). Mixed-acid digestion is a method often used for the determination of elemental analysis of sediment samples. It is crucial that efficiency details associated with the digestion method be well understood on an element by element basis. Battelle's Marine Sciences Laboratory Standard Operating Procedure for Sediment Mixed-Acid Digestions was modified to identify conditions which produce optimal recovery of elements. The parameters that were adjusted for testing were mass of sediment, mixed-acid volume, mixed-acid composition and digestion time. Digestion involves treatment of the sediment sample with mixed-acid mixtures at $135^{\circ}\text{C} \pm 10^{\circ}$ in a Teflon® digestion bomb. Typical analytical methods include Inductively Coupled Plasma–Optical Emission Spectrometry (ICP-OES) and Inductively Coupled Plasma–Mass Spectrometry (ICP-MS). Initial experiments involved determining the optimal ratio of acid volume to mass of sediment. Experiments were designed to identify the point at which insufficient acid was used to effectively digest a given mass of sediment. When the mass of sediment was varied between 0.2 and 1.0 gram using a 4 mL aqua regia acid mixture (3 mL hydrochloric acid and 1 mL nitric acid), there was no effect on the recovery of the elements Al, Ba, Ca, Co, Cr, Cu, Fe, Mg, Mn, Ni, Pb, Sr, Ti, V, and Zn. The next experiments focused on a time study to resolve the shortest digestive time for optimal elemental recovery. Two masses of sediment were investigated, 0.25 and 0.7 g, again utilizing aqua regia digestion (4 mL).

Maximum recovery was reached after 4 hours of digestion; additional digestion time released no or only minimal amounts of elements from the sediments. The final set of experiments was designed to identify optimal conditions for the total digestion of sediment using a mixture of hydrochloric acid, nitric acid, hydrofluoric acid, hydrogen peroxide, and boric acid. These experiments were designed to determine the optimal volume of hydrofluoric acid needed to achieve a total digestion. Utilizing two masses of sediment 0.25 and 0.5 g and varying the volume of hydrofluoric acid and boric acid. Total digestion was achieved with a minimum volume of 0.5 mL hydrofluoric acid and a .25 g of sediment. Future experiments incorporating the findings in these experiments will be executed using a heated carbon block as the source for thermal energy.

Determination of the Electrostatic Potential of Cytochrome c7.

BRIAN WRIGHT (*Chicago State University, Chicago, IL 60426*) **DAVID TIEDE** (*Argonne National Laboratory, Argonne, IL 60439*). Assemblies of c-type cytochromes may be capable of long-range electron transport and thus are being considered as components of electron transfer/energy storage devices. The electron transport mechanism requires the binding of a small porphyrin-like molecule to initiate the electron transfer. In order to determine the likely binding sites on the surface of c-type cytochromes, the electrostatic potential of cytochrome c7 taken from *Geobacter sulfurreducens* (Protein Data Bank entry 1OS6) and horse heart cytochrome c7 (Protein Data Bank entry 1HRC) were calculated by solving the Poisson-Boltzmann equation using Delphi, a program that is integrated into the Chimera molecular modeling program. These calculations allow the identification of electron-rich or electron-poor sites that should contribute to binding. Results with model 1HRC showed good agreement with literature values, validating the charge and radii parameters chosen for the calculation. The overall surface of cytochrome c7 in model 1OS6 is positively charged by the amino acid lysine (Lys) (electron poor). The amino acids aspartic acid and glutamic acid contribute to the negative charge (electron rich) of the 1OS6 model. One possible binding site is located near Lys-64, Lys-52, and Lys-9. Another possible binding site is near Lys-37, Lys-33, and Lys-29. These areas are being considered as binding sites because the surface may provide porphyrin-like molecules large enough areas to bind. The ability to determine which parts of the c-type cytochrome are involved in the binding will lead to an improved understanding and control of the electron transfer process.

Diffusion-controlled Apparatus' for Microgravity.

RAJENDRAN (*Stanford University, Stanford, CA 94305*) **DR. P. THIYAGARAJAN** (*Argonne National Laboratory, Argonne, IL 60439*). Large photoactive yellow protein (PYP) crystals are being grown using diffusion-controlled apparatus' for microgravity (DCAMs) for proposed neutron crystallography experiments. The basis for this experiment is that a short strong hydrogen bond (SSHB) appears to play an important role in the function of PYP in the photocycle. In order to fully understand the structure and dynamics of the SSHB, it is necessary to accurately locate the nuclear position of the proton (or deuteron) with respect to the heavy atoms involved in the hydrogen bond. Previous attempts to grow PYP crystals using the batch and hanging drop method have had limited success. The resolution of diffraction data collected from PYP crystals grown using these methods was determined to be between 0.95 Å to 1.40 Å. PYP crystallizes best between a concentration range of 2.3 M to 2.5 M. Two DCAM units have been set up. The units have a concentration of 1.6 M and 2.0 M $(\text{ND}_4)_2\text{SO}_4$ in the small chamber, respectively, and a concentration of 3.0 M $(\text{ND}_4)_2\text{SO}_4$ in the large chambers. As the higher concentration solution in the large chamber equilibrates with the lower concentration solution in the small chamber through the diffusion control plug, the concentration increases within the "button" containing the PYP sample, causing crystallization to begin. Large PYP crystals have been grown following these procedures using DCAMs.

Distribution Coefficients of Several Ion-exchange Resins for the Separation of Cobalt, Nickel, and Copper.

JILLIAN SMITH (*East Stroudsburg University, East Stroudsburg, PA 18301*) **MARGARET GOLDBERG** (*Argonne National Laboratory, Argonne, IL 60439*). A method for the separation and accurate quantification of cobalt, nickel and copper is needed for the age dating of certain irradiated substances. The separation will be completed by using ion-exchange chromatography. The objective of this project was to measure the distribution coefficients for cobalt, nickel, and copper as a function of acid concentration and resin (Chelex 100, AG 1-X8, AG MP-1 and AG 50W-X8) using batch ion-exchange. The equilibrium of the metal ions between the aqueous phase and the ion-exchange resin is represented by the distribution coefficient (KD). Initial and final concentrations of the cations were measured by using high resolution inductively

coupled plasma-mass spectrometry. The project, however, was halted when the results showed an apparent contamination of the analyzed final concentrations. With only one quarter of the samples run, further research is necessary to correct the calibration curve and to account for the interferences of the matrix before any more quantification is performed.

Effects of Microbial Activity on the Stability of Apatite. *DIANNA MANJARREZ (Pacific Lutheran University, Tacoma, WA 98447) DAWN M. WELLMAN (Pacific Northwest National Laboratory, Richland, WA 99352).* A proposed remediation technology is to immobilize uranium by injecting a soluble phosphate amendment into the contaminated soil. The addition of a soluble phosphate amendment would initially form autunite, the dominant uranyl-phosphate mineral, to directly immobilize uranium and prevent further migration through the subsurface. Secondary to this, apatite will precipitate within the subsurface serving as a long-term sink for uranium via sorption and/or precipitation of uranium phosphate minerals. The environmental stability of apatite has been the subject of numerous investigations. Although the results of these investigations have provided valuable information regarding the mechanisms and rates of apatite corrosion as a function of relevant environmental variables, the effect of microbial activity on the durability of apatite has been the subject of far fewer investigations. This investigation quantifies the effect of microbial activity on the degradation of apatite at $T = 23^{\circ}\text{C}$, pH 6-8. Preliminary results suggest pH does not affect the release of calcium or phosphorus from apatite. Also, the presence or absence of microorganisms did not have a significant effect on the reaction progress, as indexed by calcium or phosphorus, in the presence or absence of aqueous phosphorus. The formation of secondary phase formation is possible and is the subject of further investigation.

Effects of Reaction Time upon Mesoporous Carbon Self Assembly. *LAURA WANAMAKER (Middle Tennessee State University, Murfreesboro, TN 37132) SHENG DAI (Oak Ridge National Laboratory, Oak Ridge, TN 37831).* Mesoporous carbon materials, which have a wide range of applications, have previously been synthesized using silica scaffolds, which are fabricated from surfactant templates. This method, however, is very inefficient as it involves the waste of silica scaffolds and surfactant templates and the use of toxic chemicals for silica removal. Thus, a method has been developed using surfactants as direct templates for the synthesis of the carbon materials. As prescribed by this method, triblock copolymers were used as the surfactant templates and a phloroglucinol/formaldehyde copolymer was used as a carbon precursor. These triblock copolymers are ideal for use in this process as they provide for carbon through self-assembly under mild conditions. Also, they permit the production of carbon materials as monoliths, fibers, sheets, and films. In addition, this method allows for the management of pore size and structure of the carbon materials by regulation of concentration and the specific surfactant used, respectively. The purpose of the current research was to determine the optimal reaction time to produce carbon materials composed of polymers of predetermined sizes and of uniform pore size. Reaction times were varied between 20 minutes and 2 hours to determine the dependence of the self-assembly process. This process of polymerization of phloroglucinol/formaldehyde copolymers induced phase separation into an aqueous, inorganic layer, which was discarded, and an organic layer. The organic layer was separated out and dried at 80°C overnight and then at 140°C overnight prior to carbonization. Nitrogen absorption/adsorption measurements, although pending, will provide pore size, pore volume, and surface area of the produced carbon material.

Exploration of Using Starch as a Recovery Agent for Catalytic Iodine. *BEN SIKORA (Colorado School of Mines, Golden, CO 80401) JOHN VERKADE (Ames Laboratory, Ames, IA 50011).* Currently a method for conjugating soybean oil is being developed that uses Iodine as a catalyst. To help conjugated soybean oil be more economically comparable to other oils, on the industrial scale, Iodine must be able to be recycled. A survey of a variety of starches and mixtures of these starches with water at various concentrations has been conducted to obtain optimum conditions for the removal of Iodine from Hexanes, and subsequent recovery from the starch. When potato starch was used it was found that it worked best when only wetted. The wetted potato starch gave the fastest absorption time of Iodine out of Hexanes, but posed problems when trying to drive the Iodine back out of the starch by thermal decomposition of the starch-Iodine complex. "V" modified starch was found to work without an outside solvent, such as water. This helped make the removal process of Iodine much simpler by removing the need to separate another liquid from the process. The results obtained for driving Iodine out of the starch were different from

literature insight in the fact that literature suggests that Iodine will leave the starch under thermodynamic activation. Some complications are still perplexing and require future investigation, such as the best process to remove the Iodine from the starch back into the Hexanes for recycling.

Extraction of Actinide Elements. *SARA MONTGOMERY (Rochester Institute of Technology, Rochester, NY 14623) JEFF GIGLIO (Idaho National Laboratory, Idaho Falls, ID 83415).* Advanced fuel specimens of the Materials and Fuel Complex (MFC) containing Plutonium, Americium, Neptunium, and Zirconium are prepared and sent to the Advance Test Reactor (ATR) and exposed to neutron bombardment. Characterization is performed on fuel stock material products before fabrication of metallic rods, before irradiation, and post irradiation (PIE). Characterization of the fuel samples is complicated because of isobaric interferences using inductively coupled plasma mass spectrometry (ICP-MS). In addition, background complications and wavelength overlaps complicate analyses by inductively coupled plasma atomic emission spectroscopy (ICP-AES). To minimize interferences, and reduce the overall actinide content of the samples (ALARA considerations) a means of separating the actinides from each other and removal of the actinides from a sample (i.e., "Clean-up") is needed. The objective to the research was to simplify separation schemes using TRU™ resin and manual Gas Pressurized Extraction Chromatography. The removal of the actinides will allow for more accurate and safer analysis of fuel samples for trace element impurities (before irradiation) and fission products after irradiation. The TRU resin worked well for the retention of Pu and U. However, Np proved to be problematic. More work is needed to fix the oxidation state of the Np for better retention. The removal of Pu from the TRU resin was accomplished. However, the U was not removed from the resin material with the acid used. The TRU resin worked well in the "Clean-up" of the actinides.

Froth Flotation and Other Means of Separation of Plastics of Equal Density and/or Similar Characteristics. *MICHAEL MAJEWSKI (University of Pittsburgh, Pittsburgh, PA 15213) BASSAM JODY (Argonne National Laboratory, Argonne, IL 60439).* Froth flotation is a method of using the hydrophobic and hydrophilic properties of materials to selectively attach air bubbles to one type of polymer in a mix, allowing for separation. By manipulating surface tension, acidity/basicity and specific gravity of solutions, it is possible to isolate, purify, and clean polymers from various shredder residues into high value resin streams. Plastics that are of interest include polypropylene (PP), talc-filled polypropylene (PP w/Talc), polyethylene (PE), acrylonitrile-butadiene-styrene copolymer (ABS), and ABS-polycarbonate alloys (ABS-PC). After submersion in successive solutions in which some plastics float and others sink due to the previously mentioned parameters and froth flotation, individual fractions form, each with a high purity in one or more thermoplastics. After experimentation, FTIR spectroscopy, as well as some FT-Raman, is used to identify the polymers. Difficulty arises in the isolation of polymers from shredder residue, as numerous contaminants include oils, gasoline, other automotive and appliance fluids, foam, and metals. What is received as bulk shredder residue destined for a landfill can be processed, cleaned, pelletized, and re-molded. A PP/PE product has been isolated. Interior automotive plastic components, such as battery trays and knee bolsters, have been molded from the recycled material. I have spent time in the lab doing wet chemistry, including froth flotation and density separation, on various polymers, air classification using air columns, FTIR analysis to identify plastics, and measurements of the surface tension and specific gravity of solutions.

Functionalization of a Ceramic Membrane for Liquid-Liquid Extraction. *DERRICK WHITLOCK (Texas Southern University, Houston, TX 77095) SETH SNYDER (Argonne National Laboratory, Argonne, IL 60439).* Ethanol, a product available in large quantity from corn fermentation, has been proposed as a viable alternative for gasoline. However, major barriers to the successful implementation of ethanol as a major fuel source are high costs and energy consumption associated with routine distillation of aqueous mixtures. Hydrophobic membranes, which have been employed successfully in liquid-liquid extraction, should offer a viable alternative to distillation. Herein, we disclose a process using ethyltrimethoxysilane (ETMS) to functionalize ceramic membranes capable of separating ethanol from water with high flux and minimal energy costs. Overall hydrophobicity analyses conducted on functionalized ceramic test membranes indicated the development of successful and versatile hydrophobic functionalization protocol and the measurement of negligible H₂O flux.

Hydrothermal Synthesis and Characterization of Sodium Dawsonite. *DANIEL DWYER (State University of New York at Geneseo, Geneseo, NY 14454) DR. DAWN M. WELLMAN (Pacific Northwest National Laboratory, Richland, WA 99352).* Na-dawsonite

has recently been suggested as a long-term sink for storage of carbon dioxide. In order to evaluate the effectiveness of this technique the stability of Na-dawsonite must be quantified under relevant geochemical conditions. To this end, significant quantities of pure crystalline Na-dawsonite are required for testing. However, sufficient quantities are not naturally available. Hydrothermal synthesis of Na-dawsonite was conducted at a temperature of 215°C for 96 hours, with a NaHCO_3/Al molar ratio of 24:1. X-Ray diffraction (XRD) and scanning electron microscopy (SEM) results indicate this method produced highly crystalline Na-dawsonite.

***Imaging Brain Amyloid After Traumatic Brain Injury and Drug Use with [11C] 6-OH-BTA-1 (PIB).** CANDACE GIRARD (*Springfield Technical Community College, Springfield, MA 01056*) JOANNA FOWLER (*Brookhaven National Laboratory, Upton, NY 11973*). Cerebral deposition of B-amyloid present in amyloid plaque (AP) may present an early and necessary step in the pathogenesis of Alzheimer's disease (AD). Postmortem immunohistochemical analysis after traumatic brain injury (TBI) also indicates the presence of AP. Recently, [N-Methyl-11C] 2-(4-(Methylamino) phenyl)-6-hydroxy-benzothiazole (6-OH-BTA-1), commonly known as PIB, was introduced as a high affinity ligand for imaging AP with Positron Emission Tomography (PET). In the present study, the synthesis and radiolabeling of PIB was accomplished according to modified published procedures. Using PIB for in vitro autoradiography studies, assessments of AP concentration from TBI specimens were evaluated. Frozen rat brain (5=injured, 4=normal) sections were exposed to B-sensitive PhosphorImager plates for 40+ min. The exposed plates were scanned in a PhosphorImager to produce digital images indicating high densities of ligand binding in the white matter regions of normal and injured rats. The presence or absence of group differences in grey matter areas awaits quantitative and statistical analysis. Additionally, PIB was used for the first in vivo evaluation of AP concentration secondary to Methamphetamine abuse using PET imaging. A male Sprague-Dawley rat (250g) was pretreated with Methamphetamine for 5 consecutive days. [11C] PIB was administered intravenously and a 90 minute dynamic PET scan recorded PIB uptake in specific brain regions. The highest levels of labeled PIB binding were in the corpus striata. These findings are preliminary and are part of an ongoing study to develop novel therapeutic strategies for drug abuse and treatment.

Improved Sample Preparation for Metabolites of Organophosphorus Insecticides in Biological Matrices. MELISSA PURPURA (*New Mexico State University, Las Cruces, NM 88003*) JAMES A. CAMPBELL (*Pacific Northwest National Laboratory, Richland, WA 99352*). Organophosphorus insecticides are broadly used in a variety of applications. Because of their widespread use, the potential exists for both occupational and environmental exposures that may cause a variety of health problems due to the inhibition of the enzyme acetylcholinesterase. The measurement of known metabolites in biological matrices through biomonitoring is a means for determining exposure to parent organophosphorus pesticide compounds. However, biological matrices present a unique challenge for analysis due to the potential interferences from compounds they contain. For this reason, methods for the purification and analysis of three metabolites of chlorpyrifos (diethylphosphate, trichloropyridinol, and diethylthiophosphate) were studied using whole rat blood. Techniques such as liquid-liquid extraction with solvents of varying polarity, centrifugation, and filtration were used in order to purify the samples and their extracted residues. All samples were derivatized and analyzed by gas chromatography/mass spectrometry. Preliminary data suggests that recoveries of diethylphosphate were better when the sample was extracted with ethyl acetate instead of methylene chloride. Although filtration prior to liquid-liquid extraction did not result in cleaner samples, it did improve the clarity of extracted residues. Centrifugation following derivatization produced cleaner samples without loss of the target metabolites. Future work will focus on the application of these methods for the analysis of samples collected from in vitro and in vivo studies of these compounds. Application of these methods to other matrices and other organophosphorus insecticides should also be examined.

***Investigating the Physical Properties of Liquid Ionic Phosphates (LIPs).** KATHERINE URENA (*Queensborough Community College, New York, NY 11368*) DR. JAMES WISHART (*Brookhaven National Laboratory, Upton, NY 11973*). Ionic liquids (ILs) are organic salts that exhibit melting points below 100°C. They are typically composed of ammonium cations and polyatomic inorganic anions. The attractive properties of ILs, including negligible vapor pressure, high conductivity, low flammability, low melting points, and recyclable nature make them ideal as environmentally friendlier solvent alternatives. We have synthesized a series of ILs based on functionalized 1-methylimidazole

and 1-methylpyrrolidine cations and phosphate anions. The resulting ILs are referred to as Liquid Ionic Phosphates (LIPs). The structures of LIPs have been confirmed using ^1H , ^{13}C and ^{31}P Nuclear Magnetic Resonance spectroscopy (NMR). The physical properties of LIPs including polarity, conductivity, viscosity, and decomposition temperature were determined. Polarity characteristics will be examined using the ET(30) polarity scale (an empirically derived reference scale based on the solvatochromic behavior of Reichardt's dye). Conductivity measurements will be done using a conductivity meter and viscosity measurements will be done using a viscometer. In addition the decomposition temperature (which indicates the liquid range of the IL) will be done using thermogravimetric analysis (TGA). Preliminary results indicate that we have successfully synthesized 1-Methylpyrrolidinium phosphates.

***Investigating the Use of a Diffusion Flame to Produce Black Carbon Standards for Thermal-Optical Analysis of Carbonaceous Aerosols.** DIANA ORTIZ MONTALVO (*University of Puerto Rico, San Juan, PR 00931*) THOMAS W. KIRCHSTETTER (*Lawrence Berkeley National Laboratory, Berkeley, CA 94720*). Combustion generated particles impact climate and public health due to their ability to scatter and absorb solar radiation and alter cloud properties, and because they are small enough to be inhaled and deposit in the lungs where they may cause respiratory and other health problems. Specific concern is focused on particles that originate from the combustion of diesel fuel. Diesels particles are composed mainly of carbonaceous material, especially in locations where diesel fuel sulfur is low. Diesel particles are black due to the strongly light absorbing nature of the refractory carbon components, appropriately called black carbon (BC). This research project focuses on the uncertainty in the measurement of BC mass concentration, which is typically determined by analysis of particles collected on a filter using a thermal-optical analysis (TOA) method. Many studies have been conducted to examine the accuracy of the commonly used variations of the TOA method, which differ in their sample heating protocol, carrier gas, and optical measurement. These studies show that BC measurements are inaccurate due to the presence of organic carbon (OC) in the aerosols. OC may co-evolve with BC or char to form BC during analysis, both of which make it difficult to distinguish between the OC and BC in the sample. The goal of this study is to develop the capability of producing standard samples of known amounts of BC, either alone or mixed with other aerosol constituents, and then evaluate which TOA methods accurately determine the BC amounts. An inverted diffusion flame of methane and air was used to produce particle samples containing only BC as well as samples of BC mixed with humic acid (HA). Our study found that HA particles are light absorbing and catalyze the combustion of BC during TOA. It is expected that both of these attributes will challenge the ability of TOA methods in distinguishing between OC and BC, such as the simple two step TOA method which relies solely on temperature to distinguish between OC and BC. The samples prepared in this study were analyzed using two TOA methods to compare the estimates of BC concentration. Future work will focus on the preparation of a variety of BC standards and comparing measurements of the prepared samples using a range of TOA methods.

***Isolation of a Single Parameter in Ultra High Purity Electroformed Copper.** CARMEN CAPETILLO (*Heritage University, Toppenish, WA 98948*) ERIC HOPPE (*Pacific Northwest National Laboratory, Richland, WA 99352*). Ultra high purity electroformed copper has the potential to be used as shields and cryostats for low background germanium spectrometry due to its distinct properties such as high electrical and thermal conductivity. However, there remain traceable radioactive contaminants of thorium 232 and uranium 238 found in most samples of high purity electroformed copper. There are many factors effecting the electroformation of ultra high purity copper some of which include: current, voltage, concentration of solution, mixing, and electrical waveform. There is significant difficulty isolating a single parameter when such a wide variety of variables exist. In these experiments, changing the anode to cathode distance without affecting the overall surface area of the electrodes was critical. The plating was performed using a small cylindrical container, solution of sulfuric acid and copper sulfate, and a reverse pulse plating power supply. The copper anode material was cut into vertical columns and placed into plastic tubing which was used for a cylindrical form. This allowed the distance between the anode and cathode to change without varying the surface area of either. Other parameters such as voltage and waveform, stirring, volume and components of solution were held constant. As expected, the closer the anode was to the cathode a greater amount of copper was deposited over a shorter time period due to the lesser impedance of the reduced path length. An unanticipated outcome was that a

smaller distance between the anode and cathode produced copper that had a smoother surface than that at the greater distance. Various purity assays must still be completed on the copper deposits produced. Further work must also be done to determine the optimum distance between the anode and cathode.

Linking Conductivity Measurements of Composite Heteropoly Acid Proton Exchange Membranes with Membrane Compositions and Fabrication Methods. DANA LIPFERT (Colorado School of Mines, Golden, CO 80401) JOHN TURNER (National Renewable Energy Laboratory, Golden, CO 89401). Fuel cells have been proven as an efficient energy conversion device and are employed in several applications (300°C) fuel cells require a cooling and humidification system to function properly. This increases weight, size, and cost of these applications, making fuel cells impractical for them. A proton exchange membrane that functions at high temperatures will alleviate these complications and allow for mass production of fuel cells for high temperature use. Composite heteropoly acid proton exchange membranes have shown promise for high temperature use, but a chemically and mechanically stable composite membrane with sufficient conductivity has yet to be obtained. The wide variety of heteropoly acids, membrane compositions and fabrication methods allows for a plethora of composite membranes, most of which do not satisfy all requirements. The objective of this work was to associate conductivity trends with fabrication methods, conditioning methods, and weight ratios of heteropoly acids and silanes (a fixing agent for heteropoly acids). For this work 12-silicotungstic acid (12STA) and tetraethyloxosilane (TEOS) at varied weight percents were used in composite membranes fabricated by either a sol-gel solution cast method or a doctor blade film forming method. Most membranes were cured, though uncured membranes were also tested. Conductivity tests were performed at a constant cell temp of 80°C with relative humidity (RH) ranging from 50-100%. Conductivities ranged from 0.36 mS/cm to 18.7 mS/cm, the highest conductivity produced at 100% RH by a membrane with 174 weight percent (wt%) 12-STA and 56 wt% TEOS fabricated by the solution casting method. Membranes fabricated by the doctor blade method were more flexible and produced higher conductivities than membranes of the same composition fabricated with the solution casting method, which tended to be brittle. Membranes conditioned in DI water produced lower conductivities than membranes of the same composition conditioned ambiently. UV-visible absorption analysis performed on water extracts for membranes after five day soaking showed that approximately 25 wt% 12-STA were leached out of the membranes. Uncured membranes were shown to have lower conductivities than cured membranes of the same composition.

Metabolic Profiling of Carboxylic Acids and Phosphorylated Species and Using Capillary Electrophoresis-Mass Spectrometry (CE-MS). MARIJA MENTINOVA (Lawrence University, Appleton, WI 54911) GARY J. VAN BERKEL (Oak Ridge National Laboratory, Oak Ridge, TN 37831). The analysis of metabolomes covers the identification and quantification of all intracellular and extracellular metabolites which exhibit molecular masses lower than 1000 Da, using a wide variety of analytical techniques. The goal of this work is to expand the analytical tool infrastructure at ORNL for analysis of plant and microbial metabolomes. A capillary electrophoresis system was coupled with an ion trap mass spectrometer. Capillary electrophoresis-mass spectrometry (CE-MS) is an ideal analytical tool for the analysis of charged species in solution. In the present work, CE-MS was applied to the separation of various candidate charged metabolites of plant metabolomes. This approach was used for the high resolution separation and sensitive detection of metabolites in the "negative ion" mass spectrometric mode. The "negative ion" mode on the mass spectrometer was used for detecting negatively charged components. Model compounds, such as small organic acids, phosphorylated carbohydrates, and adenosine phosphates, were separated and detected. For example, a three component mixture containing malic, citric and succinic acids was separated successfully using CE in its "reverse" polarity and detected by MS. In "reverse" polarity, the injection site on the CE was a high negative polarity (e.g., -20KV), and the electrospray emitter of the MS was positive relative to that (e.g., -3KV). The resulting electropherogram contained peaks with three different migration times, corresponding to each of the acids in the mixture. Similar results were obtained using the three adenosine phosphate species, as well as fructose mono- and diphosphate. These data, taken together, suggest that more complex metabolic mixtures could be separated, the individual components detected and quantified, and their metabolic profiles created. Further studies are needed to evaluate the separating power of CE-MS using more complex mixtures. This

fundamental project on metabolic profiling of phosphorylated species and carboxylic acids using CE-MS is a step forward to developing a new analytical infrastructure for ORNL in metabolic analysis.

Microwave Plasma CVD Diamond Stripper Foils for the Spallation Neutron Source. AMANDA MCDERMOTT (University of Virginia, Charlottesville, VA 22904) ROBERT W. SHAW, LESLIE L. WILSON, CHARLES S. FEIGERLE (Oak Ridge National Laboratory, Oak Ridge, TN 37831). Many accelerators use stripper foils to convert H⁻ to H⁺ as each pulse is injected into an accumulator ring. However, traditional carbon foils would have a short lifetime in the Spallation Neutron Source (SNS), and foil replacement requires significant beam downtime. Preliminary results suggest that diamond stripper foils could last ten times longer, or more, than carbon foils. The goal of this project is to grow foils under varying conditions for testing at the SNS to determine the best procedure to transfer to SNS technicians. Silicon substrates were patterned photolithographically, producing corrugations 5–7 μm deep around the outside edge to prevent curling of the free-standing films. The substrates were roughened in a stirred diamond-particle slurry in an ultrasonic bath to create nucleation sites. Diamond films were grown via microwave plasma assisted chemical vapor deposition (CVD) with a total flow rate of 100 standard cubic cm per minute (sccm). Nanocrystalline films were grown using 90% Ar and 1000 W microwave power at 130 torr; microcrystalline films were grown without Ar at 1300 W and 50 torr. In both cases the carbon source was 1 or 2% CH₄ with H₂ constituting the remaining flow. Growth temperatures varied from about 600–750°C. Scanning electron microscopy was used to determine grain size, presence of holes, and other characteristics. Finally, the Si backing was etched from acceptable foils using HF acid, leaving some Si for mounting. Films grown with CH₄ concentrations between 1 and 2% were investigated as a phenomenon consistently observed on the surface of 2% nanocrystalline films: small black spots of unknown composition. Nanocrystalline films were grown with 2% CH₄ at pressures from 100 to 140 torr resulting in varied temperatures. Larger particle sizes occur in 1% nanocrystalline films than in those grown with 2% CH₄, and micrographs of intermediate varieties showed that the transition in particle size is gradual. The density of black spots on 2% nanocrystalline films had a positive correlation with temperature, and a hydrogen-plasma etch procedure was developed to remove them. Foils with and without spots will be included in the next foil set for the SNS. When foil lifetimes are reported in several months, it will be possible to determine the ideal grain size and film thickness and whether removing black spots enhances performance. Examination of used foils will provide insight into failure mechanisms.

Neoteric Solvents for High Performance Liquid-Liquid Extraction. SHAYLA THOMAS (Texas Southern University, Houston, TX 77004) SETH SNYDER (Argonne National Laboratory, Argonne, IL 60439). Ionic liquids are neoteric solvents that may play an integral role in increasing the efficiency of ethanol extraction. Since many ionic liquids may be synthesized, selecting the best one for ethanol extraction is a difficult task. Herein, we qualitatively explore and discuss physicochemical properties of ionic liquids influencing the feasibility of ethanol extraction using a functionalized hydrophobic membrane. As modeling standards for extractants, two ionic liquids, 1-butyl-1-methylpyrrolidinium bis(trifluoromethylsulfonyl)imide [bmpy][Tf2N] and 1-hexyl-3-methylimidazolium bis(trifluoromethylsulfonyl)imide [hmim][Tf2N], were selected. Consequently, reasonable exchange of anionic constituents and modification of cationic "R" groups of these standards resulted in the proposal of four designer ionic liquids (DILs), 1-butyl-1-methylpyrrolidinium perfluoroethyltrifluoroborate ([bmpy][CF3CF2BF3]), 1-methoxyethyl-1-methylpyrrolidinium bis(trifluoromethylsulfonyl)imide ([COe]mpy)[Tf2N], 1-hexyl-3-methylimidazolium perfluoroethyltrifluoroborate ([hmim][CF3CF2BF3]), and 1-butyl-3-methylimidazolium bis(trifluoromethylsulfonyl)imide ([bmim][Tf2N]), optimal for the extraction of ethanol from aqueous mixtures using a functionalized membrane in a membrane contactor. Of these, 1-butyl-3-methylimidazolium bis(trifluoromethylsulfonyl)imide ([bmim][Tf2N]), was selected as the best overall DIL for complete application and processing.

New Liquid Precursors for the Deposition of Molybdenum. ROBERT PASQUARELLI (Rochester Institute of Technology, Rochester, NY 14623) CALVIN CURTIS (National Renewable Energy Laboratory, Golden, CO 89401). Copper indium diselenide (CIS) solar cells have demonstrated record high efficiencies, but the technology required and number of deposition systems necessary for processing CIS solar cells makes them expensive and difficult to scale up for manufacturing. A new means of depositing molybdenum (Mo), which serves as the back contact for these devices, from liquid precursors

can help lower costs and make CIS a more viable energy alternative. Deposition was studied using the organometallic precursors bis(ethylbenzene)molybdenum and tetraallyldimolybdenum dissolved in organic solvents. These solutions were deposited on glass microscope slides at temperatures between 100 and 340°C under nitrogen atmosphere. Commercial bis(ethylbenzene)molybdenum dissolved in both tetrahydrofuran and toluene was deposited on glass substrates at 200° and 340°C via spraying to produce films metallic in appearance. X-ray diffraction (XRD) showed broad peaks that could be assigned to Mo and carbonaceous contaminants (cubic Mo₂C and hexagonal β-Mo₂C), but most of the material present appeared to be amorphous. Elemental composition should be studied in future analysis to quantify the amount of carbide and metallic Mo present. The resistivity of a sprayed film was determined using a four-point probe to be $(3.23 \pm 0.76) \times 10^{-4} \Omega\text{-cm}$, a value about two orders of magnitude greater than that of pure Mo and one order of magnitude greater than the sputtered films currently used. Tetraallyldimolybdenum was synthesized under Schlenk line conditions and deposited from solution via drop coating to produce powdery films with poor adhesion. The composition of these films could not be determined using XRD given their amorphous nature. Future work will focus on removing carbide contaminants by depositing in the presence of hydrogen and producing more crystalline material.

NO_x and NO Adsorption on CeO₂: A Combined in situ FTIR and TPD Investigation. JOHN FAIN (*Sacramento City Community College, Sacramento, CA 95822*) JANUS SZANYI (*Pacific Northwest National Laboratory, Richland, WA 99352*). The NO_x adsorption/desorption properties of a high surface area CeO₂ (ceria) (an additive in practical lean NO_x traps) was investigated using in-situ Fourier Transform Infrared Spectroscopy (FTIR) in conjunction with mass spectroscopy (MS) and temperature programmed desorption (TPD). A high surface area ceria sample, treated under various conditions (oxidation or reduction), was exposed to either NO₂ or NO. NO₂ adsorption experiments revealed the formation of large amounts of nitrates on ceria. These nitrate species desorbed in two stages, similarly to that we have observed previously on BaO, suggesting that these two desorption states may arise from the decomposition of surface (NO₂ desorption) and bulk (NO+O₂ desorption) nitrates. The amount of nitrates formed upon exposure to NO₂ was higher on the oxidized samples than on the reduced ones, probably due to the consumption of some of the NO₂ to fill oxygen vacancies present in the reduced samples. Furthermore, over the reduced ceria samples the formation of both N₂O and N₂O₃ were observed in addition to the surface and bulk nitrate species. NO adsorption experiments showed limited N₂ production during thermal decomposition, due to the presence of small number of defect sites (oxygen vacancies where NO can decompose), associated with the low temperature during reduction with H₂ prior to NO adsorption. Keywords: NO_x reduction; lean NO_x traps; ceria; NO and NO₂ adsorption; FTIR; TPD.

***Optimization of an HPLC Method for Determination of Carbon-11 Specific Activity in [C-11] Methyl Iodide.** NATALIA SHAROVA (*Contra Costa College, San Pablo, CA 94806*) JAMES P. O'NEIL (*Lawrence Berkeley National Laboratory, Berkeley, CA 94720*). We have created a "standard mass concentration curve" for determination very small concentrations of the methyl iodide in the carbon-11 labeled methyl iodide for further calculation of a carbon-11 specific activity. The stock solution of methyl iodide was prepared by weighing and volumetric dilution with several precautions such as sealing the vials with Teflon faced septa. This solution was then diluted with water to prepare 5 standards with the methyl iodide concentration range 3.0–0.03 nmoles per injection. All standards were injected in the HPLC in triplicate and the responses were analyzed by the PeakSimple data system. Collected data allowed us to create a "standard mass concentration curve" and calibrate the PeakSimple for the specific methyl iodide components. Along the experiment we came to a conclusion that standard dilutions for this experiment could be done with water; however, water as diluent had its disadvantages that limited the minimal achievable concentrations of methyl iodide and increased uncertainty of the results. In order to increase the reliability of the standard curve, the experiment should be conducted within the time period that does not exceed 12 hours, and all standard samples has to be stored in small sealed glass vials at low temperatures (~ -5°C) while not being used.

Protonation of Molybdenum Cyclopentadienyl Phosphino Chloride Complexes with Triflic Acid. SHARON LEE (*University of California–Berkeley, Berkeley, CA 94720*) R. MORRIS BULLOCK (*Brookhaven National Laboratory, Upton, NY 11973*). The conversion of ketones to alcohols has a major impact on pharmaceutical chemistry due to its application in the synthesis of drugs. Current methods require expensive transition metal catalysts based on rhodium or ruthenium.

Harsh reagents such as LiAlH₄ and NaBH₄ require stoichiometric amounts and produce significant amounts of waste. Therefore, interest in catalytic molybdenum compounds that exhibit this reactivity has been growing. To be effective in an ionic hydrogenation mechanism, such molybdenum compounds must have the ability to protonate as well as transfer a hydride to a ketone to form an alcohol. This paper introduces molybdenum compounds made through the addition of triflic acid (HOTf = HOSO₂CF₃) in dichloromethane to synthesized Cp(CO)(Ph₂PRPPH₂)MoCl (R = CH₂, (CH₂)₃, or C₆H₄, Cp = C₅H₅) compounds. The resulting product, [Cp(CO)(Ph₂PRPPH₂)MoHCl]+OTf, of interest because of its potential to increase understanding of molybdenum interaction with its attached proton and the influence of different types of phosphino ligands on protonations. This knowledge can then lead to a more efficient molybdenum catalyst that can convert ketones to alcohols. The molybdenum compounds successfully synthesized are Cp(CO)Mo(dppb)Cl (dppb = 1,2-bis(diphenylphosphino)benzene), Cp(CO)Mo(dppp)Cl (dppp = 1,3-bis(diphenylphosphino)propane), and Cp(CO)Mo(dppm)Cl (dppm = bis(diphenylphosphino)methane). After protonation with triflic acid, the following compounds were made: [Cp(CO)(dppb)MoHCl]+OTf, [Cp(CO)(dppp)MoHCl]+OTf, and [Cp(CO)(dppm)MoHCl]+OTf. Using proton and phosphorus nuclear magnetic resonance and infrared spectroscopy, all synthetic products were characterized. In the future, structural characterization using x-ray diffraction on the crystals of the protonated compounds will be performed.

Radiochemical and Elemental Analysis of Zorita Pressure Vessel Materials. MICHAEL KING (*Baker University, Baldwin City, KS 66006*) JACQUELINE FONNESBECK (*Idaho National Laboratory, Idaho Falls, ID 83415*). Despite the fact that nuclear energy has the technological capability to take the place of fossil fuel as the world's primary energy source, there is still overwhelming opposition toward nuclear energy in many countries. One particular example of recent opposition to nuclear power occurred in Spain where President Jose Luis Zapatero shut down the Jose Cabrera (Zorita) Nuclear Power Plant in April of 2006 after thirty-eight years of operation. Closure of the plant not only reduces the energy production capabilities of Spain, but it also presents a convoluted and expensive clean up effort. Before demolition of the 160 MW pressurized water reactor used at Zorita can commence, various analyses must be performed to determine the level of radioactivity present in the reactor materials. The scope of work consists of the radiochemical and elemental analysis of the reactor pressure vessel plate materials that were abstracted from the Zorita reactor. The primary focus will be determining and classifying "Greater than Class C Waste" isotopes including: H-3, C-14, Ni-59, Ni-63, Co-60, Sr-90, Nb-94, Tc-99, I-129 and Cs-137. Class C Waste materials constitute the highest level of radioactivity which can be considered low level waste and is usually stored in a landfill. Storage protocol for greater than class C waste is more stringent and is typically stored in permanent repositories. In order to determine the composition and radiological hazards associated with the pressure vessel materials, various analyses and instrumentation is required. Neutron activation experiments will be performed at Washington State University to determine the majority of the elements present in the steel samples. Additional steel samples will be dissolved at the Materials and Fuels Complex and the dissolver solution will be analyzed using various spectrometers and counting instruments including: Inductively Coupled Plasma Mass Spectrometer, Inductively Coupled Plasma Atomic Emission Spectrometer, Gamma Spectrometer, Liquid Scintillation Counter, and X-Ray LEPS. Concurrently, solid pressure vessel samples will be combusted in a LECO Carbon Analyzer. The C-14 and H-3 will be collected from the combustion process and liquid scintillation counting used to determine the quantity of each. The results from all the analyses will be compiled and the quantity of each isotope will be reported to Westinghouse Electric in parts per million.

Ruthenium Isotopic Analysis: Comparison of Separation Techniques. VALERIE STUCKER (*University of New Hampshire, Durham, NH 03824*) CHRIS BROWN (*Pacific Northwest National Laboratory, Richland, WA 99352*). Technetium-99 (⁹⁹Tc), a beta emitter with a 213,000 year half life, is a contaminant of concern at several nuclear facilities. It is difficult, however, to use ⁹⁹Tc to distinguish between different contaminant sources and waste routes since it is a mono-isotopic fission product. On the contrary, the process of nuclear fission generates multiple ruthenium isotopes. These ruthenium (Ru) fission product isotopes offer a promising substitute for ⁹⁹Tc, testing due to the commonalities related to their subsurface mobility and the fact that their presence in nature is negligible. Comparing Ru isotopic ratios from different groundwater samples and water extracts from contaminated vadose zone sediments gives insight into the source

terms and pathways of the accompanying ^{99}Tc contamination. Methods of preconcentration and pretreatment for mass interference removal were developed to evaluate their effectiveness and establish new procedures for ruthenium isotopic separations. Anion exchange resin was assessed for total analyte recovery and preconcentration of Ru. Cation exchange resin was evaluated for its ability to remove cation analytical interferences and total analyte recovery. Solutions prepared from single element Ru standards were passed through columns containing either cation or anion exchange resin and the eluents were analyzed for total Ru and Ru isotopic ratios via inductively coupled plasma mass spectrometry. 50% of the ruthenium passed directly through the anion resin column, but 94.3% of it was recovered in three elution steps. The cation exchange resin had poor recovery (11–18%), but was efficient at removing cation interferences, reducing key interferent count rates (i.e., strontium) by 3 to 4 orders of magnitude. This cation resin was used in the reanalysis of previously tested contaminated sediment samples and similar results were obtained, confirming the usefulness of column pretreatment and preconcentration. The methods described herein present an efficient way to increase detection of ruthenium isotopes and quantify natural versus fission-produced ruthenium. This work is being performed in conjunction with other research being done by the Applied Geology and Geochemistry group to discover ways to identify, remove, and eliminate long term risks of technetium contamination from the Hanford Site, Washington.

Separation and Quantification of Cobalt, Nickel, and Copper by Anion-Exchange Column Chromatography Using the Dowex AG 1-X8 Resin. TERA SLONE (Texas Southern University, Houston, TX 77004) DR. TRACEY SIMMONS-WILLIS (Argonne National Laboratory, Argonne, IL 60439). Ion exchange column chromatography is a separation technique in which ions are exchanged, and separated by virtue of the differences in their distribution ratios between a mobile phase and a stationary phase that are in contact with each other. In this experiment an aqueous solution comes into contact with a resin packed in a chromatography column and causes the solution to exhibit the property of exchanging these ions and separating them. The ions are separated based on the solution's affinity and the resin's affinity for these ions. My overall goal in performing this technique is to separate three elements that are important to the forensic analysis of dirty bombs. Analysis of cobalt (Co), nickel (Ni), and copper (Cu) is necessary for age-dating the dirty bomb materials but they must be separated prior to forensic analysis. My research involves development of a preliminary separation method using a specific resin, the Dowex AG 1-X8 anion resin. This method is performed on the basis of an ion exchange column chromatography technique in which three different acids, hydrochloric acid, perchloric acid, and hydrobromic acid, are used to determine the optimum eluent for separating cobalt, nickel and copper while using the AG 1-X8 anion resin. Once this procedure is completed and several fractions have been collected, the separated elements will be detected and quantified by an instrument known as an inductively coupled plasma mass spectrometer (ICPMS) and the efficiency of the method will be determined.

Siloxanes: A Class of Silicon Based Polymers. SHARON LEONARD (Shasta Community College, Redding, CA 96006) PAVEL HRMA (Pacific Northwest National Laboratory, Richland, WA 99352). The very first technological developments occurred in what we now know as the Stone Age. Small discoveries, possible accidental, changed the way mankind operated, developed and even thought. As metals paved the way from the Bronze and Iron Ages and into present times, so has the use of silicon in computer chips and electrical transistors has ushered us out of the Industrial Revolution and into the Information Age. Currently we live in a world that has surpassed anything our grandparents dreamed of. And much of this is made possible by this one element. Silicon is the second most common element on our planet, 27.7% of the earth's crust, and the seventh most common in the universe. It is a gray, nonmetal, lightweight, semiconductor and is a component of a vast number of everyday items, present even in many biological systems. Several species require silicon as an essential element, it is present in human skin and connective tissue, and is even eaten by some marine tide pool organisms. When silicon is incorporated into a polymer, then the material properties may be superior to organic, carbon based materials in many situations.

Single Nucleotide Polymorphism Detection Using Nucleotide and Metal Phosphate Modified Apoferritin Nanoparticles. SHAWN RIECHERS (Washington State University, Pullman, WA 99164) GUODONG LIU (Pacific Northwest National Laboratory, Richland, WA 99352). Single nucleotide polymorphisms (SNPs) are common point mutations of DNA that are of interest to several areas of research, particularly as biomarkers for predispositions to diseases. Fast

detection and quantization of these mutations would be valuable to this research. The quantization of SNPs is addressed as a continuation of previous work. In this research the use of metal phosphate loaded apoferritin nanoparticles probe, as a detection method is explored. For this detection a section of biotin modified DNA probe is bound to streptavidin modified magnetic beads. DNA containing a single cytosine-cytosine mismatch is then hybridized to this probe, after which, perfectly complementary DNA is hybridized to any remaining free probe DNA. After this process nucleotides exposed due to the c-c mismatch should be the only exposed nucleotides. Apoferritin, a hollow spherical protein, is modified to contain cadmium phosphate in the inner cavity of the protein and guanine on the surface of the protein. This modified protein is then bound to the exposed nucleotides in the presence of polymerases (enzyme). An acidic buffer is added to release the metal component from the metal phosphate core into solution. This metal is then detected using highly sensitive electrochemical stripping analysis to give a signal, which is proportional to the amount of free mismatched nucleotides. An average RSD of 8.3% and an increase of 53% above the control was obtained for the SNP detection of 10 ppb mismatch DNA. It was shown that this is a viable method for the detection of SNPs, however, further research is required to increase the signal obtained from the mismatch and to minimize the signal due to nonspecific binding.

Solvent Purification and Fluor Selection for Gadolinium-loaded Liquid Scintillator. TIGISTI KESETE, AMANDA STORM (Central State University, Wilberforce, OH 43360) DR. RICHARD HAHN (Brookhaven National Laboratory, Upton, NY 11973). The last decade has seen huge progress in the study of neutrinos, which are elementary sub-atomic particles. Continued growth in the field of neutrino research depends strongly on the calculation of the neutrino mixing angle θ_{13} , a fundamental neutrino parameter that is needed as an indicative guideline for proposed next-generation neutrino experiments. Experiments involving reactor antineutrinos are favored for the calculation of θ_{13} because their derivation equation for θ_{13} is relatively simple and unambiguous. A Gd-loaded liquid scintillator (Gd-LS) is the centerpiece of the detector and it consists of ~99% aromatic solvent, ~0.1% Gd, and < 1% fluors. Key required characteristics of the Gd-LS are long-term chemical stability, high optical transparency, and high photon production by the scintillator. This summer's research focused on two important aspects of the detector: (1) purification of two selected scintillation solvents, 1, 2, 4-trimethylbenzene (PC) and linear alkyl benzene (LAB), to improve the optical transparency and long-term chemical stability of the Gd-LS, and (2) investigation of the added fluors to optimize the photon production. Vacuum distillation and column separation were used to purify PC and LAB, respectively. Purification was monitored using UV-visible absorption spectra and verified in terms of decreased solvent absorption at 430nm. Absorption in PC at 430nm decreased by a factor slightly >10 while the absorption in LAB was lowered by a factor of ~5. Photon production for every possible combination of two solvents, four primary shifters, and two secondary shifters was determined by measuring the Compton-Scattering excitation induced by an external Cs-137 gamma source (Eg ~ 662-keV). The ideal shifter concentration was identified by measuring the photon production as a function of shifter quantity in a series of samples. Results indicate that 6 g/L p-terphenyl with 150 mg/L 1,4-Bis(2-methylstyryl)-benzene (bis-MSB) produces the maximum light yield for PC and 6 g/L 2-(4-biphenyl)-5-(4-tert-butyl-phenyl)-1,3,4-oxadiazole with 50 mg/L bis-MSB optimizes the light yield for LAB. Future work should focus on obtaining the fluorescence spectra for each of the shifters and studying the optical transparency of the LS as a function of shifter quantity.

***Stereoscopic Projections of Organic Reactions.** PETER SHIN (Bergen Community College, Paramus, NJ 07652) ROBERT BENNETT (Brookhaven National Laboratory, Upton, NY 11973). In order to help students better visualize difficult organic reactions, both stereoscopic presentations of these reactions in motion and a user-friendly mechanism through which instructors can create their own reaction animations are being prepared. Stereoscopic projectors display two polarized images, seen by the viewer through passive stereo glasses, to create an image with depth. The project began by gathering information about any visualization tools freely available through the internet. The first search item was a method to translate a reaction into a portable data format. A website, Mol4D (cheminf.cmbi.ru.nl/wetche/organic/index.html, created by Centre for Molecular and Biomolecular Informatics), was found to allow the user input certain data and obtain the plots of atoms throughout the reaction. The input is done through a set of data known as the z-matrix, which consists of atoms, bond lengths, bond angles, and dihedral angles. After the website finishes

calculating the reaction, the user is able to extract an animated XYZ file which contains the Cartesian coordinates of the atoms during each frame or state of the reaction. The next step converts this set of coordinates into a format compatible with stereoscopic output. PyMol, a molecular modeling program created by DeLano Scientific, is capable of outputting a stereoscopic image of the molecules. However, the XYZ file format proved to be problematic when used with PyMol, due to its inherent lack of explicit bonding information. In a search for a more informative molecular format, Protein Database (PDB) proved to be an ideal candidate for conversion since it contains little more than the Cartesian coordinates of atoms and the explicit bonding information between each atom. In order to make the transition from Mol4D to PyMol as easy as possible, a C++ program was written which converts an animated XYZ file into separate PDB files of each state, checking for bond connections through an algorithm based on bond lengths. With this pathway in place, several stereographic animations of organic reactions were created for educational purposes. Although molecular modeling seems to be well-established, the path from reactions to stereoscopic viewing seemed to be a tedious process. By merging the ease of creating a reaction in Mol4D with the stereoscopic output in PyMol, this path has been made much quicker for instructors to create stereoscopic presentations of organic reactions.

Sugar Yields and Rheological Changes During Enzymatic Saccharification of High Solid Biomass Slurries. EVAN MITCHELL (*State University of New York College of Environmental Science and Forestry, Syracuse, NY 13210*) CHRIS SCARLATA (*National Renewable Energy Laboratory, Golden, CO 89401*). Cellulosic ethanol production involves several steps of biomass slurry processing that include extraction of sugars using chemical and/or enzymatic reactions, fermentation of sugars to ethanol, as well as transport of slurries between unit operations. It is desirable that the amount of water in these slurries be minimized to reduce equipment size and energy input required for processing. A lower water content, however, results in "high solid slurries" which are rheologically challenging. In this investigation, we have studied the effects of solid concentrations on enzymatic conversion and have quantified the rheological property changes in high solid slurries during enzymatic saccharification. Results from digestibility studies showed that cellulose conversion decreased from 72% to 39% when initial solid concentrations were increased from 15% to 40%. It was also interesting to note that final glucose concentrations increased from 83.6 g/L at 15% solids to 159.0 g/L at 30% solids, but stayed at nearly the same level at higher solids concentrations. Further, results from rheological measurements also showed that viscosity changes were more pronounced during digestions with the lower initial solid concentrations of 25 and 30%, when compared to digestions at higher initial concentrations of 35 and 40%. The preliminary rheological characterization also showed that the material stays pseudoplastic, or shear thinning, throughout digestion. However, a more complete rheological characterization of the material was not possible due to limited capabilities of available instrumentation, and warrants further investigation. These results indicate that lower conversions at high solid concentrations are likely due to sugar inhibition of enzymes. Overall, our studies indicate that the break point in sugar release at 30% initial solid concentration correlates with rheological property measurements. At higher solid concentrations, it is likely that enzymes are inhibited either due to lack of sufficient free water or due to build up of sugars in the liquid phase. Further kinetic and rheological studies are required to better elucidate this decrease in digestibility.

Surfactant-Templated Synthesis of Nanoporous Calcium Phosphates. JANESSA HARTMANN (*Georgia College & State University, Milledgeville, GA 31061*) DAWN WELLMAN (*Pacific Northwest National Laboratory, Richland, WA 99352*). This investigation presents the method development for surfactant-templated synthesis of nanoporous calcium phosphate materials. Calcium chloride and calcium fluoride were used as the metal sources, cetyltrimethylammonium chloride (CTAC), octadecyltrimethylammonium bromide (OTAB), octadecyltrimethylammonium chloride (OTAC), cetyltrimethylammonium bromide (OTAB) were used as surfactants, and phosphoric acid as the phosphorus source. The experimental matrix included 28 different syntheses which varied the surfactant, metal, phosphorus molar ratio. Three synthetic materials demonstrated potential promise for development of nanoporous materials and are subject to further analysis.

Synthesis and Characterization of a Kläui Complex Containing a Functionalized Cyclopentadienyl Group, Na[Cp'Co{PO(OC₂H₅)₂}₃]. MICHELLE MALONE, SURRIA JAMES (*The University of the Virgin Islands, St. Thomas, VI 00802*) GREGG LUMETTA (*Pacific Northwest National Laboratory, Richland, WA 99352*). The separation

of actinide ions from complex chemical matrices is of importance in terms of radioanalytical chemistry and the management of radioactive waste materials. The work described herein is part of an ongoing study involving the synthesis and characterization of materials that can selectively extract and concentrate radioactive nuclides from complex mixtures. The Kläui salt, Na[Cp'Co{PO(OC₂H₅)₂}₃] (Cp' = C₅H₄C(O)OCH₃), was synthesized. The route chosen to synthesize the ligand is similar to that used in the original reported synthesis. The functionalized NaCp' used in the synthesis was prepared by reacting NaC₅H₅ with dimethylcarbonate (CH₃OC(O)OCH₃). This product was then reacted in situ with anhydrous CoBr₂, forming Cp'Co. The Cp'Co was then refluxed with excess diethylphosphite forming [Cp'Co{PO(OC₂H₅)₂}₃]Co. Reaction of the latter compound with NaCN in air in methanol resulted in the formation of the sodium salt Na[Cp'Co{PO(OC₂H₅)₂}₃]. The new Kläui ligand and its precursors were characterized using IR spectroscopy and mass spectrometry. Attempts were made to grow crystals of all of the products and to characterize them using single crystal x-ray diffraction. The crystal structure of [(Cp')Co{PO(OC₂H₅)₂}₃]Co indicates that the ester functional group was reduced by excess diethylphosphite to a methyl group. Further studies will investigate oxidation of the cyclopentadienyl methyl groups to a carboxylic acid functionality, with the ultimate goal to covalently attach the functionalized Kläui ligand to a polymer support and to evaluate its potential to selectively bind actinide ions. The ability of these Kläui ligands to selectively bind actinide ions has been previously reported in both liquid-liquid and solid-liquid extractions. In those studies the ligand was weakly adsorbed onto the surface of an Amberlite XAD-7 extraction resin. With the functionalized ligand prepared in this study we can covalently attach the ligand to a functionalized polystyrene support, resulting in a more robust material.

Synthesis and Characterization of Ionic Liquids Based on DABCO (Diazabicyclo-2,2,2-octane). KIJANA KERR (*Queensborough Community College, Bayside, NY 11364*) DR. JAMES WISHART (*Brookhaven National Laboratory, Upton, NY 11973*). We report here on the synthesis of a series of ether and hydroxyl containing halide salts based on DABCO diazabicyclo[2.2.2]octane, for conversion into ionic liquids with varying anions. Some of these halide salts have been converted into liquid ionic phosphates (LIPs) and bis(trifluoromethylsulfonyl)imides. The halide salts were synthesized by reacting an alkyl halide with DABCO using microwave assisted synthetic techniques and conventional methods. The corresponding ionic liquids were synthesized by anion exchange. Microwave assisted synthetic reaction conditions such as temperature, the nature of the reaction solvent and length of reaction time have been varied. Results show that quaternization has been achieved. Structure determination of these ionic liquids was done using ¹H, ¹³C and ³¹P NMR. Preliminary characterization including differential scanning calorimetry (DSC) of a homologous series of compounds is reported. Dramatic differences in melting points were observed with anion variation of DABCO compounds. Future work will focus on continuing the synthesis and characterization of these compounds.

Synthesis and Characterization of Non-Platinum Cathode Catalysts for Polymer Electrolyte Fuel Cells. JASON GOODPASTER (*University of Illinois at Urbana Champaign, Urbana, IL 61801*) XIAOPING WANG (*Argonne National Laboratory, Argonne, IL 60439*). Noble metal and transition metal alloy catalysts were prepared and studied for their activity for the Oxygen Reduction Reaction (ORR). In this work, the B-G/C* bimetallic catalysts were prepared by co-impregnation at a variety of nominal molar ratios and subsequent heat treatment in regen gas. The ORR activity was evaluated by determining the current at 0.85V from the steady state cyclic voltammograms (CVs). It was found that there is an optimal heat treatment temperature for catalysts for their activity towards the ORR. X-ray diffraction was used after heat treatment to verify if an alloy of the noble metal and transition metal had formed. Acid treatment of these catalysts can increase their performance and the possible mechanism for increased activity is discussed. The B-G/C catalysts showed activity better than B/C, which approached that of Pt/C by producing current as early as 0.90 V. *Actual names of metals is proprietary, therefore this report will make no mention of what metals were used and will refer to metals as "A" through "H" skipping "C". C was skipped since it is used to refer to Carbon.

Synthesis of Magnetic Nanoparticles. DEANNA JONES (*Brigham Young University-Idaho, Rexburg, ID 83440*) SURYA MALLAPRAGADA (*Ames Laboratory, Ames, IA 50011*). In this work, a novel biomimetic synthesis was explored to form magnetic nanocrystalline iron and iron-cobalt oxides in-vitro. Magnetite and mixed iron-cobalt oxide nanocrystals were synthesized via a room-temperature co-precipitation

method in the presence of a recombinant, iron-binding protein Mms6. This protein is thought to be involved in the biomineralization and the formation of uniform magnetite nanoparticles in magnetotactic bacteria. Synthesis was performed in aqueous polymeric gels to slow down the diffusion rates of the reagents to better mimic biological conditions. These gels included: agarose gel, thermoresponsive Pluronic® F127 gel and thermo and pH-responsive pentablock copolymer. The resulting nanocrystalline magnetic particles were comprehensively studied using Transmission Electron Microscopy, Electron Diffraction Methods, X-ray Photoelectron Spectroscopy; and magnetization measurements. The oxide particles were found to be crystalline and superparamagnetic. They had a wide size distribution, depending on the media and whether or not Mms6 was present. This method provides a bioinspired route to nanomaterials synthesis and it is now being tested in synthesis of mixed iron-ruthenium oxides.

Synthesis of Novel Crown Ethers Bearing the exo-cis-2,3-Norbornyl Group As Potential Na⁺ and K⁺ Extractants for Nuclear Waste Remediation. RACHEL ROBESON (*Earlham College, Richmond, IN 47374*) PETER BONNESEN (*Oak Ridge National Laboratory, Oak Ridge, TN 37831*). The ability to extract sodium ions (Na⁺) from alkaline nuclear tank waste containing 1-2 molar (M) sodium hydroxide and 2-3.5 M sodium nitrate is of interest as a strategy for overall waste volume reduction. Lipophilic crown ethers with high sodium binding efficiency will be needed as extractants. According to molecular modeling, crown ethers that incorporate the exo-cis-2,3-norbornyl moiety may be effective sodium extractants due to the rigidity of the norbornane framework. The rigidity allows the oxygens, attached at the 2- and 3-positions, to be directed toward the center of the binding cavity. The proposed crown ethers may be superior to existing crown ethers (such as the octamethyl-16-crown-5) that are known as being effective sodium extractants. Thus, the goal of the project was to prepare a series of novel dinorbornyl-16-crown-5 and dinorbornyl-18-crown-6 ethers for sodium extraction studies. The key starting material for both families of crown ethers, exo-cis-2, 3-norbornanediol, was successfully prepared on a large scale in 88% yield. The syn and anti isomers of the dinorbornyl-16-crown-5 ether family were prepared using diethylene glycol and 2-substituted-1,3-propyl linkages; both isomers were separated using column chromatography. A single crystal of the syn isomer suitable for X-ray crystal structure analysis was obtained, thereby confirming the syn orientation. The syn and anti isomers of the dinorbornyl-18-crown-6 ether family were successfully prepared employing a different synthetic strategy, involving the connection of two, bis-hydroxyethoxy-substituted exo-cis-2,3-norbornyl groups. Intermediates and products were checked for purity using either thin layer chromatography or gas chromatography, and characterized by proton and C-13 NMR. Future research will evaluate the sodium extraction strength of these synthesized dinorbornyl-16-crown-5 and dinorbornyl-18-crown-6 ethers as compared to the extraction performance of known crown ethers, octamethyl-16-crown-5 and dicalalino-16-crown-5.

Synthetic Clays for Chemical and Materials Applications. KENNY GUILLOTTE (*Central Missouri State University, Warrensburg, MO 64093*) KATHLEEN A. CARRADO (*Argonne National Laboratory, Argonne, IL 60439*). Contributions to the Catalyst Design Group were made concerning the development of synthetic clays for eventual catalytic and materials applications. One project provides clay supports for metal species active in catalysis. In the past the group has, for example, loaded onto such supports both cobalt-molibdenum-sulfide (CoMoS) species for hydrodesulfurization (HDS) and Pt(0) metal nanoparticles for oxidation catalysis. All of the samples prepared within this project were determined to be suitable for further testing. Another task explored clay synthesis from alternative starting materials, such as magnesium chloride salt rather than magnesium hydroxide. It was found that refluxing the precursor mixture was superior to mixing at room temperature, as had been previously published. Adding LiF mineralizing agent was also found to lead to more crystalline clay products. Finally, work towards optimizing organo-grafted materials for possible use in specialty polymer-clay nanocomposites was undertaken. The goal of this project is to combine alkoxysilanes and organoalkoxysilanes in various mixtures in order to create materials of various organo-group densities grafted to the silicate surface. Controlling the spacing between organic groups in this fashion can have effects on affinities for polymeric molecules in polymer-clay nanocomposite applications. All materials were characterized by x-ray powder diffraction (XRD) for crystallinity and thermal gravimetric analysis (TGA) to determine water and organic contents.

Task Specific Ionic Liquids. JENEE CYRAN (*Allegheny College, Meadville, PA 16335*) GARY A. BAKER (*Oak Ridge National Laboratory, Oak Ridge, TN 37831*). There are a number of advantages to performing enzymatic catalysis within ionic liquid-based solvent systems. Possible benefits include one or more of the following: reduction in water-catalyzed side reactions; reduced microbial contamination; higher activity; improved selectivity; better operational, thermal, and storage stability; elimination of solvent emissions; and clear opportunities for continuous recycling. In this work, exploration was completed on the design of task-specific ionic liquids (TSILs) deliberately engineered for use and compatibility with biocatalytic systems. Specifically, synthesis of several homologous series of TSILs with representative members from both the aprotic and Brønsted acid/base categories, including some examples containing halogen-free, pharmaceutically-acceptable anions as alternatives to the vastly popular, yet costly, bis(trifluoromethylsulfonyl)imide introduced by the battery industry. Ionic liquids were characterized using ¹H and ¹³C nuclear magnetic resonance (NMR) spectroscopy and thermogravimetric analysis (TGA). In a major segment of the project, native and chemically-modified enzymes were investigated within a range of TSILs, both those miscible and completely immiscible with water. In this aspect of this research, the solubilities, partition coefficients, secondary structure, and activities of model enzyme systems within neat TSILs and TSIL/buffer mixtures were explored. The emphasis here is shifted to the use of optical spectroscopy to interrogate well-defined enzyme systems (cytochrome c, for example) within a diverse range of TSIL-based media. UV-vis of the cytochrome c and TSIL mixtures were more stable than mixtures with organic solvents. Thus, TSILs are more compatible solvents for biocatalysis. Further studies are planned to test more TSILs and various enzymes.

Testing the Solubility of Minerals and Metallic Compounds in Deep Eutectic Solvents. STEPHEN KANE (*Suffolk County Community College, Selden, NY 11794*) MARK FUHRMANN (*Brookhaven National Laboratory, Upton, NY 11973*). The purpose of this research is to compare the solubility of various compounds in Deep Eutectic Solvents (DES) versus water. These are ionic solvents that are formed from mixtures that have a lower melting point than any of its individual components. They are drawing the attention of industry and academia for a number of applications. We concentrated on their ability to dissolve metals and minerals. The DES of particular interest is a 2:1 molar mixture of Urea to Choline Chloride. These materials are used in large quantities in agriculture; Choline Chloride (vitamin B-4) is an additive to chicken feed, and Urea is used as a common fertilizer. They were combined at 60°C and formed a viscous Ionic Liquid (I.L.) at room temperature. Once mixed < 1g of metals were added to 5 ml of I.L. and allowed to sit in the solution overnight. The samples were then placed in a centrifuge for 25 minutes. 1ml of the sample was then diluted in a 100ml volumetric flask, then analyzed using the Liberty 100, Inductively Coupled Plasma Emission Spectrometer (ICP) for solubility of iron, copper, aluminum, silicon, and zinc compounds. They were then retested at elevated temperatures. The preparation was similar at elevated temperature, with the exceptions being that the centrifuge was not utilized and the samples were placed in an oven. The ionic liquid becomes considerably less viscous at elevated temperatures enabling the samples to be filtered using a 0.7-micron filter. Altogether thirty-eight samples were tested. Of those thirty-eight only eight proved to be more soluble in water cupric chloride, copper (II) nitrate, zinc chloride, zinc nitrate, ferric chloride, ferrous chloride, ferric ammonium sulfate, aluminum chloride. At temperatures above 25°C the solubility of the I.L. seems to increase and becomes considerably less viscous making it more workable and less prone to error. The effect of temperature on solubility was varied, and although additional testing is needed it seems that each compound may have a specific temperature range for maximum solubility, or possibly more important this could be an indication that a back reaction in which a new compound is being formed.

The Effects of Boron on Uranium(VI) Adsorption on Iron Oxide. LYNDASAY TROYER (*Whitman College, Walla Walla, WA 99362*) WOYONG UM (*Pacific Northwest National Laboratory, Richland, WA 99352*). The mobility of radionuclides such as uranium(VI) released from glassified low-activity radioactive waste in radioactive waste repositories is expected to impact both environmental and human health. Because boron (or borate) concentrations have been found in accelerated glass leachate, the effects of boron on U(VI) adsorption and mobility should be considered to assess the long-term performance of the proposed glassified radioactive wastes. Previous independent studies of boron and uranium(VI) adsorption onto sediment or minerals have found a similar bell-shaped curve when plotting adsorption (%)

against solution pH. These results indicate that the two could compete with each other for the same sorption sites causing boron to affect the mobility of uranium(VI). This study uses batch experiments to look at the adsorption of boron and uranium(VI) together for the first time. Three iron oxides, hematite, goethite, and two-line ferrihydrite, were synthesized, and ferrihydrite was selected as the sorbent because of its high adsorption capacity for both B and U(VI). Sample sets were prepared containing B alone, U(VI) alone, both B and U(VI), and both with U(VI) added 24 hours after B. Boron adsorption was lower in all open sets ($P_{CO_2}=10\text{-}3.5\text{ atm}$) than in the closed sets ($P_{CO_2}=0\text{ atm}$), because of carbonate competition in the open systems. The lowest adsorption occurred in the open set containing both U(VI) and B, indicating the preferential binding of U(VI) to the sorbent surface. Because of the high solid concentration used, the majority of U(VI) samples from pH 4-8 showed 100% adsorption making comparisons difficult. With our conditions U(VI) does not appear to be affected by boron's presence, however more studies should be conducted with lower solid concentration and with higher boron concentration. Spectroscopic studies should also be performed to examine surface complexation of B and U(VI) at a molecular level.

The Effects of Surface Chemistry on the Properties of Proteins Confined in Nano-porous Materials. LATASHA GARRETT (*University of Tennessee, Knoxville, TN 37996*) HUGH O'NEILL (*Oak Ridge National Laboratory, Oak Ridge, TN 37831*). Amorphous glasses formed by the sol-gel route provide non-native environments for the investigation of the physico-chemical and structural properties of biomolecules at the biotic/abiotic interface. These studies yield important information for the design of novel bioinspired functional materials. The sol-gel process can entrap biomolecules in their active form under conditions that mimic the naturally crowded cellular environment. The biomolecules are spatially separated and 'caged' in the gel structure but solutes can freely permeate the matrix. Thus, properties such as the folding of ensembles of individual molecules can be examined in the absence of aggregation effects that can occur in solution studies. In this investigation, wild-type green fluorescent protein (GFP) from *Aequorea coerulescens* was used as a model to examine the unfolding/re-folding properties of protein in silica gels. Recombinant GFP was isolated and purified from *Escherichia coli* extracts by cell lysis, three-phase partitioning, dialysis, and anion exchange chromatography. The purity of the protein was greater than 90% via SDS PAGE gel analysis. The yield was approximately 50mg per 1 liter of cells. Sol gels were formed using a combination of alkoxide precursors such as tetramethylorthosilicate (TMOS), methyltrimethoxy-orthosilane (MTMOS), ethyltrimethoxyorthosilane (ETMOS), 3-aminopropyltriethoxysilane (APTES), and 3-glycidoxypropyltrimethoxysilane (GPS). The protein containing sol solutions were cast in plastic 1mm thick cassettes, after gelation occurred the gels were overlaid with 10 mM sodium phosphate pH 7. The entrapped properties of GFP were analyzed by UV-visible, fluorescence, and circular dichroism (CD) spectroscopies. The entrapped GFP was denatured with hydrochloric acid (HCl) and the refolding of the protein was monitored at pH 7. No renaturation was observed in gels that were made with TMOS only, and in the presence of APTES (50%), MTMOS (50%), and ETMOS (50%). However, GFP in solution and in gels that were made with GPS, the CD and UV-visible spectra indicated that the protein had refolded. Gels were made with 10%, 15%, 20%, and 25% (v/v) GPS to TMOS, but gels made with 0.15 GPS indicated a 25% activity recovery. This study highlights the importance of the surface chemistry of the silica gels for the refolding properties of the entrapped GFP. Future studies will investigate the effect of surface chemistry on the thermal and solvent stability of the entrapped protein.

Thermoset Composites from Bio-based Oils and Spent Germ from Ethanol Production. JEFFREY BAKER (*Pennsylvania State University, State College, PA 16801*) DR. RICHARD C. LAROCK (*Ames Laboratory, Ames, IA 50011*). Thermoset composites have been prepared by the use of a bio-based resin and spent germ filler, which is a byproduct from a wet ethanol production plant. The bio-based resin is prepared by the free radical co-polymerization of tung oil (TNG), methacrylonitrile (MAN), divinylbenzene (DVB), and initiated with cumene hydroperoxide (CHP). This bio-based resin is pre-cured for a few hours before being mixed with the spent germ, the filler, upon which the mixture is cured under mechanical pressure, and then post cured in an oven. The resulting composite material consists of roughly a 1:1 ratio of resin to spent germ. The crosslinked thermosets are dark brown in color, hard and brittle, and have a slight burnt odor. Thermal and mechanical analysis of the composites has been performed via thermogravimetric analysis (TGA) and tensile testing. Results from the

TGA show that the composites have a multiple stage degradation with unstable intermediates ranging from 239–304°C and 465–478°C. The tensile tests show on average the modulus values range from 915–1375 MPa and the toughness values range from 0.02–0.05 MPa.

Computer Science

3D Animation of Pancreatic Molecules. BRITTANY PETERS (*Rochester Institute of Technology, Rochester, NY 14623*) DR. PAUL CRAIG (*Brookhaven National Laboratory, Upton, NY 11973*). The pancreas is the supplier of a variety of digestive enzymes and hormones, most notably insulin. In the past a virtual animation of the pancreas has been created, showing a tour of its internal structure. To continue this animation the goal is to introduce molecular detail into this virtual model of the pancreas. We are using Maya's 3D modeling and animation capabilities to address the challenging task of providing a greater understanding of the pancreas for students, teachers and doctors. Pancreatic proteins contain hundreds or thousands of atoms; the Protein Data Bank (www.rcsb.org) contains many pancreatic proteins structures with x,y,z coordinates of each of its atoms to form a molecule that can be visualized in 3D. The challenge for molecular artists who use Maya is to model these molecules accurately because their structure is too complex to create. One easy way to provide these molecules is to download the PDB files from the Protein Data Bank and visualize them in Maya, but Maya is unable to recognize them. However, the files can be manipulated and changed to achieve the objective. The PDB file first needs to be converted to a simple text document so that the 3D program can read its written information, then it can be drawn through a Maya tool called a mel script. This script is a code that allows Maya to read the PDB file, import it, and model it. From this point the molecular structure can be rendered and animated. This procedure will help to show an up close view of a pancreatic molecule in action. We are developing techniques to display these proteins in a surface format which highlights the overall shape of each molecule, as well as a ball-and-stick format, which emphasizes the individual atoms. One of the advantages of this approach is the molecular artist can import any protein structure that is available in the PDB file format, which will enable viewers to better visualize the physiology of the human pancreas at the molecular level.

***3D Stereoscopic Fantastic Voyage of the Heart.** NATHANIEL SKINNER (*Jamestown Community College, Jamestown, NY 14702*) LEN SLATEST (*Brookhaven National Laboratory, Upton, NY 11973*). For first year Anatomy/Physiology students, the visualization of various organs and body systems can be a bit daunting. This project was designed to combat that problem. Being the first in a long string of organs this model of the heart was designed to give students a working visual knowledge of the heart. The movie starts outside the heart and shows all of the major parts of the heart in their relative positions. The movie then takes the viewer inside the heart. The inside is the part that will be the most helpful for the students, because the best they will ever see if they are lucky are cadavers and drawings. By the end of the movie those viewing this movie will have seen not only the major parts of the movie, but they will also have had a first hand experience with watching the heart beat with the proper timing of the valves. This movie was also put into a stereo version, which will greatly enhance the viewing experience. The movie was created in the 3D design and rendering program, Maya. Each part of the heart was created as a separate object, which allowed easy manipulation of the parts to get them into the right proportions to each other. The overall movie is actually composed of several smaller movies that were combine with video editing software to give the impression of one voyage through the heart. As stated above the next step is to use some of the same techniques to create various other body parts and organs. The overall long-term goal is to have a flythrough video of every system in the human body.

***3D Visualization of Angle, Frequency, and Imaginary Impedance in AC Circuits.** ANTHONY SCALI (*Alfred State College, Alfred, NY 14802*) MIKE MCGUGIN (*Brookhaven National Laboratory, Upton, NY 11973*). For most up-coming electrical engineers the understanding of alternating current (AC) circuits isn't that easy when you consider it is based one factor of frequency that will change the imaginary power/resistance in the given circuit, and that there is a angle between the voltage and current is a bit hard to understand from just crunching numbers and accepting some things to just be true. To solve this problem I will create a virtual control panel in visual basic that will allow the input of arbitrary AC component values (inductor, capacitor, and resistor and input frequency, w) which are then mathematically computed to give the power factor the angle and the current in the

circuit, it will then output a text file that can be imported into Maple (a computer program) which will be plotted in 3D imaginary impedance, frequency, and angle $Z(\omega)$ which can be directly projected as a 3D stereo object in the Alfred 3D Viz Theatre.

***A Simplified Approach to Stereoscopic Imaging of Tomographic Reconstructions in Transmission Electron Microscopy.** LAURA DEPOULI, MICHAEL LAMB, ROMAN ZRAZHEVSKIY (Nassau Community College, Garden City, NY 11530) ROBERT BENNETT (Brookhaven National Laboratory, Upton, NY 11973). In biological applications, transmission electron microscopy (TEM) enables an investigator to view a specimen at the molecular level, offering a resolving power of $\sim 0.2\text{nm}$. The two-dimensional (2-D) micrographs captured using the TEM are grayscale images in which contrast is typically achieved using heavy metal stains that limit electron transmission with respect to specimen density. In order to ascertain an adequate understanding of the structure and function of biological systems, it is important to view these structures in three dimensions (3-D), as they appear in life. Currently, there is a myriad of protocols that use various software applications for creating tomographic volumes. Moreover, the lack of a uniform approach often makes the process difficult to replicate for those with limited resources. A simple, consistent method for generating tomographic volumes of TEM micrographs to be viewed stereoscopically was investigated. Sections ranging from $\sim 60\text{-}100\text{nm}$ in thickness were collected on formvar-coated copper grids. Samples were viewed using a Philips EM300 TEM with a side-mounted goniometer stage, and images were captured with an integrated Gatan ES500W CCD camera. Common to many laboratories working with limited budgets, various challenges are faced during data acquisition and processing. Physical limitations of the goniometer have restricted datasets to a 45 degree maximum rotation in either direction about the horizontal axis. A tilt image series was digitally captured from -45 to $+45$ degrees in 1 or 2 degree increments and reconstructed into tomograms and rendered using Stanford University's EM3D software. Finally, stereoscopic visualizations of the rendered three-dimensional volumes were generated through the creation of movies that were viewed using the software application StereoMovie Maker.

***A Stereoscopic Model of a Theoretical Einstein-Rosen Bridge, i.e., Wormhole, as part of an Expedition to a Black Hole at the Center of a Supernova Remnant.** TAISSIA CARDO (Suffolk County Community College, Selden, NY 11794) DAVE STAMPF (Brookhaven National Laboratory, Upton, NY 11973). A representation of an Einstein-Rosen bridge in three dimensional space has the potential to provide the scientific community with a new educational learning tool. Maya™, a computer program designed to create three dimensional (3-D) renderings, was used to design Non-Uniform Rational B-Spline (NURBS) objects to construct a scaled version of a wormhole. Steady research shows that wormholes are created from two connected singularities, points with infinite densities, from within black holes. The tunnel is theoretically smaller than an atom and stays open for merely a fraction of a second. Kip Thorne suggested that it would be possible to travel through time if one could complete the course through a wormhole intact. Considering such theories, a scaled tunnel-like wormhole was constructed. Using the capabilities of Maya™ all breaks, tears, and/or misalignments throughout the structure were disencumbered. The resulting wormhole has arched curves with no visible attached pieces. This 3-D representation has the potential to aid the inquisitive mind of students and scientists alike in uncovering the mysteries the universe has to offer.

Adaptively Improving Long Distance Network Transfers with Logistics. DAVID LABISSONIERE (East Tennessee State University, Johnson City, TN 37614) KENNETH ROCHE (Oak Ridge National Laboratory, Oak Ridge, TN 37831). The congestion control mechanisms in the Transmission Control Protocol (TCP) severely limit the bandwidth achieved by long distance data transfers. However, it is regularly necessary to move data over great distances across the Internet. The throughput of such transfers can be improved by applying the logistical technique of breaking a single long distance transfer into multiple shorter transfers. This technique can result in significantly improved throughput while still working with the TCP congestion controls and not attempting to circumvent them. We have developed an algorithm that uses this technique to traverse the network path that approximates the best available bandwidth while the data is in flight. The algorithm couples graph techniques with real-time latency and bandwidth measurements to adaptively respond to network dynamics. The algorithm shows improvements in speed and flexibility over standard data transfer methods such as FTP. Future work includes algorithmic improvements to better predict and model network bandwidths as well

as a demonstration of the algorithm as the data transfer mechanism for a production-scale grid computation.

Adding Forward and Reverse Mode Differentiation Tools to Neos. RACHEL SISTERSON (University of Illinois, Champaign-Urbana, IL 61820) PAUL HOVLAND (Argonne National Laboratory, Argonne, IL 60439). NEOS (Network-Enabled Optimization Server) has optimization solvers that provide function and/or gradient evaluations. This is offered freely to the public and achieved with the help of automatic differentiation (AD) tools. ADIC (Automatic Differentiation in C) and Tapenade are two types of AD tools. NEOS has the ability to have more solvers and AD tools added. A NEOS solver finds an x that minimizes $f(x)$ for a user-defined function and the AD tool finds the derivatives of the user-defined function that are used by the solver algorithms for optimization. Tapenade and a newer version of ADIC were to be made available on NEOS through the BLMVM (Bound-Constrained Minimization Limited-Memory Variable-Metric Algorithm) solver. In order to add these AD tools, BLMVM's drivers, Makefiles, and XML (EXtensible Markup Language) file had to be modified. Both AD tools have to be added as an option in the XML file and pathways to the AD tools homes, libraries, and environmental variables needed to be defined within the drivers and Makefile. Future steps might be to have the ADIC upgrade and Tapenade available on solvers other than BLMVM on NEOS.

An Evaluation of Vista Performance on Current Windows Computer Systems. JAMES ARRIAGA (Big Bend Community College, Moses Lake, WA 98823) CHARLIE VERBOOM (Lawrence Berkeley National Laboratory, Berkeley, CA 94720). With the impending release of Windows Vista in January 2007, the Information Technology Division at Lawrence Berkeley Laboratory is faced with a decision involving the future transition of computers from the Windows XP operating system to the Windows Vista operating system. Research involved a review of benchmarking tools, the selection of a standard set of tests, and the application of those tests to workstation hardware in use at Berkeley Laboratory. To evaluate the impact of installing the new operating system, performance benchmarks were run on 3 desktop systems with both a standard configuration and with selected hardware upgrades. This provided a comparative analysis to determine the effects of Vista with the Authentic, Energetic, Reflective, and Open (AERO) graphical user interface and how it will react on hardware specifications as determined by Microsoft on systems commonly used at Berkeley Laboratory. The new enhanced user interface built into Vista requires more powerful hardware resources than current computers running XP can handle. The comparison of the minimum and recommended requirements for computer hardware with the Vista operating system installed indicated that legacy systems were more likely to be replaced than upgraded. Computers manufactured within the last 2 years that meet the published guidelines should run Vista with or without the AERO interface.

Automatic Detection of CRISPR Elements. KYNDALL BROWN, MICHAEL LOWE (Jackson State University, Jackson, MS 39217) NIKOS KYRPIDES (Lawrence Berkeley National Laboratory, Berkeley, CA 94720). Due to the growing interest and importance of CRISPR elements in the scientific community, there was a desire for devices that would speedily and efficiently detect CRISPRs. Initially their detection relied on tandem repeat finding tools such as PatScan, Piler, and Reputer. Unfortunately, this process required hours of manual post processing due to the software being inaccurate in distinguishing CRISPR elements. To solve this problem, the research team at the Lawrence Berkeley National Laboratory (LBNL) created a CRISPR Recognition Tool (CRT), to fast and efficiently detect CRISPR loci. CRT was implemented in Java, an object-oriented programming language. This algorithm used Boyer-Moore searching and skips techniques in locating CRISPRs. The program starts by scanning for a small region of bases that appear within the searchwindow. Assuming that the pattern is part of a CRISPR, it will appear within a range that is relative to the size of the spacer and repeat. Once the range is determined, the program searches for the pattern using Boyer-Moore and the skip method. Once the match is found, and the full repeat length is determined, it is deemed a CRISPR candidate. The program then passes the candidate through three filters with the user specified parameters. Once the candidate passes all requirements it is confirmed as a CRISPR, and the program repeats the process until all CRISPR elements are found. To determine the effectiveness of CRT, its speed and accuracy was tested against PatScan and PilerCR. As a result, the tests proved CRT to be the fastest and most accurate of the three tools. In conclusion, the algorithm efficiently detected CRISPR elements and will be a useful tool in the scientific community.

Automatic Semantic Inference and Extraction of Textual Information from Internet Resources. PHILLIP MARTIN (Clemson University, Clemson, SC 29634) THOMAS E. POTOK (Oak Ridge National Laboratory, Oak Ridge, TN 37831). The Internet is one of the largest available public collections of data. Current methods of extracting the Internet's copious amount of data by hand in a timely manner have proved inadequate. To make the untapped resources of the World Wide Web (www) more readily accessible, it is necessary to automate the data extraction of several different formats. Hyper Text Markup Language (HTML) is the most prevalent data format for the World Wide Web. However, HTML is designed for the visual presentation of data on a website and thus includes little, if any, semantic information. The Resource Description Framework (RDF) developed by the World Wide Web Consortium provides a common format that enables a user to represent low-level semantic information and structure. In addition, the Internet contains several other data formats including documents generated using Microsoft Office and Adobe PDF. The challenge is to gather HTML encoded documents and generate basic semantic data using the RDF format and to expand automatic data extraction to include other formats. To address this challenge, an RDF document is automatically generated from the basic syntax derived from an HTML document. This allows the inference of some basic semantic information from any ordinary HTML file. Text extraction is further expanded to include both Microsoft Word documents and Adobe PDFs. The results demonstrate how the methods described above can provide a broader and more robust basis for automatically gathering information from the internet.

Collection and Interpretation of Teragrid Usage Statistics. JEFFREY LEHEW (Milwaukee School of Engineering, Milwaukee, WI 53201) DANE SKOW (Argonne National Laboratory, Argonne, IL 60439). The TeraGrid network, a multi-facility parallel computing resource allows researchers to answer important questions that require large amounts of computing power. The TeraGrid is relatively new, and coherent collections of data on its usage are scarce. The goal of this project is to create tools to view and interpret existing data sources to allow developers to improve the TeraGrid infrastructure. To solve these problems, two different types of receivers were setup. One receiver was setup on a TeraGrid machine to listen for and store UDP (user datagram protocol) packets sent at the completion of activities using Globus software tools such as GridFTP and GRAM (Globus Resource Allocation Manager). In addition, a second packet receiver was started on the Juniper routers that make up the backbone of the TeraGrid network. These receivers sampled the data flow through the network, and once recorded, the data was sorted and output using the Flow-Tools toolkit. The data from these receivers was presented in a graphical format using Gnuplot, a graphing application. The uniqueness of this project is in combining these various tools to create an easily understandable metric of TeraGrid usage from a large set of unorganized data. This study is part of a larger project, and the tools developed at this stage will be integrated into a long-term study of TeraGrid usage. Future work will involve completing testing of these receivers, making some changes in the way graphical data is presented, and presenting this information in the form of a webpage.

Componentizing NetPIPE and Interfacing With GAMESS. RICHARD WANG (Carnegie Mellon University, Pittsburgh, PA 15213) MASHA SOSONKINA (Ames Laboratory, Ames, IA 50011). Common Component Architecture (CCA) allows programs written in different languages and having different interfaces to interoperate with minimal effort. As a result, complex applications with enhanced functionalities may be constructed, so that they run more efficiently and readily facilitate scientific progress. NetPIPE and GAMESS, developed at Iowa State University and Ames Laboratory, have been used to demonstrate this outcome when brought together by CCA. GAMESS is a scientific application that can be used to solve a variety of quantum chemistry computations. NetPIPE is a network evaluation program that sends messages back and forth between two a network nodes. A NetPIPE component has been created and connected with GAMESS components using a CCA framework to provide GAMESS with the knowledge of network resources availability. First, NetPIPE analyzes the current network state and checks whether it is in line with the full capacity for the given network. Second, NetPIPE's findings, GAMESS configures its communication protocols. The aim is to show that GAMESS will run more efficiently when tuned to network conditions as analyzed by NetPIPE in the preprocessing stage. In general, experiments underscore the premise of the component design that scientific applications can execute more efficiently and tackle more complex problems when implemented as components and interconnected within a component framework.

***Components for a General Purpose FPGA Implementation of Template Matching Normalized Cross-Correlation.** TIMOTHY CHAGNON (Wake Technical Community College, Raleigh, NC 27603) KEN PERRINE (Pacific Northwest National Laboratory, Richland, WA 99352). Template matching normalized cross-correlation (NCC) is a fundamental, but computationally intensive method of feature detection used in applications such as computer vision, optical character recognition, and video data extraction. An implementation of this algorithm exploiting the configurable logic, high throughput, and parallel paths available in a Field Programmable Gate Array (FPGA) is desirable for use as a PC co-processor. Compared to software development however, the design of an FPGA configuration is a time consuming and expensive process. This paper outlines parts of an FPGA implementation which were designed using mature algorithms and basic parallelism as a readily accessible tool for fast software prototyping or specific optimization. The NCC design uses the optimized multipliers and BlockRAM on a Xilinx Virtex-II device to accumulate the correlation and normalization factors for a single template placement within the image to be searched. Fixed point non-restoring square-root and division blocks are then applied to yield the normalized cross-correlation value for that template placement. High speed external ZBT SSRAM (zero bus turnaround synchronous static random access memory) and demand mode DMA (direct memory access) are used to transfer image data from the host PC. As-is, the design components can be used as building blocks for continuing work on implementations of the NCC algorithm which operate over the whole search domain. Further work to expand upon the design with coarse-grained parallelism is suggested for an application to fully utilize the FPGA hardware. The use of algorithms other than NCC, and the use of constant multiplier blocks as templates are also interesting avenues of research that could be pursued.

Content Analysis of Newswire Articles. TENISHA BARNES, SAMUEL MITCHUM (Norfolk State University, Norfolk, VA 23503) ANTONIO SANFILIPPO (Pacific Northwest National Laboratory, Richland, WA 99352). Information extraction research aims at developing tools for pattern recognition with a minimum human intervention. In order to develop a semi-supervised system, a classification approach was developed in which the cosine measure was augmented with knowledge from WordNet to provide a better matching criterion to recognize target pattern in a data sets with reference to a small set of seed patterns. The automated system was built using Java within Eclipse for programming, Connexor for parsing, Cicero Lite and LingPipe for name entity recognition. To test the system, a corpus on management succession from the sixth message understanding conference (MUC-6) was used. The results of precision, recall, and F-measure showed that the modified cosine measure provided acceptable results, but didn't perform as well as previous approaches that used WordNet to compute semantic similarity. The package offered in this study can be improved to build a system generic enough to be applied as a text mining tool in a variety of domains.

***Creating Three Dimensional Stereoscopic Animations of Organic Chemical Reactions through PYMOL for Enhanced Visualization of Reaction Mechanisms.** MARIA MATEO (Bergen Community College, Paramus, NJ 07652) ROB BENNETT (Brookhaven National Laboratory, Upton, NY 11973). Three dimensional stereoscopic animation of organic chemical reactions is an effective means for illustrating bond associations and conformational changes that would otherwise be difficult to visualize if represented as two dimensional images. Executing chemical reaction modeling requires the use of various computer programs and programming languages. The main foundation of this project is a chemical calculation program called MOPAC (Molecular Orbital Package) which estimates both the best structure and minimum energy of a molecule or a small reaction given an initial presumption on the molecular structure or reaction path. The information is input as a z-matrix which, after being calculated by MOPAC, outputs an array of digital information that is lengthy and complex. However, the Centre for Molecular and Biomolecular Informatics (CMBI) at Radboud University Nijmegen in the Netherlands created a website, called Mol4D, that presents the MOPAC data within a friendlier, GUI-based (graphical user interface) environment. This website provides the output data that are needed to create the stereoscopic version of the animation. PyMOL, a molecular modeling program, is used to animate the chemical reaction in quad-buffered stereo, which is the type of stereographic setting that is compatible with the 3D projector being used for this project. Because PyMOL functions mostly by command scripts, which can be very tedious to learn, a combination of C++ and Python was used to program a plug-in for PyMOL that, when prompted by the user, imports the correct output file from the MOPAC calculations, separates that

file into distinct movie frames, creates the overall movie script and runs it through the PyMOL viewer, and transmits the final animation in quad-buffered stereo. The intention behind creating a more user-friendly adaptation of PyMOL and using it in conjunction with the Mol4D website is so that the final outcome can be used as a valuable teaching tool for chemistry, specifically organic chemistry. The 3D stereoscopic projection of the desired reaction can help a student vividly see the discrete conformational changes that occur within an organic reaction, and thereby give the student a better understanding of the mechanism of that reaction.

Creation of Computerized Datasheets for Use in Calibrations.

RACHEL KELLER (*Hartwick College, Oneonta, NY 13820*) **PAUL ZAHRA** (*Brookhaven National Laboratory, Upton, NY 11973*). At Brookhaven National Lab (BNL) the procedures used in the Radiological Control Calibration and Instrumentation Group (Rad Con C&I Group) to guide the calibration of radiological equipment cover an entire class of instruments. These procedures provide the guidelines by which an instrument is deemed fit for use; however, the usefulness of these procedures is limited by the knowledge of the technician concerning what needs to be done and what options provided are not applicable for the unit. In addition, many paper data collection forms are used throughout the course of a single instrument calibration, making the procedure for data entry into the computer and managing the hard copy collection of results difficult and cumbersome. Using the upper level general procedures already in place as well as information from the technical manuals for the instruments undergoing revision, new, specific instructions and collections forms are being formulated. Sources that were useful in the work so far to create a computerized calibration included the manual for the Manual Met/Cal program, and the upper level procedures already created by the Rad Con C&I Group at BNL. The program Manual Met/Cal aids in the creation of computerized datasheets with accompanying instructions that match the data fields' contents. These companion pieces not only tell the technicians what to do, but also where on the forms to enter the data they have collected. Since the datasheets can be printed out to be used away from a computer terminal, the data forms will now be in the same format as the computerized version, thereby making the data entry process easier. When the data entry is complete and the sheet is saved, a standardized report form has now been created to be printed out, providing a hard copy detailing the instrument specifics, the information collected, and the status of the instrument. This is a small portion of a larger project to bring the procedures and data collection systems for calibrations up to date.

Data Encryption for Windows PC's. **BRICE LUCERO** (*Big Bend Community College, Moses Lake, WA 98837*) **CHARLIE VERBOOM** (*Lawrence Berkeley National Laboratory, Berkeley, CA 94720*). In today's society the use of mobile technology is becoming increasingly popular. The demand for the ability to secure sensitive data in a safe and easy manner on Windows operating systems is growing with the use of mobile technology. This project involved an analysis of present and future methods for data encryption for Windows operating systems: XP and the soon to be released Vista operating system. The project scope included Encryption File System (EFS) in Vista and XP along with BitLocker, a new feature that will be included in Vista. In addition two third party programs, Safe Disk and True Crypt, were reviewed. Tests were run in order to measure the time each method took to encrypt as well as the impact they had on data transfer performance. Ease of use, data recovery methods and known vulnerabilities were also taken into consideration during the review. It was determined that Windows EFS and BitLocker were effective, easy to use methods for data encryption and have reliable recovery methods when managed through a domain. Safe Disk is protected by one centralized password and has an interface that was easy to learn but offered no recovery method. It is not a recommended method. True Crypt had limited options available for data recovery and a choice of password or key files for authentication. The interface was slightly more complicated than Safe Disk and the native Windows encryption methods. True Crypt is still a recommended method for data encryption.

Database and Application Design for Integrating RFID Tracking Methods Into the Commercial Supply Chain Process for Radioactive Medical Isotopes. **JAMES HICE** (*Albion College, Albion, MI 49224*) **DAVID RESSEGUIE** (*Oak Ridge National Laboratory, Oak Ridge, TN 37831*). Current methods of tracking use line of sight bar codes which encode a number, the package's carrier tracking number, to identify each package. Each package is tracked from when the package is shipped at a carrier through final delivery. Progress of the package is marked when the bar code is manually scanned at each of the carrier's facilities and when the delivery is made. Tracking

packages containing radioactive medical isotopes and other sensitive materials beyond the standard shipping routes and carrier facilities is becoming increasingly important. A test for tracking sensitive packages using Radio Frequency Identification (RFID) tags has been created to allow sensitive package tracking without requiring manual, line of sight scanning. These RFID tags transmit a unique identification number and will be placed inside packages on each radioactive medical isotope container. Shippers register each package using a web application which inserts the information into a database. RFID readers set up at the shippers', carriers' and recipients' facilities read the packages as they pass within range and update the database with the RFID identification number, time, and location. No web application or database existed for these tests, so extensive work was done to design and create the database structure and required application. A relational database design was used to store the package, RFID, and carrier provided tracking data. The web application, which serves as the shippers' interface for inserting and managing information in the database, consists of multiple Java Server Pages. The main considerations in creating the web application's design were ease of use for shippers as well as capturing and managing the necessary data for packages of interest. Future applications will use the database information to display package information, geographic location, and compare tracking methods. Further work can be done to display the web application more dynamically, providing real-time updates from the database. The web application and database can also be used for continued tracking of shipments beyond this test, including general, non-sensitive RFID package tracking.

Design of Plotting Utilities for the Collider-Accelerator Department.

DAVID KATZ (*Alfred State College, Alfred, NY 14802*) **SETH NEMESURE** (*Brookhaven National Laboratory, Upton, NY 11973*). The Collider-Accelerator Department at Brookhaven National Laboratory has developed a mature set of C++ utilities for analyzing data. The purpose of this project is to provide a set of similar tools written in Java that allows both developers and users a similar set of functionality. The feature set that has been provided to date includes a set of curve fitting utilities, the ability to cut, paste, load, and save data sets from plots, and a flexible way to add text to any plot. There are two commercial packages being used for the development of the plotting utilities. One is a math package created by Dr. Michael Thomas Flanagan of University College London and the other is called JClass, which is a plotting package created by Quest Software. The curve fitting feature uses both of the packages to allow the user to perform essential curve fits on raw data collected. Gaussian, Gaussian with an offset, Exponential, Exponential with an offset, Polynomial, and Double Exponential are among the fitting functions supported. After the fits were coded there was extensive stress testing to determine how well each fit performs on raw data. In addition to curve fitting the Java package that has been developed provides a means for the user to open saved plots created in the existing C++ software. There is also a feature that allows the user to copy and then paste a plot onto two independent y-axis setups with different scales. Labels can also be added to the plots with a variety of looks and styles which the user can customize to their preference. The Java package has a similar graphical user interface setup as the existing C++ utilities so essentially there is no learning curve for developers and users. This package will be used at the Collider-Accelerator Department to potentially make critical decisions on the raw data collected.

Designing a Mobile Application for Purification Database Systems.

PAMILA NELSON, RAKEYA SMITH (*Governors State University, University Park, IL 60466*) **DR. ANDRZEJ JOACHIMIAK** (*Argonne National Laboratory, Argonne, IL 60439*). The Midwest Center for Structural Genomics at Argonne National Laboratory develops and optimizes integrated methods for determination of protein structures through x-ray crystallography. Scientists at the center traditionally have written down their experimental results on paper, later returning to their desktop computer to enter the data on a Web page. The objective of this project was to design and develop a personal digital assistant (PDA) exhibiting the same functionality as the Web page but providing much greater convenience and accuracy. The PDA application was developed by using Microsoft .NET technology. Specifically, user interfaces were developed with Mobile ASP.NET forms, HTML, and JavaScript. The scientific logics were implemented with C# programming language. Like the Web page, the PDA application uses Oracle 9i database for data storage. With the PDA, however, scientists can scan bar-coded purification instruments and enter the experimental values directly, updating the database in real time and comparing values with prerecorded information about volume, temperature, and concentration ranges for proteins. The PDA thus increases the

efficiency of data collection and analysis and minimizes the errors inherent in transposing data from paper to computer. In order to assist the scientists, an online user manual was also developed as part of this project. The PDA application is now available for use at Argonne. This application enables scientists to access and modify the data, in the lab or almost anywhere, while preserving the sophistication of the Web application. Moreover, the PDA provides an important step toward automation of biochemical laboratory and integration with databases.

Developing Domain Specific Ontology to Define Relational Data Flow Process Modeling. DANIELLE EVANS (*Big Bend Community College, Moses Lake, WA 99357*) MITCH PELTON (*Pacific Northwest National Laboratory, Richland, WA 99352*). The Framework for Risk Analysis in a Multimedia Environmental System (FRAMES) is a platform which allows a user to develop and simulate an ontology for a specific domain. Modules in FRAMES use a relational data structure to simulate real world processes. Each module maintains a set of ontological dictionaries, called a connection scheme. This allows FRAMES to connect modules by what they consume and produce. FRAMES has two types of dictionaries developed for data flow process modeling module input and boundary condition. Module input dictionary contains module specific information that is usually supplied by the user. The boundary condition dictionaries are the relational (ontological) data that flows between modules in FRAMES. To aid in the development of the ontological boundary condition dictionaries four categories of dictionaries were developed and used for this example ontology, they are 'selection', 'feature', 'property', and 'series' dictionaries. Selection dictionaries define the focus of the simulation. Feature dictionaries define the where conditions and are made up of geographical points, polygons and lines. Property dictionaries are the static data for models and consist of the names of variables. Series dictionaries consist of the analog signal output for a simulation. These categories helped in the management of data within a relational data flow process model. Both the dictionaries and variables for this ontology follow a domain specific naming convention. Dictionaries contain the metadata of a domain specific ontology. Ontologies represent the particular meanings of terms as they apply to a specific domain. This paper will attempt to examine an ontology developed for an environmental fate and transport modeling domain in FRAMES and make some generalizations that may aid in the development of other domain specific ontologies.

Development of 3D Stereo Visualization Tool for Teaching Introductory and Organic Chemistry Courses. JUNG MIN RYU (*Bergen Community College, Paramus, NJ 07652*) ROBERT E. BENNETT (*Brookhaven National Laboratory, Upton, NY 11973*). Substitution Nucleophilic Bimolecular (SN₂) reactions require a nucleophile to collide with an electropositive atom with an attached leaving group. Visualizing the physical displacement of molecular components in such a reaction is a key to understanding the chemistry involved. Traditional methods have relied on standard print illustrations that can directly represent any two dimensions (X-Y, X-Z or Y-Z), but which must then imply the third dimension (3-D) using a set of standard, but arbitrary symbols. There are now online and open-source software tools that make 3-D stereographic representations of such reactions possible; however, feature sets vary, user interfaces are generally clumsy and interoperability among packages is limited. This project created a tool which integrates the capabilities of a web-based visualization resource (Mol4D) and an open-source visualization product (PyMOL). Our goal has been to produce a user interface that makes the tool appropriate and effective for use in the classroom. The Mol4D (Molecules in Four Dimensions) website provides a graphical user interface that displays 3D structures and animations using a plug-in or a Java applet. One component on the web site, MOPAC (Molecular Orbital PACKage), calculates orbital energies, electron densities and molecular structure numbers, bond lengths and angles. Our group extended the capabilities of MOPAC by converting the data it generates into a format suitable for use with an open-source visualization product, PyMOL. PyMOL, which employs an embedded Python interpreter and generates high-quality molecular graphics images and animations, is not user-friendly since its functions are command scripts. Using C++ and Python, we have created a user-friendly plug-in for PyMOL that accepts converted MOPAC data files from Mol4D, separates it into frames, prompts the user to indicate bond connectivity, generates a movie script, and then outputs the final animation to the PyMOL viewing screen.

Development of a Web-Based Report Tool for User Queries Made of the Integrated Relational Model of Installed Systems (IRMIS) Control System Database at the Advanced Photon Source Accelerator. DAWN CLEMONS (*Purdue University-Calumet, Hammond, IN 46321*) DEBBY QUOCK (*Argonne National Laboratory,*

Argonne, IL 60439). The Advanced Photon Source (APS) accelerator is run by a complex and specialized control system. IRMIS, a descriptive control system relational database application, allows accelerator operations to be more easily monitored and maintained. Several IRMIS viewers (user interfaces for querying the database) present information in ways that are comprehensible and useful to those who support the accelerator. However, lacking in the viewers was the mobility of their results separate from the web interface; thus, a reporting tool was necessitated. The main achievement of this project is to provide a means for easily saving queried results. Results can be saved as text files, comma-separated (CSV) files, or viewed as printer-friendly HTML pages. Methods of software architecture were employed, as well as code qualities useful to it, such as adaptability, readability, and appropriate documentation. Because the report tool was to be adapted to an established database project, the tool required an interface design that merged with one already existing, and the code needed to be integrated into hierarchically structured viewer source code. Resources included the languages PHP 4, HTML, and JavaScript; the Zend scripting engine; and the Apache web server. The IRMIS report tool aids with APS control system troubleshooting and diagnostics. It also is a step towards providing a unified PHP viewer framework. Because the tool adds to the descriptiveness of IRMIS, it also lends itself to a desired future prescriptiveness of the database.

Enhancing Javapeño. AARON FLECKENSTEIN (*Western Michigan University, Kalamazoo, MI 49093*) DR. BRADLEY T. REARDEN (*Oak Ridge National Laboratory, Oak Ridge, TN 37831*). Javapeño is a Java-based data visualization package that is part of Oak Ridge National Laboratory's SCALE software suite. Javapeño provides a graphical interface that allows the user to visualize data in customizable plots. Javapeño was created by Dr. Bradley Rearden in 2001 as a port from plotting software called SenPlot. Originally supporting only sensitivity data from the TSUNAMI modules of SCALE, Javapeño has been improved to support additional data types. Currently, Javapeño enables visualization of data generated from SCALE modules: TSUNAMI, SMORES, KMART, and XSDRN-PM, as well as a generic 2D data type. Sponsors of SCALE development have requested that Javapeño be expanded to support visualizing neutron and gamma cross-section data in the AMPX format and cross-section-covariance data in the COVERX format. For this project these new data types required adding three dimensional (3D) plotting capabilities to Javapeño. To maintain cross-platform compatibility Javapeño's 3D plotting engine uses the OpenGL version of Java 3D, an open source Java extension. Javapeño's 3D engine is an extensively modified version of FreeHEP's Lego Plot application. After developing the 3D engine, support was added for the COVERX data type. There were conflicts with the existing methods implemented in Javapeño and the way Java handles Java 3D objects. Java 3D objects are treated as heavy-weight objects, while the rest of Javapeño is light-weight. In Java, heavy-weight objects are always placed on top of light-weight objects, even when they are not active. Thus, unless modified, the new 3D plotting capability would prevent using the existing 2D plotting capabilities of Javapeño. To address this conflict, a new interface and window manager was created. Planned future enhancements include support for AMPX data files, saving plots, and configuration files.

Information System Comprised of Oncological Data Pertaining to Methylation in Ovarian Carcinoma. WALTER LEWIS (*Cheyney University of Pennsylvania, Cheyney, PA 19319*) SEAN MCCORKLE (*Brookhaven National Laboratory, Upton, NY 11973*). Over the past decade DNA sequencing technology has vastly improved and become more affordable. Consequently DNA and protein sequencing databases have grown exponentially, and the annotation of the human genome has increased immensely. Currently existing oncological databases are sparse forcing the researcher to manually search through scores of biomedical journals and related websites. The project attempts to address this issue by creating a smaller scale information system, one that will perfectly suit the needs of cancer-methylation researchers. The system consists of three major components: data collection, the Postgresql server, and the Java user interface. The Postgresql server was first established, then data was gathered and filtered. Once the data was stored in the Postgresql server the user interface was created. This interface acts as a bridge between the biologist and the Postgresql database, allowing non-programmers to perform many of the same Postgresql search commands without knowing the language. The result is a net-based database that will aid in the research involving the methylation of CpG islands in promoter regions of genes particular to ovarian carcinoma. Via a number of sources favored by the oncological community, the database embodies a plethora of relevant data such as the gene identifiers, chromosomal position, CpG island methylation,

relevant oncological information, and hyperlinks to abstracts from related oncological studies. Data gathered in the tables can be correlated with other preexisting tables by simple queries performed by the user. While the stored data is particular enough to be very helpful to this project, it is not limited to just ovarian oncology. The database has already provided useful information for an unrelated P53 radiation damage study, proving the system can be easily augmented to assist other oncological research.

Integrating mpiP and Eclipse. JOSEPH LAMBERT (*Bucknell University, Lewisburg, PA 17837*) JEFFREY VETTER (*Oak Ridge National Laboratory, Oak Ridge, TN 37831*). Programmer productivity and efficiency have always been an important issue in software development. Current productivity levels could be improved considerably using tools developed with productivity in mind. Integrated Development Environments (IDEs) provide a solution for improving productivity by integrating editor, debugger, and compiler into one interface, usually a Graphical User Interface (GUI). Eclipse is one of the most popular IDEs today for many reasons, including the significant project management capabilities, syntax highlighting, and because of its design, powerful user-designed plug-ins. IDEs such as Eclipse are increasingly popular, and IDEs that can handle a wide variety of software development requirements are needed, including support for parallel computing. Traditional IDEs, including Eclipse, do not take into account the functionality needed for communication between tasks in a parallel program. One especially popular approach to inter-task communication is the Message Passing Interface (MPI) application programming interface, but low communication efficiency is a common hindrance that limits the performance of parallel programs including those based on MPI. To help the programmer achieve better performance in MPI programs, mpiP, a lightweight library for MPI applications, has been developed to provide the programmer with statistical information about the communication performance of MPI programs. To address part of the problem of lack of support in Eclipse for parallel programs, a plug-in was developed that integrates mpiP into the Eclipse framework. The plug-in consumes results from mpiP and displays the raw data within the Eclipse GUI to help the programmer better understand the communication performance of the program. By combining all of the necessary performance statistics within the Eclipse GUI, programmer productivity and efficiency will improve.

Logical Networks for Gene Regulatory Interaction Modeling. CHRISTOPHER LEWIS (*New Mexico State University, Las Cruces, NM 88011*) ELISSA CHESLER (*Oak Ridge National Laboratory, Oak Ridge, TN 37831*). Modeling the dynamics of gene expression levels can lead to a quantitative understanding of mechanisms in cellular processes, such as signal transduction and disease pathways. Previous studies of gene regulatory networks (GRN) have established Boolean networks as good dynamic models for GRNs. The Boolean network model regards every gene in a GRN as a binary variable whose value is a Boolean function of its regulators. In order to apply this model, continuous gene expression levels must be quantized to binary states; however, existing quantization methods discretize one gene at a time and are highly likely to miss complex interactions among genes. Furthermore, binary quantization may be insufficient to capture all interactions. To remedy these issues a novel quantization method able to capture complex interactions and a generalization of Boolean networks to multi-ary logical networks are required. The novel quantization approach creates a nonuniform grid in gene-space to encapsulate clusters of data points. Together, the grid lines form hypercubes, each representing a different state of the GRN. By using these grid lines as quantization thresholds, a logical network is constructed by finding the most statistically significant combination of regulators for every gene. Statistical significance is determined using the chi-squared test with a null hypothesis of independence between regulators and regulated genes. Quantization of several test data sets related to time course of brain gene expression following alcohol exposure have shown grid quantization to be more effective than marginal K-means clustering in capturing the true distribution and that grid quantization is effective at performing feature selection. From this quantization a statistically significant 16 node GRN was inferred. Preliminary verification of this network shows that the genes directly influenced by alcohol in the logical network are involved in pathways related to alcohol injection. The biological significance of these results is encouraging, and further refinement of these methods is merited as these methods are not specific to GRNs but applicable to any complex network. Future applications could include dynamic modeling of cerebellar development, cell response to exposure agents, and many other biological phenomena under investigation at ORNL.

Mobile Data Collection Applications: A Proof of Concept.

JONATHAN CHANG (*University of California–Berkeley, Berkeley, CA 94720*) TIM LOWE (*Lawrence Livermore National Laboratory, Livermore, CA 94550*). This project's goal is to provide a proof of concept for mobile data collection applications, and identify the best ways such applications could be implemented and used. Such an application should decrease the time and resources users now need to devote to redundant data processes, and provide an easy of locating and retrieving data at a later time. The two types of available mobile devices, Personal Digital Assistants and Tablet Personal Computers, each have their particular strengths that suggest themselves for certain types of applications. As such, parallel data collection applications have been developed, with a common web application for uploading information to the database. While these aspects have been developed and proven, it still remains to refine these applications, develop the tables to hold their data, and field-test with users for their feedback.

***Modeling a Stereoscopic Satellite as Part of a New Way to View the Fundamental Teachings of Astronomy.**

NITAI FINKELSTEIN (*Suffolk County Community College, Selden, NY 11794*) DAVE STAMPF (*Brookhaven National Laboratory, Upton, NY 11973*). Maya™, a computer software package that creates 3-Dimensional renderings of objects that a user designs, appears to be a useful tool in expressing the theories and laws utilized in Astronomy. The goal of this project was to accurately represent four astronomical scenarios using Maya's™ animations as a teaching tool. These animations were created to simulate what is believed to be occurring in astronomical phenomena. For the animations, a man made satellite was designed to travel from Earth to a super nova remnant (SNR), where it used its various instruments to study the phenomena. While traveling through the SNR, the satellite got caught by the gravitational forces of a black hole, throwing it into a wormhole. This is a theoretical tear in space-time connecting two black holes. The satellite then exited through the other end of the wormhole where it observed an explosion of a star, also known as a supernova. When studying Astronomy, it may sometimes be difficult to grasp a certain concept or fact. Teaching with the aid of 3-Dimensional (3D) animations may help students better understand what they are studying. When viewing an image of the SNR in 3D, there is depth in that image, making it easier to pinpoint and study specific parts of the SNR, something that could not be done with an ordinary 2-Dimensional image. With the modeling of the satellite using Maya™, its inner workings and how it was affected by the spatial phenomena it had encountered were able to be viewed with more ease than before. When all four scenes finished rendering, they were presented using 3-D Stereo Movie Maker. This software is used to translate videos into 3-D simulations. A special screen was needed to be used along with Stereoscopic glasses to properly view this effect. While modeling in Maya™, it was found that the animations created could be useful tools for all levels of education and scientific research. They may also be utilized as a way to interest young Americans in science and technology, furthering our hopes that our children will once again be leaders in the scientific community.

Monitoring Temperature and Fan Speed Using Ganglia and Winbond Chips.

CAITIE MCCAFFREY (*Cornell University, Ithaca, NY 14850*) YEMI ADESANYA (*Stanford Linear Accelerator Center, Stanford, CA 94025*). Effective monitoring is essential to keep a large group of machines, like the ones at Stanford Linear Accelerator Center (SLAC), up and running. SLAC currently uses Ganglia Monitoring System to observe about 2000 machines, analyzing metrics like CPU usage and I/O rate. However, metrics essential to machine hardware health, such as temperature and fan speed, are not being monitored. Many machines have a Winbond w83782d chip which monitors three temperatures, two of which come from dual CPUs, and returns the information when the sensor command is invoked. Ganglia also provides a feature, gmetric, that allows the users to monitor their own metrics and incorporate them into the monitoring system. The programming language Perl is chosen to implement a script that invokes the sensors command, extracts the temperature and fan speed information, and calls gmetric with the appropriate arguments. Two machines were used to test the script; the two CPUs on each machine run at about 65°C, which is well within the operating temperature range (The maximum safe temperature range is 77°–82°C for the Pentium III processors being used). Installing the script on all machines with a Winbond w83782d chip allows the SLAC Scientific Computing and Computing Services group to better evaluate current cooling methods.

New Algorithms for the Network Protocol Independent

Performance Evaluator. CALEB KLAPP (*Westminster College, Fulton, MO 65251*) TROY BENJERDES (*Ames Laboratory, Ames, IA 50011*). The Network Protocol Independent Performance Evaluator,

(NetPIPE) has been in development for over 5 years. As the website <http://www.scl.ameslab.gov/netpipe/> describes it, "NetPIPE is a protocol independent performance tool that visually represents the network performance under a variety of conditions. It performs simple ping-pong tests, bouncing messages of increasing size between two processes, whether across a network or within an SMP system. Message sizes are chosen at regular intervals, and with slight perturbations, to provide a complete test of the communication system." The original NetPIPE program was designed with a single-pass algorithm using exponentially increasing message sizes that exits when a time limit to transfer a message was reached. In order to improve on this design, a multi-stage algorithm was implemented. This new program uses a pan and scan method to accurately derive a representative equation for bandwidth at all message sizes. Some preliminary tests have been performed on well behaved networks where the accuracy of the program's calculations can be assessed. Comparing the experimental data with the curve generated by the program has provided strong evidence that the program produces valid performance information as well as statistical analyses of the network performance data which was not available with previous implementations.

Providing Additional Context with MapDisplay. LINDA SATO (*University of Oregon, Eugene, OR 97403*) DAVID MILLARD (*Pacific Northwest National Laboratory, Richland, WA 99352*). While an important feature of visualization and analytical tools is to give users the ability to manipulate the context in which they view their data, this functionality can normally be found to some extent in all but the most basic software tools. At the same time, the importance of having multiple representations of the data, however, can be underestimated by the designer, and its usefulness, overlooked by the user. The focus of this project was to design and implement a prototype of a map-display component for an existing software application to provide users with an alternate view of their data. To simplify the project, an existing map-based display service for the actual display was incorporated into the design. The main resource for this project was the web-based version of Operational Status Board (WebOSB). WebOSB is an application that allows users to maintain a database of information and control how that information is categorized and displayed via a spreadsheet-like interface. One existing feature of WebOSB is the ability to export a snapshot, i.e., an immediate record of the rows of a table; this was implemented as an XML document. Thus, the main goal was to create a transformation process that would transform the XML document into a format the map-display service could read; the challenge was to give users some choices in how the data was displayed, providing a very basic means of filtering their data. The solution involved creating an XML configuration file containing values defining a mapping set by the user, and using Java to parse the file and create the target display document. Currently, the software we are using for the final display is Google Earth. The addition of the MapDisplay component to WebOSB makes it possible for users to interact with their data not only in a different context, but one which is user-defined, and it is the combination of the two views that provides WebOSB users with a more complete representation of their data.

***Quality Assurance of Brookhaven National Laboratory's Accelerator Controls Division's Communications Protocols.** EDWARD D'AZZO-CAISSER (*St. Joseph's College, Patchogue, NY 11768*) DAN OTTAVIO (*Brookhaven National Laboratory, Upton, NY 11973*). The Accelerator Controls Division (ACD) manages the accelerators at Brookhaven National Laboratory (BNL). These machines, controlled by front end computers (FECs), require real-time interaction and precision to ensure the quality of retrieved information. These FECs can only be accessed remotely, using communication software (CS) which transfer information from programs to the FECs themselves. Since this software proved to be a major source of errors, we posit that targeting inconsistent behavior in program execution will reveal a variety of faults inside the CS. Traditionally, all communications testing was accomplished by visual observations and small test applications. However, using Java 2 Platform Standard Edition 5.0, we created a regression test, or suite of programs, to check the quality of ACD's Java protocols automatically. Since an exhaustive check of these protocols would result in an unfeasible amount of permutations and thus an inordinate amount of time, our regression test only interacted with higher software layers, looking for consistency and expected behavior of the CS. This is accomplished by three separate test functions: 1) a basic test to perform communication commands to a working FEC; 2) a test which communicates to a broken FEC; 3) a test which communicates to multiple FECs. The information gathered in these tests were used to locate faults within the communication software. The testing suite was finished as planned; we created the tests we intended

and we uncovered 10 faults in the CS thus far. The former system overlooked these program faults. Our new test offers a systematic way to test for inconsistencies and expedite the debugging process. We do not foresee any changes to the sweeps already in existence, and though the basic architecture will remain in tact, more automation could be implemented. The application of our regression test can help to improve the functionality of ACD's current communications software and any upgrades made to it. The regression test can also be built upon to ensure a greater versatility, ensuring its usefulness over time.

***Scientific Application of 3D Modeling and Animation Utilizing Maya to Recreate the Formation of a Supernova Remnant.** MICHAEL CASSANO, III (*Suffolk County Community College, Riverhead, NY 11954*) DAVE STAMPF (*Brookhaven National Laboratory, Upton, NY 11973*). 3-Dimensional (3D) modeling and animation software is an effective educational tool that can be used to visualize the unexplored universe. Maya™ was used to create 3D visualizations of spatial objects. When attempting to learn about an object that can't be directly observed, take all of the known data and create a visual reconstruction to aid in future studies concerning that object. When new information is acquired, simply change the attributes in Maya™ to render an updated image. A 2.20ghz workstation utilizing 1gb of 400mhz memory running Maya™ 5.0, was used to create a three dimensional visualization of a Supernova remnant (SNR). Acquisition of data was necessary to depict the relative distance that the shocked ejecta are repulsed from the core as well as the different spectrum of light the expanse shows. High and low energy x-rays define the overall expanse of the SNR. X-ray spectra are needed to show the spatially resolved spectroscopy of the ejecta. SNR1987a gave the relative symmetrical pattern that SNR exhibit. Manipulation of Maya's interface allows implementation of all data to be put into a Cartesian space to recreate a dying star. A 3D animated fly-through has demonstrated the chaos of the expelled material that forms the SNR. A 2D render has been completed to illustrate a comparison to our telescopic images of a SNR. Additionally, a 3D animated model of an SNR has demonstrated the capabilities of Maya™ to recreate this interstellar medium (ISM) for educational purposes. To expand on this experiment we could calculate the radial expanse, and visually depict the temperatures of the ejecta. Possible future studies could examine in a 3D coordinate environment, the gravitational fields that a black hole of a SNR exhibits or the effects the magnetic field has on the surrounding area of the dying star. Further examination could lead to an understanding of the affects a SNR has on surrounding star systems. This software could expedite and enhance not only the effectiveness of theoretical and experimental ideas and concepts, but also enhance learning and the effectiveness of teaching tremendously.

Shapesgui: Shapes-gui: A Graphical Front End to the Shapes Simulation Tool. JOHN DIMOND (*University of Illinois, Champaign-Urbana, IL 61820*) BOYANA NORRIS (*Argonne National Laboratory, Argonne, IL 60439*). SHAPES is a program that simulates the interaction of electromagnetic waves with twodimensional planar nano sized objects of varying composition and shape. The input for the program comes in the form of a humanreadable text file that contains all the parameters necessary to run a simulation. These parameters include particle geometries and positions, material properties, wave sources, the size and coarseness of the sampling grid, and what data should be output from the simulation. The readability of the input file makes the job of setting up and running a basic simulation relatively straightforward, but it is extremely cumbersome to input a complex simulation setup by hand. This project addressed this problem by developing an intuitive graphical program which creates the necessary input file. The SHAPES-GUI program allows the user to define the simulation domain, place objects on a grid, then resize and move them freely, as in a typical drawing application. It also provides simple dialogs that let the user set additional parameters of the simulation in a straightforward manner. This application will be expanded to create input files for the upcoming threedimensional version of SHAPES.

Simulation Environment for Digital Feedwater Control System. YURI MALITSKY (*Cornell University, Ithaca, NY 14850*) TSONG-LUN CHU (*Brookhaven National Laboratory, Upton, NY 11973*). The Digital Feedwater Control System (DFWCS) of a nuclear power plant is responsible for monitoring and controlling the flow of feedwater in the secondary coolant loops of the pressurized water reactors. This control system is also responsible for automatically responding and alerting people when something goes wrong. Because of this crucial function to the safe operation of the power plant, it is necessary to evaluate the fault tolerance of DFWCS by testing situations that can disrupt the stability of the plant and whether they will be detected and dealt with appropriately. This project created a prototype of the

simulation environment that allows the testing of the system with a virtual feedwater system (FWS) model. The system consists of two independent processes connected via network sockets. The primary process runs the original control algorithms and the second implements the input and output interface of the feedwater devices. To promote portability and modularity, the system was implemented with Java, linking to the original control algorithms through the Java Native Interface (JNI). The resulting prototype of the virtual model allows controls the input values to help identify critical situations and later the development of corresponding algorithms for analyzing the safety of the system.

SNS Beam Characterization Using Wire Scanner Analysis. BAKARI UNDEWOOD (*Tennessee State University, Nashville, TN 37209*) TED WILLIAMS (*Oak Ridge National Laboratory, Oak Ridge, TN 37831*). The Spallation Neutron Source (SNS) is the most powerful pulsed source of neutrons in the world. The SNS consists of a Linear Accelerator (Linac) that accelerates negatively charged hydrogen ions (H-) throughout the various regions of the Linac to approximately 88% of the speed of light. These regions include the Medium Energy Beam Transport (MEBT), Drift Tube Linac (DTL), Coupled Cavity Linac (CCL), Superconducting Linac (SCL), High Energy Beam Transport (HEBT), Accumulator Ring, Ring to Target Beam Transport (RTBT), and finally the Mercury (Hg) target. After the H- beam is accelerated, it is transported to the Accumulator Ring where all of the electrons in the beam are stripped off, thereby converting the beam to only protons. Once released from the Accumulator Ring, the beam then hits the Hg target and knocks out numerous neutrons from the Hg nucleus, which are used for research. Diagnostic equipment throughout the Linac provides data that are used to monitor, correct, and characterize the trajectory and shape of the beam. Some of these devices are wire scanners, which are used to measure the beam's position. Furthermore, the wire scanner data are used to set the magnetic field strengths of the quadrupole magnets; these are used to focus the beam. This is particularly important to the beam-to-target transfer process. Without correct steering, the full benefit of the beam on the target could not be achieved. Using a variety of programs, including Wireanalysis and Graphical Analysis; Gaussian and bi-Gaussian fits are calculated to measure the beam sizes. The measurements of the magnets' parameters are included in the data taken. The beam sizes and the magnets' parameters are fed into the model, and the output generated gives a plot of the sizes of the beam at various positions in the MEBT. The data is also compared on the same graph. The disparity between the two indicates how the beam changes in the MEBT. Adjustments were made to better fit the data. For example, while using wire analysis, the program was only allowed to fit the data that represented a Gaussian profile. This changed some values, but ultimately resulted in a better fit of the data. Although the beam will never be characterized without any error, there is the possibility of characterization with minimal error. Therefore, it is imperative that this research continue.

Three Dimensional Hermite Interpolation for Boundary Integral Analysis. THEODORE SAVICH (*Earlham College, Richmond, IN 47374*) LEONARD J. GRAY (*Oak Ridge National Laboratory, Oak Ridge, TN 37831*). Partial differential equations, e.g., the Laplace equation, can sometimes be transformed into integral equations on the boundary of the domain. These boundary integral equations can then be solved numerically by employing simple approximations of the boundary and boundary functions. Generally, linear (first order) polynomials have been sufficient, yielding continuous interpolations of the geometry and the boundary functions. However, for a variety of applications in heat transfer, electrostatics, and elasticity, there is interest in achieving a smoother interpolation, and this has led to the investigation of a cubic Hermite approximation. In particular, a differentiable Hermite interpolation may provide improved accuracy for moving boundary simulations wherein one would like a smooth representation of the evolving surface. Differentiability of the surface interpolation is achieved by incorporating the known normal vectors to the surface at the nodes. A differentiable interpolation for the primary function requires the function derivatives at the nodes; these are obtained by solving integral equations for the gradient of the primary function simultaneously with the original boundary integral equation for the primary function. The use of cubic elements complicates the analysis, as now the boundary integral kernels involve the square root of sixth degree rather than quadratic polynomials. As a consequence, the analytic integrations employed in the linear analysis are not immediately possible. The integrals must now be split into a non-singular piece which can be evaluated numerically and a singular piece which must be integrated analytically. The splitting for the Hermite interpolation has been developed, and test calculations on simple

problems have determined that the three-dimensional Hermite algorithm is a viable approach for determining the potential and flux in the Laplace equation. The implementation of the gradient equations is presently underway.

Upgrading the Video Crystal Centering System at the National Synchrotron Light Source. KEVIN RYAN (*State University of New York at Albany, Albany, NY 12222*) DIETER SCHNEIDER (*Brookhaven National Laboratory, Upton, NY 11973*). The National Synchrotron Light Source allows hundreds of scientists to examine the structure of biological crystals using x-ray beams and sophisticated detectors. Data collection can take hours to complete while the researcher has to adjust and recenter the crystal to ensure proper collection. Currently, an analog camera attached to the microscope lens sends video to an Axis Joint Photographic Experts Group (JPEG) engine, which inefficiently compresses the images and broadcasts them over the network. This project will install a Sony digital camera coupled to a video server, to capture high resolution images, convert them to Portable Network Graphics (PNG) format and stream them over the network. To control the camera a C program was written using the open source libdc1394 application programming interface (API) to capture the images and set camera features. From there the images will be losslessly compressed using the libpng API which was customized to output the data to a web server. This multi threaded program needs to coordinate the capture and compression precisely to create seamless image streaming from the server with only a half second delay. The advantages of using the PNG compression algorithm is the lossless compression and the existing web code for the Axis server can be reused with only slight modifications. Allowing the client to access the images through a web browser makes this project completely platform independent, eliminates the need to install unique software on the clients computer and lets us update/change the web applications functionality with ease. With this upgrade the sharper images can be more efficiently processed to provide accurate automatic crystal centering to be implemented. Completing this project will enable the researchers to collect their data more efficiently from remote locations, and the automatic centering will allow them to concentrate their attention on the important task of analyzing the data.

West Nile Virus. JOSE MARTINEZ, BRANDY SMITH (*Governors State University, University Park, IL 60466*) DR. ZHIAN LI (*Argonne National Laboratory, Argonne, IL 60439*). The West Nile is a lethal disease for which there is no helpful treatment or vaccine. The WNV has spread across the heart of the United States, causing an impact of concern among the public and federal and state public health and natural resource agencies. WNV has been involved with human deaths in the great region of the United States and has been well-known as the cause of a monstrous decline in bird populations. The swift increase of this malady and the possibility for grave medical penalty emphasizes the need to become knowledgeable of the pathways and the conditions that affect the virus's transmission. Mosquitoes become tainted when they feed on infected animals and then re-transmit the virus to other organisms during successive blood meals. In order to determine the transmission of the virus my partner and I have to study the components that are involved with the WNV. The components which are involved are the weather dynamics, mosquito population dynamics, host agent population dynamics, mosquito and host agent base habit dynamics, and human activities. The weather component which is a major process plays an important role because it affects all of the other components. Studying and gathering data of the precipitation, wind gust, soil moisture, air temperature, weather type, drought, etc. are going to help develop an input file. In the process I will study Java so the input file that I will create will be read by the compiler to help run the simulation. The weather dynamics attributes will consist of temperature, precipitation, and humidity. These attributes are spatially dispersed and temporary variables, and directly manipulate surface soil moisture, which is important in mosquito population dynamics. In developing the code for the weather dynamics which will help the researcher to simulate the transmission thereby producing a virtual laboratory to uncover the dynamics behaviors of the system as a result of the interactions among the individual components in the simulation. This code is just a small part among the interactions; research is being done to include more components like other bird species.

Windows XP (SP2) Security Settings, Windows Vista Firewall Settings and Remote Assistance. ZACHARIAH TANKO (*Big Bend Community College, Moses Lake, WA 98837*) CHARLIE VERBOOM (*Lawrence Berkeley National Laboratory, Berkeley, CA 94720*). Security is an integral part of any software deployment plans at the Lawrence Berkeley National Laboratory (Berkeley Lab). There is a template at the Berkeley Lab that contains recommended security settings for Windows

XP Professional deployment. The settings are in line with the National Institute of Standards and Technology (NSIT) recommendations. The current template is for Windows XP with service pack 1 (SP1). Most of the computers running Windows XP Professional at the Berkeley Lab have SP2 already installed. There is a need to update the Berkeley Lab's security settings template. Microsoft introduced a personal firewall as part of the operating system with Windows XP. Microsoft will soon introduce a new desktop operating system known as Microsoft Vista. In Microsoft Vista, the Windows Firewall functionality in SP2 is retained. It is important for Berkeley Lab to undertake an extensive review of the Firewall rules and settings in Microsoft Vista even before an operational version of Vista is released by Microsoft. A good understanding will make Berkeley Lab fully prepared. Remote Assistance provides a way for users to get the help they need when they run into problems with computers. It is a way for Help Desk departments to save on the cost of supporting users. The Computer Support Division at the Berkeley Lab is always looking at ways of improving user support at a reduced cost without compromising security

Engineering

A Matlab® Simulation of the Energy Recovery Linac RF Superconducting Cavity. RANDALL PLATE (*Cedarville University, Cedarville, OH 45314*) CARL SCHULTHEISS (*Brookhaven National Laboratory, Upton, NY 11973*). Linear particle accelerators (linacs) accelerate ions to near the speed of light in order to conduct experiments on particle collisions. Energy recovery linacs (ERLs) consist of both a linac radio frequency (RF) superconducting cavity and an electron ring which can be used for electron cooling. It is crucial to operate as close to the resonant frequency of this RF cavity as possible in order to maintain a proper accelerating field, but factors such as Lorentz forces and microphonics can detune the cavity. A Matlab simulation of the cavity provides the ability to analyze these affects and develop a digital control system to counteract them and retain the desired electric field gradient. A simulation of the cavities employed in Tesla, Spallation Neutron Source (SNS), and the Rare Isotope Accelerator (RIA) was analyzed and modified to be consistent with the cavity at Brookhaven's linac by changing the quality factors, resonant frequencies, and time constants of the various operating modes. This simulation and control system will be the foundation for the development of another, real-time, simulator which will be applied to the physical cavity. This paper presents the development and implementation of this simulation and discusses the implications of the results obtained.

A New GUI for Global Orbit Correction at the ALS Using MATLAB. JACOB PACHIKARA (*University of Texas at Arlington, Arlington, TX 76019*) GREGORY J. PORTMANN (*Lawrence Berkeley National Laboratory, Berkeley, CA 94720*). Orbit correction is a vital procedure at particle accelerators around the world. It is very important to have a user friendly application. The orbit correction routine currently used at the Advanced Light Source (ALS) is a bit cumbersome and this paper describes a new Graphical User Interface (GUI) developed for global orbit correction using MATLAB. The correction algorithm uses a singular value decomposition method for calculating the required corrector magnet changes for correcting the orbit. The application has been successfully tested at the ALS. The GUI display provided important information regarding the orbit including the orbit errors before and after correction, the amount of corrector magnet strength change and the standard deviation of the orbit error with respect to the number of singular values used. The use of more singular values resulted in better correction of the orbit error but at the expense of enormous corrector magnet strength changes. The results showed an inverse relationship between the peak-to-peak values of the orbit error and the number of singular values used. The plots on the GUI help the ALS physicists and operators in understanding specific behavior of the orbit. It is a convenient application to use and is a substantial improvement over the previous orbit correction routine.

Acoustic Doppler Measurement of High Speed Shearing Flow. DAVID HUBBLE (*University of Tennessee, Knoxville, TN 37916*) BRENNAN SMITH (*Oak Ridge National Laboratory, Oak Ridge, TN 37831*). The Acoustic Doppler Velocimeter (ADV) is an innovative three-dimensional flow measuring device that relates the phase shift between a transmitted acoustic signal and its reflected counterpart to fluid velocity through pulse-coherent processing. Its low cost and ruggedness make it ideal for measuring in remote locations such as rivers and tidal regions but its ability to measure high speed flow remains in question. After analyzing data from an axisymmetric jet centerline and the exit passage of a hydraulic turbine, it was determined

that an experiment was needed to improve understanding of how an ADV responds in shearing turbulent flow and to quantify the bias and errors in measurements from such flow fields. There are several problems that occur when an ADV attempts to measure shearing turbulent flow. First, due to range limitations on the speed settings, high speed flows cannot be unambiguously measured. Second, due to probe geometry, the vertical component of the velocity measurement is biased, exhibiting higher variance than the other two flow directions. To understand how an ADV reacts to shearing turbulent flow, experiments are being conducted on an axisymmetric jet at the TVA's Norris Engineering Lab. The axisymmetric jet was chosen because it creates a well understood, predictable flow field with areas of turbulence strong enough to simulate those found in a hydraulic turbine exit passage. The experimental design was determined by balancing probe resolution against the flow capacity and geometric limitations of the test flume. The geometric limitations caused concern due to the risk of boundary influence. A four inch jet was chosen. This allowed four probes to be located within the jet from 2 to 10 feet downstream with minimal flume boundary interference. There is an inherent bias in the geometry of the ADV that causes vertical measurements to contain less noise. Also, there is considerable noise at high frequencies which indicates an inability to resolve small extremely small scale turbulence. These data should help engineers decide when an ADV is appropriate for flow measurement in prototype settings.

***Addition of Wet Turbine Pod and its Related Heat Exchangers into Realistic Heavy Ion Collider Cryogenic System.** CLARENCE DZUBEY, JR. (*CUNY-Bronx Community College, Bronx, NY 10453*) TOM TALLERICO (*Brookhaven National Laboratory, Upton, NY 11973*). The Relativistic Heavy Ion Collider (RHIC) consists of two rings of super-conducting magnets to help guide and focus beams of ions during various scientific experiments. All magnets must be maintained at a temperature of 4.5 degrees Kelvin (K). The basic function of the RHIC Cryogenic System is to maintain the super-conducting magnets in the two rings of the collider at 4.5 K or below. The Cryogenics Group (CG) cycles liquid helium throughout the rings in varying amounts to keep these magnets cold at 4.5 K by removing the heat generated locally due to currents and heat leakage from its surroundings. The Cryogenic System (CS) was originally designed for the Isabelle project, another collider, which required a larger heat load (~25 kW at 3.8 K) however, it was never completed. The RHIC inherited this CS but only needs at most approximately 13 kW at 4.5 K of refrigeration power. The CG has been implementing upgrades over the last three years to achieve greater system efficiency by reducing the power usage. This year's main upgrade consisted of adding a load turbine and its associated heat exchangers that are enclosed in a cold box (CB). A turbine is an enclosed rotary engine that extracts energy from a fluid flow while a CB can be described as a low pressure vessel providing vacuum insulation for cryogenic heat exchangers, which are devices built for efficient heat transfer from one fluid to another. This upgrade would result in a 1 MW power decrease from 6 MW to 5 MW of compressor power. We worked on the planning and implementation that went into incorporating additional control and monitoring instrumentation into the existing CS for the new turbine and CB. The planning stage included engineering and design of digital and analog input and output wiring diagrams, programmable logic card diagrams, and the construction of an additional human machine interface computer screen. The implementation stage involved installation of computer racks and wiring along with analog valves, gauges and sensors.

Advanced Steam Reforming Catalysts for Generating H2 from Natural Gas. GINA FAZIO (*University of Illinois at Urbana Champaign, Urbana-Champaign, IL 61801*) DR. MAGALI FERRANDON (*Argonne National Laboratory, Argonne, IL 60439*). Reforming of natural gas at the point-of-application is one option being pursued to provide H2 for use with fuel cell systems being developed for distributed power applications. New reforming technologies will be required for these integrated fuel processor-fuel cell systems. A critical component of these fuel processors is the reforming catalyst, which promotes the conversion of the natural gas to H₂. Rhodium supported on an oxide substrate, such as alumina or ceria, is one of the most effective catalysts for reforming natural gas. Unfortunately, Rh is an expensive precious metal and, hence, the cost of a Rh based catalyst is an issue. Optimizing the Rh loading is critical to minimizing catalyst cost. The objective of this project is to investigate the effect of Rh loading on the performance of Rh supported on a lanthana-modified alumina for the steam reforming of methane, the primary component of natural gas. Three different Rh loadings were investigated: 1, 2, and 5-wt%. The catalysts were tested in a microreactor system using either a 3:1 mixture of H₂O:CH₄ or a reformate containing 1% CH₄ at 600-950°C and

gas-hourly space velocities (GHSV) of 20,000-70,000 h⁻¹. At a GHSV of 20,000 h⁻¹, similar CH₄ conversions and H₂ yields were observed for all three Rh loadings for all conditions investigated. However, at a GHSV of 60,000 h⁻¹, a significant drop-off in performance were observed with the 1 and 2-wt% but not the 5-wt% Rh catalysts.

An Investigation of the Optical Detection of Cellular Metabolic Activity. KELLY CHRISTIAN (University of Tennessee, Knoxville, TN 37996) JUSTIN BABA (Oak Ridge National Laboratory, Oak Ridge, TN 37831). The clinical challenge of preventing life-threatening vascular complications after liver and other organ transplants necessitates a means for continual post-operative monitoring for rejection, infection, and normal function assessment. Current methods, which utilize crude systemic measures such as volume of urine output and serum markers for cellular injury, are woefully insufficient. At best, these serve as indirect, time-delayed measures of tissue viability. Additionally, these techniques do not provide continuous, real-time monitoring and thus are inadequate for timely assessment that could enable life saving interventions. To address these inadequacies, the development of a device for continuous real-time tissue metabolic assessment is underway. Currently, an investigation is in progress to determine the appropriate equipment needed to produce a device that can track the ratio of two fluorescent coenzymes that are involved in cellular metabolic activity, NADH and FAD. It is anticipated that the NADH/FAD ratio will stay constant for normal function and increase considerably in the case of abnormal function. Therefore, the detection of a noticeable increase would suggest an early change in tissue viability, i.e., before irreversible organ damage occurs. Before this can be explored, an optical probe must be developed that can appropriately detect and measure the concentrations of NADH and FAD. A device was designed and tested on a spectrophotometer with several different light sources, such as a tungsten halogen, a UV fluorescent lamp, and multiple LEDs (Light-Emitting Diodes), to determine if one of the sources could detect high concentrations of the coenzymes in vitro. A model probe was also constructed, where the samples were tested with the photodiode detector. The results presented show that NADH and FAD fluorescence was visibly observed when the light sources simply illuminated the samples, however the fluorescence was unable to be detected with all but one of the light sources used. This indicates that the samples were fluorescing, but the spectrophotometer and the probe were unable to detect fluorescence due to low sensitivity in UV and near visible range. Future work must be done to determine a proper light source that can detect NADH and FAD suitably. Once the probe is complete, it must be tested for the detection of anticipated physiological concentrations in vitro and for conducting ex vivo studies using excised organs before finally proceeding to live in vivo studies.

Anemometer Standoff. NICHOLAS JOHNSON (University of Colorado at Denver, Denver, CO 80112) HAL LINK (National Renewable Energy Laboratory, Golden, CO 89401). Accurate wind speed measurements are critical in the analysis of wind turbine power performance. Common industry practice is to measure wind speed using a cup anemometer that is mounted in a position where the supporting tower distorts the measurement. It is ideal to mount the anemometer on top of the tower. Sometimes this is no practical and must be mounted on a boom, that supports it away from the tower, far enough to limit distortion errors to 1%. A theoretical model has been used to quantify where a distortion will occur with respect to the tower. However, some researchers have recently speculated that the theoretical model inaccurately predicts the distance from the tower where the 1% distortion error occurs. The objective of this project was to experimentally measure and quantify this distortion and thereby validate or disprove the model. To achieve this objective, a test was configured where one anemometer was mounted above a triangular lattice tower to measure the undistorted wind speed. On the same tower a boom-mounted anemometer was mounted below the top of the tower to measure the distorted wind speed. Data were collected by the boom-mounted anemometer at different "standoff" distances. Standoff is the ratio of the separation of the anemometer and the tower to the width of the tower. Data were sorted by wind direction in order to plot where the critical distortion occurs—when the anemometer is directly upwind of the tower. This value was reported. A second tower was requisite to quantify the vertical spacing effects between the top-mounted and the boom-mounted anemometers. This test measured distortion effects for three configurations: at a standoff of 2.31, the model predicts a distortion error of 1.6%, the test indicated 3.2%; at a standoff of 3.47, the model predicts a distortion of 0.9%, the test indicated 2.6%; at a standoff of 4.62, the model predicts a distortion of 0.6%, the test indicated 1.6%. Based on these test results, NREL has concluded that the model inaccurately predicts the distortion. To obtain accurate wind speed measurements with boom-mounted anemometers

a larger than predicted standoff is required. Results to date are limited to relatively small amount of standoff distance points, more research is needed to create an acceptable model.

Assessment of Biometrics System. KWOK WING LEE (Stony Brook University, Stony Brook, NY 11794) UPENDRA S. ROHATGI (Brookhaven National Laboratory, Upton, NY 11973). Biometric systems are used to authenticate users based on their biological characteristics such as face, voice, fingerprint, and hand geometry. This kind of identification system provides the user with logon convenience and extra protection against theft. The Russian Academy of Sciences Institute of Applied Physics is involved with the project and they are developing a software development kit (SDK), where others can use this product and create their own biometric identification system. To evaluate the quality of their product, a Biologin program was created using C++ programming and other technologies such as Microsoft Graphical Identification and Authentication Dynamic Link Library (MSGINA DLL). Communication with the Russian institute was established daily via internet, to provide them with feedback on their SDK and documentation. The goal of creating a Biologin was to determine if the SDK is useable and if the product can be sold to consumers. Product documentation is very important for a SDK but was lacking in the product and constant communication was required. Testing of the recognition system was very accurate and accounted for only a 3% error rate. It is difficult to work with another country because of language barriers and the time difference. This was a learning experience for the Russian Institute because they must develop software products that can compete with existing ones in the market.

Bipolar Plate Design and Manufacturing for Proton Exchange Membrane Fuel Cells. RACHEL BACKES (Colorado School of Mines, Golden, CO 80401) JOHN TURNER (National Renewable Energy Laboratory, Golden, CO 89401). The proton exchange membrane fuel cell (PEMFC) is the preferred candidate for future fuel cell automobiles. Metallic bipolar plates have the ability to improve this type of fuel cell. This project focuses on how stainless steel bipolar plates can be produced and designed for use in PEMFCs. The plate material considered is type 446 stainless steel. Flow patterns are designed to be stamped into the plate through application of rubber pad forming techniques. Dies are designed for the stamping process, and preliminary testing is done with substitute materials. The results of preliminary testing were successful, particularly with the softest backing material used. Seals required for implementation in a fuel cell stack are also designed. The result of this project is a set of preliminary designs for the production and use of stainless steel bipolar plates in a PEMFC.

Building an Atomic Layer Deposition (ALD) System for the Coating of Ceramic Rods. MATTHEW LEWIS (Iowa State University, Ames, IA 50013) GREGORY KRUMDICK (Argonne National Laboratory, Argonne, IL 60439). Many new types of technology are being introduced in today's world, but few of them offer a wider variety of uses than Atomic Layer Deposition (ALD). ALD makes it possible to deposit a layer of film as thin as one atomic layer on a surface and allow maximum control of thickness. With this type of layer control the technological possibilities are virtually endless. The ALD system currently being built in building 362 at Argonne National Laboratory needed to be designed to coat ceramic rods so different materials could be tested on them for strength and thermal efficiency. To accomplish this task we used the existing ALD system as a template and scaled up the new system. Many parts were fabricated by central shops using CAD drawings from Microsoft Visio that were specialized to fit the new system. The design and engineering phase of the new system is nearly complete and the fabrication phase has already begun. The system is scheduled to be finished in late January at which time it will be leak checked and ready to coat materials. The system is also being designed so that it is flexible, in that when ceramic rod testing has been completed, the system will be able to be used for many other types of applications.

Cellulose Breakdown Using a Dry Acid Catalyst. KEVIN JACKSON (University of Illinois at Chicago, Chicago, IL 60645) CHRISTOPHER MARSHALL (Argonne National Laboratory, Argonne, IL 60439). With the flux of current gas prices, energy security has become top priority for the United States in recent months. Because of current non-renewable fossil fuels located in unstable regions of the world, America is now looking into renewable alternative sources of energy to fuel our nation's automotive fleet and provide a means of cheap energy. A successful alternative energy source would allow America to become independent of the unstable regions of the world that currently produce over 80% of the world's fossil fuels. Ethanol and Hydrogen fuel cells are among the hopefuls that will one day replace gasoline as the fuel that

feeds our gas tanks. Between those two, Ethanol production is disputed to be the best option towards supplying our nation's needs. In Brazil, ethanol Production has already replaced 40% of their fueling needs. However, ethanol production is much easier in South America due to climate conditions. They use sugar cane, which is highly made up of sugars like glucose, to produce ethanol. To produce ethanol practically in the U.S. we will need a method of converting the cellulose in corn into ethanol since sugar cane can't be grown in our climate.

Characterization of Superconducting Splices. MEGAN MALLETTE (Valparaiso University, Valparaiso, IN 46383) CHRISTOPHER REY (Oak Ridge National Laboratory, Oak Ridge, TN 37831). High temperature superconductors (HTS) are materials that have no resistance to electrical current at temperatures below the transient temperature, T_c , and are therefore able to conduct much higher currents than traditional wire, in a much smaller area. HTS have the potential to greatly increase electrical efficiency in a number of applications, but it is necessary to first fully characterize the behavior of splices (i.e., electrical joints) before incorporating HTS wire into applications in order to minimize joint failure. During this investigation, splices of superconductors to be tested were fabricated by varying the type of solder, surface preparation, joint overlap area, and thermal cycle. Each splice consists of a series of seven lap joints. After fabricating each splice, a range of currents are applied to the splice and voltage measurements across each joint are used to calculate the resistance of each joint for the range of currents tested. While holding all other variables constant, the Sn60-Pb40 solder outperformed the In66.3-Bi33.7 solder in every test. Testing splices with no surface preparation resulted in poor mechanical joints that were unable to handle the stress of testing, showing the importance of surface preparation and oxide removal. Of the two types of fluxes tested, the paste flux outperformed the ruby fluid flux with all other variables constant in every test, except one splice in which the HTS was damaged by the temperature of the soldering iron. Results from varying joint overlap areas showed that larger contact areas decrease the joint resistance, as expected. Surprisingly, there was little difference between successive thermal cycles due to the stress of repeated temperature changes. Further testing on additional types of solders, fluxes, and joint overlap areas would result in a more comprehensive report on splices of HTS. Other variables that need to be considered in further testing of splices are the effects of varying magnetic fields, temperature dependence, and different types of mechanical stress.

Collection and Transmission Systems Cost and Performance Model for the Baseline Offshore Wind Farm. AMY BOWEN (Baylor University, Waco, TX 76798) JIM GREEN (National Renewable Energy Laboratory, Golden, CO 89401). The National Wind Technology Center (NWTCC) of the National Renewable Energy Laboratory (NREL) has undertaken a series of concept studies to evaluate the cost and performance of offshore wind farms. One of these studies will evaluate the power losses experienced throughout the electrical power collection and transmission systems as well as the cost of the system components and their installation. A hypothetical system was designed based loosely on the Horns Rev offshore wind farm. This system was then sent out to manufacturers with requests for electrical and cost data on the submarine cables and transformers. Upon discovering that the electrical data available for submarine cables is scarce, a very basic method of loss analysis was developed using three parameters: conductor resistance, ampacity, and power loss at capacity. The total losses are divided into two groups: losses that are modeled as a quadratic term which varies with current, and a base loss that is assumed to vary little with current, and is thus modeled as constant. In the model, both costs and losses are listed in per meter values to account for parameter variability. Power losses varied between cables from different manufacturers and also between different wind farm layouts. The cost of cables varied widely between different manufacturers as well, with one manufacturer's cable more than two times higher than another's. The results obtained in this study will be applied to the overall concept study.

Collection, Analysis, and Archiving Heavy Truck Driving Characteristics and Duty Cycles to Support the Evaluation of Benefits of Energy Efficiency Technologies. JOSEPH MASSIMINI (Purdue University, West Lafayette, IN 47906) GARY CAPPS (Oak Ridge National Laboratory, Oak Ridge, TN 37831). Despite common beliefs, commercial vehicle energy performance on highways is not well known. Ever changing hours of operation, anti-idling regulations, traffic situations and construction work make it difficult for drivers to have a true situational awareness of driving characteristics on highways. Understanding of these characteristics is often obtained through qualitative means. A quantitative profile of driving behavior of heavy

trucks does not exist. Generation of duty cycles that reflect real world driving would aid in creating such a profile. Sensors, autonomous to the driver, mounted on active fleet tractor trailers collecting kinetic, kinematics, human factor and environmental information will provide the data necessary to generate these duty cycles. Additionally, half the tractor-trailers will be fitted with Next Generation Single Tires (NGSTs) as opposed to standard dual tires to observe any improvements in fuel efficiency. This project involved extracting and analyzing the duty cycle data collected during the Pilot Test and creating and testing a prototype sensor suite for the Field Test that includes both Controller Area Network (CAN) and RS-232 type connections, requiring not only specific programming in the Data Acquisition System (DAQ), but also special CAN cables, RS-232 connectors and signal conditioning modules. ORNL worked with the DAQ vendor to specify and create the necessary software and hardware needed for integration into the prototype. This project also had to consider the fact that active fleet tractor trailers with a single driver typically operate 11 hours a day. Each channel collected and stored in the DAQ is collected at 16 bits per Hertz, thus a very large amount of data will be collected in a very short period of time. Methods were developed for formatting, organizing and archiving this large amount of data using custom Visual Basic software. At vehicle launch duty cycle data will be collected with the custom sensor suite, and will be archived and stored in an accessible location using the created software and can be used for validation, research and development of energy efficient technologies.

Compact Nanosecond High Current Pulser Design. MICHAEL MALLO (University of Oklahoma, Norman, OK 73019) SOREN PRESTEMON (Lawrence Berkeley National Laboratory, Berkeley, CA 94720). A pulser is an electronic circuit which generates a high voltage or current pulse with a very short pulse-width. Pulsers can be implemented using various topologies, such as Marx Generators, capacitor banks, coaxial transmission lines, helical lines, striplines, and Blumleins. The goal of this project was to review basic pulser theory and to design, test, and compare several pulsers using various topologies. The final design should deliver a repeatable pulse greater than 1 kA with 10 ns or less pulse-width to a 1 Ohm inductive load (high field microcoil) and be small enough to allow for insertion into an ultra high vacuum accelerator environment. The pulser topologies tested were capacitor bank, coaxial transmission line, stripline, and parallel plate Blumlein. The capacitor bank produced an output voltage of 289 V with a ringing frequency of 17.9 MHz, corresponding to a positive voltage pulse-width of 28 ns. The load impedance of this circuit is unknown. The coaxial transmission line was expected to produce an output voltage pulse of 500 V with a pulse-width of 13.2 ns; the actual output was 500 V, but with a pulse-width of 11.8 ns. The stripline was expected to produce a 1 kV 4 ns voltage pulse through a 1 O inductive load. The parallel plate Blumlein was expected to produce a 1 kV 1.2 ns voltage pulse through a 1 O inductive load. However, the stripline and Blumlein both produced far less voltage than anticipated and voltage pulse-widths of just over 10 ns. Three factors may have led to this inconsistency in predicted versus measured pulse-widths. First, the diagnostic tool used to measure the stripline and Blumlein voltage pulses was a Tektronix P5102 1 kVRMS 100 MHz 10x high voltage probe. The 100 MHz bandwidth prevents the probe from accurately measuring pulse-widths shorter than 10 ns. Second, the short lengths of these lines may have led to a greater prominence of end effects, or variations in the electric and magnetic fields at the ends of the transmission lines, in the output pulses. Third, the low 1 O load impedances combined with the stray inductances may have caused longer than expected pulse rise times. The latter two factors warrant further investigation to better understand what electrical and geometric properties lead to end effects and long rise times, and to what extent they affect the output pulse.

Comparison of Intrabeam Scattering High Energy Approximations, and Equilibrium. ALLEN OWENS, II, ROBERT OWENS (North Carolina A&T State University, Greensboro, NC 27411) MIGUEL FURAN, SEKAZI MTINGWA (Lawrence Berkeley National Laboratory, Berkeley, CA 94720). The International Linear Collider (ILC) is a particle accelerator being designed with the hopes of exploring higher energy particles in the universe that have never previously been accessible. Two of the major components of the ILC are the electron and positron damping rings, which serve the purpose of shrinking the emittances of the beams. There are several competing processes that affect the beam emittances. Synchrotron radiation damping serves to decrease the emittances. A major contributor to emittance growth is a phenomenon called Intrabeam Scattering (IBS), wherein particles within a single bunch Coulomb scatter off one another, thereby causing the beam emittance to increase.. The IBS emittance growth rates are calculated

using computer codes, and often it is too time consuming to use the full theory of IBS. In order to calculate IBS growth rates in the most efficient manner, several high-energy approximations to the full theory have been developed for the energy regime of the ILC. It is important to find the most accurate approximation. We analyzed three approximations of IBS using the software package, Mathematica; Bane's approximation, a new Diagonal Matrices approximation, and a recent CIMP one-log approximation, while attempting to develop a better two-log approximation to the CIMP formulas. We also analyzed the equilibrium emittances of the beams at different charges to determine if the transverse emittances, bunch length, and energy spread would meet the necessary requirements for the ILC. After comparing the various approximations, the Diagonal Matrices approximation proved to be the closest approximation to the full theory of IBS.

Comparison of Three-phase AC/DC Converters in a Wind to Hydrogen System. JOSHUA PRICE (University of Colorado at Boulder, Boulder, CO 80303) CHRISTOPHER PINK (National Renewable Energy Laboratory, Golden, CO 89401). Efficient production of hydrogen from wind power can be achieved by direct coupling of a variable-speed three-phase wind turbine to an electrolyzer with a high quality three-phase ac/dc rectifier interface. This paper compares three different topologies of three-phase high-quality rectifiers for use in a wind to hydrogen system. A six-pulse phase-controlled rectifier, a single-switch unidirectional ac/dc buck converter, and a single-switch ac/dc single-ended primary inductance converter (SEPIC) are developed and simulated using software-modeling techniques to calculate power output and efficiencies determined by wind turbine and electrolyzer operational characteristics. Software simulations indicate that the single-switch ac/dc SEPIC exhibits an increase in power production of 25% in the lower 25% of usable wind speeds over the single-switch ac/dc buck converter, and an increase in power production of 5% in the lower 10% of usable wind speeds over a modified six-pulse phase-controlled rectifier, with less cost and comparable efficiency. This work is part of a larger project that investigates a methodology to maximize off-grid wind to hydrogen production with a power electronics interface.

***Completing Phase III of Chipmunk Electrical Packaging Upgrade.** JULIAN DIAZ (Bronx Community College, Bronx, NY 10453) VINCENT CASTILLO (Brookhaven National Laboratory, Upton, NY 11973). Chipmunks are radiation monitoring devices used by the Collider Accelerator Department (C-AD) at Brookhaven National Laboratory (BNL) that detect radiation by means of an ionization chamber which generates a current that is proportional to the radiation. The current is converted to a frequency which is also proportional to the radiation. Different levels of radiation are used to create interlocks on the C-A machines. Chipmunks were developed at Fermi National Laboratory (FNAL) in the early 1980s and for the past 26 years have been effective as the detectors in the radiation monitoring system for the C-AD at BNL. They were designed with 1980s technology which included extensive hand-wiring and some of the components are actually obsolete. An engineering upgrade was started three years ago with the help of Community College students from the Community College Institutes (CCI) summer student program at BNL. A backplane was designed to replace hand-wiring and printed circuit boards (PCBs) were redesigned with readily available components. This project is focused on the design of circuits that will complete the upgrading process. Such circuits include a PCB for the indicators lights; a PCB for the front panel indicators; a PCB for the interlock circuits and completion of the backplane wiring. With all this circuitry in place the upgraded chipmunk will be ready for testing.

Computer Aided Engineering in the Development of the Electron Beam Ion Source Electrostatic Components in the Low Energy Beam Transport Region. GAVIN MCINTYRE (Rensselaer Polytechnic Institute, Troy, NY 12180) LOUIS SNYDSTRUP (Brookhaven National Laboratory, Upton, NY 11973). The Electron Beam Ion Source (EBIS) is the new pre-injector system for the Relativistic Heavy Ion Collider (RHIC) and will outperform the Tandem van de Graff which is the current ion source for RHIC. The EBIS is more versatile, with the ability to produce myriad stable ion species from the noble gases to uranium. Deflectors (steering/minor focusing) and quadrupoles (focusing/defocusing) ensure the beam quality and are developed using computer aided drafting and engineering software. The analysis is crucial to the success of the deflector and quadrupole designs; thus simulations constructed in analytical software (Kobra) are developed to ensure design integrity. The Adaptor Deflector is the initial steering/focus device that is mounted concentrically to the upstream ion lens. The deflector consists of electrode pairs with equivalent potentials that are mounted either parallel or alternating. Various designs were modeled using Pro/Engineer and were comprised of two to eight electrode pairs.

The investigated designs included: the split cylinder, the dual dipole (two dipoles offset from one another), and 8/16 congruent, electrode arrangements in order to ascertain the design that produces the least aberrations to the ion beam. The functionality of the deflector designs were simulated with a theoretical beam in the electrostatic analysis software, Kobra, and the 16 electrode deflector produced the most desirable qualities. Three quadrupoles are located in the Low Energy Beam Transport (LEBT) region of EBIS; the two simulated designs were a basic quadrupole triple and a Helical Electrostatic Quadrupole (HESQ). The triplet is composed of three inline quadrupoles, with electrode pairs of equivalent electric potential which focuses/defocuses the ion beam in two axial directions. The electrodes are oriented by a stainless steel framework and ceramic standoffs that act as insulators for the grounded vacuum vessel. The quadrupoles are offset from the vacuum chamber using swivel bolts that aid in mounting. The design incorporates two spring-loaded feedthroughs per quadrupole, which supply the voltages to a divided contact pad that is directly connected to the electrodes by solid wire. The HESQ has four helical electrodes held concentric in a grounded vacuum vessel and offer more locations for focusing/defocusing than the triplet while spanning a shorter length. The electric fields the quadrupoles produced were tested using the electrostatic capabilities of Kobra by applying various potentials to the electrodes; both resultant fields were adequate for focusing/defocusing the EBIS but the HESQ was superior to the triplet.

Controls Engineering for a Compact Crystal Positioning System. PRISHANTHA DUNSTAN (Columbia University, New York, NY 10027) CHRISTINA HOFFMANN (Oak Ridge National Laboratory, Oak Ridge, TN 37831). The ability to manipulate a sample for research and development has always been a basic essential. When sample size shrinks to the micro-scale and the environment for analysis proves unsuitable for direct human interference, the ability to carefully and accurately control the sample becomes much more difficult. In this case a positioning system for aligning and moving the samples remotely is desired. Such a device was constructed by Square One Systems in collaboration with the Spallation Neutron Source at Oak Ridge National Laboratory. Based on a tri-sphere approach, a series of linear actuators are employed to perform linear and spherical motions around a center point. The scope of this project was multifold: The individual motors of the instrument were calibrated and aligned. Once completed, the instrument was hardwired into a computer for control through LabVIEW software. The controls software was designed to mimic the operation of a goniometer, such that the sample could be rotated through two angles, the second angle being dependent upon the first. The equations of motion used enable sample rotation such that the crystal's position remains fixed while the motors move around it. Since the samples will be subject to neutron beam exposure with dimensions as small as 100 μ m x 100 μ m, ensuring that the crystal does not leave the beam when rotating will be essential to collect meaningful data. The controls also provide numerous calibration functions, enabling re-centering and adjustment of the sample after loading. The software calculates limits of rotation, preventing over rotation and possible dropping of the sample. Virtual images of the sample plate provide a visual for the scientist, due to the fact that the sample chamber will prevent direct view of the sample. This new instrument provides several advantages over the current sample positioner on the market (the hexapod). Using innovative Piezo motors, the instrument can manipulate the sample with zero backlash, ensuring accurate manipulation. The instrument also allows for easy sample changing, since the sample plate is not permanently fixed to the instrument. Because the software allows for repositioning of the sample, it provides much room for time-saving methods. For example, if a sample pin were used, such that 3 samples were loaded (one at the tip, one 1/3 from the tip, one 2/3 from the tip), the instrument could manipulate 3 samples sequentially without the need to reload.

Design and Construction of an RF Plasma Source. JOHN CARR (University of Illinois at Chicago, Chicago, IL 60601) RICHARD VONDRASEK (Argonne National Laboratory, Argonne, IL 60439). An RF plasma source is being developed to provide a 1+ ion beam for the Californium Rare Ion Breeder Upgrade. The 1+ beam will be injected into the Electron Cyclotron Resonance ion source, at the Argonne Tandem Linear Accelerator System, and charge bred to n+. An existing plasma source, no longer being used, was redesigned and modified to conform to new specifications. The RF plasma source consists of a 29 ml high-temperature quartz ion bottle. Gas is admitted to the plasma chamber through the ion bottle using an insulated tip and sealed with an o-ring. The bottle is mounted to a 5 inch round base, also sealed with an o-ring. Beam extraction is provided by a 30 kV puller mounted to the base opposite of the ion bottle. The source is designed to use up

to a 500 MHz RF signal to ignite the plasma and create the ion beam. Redesigning and retrofitting a currently available unit was a time and cost effective way to construct a suitable plasma source.

Design and Implementation of a High Availability Distribution Layer In a Campus Environment. MANGAL TYAGI JR. (Prairie State College, Chicago Heights, IL 60411) AJ TEMPOROSA (Brookhaven National Laboratory, Upton, NY 11973). The implementation of a robust, scalable, and fault tolerant network is dependent on logical and physical segmentation of workgroups to provide compartmentalization in event of network failure. The Cisco hierarchical model simplifies the task of building a reliable, scalable, and cost-efficient hierarchical internetwork by introducing a modular approach to the design and functionality of each network component. A distribution layer provides policy-based connectivity for workgroup access without having to route local data through the core or backbone of the network. By determining the fastest or best path to transmit data, the distribution layer will also send non-local requests to the high-end core, which will then transport the request at high data transfer rates to the correct service. Several policies provided at the distribution layer include packet filtering, quality of service (QoS), virtual LANs (VLAN), and manipulation of network traffic, which altogether contribute to exerting control over network transmissions and what goes in and out of the network. In order to improve Brookhaven National Laboratory's (BNL) network, a third distribution layer (DL-3) will be configured and deployed which will be attached to the core at high transfer rates and redistribute network data across a portion of the BNL campus. DL-3 will have redundant chassis consisting of the Cisco 6500 series, multi-layer switches, and dedicated power distribution unit (PDU) feeds. In addition, port aggregation is a technology that is implemented to provide higher bandwidth, and will also serve as a backup if a link fails. Before the deployment of DL-3, the components, such as the supervisor engines and multi-layer switches, have to be properly configured. The configuration process includes conversion of the Cisco supervisor engines from hybrid to native mode, assigning VLANs and network addresses, and establishing the spanning tree root. Once DL-3 is configured, it is connected to the network to start servicing the BNL campus similar to the other two distribution layers. The deployment of DL-3 will provide more reliable connectivity at the BNL campus by reducing the amount of hosts exposed to network failure. The work being performed is part of an ongoing effort to BNL's network reliability and performance.

Design Assistance for Renovation and New Construction at Red Rock Canyon National Conservation Area Using Building Energy Simulation. BENJAMIN BARNES (University of Illinois at Urbana Champaign, Urbana-Champaign, ILLINOIS 61801) ROBI ROBICHAUD (National Renewable Energy Laboratory, Golden, CO 89401). The Federal Energy Management Program Technical Assistance team at NREL used eQUEST software to help the Bureau of Land Management in their attempt to reach and exceed the goals of the 2005 Energy Policy Act in their new visitor center and renovated offices at Red Rock Canyon National Conservation Area. EQUEST was chosen for its intelligent defaults and its DOE-2 engine, which has been well validated against real buildings. Weather data collected on site was used for simulating external loads and visitation data from the current visitor center was used to generate internal occupancy loads while other internal loads were largely eQUEST defaults, except infiltration, which was adjusted to account for the door use patterns of a visitor center. The heating, ventilating and air conditioning (HVAC) equipment in the design involves a dedicated outdoor air system (DOAS) serving all zones and several recirculating, terminal units. The outdoor air load was simulated by assigning the DOAS to a few central zones and giving it the entire building outdoor air requirement while the recirculating units served the zones they were specified to with no OA load. Evaporative cooling (EC), on-off, two step and continuous daylighting, moveable insulation, dual speed compressors and a deeper Western overhang were all simulated. The EC and daylighting achieved the majority of the savings (21% and 8% of total building energy, respectively) while the results for the other measures suggested that they can likely be ignored. It is recommended that water conservation issues with EC be seriously investigated. Two step daylighting controls should be implemented and, if it proves feasible, combined with EC. The moveable insulation should be avoided as it would introduce maintenance issues and actually has a net detriment to energy use. The model, in the future, should be further validated concerning its HVAC approximations and used to assist in peak load management. Also, to be of greatest benefit, it must be kept up to date with current design development.

Design of Blade Rotation System for a Large Wind Turbine Blade Test Stand. MICHAEL SMITH (Portland State University, Portland, OR 97201) JASON COTRELL (National Renewable Energy Laboratory, Golden, CO 89401). Wind turbine blade testing is a key element in the development and success of the blade manufacturing industry. Testing is necessary to achieve higher reliability and meet international certification requirements. NREL (National Renewable Energy Laboratories) tests blades on both faces by mounting the blade on a test stand and applying static loads. The blades must be rotated between tests to apply loads to a second face. The objective of this study is to create and evaluate design options for a blade rotation system. Project deliverables include design specifications, graphic models, and cost estimates. The primary components of the rotational system include large adaptor plates, a rotational guide, and a drive. The focus of the study is on the design and selection of the rotational guide. Two main concepts were developed for comparison; one in which the blade is mounted to a heavy duty slewing bearing and one that uses calipers with rollers to support and guide blade during rotation. The results of this study indicate that the caliper design is likely to be a more expensive and complicated choice. However, the caliper design offers options for scalability and modularity that may make it more cost effective in the long term.

***Design Study of Temperature Stabilization of the Analyzer Array of the High Energy Resolution Inelastic X-Ray Spectrometer of the Advanced Photon Source.** JUSTIN BUELL (Montgomery College, Rockville, MD 20850) BRANISLAV BRAJUSKOVIC (Argonne National Laboratory, Argonne, IL 60439). Through the use of the high energy resolution inelastic x-ray (HERIX) spectrometer at the Advanced Photon Source (APS), vibrations in the lattice structure of various materials can be studied. The instrument consists of nine detector-analyzer pairs, a vacuum chamber, and a support structure for the entire instrument. X-rays from the APS beamline, scattered by a specimen through the vacuum chamber, are reflected and focused by the analyzers through a collimator and into a series of corresponding detectors which measure the properties of the photons. Due to the high cost of vacuum compatible components, it is more economical to place the analyzers outside of the chamber than inside it. Because thermal expansion due to temperature fluctuations in the hatch in which the spectrometer is located will compromise the geometric alignment between the optical components of the spectrometer, it is necessary to stabilize the temperature of the analyzers before the instrument can be calibrated. Using SolidWorks, a model of an enclosure and cooling channels for the analyzer array was developed. Expanded Polystyrene, a type of Styrofoam, was the selected material for the enclosure because of its optimal thermal properties. The enclosure was designed to eliminate heat transfer by free convection and minimize conduction to the analyzers. The cooling channels will consist of a copper tube through which water at a controlled temperature will flow and a series of copper pads, onto which the tube will be brazed, that will be mounted onto the support plate of the analyzers to improve thermal conduction between the analyzers and the cooling water. Finite element analysis of transient heat transfer was performed on the model assuming the hatch temperature to be a sinusoidal function of time based on measurements from a similar hatch. The results of the analysis indicated that the enclosure alone would not sufficiently stabilize the temperature of the analyzers, but that the enclosure and cooling infrastructure would maintain an acceptable degree of stability in the temperature.

Determination of the Effect of Interlayer Porosity on the Performance of Oxygen Electrodes for Solid Oxide Electrolysis Cells. PATRICK DRIEMEYER (University of Missouri-Rolla, Rolla, MO 65401) JENNIFER MAWDSLEY (Argonne National Laboratory, Argonne, IL 60439). Currently work is being done on the thermochemical cycle known as the "Westinghouse Process" in which hydrogen is produced. The step of interest in the Westinghouse Process is the decomposition of SO_3 to SO_2 using electrolysis to lower the temperature at which this reaction occurs. This step is considered a hybrid of thermochemical and electrochemical processes and reduces the highest temperature of any step to 500–600°C from 850°C. The lower temperature range opens the door for a wider array of materials to be used in construction of a hydrogen production plant. The development of an oxygen ion conducting cathode for the electrolyzer cell which exhibits low resistance is desired since it would allow free exchange of oxygen and electrons, thereby improving the performance and output of the electrolyzer cell. The production and testing of various cathode compositions along with an examination into the effect of porosity in the doped-ceria interlayer will be examined and reported on. The compositions that will be tested include $\text{La}_{0.5}\text{Sr}_{0.5}\text{CoO}_3\text{-d}$; $\text{Nd}_{0.5}\text{Sr}_{0.5}\text{CoO}_3\text{-d}$; $\text{Ba}_{0.5}\text{Sr}_{0.5}\text{CoO}_3\text{-d}$. These compositions will be produced

on site and tested in air within the temperature range of 900°C to 500°C. Their performance will be measured using electrochemical impedance spectroscopy (EIS) in which the area specific resistance (ASR) will be calculated and compared to determine the most appropriate design path. We have found that the incorporation of porosity in the doped-ceria interlayer between the oxygen electrode and the stabilized-zirconia electrolyte improves performance.

Determining the Effect of Aerosol Composition on the Accuracy of Aethalometer Real-Time Measurements of Black Carbon.

SRYAN RANGANATH (*University of California–Berkeley, Berkeley, CA 94709*) **THOMAS W. KIRCHSTETTER** (*Lawrence Berkeley National Laboratory, Berkeley, CA 94720*). Black carbon (BC), a main component of soot, is studied for its associated climatic and health effects. Filter-based light-transmission instruments are commonly used for measuring properties of black carbon. The aethalometer performs real-time measurements of black carbon concentration. Previous studies indicate that measurements produced by light transmission instruments, and the aethalometer specifically, are affected by the enhancement in particle light absorption due to the light scattering within the filters used to collect the particles. While the extent of this enhancement varies with particle loading and particle composition, the aethalometer algorithm does not consider these effects. This result could jeopardize the quality of measurements of BC concentration made with the aethalometer. This behavior was studied in the laboratory using controlled generation of BC and light scattering aerosols. An inverted diffusion flame produced BC aerosols with steady physical characteristics. A nebulizer produced salt particles which were mixed with BC from the flame. These particles were diluted with filtered air prior to sampling. The aethalometer sampled pure BC aerosols and BC + NaCl in individual experiments. In both cases, the aethalometer reported a decreasing concentration despite sampling a constant BC concentration. However, different decreasing trends in concentration were observed, depending on the composition of the aerosols sampled. This difference in instrument response means that different empirical corrections are required, which is not a practical solution to the problem. Continued investigation with aerosols of different composition is the next expected step. These results may be first steps in showing an empirical correction for the aethalometer is not practical.

Development of a Long Ion Chamber Electrometer for Particle Accelerator Beam Containment.

NICHOLAS PATE (*Tennessee Technological University, Cookeville, TN 38505*) **PAUL WRIGHT** (*Oak Ridge National Laboratory, Oak Ridge, TN 37831*). A common problem in cavity-coupled linear particle accelerators is misalignment of cavity phases resulting in particle beam loss over a short distance; when an intense beam is lost in this manner, high levels of ionizing radiation are developed that can pose a danger to both personnel and the machine itself. Long Ion Chambers (LIONS) provide a low-cost and -complexity method of monitoring radiation levels along a length such as an accelerator, potentially allowing a control system to take beam containment measures if a radiation threshold is exceeded. LION implementation in machine protection systems at the Spallation Neutron Source (SNS) requires that a standard electrometer design be developed, validated, and calibrated against other beam-loss and radiation detector systems. Circuit analysis of an existing prototype electrometer was performed to determine ideal characteristics of the design, and an experimental frequency analysis was performed to verify suitability for use under the expected measurement conditions. Because a vital piece of measurement equipment was unavailable, it was not possible to conduct a more detailed characterization of the circuit. It was determined that the maximum input signal before output clipping occurs is an order of magnitude higher than necessary, that gain drops off significantly for signals above 10KHz, and that the circuit operates as expected for relatively high input and offset currents. Further work will include a more detailed spectrum analysis, especially for small signals, determination of signal-to-noise ratio, and investigation of a small interference source that was observed during testing. This work is part of an ongoing effort to evaluate and implement LION-based radiation monitoring and beam containment in the SNS accelerator system.

Development of a Multi-Pollutant Personal Sampler (MPPS).

MARIA MINJARES (*Our Lady of the Lake University, San Antonio, TX 78207*) **LARA GUNDEL** (*Lawrence Berkeley National Laboratory, Berkeley, CA 94720*). The effects of indoor and outdoor air pollutants on human health have long been a concern to health care workers, environmental scientists, and citizens alike. Previous work has consisted of developing methods for separating and trapping particulate matter (PM) and gaseous pollutants. Currently, the multi-pollutant personal sampler (MPPS) consists of denuder with polyurethane foam coated with a ground sorbent, XAD-4, followed by a filter to collect PM < 2.5 µm

diameters (PM_{2.5}). Indoor and outdoor air sampling was conducted at Lawrence Berkeley National Laboratory to determine how much PM_{2.5} the polyurethane foam would retain. The results obtained from sampling indoor ambient air proves our hypothesis that the PM_{2.5} will pass through the 80 pores per linear inch (ppi) XAD-4 coated PUF. However, the 80 ppi XAD-coated PUF retained 30% of PM_{2.5} in its structure during outdoor air sampling. Further experimentation is needed to improve the MPPS geometry so that > 95% of PM_{2.5} passes through the XAD-coated PUF to the filter.

Development of a One-Dimensional Coal Gasifier Model Using

Fortran and UNIX. **ANDREW ELDER** (*Gonzaga University, Spokane, WA 99258*) **KEN JOHNSON** (*Pacific Northwest National Laboratory, Richland, WA 99352*). Coal gasification is a technique that is gaining attention as a clean fuel source for highly efficient power plants that are also environmentally friendly. In this process, coal is mixed with steam and a controlled amount of oxygen while under high temperatures and pressures. This environment causes the coal to break down into a synthesis gas (i.e., syngas) of hydrogen and carbon monoxide with lesser amounts of other gaseous compounds. The syngas can be used for fuel, while the waste gases can be removed easily. The goal of this project was to develop a one-dimensional computer model that would predict the heat transfer through the outer wall of the gasifier. (A one-dimensional model is one that deals with heat transfer solely in a linear fashion). Using the Fortran programming language on a UNIX machine, knowledge of conductive heat transfer and an explicit forward difference numerical method, two such one-dimensional models were developed. These models determined the heat loss through the gasifier wall and the temperature at various points through the wall. These models will serve as the foundation for future work in coal gasification modeling.

Effect of Acid Agitation on Buffered Chemical Polishing of

Niobium for Radiofrequency Cavities. **SARA MOHON** (*The College of William and Mary, Williamsburg, VA 23186*) **ANDY WU** (*Thomas Jefferson National Accelerator Facility, Newport News, VA 23606*). The performance of niobium superconducting radiofrequency (SRF) cavities can be affected by the smoothness of their inner surfaces. Smoother inner surfaces tend to result in better performance. Normally, smooth niobium surfaces are obtained by buffered chemical polish (BCP). BCP is necessary to remove the damaged layer created during fabrication and machining of the cavities. Previous experiments conducted in the Surface Science Lab at Thomas Jefferson National Accelerator Facility have shown that the morphology of niobium surfaces may be altered via different agitation constraints during BCP. The focus of this research is a systematic study of the effect of agitation on the BCP treatment of niobium. Six samples of niobium, each one square centimeter in size, were prepared using a 1:1:2 BCP mixture for 75 minutes. A control sample was also analyzed with no BCP treatment. Each BCP treated sample was agitated after a certain amount of time, varying from 0 to 75 minutes. After this treatment, the samples were examined by a 3D profilometer, where quantitative information about surface morphology was extracted. Qualitative inspection of the surface of each sample was performed a metallographic optical microscope (MOM). It was found that the surface roughness increased up to a certain asymptotic limit as the time interval between agitations increased, and that a green unidentified cloud-like material appeared above the inner surface area of niobium samples when there was no agitation. The MOM photographs show evidence that the BCP mixture attacked the grain boundaries and defect locations more than it did elsewhere, making a BCP treated surface rougher in comparison to some other polishing methods. The treated samples became smoother as the time interval between agitations decreased although they never become as smooth as the control sample. Smoother surfaces were also found in areas where the green cloud formed than in areas where it was absent. A model is proposed to qualitatively explain the experimental results. Further investigation is warranted for different BCP ratios to see if a smoother surface finish is possible and what agitation it requires. In addition, a BCP study of how larger grain samples affect niobium surface morphology is promising to the improvement of SRF cavities. These endeavors and the experimental results are useful for the BCP treatment of niobium SRF cavities to be used in particle accelerators.

Effect of Neodymium Oxide on Thermal and Mechanical Properties of Alkaline Earth Sealing Glass for Solid Oxide Fuel Cells.

BRIAN BISKIE (*Northern Illinois University, DeKalb, IL 60115*) **YEONG-SHYUNG CHOU** (*Pacific Northwest National Laboratory, Richland, WA 99352*). Earlier work on glass seals for solid oxide fuel cells (SOFCs) has shown that when fuel cells are operated over long periods, glass seals tend to react with the ferritic stainless steel interconnects at the metal/glass interfaces, and form undesirable phases. An approach for this problem was to make sealing glasses more refractory such that

the glass would be sealed at higher temperatures (i.e., 950°C) and thus be less reactive at operational temperatures of (750–800°C). In this study, a novel glass series containing Sr-CaO-Nd₂O₃-B₂O₃-SiO₂ was developed to determine the effect of Nd₂O₃ on the thermal and mechanical properties of the glass. Properties such as coefficient of thermal expansion (CTE), glass transition temperature, softening temperature, and elastic modulus were determined as the neodymium content was varied throughout the glass series. The results showed CTE increased with increasing Nd₂O₃ content up to 5 mole percent which had a CTE of 11.97 ppm/°C for as-cast glass, while the glass transition and softening points showed different behaviors. A similar alkaline earth silicate glass was used for interfacial strength testing. In addition to as-sealed coupons, samples were also aged in either air or a reducing environment to study the environmental effect on interfacial strength. The results showed the tensile strength decreased ~53% when aged in air at 850°C for 250 hours, and increased ~38% when aged 250 hours at 850°C in moist, dilute hydrogen fuel. Possible causes for the strength change were discussed.

Effect of Reactant Gases Humidification on Hydrogen Fuel Cell Performance.

FIDA ABDULLAH (State University of New York at Farmingdale, Farmingdale, NY 11706) **DR. DEVINDER MAHAJAN** (Brookhaven National Laboratory, Upton, NY 11973). Recent experimental investigations on polymer electrolyte membranes (PEM) fuel cells emphasize water management as being a critical factor in the design of an efficient cell. The current research project aims to explore the influence of humidified air and hydrogen on the fuel cell's performance. The first part of this experimental work was conducted on a five graphite bipolar plates fuel cell power stack, while operated under various loads, and involved the measurement of dry reactant gases (hydrogen and oxygen/air) humidity and temperature entering and exiting the fuel cell. The results, obtained at room temperature, indicated a substantial increase in the exiting humidity of oxygen (25.26%) despite the humidity entering the cell being relatively constant at 50% RH. The air exiting the cell plateaus at 75.15% RH (relative humidity). A comparison of the effect of both hydrogen and oxygen/air gases, under similar conditions, on the power stack performance was made. The oxygen's substantial increase in humidity was matched by a smaller increase (14.3%) from the exiting hydrogen side. When dry gases were used the power stack yielded a maximum power density of 19.43 mW/cm² and a maximum current density of 41.33 mA/cm². The second part of the experiment involved conventional methods of external-humidification of the oxygen gas/air and the humidified air entering the cell was changed in a range from 85.63% to 78.42% RH. As a result, the humidified air exiting the cell yielded a slight increase in humidity to 2.11%. Comparing humidified air versus non-humidified air a 72.77% increase in power density was observed. Since the results in the dry cell (no humidification) yielded a slight change (14.3%) in the exiting hydrogen humidity, the consequent step was to humidify circulating hydrogen and the results yielded a slighter gain of 12.87% (21.93mW/cm²) in power density. The final part of the experiment was the humidification of both reactant gases. The entering humidification of both gases yielded less improvement in performance than the previous scenarios, when each reactant gas was humidified one at a time. Also, when both entering reactant gases were humidified the exiting hydrogen humidity increased by 2.1% and the exiting air humidity increased by 11%. Initially, the humidification of both reactant gases yielded better performance than solely humidifying hydrogen but fell short of the performance of solely humidifying air. Humidification of air showed a maximum power density increased by 54.24%, and proved to be more influential than humidifying hydrogen or both gases.

Electrical Properties of Materials with a High Dielectric Constant.

CHRISTOPHER DIXON (University of Delaware, Newark, DE 19713) **STEVE HULBERT** (Brookhaven National Laboratory, Upton, NY 11973). Silicon integrated circuits are based on the Metal-Oxide Semiconductor Field Effect Transistor (MOSFET). A MOSFET uses a layer of oxide (an insulator) sandwiched between a layer of metal (gate) and a semiconductor to control the flow of electrons between the source and drain. The goal of creating a transistor using high-k dielectrics is to achieve a smaller transistor so that more transistors can be packed into a smaller area. As transistors get small, the leakage current across the dielectric increases leading to problems with battery lifetime and heat dissipation. Thus, new materials are being investigated for use as gate insulators in order to decrease the leakage current. In older electronics the gate electrode is usually a polysilicon semiconductor. Metal gates are desirable to use because they help to limit reaction at the gate/dielectric interface. The energy levels of different metals relative to the energy levels of the high k dielectrics determines the leakage current through the dielectric. Samples of the dielectric, (HfO₂)_x(SiO₂)_{1-x}

were analyzed by using ultraviolet photoelectron spectroscopy (UPS). UPS is a technique for measuring the energy spectrum of electrons emitted during the absorption of ultraviolet radiation. The relative alignment of the energy levels of the Si substrate, the dielectric film, and the gate electrode will determine the electrical properties of the transistor. This spectrum reveals the characteristic ionization energies of the component atoms and facilitates study of their chemical nature. Utilizing UPS it is possible to see the Fermi level and energy levels of the materials that are being considered. Analyses were run on the samples with different amounts of Ag and Al evaporated onto the surface of the dielectric samples. Data was recorded as a function of metal thickness for both Ag and Al depositions. The Secondary Electron Cutoff (SEC) made it possible to determine the work function of the samples being tested, and to discover whether any electric charge was transferred at the metal/insulator interface. The threshold voltage (and consequently the drain to source on-current) is determined by the work function difference between the gate material and channel material. Measurements we are undertaking will help determine which metal and dielectric are used in future generations of very highly integrated circuits.

Enhancement of Airside Heat Transfer in Air-Cooled Condensers for Binary Cycle Geothermal Power Production.

CHRISTOPHER HANNEMANN (University of California-Berkeley, Berkeley, CA 94720) **CHUCK KUTSCHER** (National Renewable Energy Laboratory, Golden, CO 89401). Binary cycle geothermal power production requires a majority of the thermal energy in the working fluid to be rejected after exiting the turbine. Because abundant sources of cool water are not available near many of these geothermal wells, air-cooled condensers must be used instead of the preferred water-cooled systems. The capital cost for these condenser arrays, as well as the parasitic power consumed to run the required fans, contributes significantly to the total cost of geothermal power. To improve the airside heat transfer in these condensers, enhanced fins are being tested at the National Renewable Energy Laboratory; slit and bent annular fins are examined in the present study. Transient testing is performed on small tube sections to determine performance improvements based on heat transfer coefficients and pressure drops as well as to select an optimum bending angle. Using the results from the transient tests, a steady-state test using a 17 tube, single pass cross flow heat exchanger is performed. The slit fins are tested unbent and bent at 12° in two different configurations, using water as the working fluid and testing each sample at four different air flow rates. The "staggered" arrangement is shown to perform the best, and the 12° bent fins are shown to outperform the unbent fins by 3–5% heat transfer per unit hydraulic power. Both the unbent and bent fins underperform model predictions, possibly due to corrosion within the tubes. Further work will focus on retesting the bent slit fins with the corrosion removed as well as examining the effects of twisting the slit fins.

Enhancing the Target Chamber for the Second Phase of the Neutralized Drift Compression Experiment.

GUILLERMO GARCIA (University of Southern California, Los Angeles, CA 90089) **MATTHAEUS LEITNER** (Lawrence Berkeley National Laboratory, Berkeley, CA 94720). The objective of a controlled fusion power plant for worldwide energy production has driven the Neutralized Drift Compression Experiment (NDCX) to investigate characteristics of ion-beam manipulation. This report focuses on enhancing the diagnostic target chamber for the second phase of the NDCX project. A target capsule, loading dock, robotic arm and target housing were developed to prepare the diagnostic target chamber for integrated compression and focusing experiments with energy transfer of 1 eV on target with a 500 MW, 1 ns ion beam. Each component was developed to incorporate the design constraints established by the diagnostic target chamber. A LabVIEW program was created to monitor and control movement of the robotic arm. The diagnostic target chamber was assembled and calibration of the robotic arm showed that the system had successful interaction between the LabVIEW program and the newly developed components.

Error Reduction in Polarization Measurement.

DONALD JONES (Acadia University, Wolfville, NS B4P 2R6) **ROBERT MICHAELS** (Thomas Jefferson National Accelerator Facility, Newport News, VA 23606). One of the greatest barriers to definitive conclusions in any scientific experiment is the accumulation of errors. Due to the precision required in parity-violation experiments, an effort has been made in Hall A at Jefferson Lab (JLab) to reduce the cumulative error by targeting specific sources. A particular focus has been placed on reduction of error in beam polarization measurements. Compton polarimetry is utilized at JLab because of its unique advantage of allowing polarization to be determined while an experiment is running, without interrupting

the beam. Electrical signals produced by scattered photons and electrons are used to determine beam polarization. The helicity of the beam is reversed every 33 milliseconds (ms) and the asymmetry that arises from pulse measurements during consecutive 33 ms intervals, is used to calculate beam polarization. While this asymmetry has been created in the past by counting photons, electrons or electron-photon coincidences, this method gives rise to many systematic errors. New methods are being sought to more accurately calculate polarization. The focus of this research has been to determine whether signal integration can be used to effectively reduce the error to under the 1% level within a feasible time frame. Extensive tests have been done to determine the reliability of signal integration across the full 33ms gate, in order to determine if the background noise is too great to make this technique useful. Because of difficulties encountered, and the lack of beam operation during the time this research was done, a pulse generator was used to simulate the electrical pulses that arise from electron scattering in the Compton polarimeter. The data from the pulse-generated asymmetry indicates that polarization can be accurately determined within three hours of beam operation. Because experiments can last for days, this is a reasonable length of time. To ensure the reliability of this technique, the results were then verified using Monte Carlo simulations. The results of this research show that this method of beam polarization measurement has great promise of being able to reduce the measurement error from the present 3%, to below 1%. This method has yet to be tested during beam operation, but its success would enhance future parity violation experiments.

Evaluation of a 4.5 kW Air-Cooled Lithium Bromide/Water Solar Powered (Hot Water-Fired) Absorption Unit. *DAVID GOODNACK (Pennsylvania State University, University Park, PA 16802) ABDOLREZA ZALTASH (Oak Ridge National Laboratory, Oak Ridge, TN 37831).* During the summer months, air-conditioning (cooling) is the single largest use of electricity in both residential and commercial buildings with the major impact on peak electric demand. Improved air-conditioning technology has by far the greatest potential impact on the electric industry compared to any other technology that uses electricity. Thermally activated absorption air-conditioning (absorption chillers) can provide overall peak load reduction and electric grid relief for summer peak demand. This innovative absorption technology is based on integrated rotating heat exchangers to enhance heat and mass transfer resulting in a potential reduction of size, cost, and weight of the "next generation" absorption units. Rotartica Absorption Chiller (RAC) is a 4.5 kW air-cooled lithium bromide (LiBr)/water unit powered by hot water generated using the solar energy and/or waste heat. Typically LiBr/water absorption chillers are water-cooled units which use a cooling tower to reject heat. Cooling towers require a large amount of space, increase start-up and maintenance costs. However, RAC is an air-cooled absorption chiller (no cooling tower). The purpose of this evaluation is to verify RAC performance by comparing the Coefficient of Performance (COP or ratio of cooling capacity to energy input) and the cooling capacity results with those of the manufacturer. The performance of the RAC was tested at Oak Ridge National Laboratory (ORNL) in a controlled environment at various hot and chilled water flow rates, air handler flow rates, and ambient temperatures. Temperature probes, mass flow meters, rotational speed measuring device, pressure transducers, and a web camera mounted inside the unit were used to monitor the RAC via a web control-based data acquisition system using Automated Logic Controller (ALC). Results showed a COP of approximately 0.58 at 35°C design condition for ambient temperature with 40°C cooling water temperature and approximately 3.7 kW capacity. This is in close agreement with the manufacturer data of 0.60 for COP and 3.9 kW capacity. This study resulted in a complete performance map of RAC which will be used to evaluate the potential benefits of rotating heat exchangers in making the "next-generation" absorption chillers more compact and cost effective without any significant degradation in the performance. In addition, the feasibility of using rotating heat exchangers in other applications will be evaluated.

Evaluation of Long-Term Brake Performance Using Performance-Based Brake Testers (PBBT). *JESSICA JOSEPH (Southern University A&M of Baton Rouge, Baton Rouge, LA 70816) GARY J. CAPPS (Oak Ridge National Laboratory, Oak Ridge, TN 37831).* Performance-Based Brake Testers (PBBTs) are devices that can evaluate the current braking capabilities of a vehicle through the measurement of brake forces developed as a vehicle engages in a braking event while on a PBBT. They are widely used for brake inspection in Europe and Australia and are beginning to emerge as both an enforcement tool and diagnostic aid for private sector maintenance and repair shops. Because of the significant benefits of utilizing PBBT technologies (time/labor savings, error reduction, objective measures, consistency,

enhanced fleet safety), Federal Motor Carrier Safety Administration (FMCSA) has an interest in assessing a vehicle's long-term brake performance using PBBT technology over time in a real-world testing environment. This will be done in conjunction with volunteer fleets (including a motor-coach), over a sufficiently long period of time, to measure (for each vehicle in the test fleet) the brake force for the overall vehicle, and for each individual wheel-end. Such an effort would provide experiential data, and would quantitatively assess benefits from long-term brake performance data. A market search was done to find manufacturers or sole distributors of PBBT devices that offer artificial axle loading (AAL) capability and research was done to understand the theory of operation of the PBBT. The different types of PBBT (roller, in-ground, portable) were evaluated to decide which PBBT with AAL would be best for research based on meeting FMCSA's Functional Specifications. An evaluation was completed for three possible vendors to determine which vendor would provide the best PBBT for research applications and a training module for use by the Tennessee Department of Safety Personnel. The vendor's PBBT must be certified and meet the FMCSA criteria in order to be a candidate to provide a PBBT. A survey and location matrix was done to compare and decide which one of three possible locations would accommodate the needs for the State of Tennessee and Oak Ridge National Lab.

Evaluation of Various New Anode and Cathode Materials for High Power Li-Ion Battery Applications. *STEPHANIE TRAN (Michigan State University, East Lansing, MI 48823) JUN LIU (Argonne National Laboratory, Argonne, IL 60439).* Since the establishment of the Partnership for a New Generation of Vehicles Program (PNGV) between the U.S. government and the U.S. Council for Automotive Research in 1993, much research has been invested into developing more efficient high power and high energy density hybrid electric vehicles (HEV). The power and performance properties of a Li-ion battery system make it an efficient source of energy for the automobile. However, high production costs of the Li-ion battery make them difficult to be accepted by automobile manufacturers. LiMn_2O_4 , Spinel and LiFePO_4 , Olivine active cathode materials are cheaper to produce and may still maintain the performance characteristics of the Li-ion system. Cycling performance tests for these materials have shown a stable battery capacity over many charge-discharge cycles in room temperature and high temperature conditions. Potential hard carbon anode materials also display the prevention of capacity loss at elevated temperatures and long term battery usage. Cost efficient battery components that can still uphold the high power and high energy qualities of a lithium-ion battery system are promising to the new generation of hybrid vehicles.

Examining the River Water and Groundwater Interface in a Hyporheic Zone Mesocosm. *CAROLINE NEWCOMBE (Arizona State University, Tempe, AZ 85287) DR. AMORET BUNN (Pacific Northwest National Laboratory, Richland, WA 99352).* The hyporheic zone of a river or stream is the area of the streambed where groundwater and surface water mix. It is an important area of study because it is an integral part of the river ecosystem with unique physical, chemical, and biological characteristics. This paper will discuss the initial steps in the design and construction of a hyporheic zone mesocosm under development at Pacific Northwest National Laboratory (PNNL). An enclosed experimental ecosystem, called a mesocosm, is well-suited for investigation of the hyporheic zone because it provides control and repeatability in the experiment. A unique feature of the hyporheic zone mesocosm under development at PNNL is that it incorporates both river water and groundwater flows into the sediment profile, whereas previous studies have only examined the effects of influent river water or influent groundwater. Since this mesocosm is using a novel approach in incorporating two types of water, it was necessary to investigate practical designs for sampling ports in the system, as well as to identify appropriate parameters for determining the distribution of groundwater and river water in the system. The hyporheic zone mesocosm consists of a sediment profile contained in a larger, insulated tank. Different configurations of sampling ports were tested by making rectangular or circular cuts in rigid high-density polyethylene tubing. Several water quality parameters of river water and groundwater were also tested in order to determine the best method to characterize the mixing of river water and groundwater within the completed mesocosm. The type of sampling port selected was a series of three 2 mm x 2 mm square cuts spread across a 5 cm length in the center of the tube. Testing several different water quality parameters showed that conductivity is the most reliable way to measure the extent of the river water and groundwater mixing in the hyporheic zone mesocosm, and further testing ensured that conductivity would not increase as a result of salts leaching from the sediment into the water. However, conductivity does not directly

relate to uranium speciation or water quality for biological growth, so water quality parameters such as alkalinity, dissolved oxygen, hardness, pH, and ORP will have to be monitored as well.

Exhaust Gas Recirculation Effects on Diesel Engine Soot Formation, Destruction, and Emissions. EDWIN HUESTIS (*University of California–Davis, Davis, CA 95616*) MARK P. B. MUSCULUS (*Sandia National Laboratory (California), Albuquerque, NM 87185*). Diesel engine manufacturers desire insight into the internal processes that affect emissions in order to design new engines that meet upcoming U.S. pollutant emissions regulations for particulate matter (soot) and nitrogen oxides (NO_x). Exhaust gas recirculation (EGR) is one available tool to reduce pollutant emissions of NO_x , and EGR has also been shown to reduce the formation of soot in fundamental combustion studies. In real engines, however, EGR can increase soot in the engine exhaust by affecting soot destruction processes after combustion. In this study, both exhaust-gas soot emissions and fundamental soot formation/destruction processes inside a diesel engine are measured to understand how these processes affect the ultimate soot emissions. The time-evolution of soot formation and destruction inside an optically accessible diesel engine is measured by analyzing the radiative emission spectrum of the combustion-heated soot. The soot radiative emission intensity is measured within two separate spectral bands, and along with high-speed luminosity movies, the soot temperature and concentration inside the engine are determined using the two-color soot thermometry technique. Gases are also sampled from the exhaust stream and drawn through a filter to collect the soot particles for exhaust-gas measurements. The measurements show that soot formation inside the engine decreased as EGR was added, but soot destruction processes decreased more rapidly, so that exhaust soot emissions increased as EGR was added. Only at very high EGR levels did the exhaust soot emissions decrease, as the soot formation processes became very slow. Finally, soot temperature measurements show that the reaction rates for soot formation and destruction depend on EGR, affecting the soot formation/destruction balance. By combining measurements inside the engine with exhaust-gas measurements, the effects of EGR on the soot formation/destruction balance were quantified in a single experimental facility. The data from this study shows that EGR decreases soot destruction processes more than soot formation processes, so that the balance is tipped toward higher exhaust soot. At very high EGR, however, soot formation processes are so slow that exhaust soot decreases, even with reduced rates of soot production. This study also identifies the tipping points where this balance shifts from increasing exhaust soot to decreasing exhaust soot.

Experimental Test of Relaxational Attenuation for Carbon Dioxide. ANGEL SANTIAGO (*University of Massachusetts–Amherst, Amherst, MA 01003*) MORRIS GOOD (*Pacific Northwest National Laboratory, Richland, WA 99352*). Attenuation is the reduction of intensity of an ultrasonic wave. Relaxational attenuation occurs when excited molecules do not exchange vibrational or rotational energy infinitely fast with translational waves. The purpose of this research is to determine relaxational attenuation can be shown experimentally. Attenuation is frequency dependent. The study of ultrasonic propagation in CO_2 was studied at 3 atmospheres in varying frequencies. The experiment was carried out using a modified pressure chamber made from a commercial paint can. Data was collected through an oscilloscope for various transducer spacing at increments of a tenth of an inch, in order to facilitate attaining the attenuation of various frequencies. All data was analyzed using Microsoft Excel and Mat lab software. Plotting the data for attenuation due to frequency I was able to match the CO_2 experimental graph and the theoretical graph. The experiment has shown the ability to obtain the relaxation attenuation of a gas. More experiments are needed with other gases to show working with the relaxation attenuation of a gas would be of practical use as an identifier of specific gases.

Heavy Truck Duty Cycle Study. MARY LASCURAIN (*Pensacola Christian College, Pensacola, FL 32503*) GARY CAPPS (*Oak Ridge National Laboratory, Oak Ridge, TN 37831*). To date, little real-world scientific data regarding long-haul, Class-8 tractors and their engine and drive train components has been collected for analysis. Of great importance to the study of this class of commercial vehicle is the understanding of how factors such as tire type and vehicle loading influence fuel efficiency. Because many variables cannot be controlled in real-world data collection, simultaneous monitoring of these variables such as weather conditions and road topography can aid in the production of useful data that can be analyzed to isolate controllable variables which influence vehicle efficiency (i.e., tire rolling resistance). Building on efficiency-related data available directly from the truck's

J1939 controller area network (CAN), an eDAQ Lite data acquisition system (DAS) was assembled to integrate several external sensors. Data from these sensors augment the duty cycle data by providing not only GPS-based information such as speed and acceleration, but also weather conditions, road topography, and weight information to increase understanding of long-haul operations. In the absence of a Class-8 truck for the earliest stages of testing, several DAS units were placed on passenger cars to collect data in normal operation for up to a week at a time. These tests, which reflected extended periods of real-world driving conditions, more closely simulated the ultimate (long-haul) application of the systems than previous bench-top testing. The results from these tests showed a discrepancy between the tilt sensor data and actual road grade. Preliminary testing also provided readings for speed and wind, which were found to differ significantly from one another. Analysis of the test data revealed that the tilt sensor readings not only were influenced by the natural vibrations of the vehicle, but also responded dramatically to vehicle tilt caused by acceleration and deceleration. Further testing will be conducted to verify that sufficient GPS altitude data can be collected to make the inclusion of a tilt sensor unnecessary. A comparison between wind and speed readings indicated that the weather station provides a sufficient indication of headwind. When a class-8 truck becomes available for instrumentation, the truck database will be integrated into the existing DAS for final testing of the system; these systems will then be installed in five to six trucks in a commercial fleet to gather data for a twelve-month study of heavy truck duty cycles.

Hydrolysis Reaction of the Copper-Chloride Thermochemical Cycle in a Vertical Reactor. DAVID TAGLER (*University of Notre Dame, Notre Dame, IN 46556*) MICHELE A. LEWIS (*Argonne National Laboratory, Argonne, IL 60439*). Thermochemical cycles have been developed to produce hydrogen at competitive energy efficiency levels while generating low greenhouse gas emissions. The copper-chlorine (Cu-Cl) thermochemical cycle is designed to split water and produce hydrogen at the relatively low peak temperature of 550°C . This cycle consists of three thermal reactions and one electrochemical reaction. This project is concerned with one of the thermal reactions, the thermal hydrolysis reaction of cupric chloride, CuCl_2 , from 350°C to 400°C at atmospheric pressure. The reaction is $2\text{CuCl}_2(\text{s}) + \text{H}_2\text{O}(\text{g}) \rightarrow \text{Cu}_2\text{OCl}_2(\text{s}) + 2\text{HCl}(\text{g})$. The goal of this experiment is to determine the optimum operating conditions (temperature, flowrate, steam ratio, and reaction time) to maximize the desired products, Cu_2OCl_2 and HCl, while minimizing the products of any competing reactions. Argon gas at 100-200 ccm is used to transport steam through a 15 inch vertical reactor containing 150-500 mg of solid CuCl_2 in a crucible with a 13 mm ID (inside-diameter) crucible for 15-60 minutes. HCl is collected in a condenser container and water trap. X-ray diffraction (XRD) is used to analyze the solid products of the reaction and determine purity. XRD analysis shows that a competing decomposition reaction of CuCl_2 to CuCl increases at temperatures greater than 350°C . The optimum temperature was found to be between 350°C and 375°C for 500 mg, and the optimum reaction time was found to be between 30 and 60 minutes. Greater sample surface area also proved to decrease the amount of CuCl produced. Thus, this experiment was successful in optimizing this reaction. Future studies need to look deeper into the effect of surface area, flowrate, temperature, and reaction time in order to further optimize this reaction.

***Increasing the Durability and Reliability of Radiation Detectors used in Radiopharmaceutical Chemistry.** SIMARJIT KAUR (*Contra Costa College, San Pablo, CA 94806*) JAMES P O'NEIL (*Lawrence Berkeley National Laboratory, Berkeley, CA 94720*). Radiation Detectors are a necessary part of radiopharmaceutical synthesis in order to determine the quantity of radioactivity throughout the synthesis, not only to determine the progress of the chemical reactions and the yield at each step but also to ensure the safety of the personnel involved in this process. Radiation detectors are usually installed in places where the potential of chemical exposure and general physical abuse is quite high. To make the radiation detectors more robust and reliable, a very easy and cost-effective method of "epoxy potting" was devised. The radiation detector is placed in a mold of appropriate dimensions and filled with epoxy (3M Scotch-Weld DP270, black). After the epoxy cures, the radiation detector is protected within a solid light resistant block. This particular epoxy was chosen for this task because it is chemically inert and provides both electrical and mechanical insulation of the detector components from the harsh surroundings of the hot cell.

***Increasing X-Ray Brightness From 3rd Generation Light Sources: Design Study of an Advanced In-Vacuum Magnet Gap Separation Mechanism for Cryogenic Permanent Magnet Undulators and Superconducting Undulators.** KOBBIANA AWUAH (*State University of New York at Binghamton, Binghamton, NY 13902*) JOHN SKARITKA

(Brookhaven National Laboratory, Upton, NY 11973). In recent years, superconducting undulators (SCU) and cryogenic permanent magnet undulators (CPMU) have been implemented in synchrotron radiation facilities in order to obtain brighter beams. Due to increasing project costs, there have been recent attempts to improve upon the versatility of the undulator design. Consequently, a chamber that can house either a CPMU or an SCU was designed to help reduce project costs encountered when shifting from a CPMU to an SCU and vice-versa. All models for the project were created using INVENTOR software. Three meter segments of each kind of magnet: superconducting magnet (SCM) and cryogenic permanent magnet (CPM) were created. Since the SCM cannot operate under ultra-high vacuum (UHV) conditions, it was placed in a vacuum-proof box before inserted into the UHV chamber. In order to generate the required magnetic field in an undulator, two magnets of the same kind are aligned to have their poles facing each other and the field is usually controlled by adjusting the gap between the two magnets. Two different gap separation mechanisms (GSM) were studied: one incorporated the use of wedges and rail bearings and the other flexure bearings. The goal was to have a mechanism that could adjust the gap between a 5-50mm range. During the studies, it was found that flexure bearings have no backlash and no friction during operation as compared to wedges and rail bearings. The latter attribute of flexure bearings makes it ideal for use in UHV environments since no oiling is required for the bearings and this reduces outgassing in the UHV chamber. Also, flexure bearings are relatively cheap and readily made. However, flexure bearings tend to be inaccurate at larger gaps mainly because the geometric center of the bearings tend to shift significantly (up to 0.5mm) during large-angle operations. Since the design could only accommodate a misalignment of the magnets in the order of microns, the flexure bearing GSM was not implemented in the final design. Instead, custom ceramic wedges and rail bearing were used in the GSM to reduce friction and springs were used to reduce backlash. Previous GSM models were usually placed on the outside of the vacuum chamber resulting in complexity and increase in project costs. The final design was able to achieve an in-vacuum GSM using less complex components: wedges and rail bearings driven by linear motors. This greatly reduced the overall size of the undulator and also the cost involved.

Indium Zinc Oxide Active Channel Layer in Transparent Thin Film Transistors. ANDREW CAVENDOR (Colorado School of Mines, Golden, CO 80401) DAVID GINLEY (National Renewable Energy Laboratory, Golden, CO 89401). Amorphous indium zinc oxide (IZO) shows promise for being the active channel layer in a transparent thin film transistor (TFT). In the last 2 years, oxide based transistors have begun to be investigated showing the promise to replace amorphous silicon (α -Si) and microcrystalline silicon TFTs to lead to transparent electronics. IZO is a lead candidate because it can be deposited at room temperature and is amorphous, making it suitable for flexible substrates. Also, IZO has higher Hall mobility (μ_h) $> 30 \text{ cm}^2\text{V}^{-1}\text{s}^{-1}$ than conventional materials ($< 1 \text{ cm}^2\text{V}^{-1}\text{s}^{-1}$), which makes faster TFT switching times possible. We used DC magnetron sputtering with O_2/Ar gas from 0–10% to optimize the active channel layer, for transistors. Addition of O_2 to the sputter gas reduces the carrier concentration (n) while preserving high mobility μ_h . Amorphous IZO films were produced at 70/30 atomic percent In/Zn with μ_h as high as $\sim 55 \text{ cm}^2\text{V}^{-1}\text{s}^{-1}$ and n as low as $\sim 10^{16} \text{ cm}^{-3}$. TFT devices were made in the gate down method through photolithography. The source and drain were produced at 84/16 atomic percent In/Zn, to achieve good conductivity $\sim 2000 \text{ S cm}^{-1}$. Films were incorporated into functional transistors which showed on-to-off current ratios $\sim 10^6$.

Inner Reflector Plug Pipe Cutter for the Spallation Neutron Source. DAVID MACNAIR (Georgia Tech University, Atlanta, GA 30332) CRAIG BRADLEY (Oak Ridge National Laboratory, Oak Ridge, TN 37831). The Spallation Neutron Source (SNS) drives high velocity protons into liquid mercury which will create the most powerful neutron scattering source in the world. When the protons hit, the neutrons are ejected and the mercury becomes radioactively activated which together with the neutrons irradiate nearby equipment. The Inner Reflector Plug (IRP) serves as a moderator and a heat sink for the mercury target and nearby components. Water fed through pipes running through the IRP absorbs the heat and transfers it to cooling equipment. After about 2 to 5 years, the components of the IRP become damaged due to intense gamma and neutron radiation. Removal must be accomplished by disassembling each layer of shielding, cutting the pipes that ran through that layer, and then repeating for the next and subsequent layers. Methods for removing the shield blocks have already been developed but the SNS needs a pipe cutter. The cutting device must withstand the high radiation environment, cut the pipes inside the IRP without leaving

a mess or deforming the pipes so as to make removal of subsequent layers difficult, transport the pipes to a shielded cask, and be used remotely. To reduce costs, not all components of the pipe cutter were designed from scratch. The inner cutter housings, for example, came from commercial tools and had to be analyzed and tested to find the amount of torque required to cut through the IRP pipes. All components were designed or modeled using the solid modeler Pro/Engineer and then analyzed using hand calculations and finite element analysis with Pro/Engineer Mechanical. Results of the calculations were verified by the Remote Systems Group of the Nuclear Science and Technology Division and the SNS Division, and finally the design drawings were completed. Due to the inaccessibility of the irradiated areas by humans during SNS operation, each component inside these environments must be carefully designed, analyzed, and tested before being put into use. Additionally, components must be easily accessible, maintainable, and maneuverable by remote handling equipment so that the SNS can continue its mission of scientific discovery even beyond the length of its original design.

Innovative Analysis and Decision Tools. MATTHEW SIMON (University of Washington, Seattle, WA 98195) HEATHER DILLON (Pacific Northwest National Laboratory, Richland, WA 99352). Decision makers in the energy sector rely heavily on modeling and scenario planning when making important decisions. These decisions could be related to initial power plant designs, policies regarding global warming, or new building code regulations, among others. Unfortunately, the future is unpredictable. Uncertainties within the models will undoubtedly cause failures in some real-world applications. Despite the problems associated with these methods, these techniques are heavily relied on to make important decisions in both design and policy. Without the techniques of modeling and scenario planning, making decisions would be extremely difficult, because there would be no efficient way to analyze the different outcomes from making one decision over another. Through several literature reviews, many current modeling software tools and techniques were examined. Each piece of software has its own strengths and weaknesses when looking at robustness. Depending on the application, some software tools are more appropriate than others. Of particular interest was a set of new software tools designed for robust analysis. These tools, developed by Evolving Logic, are the Computer-Assisted Reasoning system (CARS) and the Robust Adaptive Planning (RAP) software. Although they had not been extensively applied to many energy related applications, they are a promising set of software tools allowing for the analysis of problems dealing with deep uncertainty, allowing analysts to make more robust decisions. This paper looks at past and possible future applications of these software tools and how they can improve the decision making process.

Integrating Radiation and Radiofrequency Identification Portal to Monitor the Movement of Radioactive Materials. NATHAN ROWE (University of Tennessee, Knoxville, TN 37996) CHRIS PICKETT (Oak Ridge National Laboratory, Oak Ridge, TN 37831). Radio Frequency Identification (RFID) is a fairly new technology that allows for barcode type identification remotely over short distances. There is an interest in using this technology for tracking nuclear materials. One way of doing this is to use RFID portals at access points between materials balance areas. The inclusion of a radiation monitor to this portal would allow for a second level of confirmation of the item being moved. Radiation Portal Monitors are already in use to detect unauthorized movement of nuclear material. In order to demonstrate the integration of an RFID portal with a radiation portal, an RFID portal system was interfaced with an existing radiation portal monitor. The radiation portal monitor was connected to a local PC using a serial interface. Windows services and web services were used to log the data from the radiation portal into a remote database. The RFID web interface is then able to use the database to compare the declared radiation status of the item with its measured radiation level, and alarm if they don't match. The system shows the potential for integrating other security systems with RFID, and shows promise for using RFID for improved nuclear inventory management. Web services make a good communications system to integrate security systems of this type, because of its expandability and modularization. A similar method could be used for combining other types of systems with the RFID software as well.

Investigation of a Rhodium Catalyst in the Reduction of Carbon Dioxide and Pyruvate for Future Use in a Direct Electrochemical Methanol Production Cell. LINDSAY DIERCKS (University of Iowa, Iowa City, IA 52242) JOHN KERR (Lawrence Berkeley National Laboratory, Berkeley, CA 94720). In a world with dwindling oil reserves and increasing energy demands, reduction of carbon dioxide to methanol using solar generated electricity is a probable and environmentally conscious solution. The part of the carbon dioxide to

methanol process that this research is specifically involved in is the reduction of carbon dioxide to formate. The stereo-selectivity of Lactic Dehydrogenase (LDH) was investigated in the reduction of pyruvate to lactic acid as was the reduction of carbon dioxide to formate with only a Rhodium catalyst. Reactions were run in a glass electrochemical cell, and products of the reactions were analyzed on a Capillary Electrophoresis (CE). The pyruvate reaction showed the presence of lactic acid, however it was not certain if pyruvate was also present. The absence of pyruvate on the CE analysis of the pyruvate reaction could mean that there was a one hundred percent conversion of pyruvate to lactic acid, but that result has yet to be reproduced. The carbon dioxide reaction shows the presence of formate, but not oxalate—also a product of carbon dioxide reduction. It has yet to be determined if formate is the sole product of the reduction of carbon dioxide with a Rhodium catalyst.

Measurement of Fair Weather Air Conductivity. MONROE

DALLAS, JR., NATISSA MCCLESTER, (*Florence-Darlington Technical College, Florence, SC 29501*) **JEFFREY GRIFFIN** (*Pacific Northwest National Laboratory, Richland, WA 99352*). For the past 4 years, staff at the U.S. Department of Energy's Pacific Northwest National Laboratory have been investigating the generation, and transport of radiation-induced ions near the ground. Baseline measurements of fair weather atmospheric conductivity are required in order to estimate ions lifetimes and predict ions detectability downwind of a radioactive source. Using a Gerding condenser, atmospheric conductivity measurements were made over a two week period, July 10-21, 2006 in the 300 Area of the Hanford Site. Experimental data, during that time period, show some uniformity, with atmospheric conductivity values ranging from 1.4 to 1.8×10^{-14} S/m. These results are consistent with published values for arid rural desert regions throughout the world. Weather conditions were similar over the two weeks that the experiments were performed. Therefore; to obtain more valid background atmospheric conductivities, future experiments should look into variable weather conditions and evaluate their effects on atmospheric conductivities at the site.

Mechanizing Photoelectron Spectrometer at HERS. XIORANNY

LINARES (*University of California—Berkeley, Berkeley, CA 94720*) **ZAHID HUSSAIN** (*Lawrence Berkeley National Laboratory, Berkeley, CA 94720*). Superconductors have been a main topic of scientific research since their discovery in the 1950s. In the attempt to understand superconductors, researchers later discovered cuprates. The discovery of these "high-Tc" superconductors increased scientists' possibilities of developing room-temperature superconductors. This development would increase the efficiency of electric generation, transmission, distribution, and utilization. This would result in a reduction of generated power requirement, and thus, a decrease in greenhouse emissions to the atmosphere. However, the complexity of high-tc superconductors and their inability to follow the theories of conventional superconductors has thus far prevented the creation of room-temperature superconductors. At the Lawrence Berkeley National Laboratory, the research group under the leadership of Zahid Hussain tests high-Tc superconductors to describe their properties and how they work. They study electron systems using a state-of-the-art High-Energy-Resolution-Spectrometer (HERS) for angle-resolved photoemission experiments. In these tests, x-rays are flashed on a sample, and electrons are then emitted via the photoelectric effect. The emitted electrons are analyzed by a state-of-the-art angle-resolved electron-energy analyzer (Scienta SES-200) that rotates about the sample. The electron analyzer measures the angle and kinetic energy of the electrons, which, through the conservation of energy and momentum, determines their velocity, scattering rates, and energy. The information found is used to create a graph portraying the electron's momentum vs. its kinetic energy. This graph shows the Fermi surface of the material. The Fermi surface is the surface of constant energy in a space that at absolute zero separates the unfilled orbitals from the filled orbitals. Its shape determines the electrical properties of the metal since the current is due to changes in the occupancy of states near Fermi surface. In this way scientists can determine the properties and composition of the material. The research group's testing process is long and time consuming since they have to rotate the analyzer manually to obtain their results. To improve their process, I will make a system that rotates the analyzer automatically and collects data without the need of constant supervision. I will research the most efficient way to rotate the analyzer, make accurate drawings of the system, make the parts needed for the system, assemble it, test it, and integrate it for future use.

MEMS Optical Force Probe. KEVIN LIN (*University of California—Berkeley, Berkeley, CA 94720*) **JACK KOTOVSKY** (*Lawrence Livermore National Laboratory, Livermore, CA 94550*). This work seeks to design small and tunable optical force probes to measure compressive loads.

As the sensor will be placed between two surfaces, a major goal is to minimize the thickness of the sensor. Optical sensors based on fiber optic and Micro-electro-mechanical systems (MEMS) technology allow for small, versatile, and accurate sensors. These sensors do not use electricity, and offer numerous advantages over traditional sensors. Fiber Bragg Gratings (FBGs) are treated fibers that have a periodically varying index of refraction to give a distinct reflection and transmission spectrum. This spectrum is dependent on strain, caused either by a transducer attached to the fiber or thermal expansion. A challenge of this work is to create a MEMS structure that transduces transverse loads to fiber strain while compensating for thermal expansion. The limitations of silicon and the size of the device introduce many challenges. Finite Element Analysis (FEA) simulates the mechanical and thermal behavior of the MEMS transducer and its micro-beams to determine a suitable geometry (i.e., angle, length, and height). Various metal coatings, solders, and soldering techniques are examined to determine a repeatable and reliable method for sensor assembly. Groove cross-sections are optimized for superior fiber to silicon bonding. Novel schemes assist in the alignment and assembly of the sensor. An optical force sensor using FBGs has been designed with a total thickness of 140um (similar in thickness to a fiber optic cable), insignificant thermal sensitivity, tuneability to different applied pressures, and mass manufacturability. Its fabrication is currently underway.

Minimizing Thermal Fluctuations and Vibration Effects on a High

Resolution Beamline. ALFREDO TUESTA (*University of Notre Dame, Notre Dame, IN 46556*) **NICHOLAS KELEZ** (*Lawrence Berkeley National Laboratory, Berkeley, CA 94720*). Thermal fluctuations from the environment and vibrational impacts from surrounding equipment pose a threat to the performance of high resolution beamlines. An optimal solution is unknown because methods for addressing these issues have never been empirically tested. This research focuses on the support structures, or stands, of MERLIN (meV resolution beamline) but the results can be applied to any beamline. The team measured the ground vibrations at several locations of the Advance Light Source (ALS) where MERLIN will be installed. Two stands, one empty and one filled with Zanite® Polymer Composite (Zanite), were also tested to determine the amplification of vibrations from the ground to the top. The change in the temperature of the top and middle of the empty stand was also recorded along with the change in ambient and floor temperatures for two and a half days. The ground measurements show little change when nearby equipment is turned off. Additionally, the RMS displacement is lower than the team's goal of 0.5-1 micron. The empty stand shows voltage peaks at 40, 60, and 120 Hz, the later two which are damped in the stand filled with Zanite. The air temperature at the ALS changed 1.2 C making the stand temperature fluctuate approximately 0.8 C yielding a 9.8 microns axial deflection. This suggests that the stand must be insulated or filled with a material that will increase its thermal mass in order to decrease its deformation. Zanite should provide this thermal mass, however, more time was necessary to confirm this. Due to experimental error and equipment failure, the results for the ground vibration measurements are sometimes unclear or erroneous. More time was required to rectify these issues and to continue measurements of other methods for solving the thermal fluctuation and vibration effects at the ALS.

National Synchrotron Light Source-II (NSLS-II) Initial Conceptual

Design Report. ERIC CHANG (*Carnegie Mellon University, Pittsburgh, PA 15213*) **ALAN RAPHAEL** (*Brookhaven National Laboratory, Upton, NY 11973*). The National Synchrotron Light Source II (NSLS-II) is an anticipated \$700 million medium energy storage ring designed to deliver constant brightness and flux for hundreds of scientific experiments each year at the Brookhaven National Laboratory (BNL) in Upton, NY. Once operational, NSLS-II will have a diameter of 794 feet and be able to deliver x-rays 10,000 times brighter than the existing National Synchrotron Light Source (NSLS-I) facility. The Department of Energy granted the NSLS-II building proposal "Critical Decision Zero" (CD-0) approving of the facility, allowing site planning to begin (CD-1). The primary project objective was to draft an initial plan for utility placement and an underground emergency tunnel servicing the NSLS-II facility using AutoDesk Architectural Desktop AutoCAD software and a collection of site maps of the entire facility as drafting tools. Among the utilities that were to be supplied are electrical, communication, storm water, fire protection, sanitary, and steam. By analyzing the topography of the site as well as the underground placement of currently operational utilities, the exact depth locations and routing of the various utilities could be completed. Once all the utilities were stemmed from existing lines and drawn on the utility site maps of the facility, an updated map of the facility and in depth depiction of each line was produced. In addition to utilities, an underground tunnel was

conceptualized for the use by emergency vehicles. Using the sitemaps, utility investigations, and geotechnical reviews of groundwater history, distance calculations indicated the prime location for the tunnel and later modeled on the computer. The project is a small portion of the much larger planning stages involved for the NSLS-II construction as summarized in a Conceptual Design Report (CDR), which also outlines a budget, scheduling, and environmental/health concerns. With the updated utility maps and models produced, the CDR will be able to better plan the NSLS-II facility accounting for the utilities research and tunnel conceptualization performed. As plans for NSLS-II are finalized and sent for approval, it is expected construction will begin in 2008 and operational in 2012.

Opportunities for Direct Current Power Distribution in Commercial Buildings. PEARL DONOHOO (*Franklin W. Olin College of Engineering, Needham, MA 29492*) MICHAEL DERU (*National Renewable Energy Laboratory, Golden, CO 89401*). Direct current (DC) systems in commercial buildings have the potential for energy savings through increased motor efficiency, elimination of rectifiers, and use of distributed generation of renewable energy. These potential savings are documented through past studies on power supply efficiency, motor efficiency, and new concepts in DC distribution. Despite alternating current (AC) distribution, components of heating, ventilation, and air conditioning (HVAC) systems, fluorescent ballasts, and plug loads all use DC power. To quantify energy savings, a DC system model of the Pennsylvania Department of Environmental Protection Cambria Office building was completed. The three major building systems, HVAC, interior lighting, and plug-load were modeled, which covered 96% of building energy use. The buildings systems were modeled twice using data from a previous study of the building, first assuming one large rectifier and secondly assuming supplied DC power. The model predicted an annual average savings of \$2,700 with a rectifier and \$3,200 without.

Performance Comparison between Graphite and Metallic Bipolar Plates in Direct Methanol Fuel Cell (DMFC). RAJA CROWLEY (*Farmingdale State University, Farmingdale, NY 11735*) DR. DEVINDER MAHAJAN (*Brookhaven National Laboratory, Upton, NY 11973*). The use of Direct Methanol Fuel Cell (DMFC) is an electrochemical process without combustion as an alternative source of energy. A DMFC can produce energy constantly, unlike a Lithium battery which stores energy and after all energy is used up, a battery must be recharged for a long period of time. Since methanol is available in a liquid form, it requires minimum storage volume and is easy to transport. DMFCs have been used in different hand held applications such as cell phones and laptop computers. There are many parameters that have an effect on the performance of the DMFC such as the methanol concentrations, fluid and air flow rate, temperature, and the humidity level inside the air side of the cell. In this experiment a performance comparison between graphite and metal treated plates was studied with different methanol concentrations with and without humidification. Membrane Electrode Assembly (MEA) for DMFC with an active area of 2.54cm x 2.54cm, Pt/Ru catalyst in the anode side and Pt. catalyst in the cathode side, were used in two single fuel cells, one with graphite plates and the other with treated metal plates. The liquid methanol was fed to the cell at a rate of 6 ml/min. Methanol concentrations of 3%, 5%, 7%, and 10% diluted in distilled water were used in both cells, under room temperature, 15psi air pressure, and an air flow rate of 1.0 SCFH. 3% and 5% methanol concentrations showed an optimum performance in graphite and metallic plates respectively. The 3% methanol concentration yielded 29% higher performance in the metallic bipolar plates and the 5% methanol showed 45% higher performance in the metallic plates relative to graphite. Graphite Plates with 3% and 5% methanol concentrations with 40% humidity at the air side resulted in 16% and 21% improvement in performance respectively. While metallic plates with 3% and 5% methanol concentrations, after similar humidification was applied, showed 2%, and 9% improvement in performance respectively. Accordingly, it was concluded that the metallic bipolar plates showed higher performance than the graphite plates, and controlled humidification in the vicinity of 30% to 50% has positive influence on the performance of the cell. Humidification had more effect on the graphite plates than the metallic plates and was attributed to the surface energy of both materials. Future work will focus on optimization of the performance of the single cell and to build a stack of DMFC to power a mobile phone.

Performance of Generation 3 High-power Lithium-ion Trial Cells. AVERI ESCALONA (*University of Illinois at Chicago, Chicago, IL 60606*) IRA BLOOM (*Argonne National Laboratory, Argonne, IL 60439*). Li-ion batteries have proven to be a successful energy source for many consumer electronic devices. Research is now being done to develop

this technology for other applications, particularly as an energy source for hybrid electric vehicles. The Freedom Cooperative Automotive Research (FreedomCAR, formerly known as the Partnership for the Next Generation of Vehicles) has developed certain goals and standards for high-power, Li-ion battery cells for vehicular application. The U.S. Department of Energy's Advanced Technology Development Program addresses issues related to meeting these goals and standards. The program consists of a series of five projects, including the development of a baseline generation of cells (Generation 1) and an evaluation of it, followed by improved iterations (Generations 2 and 3) and finally low-cost packaging for the cells. The Electrochemical Analysis and Diagnostics Laboratory at Argonne National Laboratory evaluated and compared the performance of eight different trial Li-ion cell chemistries to the cell performance of a previous generation (Generation 2, or Gen2) of cells in order to determine an optimal cell composition for the next generation (Generation 3, or Gen3) of cells for a larger study. Good cell performance was evaluated in this particular study in terms of low capacity fade over time and low impedance rise over time. Characterization was done at the beginning of the study to establish a baseline for trial cell performance over time. Calendar-life aging was used as a method of cell degradation, with reference performance tests performed at four week intervals in order to gauge change in cell performance over time. Testing is still in progress, but initial results show that the capacity retention of one of the Gen3 trial chemistries, the 700-series, is better than that of Gen2, and two of the Gen3 trial chemistries, the 600- and 700-series, have a rate of impedance rise similar to that of Gen2. All Gen3 trial chemistries have both lower capacities and higher impedance than the Gen2 chemistry, but it is possible to attribute this to factors such as poor cell composition or physical damage. Based on this initial data, the 700-series cells should be considered for further study.

Performance Testing of Radio Frequency Identification Tags and Evaluation of Russian Radio Frequency-Based Tamper Indication Devices for Nuclear Safeguards. BEN PETERS (*Maryville College, Maryville, TN 37830*) CHRIS A. PICKETT (*Oak Ridge National Laboratory, Oak Ridge, TN 37831*). Two promising technologies that are being evaluated to help in nuclear material control and accountability are Radio Frequency Identification (RFID) tags and active radiofrequency (RF)-based Tamper Indication Devices (TIDs). There are both active and passive RFID tag systems. Passive RFID systems utilize a reader that induces the passive tag to transmit an RF signal back to the reader in the form of a unique digital identification number. Active tags, on the other hand, are battery powered and continuously transmit an RF signal. Two kinds of active RF-based TIDs supplied by a Russian laboratory were also tested at ORNL. The two TIDs are RF tags that utilize fiber-optic technology to create a loop-type seal, along with bolt seals, which use either a piezoelectric generator or galvanic power cell to provide power to the seals. The active RF TID tags were installed on actual radiological storage containers and evaluated in operation over several weeks. Several RFID tags and readers were characterized to determine read ranges and the effects associated with orientation and placement of the tags on metal storage containers. Ten RFID tags of each type (active and passive) were used in order to determine read range variance. Multiple trials were conducted using tags positioned at four different angles in relationship to the antenna. After multiple trials, the results illustrated that there are both benefits and limitations to using both these technologies for safeguards-related applications. The performance of the passive RFID tag system was primarily affected by the antenna size, as well as with the tag size and type. If these factors are considered during system design, an effective RFID system can be developed to maximize the read range and, therefore, the number of reads. The problems seen with the Russian TIDs were mainly associated with the design of the tag or bolt themselves. More testing and possibly some design changes will be needed before any final recommendations can be made.

Polycrystalline Ceramic Scintillators. ANDREA NORTH (*University of Tennessee, Knoxville, TN 37934*) DANNY POWELL (*Oak Ridge National Laboratory, Oak Ridge, TN 37831*). Scintillators are a vital component of radiation detection in numerous applications, including medical diagnostics and imaging, nuclear nonproliferation, and scientific research. Due to the demand for these detectors and the limitations of single-crystal scintillators, research of transparent polycrystalline ceramic scintillators has become increasingly attractive. This research has potential advantages for scintillation materials, such as the ease of fabrication and the ability for duplication. Recent studies of ZnO: Ga and Lu₂O₃: Eu have shown promise as potential transparent polycrystalline scintillators. However, additional studies are required to improve the transparency, size, and quality of the densified bodies.

After ensuring the purity of the materials, the powders are combined both manually and chemically to create a homogenous mixture. The powders are densified into a transparent ceramic through hot or cold pressing, vacuum sintering, and pulsed electric current sintering. The first method to be applied on these samples is hot press. The pellets are then tested for the important scintillation properties of decay time, light output, timing resolution, and energy resolution. Because this process is extensive and testing requires a significant amount of time, the project has not yet been completed. However, visual analysis of the ceramic after the hot pressing technique shows promise for these samples. The results from the ZnO: Ga and Lu₂O₃: Eu will enhance the knowledge of their capabilities and could also increase the abilities for radiation detection. Further work will involve different sintering techniques with these samples and also the testing of other samples. This is a very small portion of the research for improved scintillation materials that will mitigate the limitations of single-crystal scintillators.

Power Grid Dynamics: Enhancing Power System Operation through Prony Analysis. CODY RAY (Oregon State University, Corvallis, OR 97331) ZHENYU HUANG (Pacific Northwest National Laboratory, Richland, WA 99352). Prony Analysis promises to be an efficient way of recognizing sensitive lines during faults in power systems such as the U.S. Power grid. We use Positive Sequence Load Flow (PSLF) to simulate a simple two-area-four-generator system, and the dynamics the system experiences during a line fault. We then use the Dynamic System Identification (DSI) Toolbox to perform Prony analysis and use modal information to identify key transmission lines for power flow adjustment for improving system damping. We report on the success of the application of Prony analysis methods to the data obtained from PSLF, and the identification of the key transmission line for adjustment. Future work will focus on larger systems, and improving the current algorithms to deal with networks such as large portions of the Western Electricity Coordinating Council (WECC) power grid.

Power Performance Analysis of Wind Turbine Generation Systems. LAUREN COOPER (Colorado School of Mines, Golden, CO 80401) ARLINDA HUSKEY (National Renewable Energy Laboratory, Golden, CO 89401). The National Wind Technology Center (NWTC), located approximately 8 km south of Boulder, Colorado, is the premier research facility in the U.S. for wind turbine certification testing and evaluation services. NWTC provides performance, power quality, noise emissions, blade and loads testing in compliance with recognized international standards. Our research involves the power performance tests of wind turbine generation systems, which are used to determine the power performance characteristics of single wind turbines and to compare the performance of groups of turbines. Southwest Windpower, based in Flagstaff, Arizona, has partnered with NWTC to perform power performance analysis measurements of the AIR-X, a three-bladed upwind turbine rated at 400 watts. In 2003, an early version of the AIR-X was tested at NWTC. The results showed that the turbine was not performing at rated power because the shape of the blades was causing the turbine to enter stall mode at wind speeds within the turbine's normal operating range. NWTC is currently testing a version of the AIR-X with a modified blade shape. This new shape is supposed to reduce the aerodynamic fluttering that was previously causing the turbine to enter stall mode. The goal of our research was to write a power performance software program in Visual Basic for Microsoft Excel to analyze the power performance characteristics of wind turbines of all sizes and to use this program to test the performance of the new AIR-X. Our early test results indicate that the new blade shape has improved the power performance of the AIR-X by preventing the turbine from entering stall mode.

Pressure Loss in Cooling Channels Enhanced with Wire-Coil Inserts. WILLIAM O'BRIEN (Community College of Rhode Island, Warwick, RI 02886) JEFF T. COLLINS (Argonne National Laboratory, Argonne, IL 60439). Front end high-heat-load components of the insertion devices and bending magnets at the Advanced Photon Source (APS) are cooled with deionized (DI) water flowing through cooling channels that have oxygen free copper (OFC) wire-coils inserted into them to enhance convection heat transfer. The pressure loss across these cooling channels must be studied to optimize the design parameterized friction coefficients of the enhanced cooling channels and bulk fluid velocity of the DI water. One OFC test tube is used, with a 0.375 inch hydraulic diameter, made to accommodate the 13.5 inch long OFC wire-coil inserts. A matrix of OFC wire-coil inserts is fabricated in house with wire diameters ranging from 0.035–0.125 inches and different coil pitches ranging from 0.091–1.00 inches. Water is deionized, sterilized, filtered, and sent through a system of circuits designed to test flow rates across laminar, transitional, and turbulent flow regimes. Pressure loss, flow rate, and temperature readings are

collected and reduced to dimensionless quantities used to develop four equations correlating channel size, wire diameter, wire-coil pitch, mechanical fluid properties, and bulk fluid velocity of the DI water throughout laminar and turbulent flow. The correlation established will provide thermal engineers in the synchrotron light source community functions that predict coil pitch and wire size based upon design geometry and pressure loss needs.

Process Engineering for Hydrogen Production Plants Using High Temperature Steam Electrolysis. ALEJANDRO SAUCEDO, BHARAT THAKKAR, MARIBEL VALDEZ (Illinois Institute of Technology, Chicago, IL 60616) DR. RICHARD DOCTOR (Argonne National Laboratory, Argonne, IL 60439). Two process simulations for large-scale hydrogen production using High Temperature Steam Electrolysis (HTSE) have been introduced by Argonne National Laboratory (ANL) using ASPEN computer software and Idaho National Laboratory (INL) using HYSYS computer software. The economic feasibility of both processes must be determined thus a cost analysis of fluid transport and heat transfer equipment is conducted, and the energy balance is calculated. From these energy calculations, it is discovered that the optimum energy balance occurs in ANL's feed case of 50% water and 50% hydrogen. From the equipment cost analysis, it is estimated that for ANL the total process equipment cost is \$73 million, whereas for INL it is \$40 million. For both, ANL and INL systems, the total initial cost of the electrolysis unit and the nuclear reactor is about half a billion dollars. Although a HTSE hydrogen production plant will involve huge upfront investments in resources, this comparative economic analysis provides a basis for HTSE system selection.

Protein Effects on the Microstructure of Doped Silica Aerogels. BRANDI DOYLE (Texas Tech University, Lubbock, TX 79401) JAN ILAVSKY (Argonne National Laboratory, Argonne, IL 60439). Silica aerogels (AGs) are inorganic polymers with low density which are used in a wide variety of sensor applications. By doping the silica gel with cadmium sulfide (CdS) and myoglobin, a biocomposite AG used in biosensors is formed. Through better understanding of the microstructure of these porous solids, their properties can be improved and tailored towards specific applications. Silica AGs doped with a myoglobin protein in five different ratios were synthesized and then examined through ultra-small angle X-ray scattering (USAXS). Through the USAXS we expect to see an increase in the size of the protein superstructure with increasing amounts of myoglobin. The log-log plots of the Silica AGs doped with protein consistently show three structural levels, with the first pertaining to the protein superstructure. Through the comparison of the radius of gyration (R_g) which corresponds to the protein size with the percent of myoglobin in the protein mixture, the particle size of the superstructure does not show an increase, or any trend for that matter. Through future investigation we can determine if the percent myoglobin truly has no effect on size of protein superstructure or if there were other factors during sample preparation that affected their growth.

Remote Handling Tooling for the Spallation Neutron Source. DAVID MACNAIR (Georgia Tech University, Atlanta, GA 30332) CRAIG BRADLEY (Oak Ridge National Laboratory, Oak Ridge, TN 37831). The Spallation Neutron Source (SNS) will smash accelerated protons into liquid mercury which will create the most powerful neutron scattering facility in the world. When protons hit the mercury, the mercury becomes radioactively activated and the stainless steel housing for the mercury (the target) erodes. Every three months this target will be replaced, requiring the target cart to back into the target cell where manipulators, servo manipulators, and a crane change the target and perform needed maintenance. These operations require special remote handling tools to be designed, fabricated, and tested before the SNS comes online and the target cell becomes inaccessible. One of many tools worked on this semester is the lift compensator, which serves as a backup to the target cart hydraulic drive system. The compensator connects the overhead crane and the target cart backup jacks and will stretch like a spring giving the operator a gage on force applied to the jacks. Since the jacks fail at about 10,000 pounds of force, a break link was added which fails at 5,000 pounds and protects the backup jacks from damage. The spring in the compensator consists of seventy six Belleville washers stacked in series giving the operator 6.5 inches of movement between unloaded and 5,000 pounds. All components were designed using the solid modeler Pro/Engineer and then analyzed using hand calculations and finite element analysis with Pro/Engineer Mechanica. Results of the stress calculations were reviewed by the remote handling group and the SNS division, and finally the drawings were sent for fabrication. Fabrication has not finished, and no final results for the effectiveness of the design are available. Due to the magnitude of the project and the inaccessibility of the target cell by humans during SNS operation, each

component inside the target cell must be carefully designed, analyzed, and tested before the SNS starts up. Additionally, components must be easily accessible, maintainable, and maneuverable by remote handling equipment so that the SNS can enjoy scientific discovery even beyond the length of its original design.

Resource Constraint's Role in the Transition to a Closed Self Sufficient Global Nuclear Fuel Option. *TIMOTHY ROGERS (Texas A&M University, College Station, TX 77843) DAVID C WADE (Argonne National Laboratory, Argonne, IL 60439).* With uranium ore deposits estimated at about fifteen million tonnes, it is necessary to determine an optimal ore withdrawal strategy to ensure nuclear energy sustainability. Producing this strategy requires optimization of virgin ore usage so that enough fuel is available to introduce fast breeder reactors as well as secure transportable autonomous reactors. To find an optimal ore withdrawal, a classical mechanics mathematical model is used. State equations of the system form the state matrix, with the control matrix being the ore withdrawal of uranium and the transuranic fuel for each reactor type as a function of time which is simulated over the time interval chosen to find the final conditions. An adjoint solution is then found to construct the Hamiltonian variation with respect to the control matrix. This gradient is then subtracted off to produce a more optimal ore withdrawal control. This process is iterated to minimize the performance index, which is based on the power mismatch between target and actual powers, and then to maximize ore withdrawal to meet power demand. This provides the user with the best possible ore withdrawal strategy to ensure nuclear power growth. Results of this code are dependent on the user input and thus can vary over wide ranges of ore withdrawals. Output from this code shows the implications of introducing reactors that can create fuel. It also shows how early implementation of these types of reactors can help to alleviate the world's future power needs. As for future use of these results, it will be possible to use the optimal ore withdrawal as part of a high fidelity model that accounts for more factors relevant to nuclear power growth.

Rotor Design Optimization for Offshore Wind Turbines. *PAUL KREINER (Stanford University, Stanford, CA 94305) PATRICK MORIARTY (National Renewable Energy Laboratory, Golden, CO 89401).* Modern wind technology is among the most effective and profitable ways to simultaneously address global warming and meet America's growing energy needs. Nevertheless, further advancements, including the optimization of offshore wind turbines, will be necessary for continued success in the United States. This paper describes a MATLAB-based rotor design optimization program called Rotor Optimization for Offshore Turbines (ROOT) that includes both land-based and offshore cost models. The program uses MATLAB's Genetic Algorithm Tool to find the rotor radius, number of blades, chord distribution, and twist distribution that result in a minimum cost of energy (COE) for a given wind regime. To predict aerodynamic performance, ROOT uses a program developed at the National Wind Technology Center called WT_Perf, which relies on blade element momentum theory. ROOT includes a basic structural analysis as well as losses due to soiling, wind farm array effects, availability, and power conversion. Although ROOT requires further development, such as improvements in the structural and cost models, the version discussed in this paper proved to be an effective rotor design tool. ROOT consistently generates blade shapes that closely resemble existing designs, even when the program begins with a random set of geometrically unusual designs. For a wind regime near the Nantucket Sound, ROOT generated a rotor design that would improve COE by 4.6% over the baseline design.

Self-Powered Oil-Fired Heating System Based on Thermophotovoltaic Power Generation. *EVELYN MEJIA, MARTIN NOLAN (The City College of New York, New York, NY 10031) DR. THOMAS BUTCHER (Brookhaven National Laboratory, Upton, NY 11973).* Self-powered appliances, such as a home heating system, have the potential to operate independently from the electric power grid. Thermophotovoltaic (TPV) power generation is well suited for self-powering. This involves generation of electric power by converting radiant heat emitted by a high temperature emitter into electricity using photocells. Since the amount of power generated depends on how much energy is emitted, the radiant emitter becomes an important component of the TPV converter. In this project, a self-powered oil-fired heating system based on thermophotovoltaic power generation was designed and analyzed. For this project, computational and experimental analyses were used to maximize the emitter temperature, measure the emitter temperature distribution, and vary the geometry of the experimental setup in order to reach the desired temperature. The computational fluid dynamics (CFD) model simulated the heat transfer in the combustion chamber. Using the CFD model, possible changes

to the shape of the cylinder, placement of the TPV cells, and insulation thickness were explored so as to maximize the emitter temperature and exceed the target of 1300°C. From the CFD, the experimental analysis was designed; this work was part of an iterative process of adjusting the model and the experiments based on their results. The other analysis performed was experimental analysis; two geometrical cases were considered. In the first design case, the experiment was performed using a low Nitrogen Oxides (NO_x) (Blue Flame) burner with an open-end cylindrical Silicon Carbide (SiC) attached as a flame tube. The SiC emitter was selected because it can withstand temperatures above 1300°C, which is ideal for energy conversion. The emitter was wrapped with a refractory blanket to simulate the thermal resistance of the photovoltaic cells. In second design case, the flame tube was simply used to guide the flame toward a flat plate emitter, refractory blanket, and TPV cells that were placed at the open-end of the combustion chamber like a "target wall". The results for the first case showed the maximum temperature along the emitter was 1283°C and the second case, the gas temperature at the target wall reached 1569°C. Therefore, the second case was the ideal approach because it shows promise of being able to heat up the emitter above the desired temperature, 1300°C.

Single and Double Gas Electron Multiplier X-ray Gas Detector. *MARCUS MASON, ELHAG SHABAN (Southern University-Baton Rouge, Baton Rouge, LA 70813) DR. PETER SIDDONS (Brookhaven National Laboratory, Upton, NY 11973).* The purpose of this research is to present results obtained from testing of a single and a double GEM X-ray gaseous detector. The detectors have been designed, assembled, and tested at the National Synchrotron Light Source (NSLS) at Brookhaven National Laboratory (BNL). The single and the double GEM detectors are intended to provide a noise and discharge free amplification to be used for Extended X-ray Absorption Fine Structure (EXAFS) procedure. A voltage of 450 volts across the single GEM provided a maximum gain of 900. A voltage of 350 volts across the double GEMs provided a gain of 9000 without stressing the GEM and creating the possibility of discharges.

SNS Beam Characterization Using Wire Scanner Analysis. *FEDRICK REYNOLDS (Tennessee State University, Nashville, TN 37209) TED WILLIAMS (Oak Ridge National Laboratory, Oak Ridge, TN 37831).* The Spallation Neutron Source (SNS) is the most powerful pulsed source of neutrons in the world. The SNS consists of a Linear Accelerator (Linac) that accelerates negatively charged hydrogen ions (H⁻) throughout the various regions of the Linac to approximately 88% of the speed of light. These regions include the Medium Energy Beam Transport (MEBT), Drift Tube Linac (DTL), Coupled Cavity Linac (CCL), Super Conducting Linac (SCL), High Energy Beam Transport (HEBT), Accumulator Ring, Ring to Target Beam Transport (RTBT), and finally the Mercury (Hg) target. After the H⁻ beam is accelerated, it is transported to the Accumulator Ring where all of the electrons in the beam are stripped off, thereby converting the beam to only protons. Once released from the Accumulator Ring, the beam then hits the Hg target and knocks out numerous neutrons from the Hg nucleus, which are used for research. Diagnostic equipment throughout the Linac provides data that are used to monitor, correct, and characterize the trajectory and shape of the beam. Some of these devices are wire scanners, which are used to measure the beam's position. Furthermore, the wire scanner data are used to set the magnetic field strengths of the quadrupole magnets; these are used to focus the beam. This is particularly important to the beam-to-target transfer process. Without correct steering, the full benefit of the beam on the target could not be achieved. Using a variety of programs, including Wireanalysis and Graphical Analysis; Gaussian and bi-Gaussian fits are calculated to measure the beam sizes. The measurements of the magnets' parameters are included in the data taken. The beam sizes and the magnets' parameters are fed into the model, and the output generated gives a plot of the sizes of the beam at various positions in the MEBT. The data is also compared on the same graph. The disparity between the two indicates how the beam changes in the MEBT. Adjustments were made to better fit the data. For example, while using wire analysis, the program was only allowed to fit the data that represented a Gaussian profile. This changed some values, but ultimately resulted in a better fit of the data. Although the beam will never be characterized without any error, there is the possibility of characterization with minimal error. Therefore, it is imperative that this research continue.

Structure of Phosphatidylcholine Cholesterol Bilayers Using Grazing Instance Small Angle X-ray Scattering. *CHRISTOPHER LEHMANN (Texas Tech University, Lubbock, TX 79409) JAN ILAVSKY (Argonne National Laboratory, Argonne, IL 60439).* Lipid bilayer membranes isolate and protect cells in the body. The structure of

cholesterol/lipid bilayer membranes are studied to understand the manner in which molecules attach and interact at the cell membrane. This research is to determine whether the membrane lipids form ordered structure. The presence of regular lipid structures would affect the manner of drug interaction with the cell membrane and improve the understanding of the progression of many diseases associated with cholesterol. In addition, membrane organization would suggest possible behavior and design of model cell membranes in microarray and microfluidic biochips. In this work, cholesterol/palmitoyloleoyl phosphatidylcholine (Chol/POPC) bilayers on a glass substrate were studied under grazing incidence small angle x-ray scattering (GISAXS). GISAXS was used to measure the diffraction patterns and specular reflectivity. GISAXS is a useful method for lipid membrane research because it probes the area near the interface and data acquisition is fast, minimizing sample exposure to high photon fluxes. Research found the concentration of cholesterol in the bilayer mixture affects the structure of the membrane. Analysis of the collected data shows diffraction in more than one sample. For the samples that showed specular reflectivity the characteristic d-spacing observed is around 40 angstroms. Specular reflectivity suggests that the sample had regions of uniform structure. Future work should examine cholesterol concentrations in the range of 20 to 50-mol%. Membranes with higher mole percent may allow for better imaging because of the larger differences in electron density, also they closely mimic lipid/cholesterol compositions found in mammalian cells. GISAXS will be used in observing the diffraction because it proved an effective way to measure lipid bilayers at high fluxes. In addition, reflectivity data should be taken on the samples. The number of layers present from the reflectivity data would confirm whether a single uniform lipid bilayer is present.

Sulfuric Acid Materials Test Loop. DANIEL LAMONE (*The Ohio State University, Columbus, OH 43210*) STEVEN SHERMAN (*Idaho National Laboratory, Idaho Falls, ID 83415*). Several hydrogen production processes are currently under investigation by the U.S. Department of Energy (DOE) and several foreign governments, most notably France and Japan, for use in a co-located nuclear plant/hydrogen production facility. One of these processes is the Sulfur-Iodine Thermochemical Process. This process utilizes a series of chemical reactions that are driven by the thermal energy from a Very High Temperature Gas-Cooled Reactor (VHTR) to thermochemically split water into hydrogen and oxygen. The high-temperature chemical step in this process thermally decomposes sulfuric acid (H₂SO₄) at 850 °C, imposing extreme demands on the process materials. To date, little research has been conducted in the U.S. to study the long-term effects of these conditions on structural materials and components, and there are no existing facilities beyond the bench-top for performing such tests. Therefore, there is a need for a closed experimental loop containing sulfuric acid that is capable of exposing samples and integrated components (e.g., heat exchangers, valve designs, etc.) to sulfuric acid decomposition products at high temperatures (750–850°C) for long periods of time. The loop must be capable of long-term, continuous operation (hundreds to thousands of hours) under simulated operational conditions that are to be found in the actual production facility, accommodate different component prototype designs and their respective testing requirements, and operate safely during all periods of operation. This loop will be built and operated at a U.S. Department of Energy (DOE) facility or partner facility under the direction of the DOE Nuclear Hydrogen Initiative (NHI). This project provides a conceptual design for such a materials and component test loop and will serve as a starting point for more of the more detailed design and safety analysis work that will be needed once the loop is scheduled for construction and operation.

Synthesis and Electrochemistry of Composite-Structured Lithium Nickel Manganese Oxides for Lithium Batteries. JENNIFER GATES (*Fayetteville State University, Fayetteville, NC 28301*) CHRISTOPHER JOHNSON (*Argonne National Laboratory, Argonne, IL 60439*). Low weight and volume, high energy and power density, stability over many cycles, a large range of operating temperature, low cost, and safety are desired properties in all secondary batteries, but particularly those that are used in cell phones, laptops, and hybrid vehicles. Lithium's low molecular weight and very negative reduction potential place lithium-ion batteries in a good position towards meeting these goals, but much work must be done towards improving the batteries. In batteries that are currently used in cell phones, a lithium-graphite intercalation solid is the anode and the cathode is LiMn₂O₄ or LiCoO₂. We investigated (1-x)LiNi_{0.5}Mn_{0.5}O₂•xLiNi_{0.5}Mn_{1.5}O₄ composites, where x is varied from 0 to 1 in increments of 0.1, as a cathode material, in order to try to improve the capabilities of the cathode. The compositions we studied are composites of a layered and a spinel oxide phase. A composite structure may be expected to have a greater stability to lithium insertion/

extraction due to synergism between the two phases. Many new lithium metal oxides were synthesized and optimized for phase purity and structure. Electrochemical characteristics are being studied such as current rate, cycle life, stability, and safety in "coin cells". The coin cells were made using lithium metal as the anode; ethylene carbonate (EC) and ethyl methyl carbonate (EMC) in a ratio of 3:7 respectively as the solvent, and LiPF₆ as the electrolyte. The current density was 0.10 mA/cm², which gives approximately 20 h discharge or charge time.

***Testing and Development of Neutron Bubble Dosimeters for Upgrading Radiation Monitors.** PHILLIP ZELLNER (*Virginia Polytechnic Institute and State University, Blacksburg, VA 24060*) ERIK ABKEMEIER (*Thomas Jefferson National Accelerator Facility, Newport News, VA 23606*). Jefferson Lab is upgrading its particle accelerator from 6 GeV to 12 GeV to give physicists greater insight in the experiments they run. An unfortunate side effect of the upgrade, is that the experiments performed by Jefferson Lab will generate neutron radiation with much higher energy (up to 20 MeV). The ion chambers that the Lab uses to monitor the radiation dose given to the public, will not be able to detect the higher energy neutrons. In order to solve this problem, neutron bubble dosimeters are being developed to detect the higher energy neutrons. These dosimeters are the first instruments to put superheated bubbles. The ability of the neutron bubble dosimeters to detect 20 MeV neutrons has already been proven. However, this project tested the feasibility of using the neutron bubble dosimeters. The detectors were tested on Jefferson Lab's radiation range and calibrated. Then the neutron bubble dosimeters were tested side-by-side with the ion chamber dosimeters in the existing radiation monitoring stations. It was shown that the neutron bubble dosimeters could detect the higher energy neutrons. The test results from the comparison of the two types of dosimeters showed that the neutron bubble dosimeters were at least as reliable as the ion chambers in detecting the neutrons that are currently produced by the accelerator. This success ensures that a reliable radiation detection system will be in place well before the 12 GeV upgrade is complete, thereby ensuring the safety of Jefferson Lab's employees and the public.

Testing of Beam Position Monitor Calibration Software. ELI CARREIRO (*Rensselaer Polytechnic Institute, Troy, NY 12180*) THOMAS RUSSO (*Brookhaven National Laboratory, Upton, NY 11973*). New software has been developed for the Relativistic Heavy Ion Collider (RHIC) Beam Position Monitor (BPM) hardware. This software is designed, via calibration, to remove drift within the BPM motherboard, and to make only one initial time—consuming external calibration necessary. The data points from the initial external calibration are saved and utilized in remotely performed internal calibrations. Testing of the software has made use of the following instruments and experimental processes: function generators to simulate the RHIC beam signal to the BPM boards; actual RHIC beam signal; oscilloscopes to monitor electronic activity in board circuitry; resistors soldered onto certain points of the boards in order to introduce artificial drift; and finally, LabVIEW and NX Client software. NX Client software was used to read and to plot calibration data obtained from BPM boards, and LabVIEW virtual instruments were used to vary internal pulser attenuation values of the BPM boards throughout testing. After several tests and modifications to the software, the new version of code proved to be robust in maintaining calibration over a more than acceptable range of internal pulser attenuation values. Furthermore, experimentation revealed the software to be capable of calibrating out simulated drift to well within accepted error ranges. Testing of BPM boards installed in the RHIC showed the software to be operational with real beam signal. The new software is a significant improvement over past systems and, pending further testing and the implementation of a curve smoothing algorithm for calibrations utilizing the RHIC beam data, the software will be employed in all of the RHIC BPM hardware.

***The Solar Hydrogen Home.** RODRIGO PENA (*Nassau Community College, Garden City, NY 11530*) DEVINDER MAHAJAN (*Brookhaven National Laboratory, Upton, NY 11973*). As oil prices continue to escalate to levels that threaten our economy, alternative energy is starting to play an important role in our society. Hydrogen fuel cells and solar panels are alternatives that promise a non pollutant way of producing energy. A solar cell is a p-n junction, made out of silicon (semiconductor). A p-n junction is the product of two layers of the same semiconductor material that are doped with different materials to leave one free electron in a layer, and a deficit of one electron in the other layer. A photon will move this free electron from one layer to the other, inducing an electrical field at the interface of these two layers, and a current will flow when the circuit is closed. A solar energy arrangement (photovoltaic system) will be used to meet the load of an average household that requires approximately 10,000 kWhr of energy

per year. The objective of the current work is to put together a cost effective model house scaled down 1:300 of the energy required for an average residential home to conduct system and energy analysis. The photovoltaic (PV) size facing south required to meet the load of an average household is 9 kW with efficiency of 75% that counts for inverter and wiring losses of the system. In this project, two solar panels measured at 15 watts each will simulate the 9 kW PV system. These two solar panels will be used to feed the total consumption of the model house. In New York, the average sun hours per day are 4.3 hours, during which the PV system will produce the total energy needed to run the house for the whole day. The excess portion of solar energy that is not used during the 4.3 hours will be used to electrolyze water and generate hydrogen and oxygen. The hydrogen is stored in tanks to be used after the sun set to produce energy on demand by hydrogen fuel cells. The current experimental work showed that for 9 kW PV system, the hydrogen production is one fourth the total amount needed to cover the energy demand for the remaining hours of the day after sun set. This is attributed to the efficiencies of the fuel cell and Electrolyzer at the current state of technology.

The Utilization of Thermoelectrics to Capture Excess Waste Heat Produced by an Oil Burner in the Pursuit of Developing a Self-Powered Boiler. JULIAN TAWFIK (*Stony Brook University, Stony Brook, NY 11794*) DR. THOMAS BUTCHER (*Brookhaven National Laboratory, Upton, NY 11973*). Thermoelectric devices produce electric power when exposed to a ΔT (temperature difference), between the hot and cold junctions. The objective of this project is to conduct theoretical/conceptual feasibility and economic studies on the utilization of thermoelectrics and their ability to produce electricity from temperature gradients generated by an oil boiler to power its electrical components and make it electrically self-sufficient, with no need for a connection to an external power source. The most efficient installation location of the devices on the boiler and its components with the appropriate ΔT was determined (on the boiler wall/exhaust pipe) to produce the 100 watts of electricity needed to power the auxiliary boiler units. The current analysis includes the following factors: maximum temperature the thermoelectric devices could withstand, how many thermoelectrics could be accommodated on the boiler unit or its components, and cost effectiveness with return on investment (ROI). A heat sink, to prevent the overheating of the devices by maintaining the cold side at ambient temperature was designed. Two bismuth-telluride thermoelectric units were tested and an IV curve was obtained (current/voltage) to determine if they would perform under operating conditions of 155°C ΔT between the boiler wall/exhaust pipe (175°C) and ambient air (20°C). 10 units of the #219 model, 5.7-watt generators would need to be purchased at a cost of \$419.50. After 20,000hrs the ROI of the units would be \$420.00 (a 50¢ gain), which is economically unfeasible. Total burner surface area required was 291.6 cm². Results show that making an oil-burning boiler self-sufficient is possible, but uneconomical until more efficient and inexpensive materials are available. Some materials currently being researched are cobalt based and thin film superlattice thermoelectrics. In conclusion, the research here has contributed to the efficiency of oil burning boilers so that less fossil fuels are consumed to maintain a cleaner, healthier tomorrow.

Thermal Management of a PEMFC with Air Cooling. NEVILLE PERKINS (*Farmingdale State University, Farmingdale, NY 11735*) DEVINDER MAHAJAN (*Brookhaven National Laboratory, Upton, NY 11973*). The use of fossil fuel has become a major problem that has national security implications and environmental concerns. The emission of green house gasses and the need for clean renewable energy has led to the research into alternative energy sources. One of the options to replace fossil fuels is hydrogen fuel that can be utilized in a PEMFC. The PEMFC produces heat energy as a byproduct of the chemical reaction needed to produce electrical energy. The removal of excess heat produced at a rate that keeps the internal temperature constant at about 80°C is a challenge. Monitoring and controlling the external temperature of the active area of the flow field at the bipolar plate or end plate can be an economic way to keep the fuel cell within an ideal temperature range. In this project, an array of 15 thermocouples was dispersed across three bipolar plates in a fuel cell stack to monitor the internal temperature and the rate of heat production. An infrared heat sensing camera was also used to display the external surface temperature of an operating fuel cell. The output from the sixteen 15 thermocouples were connected to data acquisition software. Real-time temperature monitoring was automatically performed at predetermined time intervals. Two fans with variable air flow were used to introduce a steady stream of air to cool the external surface of the fuel cell stack. Two other sensors were used to measure temperatures up and down stream of the air flow used to

cool the fuel cell. Data was collected with the fuel cell stack operating at various power levels while establishing the air flow required to keep the internal fuel cell temperature constant at safe operating level. The heat generated by the power stack spikes and causes hot spots during periods of high demand, requiring effective cooling. It is inferred from the collected data that an economical air-cooling system could be designed for a fuel cell stack that would allow it to operate under isothermal conditions. Finding a relationship between active area, heat produced, and air flow required to remove excess heat can supply the design tool needed to configure the cooling system for any fuel cell size.

Three Dimensional Environment Models for Electromagnetic Wave Simulation. TOMAS TINOCO (*Diablo Valley College, Pleasant Hill, CA 94523*) JAMES NUTARO (*Oak Ridge National Laboratory, Oak Ridge, TN 37831*). Accurate electromagnetic wave simulation demands accurate models of the environment. New techniques that combine ideas proposed by Christiaan Huygens, transmission line theory, and the powerful capabilities of today's computers, could allow fast, accurate and large scale electromagnetic wave simulations. These techniques require three dimensional models with information of the material properties at each point in space to calculate the speed of wave propagation as well as the reflection and transmission coefficients. Therefore, such techniques can not be applied unless models with the necessary information are provided. To address this problem and create the required models, elevation data from the United States Geological Survey (USGS) was used for modeling terrain and Virtual Reality Modeling Language (VRML) was used for modeling buildings. From USGS files, information was extracted to determine the elevation points of a specific region. Subsequently, interpolation techniques were used to obtain the required resolution and a three dimensional array was allocated to store the properties of each point in space. For modeling buildings, VRML files were used as input to a conversion software that stored the physical properties of each location based on the VRML shapes present and their specifications. Using these methods, two models were created; one model using USGS elevation data for Bethel Valley and the other from a VRML model of Oak Ridge National Laboratory courtyard. The terrain model had one meter resolution and contained material properties at each location but was limited to two types of materials. On the other hand, the courtyard model was based on basic shapes but contained the required resolution and a greater variety of material types. This work allowed the creation of the necessary three dimensional models of the environment with the required information and resolution for testing an electromagnetic wave simulator. It was possible to execute the simulation in these models to analyze the time and memory efficiency and to find ways to increase the speed of simulation. Lastly, the courtyard model was used to simulate the path loss of a radio signal and the results were in agreement with measurements taken at different locations of the model. Based on the difference between simulated and measured values, the research team can increase the level of details of the model to improve the results produced by the simulator.

Transportable Radiation Monitoring Systems. JULIA MOLINE (*Columbia University, New York, NY 10027*) PAT HU (*Oak Ridge National Laboratory, Oak Ridge, TN 37831*). Malevolent use of radioactive material poses a great threat to U.S. national security. As part of U.S. Department of Homeland Security's initiative to address threats of transporting illicit radioactive materials on the national transportation network, the Oak Ridge National Laboratory (ORNL) is designing and testing a Transportable Radiation Monitoring System (TRMS). TRMS is a set of radionuclide detectors that could be set up at truck stops, rest areas, or on either side of a road to monitor vehicles passing through. The development of the TRMS will allow authorities to deploy radionuclide detectors to any site through which they believe illicit radioactive material may be traveling. It will also facilitate the necessary communication between local, state, and federal law enforcement agencies in the event that something illicit is detected. In May and June, 2006, the TRMS was tested at three sites on the grounds of ORNL. Its accuracy and efficiency were measured by observing its operational efficiency (e.g., recorded down-times) and by comparing the data the system recorded with information on shipments of radioactive material, which were provided by the ORNL Shipping Department. The data were analyzed by a number of variables, including the radionuclides carried by monitored vehicles, speed of vehicles going through the TRMS, and weather conditions at the test sites. Based on conclusions drawn from a series of statistical analyses on the data, the system and the procedures used to operate it will be improved. After the preliminary analysis of the TRMS tests is complete, the system will be tested at various sites on interstates in the Southeast. The challenges of these field tests include not only the technical

aspects of the system (accuracy of the alarms, data collection, etc.) but organizational issues having to do with the necessary involvement of various government agencies in any deployment of the TRMS.

Uncertainty of Available Energy and Available Power. SHAWN ALLRED (*University of Wyoming, Laramie, WY 82070*) JON CHRISTOPHERSEN (*Idaho National Laboratory, Idaho Falls, ID 83415*). Documenting the uncertainty analysis of the derived parameters grouped as Available Energy (AE) and Available Power (AP) for battery cells is a very complex problem. The error is an unknown combination of both linearity and offset; the analysis computes the uncertainty both ways and then the most conservative method is used (which is the worst case scenario). Each method requires the use of over 134 equations, some of which are derived and some are measured values. This includes the measurement device error (calibration error) and bit resolution and analog noise error (standard deviation error). The implementation of these equations to acquire a closed form answer was done using Matlab (an array based programming language). The uncertainty is automatically computed and will become part of the reported results for future battery testing.

Upgrade of Insertion Device Magnetic Measurement System: Motion Control and Position Measurement. JUSTIN HSU (*University of California–Berkeley, Berkeley, CA 94720*) STEVE MARKS (*Lawrence Berkeley National Laboratory, Berkeley, CA 94720*). An Elliptically Polarizing Undulator (EPU) is a storage ring insertion device that generates intense light for use in scientific experiments at synchrotron radiation facilities like the Advanced Light Source (ALS). An EPU has four individual mechanical beams, which are comprised of permanent magnets that have been arranged in a deliberate pattern of alternating pole orientations. By adjusting the position of the beams, one is able to manipulate the trajectory of an electron beam into a sinusoidal or helical path, inducing a desirable phase-coherent superposition that increases the intensity of the produced light by many orders of magnitude. Because the electron beam path depends directly on the EPU's magnetic field, errors in the magnetic field translate into out-of-phase beam trajectories, leading to degradation in brightness. To prevent this, a precision magnetic measurement system is used to measure magnetic field as a function of position. This device assesses optical phase errors and provides a basis for correcting the EPU's magnetic field. Because it had been several years since the magnetic measurement bench at the ALS had been upgraded, many of the components were obsolete. In order to maintain compatibility with newer equipment and software, a complete overhaul of the device was necessary. My task involved upgrading key components of the system. This included replacing laser interferometers with linear encoders, mechanical mounting of the linear encoders, installing an updated motor controller, building a convenient user interface to display all data, planning/implementation of the system's electrical wiring, updating the computer's software/operating system, and writing C/C++ code that facilitated communication within the entire system. Because the project is still ongoing, experimental results have yet to be determined. Future work may involve further investigation and code modification to expand system functionality.

Usability Improvements to Existing Detection Equipment. FRANKIE PONTILLO (*Purdue University, West Lafayette, IN 47906*) YOUNG SOO PARK (*Argonne National Laboratory, Argonne, IL 60439*). The goal of the project was to develop specific improvements in the method, techniques, and equipment to allow better usability of existing radiation search equipment in the field. A number of hand-held detectors were inspected. The objective was to develop concepts for hands-free operation for each of the detectors. These devices include the Identifinder, a medium weight and sized device that detects radio nuclides, the SAM-935, that is a special nuclear material detector larger in weight and size than the previous, the UDR, a handheld radioactive device that is small in size and weight and often used in the military, and the ORTEC Detective, a gamma-ray detector that is bulky in size and weighs a lot. These devices are very important both inside and outside Argonne National Laboratory. It was important to become familiar with the equipment and with the previous and alternative ideas used. Searching the internet, reviewing books, and visiting manufacturer websites, especially for these devices that we were working with, helped in developing our initial ideas of improving the devices. Looking at devices that were already marketed, but not necessarily ones that served a purpose to the radioactive search devices, shed light on our current situation and gave an idea for designing hands-free devices. Getting contact with companies and putting ideas into visuals that could be presented seemed to get the project moving in the right direction. For the UDR the device design was similar to the iPod neoprene cases, with some slight modifications. For the Identifinder a retractable locking

clip device, was used that could be purchased on the open market. For the SAM-935 ideas were taken from a car mounted DVD case, and modified to be part of a pack system that could hold the device. Lastly, for the ORTEC there is a need to come up with an idea for a way to carry the device as a front and back pack, but still be accessible. We are currently having ideas turned into prototypes, with respect to the future of this project; the main goal is that the prototypes be successful to the radioactive search industries. New casing designs were used successfully with the commercial radioactive devices. These new casings with respect to the old ones are more durable, easier to use, and make transportation of the radioactive detectors easier.

Validating Computational Fluid Dynamics Simulations of Thermodynamic Flow in the Very High Temperature Reactor Lower Plenum. MARY SPROUSE (*Kansas State University, Manhattan, KS 66506*) W.D. POINTER (*Argonne National Laboratory, Argonne, IL 60439*). The Generation IV International Forum (GIF) has been organized to address future energy needs using nuclear energy systems. The Very High Temperature Reactor (VHTR) is an advanced reactor concept undergoing engineering development. The thermohydraulics of the reactor must be modeled to ensure inherent safety in design. Engineering simulations are carried out by using computational fluid dynamics (CFD) software; CFD solves the conservation equations (mass, momentum, and energy) to predict the behavior of fluids in motion through a defined configuration. The software enables a number of turbulence models to be chosen to assess, for instance, the sensitivity of the nuclear system's thermohydraulics to a specific model. The objective of this project was to investigate the capabilities of the CFD package STAR-CD with respect to coarse-to-fine meshing options and turbulence models, with a focus on thermohydraulic flow in the lower plenum of the VHTR. The potential thermal fatigue of the lower plenum structure, as a result of poor thermal mixing, is expected to be the first standard benchmark problem proposed by the GIF VHTR Methods Project Management Board. In order to establish validity of the turbulent flow CFD approach, steady and unsteady simulations were run with various meshing options for a well-documented reference tube bank experiment. The simulation results were compared to experimental data generated by the Idaho National Laboratory's matched index-of-refraction flow experiment to evaluate the capability and packaged options (i.e., turbulence models) of the STAR-CD simulation software. To date the simulations have been found to correctly represent experimental trends. However, differences appear between the coarse-to-fine meshing approach relative to the experiment trends, in particular, between the normalized velocity over distances on the simulated reference tube bank. These differences are now being analyzed. In addition, in order to model the VHTR lower plenum, a script was developed that builds the representative geometry. Future work includes running simulations for this model and comparing the simulated and experimental data. These planned validation exercises using STAR-CD will contribute to the design engineering and safety analysis of advanced nuclear systems.

Validation of CFD Code for Heavy-Vehicle External Aerodynamics Simulation. EMILY DRINGENBERG (*Kansas State University, Manhattan, KS 66502*) W.D. POINTER (*Argonne National Laboratory, Argonne, IL 60439*). Argonne National Laboratory is using the computational fluid dynamics software STAR-CD and its ES-AERO enhancement (both Adapco) to solve the mass and momentum conservation equations as applied to the generic conventional model of a tractor-trailer vehicle. Preliminary studies show that a reduction in drag as small as 5% translates to fuel savings of about 2.5%, which can be as much as 500-1000 liters/year (~132-264 gal/year) for 150,000 km (~93,206 mi) annual highway driving for a single commercial long-haul tractor-trailer vehicle. The STAR-CD program numerically solves the turbulent flow around a tractor-trailer configuration for different turbulent flow models and under various conditions. By running simulations, information such as the coefficient of drag and pressure distribution around the vehicle is revealed. Both metrics are linked to the aerodynamic performance and hence the fuel-efficiency of the tractor-trailer. Since one defining variable of drag and pressure is the yaw, or the angle at which the flow moving over the vehicle's surface encounters the centerline of the vehicle, simulations are being carried out at yaw angles 0°, 3° (or 2.5° when 3° is problematic), and 6°. Simulations were also conducted to model underhood air flow with a standard radiator (as this is more realistic) and since it influences the overall aerodynamic performance. The information gathered from the simulations is compared to experimental data collected from a scaled tractor-trailer experiment in a wind tunnel. Major results showed an error of only ~12% for the baseline geometry at all tested yaw which confirms the ability of STAR-CD to be used in similar applications to

predict fluid flow. The V2F model suggested that for larger yaw angles, a more advanced turbulence model may be needed. The side drag and lift are typically difficult to predict but showed some tendency to follow the trend for small yaw angles. The differences and similarities resulting from this comparison have aided in determining the usefulness and accuracy of the STAR-CD and ES-AERO software as well as potential gains in fuel economy for the tractor-trailer.

Verification and Application of a Thermosiphon Solar Water Heater Model. JAY JOHNSON (*University of Missouri–Rolla, Rolla, MO 65409*) JAY BURCH (*National Renewable Energy Laboratory, Golden, CO 89401*). Rising energy prices and global warming have sparked added interest in wind, biomass and solar technologies. Solar water heating can reduce domestic water heating costs by more than half and currently new Solar Domestic Hot Water (SDHW) systems are in development and production. Thermosiphon systems are a relatively mature technology, but there are still a number of uncertainties their behavior. Thermosiphon systems use the natural buoyancy of hot water to drive flow during the day, but at night cooler ambient conditions cause reverse thermosiphoning. The National Renewable Energy Laboratory (NREL) has developed a new model using TRNSYS software, which can smoothly transition between forward and reverse flows. Two of the new NREL components in this model were verified by comparing analytical results to the TRNSYS solution. Then using this model, reverse thermosiphoning was studied and quantified in different climates and loop geometries to understand the energy penalty of the typically ignored reverse thermosiphoning phenomenon. New passive solar thermal systems have the tank nearly coincident with the collector, so the penalty from reverse thermosiphoning was of particular interest. All modeling showed some level of reverse thermosiphoning regardless of climate or tank position. Although these systems are highly dependant on hot water draws, the reverse thermosiphon mass was nine times larger in low tank configurations, forward thermosiphon mass was 80% larger with the high tank configuration and hence the high tank configuration was capable of delivering 25% more energy annually than the low tank configuration. This points to using systems with high tank configurations, but attic limitations and the inconvenience of tank mounting may not always make such geometry feasible. This work quantifies the penalty and shows that such configurations, though not optimal, produce reasonable savings.

Environmental Science

A Comparison of Water Chemistry Between Natural, Modified, and Manmade Ponds within Brookhaven National Laboratory. PRISCILLA RANDOLPH (*North Carolina A&T State University, Greensboro, NC 27411*) TIM GREEN (*Brookhaven National Laboratory, Upton, NY 11973*). Brookhaven National Laboratory (BNL) is located in the center of the Long Island Pine Barrens. Within BNL's 5,265-acre site there are 26 wetlands. Included are coastal plain ponds, vernal ponds, recharge basins, and streams, making it an ideal ecological site to study water chemistry. We tested water samples from seven coastal plain ponds on BNL: four natural (BP1, BP2, BP6, BP9), one man-modified (BP7), and two manmade (BP13a, Meadow Marsh). Five water samples were collected from each pond. An eTrex Vista Cx Global Positioning System (GPS) was used to mark each water sample point. An YSI 659 MDS meter fitted with a multiprobe was utilized to determine temperature, pH, dissolved oxygen, conductivity, and turbidity at each sample point. Water samples were analyzed for sulfate, nitrate, iron, phosphorus, chlorine, calcium, magnesium, copper, tannin-lignin, chromium, molybdenum, aluminum, and suspended solids using Hach DREL/2000 and CEL/890 water test kits. Water samples were also analyzed for eleven different elements using an ICP-AES. The pH in the anthropogenic ponds was found to be more basic than that of natural ponds. Phosphorous, tannin-lignin, and hardness were elevated in the natural ponds when compared to manmade and modified ponds, but only the difference in tannin-lignin content proved statistically significant. The natural ponds were shaded by the canopy of the surrounding forest while the manmade and modified ponds were located directly in the sun. This had an affect on water temperature. The results of this research will give environmental scientists an insight into water chemistry and interrelationships between abiotic and biotic factors and will enable BNL to optimize the management of amphibian and reptile habitats.

A Comparison of Litter Densities in Six Community Types of the Long Island Central Pine Barrens. DANA TIEVSKY (*University of Rochester, Rochester, NY 14627*) TIM GREEN (*Brookhaven National Laboratory, Upton, NY 11973*). The condition of the Long Island Central Pine Barrens has been an area of ecological concern for the past

three decades. In 2003, the Foundation for Ecological Research in the Northeast (FERN) was founded to support scientific research in the Pine Barrens. FERN's groundbreaking project is the Central Pine Barrens Monitoring Program, for which field research began during the summer of 2005 at Brookhaven National Laboratory. The purpose of this 10 year longitudinal study is to determine the current status of forest health in order to promote longevity and conservation in the Pine Barrens, as well as to learn what research should be done in the future. Litter densities from Pitch Pine, Pine-Oak, Oak-Pine, Coastal Oak, Scrub Oak, and Dwarf Pine habitats were compared in order to justify the succession of the Pine Barrens and prepare for future prescribed forest fires. Using Geographic Information System (GIS) and Global Positioning System (GPS) technology, random twenty five by sixteen meter plots of land were selected throughout eastern Long Island and then thoroughly surveyed. Litter and duff depth data were collected at four points along each of the ten line transects in the plot. Pitch Pine forests were found to have the most litter, with an average depth of 6.12 centimeters. Pine-Oak forests have an average litter depth of 6.03. Oak-Pine and Coastal Oak forests have comparable litter depths. Oak-Pine forests have an average litter depth of 5.01 while Coastal Oak forests have an average litter depth of 4.82. Scrub Oak lands have almost no litter with an average depth of 3.63 while Dwarf Pine Forests have an average litter depth of 2.49. A comparison of the vastly different litter densities of the six community types yields results that are consistent with the previously determined succession of the Pine Barrens and shows that litter density plays a key role in aiding forest succession. Data collected under the Central Pine Barrens Monitoring Program was used to determine a threshold for litter density, 4.82 cm. However, this trend is only from the first two years of research. In the future, a more accurate threshold can be determined in order to prescribe forest fires at appropriate times and preserve the Pine Barrens in the most effective manner.

***A Comparison of the Chemistry of Soil Surrounding Natural and Anthropogenic Ponds at Brookhaven National Laboratory.** SHURRITA DAVIS (*North Carolina A & T State University, Greensboro, OR 27411*) TIM GREEN (*Brookhaven National Laboratory, Upton, NY 11973*). Brookhaven National Laboratory (BNL) is located in the Long Island Pine Barrens, an area formed through decomposition and reworking of glacial materials. BNL has many wetland structures including coastal plain ponds, vernal ponds, recharge basins, and streams. Some of these serve as breeding grounds for tiger salamanders (*Ambystoma tigrinum*), a species listed as endangered by the New York Natural Heritage Program. Anthropogenic habitats need to possess suitable characteristics with respect to soil and water chemistry in order to serve as successful breeding habitat for tiger salamanders. Soil is an important factor in controlling vegetation and water chemistry. In this study five ponds were selected for a study of soil chemistry: two natural and three anthropogenic. Nine soil samples were collected from each pond, eight around the perimeter and one from the pond bottom. Global Positioning System (GPS) was used to locate the sample points and ArcGIS was used to map the ponds and sample points. Soil samples were tested for pH, nitrate nitrogen, phosphorus, potassium, aluminum, ferric iron, magnesium, sulfate, calcium, and chloride using LaMotte Combination Soil and LaMotte Soil Micronutrient Kits. Soil moisture content was also determined. Soil color, texture, structure, consistency, and mottling were also observed and recorded. Five of the nine soil samples from each pond were digested using EPA method 3050B for Acid Digestion of sediment, sludge, and soil and then tested for copper, iron, molybdenum, magnesium, cadmium, aluminum, chromium, manganese, potassium and lead using an Inductively Coupled Plasma - Atomic Emission Spectroscopy (ICP-AES). The natural ponds were more acidic than the anthropogenic ponds. The soil temperature is higher around the anthropogenic ponds (BP7, BP13, MM) than the natural ponds (BP9, BP6). Nutrient levels were low and consistent across pond types. Though these differences exist, both types of ponds accomplish the goal of providing suitable breeding sites for tiger salamanders (*Ambystoma tigrinum*). This information will serve as baseline data for BNL's natural resource manager and enable BNL to optimize the management of amphibian and reptile habitats

A Miniature Quartz Crystal-Based Device for Particulate Matter Monitoring with Real-time Data Acquisition. ZHUO HUANG (*Sacramento State University, Sacramento, CA 95819*) MICHAEL APTE (*Lawrence Berkeley National Laboratory, Berkeley, CA 94720*). Exposure to particulate matter (PM) through inhalation has been associated with adverse health problems. Accurately monitoring of the mass concentration and chemical composition of PM are necessary for exposure assessment. Many current instruments in use involve complex operation and labor-intensive work to obtain necessary data

for studies, or involve costly systems to monitor a large population. One feasible solution to address these drawbacks is to develop low-cost, compact, and miniaturized real-time devices. The miniature system for particle exposure assessment (MSPEA) developed at Lawrence Berkeley National Laboratory (LBNL) is one approach available to the aerosol research community. MSPEA PM mass detection uses a quartz crystal microbalance (QCM). All the components including the quartz crystals for this system are off-the-shelf items, and can be easily obtained. The particle deposition mechanism used by this device is thermophoresis, while particles are retained on the sensors using and van der Waals forces. The QCM is constructed using an unexposed reference crystal oscillator and a PM-exposed sensing crystal oscillator, and a mixing circuit to that combines the oscillators' outputs into a beat frequency signal. A computer is used to incorporate the data acquisition operation, but eventually a microprocessor can replace the computer to miniaturize the device for personal monitoring at low-cost. Another monitoring feature of the MSPEA system employing ultraviolet and near-infrared optics is briefly discussed in this paper.

A Study of Seedling Numbers in Relation to Canopy Cover in Six Long Island Pine Barren Community Types. EMILY EFSTRATION (University of Delaware, Newark, DE 19717) TIM GREEN (Brookhaven National Laboratory, Upton, NY 11973). Seedlings and saplings are important to forest health because they provide insight as to how the forest will develop and survive in the years to come. The canopy cover's density has much to do with how these seedlings and saplings will develop and survive. Canopy cover, density and the amount of seedlings were studied in different forest communities to help predict the future of these forests. Using a Geographic Information System (GIS) and Global Positioning System (GPS), points were selected at random and twenty five by sixteen meter plots were analyzed. By using a densitometer, the canopy cover was determined in each plot along ten transects at randomly determined intervals. Seedlings and saplings were counted in four belt transects as well as noted in the entire plot. The different communities that were compared include Pine Oak, Oak Pine, Pitch Pine, Coastal Oak areas, Dwarf Pine and Pitch Pine-Scrub Oak Woodland/Shrubland. In the Coastal Oak community, where the cover was found to be 96% hardwood cover and no pine cover, no seedlings or saplings found. On the other hand, in a Pitch Pine plot, with 72% pine cover and 1.5% hardwood cover, approximately 86 seedlings and 85 saplings were found. When this study is redone in ten years to determine the progress of the forest, the investigators will determine if human intervention is needed to aid in forest growth. If adolescent trees were found healthy and growing, this would show the progression of the Pine Barrens and would also prove that the forest is capable of recuperating without human aid.

A Study of Variations in Soil and Water Chemistry of Selected Ponds at Brookhaven National Laboratory. JAMIE BRUNGARD, NINA KEAN, GEORGIA SAWYER (North Carolina A&T State University, Greensboro, NC 27411) DR. TIM GREEN (Brookhaven National Laboratory, Upton, NY 11973). Brookhaven National Laboratory (BNL), a 5,265 acre site, contains a variety of wetlands; included are coastal plain ponds, vernal ponds, recharge basins, and streams. Wetland habitats in Pine Barrens communities serve important ecosystem functions including providing critical habitat for the state endangered tiger salamander (*Ambystoma tigrinum*) and a number of other rare species. Survey techniques were used to gather information on soil and water chemistry of seven coastal plain ponds at BNL: four natural ponds, one man-modified pond, and two man-made ponds. Each pond was tracked using Global Positioning System (GPS) technology and mapped using ArcGIS. Five water samples were collected at each pond; nine soil samples were collected at five of the seven ponds. Water samples were analyzed for iron, sulfate, total chlorine, copper, aluminum, nitrate, phosphorus, tannin-lignin, suspended solids, hardness, total chromium, and molybdenum using HACH DREL/2000 and HACH CEL/890 water test kits. Soil samples were analyzed for pH, nitrate nitrogen, phosphorus, potassium, aluminum, ferric iron, magnesium, sulfate, calcium, and chloride using LaMotte soil test kits. Soil temperature, color, texture, structure, and consistency were also determined. A YSI 650 MDS meter with multi-probe was used to field-test water temperature, pH, dissolved oxygen, turbidity, and conductivity at each sample point. Water samples and soil extracts were also analyzed using an ICP-AES. The pH and temperature of the soil around the natural ponds was significantly lower than that of the anthropogenic ponds. The pH of the water from the natural ponds was significantly more acidic and the tannin-lignin content significantly higher than that of the anthropogenic ponds. We propose that these differences in the soil and water chemistry of the ponds can be explained by the nature of the surrounding vegetation. The presence of a tree canopy and

dense shrub layer around the natural ponds reduces their exposure to solar radiation and increases the amount of leaf litter being added to the soil and water. This results in lower soil and water temperatures, lower soil and water pH, and a higher tannin-lignin content in the water of the natural ponds versus the anthropogenic ponds. The results of this study provide baseline data for monitoring pond health in the future and for assessing the suitability of ponds as breeding sites for tiger salamanders.

Adsorbent-Coated Polyurethane Foam as a Denuder and Size-Selective Inlet for Ambient Air Samplers. JEFF DUARTE (University of California-Davis, Davis, CA 95616) LARA GUNDEL (Lawrence Berkeley National Laboratory, Berkeley, CA 94720). For practical use, ambient air samplers for assessing human exposure to airborne particles must decrease in size and cost. One major step toward this change is replacement of large, adsorbent-coated glass denuders with small, cheaper adsorbent-coated PUF (polyurethane foam) denuders for capturing SVOC (semi-volatile organic compounds). The purpose of a denuder is to capture SVOC from the sampled air on its extractable adsorbent coat while allowing particles to pass through for collection on a filter. The purpose of this project was to determine if PUF could meet the latter requirement. It was hypothesized that PUF denuders could pass PM_{2.5} (particles with an aerodynamic diameter of 2.5 microns or less) and match or even exceed conventional glass denuders in SVOC capture because they have more surface area and are more compact. A bifurcated particle sampler that excluded particles larger than 2.5µm was used on multiple 24-hour sampling runs in several configurations. Data were initially collected without any denuders, then in another configuration containing glass denuders on both sides to determine the variability of particle capture between the two columns, and then lastly with glass denuders on both sides as well as a PUF denuder on one side. The PUF denuder was placed downstream of the glass denuder so as to have normal SVOC capture. This allowed the focus to be solely on whether or not the PUF was allowing PM_{2.5} through. In earlier work with PUF denuders by M. T. Minjares, it was found that the filter downstream of the PUF had one third less mass than the filter with no PUF. Minjares had no upstream glass denuders, so her result was thought to be caused by either PM_{2.5} collection by the PUF or SVOC adsorption by the Teflon filter. In this follow-up experiment, upstream SVOC was collected by the glass denuders. The average PM_{2.5} concentration difference between the filters in the two columns in a non-denuded configuration was 8.6%. The average PM_{2.5} concentration difference between the two filters in the configuration with glass denuders on both sides and the PUF denuder on one side was 10.2%. With a mass measurement uncertainty of 3.6%, the difference between these two results is insignificant. The conclusions from this project are 1) the PUF does pass PM_{2.5} well and 2) the Teflon filter adsorbed SVOC. This is contrary to the prevailing belief that Teflon does not measurably adsorb SVOC, and it was causing the artifact that Minjares observed.

An Alternative Nonvolatile Solvent to Dissolve Metals: The Mixture of Choline Chloride and Urea. DORRA KRIDIS (The Cooper Union for the Advancement of Sciences and Art, New York, NY 10003) MARK FUHRMANN (Brookhaven National Laboratory, Upton, NY 11973). The mixture of urea and choline chloride, two inexpensive, non-toxic, but high melting point organic solids in a specific ratio, produces an easy to make, colorless, and nonvolatile ionic liquid at 60°C. The prepared nonvolatile liquid is stable at room temperature. The goal of this experiment is to assess a comprehensive, environmentally friendly and efficient utilization of an ionic liquid (choline chloride and urea) and to determine the percentage of dissolved metal elements in the liquid; for example, aluminum, copper, iron, silica and zinc. In the present study, the Inductively Coupled Plasma-Atomic Emission Spectroscopy (ICP-AES) instrument is used to determine the concentration of dissolved metal in a diluted ionic liquid. The collected data is compared to the solubility of each metal in water at 25°C, 50°C and 70°C. The inexpensive ionic liquid is easily prepared where the number of moles of urea is half of the choline chloride. The reactants are the urea, and the choline chloride. The products present are an ionic liquid in the form of a salt and water. The novel ionic liquid chemical name is determined to be 3,5,5-triamino-4,6-dihydroxy-1,2,2-trimethylhexahydroimidin-1-ium chloride. The density of this salt is determined to be 1.14 g/ml. The solubility of metal oxides at 25°C, 50°C and 70°C such as copper oxide, zinc oxide, aluminum oxide and quartz are greater in ionic liquid compared to water. Solubility of elemental zinc, iron and copper also show a greater percentage over those in water. Aluminosilicate minerals also show a greater solubility in an ionic liquid compared to water. The potential structures of the formed ionic liquid suggest that it may be useful in catalysis when metals are added. The solubility results also

suggest that this ionic liquid could be applied to use as metal polishing and to remove metals from soil and other contaminated material.

Analysis of Secondary Organic Aerosols and Gas Phase Products from Ozonolysis of Alpha-Pinene in the Presence of an Organic Seed Aerosol. SHAUN GARLAND (*University of California–Davis, Davis, CA 95616*) LIZABETH ALEXANDER (*Pacific Northwest National Laboratory, Richland, WA 99352*). Ozonolysis of monoterpenes such as alpha-pinene gives rise to not only primary oxidation products, like acetone, but also secondary organic aerosol (SOA) formation. Understanding the mass budget of volatile organic compounds (VOC's) converted into aerosols and what remains in the gas phase has impact in metropolitan areas, where ozone is in higher than normal ambient concentrations and presence of existing organic aerosols, in both air quality and models that deal with pollution. Previous studies have investigated the consequence of inorganic aerosols on aerosol yields. This study uses diethyl phthalate (DOP) as a primary seed aerosol in an alpha-pinene/ozone reacting system to determine how its presence affects both SOA yield and gas phase concentrations compared to no-seed conditions. Concentrations of alpha-pinene and other primary oxidation products are tracked in real time by proton-transfer-reaction mass spectrometry to develop profiles that allow investigation into second order reaction rate constants. The presence of DOP was determined to lower organic aerosol mass yield as well as the gas phase yields of acetone. Second order reaction rates showed that DOP also does not have any kinetic impact on the alpha-pinene/ozone reaction. These results indicate that the presence of DOP aerosols provide a site for secondary reactions to take place, consuming organic matter that would normally form aerosols.

Analysis of the Habitat of Henslow's Sparrows Compared to Randomly Chosen Grassland Areas. ANITA NUNEZ (*University of Illinois, Chicago, IL 60607*) ROD WALTON (*Fermi National Accelerator Laboratory, Batavia, IL 60510*). The Henslow's Sparrow is state endangered and is at risk of extinction as a breeding species in Illinois. The population of this species has been decreasing due to the degradation and loss of grassland habitat. This is the second year of an ongoing study of the Henslow's habitat. It is important to study the vegetation of the Henslow's Sparrow's habitat in order to assess whether the land management plans at Fermilab are effective. Once the Henslow's were located, the vegetation comprising the birds' habitats was studied. Measurements of the maximum plant height, average plant height, and duff height were taken as well as ground coverage measurements (percent of grasses, forbs, duff and bare ground). For a control, randomly chosen grassland sites were located within Fermilab property. t-tests and two-sample variance tests were used to analyze the plant and duff height data, and Mann-Whitney Utests were used to analyze the ground cover data. The data suggested Henslow's Sparrows prefer areas with shorter maximum plant height than was found in the randomly chosen sites. Further, the data suggested these grassland birds prefer more duff and less bare ground when compared to randomly chosen sites. The two-sample variance tests showed there is lower variation in the maximum plant height at sites Henslow's prefer. This study's findings are in agreement with the previous study, which found Henslow's Sparrows prefer less bare ground as well as lower variance in the maximum plant height. The previous study also suggested that Henslow's prefer more grasses in their areas when compared to randomly chosen sites. For further research, this study should be repeated to further support the findings. It would also be interesting to study how large the Henslow's territories are.

Arsenic Removal from Ground Waters: An Investigation of the Effects of Temperature. MARIA MELISSA QUEMADA (*University of California–Berkeley, Berkeley, CA 94720*) ASHOK J. GADGIL (*Lawrence Berkeley National Laboratory, Berkeley, CA 94720*). Arsenic, a naturally occurring element is a major contaminant in ground waters. Approximately 40 million people in Bangladesh and tens of millions more in neighboring countries are being poisoned by arsenic in their drinking water. The World Health Organization has set a standard of 10-µg/L arsenic in drinking water, while Bangladesh standard remains 50-µg/L. In California, approximately 600,000 households use water with arsenic concentrations higher than the required standard. Lawrence Berkeley National Laboratory has developed a technology for arsenic removal using coal ash coated with ferric hydroxide (media). This process enables the arsenic bind to the iron oxide complex that is coated around the ash particles, and thus lowers the arsenic concentration in drinking water. This technology has high efficacy and very cost effective. My goal in this project is to test the performance of this technology on U.S. waters over a range of temperature values and to test the arsenic removal capacity of the media using coal fly ash that are commonly found in the U.S. The temperature values I investigated

were 4 and 35 degree Celsius. This was accomplished through a series of experiments that allowed me to find the time the process reaches equilibrium in the two temperature values I investigated. Once the equilibrium time was established, the process was repeated to obtain adsorption isotherm curves for the two different temperature values. The equilibrium times that were found were 4 and 16 hours for 4°C and 35°C respectively. The arsenic removal capacity was analyzed using an arsenic field kit test (Quick Test®) and the results were confirmed by Inductively Coupled Plasma Mass Spectroscopy analysis.

Aspen Tree Core Micro-Cat Analysis and Mutation Detection. ASHLEY NEIL (*Auburn University, Auburn, AL 36830*) LEE GUNTER (*Oak Ridge National Laboratory, Oak Ridge, TN 37831*). Among clonal organisms the actual genetic mechanism used to maintain diversity within the species is unknown; however they are suspected to have a higher mutation rate than plants propagated by seed dispersal alone. *Populus tremuloides* (aspen), with its wide distribution, persistence in the environment and extensive clonal structure, is a good model for studying this mechanism in plants. In this project, its proposed using the number of estimated somatic mutations to determine the absolute age of clonal aspen stands within Rocky Mountain National Park. Several parameters needed to be examined in order to determine if aspen has a high somatic mutation rate relative to other organisms, such as clone age, number of somatic mutations, dominant genotype, as well as the geographic distribution pattern correlated with the genetic structure. In an effort to establish clone age, individual aspen ramets were analyzed using an ultra high resolution x-ray computer tomography system. The super resolution of this system generates a clear and easily differentiated image of the rings of the collected cores. Therefore, an estimate of the clone age will be determined based on the rings reading from the image and the tree diameters. Thus far approximately 300 ramets have been examined. A correlation between the ramet ages and the diameters will need to be determined in order to calculate the age of an individual tree from its diameter. From earlier studies, it has been demonstrated that this technique is the best one to yield satisfactory results. The major objective in the genetic component of this study is to attempt to determine the rate of somatic mutation, and, if successful, to use it to estimate the absolute ages of several aspen clones in the Rocky Mountain National Park.

Assessing the Impact of the Apatite Injection Barrier on Benthic Macroinvertebrates and Periphyton at 100-N on the Hanford Reach of the Columbia River. BEN MILLER (*Birmingham-Southern College, Birmingham, AL 35244*) ROBERT P. MUELLER (*Pacific Northwest National Laboratory, Richland, WA 99352*). 100-N on the Hanford Site operated from 1963 until 1988. 100-N is unique from the other plutonium production reactors on the Hanford Site because of its multiple-pass cooling system, which circulated coolant through the reactor several times before depositing it into a series of liquid waste disposal facilities nearby. These multiple passes significantly magnified the contaminants present in the coolant, which has since leached into an unconfined aquifer adjacent to the Columbia River. In a remediation effort, an Apatite Injection Barrier (AIB) has been implemented along the shore at 100-N to impede an underground plume of Strontium-90. However, this technique is expected to release trace amounts of simple salts, as well as sodium phosphate and ammonium nitrate. To assess the impact of such a release on the Hanford Reach at 100-N, we collected communities of periphyton and macroinvertebrates from the nearshore region along vectors upstream, downstream, and adjacent to the site, as well as a reference area near the opposite shoreline of the Columbia River. A Phospholipid-Fatty Acid Analysis (PLFA) was also performed on the collected periphyton, along with a Shannon-Weiner diversity index. For the initial baseline calculations, we found very little significant difference in the composition of the benthic community between sample sites along the AIB and the reference sites across the river. Later collections of the macroinvertebrate and periphyton community will be assessed to understand what, if any, impact the AIB has on local biota.

Bacterial Diversity in Soil and Sediments From a Former Bombing Range (Vieques, PR). ERNIE PEREZ (*University of Puerto Rico at Mayaguez, Mayaguez, PR 00680*) TERRY C. HAZEN (*Lawrence Berkeley National Laboratory, Berkeley, CA 94720*). The U.S. Navy Atlantic Fleet Weapons Training Area (AFWTA) located in Vieques, Puerto Rico, includes land areas, waters and islets impacted by 63 years of military training operations. High-density universal SSU rRNA gene microarray analysis for Archaea and Bacteria were used to describe the microbial community structure of soil and marine sediment samples from Vieques and reference locations (Guánica Forest and Patillas). Total community DNA was extracted, PCR amplified and hybridized to an array encompassing 16S rRNA for over

8,900 distinguishable taxonomic units. Hierarchical clustering of the 100 most variable sub-families detected by the array demonstrated that variable sequences fell into six (6) primary response groups. Samples from sediments and soils are very similar between each of their kind. Furthermore, samples from closer geographical locations were more similar than distant sites. Higher numbers of OTU's were observed in soil samples with 193 to 318 sub-families identified in each sample. Bacteroidetes, actinobacteria and acidobacteria were the more common phyla detected in Vieques than reference samples. The presence of diverse groups of bacteria may indicate a great potential for natural or enhanced biological restoration. Understanding the function and community structure of highly disturbed ecosystems could assist environmental restoration strategies.

Baseline pH and the Variability of pH within Plots and Community Types of the Central Pine Barrens. NEAL JACK (*Pennsylvania State University, University Park, PA 16801*) TIM GREEN (*Brookhaven National Laboratory, Upton, NY 11973*). The Long Island Central Pine Barrens (CPB) is a valuable natural resource for its beauty, natural water aquifer and for being the habitat of many endangered and threatened species of plants animals and insects. The Foundation for Ecological Research in the Northeast (FERN) is an organization committed to the preservation of the Pine Barrens ecosystem by maintaining or improving the health of the forests located in the CPB. FERN, in conjunction with other organizations, implemented a ten-year longitudinal study on the health of the CPB. Data collected on the pH of the soil will provide a piece of the baseline health record for this ten-year longitudinal study. To establish a baseline health record for each forest type, several 16 x 25m plots were set up, according to established protocols, within each forest community type. Using a Kelway HB-2 Soil pH meter / moisture tester the pH of the soil was taken at eight points within each plot. The average pH of the forest types were 6.3 for Coastal Oak, Pitch Pine 5.9, Pine-Oak 6.0, Oak-Pine 5.9, Pitch Pine Scrub Oak 6.1, and 6.1 for Dwarf Pine. Analyzing this data and data collected at the end of the ten-year study will be valuable in determine the long-term health of the forest as well as the effect of human intervention such as acid rain pollution.

Benchmark Report for Homeland Security: Standards, Guidelines and Fate. MEGAN WILLIAMS (*University of New Orleans, New Orleans, LA 70148*) MARGARET MACDONELL (*Argonne National Laboratory, Argonne, IL 60439*). Because of the rise in terrorist attacks throughout the world, pre-emptive and response procedures are being identified to assure the safety of Americans. Exposure guides are being developed to support health protection of Americans for more than 150 threat contaminants that could be released into the drinking water and air following a terrorist attack. The contaminants evaluated are deemed a potential health threat by the Environmental Protection Agency-National Homeland Security Research Center (EPA-NHSRC). They consist of toxic industrial chemicals (TIC), chemical warfare agents (CWA), radiochemical agents and bacterial agents. Exposure guides which we develop are risk based concentration (RBC) reports and provisional advisory levels (PALs) reports. The RBC report identifies pre-existing benchmarks, occupational limits, fate, toxicity use and degradation products for the contaminants. The RBC report focuses on benchmarks for chronic or repeat lifetime contaminant exposure. PALs are exposure guides that answer the questions of how, what, when, where and how a contaminant will effect the drinking water and air.

Biomarkers and Treatment for Potential Contamination Response. DANIEL RAHILL (*University of Notre Dame, Notre Dame, IL 46556*) DR. MARGRET MACDONELL (*Argonne National Laboratory, Argonne, IL 60439*). The creation of Provisional Advisory Levels (PALs) for specific chemicals of possible threat was to compile valuable information regarding potential risk in preparation for possible contaminations, including those induced by terrorists. As there is risk of exposure to the PAL chemicals, indicators of exposure and treatment outlines are of great importance. Biomarkers to quickly identify a chemical contamination event have been developed in this ongoing study. Once identified either to a specific chemical or a family of chemicals, treatments are available. Both immediate treatment and more extended medical treatments have been provided. The treatments have been categorized by both severity and symptom. The treatments account for sensitive populations, children in particular. The treatments are most complete for the organophosphates, which, for example, are treated with intermittent doses of atropine and pralidoxime. The ultimate goal of the biomarkers and treatment is to prepare all populations for all severity levels in the event of a potential chemical release. Another issue of importance was the quality assurance of the PAL reports. Particularly PAL reports for methyl paraoxon and VX contained errors that needed to be addressed and corrected. The methyl paraoxon PAL

required several components of fate and toxicity to be developed, oral and inhalation PALs to be updated and corrected, and dermal PALs to be created. The VX PAL contained inhalation PAL values that should be revised. The VX document also contains improper citations with several other documents that need clarification. The corrections were flagged in this ongoing study.

Bombing Sites Used for Military Training Activities. NATALIA RAMOS (*University of Puerto Rico, Mayaguez, PR 00727*) TERRY C. HAZEN (*Lawrence Berkeley National Laboratory, Berkeley, CA 94720*). Bombing sites used for military training activities can have considerable amounts of contaminants and pose significant risks for people and the environment. Until 2003, the eastern part of Vieques, Puerto Rico, was used as a bombing range by the U.S. Navy. Since then, leaching of explosive compounds from unexploded ordnance represents a serious threat to the marine ecosystem. The contribution of microbial populations to natural attenuation of explosives, including sulfate-reducing bacteria (SRB) has been demonstrated in soils but little is known about their contribution in marine environments. Characterization assays were employed to assess the effects of explosive compounds (TNT, RDX, HMX) on *Desulfovibrio vulgaris* Hildenborough and five novel SRB isolates from marine sediments in coastal waters adjacent to the former military facilities. Pure cultures were combined with media in a covered 96-well micro plate and the opacity was monitored in real time as the bacteria grew in a temperature-controlled plate reader. A dose-response curve was used to estimate minimum inhibitory concentrations (MICs) for TNT, RDX and HMX in 0, 1.5 and 3.0% (w/v) NaCl. Some of the bacterial isolates grew better in explosive-containing environments than in regular media. The chemotactic response to nitrocompounds was evaluated for *D. vulgaris* using a Palleroni chamber. *D. vulgaris* responded positively towards TNT, but not to RDX or HMX. Elucidating the diversity and behavior of SRBs to explosives in tropical sediments could help us understand the role of these microbial populations in explosive-contaminated marine environments.

Characterization of Cytochrome Mutants of *Shewanella Oneidensis* MR-1: Study of Initial Attachment and Biofilm Growth. KYLEE MILCZAREK (*Onondaga Community College, Syracuse, NY 13215*) JEFF MCLEAN (*Pacific Northwest National Laboratory, Richland, WA 99352*). The definition of a biofilm is: a community of microorganisms and extra cellular polymeric substance (EPS) attached to a surface (plastic, glass, mineral, tissue etc.). EPS can consist of protein, exopolysaccharide and nucleic acids. Biofilms can be detrimental and hard to remove but can also be beneficial. The bacterium being studied in this investigation is *Shewanella oneidensis* strain MR-1. When *S. oneidensis* is grown into a biofilm it has enhanced capabilities to reduce metals and radionuclides from contaminated soils and waters. The scope of this project is to investigate and understand the effects that the deletion or inhibition of certain genes in the bacterial genome will have on the *S. oneidensis* strain MR-1, with respect to cell-surface attachment and biofilm formation. If the changes that occur with the deletion of certain genes can be understood, the purpose of the specific gene in question can be understood. This project investigates how these genes effect the growth of biofilms and ultimately their abilities to reduce metals and radionuclides. In order to observe these differences, the wild type (MR-1) and each of the mutants were labeled with fluorescent proteins, grown into a biofilm (which are typically 100-200µm in height), and imaged by use of a Confocal Laser Scanning Microscope (CLSM). The CLSM gives the ability to acquire three dimensional images of the biofilms and to measure their respective heights; the film height in relation to the wild type strain will be used as an indicator for how the genes effect biofilm growth as the culture grows on the sample substrate. The cultures were imaged by use of CLSM at three different time intervals: 0, 24, and 36 hours. The initial sample time point (t = 0) established the number of cells that initially attached to the substrate, the film height at t = 24 and t = 36 are then compared. Data from these images were analyzed to produce averages of the height and identify differences in the structure. The data analyzed from the mutant strain: mtrA (SO1777) shows a trend of no growth among the 24 and 36 hour time trials. This indicates that the strain mtrA (SO1777) may have a low capability to form a biofilm at any of the tested time trials. There are small indications of cell division on the later time trials but no significant growth was observed. The result presented here indicates that the gene removed from this particular strain may play an important role in the growth and formation of biofilms. Further testing is needed to confirm this result. The project seeks to achieve a deeper knowledge of how the genes involved in metal and radionuclide reduction play a role in biofilm formation. A better understanding about the genetic controls for biofilm formation in this bacterium will enable investigators to possibly engineer a form that will work best for waste

site clean-up. This type of clean-up will be environmentally friendly and cost effective.

Characterization of Immobilized Urease and the Potential for ⁹⁰Sr Sequestration. *DESIREE SWEET (University of Texas at Austin, Austin, TX 78712) YOSHIKO FUJITA (Idaho National Laboratory, Idaho Falls, ID 83415).* A new technique for ⁹⁰Sr sequestration in the subsurface is being investigated by the Idaho National Laboratory in collaboration with University of Idaho at Idaho Falls. The technique is based on the idea that urea hydrolysis, catalyzed by immobilized urease, will accelerate the rate of calcite precipitation in the subsurface. To prove the validity of this technique, the kinetics of the immobilized urease and calcite precipitation must be modeled. The effect of the precipitation on porosity and permeability must be seen, and it must be proven that the technique can capture ⁹⁰Sr. Urea Hydrolysis refers to the reaction of urea and water catalyzed by the urease enzyme. The products of urea hydrolysis are ammonia and carbon dioxide. Urease is an enzyme produced by environmental microorganisms that currently exist in the subsurface. Consequently, many problems associated with injection of a reactant can be avoided. A result of urea hydrolysis is that it increases the carbonate alkalinity, thus it is a particularly attractive remediation technique in subsurface environments which are saturated with respect to calcite, as the likelihood of calcite precipitation becomes even greater. The urea hydrolysis accelerates the rate at which calcite can be precipitated, which accelerates the rate at which ⁹⁰Sr may be coprecipitated, and removed from the subsurface.

Climate Change Effects on Decomposition Mediated by Species Composition Versus Litter Quality. *MARLENE TYNER (University of Michigan, Ann Arbor, MI 48109) AIMEE CLASSEN (Oak Ridge National Laboratory, Oak Ridge, TN 37831).* Global change is rapidly modifying our planet, including altering ecosystem nutrient cycling. Until recently, research has focused on manipulating single climate change factors such as the effects of elevated carbon dioxide (CO₂) or elevated temperature on ecosystem processes. These factors, however, will not occur independently and are likely to alter ecosystem processes differently, perhaps mediating some of the effects. This project investigated how multiple climate change factors may alter decomposition in an old-field ecosystem. Specifically, it asked if climate change (elevated [CO₂] and temperature) would have a larger impact on decomposition via indirect changes in community composition or direct changes in litter quality. Three major findings resulted from this work: 1) Litter chemical quality change due to elevated [CO₂] or temperature does not alter decomposition rates; 2) Climate-driven shifts in species composition has an effect on decomposition rates; 3) These effects occur primarily in the early stages of the decomposition process, and decline over time. Taken together, these data suggest that climate change will have a larger effect on ecosystems by causing shifts in plant communities than it will by altering litter quality. Further, these results suggest that the effects afflicted on ecosystems by changing climates may be more varied and complex than previously thought, and current databases on ecosystem process changes may need to be expanded for more accurate modeling efforts.

Cold Flow Properties of Biodiesel. *KAITLIN THOMASSEN (State University of New York at Geneseo, Geneseo, NY 14454) DR. C. R. KRISHNA (Brookhaven National Laboratory, Upton, NY 11973).* Biodiesel has become one of the most promising alternative fuels; however, its relatively high cloud point (CP) temperature is one of the reasons limiting it from replacing the widespread use of fossil fuels in today's society. Reducing the CP of biodiesel is one of the last major obstacles scientists need to overcome before the fuel can be marketed for consumers. Unfortunately, not much is known about the cold flow properties of biodiesel, their dependence on the source material from which biodiesel is made, and about methods to reduce the CP temperature. Previously, scientists have theorized that the higher the percent of saturated fatty acids in the source material from which the biodiesel is made, the higher the CP temperature. As part of this research project, samples of biodiesel made from soy, tallow, canola, and yellow grease were blended in different percent ratios to test this theory. Tallow and soy were blended together at 20%, 50%, and 80% ratios. Separately, yellow grease was blended with soy and canola was blended with tallow at these same ratios. These biodiesel samples were chosen due to the large contrast in the percent saturation. Soy and canola contain a low percent saturation, while tallow and yellow grease have a high percent saturation. The test results showed that CP temperature increased linearly as the percent of saturated components increased in the biodiesel samples. In addition, the CP temperature was found for No. 2 oil and biodiesel blends. B5, B20, B50, and B80 blends were made with yellow grease, canola, soy, and tallow-based biodiesel. The results showed that as the percent of No.2 oil increases in each

sample the CP temperature decreases. The tests also concluded that making blends of No. 2 oil and biodiesel from different sources can yield a very different CP temperature. Furthermore, in the effort to reduce the CP temperature of biodiesel, a proprietary additive was blended with several types of neat and blended biodiesel samples. What was concluded from this proprietary additive is that CP was not effectively changed however, observation indicated that the pour point (PP) temperature seemed to have been lowered. In future research, the CP of different biodiesel types will be correlated with their chemical structure.

Comparison of the Populations of Common Wood-Nymph Butterflies in Burned Prairie, Unburned Prairie, and Old Field Grasses. *MARLENE HAHN (Loyola University, Chicago, IL 60626) ROD WALTON (Fermi National Accelerator Laboratory, Batavia, IL 60510).* Common wood-nymph butterflies are found throughout the United States and Canada. However, not much is known about how they overwinter or their preferences for particular grasses and habitats. In this study, the impact of prairie management plans on the abundance of the wood-nymph population was assessed as well as the preference of these butterflies to areas with native or non-native grasses. The abundance of common wood-nymph butterflies was determined using Pollard walks. The majority of the vegetation at each of the three sites was identified and documented. Using a 1 X 3 ANOVA, it was determined that there was a significant difference ($p < 0.0005$) between the abundance of common wood-nymphs in the European grasses site compared to the burned and unburned prairie sites. There was no significant difference between the burned and unburned treatments of the prairie on the common wood-nymph population. A multiple variable linear regression generated a model in which the temperature and weather affected the observed common wood-nymph butterflies per hour ($p = 0.026$). To verify these preliminary results, future studies need to repeat this experiment. Quadrat analysis of the vegetation from all three sites should be done in order to see if there is a correlation between common wood-nymph butterfly abundance per hour and the specific types or quantity of vegetation at each site. Another area of investigation is to determine how the observer's visual field is affected by the density or height of vegetation at each site.

Creating Code for Automated Demand Response. *ARRAN BLATTEL (Stanford University, Stanford, CA 94305) MARY ANN PIETTE (Lawrence Berkeley National Laboratory, Berkeley, CA 94720).* Energy efficiency, conservation, and peak load management are important approaches to protecting the power grid, saving consumers money, and reducing impact on the environment. Demand Response (DR) is an attempt to curtail energy demand during the handful of days each year when the grid is strained. The local electric company, Pacific Gas & Electric (PG&E), created a voluntary program called Critical Peak Pricing (CPP), in which participants are asked to curb energy use for 12 independent summer days that PG&E deems are most likely to strain the grid. Participants receive lower electric rates on non-CPP days, but much higher rates during peak hours on CPP days, creating an incentive to reduce demand. Automated Demand Response (Auto-DR) is a novel approach focused on fully automating buildings participating in the CPP program, so during a CPP event their buildings will reduce its energy demands without any human interaction. The system works by using a computer program to continuously monitor CPP status posted on PG&E's server. When the program detects a CPP event in progress, it triggers pre-programmed energy saving strategies to take affect in the building such as dimming lights and reducing AC use. For buildings that are currently automated, post-event surveys are conducted to measure occupants' response to the changed environment from load reduction. This research also gives feedback to participants as soon as possible so they can see the correlation between their buildings' energy saving actions and their electrical shed. The main focus of this research is on studying the electrical demand of participating buildings evaluating how much they reduced their energy consumption. Over the past three years, this research has come to show that Auto-DR is a viable form of dynamic energy conservation, by consistently providing load sheds during CPP days. Due to the inherent lack of manual labor required to operate in this program and no reliance upon present personnel, Auto-DR may prove to be more efficient and cost-effective than DR for certain buildings.

Cumulative Risk Assessment: Environmental Fate, Physical-Chemical Properties, and Contaminant Toxicity. *JESSICA ENGLEHART (University of Maine, Orono, ME 04469) MARGARET MACDONELL (Argonne National Laboratory, Argonne, IL 60439).* In the event of a terrorist attack that utilizes chemical or biological weapons, the emergency response team needs a way to find information about the immediate risks and dangers present. In a scenario such as this,

Provisional Advisory Levels (PALs) currently undergoing preparation by Argonne National Laboratory would be of great help. These PALs are specifically designed to provide exposure guidelines for chemicals that have been deemed potential homeland security threats. If one of these chemicals were to be released to the water or air, a PAL would help first responders (e.g., individuals without an extensive scientific background) make a health-based decision about the level of danger that is present. Each PAL report is chemical specific, and multiple routes of exposure are analyzed in every document. The values for each PAL are determined by using studies from medical and scientific journals, government research, and other research publications. When as much information as possible has been compiled about each chemical, the most applicable material is used to develop the calculated PAL values that regulate the exposure guidelines. Although the derived PAL values are the designated purpose of the PAL report, other important components of the document include the chemical identification, physical-chemical properties, environmental fate, and toxicology data. The environmental fate is especially important to the report because many of the contaminants can rapidly break down into other components and chemicals. The resulting byproducts may be inert or even more toxic than the parent chemical. Specifically, the environmental fate of the nematocidal fenamiphos is undergoing analysis. While examining the fate of a chemical, it is understood that multiple chemicals may be present at any given time after a contamination occurs. This topic leads into the study of cumulative risk, which is an issue currently under national perusal. PALs are an invaluable resource in a time when chemical and biological warfare are legitimate fears; however, there is no guarantee that only one chemical will be present during a contamination or release. This is why it is vital to further investigate cumulative risk and how exposure to multiple contaminants should be handled in a time of crisis.

Detection and Quantification of Dehalococoides Strains from a Chloroethene-Contaminated Aquifer Using Quantitative Real-Time PCR (qPCR). KELLY CHO, ALMA ZHOLI (University of Michigan, Dearborne, Dearborne, MI 48128) CHRISTOPHER SCHADT, SONIA TIQUIA (Oak Ridge National Laboratory, Oak Ridge, TN 37831). Chlorinated solvents such as tetrachloroethene (PCE) and trichloroethene (TCE) are some of the most prevalent contaminants in groundwater in the United States. Recent studies have revealed that PCE and TCE can be reductively chlorinated to non-toxic ethene by specific dehalo-respiring bacteria from the genus *Dehalococoides*. While *Dehalococoides* have been found at a significant number of sites, these microbes may not be present in all groundwater environments. Hence, to promote complete dehalogenation of TCE and PCE, *Dehalococoides* are often added to contaminated sites in a process known as bioaugmentation. The present study aims to determine the presence and abundance of *Dehalococoides* strains in TCE/PCE-contaminated aquifer samples from Dover Air Force Base (DAFB) in Delaware that have undergone various treatment strategies, including bioaugmentation. Five samples were tested for the presence and abundance of *Dehalococoides* 16S rRNA genes using real-time PCR (qPCR). The composition of *Dehalococoides* in the samples were also determined by cloning and sequencing using PCR primers directed toward conserved regions of the gene within the group *Dehalococoides*. Results of the qPCR experiment revealed an abundance of *Dehalococoides* in all aquifer samples examined, indicating that this microbe may be wide spread in groundwater from DAFB, and perhaps active under each of the remediation strategies. Database searches of 16S rRNA-*Dehalococoides* partial sequences indicated that the samples were dominated by gene sequences related to *Dehalococoides* ethenogenes, *Dehalococoides* sp. CBDB1, and several uncultured *Dehalococoides* spp. This project is part of a larger effort to contribute to research and development of microbiological systems that influence parameters important to the clean up environmental contaminants such as PCE and TCE.

Determination of Aerosol Particle Size and Chemical Composition Using an Aerodyne Aerosol Mass Spectrometer. RY FORSETH (University of Wisconsin-Madison, Madison, WI 53715) YIN-NAN LEE (Brookhaven National Laboratory, Upton, NY 11973). Aerosol particles serve diverse roles in the earth's atmospheric processes including cloud formation, acid rain production and climate change through radiative forcing. In order to understand and predict aerosol's distributions and effects in the atmosphere, it is important to determine the chemical composition of aerosol particles, including nitrate, sulfate, ammonium, and organics, to elucidate their sources and formation mechanisms. Consequently, it is highly desirable to gather fast real-time data of atmospheric aerosol concentration and composition. To accomplish this, we have carried out experiments using a new real-time Aerodyne

Aerosol Mass Spectrometer (AMS) to study ambient samples as well as laboratory generated aerosol standards of known composition. We have thus gained a better characterization of the AMS regarding its ability to quantify the individual chemical components and to differentiate classes of organic compounds. Specifically, the AMS was compared with a particle-into-liquid sampler-ion chromatography (PILS) technique to gauge the quantitiveness of the AMS's analysis. In addition, since the AMS mass fragment data contain information that can be used to classify organics depending on their degree of oxidation, we have performed AMS analysis of laboratory generated organic aerosols of different oxygen to carbon ratios to provide additional data to corroborate this analysis scheme. It was found that the AMS underestimates the mass loading of aerosol particles in both ambient and lab measurements, and ambient aerosols are comprised mainly of OOA. Fresh diesel emissions were found almost completely comprised of HOA. These findings direct us to conduct further studies to probe into why there is a discrepancy between the PILS and AMS. Finally, our findings illustrate a need to use different organic species of various degrees of oxidation and functional groups to gain insights into the chemical characteristics of OOA and HOA.

Determining the Release Rate of Perfluorocarbon Tracers with Regards to Temperature. TASHA PICCOLO (Marist College, Poughkeepsie, NY 12601) JOHN HEISER (Brookhaven National Laboratory, Upton, NY 11973). Brookhaven National Laboratory uses perfluorocarbon tracers (PFTs) for atmospheric dispersion, leak detection, and measuring air ventilation rates in homes and commercial buildings. PFTs are used to tag air/gas and follow the movement of the air. PFTs are colorless, odorless compounds that consist of carbon and fluorine atoms joined by covalent single bonds. They are conserved, chemically inert, and biologically inactive. Therefore, they do not react with the atmosphere or other environments and are perfectly safe to use. One method of releasing PFTs to tag and track air is through the use of permeation sources. Permeation sources consist of a small glass vial partially filled with a PFT and fitted with a rubber membrane in its cap. The rubber membrane has a high solubility and diffusivity rate which allows PFTs to permeate through. A sampling of six different tracers were extracted and filled into permeation sources. The sources were divided into four groups; each group was contained in a constant temperature chamber with temperatures: 6°C, 20°C, 30°C, and 40°C. The 20°C temperature chamber held 15 of each tracer type, while the other temperature chambers held six of each tracer type. Every other day over a five week period, the PFT samples were weighed on a high precision balance to determine their rate of emission. The process of weighing each PFT determined the average weight loss at each weighing period and allowed calculation of the release rate at a specified temperature. As expected, the diffusion rate of each tracer was greatest in the 40°C temperature chamber. The greater release rate is due to higher vapor pressure produced in higher temperatures. By plotting the natural log (LN) of the release rate versus 1/Temperature (Kelvin), an equation was produced for each PFT which displayed the slope and y-intercept and expressed the specific release rate dependent on a given temperature. It is very important to determine the release rate of PFTs in regards to different temperatures so that the source term is well defined. Knowing the temperature dependency allows the calculation of the source term in a field experiment where the weather may change from very hot to very cold. This work is a small portion of other ongoing projects, such as the Urban Dispersion Project which uses PFTs to show how toxic gas might disperse throughout specific areas like New York City, and other projects using PFTs for ventilation and air exchange measurements in homes.

***Developing U.S. Census Bureau-Defined Regional MARKAL Modeling Energy Systems.** CHRISTOPHER TEACHEY (Stony Brook University, Stony Brook, NY 11794) VATSAL BHATT (Brookhaven National Laboratory, Upton, NY 11973). The MARKAL family of technology-rich, mathematical models is used to represent a national, regional, state, or municipal energy system while supporting long-term strategic energy and environmental planning. Because of an interest in examining energy technology options to acquire regional differences including energy resource stockpiles, energy system organization and inter-regional issues such as optimal emissions permit trading between United States regional energy systems for the purpose of reducing environmental pollution, it's now of concern to establish regional MARKAL models while using the United States Census Bureau divisions as a template. Using Microsoft Excel and the Visual Basic for Applications, the maintenance and collection of demand-side data from the Energy Information Administration's Annual Energy Outlook energy forecasts were tailored and input into each of the regional MARKAL models and the development of dynamic spreadsheets was necessary

and possible due to the extensive data to be aggregated periodically. This data was subdivided into the four primary sectors of demand which includes the residential, transportation, commercial, and industrial sectors. Among the demand data that was collected in each of these sectors includes forecasted energy projection figures and efficiencies of demand technologies. Once constructed and established, the multi-regional model will be used in an ongoing multi-year DOE project evaluating long-term impacts of the hydrogen production infrastructure on the U.S. energy market in addition to examining the key regional differences and inter-regional issues.

Development of Historical Water Table Maps of the 200-West Area of the Hanford Site (1950-1970). TEENA KINNEY (*Columbia Basin College, Pasco, WA 99301*) DUANE HORTON (*Pacific Northwest National Laboratory, Richland, WA 99352*). A series of detailed historical water table maps for the 200-West Area of the Hanford Site was made to aid interpretation of contaminant distribution in the upper aquifer. The contaminants are the result of disposal of large volumes of waste to the ground during Hanford operations which began in 1944 and continued on into the mid 1990s. Examination of the contaminant plumes that currently exist on site shows that the groundwater beneath the 200-West Area has deviated from its pre-Hanford west to east flow direction during the past 50 years. By using historical water-level measurements from wells around the 200-West Area it was possible to create water-table contour maps, which show probable historic flow directions. These maps are much more detailed than previously published water-table maps which encompassed the entire Hanford Site. The new water-table maps in this paper, focusing on just the 200-West Area, were contoured at one meter intervals and demonstrate the effects that specific waste disposal sites had on the water-table elevation and groundwater flow direction. Seven maps were created for years that would give the best representation of significant water-table changes. Time periods of significant changes were identified by examining historical water-level measurements that were taken periodically throughout the area. During the 1950s groundwater elevation and flow direction changed rapidly, so water table maps were made at two year intervals for the period 1950 to 1960. After the 1950s, far less rapid changes occurred in the water table, so maps were made at five year intervals from 1960 to 1970. The project ended with 1970 because detailed water-table maps of the 200-West Area already exist post-1970. The new series of maps show that groundwater flow direction has changed significantly over the past 50 years; shifting at some times and places 180 degrees from pre-Hanford flow directions. One may account for the past anomalies in groundwater flow direction beneath the 200-West Area by using a combination of the new map series and details about specific waste disposal sites. The new series of maps will be valuable as a reference during the clean up process of the Hanford Site.

Development of Preliminary Acute Oral Provisional Advisory Levels (PALs) for Phorate. JENNIFER MATTLER (*University of Florida, Gainesville, FL 32611*) MARGARET MACDONELL (*Argonne National Laboratory, Argonne, IL 60439*). Phorate is a highly toxic organophosphorus pesticide that inhibits acetylcholinesterase, an enzyme that degrades neurotransmitters that stimulate depolarization of nerves and muscles. Because it has been identified as a possible threat agent, concentration-based guidelines called Provisional Advisory Levels (PALs) have been developed for phorate. Draft PALs were developed using data such as the environmental fate, toxicokinetics, toxicodynamics, and symptoms of exposure in humans and animals. The preliminary PALs discussed were developed for oral exposure at three effect levels (no effect, moderate reversible effects, and lethality) for the acute (<24 hours) duration. Once a specific study dose was selected as the basis for the PAL, based on appropriateness for the given effect level it was scaled for a 70-kg adult who drinks 2 L of water per day and uncertainty factors (UFs) were applied to account for interspecies and human variation, database adequacy, exposure duration, and effect severity. The preliminary acute oral PALs 1, 2, and 3 for phorate were determined to be 0.3, 0.5, and 1.0 mg/L, respectively. These preliminary PALs are somewhat lower than the PALs for other organophosphorus (OP) compounds, which share a mechanism and general level of toxicity with phorate, indicating either possible over-conservatism in the preliminary PALs or greater toxicity for phorate compared to other OPs. With further study, the internal draft phorate PALs can be refined and also used to support extrapolations to determine PALs for other organophosphorus compounds that lack the necessary toxicological data.

Development of Sixth Grade Decomposition Curriculum to Meet National Science Education Standard: Science as Inquiry. AMY MORRIS (*Vanderbilt University, Nashville, TN 37235*) MARGARET TORN (*Lawrence Berkeley National Laboratory, Berkeley, CA 94720*).

A curriculum on decomposition was developed to meet the National Science Education Standard: Science as Inquiry by helping students acquire abilities necessary to do scientific inquiry and understandings about scientific inquiry. Additionally, the curriculum was developed to collect data on changing decomposition rates across the nation for scientists studying climate change. To meet the Science as Inquiry Standard, the students will study the carbon cycle and feedback effects in relation to climate change to identify questions that can be answered through a scientific investigation of decomposition; conduct a scientific investigation to determine the decomposition rates of local leaf litter and a common substrate; use balances, ovens, probes, and computers to gather, analyze, and interpret data; use mathematics to make data tables, graphs, and equations to describe their data; use evidence to develop explanations and predictions; and present a final project to the class. To provide data on decomposition rates for scientists studying climate change, sixth grade classrooms across the nation will follow a standard experimental protocol. The protocol will be repeated annually to provide data on how decomposition rates are changing. This summer, the experimental protocol was developed, as well as a timeline for executing the curriculum throughout the school year, sample worksheets to supplement the protocol, and a method for assessing students' abilities to do scientific inquiry and understandings about scientific inquiry. Further development of activities to teach content and experimental skills to students is needed. Students will benefit from a year-long project that emphasizes the Science as Inquiry Standard and will be able to help their world by collecting data for professional scientists to use to study climate change.

Disease Incidence of *Ustilago Bullata*, *Tilletia Fusca*, and *Pyrenophora Semeniperda* on *Bromus Tectorum* in the Hanford Site. LUIS GARCIA (*Eastern Illinois University, Charleston, IL 61920*) DR. JANELLE DOWNS (*Pacific Northwest National Laboratory, Richland, WA 99352*). In the wildland settings of the intermountain west *Bromus tectorum* is one of the most common invasive species, contributing to habitat degradation and increased wildland fire frequency. Control and eradication of cheatgrass in rangelands is a problem for many land management agencies and private land owners. Work described here is part of a cooperative effort to assess the potential use of indigenous fungal species as biocontrol organisms to this introduced annual grass. *Ustilago bullata* and *Tilletia fusca* are smut fungi that prevent seed set in infected cheatgrass plants and *Pyrenophora semeniperda* is an ascomycete fungus that kills cheatgrass seeds in the soil seed bank. To assess the incidence of the fungal pathogens in cheatgrass, three areas were surveyed in central Hanford and one site was surveyed on the Fitzner Eberhardt Arid Lands Ecology Reserve near Richland, Washington. To determine disease incidence for *U. bullata* and *T. fusca* we used a point intercept method, while extent of *P. semeniperda* infection will be assessed through examination of seed bank samples. We measured disease incidence from 40 plots at each site. No incidence of *T. fusca* was discovered at any of the sites surveyed. The average incidence of all sites of *U. bullata* was 15% and was highly variable ranging from 4%-20% and may be related to different environmental factors. Incidence of *P. semeniperda* will be determined when the seed bank samples are processed by the investigating scientist Dr. Susan Meyer at USDA Forest Service Shrub Laboratory, Provo, Utah. This research is a part of a larger study funded by the USDA Forest Service that combines data from other research areas in Washington, Idaho, and Utah.

Electrochemical Remediation of Arsenic Contaminated Groundwater. SCOTT MCLAUGHLIN (*University of California-Berkeley, Berkeley, CA 94720*) ASHOK GADGIL (*Lawrence Berkeley National Laboratory, Berkeley, CA 94720*). Arsenic in drinking water impacts 100 million people worldwide, 50 million of whom are in danger of severe poisoning. The most dire situation is in Bangladesh, where 45 million cases of arsenic related poisoning makes it the largest case of mass poisoning in human history. Available methods of treating arsenic are too expensive, not effective enough, and often difficult to implement, making them inadequate for a poor, largely undeveloped country such as Bangladesh. Electrochemistry promises an innovative, effective, and inexpensive method for arsenic remediation of drinking water. The method is an improvement upon a known method of using Fe^{3+} to remove arsenic. The Fe^{3+} combines with $As(V)$, forming an insoluble complex which then can be easily filtered out. The innovative step of electrochemistry allows for control over the amount of Fe^{3+} produced as well as electrochemical oxidation of the $As(III)$ into reactive $As(V)$ anion $[H_2AsO_4]^-$, making the method far more effective. Tests on a simple laboratory setup show a drastic improvement in arsenic removal efficiency compared to arsenic removal based on simple rusting of metallic iron. Application of 70 mA current over 10 minutes

in our electrochemical cell reduced the arsenic concentration in 850 mL synthetic ground-water from 1000 ppb to less than 5 ppb, even without system optimization. This is compared to a similar setup with a rusted iron coil without application of electrochemistry which only removed down to 250 ppb in an entire hour. We completed a major goal for this summer in understanding the effects of experimental conditions on the system so that reproducible and consistent results can be obtained. Currently, tests are being performed at various current densities and durations to find the optimal electrochemical parameters for efficient oxidation of Fe into Fe³⁺ and effective removal of arsenic. Once the process is well understood, the method will be able to be very efficiently applied to a water filter applicable to areas with arsenic in the groundwater.

Endocrine Disrupter Effects on Fish Reproduction: The Evaluation of the Toxicity of PFOA, PBDE-47, and its Metabolite 3-OH BDE-47 in Fathead Minnows (*Pimephales Promelas*). DANIEL HASKELL (University California–Santa Barbara, Santa Barbara, CA 93106)

IRVIN SCHULTZ (Pacific Northwest National Laboratory, Richland, WA 99352). Polybrominated diphenyl ethers (PBDEs) are commonly used as flame retardants in many consumer products and reports of their occurrence in fish and humans has steadily increased. Tetra- and penta-bromo congeners such as PBDE-47 are more bioaccumulative, but may also be metabolized into hydroxylated forms such as the PBDE-47 metabolite 3-OH BDE-47. It is unknown whether PBDE hydroxylated metabolites are more toxic to fish. Another compound that has become ubiquitous in the environment is perfluorooctanoic acid (PFOA). It is also widely used in industrial and commercial applications such as stain resistant carpeting. PFOA is very stable and is not known to be metabolized in animals and wildlife. In this study, I measured the effects of these contaminants on reproduction in fathead minnow breeding pairs orally exposed to each test chemical. Each treatment group was dosed via controlled feedings of brine shrimp (*Artemia sp.*) that previously had been incubated with each test chemical. Fecundity was tracked daily and used as an endpoint to evaluate reproductive toxicity. At the end of the exposure minnows were dissected and the gonads removed. The gonado-somatic index (GSI) and the condition index (CI) were also recorded to determine if there were any differences between treatment groups. Analysis of the results indicated there was no effect on reproductive performance or CI and GSI.

Evaluating Changes in Black Carbon Concentrations from California Diesel Emissions. JEFFERY AGUIAR (University of the Pacific, Stockton, CA 95211)

THOMAS KIRCHSTETTER (Lawrence Berkeley National Laboratory, Berkeley, CA 94720). In this paper we show how changes in diesel fuel properties influenced black carbon (BC) concentrations and emission factors during the past 37 years. In our analyses we use data from the San Francisco Bay Area, where diesel traffic can be considered the primary source of BC aerosol. We estimate BC concentrations from archived Coefficient of Haze (COH) data, collected routinely since 1967 at a number of Bay Area locations. COH values are a measure of the attenuation of light by the collected filter deposit and are proportional to BC concentrations measured by commonly used optical methods. Our analyses of monthly and annual COH-derived BC concentrations show that the Bay Area BC mass concentration is an order of magnitude greater in winter than in summer. Our estimated diesel BC emission factors changed from about 10 g kg⁻¹ in the late 1960s to less than 1 g kg⁻¹ in 2000. The seasonality is caused by unchanging monthly diesel BC emissions modulated by synchronous area-wide changes in inversion heights. Despite the continuous increase in diesel fuel consumption, annual area-wide BC concentrations decreased from 3.5 µg m⁻³ in 1967 to about 0.9 µg m⁻³ in 2000. We attribute the BC concentration decrease to the changes in diesel technology and fuel composition—particularly sulfur content that occurred in the period. BC emission factors are possibly more influenced by fuel property than engine technology. The intention for the diesel sulfur reduction was to reduce the emissions of sulfur oxides, which lower the effectiveness of exhaust particle control devices. The observed BC reduction is, therefore, an unintended benefit of the fuel sulfur reduction and steady improvements in diesel technology.

***Generating Wind Rose Plots to Predict Weather Behavior within New York City.** KATIE JOHNSON (St. Joseph's College, Patchogue, NY 11772) VICTOR CASSELLA (Brookhaven National Laboratory, Upton, NY 11973). Every day, the public accesses weather information collected by a vast network of cooperative observers. A wind rose gives a very concise view of how wind speed and direction are distributed at specific locations to show wind character for a particular event or purpose. Within the New York City Urban Dispersion Program (UDP), a multi-National Laboratory and multi-Federal Agency research project, the major objective is to study how air flows in a city environment.

The deep canyons beneath the tall buildings of New York City create challenges in predicting air flow. To study these air flow problems, Brookhaven National Lab (BNL), with help from the UDP, set up weather stations all around New York City to allow better estimates of where contaminants may travel and to enhance the city's emergency response capabilities. The objective is to have BNL continuously collect and store the data that is being sent from these weather stations, groups the information to create graphical wind roses using PERL programming and Lakes Environmental WRPLOT view software. In order for meteorologists to predict the different seasonal wind patterns more accurately at specific locations for the future to come, these wind roses show past to present weather behavior. The data is used to provide the scientific community with a better, more thorough understanding of local climate regimes and long-term trends in weather. Over time, the results and patterns of the winds at the observed locations are predicted more precisely by meteorologists to give the public a more accurate forecast in the future.

High Temperature Electrolysis for Production of Hydrogen.

PRISCILLA ZELLARCHAFFERS (Illinois Institute of Technology, Chicago, IL 60619) DR. RICHARD DOCTOR (Argonne National Laboratory, Argonne, IL 60439). Hydrogen fuel production is a stepping-stone towards eliminating dependency on fossil fuels. A potential method for mass production uses High Temperature Steam Electrolysis (HTSE). HTSE is a thermo-chemical process that splits a water molecule into hydrogen and oxygen. It requires a solid oxide electrolysis cell (SOEC) that operates at 1100 K with an yttrium-stabilized zirconium electrolyte. Potentially, the Gen IV nuclear reactor will be used as a power source to meet temperature requirements without greenhouse emissions. Currently, two process simulations for large-scale hydrogen production using HTSE have been introduced by Argonne National Laboratory (ANL) using ASPEN computer software and Idaho National Laboratory (INL) using HYSYS computer software. The economic feasibility of both processes must be determined thus a cost analysis of fluid transport and heat transfer equipment is conducted, and the energy balance is calculated. From these energy calculations, it is discovered that the optimum energy balance occurs in ANL's feed case of 50% water and 50% hydrogen. From the equipment cost analysis, it is estimated that for ANL the total process equipment cost is \$73 million, whereas for INL it is \$40 million. For both, ANL and INL systems, the total initial cost of the electrolysis unit and the nuclear reactor is about half a billion dollars. Although a HTSE hydrogen production plant will involve huge upfront investments in resources, this comparative economic analysis provides a basis for HTSE system selection.

Human Health Risk Assessment in the Hanford Area. CHRISTINE

SCHULTZ (Washington State University, Pullman, WA 99163) TERRI MILEY (Pacific Northwest National Laboratory, Richland, WA 99352). One of the goals of the City of Richland is to eventually use parts of the Hanford Site for non-industrial purposes, possibly as a golf course or a residential area. Although there has been an ongoing decontamination effort, the area is still too polluted to support these uses. In order to make predictions about future risk to humans in the Hanford Area and the City of Richland, and so the city can start making its growth plans, a thorough assessment of the current risk in the area is needed. Many types of data are gathered, and these data are run through various computational models. The parameters for the computer codes that implement the computational models are defined by an assortment of exposure scenarios. There are seven scenarios for how different people could be adversely affected by contaminants in the environment: drinking water (surface water and groundwater) only, residential farming, avid recreation, casual recreation, child recreation and an industrial worker. Each of the scenarios produces different results, as expected because of their distinct parameters. The scenarios are meant to reflect how various lifestyles can affect people's risk levels differently. Levels of risk for each scenario in each appropriate region were determined. Using maximum measured environmental concentrations, most of the scenarios were over the safe limit of risk in at least one sub-region, showing that the area is not yet safe for these exposures. With these results, and by comparing them with results of a similar study from the early 1990s, predictions for when the area will be safe can be updated. It is important this study be done frequently because the natural attenuation of contaminants is occurring at a slower rate than initially predicted.

Improving Lithofacies Interpretation through Systematization

and Quantification of Borehole Geologic Data. JAMES REIDER (Lock Haven University of Pennsylvania, Lock Haven, PA 17745) GEORGE LAST (Pacific Northwest National Laboratory, Richland, WA 99352). Simulations of vadose zone flow and transport are a fundamental component of studies aimed at determining the extent

of waste contamination and movement beneath the Hanford Site. Historically, these simulations and models have represented the geologic framework and associated flow and transport properties through simple homogenous and horizontally stratified hydrogeologic units. Capturing the heterogeneity, small scale variability, and uncertainty within numerical models is receiving more emphasis due to increasing capabilities of computer systems and the need to develop more detailed and complete depictions of contaminant transport. The ability to improve resolution of numerical models and simulations is limited by the availability of data in a form favorable to computer processing. Geologic borehole information is, for the most part, qualitative in nature and not readily amenable to numerical analysis. Thus, efforts are being made to systematize borehole geologic data, to be used in a more quantitative manner. Detailed procedures have been developed to translate qualitative descriptive information into discrete semi-quantitative parameters, and to translate inconsistent quantitative and semi-quantitative data sets into common parametric data sets. A geologic data management system is being developed to manage these new "translational" data sets and integrate them with existing databases to support their synergistic analysis and improved numerical representation of the subsurface geology. Detailed procedures and uniformed translational processes allow for qualitative data from a variety of sources to be represented in a semi-quantitative and computer accessible form that is thorough, uniform, traceable, and defensible. This process is leading to the creation of a detailed representation of the geologic relationship between flow and transport properties of lithofacies and the stratigraphic sequence of those lithofacies beneath the waste disposal facilities at the Hanford Site.

Indoor Air Quality Study-Vapor Intrusion of Volatile Organic Compounds. FRANK OGERO (*Medgar Evers College, Brooklyn, NY 11225*) DERECK SKEETE (*Brookhaven National Laboratory, Upton, NY 11973*). Growing response to residential exposure to Volatile Organic Compounds (VOCs) and Semi Volatile Organic Compounds (SVOCs) have prompted concern by the EPA to promulgate regulatory limits for VOCs in residential homes. A major source of these fugitive VOCs are dry cleaners, service stations and leaking underground storage tanks. An immediate threat can be realized from the vapors that migrate into residences. This threat can pose chronic health risk for residents if the detectability level is low. The objective of this project is to validate the Johnson-Ettinger (JEM) model and other 2-dimensional and 3-dimensional models using the Brookhaven National Laboratory Air Infiltration Measurement System (BNL/AIMS) technique to determine the subsurface contribution of VOCs intrusion in buildings. Four PFT sources were deployed in building 830. Sources were left for approximately 48 hours in six zones. Passive samplers were used to trace the infiltration and exfiltration of PFT sources. Analysis of the samplers in the laboratory showed that the flow rate in three of the six zones were quite comparable. The hallway (zone5) had a relatively high concentration rate upwards of $6\text{m}^3/\text{h}$. However, the crawl space had low source rates hence there was little detection of PFT sources. This miniature source and sampling tracer kit can measure infiltration rates on the order of 0.2 to 5 changes per hour over time-averaged periods of 1 day to several months or years.

Indoor Vapor Intrusion of Volatile Organic Compounds. DERECK SKEETE (*Pennsylvania State University, State College, PA 16801*) JOHN HEISER (*Brookhaven National Laboratory, Upton, NY 11973*). Growing response to residential exposure to Volatile Organic Compounds (VOCs) and Semi Volatile Organic Compounds (SVOCs) have prompted concern by the EPA to promulgate regulatory limits for VOCs in residential homes. A major source of these fugitive VOCs are dry cleaners, service stations and leaking underground storage tanks. An immediate threat can be realized from the vapors that migrate into residences. This threat can pose chronic health risk for residents if the detectability level is low. The objective of this project is to validate the Johnson-Ettinger (JEM) model and other 2-dimensional and 3-dimensional models using the Brookhaven National Laboratory Air Infiltration Measurement System (BNL/AIMS) technique to determine the subsurface contribution of VOCs intrusion in buildings. Four perfluorocarbon tracers (PFTs) sources were deployed in building 830. Sources were left for approximately 48 hours in six zones. Passive samplers were used to trace the infiltration and exfiltration of PFT sources. Analysis of the samplers in the laboratory showed that the flow rate in three of the six zones were quite comparable. The hallway (zone5) had a relatively high concentration rate upwards of $6\text{m}^3/\text{h}$. However, the crawl space had low source rates hence there was little detection of PFT sources. This miniature source and sampling tracer kit can measure infiltration rates on the order of 0.2 to 5 changes per hour over time-averaged periods of 1 day to several months or years.

***Investigation of Lyme Disease Spirochete, Borrelia burgdorferi and Babesiosis Transmitted by Amblyomma Americanum.**

MELISSA TORRES (*State University of New York at Stony Brook, Stony Brook, NY 11794*) ROBERT SELVEY (*Brookhaven National Laboratory, Upton, NY 11973*). Brookhaven National Laboratory is the home of three species of ticks: *Ixodes scapularis* (Deer Tick), *Amblyomma americanum* (lone-star tick), and *Dermacentor variabilis* (Dog tick). Lone-star tick is a species of tick that was almost non-existent at Brookhaven National Laboratory in the late 1980s. The ratio of Deer ticks to Lone-star ticks has dramatically changed within the past fifteen years due to the vast population of deer at Brookhaven National Laboratory. This is a concern for the employees and visitors at BNL because they may be at a higher risk of contracting lyme disease. Lone-star ticks are known carriers of ehrlichiosis and a spirochete called *Borrelia lonestari* which gives a rash similar to the rash associated with *Borrelia burgdorferi*; however lone-star ticks are not known carriers by the State of New York Department of Health to carry the lyme disease spirochete or babesiosis. The known transmitter of lyme disease and babesiosis are deer ticks. Since both species of ticks feed off of the same infected mice and deer, this increases the possibility of the lone-star ticks acquiring and being able to transmit the lyme disease spirochete. Using Polymerase Chain Reaction (PCR) methods of locating specific DNA fragments we are able to analyze lone-star ticks for the *Borrelia burgdorferi* spirochete as well as babesiosis. We had a small sample size but according to our results all of the lone-star ticks returned negative for the lyme disease spirochete but surprisingly instead of an expected zero percent lone-star returned 10% positive for Babesiosis. We also tested deer ticks and they returned 10% for the lyme disease spirochete and another 10% positive for babesiosis. Due to the way we sent our samples out for analysis it was impossible to find out if there was a correlation with the two diseases. Our results did not return as expected and we now conclude that employees and visitors at BNL should be more aware of babesiosis since it is carried by two different species in the area.

Investigation of the Characteristics of Ponds and Vernal Pools used by Eastern Tiger Salamanders and Their Effects on Juvenile Recruitment. CHAUNCEY LEAHY (*Community College of Rhode Island, Providence, RI 02903*) VALORIE R. TITUS (*Brookhaven National Laboratory, Upton, NY 11973*). The Eastern Tiger Salamander (*Ambystoma tigrinum*) is endangered due to rapid over-development on Long Island. In order to protect this species, protocols must be developed to identify suitable habitat and habitat preservation requirements. Egg mass surveys can be used to evaluate the optimum conditions of ponds and vernal pools (i.e., temperature, pH, conductivity, etc.) used by tiger salamanders in order to reproduce. Linking egg mass surveys with juvenile recruitment can assist in creating models that predict how productive a pond/vernal pool has the potential to be. This research investigated the characteristics associated with ponds and vernal pools used by tiger salamanders for breeding to determine which ponds are the most productive and which ponds result in the greatest amount of surviving larva. Egg mass surveys were conducted 2000 through 2006 at thirty-seven pond and vernal pool locations throughout the Brookhaven National Laboratory property and juvenile recruitment data was collected at four of the ponds via drift fences and seining data. This is an ongoing project and more data is needed before a conclusion can be made.

Isolation of Lactate Dehydrogenase from a Filamentous Fungus.

JEANNENE RAVET (*Walla Walla Community College, Walla Walla, WA 99362*) ELLEN PANISKO (*Pacific Northwest National Laboratory, Richland, WA 99352*). Lactate dehydrogenase is the enzyme responsible for catalyzing the production of lactate from the substrate pyruvate and causing the oxidation of nicotinamide adenine dinucleotide, reduced form (NADH) to nicotinamide adenine dinucleotide, oxidized form (NAD). In order to attain the production of high levels of lactic acid, the ideal growth conditions and strain of fungus must be determined. Through the use of a lactate dehydrogenase assay, the conversion of NADH to NAD from various fungal extracts is observed by spectrophotometry and recorded over a five minute period. From these results, the activity of the enzyme can be determined. Results did not consistently show lactate dehydrogenase or significant enzyme activity when uncharacterized fungal isolates CKF120 and CKF394 were tested against a control lacking the substrate sodium pyruvate. Various methods were tested to produce results; however, the possibility of contamination and the variability of filamentous fungi could contribute to the lack of lactate dehydrogenase activity. Currently, testing is being done on different conditions to determine which will cause lactate dehydrogenase to be highly expressed. Once found, the enzyme will be isolated from the cell

for further study, to potentially obtain the protein sequence, providing information to help achieve hyper productivity.

Linking Water and Energy Models to Acquire a Better Understanding of the Interrelation Between Energy and Water.

CARISSA SALVATO (Binghamton University, Binghamton, NY 13902) KENYA CROSSON (Brookhaven National Laboratory, Upton, NY 11973). It is important to consider the amount of energy and water available when implementing new technologies. When investigating innovative energy technologies, water supply and water quality data are often overlooked, and energy is often assumed to be an unlimited resource for water treatment and conveyance. Markal Allocation (MARKAL) is an energy, environment and economic analysis linear programming model that is technology-rich and capable of assessing multi-scale energy systems over a user-defined time period. MARKAL is currently used to model energy demands and technologies in over 55 countries. Brookhaven National Laboratory is currently incorporating water supply and conveyance, water and wastewater treatment, and the associated technologies into a New York City version of MARKAL. However, an in depth analysis of watershed conditions (meteorology, land use, point and non-point sources, etc.) that significantly affect water supply and water quality cannot be accomplished with the MARKAL model framework. Thus, it is necessary to link a watershed model with MARKAL to create a decision support network that addresses energy-water issues. Research was conducted to find the most suitable watershed model. After reviewing the qualities of many different models, one was chosen. The model chosen was the Watershed Analysis Risk Management Framework (WARMF) because it could be easily obtained in Windows format and also due to its ability to integrate water quality, DEM and GIS. Data necessary to run the WARMF model was obtained from sources such as USGS (United States Geological Survey), EPA's STORET (Storage and Retrieval) and NADP (National Atmospheric Deposition Program). All necessary information has yet to be obtained in order to run the WARMF model, warranting further data searches. In further studies the WARMF model will be linked with the New York City MARKAL model. The economic and environmental results of these studies will illustrate the interrelationship between energy and water systems in metropolitan areas and lead to better management of energy and water resources, improved policies/regulations, and a better understanding of the economic and environmental impacts of energy and water technologies.

Lipid Production by *Dunaliella Salina* in Batch Culture: Effects of Nitrogen Limitation and Light Intensity.

CHAD WELDY (Western Washington University, Bellingham, WA 98225) MICHAEL HUESEMANN (Pacific Northwest National Laboratory, Richland, WA 99352). Atmospheric carbon dioxide (CO_2) concentrations are increasing and will cause unknown deleterious environmental effects if left unchecked. The Intergovernmental Panel on Climate Change (IPCC) has predicted in its latest report a 2°C to 4°C increase in global temperatures even with the strictest CO_2 mitigation practices. Global warming can be attributed to in large part to the burning of carbon-based fossil fuels, as the concentration of atmospheric CO_2 is directly related to the burning of fossil fuels. Biofuels which do not add CO_2 to the atmosphere are presently generated primarily from terrestrial plants, i.e., ethanol from corn grain and biodiesel from soybean oil. The production of biofuels from terrestrial plants is severely limited by the availability of fertile land. Lipid production from microalgae and its corresponding biodiesel production have been studied since the late 1970's but large scale production was determined to be economically unfeasible due to the large costs of sterile growing conditions required for many algal species. This study focuses on the potential to use the halophilic microalgae species *Dunaliella salina* as a source of lipids and subsequently for biodiesel production. The lipid production rates were compared for *D. salina* cultured in replicate photobioreactors under high light and low light as well as nitrogen sufficient and nitrogen deficient culture conditions. The results show (a) cellular lipid content ranging from 16 to 44% (wt), (b) a maximum culture lipid concentration of 450 mg lipid/L, and (c) a maximum integrated lipid production rate of 46 mg lipid/L culture*day. The high amount of lipids produced suggests that *D. salina*, which can be mass-cultured in non-sterile outdoor ponds, has a strong potential to be an economically valuable source for renewable oil and biodiesel production.

Litter Position Appears to be the Most Important Driver of Decomposition at ORNL FACE. REBECCA ROHA (Gettysburg College, Gettysburg, PA 17325) AIMEE CLASSEN (Oak Ridge National Laboratory, Oak Ridge, TN 37831). Levels of atmospheric $[\text{CO}_2]$ (carbon-dioxide concentration) are expected to double in the next century, therefore it is important to understand the effects of CO_2 on ecosystem processes such as decomposition. Decomposition plays an

important role in the global carbon cycle, and will likely be impacted by climatic change. The Free Air Carbon-dioxide Enrichment (FACE) site at Oak Ridge National Laboratory (ORNL) provides a unique opportunity to investigate the effects of elevated $[\text{CO}_2]$ on decomposition and carbon cycling. ORNL FACE is a sweetgum plantation consisting of two rings of elevated $[\text{CO}_2]$ and three rings of ambient $[\text{CO}_2]$. This decomposition study was constructed to examine how changes in atmospheric $[\text{CO}_2]$ may alter decomposition and carbon cycling in forested ecosystems. Three parameters were measured: (i) litter quality, (ii) decomposition environment, and (iii) decomposition position. Treatments include leaves that were naturally grown under either elevated or ambient atmospheric $[\text{CO}_2]$. Leaves from elevated and ambient rings were decomposed in like rings to test how $[\text{CO}_2]$ might alter litter quality and decomposition. In an adjacent "common substrate" experiment, leaves from ambient rings were decomposed in all elevated and ambient rings to test if the effects of $[\text{CO}_2]$ on microclimate or microbial communities would alter decomposition. Finally, leaves from ambient and elevated rings were buried in the soil profile to test if litter position impacted decomposition. Decomposition rates were determined by comparing the mass before and after decomposition (percent mass loss). This research resulted in three major findings: 1) The effects of elevated $[\text{CO}_2]$ on litter quality had no impact on litter decomposition; 2) Decomposition of a common substrate did not differ between ambient and elevated plots, suggesting the change in soil environment due to elevated $[\text{CO}_2]$ does not alter decomposition; 3) Due to earthworm activity, belowground decomposition occurred much faster than aboveground decomposition; thus, litter position appears to be the most important driver of decomposition at FACE. These data are important because modelers can use them to better predict the effects of elevated $[\text{CO}_2]$ on forest carbon cycling in the future.

MARKAL Modeling for Energy in Census Regions and Divisions of the United States.

KIN MAN LEI (State University of New York at Stony Brook, Stony Brook, NY 11794) VATSAL BHATT (Brookhaven National Laboratory, Upton, NY 11973). MARKAL, short for MARKet ALlocation, is a comprehensive energy/economic model that simulates a nation, region, or state's energy system by representing the technologies and demands for energy services that comprise it. The model finds the least-cost way to meet a given set of demands for energy services within the constraints of a user's available technologies and any environmental limits. Developing MARKAL involves building a bottom-up model of the region's energy system, and thus requires a tremendous amount of technical input data. These data are divided into two main parts, the supply side and the demand side. The supply side consists of data related to the resources used in each state to produce energy, such as natural gas, biomass, coal, oil and others. While the demand side consists of data regarding the technologies in use, their costs, and the assumption of their efficiencies. Most of the data can be collected from the Energy Information Administration, U.S. Census Bureau, U.S. Department of Energy and others. For the supply side data, each resource defines its own regions without reference to each other or to the national census regions. Consequently all supply side data for each resource must be converted to a uniform standard, which is the national census regions. After collecting all these data, they are inputted into the ANSWER software. This processes the input data, draws Reference Energy Systems diagrams, submits model runs, handles the numerous scenarios needed during an assessment, and facilitates analysis and interpretation of the model results. When the MARKAL model is formed, it can identify costs and benefits of alternative energy scenarios for future use, and also estimate the relative merits of specific technologies that are applied in an energy system of each census region.

Mercury Deposition on the Forest Edge and Beyond.

CHELSEA CAMPBELL (Western Kentucky University, Bowling Green, KY 42101) TERRY SULLIVAN (Brookhaven National Laboratory, Upton, NY 11973). Mercury is a neurotoxin that, if ingested at high concentrations, can significantly effect physical, psychological, and behavioral problems including sleeping disorders, memory loss, and chronic fatigue. The Environmental Protection Agency has set many precautionary restrictions on fish consumption due to these health issues. Mercury is naturally occurring in the earth's crust, and therefore, is found in many minerals such as coal. Coal-fired power plants are the largest human contributors of mercury. As part of a larger program to investigate the impact of mercury releases from coal-fired power plants, a study is being conducted on mercury concentrations in tree leaves at Brookhaven National Laboratory (BNL). It is hypothesized that the mercury deposition could be higher in the trees on the forest edge, and therefore, acts as a shield to the trees inside the forest. To examine the impacts of forest edges and heavily traveled roads on mercury concentration in tree leaves, five locations within three

transects around BNL were designated sample sites. At each location, three types of trees were studied: Red Oak (*Quercus rubra* L.), White Oak (*Quercus alba* L.), and Scrub Pine (*Pinus rigida* mill.). The three transects were William Floyd Parkway, I-495, and a clearing at the BNL biology testing fields. The first location in each transect was taken on the perimeter, while the other four locations were set at 100-yard increments progressing into the forest. The samples were taken by hand from selected trees with low branches resulting in a deficiency of pine samples in some locations. Weekly collections were done for six weeks including a collection of leaf litter. Blind Duplicates were taken in the field and approximately 90 samples were collected in every round. Samples were measured in duplicate for quality assurance, and if necessary, triplicate measurements were taken, with a result of over 1,000 samples being analyzed. The moisture content was calculated after drying the samples at 60°C overnight. The Red Oak moisture content was found to be around 61% while the White Oak had a moisture content of 65%, and the pine was found to contain about 55% moisture. A Direct Mercury Analyzer (DMA-80) was used to determine the concentration of mercury in the leaf samples. The data analysis has begun on the first and second round of sampling to investigate comparisons between the rounds and the spatial trends.

Methodology Development for Monitoring the Diatom *Pseudo-nitzschia* Spp. in Coastal and Estuarine Waters of the Pacific Northwest. ELYSE WALKER (University of South Carolina, Columbia, SC 29208) DANA WOODRUFF (Pacific Northwest National Laboratory, Richland, WA 99352). *Pseudo-nitzschia* spp., a harmful algal specie found in Pacific Northwest waters can produce domoic acid, a neurotoxin that affects shellfish, marine mammals, birds, and humans if ingested in high doses. Instruments and techniques that can rapidly detect harmful species for screening purposes are useful as early warning tools. The goal of this study was to develop and test a procedure for identifying *Pseudo-nitzschia* spp. blooms in Sequim Bay, Washington. Weekly samples were taken from both an incoming and outgoing tide at the mouth of Sequim Bay and analyzed using an image analysis system, the FlowCAM®. These data were analyzed to create a protocol for monitoring *Pseudo-nitzschia* spp. and determining if bloom conditions were present. Based on knowledge of a June 2006 *Pseudo-nitzschia* spp. bloom in Sequim Bay, results indicate that a bloom may be occurring when more than 92% of particles <0.08 in aspect ratio are *Pseudo-nitzschia* spp. Based on this preliminary data, the FlowCAM® appears to be a useful tool for pre-screening of *Pseudo-nitzschia* spp. bloom conditions.

Non-Invasive Species Confirmation of Fox Populations at Brookhaven National Laboratory. WENDY FINN (University of Rhode Island, Kingston, RI 02874) DR. TIMOTHY GREEN (Brookhaven National Laboratory, Upton, NY 11973). Information regarding the present day status of Fox populations on Long Island, NY is essential for an understanding of species diversity. Historically, Red Fox (*Vulpes vulpes*) and Gray Fox (*Urocyon cinereoargenteus*) occurred sympatrically on Long Island, NY. Although current population size estimates have not been established for either species it is speculated that the Red Fox has adapted to anthropogenic disturbances better than the Gray Fox. After the discovery of a deceased Gray Fox in the Relativistic Heavy Ion Collider at Brookhaven National Laboratory (BNL) in October of 2004, questions arose concerning the presence of this species in the area. To determine if the Gray Fox is utilizing areas of BNL as a home range, this study focused on observing mitochondrial DNA markers in feces, which enable us to distinguish between the two species. A positive scat sample and camera trap shot have confirmed the presence of gray fox at BNL.

Potential for *Amblyomma Americanum* to Carry *Borrelia burgdorferi*, and *Babesia*. ZARREA PRADHAN (Stony Brook University, Stony Brook, NY 11794) ROBERT SELVEY (Brookhaven National Laboratory, Upton, NY 11973). Long Island is the home to three species of tick: the deer tick *Ixodes scapularis*, the American dog tick (*Dermacentor variabilis*), and the Lone Star tick (*Amblyomma americanum*). Over the past few years the tick population has become dominated by *Amblyomma americanum*. The ratio of *Amblyomma americanum* to *Ixodes scapularis* at Brookhaven National Laboratory is about 8 to 1. New York State Center for Disease Control does not recognize *Amblyomma americanum* as a carrier of Lyme disease or *Babesia*, a protozoan that causes intestinal discomfort. Due to the increasing population of this species of tick, it would be beneficial to test for the presence of *Borrelia burgdorferi*, which is the bacterium that causes Lyme disease. *Amblyomma americanum*, are known to carry other *Borrelia* bacterium, specifically *Borrelia lonestari* which only causes a minor rash. In an attempt to determine if this species carries the spirochete *Borrelia burgdorferi*, several samples have been

obtained at Brookhaven National Laboratory. The samples that have been collected have been sent to a lab where they were analyzed using PCR (polymerase chain reaction), a DNA amplification process, which tests the DNA for the spirochete bacterium *Borrelia burgdorferi*. Using the 609 ticks collected over a two and a half week period from various locations around the site, random samples were chosen for testing. These samples consisted of 10 *Ixodes scapularis* nymphs, 10 adult *Amblyomma americanum* females, 10 adult *Amblyomma americanum* males, and 10 *Amblyomma americanum* nymphs. The testing performed detected the presence of *Borrelia burgdorferi* and *Babesia*. The results showed the *Amblyomma americanum* that had been tested (a total of 30 ticks) were negative for the presence of *Borrelia burgdorferi*. The results also showed 6% of *Amblyomma americanum* were positive for the presence of *Babesia*, which they had not been know to carry prior to the testing. Of the 10 *Ixodes scapularis* tested, 10% were positive for *Borrelia burgdorferi* and 10% were positive for the *Babesia*. It should be noted that the sample size used in this study was very small. Only 4.9% of the ticks collected were tested due to funding limitations. In order to further support the claim that *Amblyomma americanum* does not carry *Borrelia burgdorferi*, further testing should be done using a larger sample size. In addition, further testing should also be done to try and estimate the percentage of *Amblyomma americanum* infected with *Babesia*.

Processing of Numerical Simulations of Fluid and Chemical Transport to Determine Kinetic Coefficients Using an Inverse Solution Algorithm. SCOTT CESAR (Western Michigan University, Kalamazoo, MI 49006) JACK PARKER (Oak Ridge National Laboratory, Oak Ridge, TN 37831). Chemical reaction kinetics and physical mass transfer can be described as rate equations that are dependant on such factors as mass transfer, permeability and dispersivity while also being affected by flow. Through modeling, the rate of a certain process may be conceptualized at a specific scale when seen at a given time. Computation models do not necessarily scale to a larger or smaller dimension readily and therefore complex coefficients are necessary for accurate modeling. Through refinement of variables, model accuracy can be determined with much greater efficiency. The purpose of this study is to model processes at different scales using scale-independent mathematical formulations with scale-dependant coefficient values or functions with scale-dependent intrinsic error. Laboratory data of batch and column experiments with specific fluid flows through porous media (weathered, fractured shale saprolite and pyrolusite) was obtained from previous research. The data was then manipulated through the use of Sigma Plot and Microsoft Excel to provide a suitable output form for further use. The new data structure was used to construct files for input into HydroGeoChem. The code was then modified through use of Fortran 95 to create an inverse solution algorithm for further modeling. The data files and Fortran code are then run using VisualPest to derive estimation of parameters to formulate mass transfer rate and correlations of coefficients for further statistical analysis. The first and only set of data analyzed at this point deals with the mass transfer of bromine through columns with soil sample collected locally. Two saturated undisturbed column experiments were performed and the results were analyzed. Simulation 1 gives an estimation of mobile zone porosity → and geometry factor a which utilized together with different scale experiments and simulation will be used to determine the scalability. In Simulation 2, no non-reactive tracer drop was seen during flow interruption, so mobile-immobile mass transfer simulation was not performed. No conclusion can be made from the data due to the limited number of viable analyses performed. More simulations must be conducted before substantiated results may be established.

Raman Spectroscopic Studies of Plant Species. LAURA ROSSIER (Stony Brook University, Stony Brook, NY 11794) WEI WANG (Oak Ridge National Laboratory, Oak Ridge, TN 37831). This study examined the Raman spectra of leaves, flowers, and fruits at varying stages of decay in an attempt to identify various plant pigments and species based on their chemical and structural signatures. All Raman spectra were collected using a Renishaw micro-Raman system with a 300 mW near-infrared diode laser with 785 nm wavelength of excitation. Seven main vibrational bands occurred at ~1526, 1188, 1157, and 1602, 1326, 1287, 744 cm⁻¹ for all samples; these bands were assigned to the C-C stretching mode, as well as other carbon bonding, of carotenoid and chlorophyll. The spectral peaks can act as references for the color of the plant material, regardless of the species of plant or plant part. Using the relative intensities of peaks associated with chlorophyll and carotenoids, samples can be roughly classified according to color. This study also observed a red carnation at different times over the course of a week as it was removed from water and allowed to decay. Over time the relative intensities of peaks distinctly changed. For the red carnation, the ratio

of the highest intensity peaks (l1188(carotenoid)/l1602((chlorophyll)) increased steadily with time and lack of water. Future studies will illuminate the nuances of the relationship between spectra of pigment and observed color by expanding the spectral database of colored plant material. In addition future studies will determine more exactly the rate of change for relative peak intensities, as well as determining the variation in the relative intensity of chlorophyll and carotenoid peaks for a variety of decaying plant materials. Potentially, surface enhanced Raman spectroscopy could enable identification of other plant molecules as well as providing a method for plant classification by species.

***Redesign and Update of the Brookhaven Atmospheric Tracer Sampler (BATS).** MIGUEL LOPEZ, RAMON FERNANDEZ (Bronx Community College, Bronx, NY 10453) JOHN HEISER (Brookhaven National Laboratory, Upton, NY 11973). The Brookhaven Atmospheric Tracer Sampler (BATS) is a versatile air-sampling instrument used to capture perfluorocarbon tracers (PFT) used in air infiltration and atmospheric transport studies. The updated BATS includes a new power control module (PCM), which can be programmed by computer via either serial connection or wirelessly through the World Wide Web. These units are assigned an IP Address so that they can be accessed from any computer terminal with an Internet connection, providing access to the functionality of the BATS at any time and distance. Each unit is equipped with a digital LCD screen with a real-time clock, date, and temperature meter, to allow for manual calibrations or changes in data collection settings. With unique timing, triggering, wireless capabilities and pumping modules, the BATS has now become a more efficient tool for precise tracer sample acquisition. Whereas outdated units were programmed to pull air through these tubes for a certain time period, renovated units are capable of pulling a measured volume of air through any of the 23 sampling tubes at a specified time, date and rate. In addition, the introduction of mass flow control reduces the time and cost involved in data analysis and greatly improves QA/QC. Each independent battery-operated BATS unit can be programmed to cycle on and off within a 24-hour period over seven days to provide time sequential sampling. The sampler consists of two modules—the pump control module and the interchangeable sampling module—located in the base and lid respectively. The lid or Air Flow Module (AFM) contains the sampling tubes, selector valve, and drive solenoid, while the PCM contains the batteries, control, and sampling pump. The AFM consists of 23 sampling catch tubes, each containing a carbonaceous adsorbent. The major differences between the old and new BATS are the new BATS has a web based microprocessor controller, mass-flow measurement, variable sampling intervals and flow rate with wireless internet access. We are in the process of bench testing new units prior to deployment in the field.

Relative Abundance of Anurans on the Hanford Reach National Monument. SHANNON BLACKBURN (Columbia Basin Community College, Pasco, WA 99301) JAMES BECKER (Pacific Northwest National Laboratory, Richland, WA 99352). Breeding sites of three anurans, the bullfrog (*Rana catesbeiana*), Great Basin spadefoot (*Spea intermontana*), and Woodhouse's toad (*Bufo woodhousei*), a Washington state monitor species, were identified during call surveys at 23 pools and river shoreline locations along the south and west shorelines of the Hanford Reach of the Columbia River in Benton County. Call surveys were conducted from the beginning of February through mid-August to identify breeding sites for these species, breeding chronology, and establish baseline relative abundance. All three species used pool locations almost exclusively, with very little use of river shoreline locations. A total of 1,301 individuals of all three species were heard calling during the study period. The Great Basin spadefoot was the first species to begin calling, in late April, reaching its peak calling period in late May, and tapering off in early July. Woodhouse's toads began calling in early May, peaked during mid-May, and continued calling into late July. The bullfrog called from early May but did not peak until late July through mid-August. Great Basin spadefoot calls were most abundant, comprising 44.2% of the total, followed by Woodhouse's toad at 41.8%, and the bullfrog at 14%. Given general downward trend in anuran population numbers worldwide and the increase in species extinctions, it may be beneficial to continue monitoring populations at the Hanford Reach in order to follow long term population trends.

Removal of Arsenic from Contaminated Water by Means of Electrochemistry. KRISTIN KOWOLIK (Santa Monica College, Santa Monica, CA 90405) ASHOK GADGIL (Lawrence Berkeley National Laboratory, Berkeley, CA 94720). Millions of people worldwide do not have access to clean water. This problem is especially severe in Bangladesh where water is severely contaminated with arsenic. Chronic arsenic exposure has devastating health effects: cardiovascular

diseases, cancers, and eventually death. Many methods of arsenic removal have been studied but most of these are too expensive and impractical to be implemented in poor countries such as Bangladesh. This project investigates electrochemistry as an affordable means of removing arsenic. Experiments are performed using a galvanic cell with iron and copper electrodes. These are immersed in synthetic ground-water spiked with an arsenic concentration of 1 ppm. Current is applied to the system and iron metal is oxidized to Fe(III). As an ionic species, iron will bind free arsenic in solution. After the electrochemical process, the treated water is filtered by means of vacuum filtration. One of the significant major tasks of the project was to develop an experimental protocol (methods, measurement techniques, experimental conditions) to obtain reproducibly consistent results, so this process can be investigated further. We showed that if certain conditions are met such as (1) optimal current density, (2) sanded iron electrode and (3) specific amount current and time, consistent results are obtained. An initial arsenic concentration of 1 ppm can be reduced to a final concentration as low as 5 ppb or less, in 1 L water by application of 90 mA current in 10 minutes. These results are very encouraging and provide great promise that electrochemistry is a powerful, and most importantly, an affordable tool in the remediation of arsenic from contaminated groundwater.

Reproductive Toxicity of PCB-77 and 4-OH PCB-66 in. MARIO DELGADILLO-LARIZ (Cabrillo Community College, Aptos, CA 95003) IRV SCHULTZ (Pacific Northwest National Laboratory, Richland, WA 99352). The reproductive toxicity of 3',3',4,4'-tetrachlorobiphenyl (PCB-77) and a representative hydroxylated metabolite, 4-OH PCB 66, was studied in fathead minnows (*Pimephales promelas*). The study consisted of three groups of sexually mature and actively spawning fathead minnows (FHM). One group of FHM's was orally exposed to PCB-77 by bioencapsulation in brine shrimp, *Artemia sp.* Bioencapsulation was achieved by placing adult *Artemia* in a flask coated with the test chemical. A second group of FHM pairs were orally exposed to 4-OH PCB-66, also by bioencapsulation. The exposure lasted 21 days. Their reproductive performance was tracked daily by measuring fecundity and compared to a third group of unexposed FHM's. At the end of the exposure they were terminated, their gonadosomatic index (GSI) and their condition index (CI) were calculated as a general measure of the overall health of the fish. My results show that PCB-77 and 4-OH PCB-66 had no reproductive toxicity; at no time during the exposure did any of the groups stop or even reduce spawning frequency. The GSI average for male FHMs exposed to PCB-77 and the male FHMs exposed to 4-OH PCB-66 was well within the typical GSI values: ~1% to 2% (1). The same is true for the female FHMs, the typical GSI values are: ~8% to 12% (1), which is what I observed. GSI and CI results show that all three groups of fish were at seemingly similar conditions which, was verified by their reproductive performance.

Risk-Based Assessments for Homeland Security Planning and Response. MEGAN WILLIAMS (University of New Orleans, New Orleans, LA 70148) MARGARET MACDONELL (Argonne National Laboratory, Argonne, IL 60439). As the potential threat of terror attacks elevates widespread concern throughout the United States, prevention and rapid response measures are being put in place to assure the security of Americans. Risk-based assessments are being conducted and provisional advisories levels (PALs) are being set for potential threat contaminants that may be released into the public drinking water supply and/or air. Risk-based assessments include the evaluation of new standard, existing standards and guidelines, fate and detection of contaminants and their degradation as they are often a precursor to the development of PALs. The contaminants in which we assess range from toxic industrial chemicals to radionuclides. PALs are advisories that answer the questions of who, what, when, where and how a contaminant will effect the drinking water and/or air if released. These contaminants identified are those that the Environmental Protection Agency-National Homeland Security Research Center (EPA-NHSRC) have deemed as a potential health threat to the American public.

Spatial Distribution of Iridovirus in the Eastern Box Turtle Population at Brookhaven National Laboratory: Implications for Transmittance Based on Home Range Size. SARAH SNYDER (Unity College, Unity, ME 04988) VALORIE TITUS (Brookhaven National Laboratory, Upton, NY 11973). There are currently four recognized genera of the icosahedrally symmetric iridoviruses that infect both invertebrates (Iridovirus and Chloriridovirus) and poikilothermic vertebrates (Lymphocystivirus and Ranavirus). Ranaviruses have only been documented in a relatively few number of reptiles when compared to the number of viruses that have been documented in amphibians and fish. Relatively recent detection of ranaviruses in five species of

chelonians, including a virus outbreak in a population of Eastern box turtles (*Terrapene carolina carolina*) at Brookhaven National Laboratory, is especially alarming. This discovery poses a threat to box turtles in surrounding areas since the species is listed as Special Concern in the state of New York. To ascertain the current distribution of infected turtles at Brookhaven National Laboratory, cloacal and oral samples were collected and virus testing was performed using molecular genetic techniques. To further explore the potential transmission of the ranavirus within the box turtle population, determining individual home range size was necessary. Habitat quality, structure, diversity, individual preference, and population density all account for variation in size and spatial structure of box turtle home ranges. Due to this variability, it was crucial to determine home range size specific to the study area in question. Radiotransmitters were attached to 5 box turtles inhabiting the area of Ranavirus discovery and their daily movements and habitat preferences were recorded. Geographic Information Systems (GIS) was used to digitally map home range area in order to determine Ranavirus dynamics and the potential for disease spread within the box turtle population. Preliminary results indicate that the virus is likely present in the box turtle population at Brookhaven National Laboratory. Home ranges of turtles appear to be relatively small but overlapping which suggests favorable conditions for virus spread, depending on encounter rates and mode of transmission.

Successional Assessment of Columbia River Periphyton. NINA SOVIK (Johns Hopkins University, Baltimore, MD 21218) AMORET BUNN (Pacific Northwest National Laboratory, Richland, WA 99352). The Columbia River's hyporheic zone is an area of high biodiversity where river and groundwater mix. Periphyton is found at the surface/water interface and forms the basis of the food chain for the entire river. The periphyton community consists of the primary producers in the river environment, and the community includes photosynthetic organisms, such as diatoms and algae, bound together in a polysaccharide matrix. The composition of species succeeds, or changes, naturally over time. The presence of contaminants in the surface/water interface may affect some or all of the species comprising the periphyton community. Contaminants may change the succession of these organisms and the ultimate structure and function of the community. To understand the development of the community, a laboratory growth system was used to monitor succession without the presence of contaminants. Cleaned microscope slides were added to bins with flowing Columbia River water. They were exposed to a light cycle of 16/8 hours light/dark photocycle. The slides were colonized by organisms in the river water. Using a light microscope, slides were examined for a total of ten days, including every 24 hours for five consecutive days. They were photographed to document natural successional changes and trends in microbial diversity. It was found that the amount of biomass increased over time, and slides were completely obscured from view within two weeks. The increase in biomass corresponded to changes in species composition. During the early successional stages, the species composition was primarily diatoms (*Navicula*) and a few types of filamentous algae. After three days, more algal species and consumers (protozoans and rotifers) were observed. There was also an increase in filamentous diatoms (*Cyclotella*), and in the frequency of cell division among certain diatoms (*Synedra ulna*). This work is part of a larger study being done to understand the hyporheic regions of the Columbia River and how those regions may be affected by the presence of groundwater contamination at the surface/water interface.

The Adaptation of Soybean Plant Antioxidant Enzyme Activity Assays for a 96-Well Microplate. BINGJIE LING (University of Virginia, Charlottesville, VA 22904) ALISTAIR ROGERS (Brookhaven National Laboratory, Upton, NY 11973). Reactive oxygen species (ROS) such as superoxide, hydrogen peroxide, and the hydroxyl radical are produced in plants in response to stresses such as ozone, UV light, microbial attack, and low temperatures. To reduce oxidative damage to the cell, the plant produces antioxidant enzymes such as superoxide dismutase, catalases, peroxidases, and glutathione reductase to directly or indirectly detoxify ROS. There has been a tremendous tropospheric O₃ increase since the Industrial Revolution, and soybean plants are one of the most sensitive crops, with yields decreasing by nearly 50% at high concentrations of ozone. However, the response of plants to this rise in ROS under different conditions is unknown. Current methods for analyzing these enzymes use single-sample assays, but in order to analyze enzyme activities in large-scale field experiments, there is a need to increase the capacity and throughput. The aim of this project was to adapt these methods for a 96-well microplate. Similar concentrations of the assay components were used, but due to the significantly smaller volume employed by the microplate, these amounts were adjusted accordingly after every trial experiment. Other changes

involved using different buffers, temperatures, and timing to optimize the reaction for small volumes. Kinetic absorbance data were obtained from a Bio-Tek® Microplate Reader and standard curves of concentration vs. absorbance were used. Enzyme activity was calculated and expressed in nmol min⁻¹ mg⁻¹ protein. Microsoft Excel templates were also created to facilitate data interpretation for future experiments. The five enzymes chosen for which to produce these high throughput assays were catalase, ascorbate peroxidase, dehydroascorbate reductase, monodehydroascorbate reductase, and glutathione reductase. These have been identified as important enzymes in ROS detoxification and the methods developed will provide a way to simultaneously assay many samples and determine the effects of ROS on the plant in various conditions. Eventually, programs can be designed for the Evolution P3 Precision Pipetting Platform, a robot that can further increase assay throughput.

The Effect of Climatic Warming on Forest Growth. DANIEL WRESCHNIG (Albion College, Albion, MI 49224) CARLA GUNDERSON (Oak Ridge National Laboratory, Oak Ridge, TN 37831). Climatic warming is predicted to affect forest migration, succession and growth, according to many computer models. The success of a modeling approach in understanding the effects of climatic warming has been hampered, however, by an incomplete understanding of the role acclimation-the adjustment of individuals to changes in environment-will play in the responses of trees subjected to future warming. To better understand the interaction between warming, acclimation, and growth, individuals from three species native to different temperature regimes (*Quercus rubra*, *Betula alleghaniensis*, and *Liquidambar styraciflua*) were grown together in open-topped warming chambers maintained at ambient, +2, and +4°C. Seedling height and diameter were measured intermittently during the growing season for four years, and average relative growth rates (RGRs) for each interval were calculated based on D2H (diameter X diameter X height) for each species by treatment. RGRs were tested via multiple regressions against condition variables, including growing degree days, average rainfall, average temperature, vapor pressure deficit, and photosynthetically active radiation (PAR). Initial results indicate that while temperature promotes growth in two of three species (including, unexpectedly, *B. alleghaniensis*, which models predict should not have grown under these experimental conditions at all), the strongest influence on growth may be PAR. Further study of warming and acclimation in trees will be necessary, as there is much species-specific information to be collected. While this study focused on three species, forest succession models contain many more, and it will be important to determine how plastic trees are in their response to warming to correctly predict their disposition over the next hundred years of climate change. It may be equally important to test different genotypes within species to understand how the character of species themselves may change as the climate warms.

The Effects of Drought on the Composition of Vegetation in Mitigation Wetland R at Argonne National Laboratory, Illinois. JAMIE MODERHACK (Illinois State University, Normal, IL 61761) DR. KIRK LAGORY (Argonne National Laboratory, Argonne, IL 60439). Wetlands are unique and vanishing habitats for plants and animals. In 1990, the construction of the APS facility at Argonne National Laboratory, Illinois led to the destruction of three wetlands in the area. A new 1.8 acre wetland was built to replace the three that were destroyed. This new wetland, Wetland R, has been previously monitored from 1992-1996 and 2002-2005, to ensure that its plant composition and diversity is comparable to the destroyed wetlands. During the 2005 monitoring process, the low levels of precipitation led Wetland R to dry up. Changes in hydrology can have a strong impact on the plants of a wetland, and thus the purpose of this year's study was to monitor Wetland R for changes in hydrology and vegetation with a specific focus on the effect of previous year's drought on plant composition. Ten transects were marked and five quadrats were randomly assigned to each transect. Each of the fifty quadrats was sampled and species name and percent cover were identified. The native status, the coefficient of conservatism or {C}value, and wetland status for all species identified were also documented. A total of 80 plants were identified during the sampling period. The number of species identified in Wetland R has continued to rise during the previous ten year monitoring period. In 2005 40% of the species identified were obligate wetland plants. In 2006 only 33% of the plants that could be identified by wetland status were obligate wetland species. Although Wetland R was able to support new vegetation and increase its species diversity in 2006, most of the vegetation was either facultative or upland species. As evidenced in previous studies, as water levels drop, facultative or upland plant species flourish while obligate wetland species tend to decline. This correlation was observed in the 2006 monitoring of

Wetland R. It is suggested that Wetland R continued to be monitored for diversity and whether the low water levels of 2005 will continue to affect the species composition and distribution in the future.

***The Effects of Hypoxia on the Growth of Eelgrass (*Zostera Marina*).** MIA PRINZEN (Long Beach City Community College, Long Beach, CA 90808) MICHAEL BLANTON (Pacific Northwest National Laboratory, Richland, WA 99352). Dead Zones are areas where dissolved oxygen levels are so low that fish and shellfish cannot live and can cause mass mortalities of marine organisms. Since 2002, monitoring data from Hood Canal, Washington reveal that the zone of hypoxia (oxygen depletion) has increased in magnitude. Fish kills are more commonly reported than prior to 2002 due to hypoxia. If hypoxic conditions reach shallow subtidal and low intertidal zones, eelgrass (*Zostera marina*) in Hood Canal could be negatively impacted by decreases in growth and productivity. To assess whether hypoxia could affect the growth of *Z. marina*, two 10-gallon aquaria were set up with 10.5 liters each of sediment from Sequim Bay and planted with 30 *Z. marina* shoots. One tank contained flow-through raw seawater and supplemental air to increase dissolved oxygen levels. The second tank contained stagnant raw seawater to decrease dissolved oxygen levels. Temperature, salinity, dissolved oxygen, and pH were monitored five times per week using a water quality sonde. Light intensity was maintained above 200 $\mu\text{mol}/\text{m}^2\text{s}$ of Photosynthetically Active Radiation (PAR). During daylight hours, all shoots were cut at a uniform height before transplantation. The new leaf growth was removed by cutting at the height at which the initial cut was made. Then, all shoots with new growth within each tank were dried, weighed and averaged. *Z. marina* growth was gauged weekly. The *Z. marina* in the flow-through tank grew at twice the rate of the *Z. marina* in the stagnant tank for the first seven-day period and in the second seven-day period it grew thirteen times faster than the *Z. marina* in the stagnant tank.

The Role of Dead Trees in a Healthy Forest: Quantifying the Abundance of Snags in Six of the Central Pine Barrens Communities. WENDOLIE AZCONA (Bronx Community College, Bronx, NY 10453) TIMOTHY GREEN (Brookhaven National Laboratory, Upton, NY 11973). The Long Island Central Pine Barrens (CPB) has a variety of forest communities including Coastal Oak Forest, Oak-Pine Forest, Pine-Oak Forest, Scrub Oak Forest, Dwarf Pine Forest, and Pitch Pine Forest. To determine the future management practices the Foundation for Ecological Research in the Northeast (FERN) started, a forest health-monitoring project in 2005 to evaluate Pine Barren forest health indicators including snags. To assist land managers in preserving and protecting this natural resource many forest health's indicators were recorded but not limited to pH, canopy cover, sapling numbers and snags. Snags are standing dead trees which are an important forest health indicator because they provide habitat for wildlife. The purpose of this research is to quantify the abundance of snags in six forest community types to determine in which community type they are most prevalent. Using Global Positioning System (GPS) and Geographic Information System (GIS) technology, random plots (16 x 25 meters) were selected. The quantity and average diameter at breast height (dbh) of snags in each community type were recorded for each plot. Results show that among the six community types, snags are more likely to be found in Oak pine forest followed by Coastal oak, Pitch pine, Pine oak, Scrub oak, and Dwarf pine Forest. Oak-pine and Coastal oak are two of the community types in which the greatest average dbh exist. The research of 2005/2006 will be repeated in 2015 to determine changes over time. This will serve as a baseline data to show changes over time and provide data for the management of the CPB of Long Island.

The Use of 16S rDNA Gene Libraries to Describe Microbial Communities in a Uranium Contaminated Sites. KELLY CHO (University of Michigan-Dearborne, Dearborne, MI 48128) CHRISTOPHER SCHATZ, SONIA TIQUIA (Oak Ridge National Laboratory, Oak Ridge, TN 37831). Libraries of 16S ribosomal DNA (rDNA) genes provide powerful insights into microbial ecology. Previous studies have demonstrated that consortia of microbes can effectively promote the precipitation and removal of uranium from contaminated groundwaters. The Field Research Center at Oak Ridge National Laboratory contains field-sites contaminated with various levels of metals and radionuclides, nitrate and of varying geochemical characteristics. To characterize the composition and diversity of the resident microbial communities in the groundwater samples at the site, a PCR-based cloning approach was used. Four sampling sites (GW-835, GW-836, FW113-47 and FW-215) that encompass a wide range of uranium concentrations and geochemistry were studied. Bulk community DNA was directly extracted from the groundwater samples. The 16S rRNA fragments were amplified from the bulk community DNA

using PCR primers directed toward conserved regions of bacterial rDNA. Amplicons were then cloned and sequenced. Altogether, 800 representative 16S rRNA clones were sequenced. The 16S rRNA partial sequences for each gene library were aligned using ClustalW multiple sequence alignment, and were used for phylogenetic analyses. BLASTn similarity searches were also carried out to compare 16S rRNA sequences to those previously known and available from GenBank. The most highly contaminated groundwater source site, FW113-47 (pH 3.47; 23,409 mg nitrate L^{-1} ; 60.36 mg uranium L^{-1}), had limited diversity with diversity increased along the contaminant gradient in the shale pathway with decreasing contaminant levels. Overall, our preliminary results indicate that there is enormous heterogeneity in the microbial communities across the FRC and that their composition is strongly influenced by pH and contaminant (i.e., nitrate, uranium) levels. This work is a small portion of a much larger project to develop a framework that will allow for the comprehensive discovery, visualization and understanding of how microbial population and community structures, geochemical factors, as well as the types and extent of contamination interact, to influence field scale natural attenuation processes.

The Use of Mark-Recapture to Estimate a Population of Cherry-Faced Meadowhawk (*Sympetrum Internum*) at a Vernal Pool on Brookhaven National Laboratory. DIANNA RODRIGUEZ (Suffolk County Community College, Brentwood, NY 11717) TIM GREEN (Brookhaven National Laboratory, Upton, NY 11973). Dragonflies are insects of the order Odonata, suborder Anisoptera. Of the 3000 species known world wide, more than 100 species occur in the state of New York and 32 have been identified at Brookhaven National Laboratory. Odonates play a role in maintaining the delicate ecosystem of vernal pools and other bodies of water such as marshes, streams, and wetlands. Tracking and monitoring Odonates can be extremely difficult due to their relatively short lifespan, numerous populations, and extraordinary flight speed. To observe and monitor Odonates, the use of a tracking system is needed to keep accounts of specific species populations. Using a simple form of Mark-Recapture, the Odonates are caught in nets, and marks are drawn on their wings with non water-soluble markers. During a course of ten weeks, the method of Mark-Recapture was employed and perfected, considering there has been no previously documented use of it on Odonates there was a necessity to perfect the method to optimize results. Once perfected the system was used during the final four weeks, concentrating on one species, the Cherry-Faced Meadowhawk (*Sympetrum internum*) at one pond. Using the Mark-Recapture method we have found that the method can be successfully employed on Odonates with positive results. A total of 168 Cherry-faced Meadowhawks were captured with 32 individuals recaptured at least once. Using the program NOREMARK, two population estimates were generated, one estimate using the numbers of captured and recaptured Cherry-faced Meadowhawks, and one that also added a variable to account for emigration and immigration. The program estimated about 300 Cherry-faced Meadowhawks inhabit pond 7, without including emigration and immigration. Including the variable for immigration and emigration, the program estimated the population to be over 500 Cherry-faced Meadowhawks inhabiting pond 7. The method of Mark-Recapture has proven useful in the study of Odonates and may be used for future population estimates of other Odonate species. This research is part of an ongoing project that was started in 2003 to observe the Odonate populations of the Brookhaven National Laboratory and will be continued until an accurate account of species is created. Additionally, three new species of Odonates, not previously documented, were added to the list of those found at Brookhaven National Laboratory.

Thermophoresis and its Thermal Parameters for Aerosol Collection. ZHUO HUANG (Sacramento State University, Sacramento, CA 95819) MICHAEL APTE (Lawrence Berkeley National Laboratory, Berkeley, CA 94720). The optimal particle collection efficiency of a prototype environmental tobacco smoke (ETS) sampler based on the use of thermophoresis was determined with a particle phase "titration" in a 24 m^3 environmental chamber. This sampler's heating element was made of three sets of thermophoretic (TP) wires of 25 μm in diameter suspended across a channel cut in a printed circuit board. Two collecting surfaces were mounted, one on each side, to form a flow channel of 1 mm high with the TP wires suspended in the middle, 500 μm from each surface. The separation of between the heating element and the room temperature collection surface was determined in a numerical simulation based on Brock-Talbot model. Other thermal parameters of this TP ETS sampler were predicted by the Brock-Talbot model for TP deposition. The theoretical thermal parameters were examined and were used to characterize the TP ETS sampler's collection mechanism. In addition, by heating the wires we determined

their temperature-resistance relationship. From the normalized results the optimal collection ratio was expressed in terms of applied voltage and filter mass. We raised the operational voltage from 1.0 to 3.0 V, and we found that the collection efficiency was increased by a factor of five for both theory and experiment.

Toxicokinetics of PBDE-47 in Fathead Minnows (*Pimephales promelas*). DANIEL HASKELL (*University of California–Santa Barbara, Santa Barbara, CA 93116*) IRVIN SCHULTZ (*Pacific Northwest National Laboratory, Richland, WA 99352*). Polybrominated diphenyl ethers (PBDEs) are commonly used as flame retardants in many consumer products and reports of their occurrence in fish and humans has steadily increased. In this study, we experimentally measured the uptake, retention and maternal transfer of PBDE-47 in fish. Minnows were orally exposed to PBDE-47 by controlled feedings of brine shrimp (*Artemia sp.*) that previously had been incubated with PBDE-47. Female minnows were given a single oral dose and terminated at selected times to characterize the uptake and tissue distribution of PBDE-47. A separate group of PBDE-47 dosed females were used to study the maternal transfer of PBDE-47 to eggs. The latter experiment paired a dosed female minnow with a control male to induce spawning. My results indicate that PBDE-47 is rapidly and well absorbed from the minnow gastrointestinal tract. Peak blood plasma and carcass levels occurred around 12-24 hrs after dosing although smaller amounts were detected after the first sampling time of 0.5 hr. Measurement of the maternal transfer of PBDE-47 to eggs indicates this is an important elimination route for females, with approximately 11% of the body burden being eliminated in a typical spawn. In contrast, non-spawning females appeared to have a greatly reduced capacity to excrete PBDE-47.

Validity of Observing Fine Root Density Using Minirhizotron Tubes. JOEY ROBERTS (*Middle Tennessee State University, Murfreesboro, TN 37132*) DR. RICHARD J NORBY (*Oak Ridge National Laboratory, Oak Ridge, TN 37831*). Minirhizotron observation tubes allow nondestructive, in situ, estimates of fine root dynamics in natural ecosystems. All minirhizotron users make a major assumption: that root length measured by the minirhizotron tube is representative of root production at the site. Root production and turnover measurements are important components of C sequestration and are frequently used at many sites, including Oak Ridge National Laboratory's Free-Air CO₂ Enrichment (FACE) facility. This study aimed to answer the question: are there altered root patterns along minirhizotron tubes when compared to root production in the bulk soil? This study took advantage of a unique opportunity to destructively sample unused minirhizotron tubes that have been in place for 9 years at the facility. Fine (=2mm diameter) root biomass density (mg dry weight cm⁻³) measurements were destructively collected along the minirhizotron tube-soil interface on three tubes and in the adjacent bulk soil. First, intact soil cores were collected by coring straight through the butyrate tube. Correspondingly, soil cores were taken 5 cm away from each tube in the adjacent soil. Sampling was done at a vertical depth of 40 cm. In all, two soil cores were taken per plot for a total of six samples. Soil disks (2 cm by 2.54 cm) were sliced off at the soil-tube interface, and fine-root biomass density was quantified. Results from this study showed that in all three plots, fine root biomass was lower at the tube-soil interface than in the bulk soil. These data suggest that the presence of the minirhizotron tube may be underestimating root density at ORNL FACE.

Vineyard Optimization through Novel Characterization and Cluster Analysis: Applications of Geographic Information Science in Precision Viticulture. JAMES WOLF (*University California–Santa Barbara, Santa Barbara, CA 93106*) SUSAN HUBBARD (*Lawrence Berkeley National Laboratory, Berkeley, CA 94720*). With viticulture and other agriculture comprising a significant portion of the California economy and water budget, accurate and precise information regarding soil and hydrological characteristics is crucial. With regards to viticulture, the science of growing wine grapes, 90% of the United States' wine is produced within California. Furthermore, California is the nations greatest consumer of developed water, with roughly 80% of that water allocated to agricultural production. This research combines a wide array of data collected from both traditional and novel techniques into a single analysis. Traditional data acquisition techniques explored in this project include surveying of topography for elevation, slope, and aspect analysis, soil pit drilling for analysis of soil texture and chemical composition, and Time Domain Reflectometry. These traditional techniques offer discrete sampling which necessitates interpolation between sample points. Novel techniques, on the other hand, provide more continuous data collection. Such techniques include Ground Penetrating Radar, electromagnetic measurements, Cone Penetration Testing for soil behavior types, and Normalized Difference

Vegetation Index. From these data, properties that are important to the production of wine grapes such as soil moisture and texture can be estimated. To manage the data collected, a Geographic Information System was developed. Then the Hierarchical Ordered Partitioning And Collapsing Hybrid algorithm was applied to look for clusters of similar values, with the ultimate goal of delineating management zones within a single vineyard. In this way, a wine grower can optimize production by precisely planning where higher quality grapes will be most suitable for planting. Also, in order to optimize water resource management, water balance simulations can be performed within the defined management zones to explore the impact of different irrigation strategies.

Wind Energy: Changing the Future One Gust at a Time. SHARLA BOARDMAN (*Brigham Young University, Provo, UT 84606*) GARY SEIFERT (*Idaho National Laboratory, Idaho Falls, ID 83415*). This project was focused on improving the possibilities of wind power in southeast Idaho. The main objectives were to set up anemometers, calculate wind data, create a kiosk proposal for a local wind farm, and accumulate lesson plans and activities for the Idaho National Lab (INL) wind outreach program. In order to accomplish the objectives the team went into the field to set up an anemometer tower. An anemometer is an electronic device that measures the constant wind speed for one month's time. Over a years time the team would return to the site each month to replace the chip and collect the previous month data from the chip. The data was then recorded into a program called Symphonie Data Retriever which uploaded the information to the INL website. The next step in the project was to take this knowledge about anemometers and correlate it with lessons and activities for elementary and secondary education students. These lessons provided students the basic concepts about wind power and renewable energy. These concepts are found in most state education standards. The Outreach website now houses lesson plans for grades K-12. A college lesson plan curriculum is currently under development. Another focus for this summer included the proposal for the Wolverine Creek Wind Farm. This kiosk includes design plans for a visitors' information center, as well as the information that would be most beneficial to the viewers. The idea for the kiosk was presented without any design or cost constraints. Initially, a brainstorming session was held to determine possible structure layouts for the informational area. Once several plans were formulated, cost analysis as well as feasibility was required to compile and create a professional proposal. The Outreach website provides critical wind energy information to students at all educational levels. Once the students obtain this wind energy education, they are better prepared to make future decisions that affect the environment.

General Sciences

An Analysis of Chlorine Gas Release. KARA BROWN (*University of California–San Diego, La Jolla, CA 92092*) GEORGE FULTON (*Lawrence Livermore National Laboratory, Livermore, CA 94550*). Chlorine is an extremely reactive and harmful gas that can cause a myriad of health problems within seconds of exposure. This report is an analysis of current chlorine safety regulations in place at Lawrence Livermore National Laboratory for Building 153. It was found that the rapidity at which usable amounts of chlorine gas could be released into the main workspace of the building that the emergency response alarm for a leak needed to remain active. The calculations go through a series of different possibilities including the concentration of chlorine gas with multiple size cylinders, the difference that ventilation makes, and the amount of time it would take the ventilation to get the concentration of chlorine gas down to different airborne exposure standards such as the IDLH, STEL, 8-Hour TLV, or Mean Odor Threshold.

***Arc Flash.** YEVHEN RUTOVYTSKYI (*Three Rivers Community College, Norwich, CT 06360*) SWAPNA MUKHERJI (*Brookhaven National Laboratory, Upton, NY 11973*). Analyzing BNL electrical distribution system. Determine the incident energy, boundary requirements, and the personal protective equipment necessary in order to minimize the possibility of electric shock to personal. All the calculations are done by using PTW (Power Tools for Windows) software and based on measured data or information, obtained from the manufacturers labels (such as: operating voltage, breaker size, size of the wire etc.) After completing this project we expect to come up with a universal label that will be posted on all electrical equipment that exists at BNL. New label will contain the name of the panel, warning statement "Arc Flash Hazard!!!" and category PPE (Personnel Protective Equipment).

Assessing the Impact of Aerosols on the Radiation Budget in the Sahel Using the Shdompp Radiative Model. NIMISHA GHOSH ROY (*University of Washington, Seattle, WA 98006*) TOM

ACKERMAN (*Pacific Northwest National Laboratory, Richland, WA 99352*). To understand Earth's dynamic climate system, scientists are developing global climate models. Currently there are various climate models that scientists are continuously trying to understand and refine. Current difficulties include the ability to correctly include the effect of aerosols and clouds in global climate models. The purpose of this project is to work on calculating the effect of aerosols (particles in the atmosphere) on the Earth's radiation budget (the balance of incoming and outgoing solar radiation). This project focuses on the effects of aerosols in the Sahel (south of the Sahara Desert) with hopes of refining the way global climate models currently model the Sahel and similar regions. The instruments used are part of the Department of Energy's Atmospheric Radiation Measurement Program's mobile suite of instruments located in Niamey, Niger. The Sky Radiometer, Total Sky Imager and Micropulse Lidar were used to identify periods of clear skies on a time scale of fifteen minutes. Clear sky sets of data were critical because the presence of clouds in the data set would introduce too many variables. Various atmospheric properties were collected from a variety of instruments (also at Niamey, Niger) over the same periods of clear skies. Data used were from January 1–31st, 2006. The data was put into the SHDOMPP (Spherical Harmonics Discrete Ordinates Model, Plane-Parallel Version) Radiative Transfer Model. The model was run with two scenarios: 1) Clear Skies with Aerosols and 2) Clear Skies without Aerosols. Comparing the SHDOMPP model results with observed data from ground instruments provides a measure of the accuracy of the model. Initial results show a 1–5% agreement between modeled and observed calculations of total down welling shortwave flux. The two model runs (with and without aerosols) were compared to each other to understand the effect of the aerosols. Initial results show the presence of aerosol lowers the total down welling shortwave flux by 32–120 w/m². Problems with the treatment of some input parameters have been identified. The next step in developing an understanding of the effect of aerosols will involve refining the assumptions and parameters input to the SHDOMPP model.

Focal Mechanisms and Stress Axes of Microearthquakes

in Southeastern Washington State. STEFANY SIT (*Lawrence University, Appleton, WI 54911*) ALAN ROHAY (*Pacific Northwest National Laboratory, Richland, WA 99352*). The Hanford Seismic Network combined with the Eastern Washington Region Network covers eastern Washington State with forty-one seismograph stations. Routine analysis monitors and locates local seismic events dominated by shallow depth microearthquakes. However, regular study does not include investigations into the mechanisms of earthquakes. This report uses seismograms from 2000 to 2006 to develop constraints on fault and auxiliary planes of seismic activity occurring in southeastern Washington State. Through the proper identification of planes, the principal axes of stress can then be extrapolated. Using a SUN system and Focal2 software, focal mechanisms were developed according to the procedure provided by Oppenheimer (1996). A significant portion of the mechanisms showed a general maximum compression in the north-south direction with a low angle of plunge. The axis of minimum compression showed varying orientations with no conclusive pattern. These results are in agreement with previous studies done in the area and show no deviance from the historical pattern.

Inquiry-Based Learning at Its Best. SARAH BAUM (*Lesley University, Cambridge, MA 02138*) MARY CONNOLLY (*Lawrence Berkeley National Laboratory, Berkeley, CA 94720*). The Lawrence Hall of Science (LHS) is one of the leading forces in the inquiry-driven, direct experience approach to science and mathematics instruction for grades K-12. LHS has developed several inquiry-based curriculum projects that are used throughout the United States. This public science center also provides educational exhibits and classes, year-round outreach programs, as well as diverse summer camp programs for children of the region. The investigative approach stems from human beings' natural curiosity to explore what is seen on a daily basis. This strategy when applied to a classroom helps students connect concrete ideas to their own experiences through open-ended investigations and discussions. My goal throughout the summer was to observe how instructors use guided inquiry techniques with a variety of age groups to delve into life, physical, and earth science. My research reflects an exploratory sample of age groups and content areas. Working alongside LHS instructors has allowed me to study inquiry-based education by observing, comparing, analyzing, and applying themes and elements central to the process.

Qualitative Testing of Social Network Analysis Biowarfare Taxonomy: An Analysis of LLNL Open Source Publications. LIRAN GOLDMAN (*University of California—San Diego, La Jolla, CA 92093*) DEBORAH YARSIKE BALL, DALE K. BREARCLIFFE (*Lawrence*

Livermore National Laboratory, Livermore, CA 94550). The Dynamic Network Engineering Group takes a network-centric approach to discover and characterize organizational expertise and relationships of state and non-state actors intent on creating and using weapons of mass destruction (WMD). This approach utilizes a taxonomy that can identify and extract key actors from large, unstructured data sources. In this project, a taxonomy was developed and tested on a known entity: Lawrence Livermore National Laboratory (LLNL). The goal was to discover and qualitatively describe the results of a specific taxonomy when combined with the dynamic network analysis methods. The data used in this test analysis include a list of Livermore Laboratory employees who have a pager assigned to them, online versions of LLNL's Science & Technology Review (S&TR), and a potential biowarfare taxonomy. After the S&TR issues were downloaded, the data were uploaded and processed in Automap, a program capable of extracting and analyzing computer based text by creating links among words then constructing a network. Next, the words of interest were extracted from the S&TR articles, and evaluated in Organization Risk Analyzer (ORA), a program capable of statistically analyzing dynamic networks. The analysis completed by ORA on this dataset revealed some key findings: the years 2003 and 2004 were prominent for biology related publications. Also, pathogens and anthrax were consistently the top areas explored. Follow-up analysis of these results indicates that this process is successful at singling out pertinent actors, but the results should be viewed with caution. A few drawbacks include Automap's failure to extract variations of words the program is instructed to locate. Additionally, not all of the relationships established by Automap are valid due to its inability to distinguish between unrelated, yet adjacent articles. Furthermore, reporters who wrote the publications used in this test case became part of the data set. Also, the inclusion of projects and people is not a complete representation of ongoing research at LLNL. This latter issue is somewhat mitigated when examining external organizational expertise and relationships because the publications assessed are usually authored by the researchers themselves. These matters will be considered when applying this process to other datasets.

***The Effect of Fire on Soil Carbon Storage in a Prairie Ecosystem: Implications for Global Climate Change and Ecosystem-Climate Feedbacks.**

RYAN SMITH (*California State University—Fresno, Fresno, CA 93740*) MARGARET TORN (*Lawrence Berkeley National Laboratory, Berkeley, CA 94720*). The increasing concern around the topic of global warming is reason to assure climate change models be accurate. A potentially important omission from current models is CO₂ feedbacks between climate and soils. Natural fire and managed fire both play an important role in maintaining the prairie ecosystem. If warming increases the frequency of fire it will be important to know the effect fire has on the storage of carbon in soil. The goal of this project was to investigate the effect of fire on soil carbon stocks in a prairie of the Southern Great Plains. Our null hypothesis was: no change in carbon content of grassland soil due to the fire treatment. The alternative hypothesis was that carbon content of the soil will decrease due to the treatment of fire. The USDA Grazing Research Laboratory in Oklahoma collaborated in this project and provided soil samples for analysis. Ten soil cores, 1 meter deep, were collected from two adjacent prairie fields in March 2005. Shortly after collection, the north field was treated with fire while the south field was left unburned to function as the experimental control. In August 2005, 10 more cores were collected from each of the two fields. Each core was divided into 10 cm depth increments from 0–50 and 25 cm increments below that, to look at the change in carbon content with depth. One half of the core was used to determine bulk density. The other half was used to test for carbonates and determine carbon content. No core tested positive for carbonates. For carbon analysis, the soil was homogenized and roots were removed. The carbon analysis showed that the content of carbon decreased with depth and that the greatest variability among cores was in the top 10 cm. Between March and August, the south field (unburned control) lost, 0.31 kg Carbon/m² ($p < 0.14$ for the difference). In contrast, the north field showed an average total carbon stock loss of 1.1 kg Carbon/m² after the treatment of fire. The loss of soil carbon in the burned field was highly significant (one-tailed $p < 0.034$) Assuming that the lost soil carbon was released to the atmosphere as CO₂, these results suggest that there could be a strong positive feedback effect if warming increases fire frequency in prairie. Continued research on the rates of inputs and outputs of carbon into the soil-and the effect of fire on them-needs to be done to make whole conclusions.

The Laboratory Assessment Worksheet—A Risk Comparison of Biological and Chemical Hazards in the Laboratory. REBECCA WILLIAMSON (*University of Virginia, Charlottesville, VA 22556*) GERALD SCHWEICKERT (*Lawrence Livermore National Laboratory,*

Livermore, CA 94550). Biological hazards and chemical hazards are commonly found within the same project at Lawrence Livermore National Laboratory (LLNL), however no established system currently exists to do a comparative analysis of the degree of implementation of safety controls for both types of hazards. A Laboratory Assessment Worksheet was created to devise a way to quantitatively compare the hazards, controls, and the degree of risk management actually present. Four numerical values—a biological hazard score, a chemical hazard score, a biological control score, and a chemical control score—were calculated to accomplish the comparison. The worksheet utilizes the Centers for Disease Control and Prevention's biosafety levels as a score for biological hazards; Sax's Dangerous Properties of Industrial Materials hazard ranking in combination with an exposure potential evaluation for the chemical score; and a percentage of a standardized list of controls for the control scores for both hazards. Once scores for each of the four categories are tabulated, the ratio of the hazard score to the control score can be used to decide whether the controls are appropriate for the particular hazard, i.e., the degree of risk management. Upon further development this worksheet will become a unique tool for the Hazards Control Department at LLNL because it will serve as an initial screening tool with the ability to compare biological and chemical hazards in a single experiment as well as biological and chemical hazards across multiple experiments.

Material Sciences

A Novel Approach to Estimating Thermal Conductivity. GORDON WU (University of California—Berkeley, Berkeley, CA 94720) TIM KNEAFSEY (Lawrence Berkeley National Laboratory, Berkeley, CA 94720). Scientists at Lawrence Berkeley National Laboratory (LBNL) are currently researching natural gas recovery from gas hydrates in hopes that this will one day become a viable source of energy. Natural gas hydrates are water crystals located below permafrost and submarine environments that contain methane gas. Knowledge of heat flow through the hydrate-bearing reservoir must be understood and thermal conductivity is a fundamental property of a material that indicates its ability to conduct heat. The technique for estimating thermal conductivity calls for applying a temperature changes and using thermocouples to accurately measure the rate of temperature change. The thermal data were analyzed using Microsoft Excel and iTOUGH2. The program iTOUGH2 computes a best-fit to our measured data by optimizing the thermal conductivity through automatic model calibration. iTOUGH2 estimates the thermal conductivity based on previous output values and given parameters. The four materials used were dry sand, polyvinyl chloride (PVC), high density polyethylene (HDPE) and Pyrex borosilicate glass, and were chosen because they have thermal conductivities close to that of hydrate bearing sand (2.7 W/m K). Good matches were obtained between the simulations and the measured data showing the validity of the technique. It is important to realize that the substances that we were using can vary in thermal conductivity depending on the temperature, the porosity of the particular substance, and the composition of the sample. Now that the technique is validated, it can be used in other experiments to measure thermal conductivities.

Atomic Layer Deposition of Tin (IV) Oxide and Indium Tin Oxide Using Tetrakis(Dimethylamino)Tin Precursor. DAVID BAKER (University of Illinois at Urbana Champaign, Urbana, IL 61802) GREGORY KRUMDICK (Argonne National Laboratory, Argonne, IL 60439). Thin films of tin oxide were deposited on silicon wafers (001) and glass by Atomic Layer Deposition (ALD) using alternating pulses of Tetrakis(Dimethylamino)Tin and an oxidizing precursor. Doping tin oxide films with various reagents, such as indium, can create smooth, optically transparent and conductive coatings with applications in solar cell, gas sensor, and flat panel display technologies. Using deposition temperatures between 100–400°C, and exposure times ranging from 0.5 to 8 seconds, growth of a film was evident on Al₂O₃ coated substrates. For the silicon and glass substrates, measurements from the spectroscopic ellipsometer showed the thickness of the film increased with temperature and increased linearly with the number of cycles (maximum of 1.5 Å per cycle) during the ALD growth. At lower temperatures, extending the exposure times of each precursor demonstrated a self-limiting reaction. Growth at higher temperatures did not demonstrate a self-limiting reaction. This precursor was also used to create Indium Tin Oxide (ITO) films also by ALD. As evident from 4-point probe resistivity measurements, tin oxide and ITO films are excellent conductors with good optical transmittance. Characterization of the films was furthered by x-ray diffraction (XRD), x-ray photoelectron spectroscopy (XPS), x-ray fluorescence (XRF), and scanning electron

microscope (SEM). Tetrakis(Dimethylamino) tin precursor demonstrated consistent ALD growth on glass and silicon surfaces coated with Al₂O₃.

Characterization of Nano-Particles in Mesophase Pitch Derived Graphite Foams. JENNIFER MUELLER (Virginia Polytechnic Institute and State University, Blacksburg, VA 24060) JAMES KLETT (Oak Ridge National Laboratory, Oak Ridge, TN 37831). The addition of nano-particles to a raw material can significantly alter the structure and therefore properties of a material. A characterization study was conducted to explore the effects of nano-particle additions on graphite foam, a material that exhibits very high thermal conductivity and low density. Carbon nano-particles were added to mesophase pitch in varying amounts and processed to create graphite foam. Image analysis was conducted on each sample by using an optical microscope, Scanning Electron Microscope (SEM), and Transmission Electron Microscope (TEM). Other analyses included density measurements, compression tests, permeability tests, and flash diffusivity tests. Results showed that there were overall trends of decreasing density, thermal conductivity, and strength with an increasing amount of carbon nano-particles, but the permeability increased. Through optical image analysis, it was determined that the ligament size of the graphitic matrix decreased and that there was a significant disruption of graphitic plane alignment with greater additions of carbon nano-particles. Additionally, it was seen with the SEM that the number and size of open pores increased with an increasing amount of carbon nano-particles. Overall, the decreased ligament size and disruption of graphitic alignment explains the decreased strength and thermal conductivity, respectively. Also, the addition of the nano-particles increased the open porosity and, therefore, increased the permeability of the foam. As a result, the graphite foams characterized through this study are suitable for applications where higher permeability foams are desired. Since the mixture with the greatest amount of nano-particles had the highest permeability, a further study should be conducted to determine what mixture results in the maximum permeability of the graphite foam without a significant loss in thermal and mechanical properties.

Characterization of Sub-diffusion within Benard-Rayleigh Advective Cells by Examination of a Velocity Field with Additive Noise. MARSHA LAROSSEE (University of Michigan, Dearborn, MI 48128) BEN CARRERAS (Oak Ridge National Laboratory, Oak Ridge, TN 37831). Normal diffusion worked out by Einstein and Taylor is modeled by averaged particle 'Brownian motion' such that a given particle's motion is determined by random collisions with surrounding particles. Less well understood is the subject of anomalous diffusion, which is studied in many fields where diffusion influences the system (e.g., heat, fluids, chemical kinetics). The distinction between normal diffusion, a random mechanism and anomalous diffusion, that is a mixture of random and deterministic processes, is the time scale at which the transport occurs. Both diffusion and anomalous diffusion follow a power law relation $\langle \Delta r^2 \rangle \sim t^q$, where $q(s) = 1/2, < 1/2, > 1/2$ for diffusion, sub-diffusion, and super-diffusion. Thus, sub-diffusion and super-diffusion scale with time differently than random motion predicts. In order to study sub-diffusion a deterministic model must be used while adding randomness, or noise to the system. A model referred to as the random walk with pauses or trapping events was investigated in order to characterize sub-diffusion in a fluid system. The system that was studied is an array of Benard Rayleigh advective cells where the velocity fields cause 10,000 tracer particles to circulate within a cell. Noise added to the velocity field causes diffusion between cells. Moments of the displacement were calculated as a function of time while varying the frequency and magnitude of noise in order to magnify the region where sub-diffusion is observed. Frequency of the additive noise extended the time frame in which sub-diffusion was observed and appears to extend the time frame non-linearly. Moments of the displacement show that the diffusive exponent $q(s)$ is the same for all higher moments which indicates scale invariance, or $q(s) = \text{constant}$. This property is characteristic of both anomalous and normal diffusion. The exponent observed $q(s) \sim 0.4$, was larger than the typical exponent of sub-diffusive systems $q(s) \sim 1/3$. The reason for this is undetermined but may indicate an influence of normal diffusion within the system and future investigation is planned.

Composition of Stainless Steel Slurries for Enhanced Structural Support of the TuffCell. LAURA JANE ELGASS (College of DuPage, Glen Ellyn, IL 60517) J. DAVID CARTER (Argonne National Laboratory, Argonne, IL 60439). The "TuffCell" is a bipolar plate-supported solid oxide fuel cell that produces electrical power by the galvanic combination of oxygen with hydrogen or other fuel. The SOFC anode support must be both conducting and porous. Porosity is required to ensure that hydrogen gas can flow through the anode support. SOFC anode supports have traditionally been composed of nickel, but the

use of stainless steel as a support while also using a thinner anode will provide increased structural integrity. The process for building the support layer starts with making a stainless steel slurry. The slurry composition includes stainless steel powder, binder, plasticizer, solvent, and in some cases pore former. The slurry is allowed to mix thoroughly and is then made into a tape cast using a doctor blade. The tape cast is dried and then placed into the dilatometer for twenty hours where it is exposed to air, nitrogen, and hydrogen to sinter. The weight percent of each slurry component must be such that the slurry meets certain criteria when cast and sintered. In casting, these criteria include an even cast (i.e., the stainless steel cannot separate from the other components during the cast), a strong and flexible dried cast, and a slightly grainy texture. In sintering, the stainless steel layer must not shrink more than the other layers of the cell and must also be porous, with pores approximately 20 microns in diameter. An even cast is the result of optimal slurry viscosity for the given components. Modification of flexibility and strength is accomplished by varying the binder to plasticizer ratio. Porosity can be achieved with a large stainless steel powder particle size and no pore former, or with smaller particles plus pore former (this method warrants varying the volume ratios of stainless steel and pore former to find the optimal porosity). In addition to finding the optimal weight percents of each of the slurry components, it is necessary to determine which plasticizer/binder/solvent trio best casts, sinters, and interacts with the other components of the cell. When xylene/butanol is used for a solvent, compositions with a combination of large stainless steel mesh size and smaller stainless steel mesh size in conjunction with 12% solvent and a plasticizer to binder ratio of 1:5 or 1:7 have proved most successful.

Controlled Assembly of Protein-Mediated Lipid Multi-Bilayers. *CONSTANCE ROCO (University of Virginia, Charlottesville, VA 22904) GABRIEL MONTAÑO (Los Alamos National Laboratory, Los Alamos, NM 87545).* Protein-mediated multilamellar lipid assemblies were created using biotin-streptavidin conjugation. We are interested in using these assemblies as a platform for investigating membranes and membrane-protein properties, as well as towards understanding the relationship between structure and function in biological multilamellar assemblies, such as the neuron insulating myelin sheath. Successive lipid bilayers, containing a fraction of biotinylated lipids, are held together using an intermediate layer of streptavidin. Control over lipid bilayer assembly was determined using atomic force microscopy and spectroscopic ellipsometry. Lateral fluidity of individual layers was characterized by fluorescence recovery after photobleaching (FRAP). Three successive bilayers, with each successive bilayer exhibiting fluidity, have been created. We are currently determining effects of protein concentration and numbers of bilayers on fluidity by comparing rates of diffusion under the various conditions. There are many other properties, such as the substrate and lipid composition, that can affect membrane interactions that can be altered and studied in future work. The investigation of these biomimetic assemblies illustrates how guided molecular self-assembly at the nanometer length scale can improve our understanding of complex biological systems.

Crystallographic Descriptors of a Metal Surface Along a Fracture Line. *RYAN GLAMM (Ohio State University, Columbus, OH 43210) BARBARA K. LOGRASSO (Ames Laboratory, Ames, IA 50011).* This work investigated the feasibility of using electron back scattered diffraction (EBSD) to associate, or differentiate, metal fracture fragments. The objective of this work was to determine an empirical basis for the hypothesis that a minimum sequence of grains can be used to identify a metal fracture line beyond a reasonable doubt. Crystallographic misorientations between individual grains were determined using EBSD along several lines (point-to-origin vectors) of metal crystals within the microstructure of a 304 stainless steel. From a given starting crystal, a grid of vectors was used to do relative referencing comparison of the grain orientation profiles along each vector. A radial grid was used with 5 spacing between vectors at a radius of 11.5 times the average grain diameter. Misorientation angle between grains was calculated by averaging the misorientation angles within a single grain and referencing this average misorientation angle back to the origin grain. The average vector matched 2.6 ± 2 grains with adjacent vectors out of 16.9 ± 7 grains characterized per vector. In point by point matching, vectors placed 5 apart had $83 \pm 11\%$ of data points match in the first 2.5 grains away from the origin, with that falling to $36 \pm 10\%$ in the last 2.5 grains characterized in the vector. The extent of point to point matching confirms that this method can properly identify when similar or dissimilar profiles are being compared. This leads to the conclusion that a relatively low number of grains need to be analyzed to uniquely characterize a fracture line by relative crystallographic

orientations. It also opens the possibility to a more extensive statistical review of concepts and data.

Design, Fabrication and Measurement of Nb/Si Multilayers and Niobium Transmission Filters. *SUNEIDY LEMOS FIGUERO (University of Puerto Rico, Rio Piedras, Rio Piedras, PR 00931) ERIK GULLIKSON (Lawrence Berkeley National Laboratory, Berkeley, CA 94720).* The extreme ultraviolet (EUV) region of the electromagnetic spectrum is being used in multilayer optical systems to design technology projected for use in the fabrication of nano-electronics. Multilayer optical systems with high reflectivity have been produced in the soft x-ray and EUV regions of the spectrum. Due to the limited understanding of the Nb/Si optical systems, our research group fabricated and measured Nb/Si multilayers and Nb transmission filters for the soft x-ray and EUV regions. Multilayer optical systems are used in applications ranging from EUV lithography to synchrotron radiation. The films were deposited using dc magnetron sputtering in the Center for X-Ray Optics at the Lawrence Berkeley National Laboratory. Reflectivity and transmission measurements were performed at the Advanced Light Source beamline 6.3.2. The Nb/Si multilayer mirrors fabricated have a reflectivity of approximately 65% in the extreme ultraviolet region, which makes these systems practical for applications where a high reflectivity is required, such as Astronomy and instrumentation development. Transmission measurements of up to 90% were observed in the soft x-ray and EUV regions as well. Future work in the research group includes the design and fabrication of an Nb/Si multilayer with a B4C interface. The Nb/B4C/Si optical systems are expected to have a higher reflectivity than Nb/Si systems.

Detection of Botulinum Toxin with an Automated Fluidics System Using Quantum Dots as the Fluorophore. *ABBY TYLER (Utah State University, Logan, UT 84321) MARVIN WARNER (Pacific Northwest National Laboratory, Richland, WA 99352).* New technologies able to detect biotoxins are in demand as the threat of bioterrorism grows. Effective detection systems have a high sensitivity, allow rapid detection and be automated and accurate. Automated fluidics systems are being developed at PNNL to fulfill all these requirements. The fluidics system performs a sandwich immunoassay that utilizes high affinity antibodies to detect botulinum toxin. A column of beads, which are conjugated to an antibody specific for a single epitope on the botulinum neurotoxin, are packed above a rotating rod. Next, a liquid sample containing the toxin analyte is perfused over the column. As the sample passes over the column toxin molecules bind to the antibodies on the beads. Then, a dye-labeled antibody that is specific for a second epitope on the toxin is perfused over the column to facilitate binding to the toxin immobilized on the column. Unbound dye is flushed off the column with buffer. Finally, the column is exposed to light to excite the dye and signal the absence or presence of the target toxin. A photo multiplier tube is used to measure the fluorescence of the dye particles left in the column. Many fluorescent dyes are available, and in a series of parallel experiments we have been investigating the use of semiconductor quantum dots as the fluorophore in this detection system. Quantum dots, or semiconductor nanocrystals, are a fluorophore that is becoming widely used in bioimaging though their use in biodetection is relatively new. Some of the advantages that quantum dots have over molecular dyes are that they have a broad excitation spectrum and a narrow emission spectra that is highly red-shifted compared to the excitation wavelength. Further, the wavelength at which they emit can be controlled by the size of the quantum dot. Detection of botulinum toxin using quantum dots in an automated fluidics system was the goal of this research, and is currently under development. Future work will involve improving the overall performance of the system by investigating characteristics such as the non-specific binding of the quantum dots to the column as well as the stability of the antibody coupled materials.

Determining Valence Band Maxima for Photovoltaics Using Ultraviolet Photoelectron Spectroscopy. *SAKA OKYERE-ASIEDU (University of Delaware, Newark, DE 19050) DR. STEVEN HULBERT (Brookhaven National Laboratory, Upton, NY 11973).* Photovoltaic solar cells (PVs) consist of semiconducting materials, which directly convert sunlight into electricity. In order to make high efficiency solar cells there is the need to maximize the transport of charge carriers—thus experiments should reveal energy levels of electrons in the device. Ultraviolet Photoelectron Spectroscopy (UPS) allows for probing these energy levels. In UPS, vacuum UV (10–45 eV) radiation is used to examine valence levels by exciting electrons from those levels. The valence band is defined as the highest electron energies where electrons are normally present and determines the conductivity of the semiconductor. For the experimentation we set three principal goals. The first was to understand the operation of the U4A beamline on which the experiments were run. Since the objective was to study bulk not

surface phenomena, it is necessary to understand how to minimize the effects of surface treatment on the measurement. The second goal was then to determine the effect of HF surface treatment on valence bands. Under this goal we needed to identify features in a valence band spectra belonging to the Si substrate, as well as H, O and defects in the Si film. Also, the cross-section for electron excitation and the electron path lengths are incident photon energy dependent. The third goal was to determine the valence band maximum (VBM) for a series of candidate materials for solar cells. This series includes amorphous (a) and crystalline (c) Si, with n-type (n), p-type (p), or intrinsic (i) doping. The series of i-a-Si, n-a-Si, and p-a-Si was analyzed with varying energy photon 30eV – 120eV. For experimental controls, we started with samples of n-c-Si and p-c-Si with expected $EF - EV = 0.87\text{eV}$ and 0.225eV . We then compared a-Si films of different p- and n-doping as well as standard i-layer. Future experiments seek to maximize the efficiency of solar cells by adjusting the valence bands using various deposition techniques and doping.

Does an Indentation Size Effect Exist in Nickel Titanium Shape Memory Alloy? ERIN DONOHUE (Brown University, Providence, RI 02912) EASO P. GEORGE (Oak Ridge National Laboratory, Oak Ridge, TN 37831). Hardness is usually measured by indentation and is considered to be an intrinsic property of a material. Recently, however, an indentation size effect (ISE) has been observed, which is manifested as an increase in a material's hardness with a decrease in the volume of material probed. This phenomenon has previously been studied in a variety of materials and is due to the creation of geometrically necessary dislocations (GND) and work hardening. In this new work, shape memory alloys (SMA) are examined to determine if they demonstrate an ISE. After elastic deformation, instead of going directly into the plastic regime, deformation in a SMA occurs by the reorientation of the variants of the martensite phase. As a result, when the SMA is heated above its martensite-to-austenite transformation temperature, the material returns to its original shape. Nickel titanium (NiTi), a common SMA, is the material chosen for this study. Using an Instron machine, a uniaxial compression test is performed to determine the stress-strain behavior of a bulk sample of NiTi. Another NiTi sample is tested with spherical indenters in the Nano Indenter XP. By making indents at a variety of maximum depths for each of the five indenters of different radii, it is possible to characterize the size dependence of hardness in NiTi. Fused silica, a material whose elastic properties are well known, is used to calibrate the size of each indenter. The indents are also imaged and measured by the MicroXAM Interferometric Surface Profiler. Finally, the sample is placed in hot water to see which indents are able to recover. There is a clear trend of increasing hardness with decreasing radii of the indenters, i.e., an indentation size effect. However, the hardness values obtained with the two smallest spheres were similar, indicating that the size effect breaks down at small length scales. The hardness values obtained with the two largest spheres agree with the hardness deduced from uniaxial compression, indicating that they correspond to the macroscopic hardness of the material. Indent sizes measured with the Nano Indenter and the Profiler correlate well and there is no time-dependent shape recovery. When placed in hot water, all of the indents experience some degree of recovery, with some of the smaller indents disappearing completely. These results indicate that the observed ISE cannot primarily be due to a dislocation mechanism.

Effects of Annealing on DC Sputtered Gold Catalyst for Growth of Pinning-Effective Nanostructures in YBCO Film. JONATHAN HEBERT (University of South Alabama, Mobile, AL 36688) DAVID CHRISTEN (Oak Ridge National Laboratory, Oak Ridge, TN 37831). As high temperature superconductors move more from the laboratory to industry, it is critical to improve the current carrying capacity. One way to do this is to introduce controllable flux pinning sites, which prevent the dissipative motion of superconducting vortices. A method for this of current interest at ORNL is to embed an ordered array of nanorods within a superconducting film. In order to be effective, this method should produce pinning sites with appropriate sizes in densities comparable to important flux densities, which for most applications is on the order of one tesla. Also, the nanorod material must be nonreactive to the superconductor and, in order to be grown perpendicular to the substrate, have a similar crystal structure to the substrate material. Magnesium oxide (MgO) is an ideal material for these nanorods for use with the superconductor yttrium barium copper oxide (YBCO). Another prerequisite for nanorod growth is the presence of a catalyst, from which the nanorods will nucleate. One such catalyst for MgO is gold. Through the method of DC sputtering, thin films of gold have been fabricated, and by annealing these films, "nanodots" were created. It is known that four main factors affect the size and density of these

nanodots: film thickness, substrate material, annealing time, and annealing temperature. In this project the effect of different annealing times was studied for a sputtering time of eight seconds, a sufficient time for the growth of a continuous film, and an annealing temperature of 900°C , the processing temperature of MgO nanorods. Interestingly, the as-deposited film appears to consist of layers of nanoparticles, each around 100 nm in size, implying that the gold is deposited as fairly uniformly sized particles instead of atomically. Analysis of the films and nanodots is carried out using atomic force microscopy and scanning electron microscopy. The results show that an annealing time on the order of tens of minutes is needed for nanostructures to agglomerate from continuous film. In addition, the smallest particles were obtained with an annealing time of 60 minutes, while annealing for 30 minutes produced the most uniformly sized particles.

Electrochemical Characteristics of Secondary Lithium Metal Batteries Containing $(x)\text{LiNi}_0.5\text{Mn}_0.5\text{O}_2 \cdot (1-x)\text{LiNi}_0.5\text{Mn}_1.5\text{O}_4$ as the Active Material in the Cathode. JACOB HENDRICKS-HOLTZ (Fayetteville State University, Fayetteville, NC 28301) CHRISTOPHER JOHNSON (Argonne National Laboratory, Argonne, IL 60439). As technology progresses, a search for improved batteries that have higher energy content is needed to implement Li-ion chemistry in hybrid electric vehicles. The $(x)\text{LiNi}_{0.5}\text{Mn}_{0.5}\text{O}_2$ (layered) $\cdot (1-x)\text{LiNi}_{0.5}\text{Mn}_{1.5}\text{O}_4$ (spinel) ($0 \leq x \leq 1$) composite-structure materials were synthesized and evaluated as cathodes in lithium metal secondary cells. Various lithium metal oxides were synthesized and optimized for phase purity and structure. Electrochemical characteristics are being studied such as current rate, cycle life, stability, capacity, and safety in "coin cells". The synthesis method used was precipitation of the metal hydroxide salts in basic solution, followed by heating the solid with Li_2CO_3 to 900°C in air. For the battery testing the anode was lithium metal, and the electrolyte was a 1.2M of LiPF₆ in ethylene carbonate (EC) and ethyl methyl carbonate (EMC) in a ratio of 3:7 respectively as the solvent. Ten charge/discharge cycles were used, with a fully-charged voltage of 4.8V and a fully discharged voltage of 2.8V. The current drawn was 0.16mA with and has a current density of 0.10 mA/cm^2 . We used X-Ray Diffraction (XRD) of each metal oxide, $(x)\text{LiNi}_{0.5}\text{Mn}_{0.5}\text{O}_2$ (layered) $\cdot (1-x)\text{LiNi}_{0.5}\text{Mn}_{1.5}\text{O}_4$ (spinel) ($0 \leq x \leq 1$), indicated that composites were formed. The composites have broad peaks showing crystal strain in their structure

Electrodeposition of Cobalt and Cobalt-Vanadium Alloy Films on Copper and Iron Substrates. BENJAMIN TAYLOR (Tennessee Technological University, Cookeville, TN 38505) MARIAPPAN PARANS PARANTHAMAN (Oak Ridge National Laboratory, Oak Ridge, TN 37831). Cobalt (Co) and its alloys have magnetic and electrical properties that are very attractive for technological applications. Low coercivity, high magnetic permeability and relatively high saturation magnetization and electrical resistivity allow these materials to be used in technical devices such as transformers, thin film inductors, giant magneto-impedance sensors, etc. One of the major advantages of Cobalt-Vanadium (Co-V) alloys is that they can be prepared on different shaped substrates with controlled composition and magnetic properties by electrodeposition methods. This study concentrates on developing successful electrodeposition techniques to grow thin films of Co and Co-V alloys on flat Copper and Iron substrates and transform the techniques to round wires. The controlling parameters for electrodeposition of Co and Co-V alloys on Copper and Iron substrates were investigated; these are temperature, pH, current density, electrolyte composition, and time. The compositional, magnetic, electrical, and structural properties of the electrodeposited films were studied. The electroplated samples were characterized using x-ray diffraction (XRD), x-ray fluorescence, scanning electron microscopy (SEM), optical microscopy, atomic force microscopy, and energy dispersive x-ray diffraction. XRD analysis shows that electrodeposited Co forms hexagonal close packed (h.c.p.) and face centered cubic (f.c.c.) structures under the various deposition conditions used in this study. The addition of vanadium (V) and a divided electrolytic cell with very negative current densities forms slightly textured Co films in the (110) and (100) orientations. The division of the cell increases the current efficiency in solutions containing V. Co film thickness is found to have linear relationships with both current density and time. SEM images show dense, uniform Co films without cracks or porosity. Grain size variation is observed with changes in current density and time. More negative current density causes the electrodeposited Co to be deposited f.c.c., which is more magnetically reversible than the h.c.p. structured Co. The coercive field is also significantly less in the f.c.c. electrodeposited cobalt than in the h.c.p. The electrical and magnetic performances of the electrodeposited wires will be compared with

commercially available Copper and Iron wires. Research efforts are underway to optimize the growth of Co film alloyed with 2–3 atomic % V.

Examination of Dislocations in Lattice Mismatched GaInAs/GaAs for III-V Photovoltaics. ALEJANDRO LEVANDER (*Pennsylvania State University, State College, PA 16802*) JOHN GEISZ (*National Renewable Energy Laboratory, Golden, CO 89401*). Dislocations act as sites for nonradiative electron/hole pair recombination, which reduces the efficiency of photovoltaics. Lattice-matched materials can be grown on top of one another without forming a high density of dislocations. However, when the growth of lattice-mismatched (LMM) materials is attempted, many dislocations result from the relaxation of strain in the crystal structure. In an attempt to reduce the number of dislocations that propagate into a solar device when using LMM materials, a compositionally step-graded buffer is placed between the two LMM materials. In order to confine the dislocations in buffer layer, and therefore increase material quality and device efficiency, the growth temperature and thickness of the buffer layer were varied. A GaInP compositionally graded buffer and GaInAs p-n junction were grown on a GaAs substrate in a metal-organic chemical vapor deposition system. A multi-beam optical stress sensor (MOSS) and X-ray diffraction (XRD) were used to characterize the strain in the epilayers. Electrical and optoelectronic properties were measured using a probe station and multimeter setup, solar simulator, and a quantum efficiency instrument. It was determined that device functionality was highly dependent on the growth temperature of the graded buffer. As growth temperature increased, so did the dislocation density in the device despite an increase in the dislocation velocity, which should have increased the dislocation annihilation rate and the diffusion of dislocations to the edge of the crystal. The thickness of the graded buffer also affected device efficiency with thinner samples performing poorly. The thinner graded buffer layers had high internal resistances from reduced carrier concentrations. The empirically derived recipe developed at the National Renewable Energy Laboratory (NREL) produced the highest quality cells. Future work will concentrate on further determining the scientific theory explaining dislocation propagation in LMM buffer layers, possibly by examining the effect of dopant type.

Influence of Charge State and Crystal Structure on Properties of Transparent Conducting Oxide Spinel. ADRIANA TEODORO-DIER (*Lawrence University, Appleton, WI 54912*) GREG EXARHOS (*Pacific Northwest National Laboratory, Richland, WA 99352*). Solution and vacuum based deposition approaches have been used to prepare thin transition metal oxide films that are electrically conductive. To achieve high conductivity in these materials, processing methods that drive polaron formation in the oxide have been explored. Research reported here is focused on optimizing the transparency and conductivity of NiCo_2O_4 and the new polaron conductor CuMn_2O_4 by manipulating film deposition parameters. This has been achieved by changing the resident metal cation charge states. Pulsed Laser Deposition (PLD) from a NiCo_2O_4 target with high substrate temperature and high oxygen partial pressure followed by post-deposition annealing produced spinel films with resistivities as low as $4.0 \times 10^{-1} \Omega \text{ cm}$. In the CuMn_2O_4 system, infrared transparent films were deposited from alcoholic or aqueous solutions using spin deposition and PLD. Films deposited from aqueous solutions displayed resistivities of $2.69 \Omega \text{ cm}$ while those obtained from alcohol solutions were insulating. Although the insulating films became conductive when heated in air, the optimum cation oxidation states to promote conductivity in the films derived from alcohol solutions have not been realized. PLD films of CuMn_2O_4 created under conditions similar to those used to deposit NiCo_2O_4 films displayed resistivities around $0.5 \Omega \text{ cm}$. XRD, XPS, Hall measurements, Raman and transmission spectra were used to further characterize resident properties. Ongoing work involves optimization and refinement of deposition conditions for the CuMn_2O_4 PLD films in order to achieve the appropriate mixture of cation oxidation states associated with optimum conductivity.

***Multilayer Mirrors for Extreme Ultraviolet Lithography.** JONNY RICE (*Norfolk State University, Norfolk, VA 23504*) DAVID ATTWOOD (*Lawrence Berkeley National Laboratory, Berkeley, CA 94720*). Extreme Ultraviolet (EUV) lithography promises to be an efficient way to manufacture faster and more powerful microchips. Using light of wavelength 13–14 nm instead of the currently used range of ~200 nm results in the ability to produce smaller feature sizes for the silicon network that makes up the microchip. However, the normal lithography optics cannot be used with this range of light because the scattering of light at this wavelength reduces the rate of success of the process. The answer is multilayer mirrors, mirrors coated with alternating layers of optical materials, since the internal reflections between the individual layers and off-phase refractions within them cause interference that

reduces the scatter. The most efficient multilayer optics reflect at ~70%, which means a multilayer mirror must have a high reflectance and be durable enough to withstand the intense energy required for the process, since the initial energy wave will be reduced by 60–70% at each interaction with one of several multilayer optics within the system. Current testing for EUV lithography involves measuring peak reflectance and uniformity of reflectance of mirror samples as well as reductions in reflectance caused by prolonged exposure to radiation. Future research will involve testing new combinations of materials for multilayers as well as testing coating layers designed to lengthen the lifespan of the multilayer optics.

Multiple Differential Aperture X-Ray Microscopy. OMBREYAN BROADWATER, VIRGIL GREENE (*South Carolina State University, Orangeburg, SC 29117*) DR. GENE ICE (*Oak Ridge National Laboratory, Oak Ridge, TN 37831*). A truly non-destructive tool (X-ray microbeam) for three-dimensional (3-D) characterization of mesoscopic and nanoscopic material structures has been developed and is in use. A major breakthrough towards the study of crystal structure distribution in 3-D is the development of Differential Aperture X-Ray Microscopy (DAXM). It provides a way to decode the location of scattering from sites along the incident x-ray microbeam. A single wire DAXM is currently in use. This method has one major drawback; it requires a huge increase in data collection time. In this project, a multiple wire DAXM has been designed and constructed to accelerate 3-D measurements of crystal structure. The design considers beam penetration-depth into the sample, angle of sample surface with respect to beam direction, spacing between the sample surface and the wires, wire size, and wire spacing. An appropriate holder that allows all reflected rays to be detected by the X-ray area detector without interference was also designed and constructed. For a 50- μm diameter size wire, theoretical and computer program data show that data collection time is accelerated by at least a factor of 2.5 compared to a single wire for a 1- μm resolution. Also, a 30 degree angle between sample surface and beam direction resulted in fewer steps and lower minimum wire spacing compared to the 45 degree angle that is currently used. A similar effect is observed as the wires move closer to the sample surface. Multiple-wire Differential Aperture X-ray Microscopy not only accelerates data collection time, but also allows studies of dynamic processes in which short data collection time enables real time resolution. It provides better signal-to-noise-ratio conditions and less sensitivity to instabilities compared to a single wire. This system was tested on the 3D X-ray crystal microscope (station 34-ID-E) at the Argonne National Laboratory's Advanced Photon Source and it worked as designed. Detailed analysis and development of software to decode the diffraction information is underway. This result further illustrates the potential for accelerated data collection with multiple differential apertures.

Nitride Membranes: Surface Debris Prevention and Strength Testing. PATRICK BENNETT (*University of California–Berkeley, Berkeley, CA 94720*) ERIK ANDERSON (*Lawrence Berkeley National Laboratory, Berkeley, CA 94720*). Fresnel Zone plate lenses are used to focus soft x-rays through a series of alternating zones of opaque and transparent material. Nitride membranes act as a support upon which zone plates are manufactured. The membranes are created by coating a silicon wafer with nitride and then etching away the silicon with potassium hydroxide (KOH) to form a window. Since window strength is an important factor in throughput, it would be desirable to identify and optimize production factors that affect strength. To perform analysis of window strength, an apparatus was designed and constructed that would increase pressure on nitride membranes until breakage, allowing for comparative analysis between different production steps. During testing, it was found that the windows being produced were contaminated with debris. In order to reduce contamination, sources were identified using a process of elimination. By replacing contaminating production steps, surface debris was greatly reduced. Furthermore, debris was eliminated completely using a solution of hydrogen peroxide and sulfuric acid. This is not an ideal solution, however, as it is hazardous and its effects on window strength are unknown. Preliminary results from pressure testing indicate that strength of membranes is dependant on mount orientation. While these results were unexpected, more testing needs to be done to determine the nature of this relationship. Most likely, window strength will be related to both the absolute window size as well as the relative size of window to surrounding silicon support frame.

Non-Destructive Measurement of Residual Stresses in Finished Carburized Gears Using X-ray Diffraction. BRYAN BOGGS, JEFFREY BUNN (*University of Tennessee at Martin, Martin, TN 38238*) DR. CAMDEN HUBBARD (*Oak Ridge National Laboratory, Oak*

Ridge, TN 37831). Carburization is a common method for improving fatigue strength and wear resistance of gears found in transportation systems. Compressive residual stresses develop as a result of phase transformations from post carburization heat treatments, which improve fatigue strength. Conversely, these phase transformations cause surface distortions to develop in the gear geometry and a loss of surface finish. A finishing process such as grinding or skiving is implemented in order to remove these distortions and improve the finish. This research seeks to quantify the change in residual stress in a carburized gear as it progresses through the finishing process. X-ray diffraction was used to characterize both a finished and unfinished carburized gear to map the residual stresses across and along the face width of a gear tooth. At ten radial positions along the gear tooth, the compressive stresses were measured across the width of the tooth. The unfinished gear showed little variation of residual stresses while the finished gear showed a significantly larger variation of residual stresses. In the unfinished gear the average of the stresses varied slightly and had an average value of 150 ksi compression. However, the finished gear yielded an average compressive residual stress at each radial position that varied linearly from 70 ksi to 130 ksi and then back to 70 ksi. This significant variation is presumed to be a result of the amount of material removed during grinding. Additional tests are planned to determine whether the trends observed from these tests are repeatable for other gear samples. Metrology studies are also in progress to determine the amount of material removed by grinding, with the intent to correlate this loss to the change in residual stress. This research is part of a larger research project in which neutron diffraction will be used to penetrate deeper into the specimen and to compliment the near surface x-ray stress data.

Preparation and Characterization of Self-Assembled Molecular Films. KYAL WRIGHT (Norfolk State University, Norfolk, VA 23504) MIQUEL SALMERON (Lawrence Berkeley National Laboratory, Berkeley, CA 94720). Industrial laboratories and semiconductor manufacturing companies have implemented an initiative to investigate the structure-property relationships, specifically the electrical and mechanical property relationships, of island structures (islands) of organic ultra thin films. Before these properties can be studied, reproducible methods of island formation must be developed to promote controlled structure-property studies. This project will study island formations from alkanethiol self-assembled monolayers (SAM) and conduct preliminary mechanical property tests. There are many parameters that affect the formation of SAM islands. Some of these parameters include the surfactant concentration in solution, the solution temperature, the substrate cleanliness, the substrate's grain sizes and the duration of deposition. This project used Atomic Force Microscopy (AFM) to investigate the relationships between solution concentrations, substrate deposition times, and substrate grain sizes for the control of SAM island domains. To test the effects of deposition time and material concentration on the formation of the SAM islands on gold substrates, alkanethiol molecules in ethanol solution were used in 2 μM , 5 μM , 10 μM and 20 μM concentrations. Experiments dependent on deposition time used time periods ranging from 30 seconds to 6 minutes. Preliminary tests on the effects of flame annealed gold substrates resulted in the use of substrates annealed for 45 passes at one pass per hertz for the tests involving solution concentration and deposition time. The results of the preliminary substrate investigation and structural investigations support that SAM island domains larger than 100nm can be formed on annealed gold substrates when alkanethiol solutions greater than 10 μM concentration are deposited on the substrate between 45 seconds and one minute. Results from the mechanical property investigation indicated that the islands formed from 20 μM solution at a deposition time of 45 seconds are quite robust when a maximum load corresponding to 8 volts from the AFM system was applied to a 150nm region. While the results from all the investigations support the theory that the first phase of SAM island formation can be controlled, further investigations and trials for each experiment are still needed to confirm this claim.

Processing and Analysis of YBCO Film Spectroscopy Data Using the GRAMS Series of Computer Software. MICHAEL DUITSMAN (University of Evansville, Evansville, IN 47722) VICTOR MARONI (Argonne National Laboratory, Argonne, IL 60439). The Superconductivity for Electric Systems Program at Argonne is performing detailed characterization studies on $\text{Y}_2\text{Ba}_2\text{Cu}_3\text{O}_7$ (YBCO) superconducting films deposited on long-length metal substrate tapes. One of the important tools used in this research is Raman microspectroscopy, which makes it possible to determine phase composition and texture quality of the YBCO films. A large number of Raman spectra are collected in this program and each one has to

be processed to remove background effects, so that a pure Raman spectrum extrapolated to a horizontal baseline can be obtained for further analysis. Due to the long period of time required to perform even simple mathematical processes on spectroscopy data, there have been many computer programs created to assist in the performance of these tasks. This report discusses the use of one such series of programs—the GRAMS series. The work focused on processing groups of spectra from step-milled samples by applying the software for baselining, noise smoothing, spectral subtraction, and curve-fitting of such spectra. The results show that the GRAMS series facilitates rapid, simple, reproducible processing of spectral data of the type generated by Raman microspectroscopy. The processing of many sets of spectra from a group of six related samples has shown an interesting correlation between the performance behavior of the superconductor and certain types of defects that Raman can detect.

Production of Micro- and Nanocrystalline Diamond Stripper Foils for the Spallation Neutron Source Using Microwave Plasma Chemical Vapor Deposition. MARK JENSEN (Brigham Young University, Provo, UT 84602) ROBERT W. SHAW (Oak Ridge National Laboratory, Oak Ridge, TN 37831). Preliminary testing at Brookhaven National Laboratory predicted that diamond stripper foils will have a longer lifetime in the Spallation Neutron Source (SNS) H⁻ beam (38 mA at 1 GeV) than conventional carbon stripper foils. The design of the SNS requires that foils be supported by a single 12 mm edge and extend 20 mm of freestanding foil. Also, the SNS design estimates the ideal areal density to be 280 $\mu\text{g}/\text{cm}^2$ or $\sim 0.8 \mu\text{m}$ thick. However, testing at Los Alamos National Laboratory showed that increasing foil thickness should provide increased stripping efficiency. Foils were produced using microwave plasma chemical vapor deposition (MPCVD) onto silicon substrates. Substrates were pretreated by the use of ultrasonication in a diamond-methanol slurry. The slurry consisted of 0.3 g each of 35 μm and 4 and 98–99% H₂, at 50 torr. Nanocrystalline diamond films were grown at 900–1000 W in an atmosphere of 1–2% CH₄, 8–9% H₂, and 90% Ar at 130 torr. The foils' substrates were then etched using a standard Nitric-HF-Acetic Acid etching solution. Due to thermal expansion mismatch of diamond and silicon, foils originally scrolled upon etching the silicon. To keep the freestanding foil flat, a photolithography technique was used to pattern $\sim 6 \mu\text{m}$ deep U-shaped channels in the substrate before pretreatment. The channels terminated on the supported edge. Foils showed inconsistent and low nucleation densities that resulted in pinholes and weak areas. Nucleation density increased and became more uniform by frequent stirring of the diamond slurry during pretreatment. This enhancement of the scratching procedure resulted in smoother surfaces and decreased the likelihood of holes. It is anticipated that the usable lifetime of both micro- and nanocrystalline diamond foils will greatly exceed that of conventional stripper foils. The performance of different foils in the SNS will provide direction into which properties and crystal size are the most important for long lasting foils.

Protection of Aluminum from Saltwater Corrosion by Superhydrophobic Films. PHILIP BARKHUDAROV (Utrecht University, Utrecht, ND 00000) JAROSLAW MAJEWSKI (Los Alamos National Laboratory, Los Alamos, NM 87545). The damaging effects of corrosion cost billions of dollars each year in metal replacements and repairs. Unfortunately, corrosion cannot be completely stopped; the natural state of most metals on earth is in oxide form. Fortunately, it is possible to slow the oxidation process or to redirect it, and with ever more advanced technology, especially on the nano-scale, corrosion prevention is becoming more and more effective. This research focused on the corrosion of aluminum in salt-water environments. In dry air, aluminum develops a thin surface oxide layer that prevents further corrosion. However, in the presence of water and salt, this layer is broken and rapid corrosion ensues. In this study, superhydrophobic films were layered onto the metal, repelling water and slowing corrosion. These superhydrophobic films consisted of a highly nano-porous silica framework together with hydrophobic organic ligands. To study the effectiveness of such protective layers, the neutron reflectometry method was used. By taking neutron reflection measurements over time on samples of layered aluminum/superhydrophobic film/salt-water, it was possible to observe and quantify the rate of oxide growth in the aluminum. From the relatively short period of measurement, it was possible to predict corrosive behavior on a longer time scale and to show the effectiveness and feasibility of using superhydrophobic films to protect aluminum in marine environments, i.e., ships, off-shore platforms, aircraft, and coastal regions.

Pulsed Laser Deposition of Precursors for Ex Situ BaF₂ Growth of YBCO Superconducting Film. ALI MORADMAND (University of South Alabama, Mobile, AL 36688) DAVID CHRISTEN (Oak Ridge

National Laboratory, Oak Ridge, TN 37831). Various methods exist for the deposition of thin films used in materials research of yttrium barium copper oxide (YBCO) superconductors. One common method is in situ pulsed laser deposition (PLD), in which a target is subjected to a pulsed laser beam and ablated into a plume of particles which deposit reactively on a substrate. Another technique used to make high-quality YBCO film for the application of so-called "coated conductor" technology is the ex situ physical vapor deposition of precursors containing BaF₂ at room temperature—unlike in situ PLD where the deposition takes place at elevated temperatures. The precursors are then converted in a furnace to form superconducting YBCO. The focus of this study is to develop a new ex situ PLD method, in which the substrate is kept at room temperature and the deposition of the fluoride-containing YBCO is done using PLD. By optimizing parameters such as ambient gas species, chamber pressure of background gas, and laser energy, YBCO precursors can be formed with the desired thickness, surface morphology, and ratio of the elements in the precursor. The converted films are analyzed for the crystalline YBCO structure using x-ray diffraction and the surface is imaged using atomic force microscopy and scanning electron microscopy. The samples are then tested for superconductivity in a superconducting quantum interference device. Analysis on various samples deposited under different conditions shows that lower laser energy and introduction of background gas can produce film with more favorable surface structure for conversion. Reduction of laser power by modifying the optics reduces the problem of "splashing", which is a known obstacle in PLD. Under an optical microscope, reduction of laser energy shows a significant decrease in surface irregularity. Magnetometry tests show a critical temperature of 88K for these converted YBCO precursor films and critical current densities of 2.9 mA/cm² at 5K. Future goals are to further improve film uniformity and quality to increase these values. Because PLD can also make good multilayering films, the long-term goal is to conduct rare-earth substitution into the precursors. Alternating layers of rare-earth material can be deposited in the precursor, and the substitution of the yttrium in YBCO with other rare earth elements has been known to improve flux pinning and raise the critical temperature of such superconductors. By optimizing the parameters for ex situ PLD of a single layer, the method can be extended to rare-earth substituted multilayered precursors as a versatile method of deposition of precursors for high-quality high temperature superconducting films.

Purification of N@C60. CHANDA ROGERS (Benedict College, Columbia, SC 29204) DR. JOHN SCHLUETER (Argonne National Laboratory, Argonne, IL 60439). Currently, research is being conducted to produce and purify the endohedral molecule N@C60, which will act as the basic quantum bit (qubit) for the next generation of computers. With these qubits, quantum computers will become more effective in the areas of large database searches, large number factorization, and quantum mechanical simulation of physical systems. Therefore, there is a need to develop methods to increase the yield and purity of N@C60. The method that was chosen for the purification of N@C60 was high performance liquid chromatography (HPLC). Electron paramagnetic resonance (EPR) was used to confirm the presence of N@C60. In utilizing these two methods together, the sample of N@C60 in C60/toluene was separated with the HPLC instrument, and then each fraction from the fraction collector was concentrated down to about 1mL of solution and placed inside of EPR tubes. Next, an EPR spectrum was recorded, and the fraction that gave an EPR spectrum of the clearly defined triplet characteristic of N@C60 was reinjected into HPLC. This will be continued until a pure sample of N@C60 is identified. It will then enter into the next stage of the research, which includes it being formed into the qubits.

Search for Mechanically-Induced Grain Morphology Changes in Oxygen Free Electrolytic (OFE) Copper. JENNIFER SANDERS (Westminster College, Fulton, MO 65251) ROBERT KIRBY (Stanford Linear Accelerator Center, Stanford, CA 94025). The deformation of the microscopic, pure metal grains (0.1 to > 1 millimeter) in the copper cells of accelerator structures decreases the power handling capabilities of the structures. The extent of deformation caused by mechanical fabrication damage is the focus of this study. Scanning electron microscope (SEM) imaging of a bonded test stack of six accelerating cells at magnifications of 30, 100, 1000 were taken before simulated mechanical damage was done. After a 2–3° twist was manually applied to the test stack, the cells were cut apart and SEM imaged separately at the same set magnifications (30, 100, and 1000), to examine any effects of the mechanical stress. Images of the cells after the twist were compared to the images of the stack end (cell 60) before the twist. Despite immense radial damage to the end cell from the process of twisting, SEM imaging showed no change in grain morphology from

images taken before the damage: copper grains retained shape and the voids at the grain boundaries stay put. Likewise, the inner cells of the test stack showed similar grain consistency to that of the end cell before the twist was applied. Hence, there is no mechanical deformation observed on grains in the aperture disk, either for radial stress or for rotational stress. Furthermore, the high malleability of copper apparently absorbed stress and strain very well without deforming the grain structure in the surface.

Solid Oxide Fuel Cell Based on Proton Conductor. KATHRYN FENSKE (University of Illinois at Urbana Champaign, Champaign, IL 61820) DR. U. BALACHANDRAN (Argonne National Laboratory, Argonne, IL 60439). Thin films of SrCe_{0.95}Yb_{0.05}O_{3-d} (SCYb5) are prepared on porous substrates of SCYb₅/NiO by a casting method. Dense, crack-free SCYb₅ substrate films with a thickness of approximately 10–30µm are successfully deposited on porous NiO/SCYb5 substrates. Scanning Electron Microscopy (SEM) shows uniform thickness of the films and is bonded to the substrate. The prepared cells were tested to determine their performance as a fuel cell at 800°C.

Solvent-Induced Bandgap Effects in Poly(3-hexylthiophene). RENEE GREEN (University of Pittsburgh, Pittsburgh, PA 15213) GARRY RUMBLES (National Renewable Energy Laboratory, Golden, CO 89401). Poly(3-hexylthiophene) is a well-studied semiconducting polymer whose absorbance, and thus, optical bandgap, can be altered via formation of thin films or addition of poor solvent. These methods are known to change the color of the polymer from yellow ("Y-form") to red ("R-form"). The change in absorbance of the two forms of polymer results in the widening of its optical bandgap, but the resulting alteration of the electrical bandgap is poorly understood. Absorbance spectra were taken on dilute solutions of poly(3-hexylthiophene) dissolved in THF as methanol was added to bring about the absorbance transition. The resulting absorbance wavelengths were then converted into electron-volts to determine the polymers' optical bandgaps. Cyclic voltammetry was then performed on the solutions containing varying methanol volume fractions to evaluate the polymers' electrical bandgaps. Y-form polythiophene was found to have an approximate optical bandgap of 2.3eV, while that of the R-form was found to be 1.9eV. The electrical bandgap of only the Y-form of the poly was able to be determined, at approximately 1.8eV. Solvent oxidation interference is suspected to be the cause of poor R-form electrochemical data, thus other solvents will be tested. Furthermore, while it is assumed that both phases of R-form polythiophene are energetically analogous, we aim to eventually demonstrate this concept by comparing the electrical and optical bandgap data of the polymer in solution and in thin-film.

Stainless Steel Support Layer for Solid Oxide Fuel Cells (SOFC). MATTHEW HAMEDANI (College of DuPage, Glen Ellyn, IL 60137) DAVE CARTER (Argonne National Laboratory, Argonne, IL 60439). The solid oxide fuel cell (SOFC) is a type of fuel cell that operates at high temperatures and employs ceramics as functional elements of the cell. Each cell is composed of a cathode and an anode separated by a solid impervious electrolyte, which during operation conducts oxygen ions produced by reduction of oxygen from the cathode to the anode where they react with hydrogen gas supplied to the anode. This investigation focuses primarily on developing a reliable cell support using stainless steel 434 (SS 434) instead of a nickel cermet support because it is expected to be more cost effective and structurally and chemically durable in hydrogen/steam atmosphere. Ultimately, the cell support layer should have the combined properties of porosity and high electrical conductivity. Layers were made by tape casting onto a Mylar sheet from a pre-made slurry containing metal particles, solvent, binder, plasticizer, and pore former when needed. The binder holds the cast together and makes it viscous, the plasticizer makes the cast flexible, and the pore former which generates porosity in the metal layer once it is sintered. The composition of the slurry was changed so that the cast from it would exhibit the desirable properties of being flexible, smooth, porous, electrically conductive, and sturdy. We found such slurries to be well dispersed, free from foaming and air bubbles, chemically stable, and rheologically optimal for casting. Shrinkage of casts that exhibited desirable properties was measured using a dilatometer. Results indicate that slurries made using butanol as the solvent and B-79 as the binder gave more flexible and sturdy casts than slurries made with Xylene/Butanol as the solvent and AT 746 as the binder. Successful fabrication of multilayer cells containing an electrolyte, anode layers, and two layers of a metal slurry was achieved. Sintering of these multilayer cells at high temperature under controlled atmosphere yielded products in which the electrolyte layer was impervious and free of cracks, while the stainless steel layer displayed the high porosity. Further work will optimize slurry composition and tape casting process.

Structural Investigation of Voids and Al Nanoparticles in 20% Al-80% MoO₃ Thermite Pellets. JOSHUA HAMMONS (Texas Tech University, Lubbock, TX 79409) JAN ILAVSKY (Argonne National Laboratory, Argonne, IL 60439). Aluminum and molybdenum tri-oxide thermites have a very high energy density and thus are a very attractive energetic material. Explosion of these thermites is a result of the oxidation of Al by MoO₃ and some O₂. To enhance the contact of Al particles with the MoO₃, a mixture of 80% MoO₃ and 20% Al was compressed into pellets. When the Al and MoO₃ powders were compressed into pellets, burn rates decreased. The purpose of this research is to gain some insight into the structure of the Aluminum particles and or voids that are in the pellet. Scanning electron microscopy was used to examine the surface of the pellets and compared to ultra-small angle x-ray scattering (USAXS) data performed at Argonne National Laboratory (33-ID beamline). Results indicate the possibility that low density samples contain two separate void phases; the two phases consist of one large void population that is separate from much smaller voids that surround the Al nanoparticles. As the density is increased, the Al particles may penetrate these large voids resulting in a random dispersion of the Al particles in a single void phase. To verify these conclusions additional information is needed. BET analysis should provide additional information about the surface to volume ratio of the void space in these samples. Additional USAXS data should also be obtained on samples that range from 30% TMD to 100%TMD.

Superplastic Forming of Structures Fabricated Using Friction Stir Welding and Friction Stir Spot Welding. CASSANDRA DEGEN (South Dakota School of Mines and Technology, Rapid City, SD 57701) GLENN GRANT (Pacific Northwest National Laboratory, Richland, WA 99352). Superplastic forming (SPF) is becoming an increasingly popular metal forming process as parts with more complex shapes are needed. SPF exhibits the ability to form complex near-net shapes, reducing both cost and weight. Welded structures can also be superplastically formed, however the welding method used is critical to the success of the later forming operation. Fusion welded aluminum cannot be superplastically formed because the fusion weld metal is not superplastic. Friction stir welding (FSW) is a new joining method in which the metal is not melted and the microstructure remains fine after welding, an essential requirement for later SPF. In this work, the feasibility of fabricating complex structures using FSW and friction stir spot welding (FSSW) prior to SPF was studied. Coupons of FSW and FSSW were made using different parameters. The coupons were tested in tension at the SPF conditions. Multisheet packs were also made using FSW and FSSW. The packs were then superplastically formed in a superplastic forming press. The results of the coupon and multisheet testing were analyzed and compared to the metallurgy of the welds before and after SPF. Nearly all samples showed abnormal grain growth (AGG), a condition detrimental to the superplastic forming of the weld metal, resulting in low deformation of the weld metal as compared to the parent metal. From these results, recommendations are given concerning which FSW and FSSW parameters should be used to give the best superplastic formability. Future work will include optimizing the weld parameters for SPF and performance testing of the multisheet structures.

Synchrotron X-Ray Diffraction Studies of Single Crystals with Varying High Pressure. DANIEL SCOTT (Eastern Illinois University, Charleston, IL 60193) YU-SHEN CHEN (Argonne National Laboratory, Argonne, IL 60439). Three single crystals were studied using a synchrotron resource to understand the change in lattice structure with varying high pressures. The crystal compositions of H₂C₂O₄·2H₂O, Na₄SiO₄, and C₄₉H₄₀N₃PS were determined by their X-ray diffraction patterns while in the synchrotron beam. The cell parameters of each crystal came out as expected and verified previous research [H₂C₂O₄·2H₂O: a = 6.100(12), b = 3.500(7), c = 11.850(2), β = 104.0(3), Na₄SiO₄: a, b, c = 24.875(2), a, β, γ = 90.00, C₄₉H₄₀N₃PS: a = 14.624(3), b = 27.343(6), c = 9.982(2), β = 102.31(3)]. To apply high pressure to the crystals, ruby fluorescence from an Argon laser was used to determine the pressure calibration of a four-screw Diamond Anvil Cell (DAC). The DAC was calibrated to apply 13.610(5) GPa of pressure over a spectrographic shift of 4.851(7) nm. Due to equipment complications with the DAC, the high pressure lattice determination could not be finished in the specified research time. Future extensions of this research will be to observe how the unit cell of each crystal changes when inside the DAC while being exposed to a synchrotron source.

Temperature Measurements of Large-Area TCOs under Vacuum. JENNIFER GADDIS (University of Illinois at Urbana Champaign, Urbana, IL 61801) BRENT NELSON (National Renewable

Energy Laboratory, Golden, CO 89401). The National Center for Photovoltaics (NCPV) has developed new standards for deposition and characterization tools in order to facilitate process development and integration. The first tool designed to these specifications is a sputtering tool for transparent conducting oxides. One such specification dictates that all systems must hold 6" x 6" substrates. Concerns were raised internally at the NCPV about temperature uniformity across the substrates and the performance of large-area heaters. In this study, large area heater characteristics were studied using Type-K thermocouples and an Infrared camera; preliminary work on verifying temperature uniformity and creating intentional non-uniformity was also conducted. Both optical and direct contact measurement techniques were used to create a heater calibration curve for Corning 1737F glass substrates. However, the temperature measured optically was significantly higher due to radiation from the back-plate of the substrate holder. Using the thermocouple measurement, the temperature of the glass was found to achieve only about one half of the heater temperature (°C). For combinatorial deposition, the ability to produce both uniform and intentionally non-uniform heating is desired. An infrared camera was used to create temperature maps of glass substrates. The uniformity of the substrates from 100–400°C was verified to within a standard deviation of 2.6% of the substrate temperature. Intentional temperature reduction of 15% over a specified area of the substrate was produced using a Tantalum radiation shield. Future work will focus on creating a standard temperature measurement method for 6" x 6" substrates, exploration of other materials and thicknesses for the substrate platen, and manipulations of temperature for combinatorial deposition.

The Effect of Phthalocyanines on Solution-Processed Organic Photovoltaic Devices. TALIA GERSHON (Massachusetts Institute of Technology, Cambridge, MA 02139) DR. SEAN SHAHEEN (National Renewable Energy Laboratory, Golden, CO 89401). Organic photovoltaics (OPVs) are one mode of renewable energy utilization that promises to provide a cleaner energy alternative to fossil fuels. Initial devices called bulk heterojunctions are commonly made using an active layer composed of a blend of a p-conjugated polymer and a fullerene, in our case poly(3-hexylthiophene) (P3HT) or Poly[2-methyl,5-(3',7'-dimethyl-octyloxy)]-p-phenylene vinylene (MDMO-PPV) and [6,6]-phenyl C61 butyric acid methyl ester (PCBM). These devices have optical band gaps approximately equal to 1.9 eV where an optimal device would have a band gap closer to 1.4 eV, thus adding a third component to red-shift absorption should increase the amount of light absorbed as well as improve the efficiencies of these devices. Liquid crystalline zinc-phthalocyanine (Zn LC PC) and liquid crystalline copper phthalocyanine (Cu LC PC) are materials that have peak absorbances around 650 nm, which would enhance absorption in the active layer in this way; because of their liquid crystalline morphologies, these materials may also improve ordering and, thus, improve transport and efficiency in OPV devices. Other non-liquid crystalline materials that have similar optical densities have also been considered, including a Titanyl Phthalocyanine (TiO PC) and a Free Base Phthalocyanine (Free Base PC). Our research explored the effects of adding such materials to the P3HT:PCBM or MDMO-PPV:PCBM active layers in the bulk heterojunction. Though there is some evidence indicating an improvement in absorption and transport with these materials, no increases in cell efficiency have been observed to date.

The Theoretical Calculation of Phase Diagrams and Thermophysical Properties of Potential Nuclear Fuel Alloys. COREY WESTFALL (Albertson College of Idaho, Caldwell, ID 83605) IRINA GLAGOLENKO (Idaho National Laboratory, Idaho Falls, ID 83415). With the increase of nuclear power plants, nuclear waste is becoming an increasing environmental concern. By transmuting the Actinides in a burner reactor, the amount of nuclear waste can be decreased significantly. Zirconium based alloys have been considered for use in burner reactors, but due to the rarity and dangers of the Actinides, little, if any, Actinide-Zirconium alloy data exists. To supplement this data, Thermo-Calc[®], a thermodynamic modeling software, was used in conjunction with TCNF2[®], a nuclear fuel database, to create phase diagrams and property plots for the Actinide-Zirconium binaries, a pseudo-binary for Am-Pu-Zr, and multiple ternaries for U-Pu-Zr. The graphs were then compared to experimental plots to identify errors in TCNF2[®] and to determine the alloy data needed to correct the database. The melting temperatures were calculated for multiple alloys of interest in burner reactors. Thermo-Calc[®] was shown to perform very well calculating the melting temperatures and most of the binaries, but TCNF2[®] was shown to be lacking data for Np-Zr, most Americium alloy data, and ternary data.

Future work includes the characterization of the recommended alloys and that incorporation of this data into TCNF2®.

Ultrasonic Testing of High Attenuation Materials with Pulse Compression Techniques. LISA DEIBLER (*Washington State University, Pullman, WA 99164*) BRIAN TUCKER (*Pacific Northwest National Laboratory, Richland, WA 99352*). Homeland security and industry widely employ ultrasonic non-destructive evaluation (NDE) because of sound's ability to non-invasively characterize a variety of materials. However, the capabilities of conventional ultrasonic NDE are severely limited in many materials due to high attenuation and scattering of ultrasound. In addition, most ultrasonic techniques require contact with the specimen either by immersion or direct coupling, which can present issues for moisture-sensitive materials and/or materials in a high-speed process line. Recent advances in air-coupled transducers have enabled the efficient transmission of broadband ultrasonic (between 20 kHz and 1.5 MHz) waveforms through air, eliminating the need for specimen contact. Additionally, pulse compression, a technique commonly used in RADAR applications, provides a higher signal-to-noise ratio (SNR) for accurate measurements. Combining air-coupled transducers with pulse compression shows great promise for characterizing ultrasonically difficult materials without the need for specimen contact. Comparison of two pulse compression techniques, cross correlation (XCorr) and swept frequency multiplication (SFM), by computer simulations and experimental testing revealed a more robust and accurate response from XCorr. Using air-coupled transducers and the XCorr pulse compression method, SNRs up to 28.3 dB (increase of 26 times in signal strength) over conventional ultrasound were observed. This method was used to successfully detect a defect in a thick (10mm) carbon fiber laminate without the need for direct specimen contact. Combining advanced signal processing techniques with the capabilities of broadband electrostatic transducers is shown to be a highly promising non-contact method for characterizing difficult materials in air.

X-ray Photoelectron Spectroscopy of GaP(1-x)N(x) Photocorroded as a Result of Hydrogen Production Through Water Electrolysis. MARIE MAYER (*University of Illinois at Urbana Champaign, Urbana-Champaign, IL 61801*) ANDERS NILSSON (*Stanford Linear Accelerator Center, Stanford, CA 94025*). Photoelectrochemical (PEC) cells produce hydrogen gas through the sunlight driven electrolysis of water. By extracting hydrogen and oxygen from water and storing solar energy in the H-H bond, they offer a promising renewable energy technology. Addition of dilute amounts of nitrogen to III-V semiconductors has been shown to dramatically increase the stability of these materials for hydrogen production. In an effort to learn more about the origin of semiconductor photocorrosion in PEC cells, three samples of p-type GaP_{1-x}N_x (x = 0, 0.002, 0.02) were photocorroded and examined by X-ray Photoelectron Spectroscopy (XPS). GaPN samples were observed to be more efficient during the hydrogen production process than the pure GaP samples. Sample surfaces contained gallium oxides in the form of Ga₂O₃ and Ga(OH)₃ and phosphorus oxide (P₂O₅), as well as surface oxides from exposure to air. A significant shift in intensity from bulk to surface peaks dramatic nitrogen segregation to the surface during photoelectrochemical hydrogen production. Further investigations, including using a scanning electron microscope to investigate sample topography and inductively coupled plasma mass spectroscopy (ICP-MS) analysis for solution analyses, are under way to determine the mechanism for these changes.

X-ray Reflectivity Characterization of Structural Damage Induced by Xe⁺ Bombardment in Thin Film EUV Collector Mirror Optics. DOUGLAS DETERT (*University of Wisconsin-Madison, Madison, WI 53711*) JEAN-PAUL ALLAIN (*Argonne National Laboratory, Argonne, IL 60439*). Xe⁺ ion bombardment produced by extreme ultraviolet (EUV) plasma-based sources degrades the surface and limits the operational lifetime of single layer and multilayer thin film collector optics used in 13.5 nm wavelength EUV lithography. The objectives of this experiment are twofold: to use specular Cu Kα₁ (α=1.54 Å) X-ray reflectivity (XRR) analysis to characterize and quantify the structural damage induced by Xe⁺ bombardment in multilayer mirrors, and to predict the 13.5 nm wavelength (EUV) reflectivity performance of both single layer and multilayer mirrors using traditional 1.54 Å wavelength XRR. Si/Mo multilayer films were subjected to 1 keV Xe⁺ fluences ranging between 10¹⁶ to 10¹⁸ Xe⁺/cm² at temperatures of 294 and 473 K. In addition, both EUV and Cu Kα₁ wavelength XRR analyses were performed on non-irradiated Ru/Ti single layer films. A systematic comparison of XRR simulations using IMD software and measured XRR data at a wavelength of 1.54 Å reveals that while the simulations provide useful insight into the interaction of thin films and X-rays, the specific scheme used may be inadequate for obtaining accurate structural information

about the irradiated mirrors or reflectivity behavior at 13.5 nm. The behavior of single layer mirror reflectivity at Kα₁ scales well in IMD simulations to predict the measured EUV reflectivity performance at 13.5 nm. This work is part of an ongoing study that seeks to understand the EUV reflectivity performance of thin film collector mirrors and the combined effects of damage in EUV lithography optics from energetic ion-bombardment, thermal deposition of neutral particles, and off-band radiation produced by Xe⁺ and Sn⁺ plasma-based light sources.

Medical and Health Sciences

A Noninvasive Method to Assess Left and Right Ventricular Fractional Area Change in Genetically Altered Mice. MEGAN GREEN (*La Salle University, Philadelphia, PA 19141*) HELENE BENVENISTE (*Brookhaven National Laboratory, Upton, NY 11973*). The techniques which allow a comprehensive assessment of cardiovascular performance in small animals are still limited. The development of a noninvasive cardiac MRI-based method to facilitate the analysis of both right and left ventricular function in a mouse heart is essential in a cardiac study. The use of animals with genetic modifications, which lacks the ability to produce vasointestinal peptide (VIP), and important cardiovascular regulatory factor. The use of these animals with genetic modifications allows for a more precise assessment of cardiovascular failure development. Changes in myocardial VIP concentration or with alteration of physiological responsiveness of VIP receptors have been links to the development of severe cardiovascular disorders, such as myocardial fibrosis, heart failure, cardiomyopathy and pulmonary hypertension. The goal of this study was to compare the left and right ventricle to see if they are both equally involved in the development of cardiomyopathy in VIP-deficient mice. The cardiac image was performed in five anesthetized animals using several different Flash_movie sequences in a 9.4T MicroMRI system. Once the images were obtained Amira Imaging software was utilized to make outlines of the left and right ventricular cavities and areas for each ventricle were obtained during different phase of the cardiac cycle. A transactional view through the midpapillary level was used for analysis. Functional ventricular assessment was performed by calculating the fractional area change (FRAC) during systole. Data showed that there was not a significant difference between the left ventricle (53.87 +/- 13.66%) and the right ventricle (52.90 +/- 15.01%) FRAC. Both sides developed significant hypertrophy of the myocardial wall. In summary, the VIP-deficient mouse, the development of cardiomyopathy was shown to similarly affect both the left and right ventricular function. We were able to develop a noninvasive method for advanced characterization of cardiac function in the murine model. This will help to facilitate longitudinal study of the heart disease process. The long term goal of this study is to map the development of heart disease.

An Examination of Perseveration in Cocaine Abusers. TANYA LUKASIK (*Stony Brook University, Stony Brook, NY 11794*) RITA GOLDSTEIN, PH.D. & PATRICIA WOJCIK, PH.D. (*Brookhaven National Laboratory, Upton, NY 11973*). Drug addiction is associated with executive deficits that are typically attributed to dysfunction in prefrontal brain regions (e.g., the ventromedial region of the orbitofrontal cortex and dorsolateral prefrontal cortex). Cocaine-addicted individuals exhibit mild performance deficits on neuropsychological tasks that require set shifting, instead, perseverating on previously rewarded behavior. However, the research reported is inconclusive possibly due to the heterogeneity among cocaine-abusing populations. In the current study, cocaine abusers were compared to healthy control subjects on the Wisconsin Card Sorting Task, (WCST); a classical neuropsychological task that assesses concept formation, cognitive flexibility and set shifting. Cocaine abusers were grouped according to their ability to complete all categories on the WCST (high functioning versus low functioning). Compared to higher functioning cocaine subjects, lower functioning cocaine abusers were associated with more positive urine screens. Lower functioning cocaine subjects also scored lower on indices of general intelligence and traditional indices (total scores) of the WCST as compared to higher functioning cocaine subjects and controls. In contrast, higher functioning cocaine abusers scored similarly to controls on total scores of the WCST, however, an examination of performances at the category level suggests a different pattern of learning, specifically a tendency to perseverate in the first sequence of the task. Results suggest two patterns of executive dysfunction in cocaine abusers; one associated with lower functioning cocaine abusers that is more severe and possibly related to acute withdrawal (recent cocaine use) and another associated with higher functioning cocaine abusers characterized by mild perseverative deficits.

Analysis of Sharps Safety Procedures and Injury Prevention Methods at Lawrence Livermore National Laboratory. NICOLE SADLER (University of California–Davis, CA 95616) LESLIE HOFHERR (Lawrence Livermore National Laboratory, Livermore, CA 94550). Today's hazardous world demands safe work practices. An employee's risk of injury and infection increases significantly when he handles sharps. To assess sharps use and compliance with correct safety controls and practices, the author generated a survey form. This form was based on current safety standards and used to conduct face-to-face interviews of Lawrence Livermore National Laboratory (LLNL) personnel who were using biological materials and sharps in research projects. At LLNL, current safety standards are summarized in what is known as the Environmental Safety and Health (ES&H) Manual. Close scrutinization of the ES&H manual confirmed consistency with the current sharps use standards. The Occupational Safety & Health Administration (OSHA) Bloodborne Pathogens Standard mandates that employers maintain a sharps injury log. The survey was designed to determine if any discrepancies between the number of sharps injuries sustained and those reported existed. However, the LLNL sharps injury log was not currently available but will be available in the future, and therefore such comparisons were not performed as part of this analysis. Twenty percent of the facilities using sharps at LLNL were evaluated. During the assessments, almost sixty percent of the labs had an observable sharps safety hazard. These safety breaches fell into one of the following three categories: improper recapping technique, presence of an exposed or improperly discarded sharp, or overfilled sharps container. Nearly twenty percent of the individuals interviewed either had injured himself with a sharp or knew of someone affiliated with his particular lab that had been injured. Seventy-five percent of the reported injuries occurred in a BSL-2 lab. Most researchers at LLNL use scalpels and needles. Half of the researchers reuse their sharps, a practice that should be avoided. The statistical results of the surveys alerted safety personnel to the need for sharps training and further evaluation of sharps use at LLNL.

Analyzing Intensive Care Unit (ICU) and Emergency Room (ER) Unit Records. LAKEISHA MELTON (Texas Southern University, Houston, TX 77004) JONATHAN YOUNG (Pacific Northwest National Laboratory, Richland, WA 99352). By analyzing Intensive Care Unit (ICU) incident reports and Emergency Room (ER) Unit medical records using data analysis, data mining, and cluster analysis, a statistical representation and a data visualization of the analyzed data can support the discovery of complex and unanticipated relationships extant in the data. The primary focus of this project is to identify potential weaknesses and systematic problems throughout the datasets of patient medical records and potential unanticipated process behavior in order to potentially sustain improvements in the reduction of patient medical errors and the enhancement of healthcare facility performance. A tool called IN-SPIRE™, is used to explore each type of data (incident reports and medical records) individually and thoroughly to find the complex relationships in the records. The analysis tools were also used to analyze clusters of records, categorize and group those records in order to potentially produce data visualizations and statistical representations of the analyzed data.

Detection of Cocaine-Induced Cerebral Hemodynamic and Neuronal Function Changes in vivo Using Laser Doppler Flowmetry. MELISSA TULLY (Stony Brook University, Stony Brook, NY 11794) CONGWU DU (Brookhaven National Laboratory, Upton, NY 11973). Cocaine abuse increases the risk of life-threatening neurological complications such as stroke, seizures and transient ischemic attacks. Further, chronic intake leads to long lasting cognitive and behavioral changes. Cocaine has vasoconstrictive properties and also decreases the cerebral metabolism. However, the exact pathophysiological mechanisms underlying cocaine's neurotoxic effects remains incompletely understood. In this study, Laser-Doppler flowmetry (LDF) was used to characterize the effects of cocaine on the cerebral blood flow (CBF) in the rat brains in vivo and compare these changes with CBF changes elicited in the same animal in response to forepaw electrical stimulation before and after the acute cocaine challenge. The rats were anesthetized, intubated, mechanically ventilated, and catheterized to monitor the physiological parameters. The rats were then positioned in a stereotaxic frame and a craniotomy was performed above the left somatosensory cortex. The LDF probe was then mounted upon the exposed brain surface in the somatosensory cortex area, and the changes in the local cerebral blood flow (LCBF) along with the changes in the red blood cell concentration and speed were recorded using the LDF. Electrical stimulations were then administered to the right forepaw subcutaneously to induce a neuronal activation in the left somatosensory cortex with the various

stimulation frequencies (1, 2, 3, 5 & 8 Hz). Cocaine (1mg/kg) was then injected via the venous catheter and the series of stimulations was repeated 5 minutes after the injection until a neuronal response was obtained and LCBF was continually recorded during the experiment. Our preliminary results indicate that cocaine has different effects on the amplitude of response to forepaw electrical stimulation depending upon the stimulation frequency. There was a 25% increase in CBF immediately following the cocaine administration. The mean arterial blood pressure (MABP) also increased to 115 mm Hg from a baseline of approximately 95 mm Hg. The CBF as well as the MABP increase induced by cocaine were transient and recovered to baseline 5 minutes and 8 minutes, respectively after cocaine. However, a neurological response was not obtained until 40 min after the injection. After this time had elapsed, cocaine did not appear to affect the neuronal response at a stimulation frequency of 3 Hz. The present results elucidate the time course of cocaine's acute cerebrovascular and neurological effects and provide a better understanding of the etiology of cocaine-related stroke and transient ischemic attacks.

Developmental Assessment of the D4 Receptor Mice: Part I — Locomotor Activity. NATALIA LONDONO (Stony Brook University, Stony Brook, NY 11794) DR. PANAYOTIS, PETER K. THANOS (Brookhaven National Laboratory, Upton, NY 11973). Dopamine, a neurotransmitter that regulates cognition, movement, pleasure, and motivation, is related to the physiological and behavioral changes that are important aspects of aging, such as the loss of independence because of the deterioration of motor functions. This study investigated the relationship between locomotor activity and development in dopamine D4 receptors mice that were either single or group housed. Wild-type, Heterozygous, and Knockout D4 mice were used for this experiment (from age 10–100 weeks). Group housed mice were provided with an enrichment environment and single housed were in standard conditions. Their locomotor activity was recorded weekly. While the results are still in progress, the study will examine the change (if any) in locomotor activity across D4 genotype and in single versus group housed mice. These results will also examine the interaction of the D4 genotype with environment and locomotor activity. Future experiments will compare these findings in other dopamine receptors in mice.

Effect of Inhibitors on bFGF Signal Transduction Pathways in Human Endothelial Cells. AMANDA VREELAND (State University of New York at Stony Brook, Stony Brook, NY 11794) LOUIS A. PENA (Brookhaven National Laboratory, Upton, NY 11973). Ionizing radiation, such as that used in radiation therapy, causes cells to undergo apoptosis or programmed cell death. Basic Fibroblast Growth Factor (bFGF) has been shown to inhibit irradiated cells from undergoing apoptosis. bFGF promotes cell growth through several signal transduction cascades: Mitogen Activated Protein Kinase/ Extracellular-Signal Regulated Kinase (MAPK/ERK), Protein Kinase C (PKC), and Protein Kinase B (AKT/PKB) pathways. Conversely, the p38 MAPK pathway, which signals for a cell to undergo apoptosis, is activated when cells are placed under stressful conditions such as those experienced after a dose of ionizing radiation. When bFGF is added to Human Umbilical Vein Endothelial Cells (HUVEC), the level of radiation-induced apoptosis is reduced. If inhibitors of these signaling pathways are added, they will block the protective bFGF effect and restore the high levels of radiation-induced apoptosis. However, before these experiments can be performed, the effective dose range of the inhibitors and bFGF in HUVECs must be established. To determine this, we employed a reliable bioassay in a convenient format: cell proliferation measured by XTT cleavage in a 96-well plate. Cells are seeded and changed to low serum medium. The AKT/PKB pathway can be blocked with LY294002 hydrochloride which inhibits the activity of Phosphatidylinositol 3-Kinase (PI3K). The PKC pathway can be inhibited with U73122, which blocks the activation of phospholipase C-gamma (PLC γ). SB202190 inhibits the alpha and beta isoforms of p38 and induces apoptosis. bFGF is effective in the range of 5-10 ng/mL for this cell type. The IC50 for LY294002, U73122, and SB202190 are 3.3 μ M, 1.0 μ M and 33.0 μ M, respectively. The goal of this study was to optimize the dose of inhibitors that may block the proliferative and protective effects of bFGF in HUVECs. The results of this study are being used in ongoing radiation induced apoptosis assays, where the effects of inhibitors to bFGF radioprotection are being quantified.

Efficacy of Sub-Chronic Low-Dose S-gamma-vinyl GABA (GVG) in Inhibiting Methamphetamine-Induced Increases in [18F]Fluoro-Deoxyglucose Uptake. JESSICA PAI (New York University, New York, NY 10003) STEPHEN DEWEY (Brookhaven National Laboratory, Upton, NY 11973). In previous studies, gamma-vinyl-GABA (GVG, vigabatrin) has been shown to effectively inhibit methamphetamine-

induced increases in nucleus accumbens dopamine, demonstrating that GVG could serve as a potential treatment for methamphetamine (METH) addiction. In this study, the effect of sub-chronic low-dose S-GVG was examined to determine if a sub-chronic treatment schedule could successfully reduce [¹⁸F]fluoro-deoxyglucose (18FDG) uptake in brain regions where elevated metabolic activity is due to METH administration. Male Sprague-Dawley rats (n=10) received a static scan following a 45 minute awake 18FDG uptake using an R4 microPET imaging (Concorde Microsystems). Animals received a baseline scan (scan 1; mean weight = 136.6 ± 10.8g) and then after two days (scan 2) following an acute METH challenge (1 mg/kg). Over the course of the next 11 days, rats received METH and/or saline (5 pairings) intraperitoneally (I.P.) on alternate days. Animals (206.5 ± 17.9g) were again imaged (scan 3) following a METH challenge. Next, a sub-chronic low-dose GVG (75 mg/kg) schedule was administered I.P. for five consecutive days, then animals (238.6 ± 20.2g) received their final scan (scan 4) following a METH challenge. Results show global increases (18.9 ± 2.7%) in 18FDG uptake in specific brain regions of the brain previously demonstrated to respond to an acute METH challenge. Following the sub-chronic METH administration, increases in 18FDG uptake appeared to be regionally specific, with the greatest increase in the primary motor cortex (5.6%) and decreases occurring in the thalamus (7.9%) and cerebellum (6.4%). Images obtained following the 5-day S-GVG treatment showed global decreases (13.2 ± 4.3%) in 18FDG uptake in specific brain regions. These results indicate that sub-chronic low dose S-GVG effectively inhibits METH-induced increases in 18FDG uptake as seen by the hypometabolism in brain regions activated by METH administration. These findings support the potential use of S-GVG for the treatment of METH addiction.

*Functional Somatosensory Activation in Control and Wild Rats.

JOEL URENA (State University of New York at Buffalo, Buffalo, NY 14260) HELENE BENVENISTE (Brookhaven National Laboratory, Upton, NY 11973). For the past decade, scientists have studied rodent somatosensory (SS) function and have been able to localize external physical stimuli, such as electrical stimulation, to specific regions of the brain, particularly the SS cortex. One method of measuring SS activation is by using Blood-Oxygen-Level-Dependent (BOLD) functional Magnetic Resonance Imaging (fMRI). Neural activation corresponding to electrical stimulation results in a significant change in blood perfusion levels that can be measured via BOLD fMRI. The aim of this study is to measure and compare SS cortex activation elicited by forepaw and hind paw electrical stimulation between wild and laboratory Norway rats via BOLD fMRI. Because the common wild rat found in the North American region is of the Norway strain, SS activation in laboratory-housed Norway rats will be investigated to allow for comparison. It is hypothesized that SS activation in wild rats will be smaller and sharper because wild rats have to adapt to various environments, avoid predators and search for their own food. The rats were first anesthetized with isoflurane followed by a continuous IV infusion of a-chloralose. Electrodes were inserted in both forepaws and the left hind paw. One paw was stimulated at a time with the following paradigm: 69 seconds of rest, 30 seconds of stimulation, and 90 seconds of rest while MR images were acquired. Data was analyzed using the software STIMULATE. A Student's t-test was used to construct statistical activation maps. The average increase in BOLD signal corresponding to left forepaw stimulation among six control rats was 4.7%. The average increase in BOLD signal corresponding to right forepaw stimulation among five control rats was 5.6%. Recent attempts have been made to capture wild rats. However, the attempts were unsuccessful due to the small wild rat population on the Brookhaven National Laboratory campus. Plans will be made to capture wild rats off-campus.

Imaging Nanoparticles in Living Systems. JOSEPH CARRION (The City College of New York, New York, NY 10034) WYNNE SCHIFFER (Brookhaven National Laboratory, Upton, NY 11973). Nanotechnology and Quantum Dots in particular hold much promise for biomedical engineering since, by virtue of their size, nanomaterials can permeate many of the body's natural barriers. It is not, however, known how these nanometer-sized particles will disperse within living systems, nor has it been established what physiochemical properties such as size, surface modification, and core material will alter this in-vivo dispersion. In this study we use in-vivo imaging to look at the effects of [¹¹¹C] Cadmium Selenide/Zinc Sulfur (CdSe/ZnS) and [¹¹¹C] Gold nanoparticles (Au). Ten Swiss-Webster (SW) mice were injected with an intravenous bolus of thiol conjugated [¹¹¹C] Cadmium Selenide/Zinc Sulfur quantum dots (QDs) at two concentrations, both coated and uncoated with the surfactant Tween 80. Five of these mice were sacrificed immediately, and five were sacrificed after 6 weeks as part of the comprehensive

imaging studies. All mice organs harvested were placed in a 4% Formaldehyde/1% glutaraldehyde in phosphate buffer with 5% Sucrose added for Transmission Electron Microscopy visualization. The kidney and liver of the mice were cryosectioned and nanoparticle distribution at a light microscope level was visualized using the fluorescent properties of QDs to estimate accumulation. There appears to be a concentration dependent distribution in the mouse kidney and liver: animals injected with smaller concentration of QDs show less fluorescence at 470nm in kidney compared to animals receiving higher concentrations. High Performance Liquid Chromatography (HPLC, computer automated BAS System) with electrochemical detection was used to estimate concentration of CdSe/ZnS nanoparticles of 2 nanometer and 10 nanometer sizes. These studies used in-vivo imaging together with light microscopy to explore the effect of variations in size and surfactant coating on the dispersion of these particles in living systems. Image-guided localization with Micro-PET allows the modeling of distribution of [¹¹¹C] CdSe/ZnS nanoparticles of 2nm and 10nm size in a living system.

Parallel Changes in Behavior and Neurochemistry Resulting From Surgical Implantation into the Brains of Rats. DAVID FRUMBERG (Cornell University, Ithaca, NY 14853) WYNNE SCHIFFER (Brookhaven National Laboratory, Upton, NY 11973). Surgical implants into the brain can cause long-term behavioral and functional deficits in vivo. Using a routine surgical procedure, intracerebral stylets were stereotaxically inserted into the right striatum of anesthetized rats. Novel object recognition (NOR) tests were administered to subjects 3 days prior to and 3, 7, 14, and 56 days after surgery to assess intellectual performance. Metabolic imaging with 18F-fluorodeoxyglucose (18FDG) occurred 28 and 57 days after surgery. Behavioral deficits significantly appear 3 days post-injury, where performance has decreased by 17.3%; performance decreased by 24.3% after 7 days, 38.0% after 14 days, and 41.7% after 56 days. Subjects that did not receive implants devoted a mean of 57.1% of their investigation time with the novel object, while the mean for subjects that received implants was 50.2%. This observation suggests that animals with implants failed to recognize the familiar object as such. Normalized PET analyses demonstrated a significant decrease in glucose uptake after surgery in the entire hemisphere ipsilateral to the implant relative to the contralateral hemisphere. Greatest metabolic deficits occurred in the motor cortex (-16.4%; p=.0005), sensory cortex (-10.3%; p=.009), dorsal striatum (-13.7%; p=.007), and thalamus (-9.2%; p=.006) of the side of implantation compared to the intact side. Metabolic deficits in the motor cortex significantly correlated with a decline in general locomotion observed three days following the surgical implant (R²=0.63). No metabolic recovery was observed over the two-month period. These results imply that the window for treatment of open head injury in humans is much shorter than previously believed.

Rehabilitation and Implementation of Scintimammography Gamma Camera Integrated into a Stereotactic Core Biopsy Digital X-ray System. CLARISSA FREEMAN (Hampton University, Hampton, VA 23606) STAN MAJEWSKI (Thomas Jefferson National Accelerator Facility, Newport News, VA 23606). Biopsies are used to accurately confirm the presence of breast cancer when suspicious lesions are found. A biopsy is a small sampling of tissue that can be tested to determine whether there is malignancy. Approximately three out of every four women still have unnecessary biopsies. A scintimammography gamma camera integrated into a stereotactic core biopsy digital x-ray system may be used to reduce unnecessary biopsies. The scintimammography gamma camera is a custom-built mini gamma camera with an active area of 5.3 cm by 5.3 cm. It is based upon a 2 by 2 array of position-sensitive photomultiplier tubes made by Hamamatsu. The system obtains dynamic scintimammographic data by performing dynamic radiopharmaceutical uptake studies; these images can confirm or negate the need for a biopsy, leading to fewer unnecessary procedures. The objective of the project was to remove the system out of its clinical setting for repair and calibration. It has a primary detector head for most clinical settings, as well as a second detector to be used as an auxiliary. A new crystal map was created for the system, detector head energies were calibrated, and corrected images were taken. In addition, electrical components were replaced and appropriately labeled. For optimal stability, calibrations were performed using Kmax Sparrows NT development package. A dynamic energy range for detector head one was found to be 540 volts, and the second detector range was found to be 580 volts. The system was tested once all repairs were complete and calibrations were finalized. In the coming months, the system will be put into a clinical environment so that its performance can be tested against traditional detector systems.

The Efficacy of the National Ignitions Facility's Ergonomic Program. NAOMI SHAH (*University of California—San Diego, La Jolla, CA 92092*) STEVEN MCCONNELL (*Lawrence Livermore National Laboratory, Livermore, CA 94550*). Ergonomic injuries have become an increasing concern for office workers and their employers due to the rise in computer-based work. These injuries, as with all chronic injuries, are most prevalent in the older members of the work force due to a longer exposure to chronic insults to their bodies. In 2005, over half of the recorded illness/injury cases at the National Ignitions Facility (NIF) at Lawrence Livermore National Laboratory (LLNL) were ergonomic cases. In order to reduce the number of such cases and their associated costs, NIF has implemented an ergonomic program in which the goal is to evaluate their 1,200 employees. The current process of creating a list of employees who need an evaluation, making an appointment with the employees, performing the evaluation, and following up afterwards proved to have some problems which inhibit efficiency. To enhance the process of forming a list of employees for evaluations, a new database has been developed and is being tested. This allows the evaluator to receive daily updated lists. In order to easily set up appointments and yield a larger response rate, it was found that a Meeting Maker proposal followed by an Email works the best. The evaluator uses the NIF Comfort Survey to help assess the employee's work space; this survey proves to be sufficient in identifying the needs of the employee. Overall, the ergonomic program has made a good start in preventing further ergonomic injuries, and with implementation of the new recommendations, will prove to be an efficacious program.

***Tolerance of Rat's Spinal Cord to Dose-Fractionated Irradiation with Arrays of Parallel X-ray Microbeams.** SASHEEN FERGUSON (*Stony Brook University, Stony Brook, NY 11794*) AVRAHAM DILMANIAN (*Brookhaven National Laboratory, Upton, NY 11973*). It has been shown that single-exposure to arrays of parallel, synchrotron-generated x-ray microbeams is well tolerated by normal tissues in laboratory animals at doses up to several hundred Gy. The tissues studied include the brain and spinal cord of the rats. We examined such a tolerance to dose-fractionated irradiations with microbeam arrays. Rats were irradiated daily for four days with microbeam arrays made of 27- μm beams spaced 200 μm on-center. The daily in-beam incident dose was 400 Gy. The angles of the irradiations were 45° apart from each other. The animals were monitored by weighing and the behavioral test of "Open Field" to evaluate any potential loss of sensorimotor performance, and the results were compared to those in unirradiated controls. As of 15 days after the last irradiation the rats are gaining weight and performing normally in the Open Field test. They will be kept for one year. Afterwards these animals will be euthanized for histology.

Nuclear Sciences

Analysis of the Infrastructure That Will Support a Transition to a Hydrogen. TROY MITCHELL (*Roane State Community College, Harriaman, TN 37748*) JUAN FERRADA (*Oak Ridge National Laboratory, Oak Ridge, TN 37831*). The transition to a hydrogen economy is assumed to begin in 2020 with a total of 2.5 million hydrogen cars in seven cities including: Atlanta, Miami, San Francisco, Detroit, Houston, Chicago, and Los Angeles. Factors that affect the transition to a hydrogen economy are production, delivery, storage, and dispensing the hydrogen. Using data from the Department of Energy's Hydrogen Analysis (H2A) models, FLOW[®], a simulation program developed at Oak Ridge National Laboratory, can simulate the entire hydrogen economy for each one of the cities used in the analysis. Sensitivity and uncertainty analysis are applied to determine the affects of fluctuating feedstock prices and demand for hydrogen. According to the results of the H2A models, trucking of gaseous hydrogen was not a practical method of delivery. During this research it was found that Python™ is a user friendly object-oriented programming language. In terms of unit cost, natural gas reforming was found to be an effective production method at lower demands for hydrogen, and coal gasification was found to be more effective with higher demands of hydrogen. Steam methane reforming is an effective method of production and distribution, in terms of unit cost. Piping is an effective method to distribute hydrogen at low demands. Trucking is more cost effective when hydrogen demand is higher. Results of the analysis will be used to provide recommendations for the required infrastructure that will provide a better transition to a hydrogen economy from the current fossil fuel economy.

Candidates for New Transitions in ²⁵⁴No. DAVID GRAYSON (*University of Illinois at Urbana Champaign, Urbana, IL 61801*) TENG LEK KHOO (*Argonne National Laboratory, Argonne, IL 60439*). Several candidates for transitions in ²⁵⁴No have been observed in an

experiment performed at Argonne National Laboratory. The reaction ²⁰⁸Pb(⁴⁶Ca,2n)²⁵⁴No was used at beam energies of 219 and 223 MeV. In this report, gamma-gamma matrices were examined to find candidates that were coincident with previously known transitions in the ground state band of ²⁵⁴No. The candidates found were only evident at 223 MeV, which suggests that they come from parent states with high energies that are not populated at the lower 219 MeV beam energy. The strongest candidate was 469 keV. If this transition feeds in to the top of the previously observed ground state band, then it breaks the pattern of transition energies, which implies a change in structure at that energy. This would have implications for the width of a specific neutron "magic gap", and would help test theories of nuclear structure.

Development of a Beam Profile Diagnostics Device for the VENUS ECR Ion Source Beam Line. CARY PIINT (*University of Northern Iowa, Cedar Falls, IA 50614*) DANIELA LEITNER (*Lawrence Berkeley National Laboratory, Berkeley, CA 94720*). This work describes the design and development of the instrumentation for a beam profile diagnostics unit for the low energy beam transport line of the superconducting Electron Cyclotron Resonance (ECR) ion source VENUS (Versatile ECR ion source for Nuclear Science). VENUS is currently being commissioned at LBNL and serves as the prototype ECR injector source for next generation heavy ion accelerators. In order to enhance simulations of beam transport from extraction in VENUS, a measurement device (called a harp) consisting of a grid of thin conducting wires is placed into the beam line, directly downstream from extraction, to measure the beam profile. Utilizing the diagnostics unit developed and described in this work, the first measurements of the beam profile for a simple helium beam are presented. By changing the Glaser current to focus the ion beam onto the harp, the helium beam profiles illustrate that the extracted beam has the same symmetry as the plasma surface from which they are extracted, and not the uniform circular symmetry that is assumed in most simulation models. These results give quantitative insight into the enhancement of initial conditions needed for using simulations to give a physically accurate description of beam transport from extraction of an ECR source.

Directed Long Range Thermal Neutron Detection System. JEFFREY MAGEDANZ (*Oregon State University, Corvallis, OR 97333*) DR. RAYMOND KLANN (*Argonne National Laboratory, Argonne, IL 60439*). A long range thermal neutron detection system could be useful for determining whether a suspected location contains a neutron source. At long ranges, the flux of neutrons from the source becomes small compared to the flux of background neutrons. A bundle of collimator tubes made of a neutron absorbing material could be used to minimize the effect of background neutrons by only allowing neutrons coming from the direction of the source to reach the detector. Monte Carlo N-Particle transport code (MCNP) version 4c was used to simulate a detector with such a collimator bundle in order to study its potential and optimize the design. The simulations determined the response to a moderated californium-252 source at several distances as well as the response to background neutrons. It was determined that cadmium was not an adequate shielding material while materials containing boron, particularly enriched boron, performed well. A 100 cm² detector with a collimator was found to be reasonably certain to detect a source producing 105 neutrons per second at 30 meters in less than a half hour. However, for greater distances, the time required for detection becomes large. Further research will compare the simulation results to experimental results.

Gamma-Ray Spectroscopy of Dysprosium-152. JASON KOZEMCZAK (*Greenville College, Greenville, IL 62246*) ROBERT V. F. JANSSENS (*Argonne National Laboratory, Argonne, IL 60439*). Nuclei at high excitation energy and spin go through shape deformations, which are a result of interplay between collective and single-particle effects, as they decay to their ground states. Of particular interest are the super-deformed (SD) bands in the A~150 region. In order to assign correct excitation energy, spin, and parity to these SD bands, linking transitions must be observed between the SD bands and the lower-lying normal deformed (ND) bands. ¹⁵²Dy is one of only a few nuclei where these linking transitions have been observed. The GAMMASPHERE group at Argonne National Laboratory wishes to map the complete decay process of this isotope so that it can be used to develop a realistic model of this process that will give good predictions of the spins and excitation energies of SD bands where linking transitions have not been observed. To correctly model the decay, the single-particle spectra in ¹⁵²Dy have been analyzed to map out the yrast line to the highest angular momentum state possible. The fusion reaction ¹⁰⁸Pd(⁴⁶Ca,4n)¹⁵²Dy with a beam energy of 191 MeV was used to populate the ND and SD bands in ¹⁵²Dy, and the single-particle level scheme was constructed using triple and quadruple coincidence events.

Angular distribution data have been analyzed to determine the spins of these states. The analysis indicates that the single-particle states stay competitive with the collective states up to very high excitation energy and spin (at least 20 MeV and 48h, respectively). Furthermore, the coincidence analysis has raised questions concerning the placement of a linking transition from a triaxial band to the ND states. Further analysis is needed to place this transition, as such linking transitions allow proper spin and excitation assignment to the triaxial states in question.

Investigating Applications for the Three-Dimensional Design Information Verification System at Department of Energy Facilities in the United States. AARON HANSON (*Minnesota State University, Mankato, Mankato, MN 56055*) CAMERON COATES (*Oak Ridge National Laboratory, Oak Ridge, TN 37831*). The current method used for the annual verification of design information for nuclear facilities under International Atomic Energy Agency Safeguards can be labor intensive since this involves manually verifying that a facility has not been altered over the period of time. This process generally involves comparing new pictures of the facility to previous pictures which can require a great deal of time and effort. A new method was proposed, developed by the European Union's Joint Research Center, which involves using a Three-Dimensional Design Information Verification system. This system uses a laser scanner to take panoramic images of an environment. These two-dimensional images can be made into three-dimensional meshes using accompanying software. The software can automatically compare two three-dimensional images of the same environment and find differences between them. The first of the scans is considered to be a reference scan. The later scan is used for verification, and the verification scan is compared to the reference scan to determine how the environment has changed since the reference scan was taken. In this project, three different environments were set up in order to test the systems capabilities. The first environment was used to determine how well the system could detect large movements (0.5m to 1m) of objects within the environment. The second environment was used to determine how well the system could detect small movements (0.002m to 0.02m) of objects within the environment. The third environment was used to determine if the system can detect the addition of objects to a processing environment. Different conditions were also incorporated into the environments such as making the laser scan through glass and/or water. An analysis of the resulting data showed that the system was able to detect both small and large movements to an accuracy of approximately 4mm, as well as find new objects that were added to the environment. The system is capable of scanning through glass, but not water. The high level of accuracy and the automatic capabilities of the system mean that it will be a significant improvement on the current methods of design information verification for nuclear facilities, although the inability of the system to scan through water might lead to difficulty in some areas that hold large amounts of liquid. Further studies should focus on overcoming this difficulty.

Optimization of the CLAIRE Ion Beam Extraction and Transport System Using Computer Simulations. NAN XU (*University of California-Berkeley, Berkeley, CA 94720*) DAMON S. TODD (*Lawrence Berkeley National Laboratory, Berkeley, CA 94720*). Center for Low Energy Astrophysics and Interdisciplinary Research (CLAIRE) is a proposed nuclear astrophysics facility under design at the Lawrence Berkeley National Laboratory. The facility will measure cross sections relevant to stellar burning, namely ${}^3\text{He}({}_4\text{He},\alpha){}_7\text{Be}$, a reaction which is one of the leading sources of uncertainty when correlating solar neutrino data with theoretical solar models. A beam line concept has been developed to extract and transport a tightly focused (sub-centimeter), high current (100 mA), low energy (50 keV-300 keV) ${}^3\text{He}^+$ ion beam to a high density gas jet target. The beam is first extracted from a plasma ion source, and is then focused by two solenoid lenses. An acceleration column is placed to accelerate the beam to a higher energy. The envelope of the accelerated beam is kept as small as possible by another lens before going through a 60 analyzing magnet for filtering. The last focusing solenoid lens produces the desired beam size on the target. An extensive simulation program was employed to optimize the extraction and the transport of a 100 mA, ${}^3\text{He}^+$ beam at 50 keV. The source extraction electrodes will have to undergo further shaping including rounding of corners, but provide the preliminary source configuration that can be used to design the remainder to the beam transport system. Initial work was done on the acceleration column to insure that accelerated beams can arrive at the source with similar qualities, but further modifications of the simulation are needed and further fine tuning must take place for the final design. The detailed analysis of this simulation will be shown and discussed.

Previous, Current, and Predicted Trends for Applications Using Source Material as Covered by the U.S. Nuclear Regulatory Commission General License. CASSANDRA BEATTY (*Cornell University, Ithaca, NY 14850*) EVA HICKEY (*Pacific Northwest National Laboratory, Richland, WA 99352*). With sensitivity to terrorism having heightened since 9/11 and the nuclear energy industry planning to expand in the near future, monitoring the use of fissile and fissionable materials is becoming ever more important. The products and processes that use naturally occurring radioactive materials must be reviewed not only to protect worldwide radioactive resources but the general public as well. The U.S. Nuclear Regulatory Commission (NRC) provides a general license for agencies to use and transfer not more than 15 pounds of materials that contain 0.05% by weight uranium, thorium, or any combination thereof. Regardless, current industrial trends indicate a general decline in the use of thorium and uranium. Thorium was traditionally used in ceramics for refractory purposes but now is primarily used in scientific research and a few electrical applications. Uranium, once popular in pigments and glazes, is now almost entirely limited to military applications that require special licensure and scientific research. Industry substitutes and alternate processes that do not involve uranium and thorium are becoming increasingly popular. If regulatory pressure and public sentiment continue to impede the ease of use of naturally occurring radioactive materials, the NRC general license may become obsolete with respect to uranium and thorium.

Proton Recoil Detectors and Fission Ionization Chambers for Neutron Dosimetry. BRENT WILSON (*Merced College, Merced, CA 95340*) PEGGY MCMAHAN (*Lawrence Berkeley National Laboratory, Berkeley, CA 94720*). Neutrons are ionizing particles, which cause damage to human cells, including astronauts, and electronics. They are difficult to directly detect due to a neutral charge; however, there are several different ways to develop a neutron detector to measure neutron flux indirectly. This research involved the creation and development of two neutron detectors: the prototypes of a proton recoil detector and a fission ionization chamber. The intention was to measure neutrons of 5 to 30 MeV, but since the neutron beam was not available, a proton beam was used instead. A proton recoil detector is composed of a solid-state detector, which electronically counts how many protons are being recoiled out of a plastic medium to determine the incident number of neutrons. In this particular prototype, a 50.0 MeV proton beam was used to show that this prototype worked for the first phase of testing. The next phase of testing will include neutron beams with energies between 5 and 30 MeV for actual proton recoil and a plastic medium containing an ample amount of hydrogen, like polyethylene terephthalate (Mylar). A fission ionization chamber indirectly counts the number of neutrons by means of a gas-filled chamber and fissile foil (e.g., thorium), in which fission fragments produce ion charges, so that measuring the total charge count leads to a calculation of neutron flux. In this particular prototype, an americium-beryllium source was used as a neutron emitter for testing the ion charge collection. The chamber was filled with nitrogen gas at one atmosphere pressure and contained two electrodes, biased to -325 V, and the other used for ion collection to electronics. The prototype fission ionization chamber has just been completed, and tests for functionality are currently being conducted. The next prototype of the fission ionization chamber will include evaporation of the ${}^{232}\text{Th}$ onto a window and neutron tests from 5 to 30 MeV in beam.

Study of Beam Spin Asymmetry in Exclusive π^+ Production. IAN HOWLEY (*The College of William and Mary, Williamsburg, VA 23186*) HARUT AVAKIAN (*Thomas Jefferson National Accelerator Facility, Newport News, VA 23606*). Describing and understanding atomic nuclei is a puzzle that has intrigued scientists for decades. Approximately ten years ago, a way to describe nucleon structure, referred to as Generalized Parton Distribution (GPD), was introduced. GPDs are a way of describing scattering and production processes in a single framework. Deeply Virtual Compton Scattering (DVCS) is a process that scatters a photon from a proton and detects a scattered electron, a proton, and one photon in the final state. From DVCS, GPDs can be extracted in order to lead us to a more complete picture of nucleon structure. The focus of this study is to understand the beam spin asymmetry (BSA) of the neutral π^0 meson, a main source of background during the DVCS process. To calculate the BSA, the number of π^0 events with positive helicity (spin) and negative helicity were counted by integrating histograms with Gaussians fits. It is shown that there is a significant non-zero BSA in production of exclusive π^+ , namely 0.0655 ± 0.0022 . In the analysis of previous experiments, the BSA of π^+ was assumed to be zero and therefore ignored. Now, since it is proven to exist, it can be taken into account in future DVCS studies.

A deeper understanding of background processes (π^+) in the DVCS will allow precision measurements of GPDs, providing new insight concerning the structure of nucleons.

System Dynamics. JAIMEE WILLIAMS (*Brigham Young University, Provo, UT 84602*) JACOB JACOBSON (*Idaho National Laboratory, Idaho Falls, ID 83415*). VISION (Verifiable Fuel Cycle Simulation Model) is a dynamic model of the nuclear fuel cycle developed at the Idaho National Laboratory (INL). The model tracks the mass of useable fuel, dangerous isotopes, and weapons useable material for adding different types of fuel cycle scenarios to the U.S. reactor fleet. Speed and ease of use differentiate VISION from other more complex models. VISION was developed in a modeling program called POWERSIM, which has uncertainty analysis built in which is necessary to gain a valuable estimation of the cost associated with nuclear fuel cycle. Unfortunately POWERSIM's sampling method fails to distinguish the economic sub-model from the main VISION model. A consequence is that POWERSIM reruns the entire model each time the economic sub-model is run; although no new information is gained. A good sampling size of 10,000 runs at thirty seconds per run would take three and a half days. The objective of this project was to develop a simple sampling method implementing a Latin hypercube algorithm. Latin Hypercube Sampling (LHS) is a stratified sampling technique where the random variable distributions are divided into equal probability intervals. A probability is randomly selected from within each interval for each basic event. Generally, LHS will require fewer samples than simple Monte Carlo Sampling. However, due to the stratification method used, it may take longer to generate a value than for a Monte Carlo Sampling however, the LHS technique will give us a more accurate cost analysis. The Latin hypercube algorithm we implemented works by dividing up the cost distributions into two hundred equally probable events and randomly sampling from them. The key to our approach was decoupling the economic sub-model from the main model, meaning we only ran the VISION model once for numerous iterations on the economics sub-model. Our new approach allowed us to sample 10,000 runs in two minutes, which is a vast improvement over the old sampling methods. The approach implemented allows VISION users to easily access cost analysis data without waiting for extended periods of time. This is in keeping with the objectives sought by VISION; speed and ease of use.

The Optimization of Environmental Sample Data Analysis and Visualization. MATTHEW ANDERSEN (*Southern Adventist University, Collegedale, TN 37315*) DIANE FISCHER (*Oak Ridge National Laboratory, Oak Ridge, TN 37831*). For the last 10 years, the International Atomic Energy Agency (IAEA) has been collecting, organizing, and storing vast amounts of environmental sampling (ES) data. ES data are used by the IAEA to detect undeclared nuclear activities all across the world. Currently, the analysis of this data is time-consuming and inefficient due to a lack of integrated data evaluation tools. The first objective in providing a solution to this problem was to evaluate multiple software suites used in data modeling. The second objective was to develop an easy-to-use, multifunctional graphical user interface (GUI) that allows quick customization and visualization of ES data analysis information using one, or a combination of several, of the options explored in the first objective. The evaluation process included examining the software's documentation; downloading and testing freeware, trialware, or full versions of the software; and attending software tutorials. Initial models for the interface were based upon current IAEA methodologies and inquiries concerning desired features for the data analysis and visualization output. Several books on nuclear forensics and programming were used in the maturing of the GUI's design and functionality. The finalized GUI was developed for the Microsoft Excel 2003 software package using Excel's integrated Visual Basic for Applications programming language. This new interface allows users to more efficiently add to or modify the visualization of the data. Fast access to functionality not previously available was also incorporated. New features include the ability to plot multiple data sets on the same graph, based on country, facility name, facility code, material balance area, location, or any combination of these, as well as the ability to remove specific data sets from a given graph. This new GUI gives the IAEA a graphical tool that will aid in understanding and analyzing ES data. The improvements offered by the software will allow personnel to make more efficient use of their time while having the tools needed to help them make more-informed decisions. The customization and functionality of this new model permits adaptation to many other data analysis and visualization scenarios, not just those involved with nuclear safeguards data. As with any software, future work will include adjustment to new technology and the implementation of additional features as output requirements change.

The Standardization and Upgrade of Isotopic Enrichment Measurement Software through the Analysis of Enriched Uranium Standards. LINDSAY OWENS (*Brigham Young University-Idaho, Rexburg, ID 83460*) MARY D. EIPELDAUER (*Oak Ridge National Laboratory, Oak Ridge, TN 37831*). There are many accepted isotopic enrichment measurement software packages used to identify and measure levels of enriched uranium and plutonium. The basis for the following project has come about in response to inconsistencies in the types and versions of software being used. In addition to comparing the accepted software, the goal is to decide on a single international standard. The United States Department of Energy/National Nuclear Security Administration through Oak Ridge National Laboratory (ORNL), Lawrence Livermore National Laboratory, Los Alamos National Laboratory, in conjunction with the Brazilian-Argentine Agency for Accounting and Control of Nuclear Materials, are testing and evaluating isotopic enrichment measurement software packages to identify the most effective software. The software packages undergoing testing at ORNL are: WinU235, NaIGEM, MGAU (v3.21 and v4.0), and ISOTOPIC. In order to test these software programs, the Safeguards Laboratory at ORNL is conducting eight experiments. The setups for the experiments consist of germanium and sodium iodide detectors in combination with a variety of multi-channel analyzers. The experiments have been prearranged to include a variety of different measurement distances, attenuator materials, and thicknesses of attenuators. The eight uranium standards used range from depleted uranium (0.31% enriched) up to highly enriched uranium (93.17% enriched). For each standard, spectra are collected for 1000 seconds and repeated for six trials. In Experiment 1, which used a Canberra Planar germanium detector with a MCA-166 multi-channel analyzer, the spectra were analyzed using MGAU v3.21, and the six trials for each spectrum were condensed by calculating the averages for the following categories: Measured Percentage of U-235 - Declared Percentage of U-235, Standard Deviation [Measured - Declared/Declared Weight Percentage], Measured Percentage of U-235, Absolute Error, and Percent Error. The work completed thus far is a small part of a much larger project, and thousands of spectra remain to be analyzed. In order to better understand how the software programs compare to each other and eventually decide upon a single international standard, the data gleaned from analyzing the spectra must be compressed and organized in such a way that a comparison can be made. A significant amount of work remains in the present efforts to standardize and upgrade existing isotopic enrichment measurement software.

Thermo-hydraulic Design and Analysis of Lead Coolant Test Facility (LCTF). RYAN DALLING (*Brigham Young University-Idaho, Rexburg, ID 83440*) SOLI KHERICHA (*Idaho National Laboratory, Idaho Falls, ID 83415*). The Lead Fast Reactor (LFR) is one of the six concepts selected on the Generation IV Road Map by the Generation IV International Forum. If certain technical innovations can be proven in the LFR reactor concept, it will provide a unique and attractive nuclear energy system. Thus, advancement of the LRF beyond the conceptual phase will require lab demonstrations and tests involving many research and development issues. The Idaho National Laboratory (INL) is working on such test loops by further developing the LCTF. The laboratory demonstration of key attributes of the LFR design can be provided by the LCTF which would conduct such tests on certain issues. The thermo-hydraulic tests will allow the LCTF to prove the functionality of the many attractive attributes provided by the LFR. In order to build the LCTF, a thermo-hydraulic analysis of the LCTF was conducted to produce a proposed preliminary design and concept. This analysis was first conducted using a Microsoft Excel spreadsheet with lead as the primary coolant, and then conducted in RELAP5-3d with lead-bismuth as the primary coolant. An envelope of variation of various LCTF parameters providing different design options was created using the results of these analyses, which will facilitate any further R&D needs in the future when the LCTF is to be further developed. The two models (Excel, RELAP5-3d) provide sufficient, valuable information to make preliminary design decisions of the LCTF.

Tritium Diffusivity in Metals; Response of a Tritium Monitor To Cs-137 Gammas; Dose-Response Relationship Function of Species Mass, DNA Content and Chromosomes. CHRISTOPHER COPELAND (*Morehouse College, Atlanta, GA 30314*) MICHAEL SINGH (*Lawrence Livermore National Laboratory, Livermore, CA 94550*). Tritium will be used as a fuel for the NIF ignition experiments. Understanding its behavior in various materials is important to evaluate inventory and to develop safety plans for handling tritiated hardware. Since tritium monitors will be used for evaluating airborne tritium concentration, the response of tritium monitor, an ion chamber, was calculated as a function of distance from the center of the chamber

to the source location. A Cs-137 gamma check source was used to determine the experimental response of the meter as a function of distance from the center of the chamber. Cs-137 emits beta radiation (95% – 0.514 MeV, and 5% – 1.18 MeV; with 0.661 MeV gammas). Its half-life is about 30.07 years. By correlating a simple relationship between the tritium energy deposition and gamma energy deposit in the chamber volume, an external gamma source can be used to both check the response and calibrate the meter precisely. Also had a brief opportunity to study the radiation dose-response relationship, primarily for acute doses, for various species as function of DNA content, number of chromosomes, body mass, etc. Some discussions were held in the areas of radiobiology and nuclear medicine.

Physics

²⁴Al Level Structure and the Corresponding ²³Mg(p, α) ²⁴Al Astrophysical Reaction Rate. CHRISTOPHER DEATRICK (*Western Michigan University, Kalamazoo, MI 49008*) DARIUSZ SEWERYNIAK (*Argonne National Laboratory, Argonne, IL 60439*). In order to better understand the processes involved in heavy nuclide production in explosive stellar environments, the breakout process from the CNO cycles to the NeNa cycle and to the MgAl cycle must be quantified. Better numerical values of proton capture rates are deduced for the ²³Mg(p, α) ²⁴Al reaction by studying nuclear energy levels in ²⁴Al above the proton capture threshold using high-resolution α -ray spectroscopy and α -ray angular distribution analysis. ²⁴Al nuclei were produced by colliding an ¹⁶O beam delivered by the Argonne Tandem-Linac Accelerator System with a ¹⁰B target. Excited states in ²⁴Al were populated after evaporating two neutrons from the compound system. Gamma rays emitted from these states were detected with the GAMASPHERE array of Compton-suppressed Ge detectors. The Argonne Fragment Mass Analyzer was used to separate reaction products from the beam and assign mass and atomic numbers. As a result, states above and below the proton threshold were studied in detail resulting in an improved ²⁴Al level scheme. The analysis of the first state above the proton threshold indicates that the reaction rate contribution of this state could differ by a factor of up to 9 from that of previous calculations in the 0.1–0.5 GK temperature range.

3D Simulation for the ATLAS Education and Outreach Group. BRIAN AMADIO (*Rensselaer Polytechnic Institute, Troy, NY 12180*) MICHAEL BARNETT (*Lawrence Berkeley National Laboratory, Berkeley, CA 94720*). ATLAS is a particle detector under construction at the Large Hadron Collider facility at the CERN Laboratory in Geneva, Switzerland. The project will be the most expansive physics experiment ever attempted. The ATLAS Education and Outreach Group was started to provide information to students and the general public about the importance of this project. A three-dimensional interactive simulation of ATLAS was created, which allows users to explore the detector. This simulation, named the ATLAS Multimedia Educational Laboratory for Interactive Analysis (AMELIA), allows users to view detailed models of each part of the detector, as well as view event data in 3D. A similar project is called ATLANTIS, which allows users to examine events in only two dimensions. Currently ATLANTIS allows more sophisticated analysis of events. AMELIA will provide similar functionality, but in a more intuitive way, which will be much friendlier to the public.

A Catalog of Candidate High-Redshift Blazars for GLAST. TERSI ARIAS (*San Francisco State University, San Francisco, CA 94132*) JENNIFER CARSON (*Stanford Linear Accelerator Center, Stanford, CA 94025*). High-redshift blazars are promising candidates for detection by the Gamma-ray Large Area Space Telescope (GLAST). GLAST, expected to be launched in the Fall of 2007, is a high-energy gamma-ray observatory designed for making observations of celestial gamma-ray sources in the energy band extending from 10 MeV to more than 200 GeV. It is estimated that GLAST will find several thousand blazars. The motivations for measuring the gamma-ray emission from distant blazars include the study of the high-energy emission processes occurring in these sources and an indirect measurement of the extragalactic background light. In anticipation of the launch of GLAST we have compiled a catalog of candidate high-redshift blazars. The criteria for sources chosen for the catalog were: high radio emission, high redshift, and a flat radio spectrum. A preliminary list of 307 radio sources brighter than 70mJy with a redshift $z = 2.5$ was acquired using data from the NASA Extragalactic Database. Flux measurements of each source were obtained at two or more radio frequencies from surveys and catalogs to calculate their radio spectral indices α . The sources with a flat-radio spectrum ($\alpha = 0.5$) were selected for the catalog, and the final catalog includes about 200 sources.

A Geant4 Simulation of the COUPP Bubble Chamber. CHARLES CAPPS (*Carnegie Mellon University, Pittsburgh, PA 15289*) ANDREW SONNENSCHNEIN (*Fermi National Accelerator Laboratory, Batavia, IL 60510*). It is known that a sensitivity on the order of 1 event per year per ton of detector material is necessary to detect a WIMP (Weakly Interacting Massive Particle) dark matter candidate. After successful veto of cosmic radiation, the neutron background will become the greatest obstacle for COUPP (Chicagoland Observatory for Underground Particle Physics) to achieve this level of sensitivity. Thus, understanding the COUPP bubble chamber's response to low-energy neutrons (< 50 MeV) is crucial. A Geant4 simulation of the COUPP bubble chamber response to an Am/Be neutron source is described. The recoil energy spectra given by the simulation are presented. Simulation results of event rate as a function of chamber pressure are compared to experimental data. Moreover, multiple bubble events—indicative of neutrons—are examined. The ratio of single to multiple bubble events is determined for different energy thresholds. To verify Geant4 for neutrons in this energy regime, cross-sections and differential cross-sections are computed from the simulation and compared to the JENDL, JEFF, and ENDF nuclear databases. Elements present in the COUPP experiment are considered. Good agreement is found between simulation cross-sections and the above nuclear databases.

A Numerical Model of the Critical Charge Density Surface of Ultra High Energy Cosmic Ray Induced Extensive Air Showers Using the SCILAB Programming Language. ALLEN SHARPER (*Florida A&M University, Tallahassee, FL 32301*) HELIO TAKAI (*Brookhaven National Laboratory, Upton, NY 11973*). A numerical model of the critical charge density surface of ultra high-energy cosmic ray (UHECR) induced extensive air showers (EAS) has been computed. The critical charge density surface defines the surface for specular reflection of radio waves with frequency less than the natural oscillation frequency (plasma frequency) of the EAS charges. Using a numerical model to understand how radio waves reflect from the air shower will help improve the design of devices (antennas, arrays) used to detect the reflected waves. The numerical model will allow the power and direction of the reflected waves to be calculated which will provide a map of the spatial distribution of reflected wave power and polarization incident to the surface of the earth. The program of the numerical model, written in the SCILAB language, calculates the density of ionization electrons as a function of radial distance from the shower axis and location along the axis. The cosmic ray tracing model is part of the Mixed Apparatus for Radar investigation of Cosmic-rays of High Ionization (MARIACHI) project. The MARIACHI project, consist of research that investigates an unconventional way of detecting UHECR. Based upon a method successfully used to detect meteors entering the upper atmosphere. Mariachi seeks to listen to television signals reflected off the ionization trail of an UHECR.

A Plasma Gun for the Next Generation of Spallation Neutron Source H⁻ Ion Sources. JUSTIN CARMICHAEL (*Worcester Polytechnic Institute, Worcester, MA 01609*) ROBERT F. WELTON (*Oak Ridge National Laboratory, Oak Ridge, TN 37831*). The ion source for the Spallation Neutron Source (SNS) is required produce 40-50 mA of H⁻ current depending on emittance with a duty factor of ~7% for baseline facility operation. The SNS Power Upgrade Project requires this current to be increased to 75–100 mA at the same duty factor. In its present form, the baseline SNS ion source is unable to deliver this performance over sustained periods of time. A new generation of RF-driven, multicusp, ion sources based on external antennas are therefore being designed to meet these requirements. It was found that by injecting a stream of plasma particles from a simple, steady-state, DC glow-discharge into the RF-plasma (i) H⁻ production can be dramatically increased and (ii) H⁻ pulse rise time can be significantly reduced. The design of a suitable plasma gun is presented which features a hollow anode and mechanical compatibility with the new ion sources. The Finite Element Method (FEM) has been employed to optimize the design: coupled fluid dynamic, heat transfer, mechanical stress and deformation, and ion/electron trajectory simulations were performed. Several design improvements over earlier versions were implemented such as the addition of an extraction system. The FEM simulations showed that the design of the new plasma gun is sufficient to handle the thermal stresses resulting from a 1 kW load on the cathode face. The ion/electron simulations demonstrated a high degree of control over the plasma beam, allowing for manipulation of the intensity, mean energy, and divergence of the streaming plasma. The extraction system also allows for selective emission of electrons or ions. It is anticipated that the plasma beam can be optimized with the extraction system to significantly increase the H⁻ current in the new ion sources.

A Portable Water Cherenkov Detector: Measuring Particle Flux at Different Altitudes. LUKAS BAUMGARTEL (*University of New Mexico, Albuquerque, NM 87131*) BRENDA DINGUS (*Los Alamos National Laboratory, Los Alamos, NM 87545*). High-energy cosmic particles initiate extensive air showers (EAS) as they interact with the air molecules in Earth's upper atmosphere. If the primary particle carries sufficient energy, the shower reaches the ground. With an array of photo-multiplier tubes (PMT's) located in a pool of water, the direction and energy of the primary particle can be reconstructed from the Cherenkov light generated as the EAS hits the detector. Milagro is one such detector, and has observed high energy (~1TeV) gammas and protons from high energy cosmic phenomena such as active galactic nuclei and supernova. A new detector called HAWC (High Altitude Water Cherenkov), similar to Milagro but with new electronics and high-altitude location (4000m), data was taken at University of New Mexico to perfect the measurement method and to characterize how other factors, such as weather, tank configuration, and power sources affect count rates. Once these variables were well understood, the detector was used to measure particle flux at four different altitudes: 1540m, 2650m, 3231m, and 4308m. The rates of the low energy electromagnetic particles were found to increase with altitude, and had values of 4.38 kHz, 4.82 kHz, 5.50 kHz, and 6.92 kHz, respectively. The 2650m data was taken at the Milagro site as a reference point. Based on the current data acquisition and analysis algorithm used for Milagro, singles rates at the HAWC site should be less than a factor of two greater than they are at Milagro. The rates measured at >4000m were 1.44 times greater than the rates at Milagro, leading to the conclusion that singles rates at a HAWC site >4000m will have a negligible effect on triggering and pulse height measurement.

A Preliminary CCD Cosmetic Grading System for the Dark Energy Survey Camera Focal Plane CCDs. SARAH CARLSON (*DePauw University, Greencastle, IN 46135*) JUAN ESTRADA (*Fermi National Accelerator Laboratory, Batavia, IL 60510*). The Dark Energy Survey (DES) is a 5000 sq-degrees sky survey that will strive to make more precise measurements of dark energy. The DES team at Fermilab is responsible for the construction of the Dark Energy Camera (DECam) that will be mounted along with corrective optics and electronics on the Blanco 4-meter telescope at the Cerro Tololo Inter-American Observatory (CTIO) in Chile. The camera will be comprised of 62 image charge-coupled devices (CCDs) and 8 guiding, focusing and aligning CCDs. These CCDs are made of silicon and manufactured at Lawrence-Berkeley National Laboratory (LBNL). Part of the task of building the DECam is understanding how each CCD functions. This understanding includes knowing the limitations of each CCD. Cosmetic defects can be crippling to the performance of a CCD. Cosmetic defects include white and dark pixels, bad columns, as well as defects caused by dark current and quantum efficiency (QE) non-uniformity problems. Dark current is a small electric current generated by the thermal motion of the silicon atoms in the CCD. QE is the measure of the CCD's sensitivity to a certain wavelength. Using the popular astronomical source detection program Source Extractor we make two separate analyses: a flat-fielding analysis and a uniformity analysis which includes both the dark current and QE uniformity. Catalogs of all the defects found are created for each analysis and analyzed. To be an acceptable candidate for the DECam focal plane, each CCD must meet the requirement of no more than 5% non-usable image area. Using this requirement as a starting point, we have devised a preliminary cosmetic grading system to be used for each CCD. Each CCD will be given two grades, one for the flat-fielding analysis and one for the uniformity analysis. The CCD will receive a grade of 0 if the affected area is 2.5% or less of the total CCD area. A grade of 1 will be given if the affected area is between 2.5% and 5% of the total CCD area. A grade of 2 will be given if the affected area is 5% or more of the total CCD area. Our logic for giving each CCD two grades instead of one overall grade is that we will be able to better characterize CCDs, and if the occasion should arise that we need to pick between groups of CCDs for the DECam focal plane the two grades will assist us in making our choice.

A Study of Gas Electron Multiplier (GEM) Foils. MATTHEW RUMORE (*Worcester Polytechnic Institute, Worcester, MA 01609*) CRAIG WOODY (*Brookhaven National Laboratory, Upton, NY 11973*). Advances have been made in the field of high-energy nuclear physics due to the increased usage of Gas Electron Multiplier (GEM) foils, which are known for their versatility and their ability to detect and amplify charge. For instance, GEM foils will be implemented in the Pioneering High Energy Nuclear Interaction eXperiment (PHENIX) and Solenoidal Tracker At RHIC (STAR) experiments at the Relativistic Heavy Ion Collider (RHIC) for the detection of signals from high-energy particle interactions. The reliable production of GEM foils depends on

a study of their properties and operating conditions. Two of the most important properties are the absolute gain and the gain stability over time. To test the gain, each foil is placed in an Argon/Carbon Dioxide environment in the ratio of 70:30. An alpha particle emitted above the foil by an Americium-241 source ionizes the gas and produces a cluster of electrons. This primary charge is then collected and amplified by the GEM foil. The amplified signals are read out through a conductive pad on the bottom of the GEM detector using a digital oscilloscope. Because the amount of primary charge is known, the absolute gain will be calculated for each GEM foil as a function of voltage. The gain stability measurements entail taking successive gain measurements over time for a constant voltage. The manufacturing process strongly influences the performance of each GEM foil. As a result, a number of foils produced under different manufacturing conditions were studied in terms of their overall gain and gain stability. This study, which will mostly likely continue until August 2006, will allow the scientific community to understand the properties of the GEM foils and improve the ability to manufacture better foils in the future.

A Twin Ionization Chamber Arrangement for the Study of $^{12}\text{C}(\alpha,\alpha)^{16}\text{O}$ Through the β -Delayed a Spectrum of ^{16}N . ALESSANDRO LAURO (*University of Chicago, Chicago, IL 60637*) ERNST REHM (*Argonne National Laboratory, Argonne, IL 60439*). The most fundamental reactions that describe the complex process of helium burning during stellar evolution include the $^{12}\text{C}(\alpha,\alpha)^{16}\text{O}$ reaction and the $3\ ^4\text{He} + \alpha$ reaction. While the latter has been studied quantitatively over the last decades, the properties of the $^{12}\text{C}(\alpha,\alpha)^{16}\text{O}$ are surrounded by a great deal of uncertainty due to its very small cross section of $10^{-41}\ \text{cm}^2$. Despite this restriction, the $^{12}\text{C}(\alpha,\alpha)^{16}\text{O}$ reaction can be studied indirectly by observing the β -delayed a spectrum of ^{16}N . While it is energetically impossible for ground state ^{16}O to a decay to ^{12}C , it is possible to examine $^{16}\text{O}^*$, excited states of ^{16}O , that result from the β -decay of ^{16}N . Even though the branching ratio of this reaction favors a decay over a decay by a factor of about 10^5 , a precise measurement of a-particles can be carried out by a specially designed dual twin ionization chamber located at the Argonne Tandem Linear Accelerator System (ATLAS) at Argonne National Laboratory. An important step in this experiment involves the calibration of the ionization chamber using a Pu-Be neutron source in order to test the a emission produced by the $^{10}\text{B}(n,\alpha)^7\text{Li}$ and $^9\text{Li}(n,\alpha)^7\text{t}$ reactions. It is from this procedure that a new method of obtaining information about the emission angle of a-particles from the source has been found.

Afterglow Radiation from Gamma-Ray Bursts. HUGH DESMOND (*Katholieke Universiteit Leuven, Leuven, BELGIUM 03000*) WEIQUN ZHANG (*Stanford Linear Accelerator Center, Stanford, CA 94025*). Gamma-ray bursts (GRB) are huge fluxes of gamma rays that appear randomly in the sky about once a day. It is now commonly accepted that GRBs are caused by a stellar object shooting off a powerful plasma jet along its rotation axis. After the initial outburst of gamma rays, a lower intensity radiation remains, called the afterglow. Using the data from a hydrodynamical numerical simulation that models the dynamics of the jet, we calculated the expected light curve of the afterglow radiation that would be observed on earth. We calculated the light curve and spectrum and compared them to the light curves and spectra predicted by two analytical models of the expansion of the jet (which are based on the Blandford and McKee solution of a relativistic isotropic expansion; see Sari's model and Granot's model). We found that the light curve did not decay as fast as predicted by Sari; the predictions by Granot were largely corroborated. Some results, however, did not match Granot's predictions, and more research is needed to explain these discrepancies.

Analysis of Beam Deviation Due to Quadrupole Misalignment Caused by Ambient Ground Motion in the Relativistic Heavy Ion Collider. BRANDON BELEW (*Rensselaer Polytechnic Institute, Troy, NY 12180*) CHRISTOPH MONTAG (*Brookhaven National Laboratory, Upton, NY 11973*). Within the Relativistic Heavy Ion Collider (RHIC) and particle accelerators in general, proper alignment of the focusing and defocusing quadrupole magnets is essential to maintaining a stable beam orbit. However, it is also a fact that there will always be some misalignment due to ambient ground motion. The extent of this displacement is given by a simple linear formula of time, distance and a site-specific constant (the 'ATL Rule'). Using known values of the beta function, phase advance, and focusing strength at the RHIC quadrupoles, code was written to simulate expected beam deviation at specific monitor points according to the ATL rule, for arbitrary values of the constant A. This expected deviation was then compared with actual logged beam data over the course of several months to arrive at the site-specific value of A. The end result, the constant of ambient ground motion specific to the RHIC location, was calculated to be around $3e^{-11}$

mm²/m*s. Knowing this value will allow for more accurate predictions of future beam deviation, and facilitate the proper application of correcting dipole magnets to counteract these effects.

Analysis of Creep in Polyvinyl Chloride for the NOvA Detector.

CHRISTINE MIDDLETON (*Wesleyan University, Middletown, CT 06459*) **HANS JOSTLEIN** (*Fermi National Accelerator Laboratory, Batavia, IL 60510*). This analysis is an attempt to predict creep in the NOvA detector, a proposed electron neutrino detector for the NuMI beamline at Fermilab. The NOvA detector is constructed of large PVC extrusions which contain 25 ktons of scintillating oil. Due to the scale of this detector and the proposed experiment length of 20 years, creep in the structural PVC of the detector is a concern. Creep data was taken on 18 samples over 188 days. Stress levels ranged from 500 PSI to 2100 PSI, with 2 samples being tested at each stress. A variety of models and fit functions from the literature were used, however a best fit function was not readily apparent. Although the data could be fit reasonably well, these functions were unable to give a reasonable prediction for the creep after 20 years. In order to improve these results, more data is needed which represents the secondary and tertiary creep stages. We anticipate being able to study this behavior using accelerated high temperature creep tests.

Analysis of Off-Nuclear X-Ray Sources in Galaxy NGC 4945.

SARAH HARRISON (*Massachusetts Institute of Technology, Cambridge, MA 22901*) **GRZEGORZ MADEJSKI** (*Stanford Linear Accelerator Center, Stanford, CA 94025*). Recently, X-ray astronomy has been used to investigate objects such as galaxies, clusters of galaxies, Active Galactic Nuclei (AGN), quasars, starburst superbubbles of hot gas, X-ray binary systems, stars, supernova remnants, and interstellar and intergalactic material. By studying the x-ray emission patterns of these objects, we can gain a greater understanding of their structure and evolution. We analyze X-ray emission from the galaxy NGC 4945 using data taken by the Chandra X-ray Observatory. The Chandra Interactive Analysis of Observations (CIAO) software package was used to extract and fit energy spectra and to extract light curves for the brightest off-nuclear sources in two different observations of NGC 4945 (January, 2000 and May, 2004). A majority of sources were closely fit by both absorbed power law and absorbed bremsstrahlung models, with a significantly poorer X²/dof for the absorbed blackbody model, and most sources had little variability. This indicates that the sources are accreting binary systems with either a neutron star or black hole as the compact object. The calculated luminosities were about 10³⁸ erg/s, which implies that the mass of the accreting object is close to 10 solar masses and must be a black hole.

Analysis of the Properties of Particles Emerging From Deep Inelastic Scattering off a Range of Nuclei.

SÉRÈRES JOHNSTON (*Andrews University, Berrien Springs, MI 49103*) **KAWTAR HAFIDI** (*Argonne National Laboratory, Argonne, IL 60439*). Hadronization, the process by which a struck quark evolves into a hadron, is not well understood in the nuclear medium. Experiments done with medium energy electron beams and multiple nuclear targets can investigate hadronization at nuclear scales. Understanding this process would provide insight into the confinement property of the nuclear strong force. The data collected by the E02-104 Nuclear Semi Inclusive Deep Inelastic Scattering experiment, performed at Jefferson Laboratory with a 5 GeV electron beam, can be used to characterize hadronization as a function of multiple variables. E02-104 ran with several solid targets of differing atomic radius and the data taken is sensitive to early hadronization processes. Programs were written which compared the hadron attenuation and transverse momentum broadening in the three nuclear targets, carbon, iron, and lead. Greater attenuation is observed in large nuclei. Hadron attenuation is described by the multiplicity ratio, R_{hM}, which is a multivariable function. The high statistics of the E02-104 data allowed its dependence on four different variables to be examined in detail. The quark energy loss indicated by the transverse momentum broadening is seen to increase with the square of the nuclear distance traveled. This agrees with QCD predictions based on quark energy loss through gluon radiation. There is also some evidence that the transverse momentum broadening approaches a limit in larger nuclei. Not enough nuclear targets were examined for this last result to be definitive.

Analysis Strategy of Powder Diffraction Data with 2-D Detector.

ABHIK KUMAR (*Austin College, Sherman, TX 75090*) **APURVA MEHTA** (*Stanford Linear Accelerator Center, Stanford, CA 94025*). To gain a clearer understanding of orientation and grain deformation of crystalline materials, x-ray powder diffraction has played an integral role in extracting three-dimensional structural information from one-dimensional diffraction patterns. Powder diffraction models identical

geometry to the intersection of a normal right cone with a plane. The purpose of this paper is to develop a general expression defining the conic sections based on the geometry of a powder diffraction experiment. Applying the derived formulation of a diffraction arc to experimental data will give insight to the molecular and structural properties of the sample in question. Instead of using complex three-dimensional Euclidian geometry, we define the problem solving technique with a simpler two-dimensional transformation approach to arrive at a final equation describing the conic sections. Using the diffraction geometry parameters, we can use this equation to calibrate the diffractometer from the diffraction pattern of a known reference material, or to determine the crystalline lattice structure of the compound.

Analytical Data Acquisition via Radar of Ionization Electrons in Cosmic-ray Extensive Air Showers.

JEREMY MARTIN (*FAMU-FSU College of Engineering, Tallahassee, FL 32310*) **HELIO TAKAI** (*Brookhaven National Laboratory, Upton, NY 11973*). Ultra-high-energy cosmic-rays initiate cosmic showers of high-energy, electrically charged particles upon interaction with the atmosphere of the earth. Evidence of radio wave reflection is collected from ultra-high-energy cosmic-ray (UHECR)-induced extensive air showers (EAS) of high energy electrically charged particles when entering the stratosphere. Optimal detection of UHECR entails facilitating a more pertinent understanding of the high-energy particle and its celestial origin. The challenge is using a type of radar detection to separate the radio signals reflected by EAS from radio waves reflected from other sources (i.e., clouds, meteor trails, air crafts, emissions from lightning). This requires an approach involving Fourier transform, power spectrum analysis, as well as other series evaluation techniques to discriminate between the EAS reflected waves which contain data from high ionization particle interaction and oscillations that are irrelevant to this research. To distinguish EAS radio waves from other atmospheric sources of radio waves, a set of software tools were developed. Using this uniquely developed data acquisition software, randomly reflected radio waves about the atmosphere can be manipulated from their intrinsic state to isolate the power spectrum of the EAS waveforms in an attempt to efficiently identify these particular signatures of undulation in greater proportion. By analyzing the frequencies of these signals the intention is to later demonstrate a correlation between the radio waves occurring in specific VHF radio frequencies and cosmic-ray events detected by other means. This research is a portion of a process in which the goal is to develop a basis for further study of UHECR within the Mixed Apparatus for Radar Investigation of Cosmic-rays of High Ionizations (MARIACHI) project, which seeks to develop radar detection techniques for related studies of high energy physics.

Calculation of Particle Bounce and Transit Times on General Geometry Flux Surfaces.

DOUGLAS SWANSON (*Yale University, New Haven, CT 06520*) **DR. JONATHAN MENARD** (*Princeton Plasma Physics Laboratory, Princeton, NJ 8543*). Minimizing magnetohydrodynamic (MHD) instabilities is essential to maximizing the plasma pressure and the fusion power output from toroidal plasmas. One such instability is the resistive wall mode (RWM). Plasma rotation above a critical frequency has been observed to stabilize the RWM. The critical frequency is predicted in some theories to depend strongly on characteristic bounce and transit times particles take to complete orbits. Bounce times are orbit times for particles with large magnetic moments that are trapped poloidally in banana orbits. Transit times are orbit times for particles with small magnetic moments that are able to complete full poloidal circuits around the plasma. Previous calculations of these bounce and transit times have assumed high aspect ratio and circular flux surfaces, approximations unsuitable for the National Spherical Torus Experiment (NSTX). Analytic solutions for the bounce and transit times were derived as functions of particle energy and magnetic moment for low aspect ratio and elliptical flux surfaces. Numeric solutions for arbitrary aspect ratio and flux surface geometry were also computed using Mathematica and IDL and agree with the analytic forms. The solutions were found to scale as the elongation at low aspect ratio, and as the square root of the elongation at high aspect ratio. For typical values of the parameters the bounce and transit times can differ from the high aspect ratio, circular results by as much as 40%. Analytic transformations to map the high aspect ratio, circular solutions into the general geometry solutions are being investigated. Such transformations could be easily incorporated into existing stability codes such as MARS to refine models of RWM rotational stabilization.

Calibration of Small Pb-Glass Photomultiplier Cells in the FPD (Forward Pion Detector).

SHAWN PEREZ (*State University of New York at Stony Brook, Stony Brook, NY 11790*) **LESLIE BLAND** (*Brookhaven National Laboratory, Upton, NY 11973*). The FPD (Forward

Pion Detector) at Brookhaven National Lab, consists of two matrices of Pb-glass bars viewed by photomultiplier tubes that are positioned left and right of the colliding beam axis. These detectors are used to explore transverse single spin asymmetries through analysis of forward pion production and its corresponding jet shape. In order to extract information from polarized proton–proton collisions, the FPD had to be calibrated cell by cell. Reconstructed di-photon invariant mass is associated with the highest energy cell in the inner matrix. Distributions of high tower invariant mass are fit by a Gamma function to describe background in the detectors and a Gaussian to describe the $\text{P}\pi^0$ peak. The absolute gain of each tower is then varied until the $\text{P}\pi^0$ peak is centered at its known position of .135 GeV/c². Once the relative gain correction factors of each iteration performed have converged, the cells have been calibrated. Currently the Small cells of the FPD are calibrated within an accuracy of 2%, while the large cells still need to be calibrated. Comparing the summed energy spectra of polarized up and down proton collisions in the west-north and west-south modules of the FPD, will reveal more information about transverse single spin asymmetries and possibly the relative contributions from the Collins and Sivers effect toward these asymmetries observed in forward pion production. The Collins and Sivers effect are theoretical models developed to explain transverse single spin asymmetries, dependent on spin and transverse momentum distribution functions or fragmentation functions. Analyzing the pseudorapidity ($-\ln(\tan(\alpha/2))$) dependence on particle production will explore parton distributions within the proton.

CCD Quantum Efficiency Characterization for LSST. XIAOQIAN ZHANG (Cornell University, Ithaca, NY 14853) JAMES S. FRANK (Brookhaven National Laboratory, Upton, NY 11973). The optical performance of charge coupled devices (CCDs), the fundamental units used for digital cameras, can be characterized by their quantum efficiency. The Large Synoptic Survey Telescope (LSST) project, an ongoing project aiming for completion in 2013, needs a high-efficiency digital camera with 3.2 Giga-pixels of CCDs for its acquisition of astronomical images. The CCDs used in this camera need to attain nearly 50 % quantum efficiency in the near-infrared (1000nm) while operating in a vacuum Dewar at a temperature of 173K. To test this requirement, instrumentation of a device that measures quantum efficiency of manufactured CCDs is under development at Brookhaven National Laboratory (BNL) and is based partially on the similar instrumentation developed in 2004 and 2005 in the Lawrence Berkeley National Laboratory (LBNL). This device consists of multiple light sources, a shutter, several filters, a coupled monochromator, a 12-inch diameter integrating sphere, a black box, and a dewar where the cooled CCD is to be placed. The equipment is assembled in the order listed above so that the monochromator first selects the desired wavelength of light emitted from the light source. This beam is then monitored in the integrating sphere, and made uniform through the black box before it reaches the CCD in the dewar. Picoammeters and photodiodes are placed in several locations for light intensity measurements. After examining the light leakage of the integrating sphere, calibration of the coupled monochromator was performed using a Hg light source. Properties of gratings, filters, and slits were studied by comparing measured spectral lines of Hg and Xe light source. A LabView program was developed and used to operate the assembled devices and take readings from the photodiodes. These programs, devices, and data will be used to measure the quantum efficiency as a function of wavelength in CCDs currently under development for LSST.

Centrality Determination in Heavy Ion Collisions for the Pioneering High Energy Nuclear Interaction eXperiment (PHENIX) at the Relativistic Heavy Ion Collider (RHIC). ELI LANSEY (Yeshiva University, New York, NY 10033) ALEXANDER MILOV (Brookhaven National Laboratory, Upton, NY 11973). In the physics of Relativistic Heavy Ions (RHI), the centrality related parameters (such as the number of participating nucleons or number of binary collisions between nucleons) are the essential characteristics of the collisions. The majority of publications from all four RHIC experiments related to RHI physics present their results as functions of one or more centrality-related parameters. Centrality's precise determination is therefore critical to understand most of the RHI results. The distribution of the number of participating nucleons can be obtained with the commonly used Glauber model. In the PHENIX experiment, this distribution is related to the number of particle hits in the Beam-Beam Counters via statistics of the Negative Binomial Distribution (NBD). These properties allow us to achieve two principle goals: to validate the commonly used theoretical model and to establish an accurate relationship between the observable quantity (number of hits) and the number of participating nucleons. Using the data collected during full energy (200 GeV) Au-Au Run4 of the PHENIX experiment we studied the parameters of the

NBD, their systematic dependencies and accuracy to which they can be determined. The work is done by using the MINUIT minimization tool in the ROOT environment. This work will contribute to future analysis by many members of the PHENIX collaboration, yielding better measurements of the centrality-related parameters.

Characterization of an Electromagnetic Calorimeter for the Proposed International Linear Collider. MERIDETH FREY (Wellesley College, Wellesley, MA 02481) NORMAN GRAF (Stanford Linear Accelerator Center, Stanford, CA 94025). The International Linear Collider (ILC) is part of a new generation of accelerators enabling physicists to gain a deeper understanding of the fundamental components of the universe. The proposed ILC will accelerate positrons and electrons towards each other with two facing linear colliders, each twenty kilometers long. Designing and planning for the future accelerator has been undertaken as a global collaboration, with groups working on several possible detectors to be used at the ILC. The following research at the Stanford Linear Accelerator Center (SLAC) pertained to the design of an electromagnetic calorimeter. The energy and spatial resolution of the calorimeter was tested by using computer simulations for proposed detectors. In order to optimize this accuracy, different designs of the electromagnetic calorimeter were investigated along with various methods to analyze the data from the simulated detector. A low-cost calorimeter design was found to provide energy resolution comparable to more expensive designs, and new clustering algorithms offered better spatial resolution. Energy distribution and shape characteristics of electromagnetic showers were also identified to differentiate various showers in the calorimeter. With further research, a well-designed detector will enable the ILC to observe new realms of physics.

Characterization of Long Cosmic Ray Muon Tracks in IceCube Detector at South Pole. DANIEL HART (Southern University, Baton Rouge, LA 70813) AZRIEL GOLDSCHMIDT (Lawrence Berkeley National Laboratory, Berkeley, CA 94720). IceCube is studying high-energy neutrino astronomy. IceCube uses an array of optical modules to detect faint Cerenkov light produced by muons. These muons are the result of neutrino interactions with matter. Using the information received from data acquisition systems at the South Pole, software was developed using the C language to read this data and use it to produce possible muon paths. Events were filtered through by placing cuts on the calculated paths that passed through the full geometry of IceCube, had velocity within 5% of the speed of light, and were of low multiplicity. This resulted in path distance distributions that showed exponential decay of modules to receive light as a function of distance. The probability curves produced, followed along the same traits. However, the distance distributions were not exactly smooth as would be expected, and the selection of paths that were to be considered as neutrino candidates behaved similarly. These impurities are interpreted as the integration of multiple muons in a single event. In further studies, the plan is not only to add in more data from additional days, but also to employ more sophisticated methods for separating true events from those produced by multiple muons.

Characterizing the Charge Collection of the 0.13 μm IBMPIX Prototype Pixel Detector. ANJALI TRIPATHI (Massachusetts Institute of Technology, Cambridge, MA 02139) RONALD LIPTON (Fermi National Accelerator Laboratory, Batavia, IL 60510). Central to collider physics experiments are silicon detectors, which track the trajectory of particles produced during collisions. With the drive for ever more precise resolution in particle tracking, a prototype pixel detector (IBMPIX) manufactured by IBM in a 0.13 μm RF CMOS process, was investigated to understand its charge collection and individual pixel behavior. As a Monolithic Active Pixel Sensor, it was comprised of arrays of pixels (10 μm by 150 μm) divided into three diode types—a standard N-well, a deep (or triple) N-well, and a control without a diode. To measure the pixel to pixel variations from the readout electronics, a signal generator pulsed charge directly into the analog circuitry, bypassing the diodes, at different threshold settings. Upon characterizing the response of the readout electronics for each pixel, a pulsed 1.06 μm Nd:YAG laser was used to determine the relationship between the input charge and the output pulse width. This pulse width was the amount of time that the input charge was above a set threshold. With the data from both the laser and the signal generator, a mathematical model was made for charge diffusion across the chip. From the signal generator tests, the readout electronics showed significant pixel to pixel variation. This variation was nearly proportional to the threshold current setting. Additionally, testing of the diodes yielded a precise equation relating pulse-width to charge. For an idealized laser beam of zero width, a diffusion length of approximately 80 microns was determined. The source of the pixel to pixel variation

can be attributed to gain variations due to the fabrication. Further studies should employ a laser with a spot size contained within one pixel, include a diffusion model incorporating variable beam width, and use an additional current source to set the threshold value.

Comparison of Non-Redundant Array and Double Pinhole Coherence Measurements with Soft X-rays. GABRIEL WEIL (Northwestern University, Evanston, IL 60201) JAN LUNING (Stanford Linear Accelerator Center, Stanford, CA 94025). Experiments on the future Linac Coherent Light Source (LCLS) and other Free Electron Lasers will need to be performed on a single-shot basis. The double pinhole method of measuring spatial coherence requires a separate measurement, with a different pinhole separation distance, for each length scale sampled. This limits its utility for LCLS. A potential alternative uses a Non-Redundant Array (NRA) of apertures designed to probe the coherence over the range of length scales defined by their physical extent, in a single measurement. This approach was tested by comparing diffraction patterns from soft x-rays incident on double pinhole and NRA absorption mask structures. The double pinhole fringe visibility data serve as discrete reference points that verify the continuous spectrum of the NRA coherence data. The results present a quantitative analysis of the double pinhole coherence measurements and a qualitative comparison to the NRA images.

Construction and Commissioning of a Micro-Mott Polarimeter for Photocathode Research and Development. APRIL COOK (Monmouth College, Monmouth, IL 61462) MARCY STUTZMAN (Thomas Jefferson National Accelerator Facility, Newport News, VA 23606). Thomas Jefferson National Accelerator Facility uses polarized electrons to further the understanding of the atomic nucleus. The polarized source produces electrons by directing laser light onto a specially prepared gallium arsenide (GaAs) photocathode. During the course of this project, an off-beamline micro-Mott polarimeter has been built and commissioned within the Source Lab for photocathode research and development. A polarimeter measures the polarization, or spin direction, of electrons. The micro-Mott runs at 30 keV and can be used directly in the Source Lab, off of the main accelerator beamline. Construction of the Mott system began with a polarized source, which consists of a vacuum chamber complete with a cesiator and nitrogen trifluoride (NF₃) to activate the photocathode, residual gas analyzer (RGA), ultra-high vacuum pumps, an electrostatic deflector to bend the electron beam 90 degrees, and electrostatic lenses. The polarimeter is housed in an adjacent vacuum chamber. The circularly polarized laser light enters the polarized source, hits the GaAs photocathode, and liberates polarized electrons. The original longitudinally-polarized electrons are transformed into transversely-polarized electrons by the electrostatic bend. They are then directed onto a gold target inside the Mott and scattered for data analysis. The polarized source has been commissioned, achieving photoemission from the activated GaAs crystal, and the electrostatic optics have been tuned to direct the electrons onto the gold target. Nearly ten percent of the electrons from the photocathode reach the target, giving adequate current for polarization measurement. The micro-Mott polarimeter will aid in photocathode research and pre-qualification of material for use in the injector.

Construction of the La-Bi-O Phase Equilibria: The Search for Inorganic Scintillators. STEVEN VILAYVONG (North Carolina A&T State University, Greensboro, NC 27411) YETTA PORTER-CHAPMAN (Lawrence Berkeley National Laboratory, Berkeley, CA 94720). Scintillators have been around forever, however the demand for scintillators has risen exponentially since World War II. This need for viable scintillators to be used in the detection of ionizing radiation has spurred research around the world. The New Detector Group of the Department of Functional Imaging in the Life Sciences Division of Lawrence Berkeley National Laboratory conducts systematic searches of various compounds to find the most effective scintillator. Much of their work focuses on compounds that contain Bismuth (III) and Lanthanum (III) ions. Bismuth (III) ions have the capability to be luminescent sometimes providing intrinsic scintillation as seen in the commonly used scintillator, Bi₂Ge₂O₇, (BGO). Phases containing lanthanum (III) ions are also investigated to utilize their sites for cerium (III) (another luminescent ion) doping. In this work, various molar ratios of La₂O₃ and Bi₂O₃ were reacted by solid state chemistry techniques to find phases that may exhibit scintillation. To be classified as a good scintillator, one must characterize these phases by x-ray diffraction (XRD), fluorescence spectroscopy, and pulsed x-ray measurements. Four La-Bi-O phases, La_{0.176}Bi_{0.824}O_{1.5}, La_{0.12}Bi_{1.88}O₃, La₄Bi₂O₉, and an unknown phase were found however, none are good scintillators.

Design, Fabrication and Measurement of Nb/Si multilayers and Nb Transmission Filters. SUNEIDY LEMOS FIGUEROE (University of Puerto Rico, Rio Piedras, P.R 00979) DAVID ATTWOOD (Lawrence Berkeley National Laboratory, Berkeley, CA 94720). The extreme ultraviolet (EUV) region of the electromagnetic spectrum is being used in multilayer optical systems to design technology projected for use in the fabrication of nano-electronics. Multilayer optical systems with high reflectivity have been produced in the soft x-ray and EUV regions of the spectrum. Due to the limited understanding of the Nb/Si optical systems, our research group fabricated and measured Nb/Si multilayers and Nb transmission filters for the soft x-ray and EUV regions. Multilayer optical systems are used in applications ranging from EUV lithography to synchrotron radiation. The films were deposited using dc magnetron sputtering in the Center for X-Ray Optics at the Lawrence Berkeley National Laboratory. Reflectivity and transmission measurements were performed at the Advanced Light Source beamline 6.3.2. The Nb/Si multilayer mirrors fabricated have a reflectivity of approximately 65% in the extreme ultraviolet region, which makes these systems practical for applications where a high reflectivity is required, such as Astronomy and instrumentation development. Transmission measurements of up to 90% were observed in the soft x-ray and EUV regions as well. Future work in the research group includes the design and fabrication of an Nb/Si multilayer with a B4C interface. The Nb/B4C/Si optical systems are expected to have a higher reflectivity than Nb/Si systems.

Determining Micromechanical Strain in Nitinol. MATTHEW STRASBERG (Cornell University, Ithaca, NY 14850) APURVA MEHTA (Stanford Linear Accelerator Center, Stanford, CA 94025). Nitinol is a superelastic alloy made of equal parts nickel and titanium. Due to its unique shape memory properties, nitinol is used to make medical stents, lifesaving devices used to allow blood flow in occluded arteries. Micromechanical models and even nitinol-specific finite element analysis (FEA) software are insufficient for unerringly predicting fatigue and resultant failure. Due to the sensitive nature of its application, a better understanding of nitinol on a granular scale is being pursued through X-ray diffraction techniques at the Stanford Synchrotron Radiation Laboratory (SSRL) at the Stanford Linear Accelerator Center (SLAC). Through analysis of powder diffraction patterns of nitinol under increasing tensile loads, localized strain can be calculated. We compare these results with micromechanical predictions in order to advance nitinol-relevant FEA tools. From this we hope to gain a greater understanding of how nitinol fatigues under multi-axial loads.

Development of Charged-Coupled Devices for Precision Cosmology and the Supernova Acceleration Probe Satellite. JESSICA WILLIAMSON (University of Alabama in Huntsville, Huntsville, AL 35899) DR. NATALIE ROE (Lawrence Berkeley National Laboratory, Berkeley, CA 94720). Dark energy, which is believed to be a cosmic energy density that is gravitationally repulsive and does not appear to cluster in galaxies, has been invoked to account for the recent measurement that the rate of the universe's expansion is accelerating. To better understand these phenomena, scientists utilize type Ia supernovae as calibrated candles. Lawrence Berkeley National Laboratory (LBNL) is developing the Supernova Acceleration Probe (SNAP), a space-based telescope that will be used to identify and measure supernovae. The SNAP focal plane will consist of an innovative camera that integrates two cutting-edge imaging sensor systems, one of which is the LBNL high purity charged coupled device (CCD) for the visible light range. We report on the development of a novel technique for extending the spatial and photometric fidelity performance of the LBNL CCDs. Presented are our results obtained from measurements using a 10.5 μm pixel pitch, 1.4k×1.4k format, p channel CCD fabricated on high-resistivity silicon at LBNL. The fully depleted device is 300 μm thick and backside illuminated. Measurements of the device's transverse diffusion of charge carriers, pixel to pixel uniformity and intrapixel uniformity will be reported. will be reported. Also presented are new, preliminary results from the first implementation of CCD Phase Dithering, a novel technique for achieving sub-pixel spatial resolution in undersampled, pixelated image data as will be obtained by the SNAP satellite.

Development of Emittance Analysis Software for Ion Beam Characterization. MARIANO PADILLA (Fullerton College, Fullerton, CA 92832) YUAN LIU (Oak Ridge National Laboratory, Oak Ridge, TN 37831). Transverse beam emittance is a crucial property which describes the angular and spatial spread of charged particle beams. It is a figure of merit frequently used to determine the quality of ion beams, the compatibility of an ion beam with a given beam transport system, and the ability to suppress neighboring isotopes at on-line mass separator facilities. Generally a high quality beam is characterized

by a small emittance. In order to determine and improve the quality of ion beams used at the Holifield Radioactive Ion beam Facility (HRIBF) for nuclear physics and nuclear astrophysics research, the emittances of the ion beams are measured at the off-line Ion Source Test Facilities. In this project, an emittance analysis software was developed to perform various data processing tasks for noise reduction and to evaluate root-mean-square emittance, Twiss parameters, and area emittance of different beam fractions. The software also provides 2D and 3D graphical views of the emittance data, beam profiles, emittance contours, and ellipses. Noise exclusion is essential for accurate determination of beam emittance values. A Self-Consistent, Unbiased Elliptical Exclusion (SCUBEE) method is employed. Numerical data analysis techniques such as interpolation and nonlinear fitting are also incorporated into the software. The software will provide a simplified and fast tool for comprehensive emittance analyses. The main functions of the software package have been completed. In preliminary tests with real experimental emittance data, the analysis results using the software were proven to be correct.

Development of Nanofluidic Cells for Ultrafast X-ray Studies of Water. MELVIN IRIZARRY (*University of Puerto Rico, Mayaguez, PR 00667*) AARON LINDENBERG (*Stanford Linear Accelerator Center, Stanford, CA 94025*). In order to study the molecular structure and dynamics of liquid water with soft x-ray probes, samples with nanoscale dimensions are needed. This paper describes a simple method for preparing nanofluidic water cells. The idea is to confine a thin layer of water between two silicon nitride windows. The windows are 1 mm × 1 mm and 0.5 mm × 0.5 mm in size and have a thickness of 150 nm. The thickness of the water layer was measured experimentally by probing the infrared spectrum of water in the cells with a Fourier Transform InfraRed (FTIR) apparatus and from soft x-ray static measurements at the Advanced Light Source (ALS) at Lawrence Berkeley National Laboratory. Water layers ranging from 10 nm to more than 2 μm were observed. Evidence for changes in the water structure compared to bulk water is observed in the ultrathin cells.

Development of Powder Diffraction Analysis Tools for a Nanocrystalline Specimen: An Emphasis upon NiTi (Nitinol). ERICH OWENS (*Albion College, Albion, MI 49224*) APURVA MEHTA (*Stanford Linear Accelerator Center, Stanford, CA 94025*). Powder diffraction is a specialized technique whose investigatory limits are constrained by the scale of the crystallized substance being scanned versus the probe beam used. When disparate in scale, with the photon spot size larger than the crystal being probed, many are employed, the resulting diffraction image being cast from all possible incident angles, constructing α-arcs containing information about the crystalline structure of the material under examination. Of particular interest to our collaboration is the structure of Nitinol, a superelastic Nickel-Titanium alloy, whose phase transformations and load bearing deformations can be studied by usage of diffraction, with wide sweeping biomedical uses. Analysis of this data is complicated by phase transformation and material fluorescence, which make difficult the computational modeling of the peaks within concentric α-arcs. We endeavored to construct a series of computational tools (the amalgamation of them known as 2DPeakFinder) for refining and extracting this relevant data, toward the end of employing previously developed algorithms in the material's structural analysis. We succeeded to a large degree with the use of an iterative algorithm to navigate radial complexity of the signal and manage to retain a distinction between useful signal and superfluous background noise. The tools developed in this project are a small step in readily streamlining the analysis and physical modeling of a Nanocrystalline material's structural properties.

Eddy Current Non-destructive Inspection Using Giant Magnetoresistive Technology. STEVEN GARDNER (*Brigham Young University-Idaho, Rexburg, ID 83460*) DENNIS C. KUNERTH, PH.D. (*Idaho National Laboratory, Idaho Falls, ID 83415*). A prototype eddy current probe utilizing giant Magnetoresistive technology was found to have the following benefits: 1. It functions at very low frequencies (DC to 30 kHz) and deep sample depths. 2. The probe can be characterized to reveal thickness of an aluminum sample up to 10 mm thick, and much thicker in stainless steel and other less conductive metals. 3. The probe design uses a noise reduction coil and shield system which increases signal to noise ratio by nulling drive coil noise. This probe would be ideal for testing thickness of metals with low magnetic permeability. It is also effective at locating defects greater than 0.25 mm on the surface or within the depth of penetration as determined by the relationship depth (m) = $v(1/(p \cdot f \cdot \mu_0 \cdot \mu_r \cdot s))$ where μ_0 is the permeability of free space, μ_r is the relative magnetic permeability and s is the electrical conductivity. Its limitations include: 1. It was unable to function at frequencies greater than 30 kHz. 2. It was not able to detect defects

smaller than .25 mm or surface defects which did not extend this same distance or more into the metal. Attempts were also made to operate the probe using pulse and linear sweep drives. These attempts did not create satisfactory results. Much of the lack of success could be due to the fact that it was not possible to null the drive signal using the noise reduction coil for either the pulse or the sweep drive methods. The inability to resolve small defects, and the limitations on the frequency range appear to be caused by the large coil geometry and the inductance change introduced by the iron shield.

Effects of UV Light on a Fluorescent Dust Cloud. ENRIQUE MERINO (*Ramapo College of New Jersey, Mahwah, NJ 07430*) ANDREW POST-ZWICKER (*Princeton Plasma Physics Laboratory, Princeton, NJ 08543*). Dusty plasma research has applications ranging from microchip fabrication to the study of planetary rings. Typically, the behavior of laboratory dusty plasmas is studied by laser scattering techniques. A new diagnostic technique developed at the Science Education Laboratory at the Princeton Plasma Physics Laboratory uses a 100W ultra-violet (UV) light to illuminate a fluorescent organic dust cloud created in an argon DC glow discharge plasma. By using the UV light, the fluorescent particles can be clearly seen during and after cloud formation and their 3D properties analyzed. This technique has been successfully used to study formation and transport of the dust cloud. Observations have shown that after the dust cloud has formed, the UV light causes rotation of the edge of the cloud (~ 3mm/s), while particles in the center of the cloud remain stable. Displacements of several millimeters up and towards the UV light have also been recorded by modulating the UV light. Through the use of a Langmuir probe, changes in the charge of the plasma were recorded whenever UV light was introduced. These changes occurred both in the presence of a dust cloud and with a clean plasma as well. Although these experiments were helpful in demonstrating that UV light had an effect on the plasma, it is left as future work to determine the effect of UV light on the dust particles themselves and propose analytical models for the displacements experienced.

Energizing a Superconducting Solenoid for Applications in Precise Mass Measurements. DAVID DANAHER (*Monmouth College, Monmouth, IL 61462*) GUY SAVARD (*Argonne National Laboratory, Argonne, IL 60439*). The precise mass measurement of ions is the main objective of the Canadian Penning Trap (CPT) collaboration at Argonne National Laboratory. The mass measurements require a beam from the Argonne Tandem Linear Accelerator System (ATLAS) to fuse with a target to create the desired reaction products. A new beamline has nearly been completed in Area II of ATLAS for the purpose of taking mass measurements of ions with greater divergence angles that were previously hard or nearly impossible to measure, which diverge due to alpha decay and are refocused for later measurement. A solenoid can be used to refocus the ions before they can be sent through the rest of the system and, consequently, measured. This component of the new beamline in Area II is a superconducting solenoid with a 68 centimeter inner bore and a central field of 1.5 Tesla, weighing over 10 tons with all of the necessary shielding and support in place. For the solenoid to produce a magnetic field, it must be energized and continually carry a current of about 200 Amps within its coils. The process of energizing such a device is a subtle exercise and requires creating a vacuum within the solenoid, pre-cooling of the cryostat with liquid Nitrogen, filling the cryostat with liquid Helium, running a cryo-compressor to limit Helium boil-off, and well-regulated power sources to bring the solenoid to maximum field. Once carefully assembled, however, the components of the energization process may be used to safely energize and de-energize the system time and time again. My project was to help locate all the components of the energization process, facilitate the interconnections between components, and, finally, to aide with the powering of the magnet.

Experimental Studies of Electrode Biased Compact Toroid Plasmas in the Magnetic Reconnection Experiment. ELIJAH MARTIN (*North Carolina State University, Raleigh, NC 27609*) DR. MASAAKI YAMADA (*Princeton Plasma Physics Laboratory, Princeton, NJ 8543*). Compact Toroid (CT) plasmas such as Field-Reversed Configurations (FRC's) and Spheromaks are known to exhibit a global instability known as the tilt mode, where the magnetic moment of the CT tilts to align itself with the external magnetic field, as well other non-rigid body instabilities. Possible tilt stabilizing mechanisms for these instabilities include external field shaping, nearby passive stabilizers, and plasma rotation. This research focuses on reducing the growth of the tilt instability by introducing toroidal rotation in spheromaks formed in the Magnetic Reconnection Experiment (MRX). Rotation is introduced by the use of interior and exterior electrodes; the result is a $J_{\text{bias}} \times B_{\text{internal torque}}$ on the CT plasma which in turn leads to toroidal

rotation of the CT plasma. In order to power the bias electrode a 450 V 8800 μF capacitor bank capable of delivering up to 450 amperes was constructed along with the required control and triggering circuitry. Solid state switches allow for fast turn on and turn off times of J_{bias} . The bias current and the voltage drop across the electrodes are measured using a current shunt and voltage divider respectively, and the resulting flow in the CT plasma is measured with a Mach probe. Internal arrays of magnetic probes and optical diagnostics will be used to parameterize the performance of the CT plasma during bias. Construction and testing of all necessary components and diagnostics is complete; preliminary experiments were designed such that the resistivity of the plasma could be determined. It was found that a typical CT plasma has a resistivity of 34.1 ± 3.6 ohm m, a leaky capacitor model of the CT plasma was applied to determine the resistivity theoretically. A theoretical resistivity of 4.9×10^{-3} ohm m was calculated based on conditions of a typical CT plasma. The strong disagreement between experimentally and theoretically determined values is hypothesized to be due to non-optimal control of CT plasmas formed in MRX. The focus of future research will be optimizing control of the CT plasma; agreement between the model and experiment will then be studied as well as experiments designed to induce toroidal rotation.

Formation and Transport of a Fluorescent Dust Cloud: a New Diagnostic Technique in Dusty Plasma Research. ENRIQUE MERINO (*Ramapo College of New Jersey, Mahwah, NJ 07430*) ANDREW POST-ZWICKER (*Princeton Plasma Physics Laboratory, Princeton, NJ 08543*). Dusty plasma research has applications ranging from microchip fabrication to the study of planetary rings. Typically, the behavior of laboratory dusty plasmas is studied by laser scattering techniques which give a 2D slice of the dust cloud or by the use of 3D particle image velocimetry methods (PIV). Although these diagnostic techniques allow for the study of cloud formation, they require extensive computer processing or simulations to study the formation processes. A new diagnostic technique has been devised to study 3D behavior and cloud formation, without the need for the complicated and usually expensive methods mentioned above. A fluorescent organic dust is used to create a cloud in an argon DC glow discharge plasma, illuminated by a 100W ultra-violet (UV) light. By using UV light, the fluorescent particles can be clearly seen during cloud formation and their 3D properties analyzed. One question remaining, however, is whether the UV light perturbs the plasma by changing the local charge balance or actively changing the dust cloud charge by photoelectric emission. In fact, initial observations show that particles in the back of the dust cloud experience a displacement towards the UV light, while particles in the front move away from it. Velocities ranging in the order of 1.5 mm/sec to 3 mm/sec were recorded for different areas of the cloud. Future work will use a Langmuir probe to separate changes in plasma parameters from changes in dust charge.

Gain Mapping and Response Uniformity Testing of the Hamamatsu R8900 Multianode Photomultiplier Tube and the Burle Planacon Microchannel Plate Photomultiplier Tube for the Picosecond Timing Project. MELINDA MORANG (*University of Chicago, Chicago, IL 60637*) KAREN BYRUM (*Argonne National Laboratory, Argonne, IL 60439*). Research is currently underway for the development of a microchannel plate photomultiplier tube with picosecond timing capabilities, a property that would be extremely useful in many fields of physics and in radiology. It is important in a research and development study such as this one to fully understand the currently available technology, and the study presented in this paper focuses on characterizing gain and response uniformity in the Hamamatsu R8900-00-M16 multianode photomultiplier tube (R8900) and the Burle Planacon 85011-501 microchannel plate photomultiplier tube (MCPMT). The tubes were tested using a dark box setup in which a moveable fiber carrying an LED pulse could be directed into each pixel in the tube. The gains for each pixel of ten R8900 tubes and for part of an MCPMT were calculated, and a horizontal scan in 1mm steps was performed across the breadth of the R8900 and across one quadrant of an MCPMT. Plots showing the signal output in the horizontal scans showed that the MCPMT had much greater response uniformity across the tube, but due to time and equipment restraints, these results are only preliminary, and more extensive study of uniformity is necessary, as is study of many other properties of these tubes.

GEANT Simulations of the Preshower Calorimeter for CLAS12 Upgrade of the Forward Electromagnetic Calorimeter. KRISTIN WHITLOW (*University of Florida, Gainesville, FL 32612*) STEPAN STEPANYAN (*Thomas Jefferson National Accelerator Facility, Newport News, VA 23606*). Hall B at the Thomas Jefferson National Accelerator Facility uses the CEBAF (Continuous Electron Beam Accelerator Facility) Large Acceptance Spectrometer (CLAS) to study the structure

of the nucleon. The accelerator is currently planning to upgrade from using a 6 GeV beam to a 12 GeV beam. With the beam upgrade, more high-energy pions will be created from the interaction of the beam and the target. Above 6 GeV, the angle between the two-decay photons of high-energy pions becomes too small for the current electromagnetic calorimeter (EC) of CLAS to differentiate between two photon clusters and single photon events. Thus, a preshower calorimeter will be added in front of the EC to enable finer granularity and ensure better cluster separation for all CLAS experiments at higher energies. In order to optimize cost without compromising the calorimeter's performance, three versions of the preshower varying in number of scintillator and lead layers were compared by their resolution and efficiency. Through the use of GSIM, a GEANT detector simulation program for CLAS, π^0 's and single photons were passed through the CLAS detector with the added preshower calorimeter (CLAS12 EC). The resolution of the CLAS12 EC was calculated from the Gaussian fit of the sampling fraction, the energy CLAS12 EC detected over the Monte Carlo simulated momentum. The single photon detection efficiency was determined from the energy and position of the photon hits. The resolution measured in the five-modules version was 0.0972, the four-modules version was 0.111, and three-modules version was 0.149. Both the five- and four-modules versions had 99% efficiency above 0.5 GeV while the 3 module version had 99% efficiency above 1.5 GeV. Based on these results, the suggested preshower configuration is the four-modules version containing twelve layers of scintillator and fifteen layers of lead because it is the most realistic choice to construct in resolution, efficiency and cost. The next step will be to do additional GSIM simulations to verify that the four-modules version has acceptable π^0 mass reconstruction and continue Research and Development (R&D) analysis on the preshower calorimeter.

Generation of Theoretical Spectra for Hot Dense Matter. ELIAS ALLISON, MATILDA FERNANDEZ (*Northern New Mexico Community College, Espanola, NM 87532*) DR. RICHARD W. LEE (*Lawrence Livermore National Laboratory, Livermore, CA 94550*). The focus of this project is to use computer codes to generate spectroscopic data for plasmas and hot dense matter, and to use these theoretical spectra to interpret experimental data. These theoretical spectra are important because of their applications in the study of ionized matter and magnetic fields near the surfaces of the sun and the stars, the origin of cosmic rays, the dispersion and broadening of signals traveling through interstellar space, the realization of controlled release of nuclear fusion energy, and the development of new electronic devices, among others. The computer codes model requested data for elements ranging from Helium to Iron, with a particular interest in the lithium-like, helium-like, and hydrogenic ionic species. Some of the important scattering events included in the model are collisional ionization and recombination, radiative bound-free processes, bound-bound processes, autoionization and electron capture. At present, the focus of the project is the design and implementation of a good dynamic interface to improve the ease of use of the existing codes.

Hold-up Time Measurements for Various Targets. EMILY PRETTYMAN (*DePaul University, Chicago, IL 60614*) KEN CARTER (*Oak Ridge National Laboratory, Oak Ridge, TN 37831*). At Oak Ridge National Laboratory the Holifield Radioactive Ion Beam Facility (HRIBF) produces radioactive ion beams (RIBs) typically by proton-induced fission on an actinide target. The RIB yields depend on the chemical and physical properties of the target used, such as the chemical compound, density and temperature. The rates at which chemical elements are released from the target ion source, called hold-up times, can give yield information and information about the movement of chemical elements within the target material and the ion source. This information may be useful in designing optimal targets and choosing operating conditions to maximize production of specific isotopes. Hold-up times are measured using the UNISOR isotope separator, connected to the tandem accelerator. Typically, the proton beam is left on until the element of interest reaches equilibrium between production and release. The proton beam is then turned off and the decrease of the release is observed using a moving tape collector and a germanium detector. Hold-up times have been measured using a pressed-powder Uranium Carbide (UCx) target at different temperatures for four elements: ^{78}Ge , ^{92}Sr , ^{128}Sn , and ^{130}Sb . In addition, hold-up times have been measured using two ThO_2 targets of different densities for ^{132}Te . For the various elements measured, as the temperature increases the hold-up times tend to decrease as expected. In addition, the denser ThO_2 target has drastically longer hold-up time than the less dense ThO_2 target for ^{132}Te . The current analysis was done by fitting the data with two exponential decay functions and as expected the hold-up times decrease as target temperature increases and the porous ThO_2

target has shorter hold-up times and higher yields than the denser ThO₂ target. Another attempt to fit the data would be to use equations which take into account diffusion and effusion with the goal of determining the ratios between diffusion and effusion to see which process dominates. There is still more work that must be done before conclusions can be drawn about the best design of a target and the most efficient operating conditions to maximize the yields.

Host Galaxies of X-Shaped Radio Sources. ALESSONDRA SPRINGMANN (*Wellesley College, Wellesley, MA 02481*) TEDDY CHEUNG (*Stanford Linear Accelerator Center, Stanford, CA 94025*). The majority of radiation from galaxies containing active galactic nuclei (AGNs) is emitted not by the stars composing the galaxy, but from an active source at the galactic center, most likely a supermassive black hole. Of particular interest are radio galaxies, the active galaxies emitting much of their radiation at radio wavelengths. Within each radio galaxy, an AGN powers a pair of collimated jets of relativistic particles, forming a pair of giant lobes at the end of the jets and thus giving a characteristic double-lobed appearance. A particular class of radio galaxies have an "X"-shaped morphology: in these, two pairs of lobes appear to originate from the galactic center, producing a distinctive X-shape. Two main mechanisms have been proposed to explain the X-shape morphology: one being through the merger of a binary supermassive black hole system and the second being that the radio jets are expanding into an asymmetric medium. By analyzing radio host galaxy shapes, we probe the distribution of the stellar mass to compare the differing model expectations regarding the distribution of the surrounding gas and stellar material about the AGN.

Hydrocode Simulations of Mach Stem Formation. STEPHEN DAUGHERTY (*Vanderbilt University, Nashville, TN 37235*) DENNIS PAISLEY (*Los Alamos National Laboratory, Los Alamos, NM 87545*). The study of shock waves often makes use of metallic disks propelled at high velocities to act as impactors. There are a number of ways to supply flyers with energy, but it takes some scheming to achieve extreme accelerations; a laser can focus a large amount of energy into a small area, but at some point thermal effects will take over, scattering much of the pulse energy and heating the sample. One solution is to strike a cone with a high-energy pulse and allow the resulting shock to converge toward the center. The shock reflected from the center will move at supersonic speed behind the incident shock, causing a flat energy disk—a Mach wave—to propagate through the center of the cone. The Mach wave will carry a high energy density to the base of the cone, where it can be transferred to a flyer.

Improvement of PEP-II Linear Optics with a MIA-Derived Virtual Accelerator. BEN CERIO (*Colgate University, Hamilton, NY 13346*) YITON YAN (*Stanford Linear Accelerator Center, Stanford, CA 94025*). In several past studies, model independent analysis, in conjunction with a virtual accelerator model, has been successful in improving PEP-II linear geometric optics. In many cases, optics improvement yielded an increase in machine luminosity. In this study, an updated characterization of linear optics is presented. With the PEP-II beam position monitor (BPM) system, four independent beam centroid orbits were extracted and used to determine phase advances and linear Green's functions among BPM locations. A magnetic lattice model was then constructed with a singular value decomposition-enhanced least-square fitting of phase advances and Green's functions, which are functions of quadrupole strengths, sextupole feed-downs, as well as BPM errors, to the corresponding measured quantities. The fitting process yielded a machine model that matched the measured linear optics of the real machine and was therefore deemed the virtual accelerator. High beta beat, as well as linear coupling, was observed in both LER and HER of the virtual accelerator. Since there was higher beta beating in LER, focus was shifted to the improvement of this ring. By adjusting select quadrupoles of the virtual LER and fitting the resulting beta functions and phase advances to those of the desired lattice, the average beta beat of the virtual machine was effectively reduced. The new magnet configuration was dialed into LER on August 10, 2006, and beta beat was reduced by a factor of three. After fine tuning HER to match the improved LER for optimal collision, a record peak luminosity of $12.069 \times 10^{33} \text{ cm}^{-2} \text{ s}^{-1}$ was attained on August 16, 2006.

Initial Hydrodynamic Data for a Free-Surface Liquid Gallium. KARL MCMURTRY (*Occidental College, Los Angeles, CA 90041*) HANTAO JI (*Princeton Plasma Physics Laboratory, Princeton, NJ 8543*). Free-surface Magnetohydrodynamic (MHD) shear flows have application to both astrophysics and fusion plasmas, but very little relevant experimental research has been done on them. To measure and observe physics relevant to these topics, a channel has been fabricated for the free surface flow of magnetized liquid gallium. This

channel is 16cm wide, 2cm deep, and 70cm long. As a benchmark, initial water data was taken using Laser Doppler Velocimetry (LDV). Several programs were written in Matlab to analyze the large amounts of LDV data. Average flow profiles and fluctuations were measured as a function of Reynolds number with values between 7,000 and 12,000. Average Froude numbers showed that diamond-shaped surface wave patterns were related to supercritical flow regimes.

Investigating the Polarization Effects of Free Electrons Through a Longitudinal Stern-Gerlach Apparatus. RACHEL SPARKS (*Old Dominion University, Norfolk, VA 23517*) DR. DOUGLAS W. HIGINBOTHAM (*Thomas Jefferson National Accelerator Facility, Newport News, VA 23606*). Otto Stern and Walther Gerlach completed an experiment in 1922 that opened many important questions and discoveries about the quantum mechanical world. Known as the Stern-Gerlach experiment, a beam of neutral silver atoms was passed through an inhomogeneous transverse magnetic field and then projected onto a screen. Classically, one would expect the screen to display a single blob of silver atoms; however, two blobs appeared. The breakthrough from this experiment was that the electron has an intrinsic spin, similar to a rotating top. Attempts have been made to conduct the Stern-Gerlach experiment with a beam of free electrons; but the Lorentz force, along with the Heisenberg uncertainty principle, blurs the splitting of the beam. In 1928, Brillouin suggested that a longitudinal Stern-Gerlach apparatus would minimize the effect of the Lorentz force. While this idea was dismissed in 1930 by Wolfgang Pauli, recent papers have shown that Brillouin's idea may have been valid. A computer simulation for an experiment to use the longitudinal Stern-Gerlach was completed this summer by analyzing the effect of different spin separations of the beam. Enhancement of the polarization was seen even using a realistic spread in the electron's momentum. Thus, it appears feasible to conduct an experiment that will investigate Brillouin's idea. In the future, this could be done in the Jefferson Lab test cave with equipment that is readily available.

***Investigation of the Optical Properties of Light-Emitting Diodes for Use in Fluorescence-Based Detection of Biological Threat Particles.** SHAWN BALLENGER (*Florence-Darlington Technical College, Florence, SC 29501*) NORM ANHEIER (*Pacific Northwest National Laboratory, Richland, WA 99352*). The optical properties of ultra-violet (UV) light-emitting diodes (LEDs) are being investigated to determine the LEDs' applicability in detecting biological particles using intrinsic fluorescence. When a biological material fluoresces it gives off a specific spectrum. This spectrum can be analyzed to identify threat particles from the background interferents. Pulsed laser excitation has previously been used to induce fluorescence in biological materials; however, the continued improvement in LED technology has made LEDs a viable alternative to lasers, which would enable the development of economical detectors for biological threats. Digital logic pulsing techniques were used to drive the LEDs, and an integrating sphere was used to measure the LEDs' average optical power as the duty-cycle and pulse repetition frequency (PRF) was varied. The digital logic pulsing techniques were successful in driving the LEDs; however, alternative pulsing techniques need to be developed to extract additional optical power from the LEDs. Once the LED driver circuit is properly developed, experiments investigating the LEDs' ability to produce fluorescence in biological particles can be done to determine if the LED is a viable alternative to the more costly laser source.

Java Based Interface for Particle Fragmentation Studies at the NASA Space Radiation Laboratory. JENNIFER MABANTA (*St. Joseph's College, Patchogue, NY 11772*) DR. MICHAEL SIVERTZ (*Brookhaven National Laboratory, Upton, NY 11973*). Before extended space missions can occur, protective measures must be in place for astronauts as prolonged exposure to radiation fields can have harmful and sometimes permanent effects. The purpose of the research done at the NASA Space Radiation Laboratory (NSRL) at Brookhaven National Laboratory (BNL) is to gain a better understanding of the cosmic rays in space and develop the most efficient countermeasure for the voyagers. Proton and heavy-ion beams from the BNL Booster accelerator are directed along a beam line to NSRL. By mimicking cosmic rays with the beam, the lab provides a controlled area in which to study the effects of the rays. The most harmful of the rays is iron, and the least destructive and most abundant is hydrogen. Of particular interest to NASA is the process of fragmentation, or the way in which heavy ions, like iron, break up into lighter less dangerous ions, such as protons. Currently, the methods used by the scientists to conduct analysis on fragmentation data are cumbersome at best. A program needed to be created to facilitate the studies being conducted at NSRL. A program called "Fragmentation Process" was developed which provides a graphical user interface (GUI) for the scientists interested in fragmentation

data. This Java-based program, written using an Emacs text editor, allows the user to collect data while the beam is on and provides graphs generated by the data in real time. These graphs can be made while data is still being taken or at the end with the total data sample collected. The graphs are displayed using a program called Ghostview and provide the scientist with a measure of the fragmentation in the beam. Prior to this, the work required to generate these graphs could take up to a week. Now, by utilizing the program, the calculations and resulting graphs are done immediately. Comparison of these graphs and the graphs generated prior to the creation of the GUI show that the program is displaying accurate information. The increased efficiency in studying fragmentation data at NSRL will be of great value to NASA and researchers will be able to gain a deeper understanding of fragmentation and develop the most effective shielding or other countermeasures for our astronauts.

Jet-Like Event Simulations for the FPD++ Calorimeter at STAR.

CHRISTOPHER MILLER (*Stony Brook University, Stony Brook, NY 11794*) **LES BLAND** (*Brookhaven National Laboratory, Upton, NY 11973*). The Forward Pion Detector upgrade (FPD++) to the STAR experiment at Brookhaven National Laboratory is capable of detecting photons at high rapidity. Most of these photons are produced from the decay of neutral pions (π^0) which are fragments of quark or gluon jets that have undergone small angle scattering in proton-proton collisions. My project was to quantify the average production of these photons with azimuthal symmetry about the forward jet axis. Asymmetries can arise in the fragmentation of forward scattered quarks and gluons from particles produced by spectators to the quark/gluon scattering. These asymmetries can serve as backgrounds to measurements that aim to establish the spin dependence of forward jet production. In order to accomplish my goal, I used a Monte Carlo generator called PYTHIA 6.222 to simulate the particle production at a total center of mass energy of 200 GeV. The correlation between the energy of each photon and its distance from the thrust axis, calculated from the photon's momentum sum vector, was histogrammed. The results were averaged over many events and a visualization of the jet shape was created, which allowed for a further analysis to quantify its azimuthal symmetry. In the end, the computer generated simulation showed a falling exponential trend of the jet shape from the leading pion and a small asymmetry between the left and right section of the jet. These results give an estimation of the underlying event background.

Jovian Planet Formation in 50 AU Binary Star Systems.

CHRISTIAN LYTLE (*University of St. Thomas, St. Paul, MN 55105*) **ANDY NELSON** (*Los Alamos National Laboratory, Los Alamos, NM 87545*). The detection of Jovian planets in large-separation binaries (>100 AU) has motivated investigation into the probability of planet formation in approximately 50 AU and smaller systems. We have run smoothed-particle hydrodynamics (SPH) simulations of binary systems with circumstellar disks and compared our results with others in the literature. Cooling based both on a fraction of the orbital period and a fully radiative model are implemented, but neither produce gravitational instabilities of the magnitude required for long term fragmentation of the disks, due primarily to the strong heating which occurs when the disks are near periape. These results are in conflict with simulations from the literature that have produced fragmentation in disks with morphologies similar to ours. We propose that the inconsistencies are attributable to numerical deficiencies (low resolution and fixed gravitational softening) and unrealistic initial conditions present in the previous work.

Laser Induced Fluorescence Motional Stark Effect Control & Data Acquisition Application.

PATRICK MALONEY (*Carleton College, Northfield, MN 55057*) **JILL FOLEY** (*Princeton Plasma Physics Laboratory, Princeton, NJ 8543*). The motional Stark effect (MSE) is a standard technique for measuring spatially resolved magnetic fields in plasma experiments. These fields are found with a beam of neutral hydrogen atoms which when traveling through a magnetic field perceive a Lorentz electric field in their own frame. The resulting electric field causes observable line splitting in hydrogen's spectral lines, which is proportional to the electric field. The polarization of the lines gives the field direction. However, while MSE is extremely effective for fields > 1 T, it can be difficult to measure weaker fields as a consequence of spectral line overlap. A dominant source of the overlap is from different emission lines being red and blue shifted across finite sized collection optics, an effect referred to as geometric broadening. To counter this effect, a method using Laser-Induced Fluorescence (LIF) to excite a single atomic transition at a time in the hydrogen beam has been proposed. Using this technique, the exact energy and thus wavelength of incoming photons is set by the laser, allowing geometric broadening effects to be completely ignored. Already the combination of MSE and LIF has been able to measure magnetic fields on the order of tens

of Gauss in neutral gases but has yet to be tested on plasma. The purpose of this project has been to implement a data acquisition and control system with LabView for the MSE-LIF development laboratory, including the new Spiral Antenna Helicon High Intensity Background (SAHHIB) experiment, a plasma test bed for LIF-MSE. The resulting program displays and records a variety of measurements including pressures at critical points in the vacuum system, laser and RF power characteristics, and most importantly, time dependent LIF signals used to find magnetic field magnitude and direction. The program is useful because previous measurements were primarily taken by hand making the collection of experimental parameters tedious. The data acquisition and control application developed to study LIF-MSE may also be employed for studying different instabilities in the helicon plasma source SAHHIB. Should the LIF-MSE device on SAHHIB prove successful, it will eventually be employed at the National Spherical Torus experiment (NSTX).

Limited Streamer Tube System for Detecting Contamination in the Gas Used in the BaBar Instrumented Flux Return.

LAURA HUNTLEY (*Franklin & Marshall College, Lancaster, PA 17603*) **MARK CONVERY** (*Stanford Linear Accelerator Center, Stanford, CA 94025*). The Resistive Plate Chambers (RPCs) initially installed in the Instrumented Flux Return (IFR) of the BaBar particle detector have proven unreliable and inefficient for detecting muons and neutral hadrons. In the summer of 2004, the BaBar Collaboration began replacing the RPCs with Limited Streamer Tubes (LSTs). LST operation requires a mixture of very pure gases and an operating voltage of 5500 V to achieve maximum efficiency. In the past, the gas supplies obtained by the BaBar Collaboration have contained contaminants that caused the efficiency of the IFR LSTs to drop from approximately 90% to approximately 60%. Therefore, it was necessary to develop a method for testing this gas for contaminants. An LST test system was designed and built using two existing LSTs, one placed 1 cm above the other. These LSTs detect cosmic muons in place of particles created during the BaBar experiment. The effect of gas contamination was mimicked by reducing the operating voltage of the test system in order to lower the detection efficiency. When contaminated gas was simulated, the coincidence rate and the percent coincidence between the LSTs in the test system dropped off significantly, demonstrating that test system can be used as an indicator of gas purity. In the fall of 2006, the LST test system will be installed in the gas storage area near the BaBar facility for the purpose of testing the gas being sent to the IFR.

Measurement of Fair Weather Air Conductivity.

NATISSA MCCLESTER, **KAMIL ZAKHOUR** (*Florence-Darlington Technical College, Florence, SC 29501*) **BRUCE WATSON**, **PAUL SABIN**, **SAKHER KHAYYAT**, **JEFF GRIFFIN** (*Pacific Northwest National Laboratory, Richland, WA 99352*). For the past 4 years, staff at the U.S. Department of Energy's Pacific Northwest National Laboratory have been investigating the generation, and transport of radiation-induced ions near the ground. Baseline measurements of fair weather atmospheric conductivity are required in order to estimate ions lifetimes and predict ions detectability downwind of a radioactive source. Using a Gerdien condenser, atmospheric conductivity measurements were made over a two week period, July 10-21, 2006 in the 300 Area of the Hanford Site. Experimental data, during that time period, show some uniformity, with atmospheric conductivity values ranging from 1.4 to $1.8 \times 10^{-14} \text{ S/m}$. These results are consistent with published values for arid rural desert regions throughout the world. Weather conditions were similar over the two weeks that the experiments were performed. Therefore; to obtain more valid background atmospheric conductivities, future experiments should look into variable weather conditions and evaluate their effects on atmospheric conductivities at the site.

Measuring the Point Spread Function of a High Resolution Charge-Coupled Device.

ANNA DERBAKOVA (*University of North Carolina-Chapel Hill, Chapel Hill, NC 27028*) **PAUL O'CONNOR** (*Brookhaven National Laboratory, Upton, NY 11973*). When a diffraction-limited point source of light passes through an optical system, it acquires aberrations from imperfections in the optics and becomes blurred due to lateral diffusion of photogenerated charge within the semiconductor detector. The quality of the optical system is characterized by the point spread function (PSF) which measures the amount of blurring that is present. The purpose of this experiment was to produce a light spot much smaller than a CCD pixel ($15 \times 15 \mu\text{m}$ square), characterize this light spot, and then use it to measure the PSF of a high resolution prototype charge-coupled device (CCD), which will later form the basis of the CCD camera in the Large Synoptic Survey Telescope (LSST). The point source for this experiment was obtained by coupling a diode laser to an optical fiber 4 μm in diameter. A light spot was obtained by imaging this point source using a long working-distance microscope

objective. In order to characterize this light spot, the knife-edge scan technique was used. Here, the point source was directed at a detector (photodiode) and a razor blade was scanned laterally through the focal region in increments of $0.1 \mu\text{m}$ at various axial positions. The amount of light incident on the detector was measured as a current using a picoammeter. The intensity was plotted versus position and fitted with an Erf function from which the rms spread, s , of the spot was determined. The rms spread of the light spot was measured to be: $s = 1.18 \mu\text{m}$. This spot was then projected onto the surface of the CCD and images were acquired as the point source was stepped across the CCD in sub-pixel increments. By summing the intensity in a fixed pixel window as the light spot is scanned across the edge of the window, the PSF can be obtained ("virtual knife-edge" technique). Subtracting the light-spot size in quadrature from the width of the fit to the virtual knife edge scans results in an estimate for the PSF of the CCD. The result in this case is $s = 7.25 \mu\text{m}$ or a FWHM of $17.06 \mu\text{m}$ which is the contribution of charge diffusion to the broadening of the image in the CCD. The results of this experiment will be useful in determining the optimum parameters for future prototype CCDs that will be used in the LSST high resolution CCD camera.

Mixed Apparatus Radar Investigation of Atmospheric Cosmic Rays of High Ionization Via the Triple Inverted V Array Antenna. ALISHIA FERRELL (Florida A & M University, Tallahassee, FL 32307), HELIO TAKAI (Brookhaven National Laboratory, Upton, NY 11973). The observation of ultra high energy cosmic rays (UHECR) is an ongoing mystery. There are two main issues surrounding these subatomic mechanisms. The first of the two is how do these mechanisms accelerate to such high energies? The second question is where are these mechanisms located in our universe? By studying these intense mechanisms we are only brushing the tip of the iceberg to our elusive universe. The Mixed Apparatus for Radar Investigation of Atmospheric Cosmic Rays of High Ionization (MARIACHI) will search for UHECR by detecting radio signals reflected from the extensive air showers (EAS) of charged particles created when the UHECR interacts with the earth's atmosphere. The task given was to design and build a portable, reconfigurable receiving antenna that is tunable to multiple Very High Frequency (VHF) frequencies. This receiving antenna also known as the Triple Inverted V Array Antenna (TIVAA) is based on a half-wave inverted v dipole design. TIVAA consists of three dipoles using metal tubes. The length of each dipole is variable leading to a change in the optimally detected frequency. Additionally, the angle of each v can be altered; orientation of the dipole array may also be altered as well. Mounted on a patio umbrella frame that was modified specifically as the antenna frame, which can be folded downward in a straight line for ease of portability the TIVAA is positioned at a specific location above the ground to minimize destructive interference with ground reflected waves. The TIVAA has special features which make it unique. The orientation of this receiving antenna can be altered, as well as the polar angle of each quarter wave element. The design has been chosen to optimize detection of radio signals which may consist of multiple polarizations. The results (to produce radio signals from local television and FM radio stations) aid the TIVAA in demonstrating the ability to tune well, to gain good isotropic reception, as well as attract other phenomena such as meteors and lightning. The TIVAA design may form the basis of a future array of antennas providing timing, direction, and ranging information for UHECR induced EAS.

Modeling X-ray Imaging with Monte Carlo N-Particle Software. JEREMIAH RUESCH (California State University-Chico, Chico, CA 95929) DR. TIMOTHY RONEY (Idaho National Laboratory, Idaho Falls, ID 83415). Monte Carlo simulation uses stochastic (random sampling) processes to solve equations that are difficult to solve by other means. For radiation transport the Boltzmann equation may be solved by Monte Carlo methods. Monte Carlo N-Particle (MCNP), a stochastic approach to solving the Boltzmann equation is utilized for our study. To ensure accuracy between the output of MCNP and known analytic results, a simple geometry is created with a monoenergetic pencil beam source shooting through a homogeneous material to a single detector element. The simulation was performed for three material thicknesses. The simulated detector response is used to derive the x-ray linear attenuation coefficient (LAC) of the material from Beer's Law and compared to the known LAC of the material for the energy of the source. The processed MCNP results were less than one percent different from the known LAC. To begin modeling the radiographic imaging process the material was changed to be spatially varying, the single detector element was replaced by a linear detector array of six elements, and the source changed from a pencil beam to a cone-beam configuration. The source was centered vertically on the linear detector array with the face of the array perpendicular to the source.

The distance between source and detector is held fixed. The object is defined as a rectangular block of iron with a rectangular aluminum insert. The object is located so that its face is perpendicular to the source, a distance of two centimeters from the detector array, and is then held fixed in this location. Moving the source and detector array to one end of the object, a run of MCNP is taken, creating a single vertical line of image data. The source and detector array are then moved a distance of one detector width and the simulation is repeated yielding an adjoining detector line. This process is repeated until the entire object is scanned and a two-dimensional image is produced. The images produced in this manner appear to have qualitative spatial and contrast features in agreement with our intuition. We have demonstrated the potential for using a stochastic particle transport modeling code (MCNP) to simulate x-ray imaging and have developed confidence in the numerical results by comparing derived quantities with known quantities (linear attenuation coefficients). Comparisons with experimental data are needed to validate the methods employed. This will be our next step.

Monitoring Displays for GLAST: Building ISOC Status Displays for the Large Area Telescope Aboard the Gamma Ray Large Area Space Telescope (GLAST) Observatory. CHRISTINA KETCHUM (Lewis and Clark College, Portland, OR 97219) ROB CAMERON (Stanford Linear Accelerator Center, Stanford, CA 94025). In September 2007 the Gamma Ray Large Area Space Telescope (GLAST) is scheduled to launch aboard a Delta II rocket in order to put two high-energy gamma-ray detectors, the Large Area Telescope (LAT) and the GLAST Burst Monitor (GBM) into low earth orbit. The Instrument Science Operations Center (ISOC) at SLAC is responsible for the LAT operations for the duration of the mission, and will therefore build an operations center including a monitoring station at SLAC to inform operations staff and visitors of the status of the LAT instrument and GLAST. This monitoring station is to include sky maps showing the location of GLAST in its orbit as well as the LAT's projected field of view on the sky containing known gamma-ray sources. The display also requires a world map showing the locations of GLAST and three Tracking and Data Relay Satellites (TDRS) relative to the ground, their trail lines, and "footprint" circles indicating the range of communications for each satellite. The final display will also include a space view showing the orbiting and pointing information of GLAST and the TDRS satellites. In order to build the displays the astronomy programs Xephem, DS9, SatTrack, and STK were employed to model the position of GLAST and pointing information of the LAT instrument, and the programming utilities Python and Cron were used in Unix to obtain updated information from database and load them into the programs at regular intervals. Through these methods the indicated displays were created and combined to produce a monitoring display for the LAT and GLAST.

Nanosecond-Length Electron Pulses for a Time-of-Flight Mass Spectrometer. LIANNE MARTINEZ (University of Nevada-Las Vegas, Las Vegas, NV 89123) HERBERT FUNSTEN, PAUL JANZEN (Los Alamos National Laboratory, Los Alamos, NM 87545). The Spatially Isochronous Time-of-Flight (SITOF) mass spectrometer is a rapid mass analysis of gaseous samples at a high mass resolution in a small volume. The mass spectrometer incorporates a pulsed electron ionization source within the drift region itself, eliminating a separate ion source and its associated mass, power, and volume resources. Gas in the drift region is ionized at the same time by the pulsed electron source, and the ions are accelerated by a linear electric field in the drift region so that their time-of-flight in the drift region is independent of the location at which they were ionized. The current proof-of-concept pulsed electron source uses a channel electron multiplier stimulated by a weak radioactive source to produce electron pulses approximately 10 ns long. These pulses have been characterized, and development has started on a pulsed electron source which uses a microchannel plate stack to multiply photoelectrons produced from a fast ultraviolet LED. This method produces electron pulses of a shorter duration, over a larger area, at a controllable frequency. We discuss the time dispersion of the pulsed electron source, its dependence on detector bias and gain, and its impact on the mass resolution of the SITOF mass spectrometer.

Novel Coarsening of Pb Nanostructures on Si(111) 7 X 7. CHARLES PYE (University of Kansas, Lawrence, KS 66044) MICHAEL TRINGIDES (Ames Laboratory, Ames, IA 50011). In order to study a possible means of controlling the growth of a self-assembled nanostructure grown epitaxially, Pb/Si(111) was analyzed. The experiments were performed with a Scanning Tunneling Microscope (STM) on a Si(111) 7 X 7 crystal prepared atomically clean under Ultra High Vacuum (UHV) conditions followed by Pb deposition. The islands were monitored in time to see how they coarsen and whether

the classical theory of Ostwald ripening is applicable. STM Images of the resulting Pb islands were taken as they evolved in time. Height measurements indicated that initially, the majority (25 out of 33 islands) were 4 or 5 layer islands, but by the end of the experiment 68 minutes later, the majority (18 out of 24 islands) were 7 or 9 layer islands. Additional measurements of the area indicate that the total area of all the islands was reduced by 10%, but the total volume increased by ~40%, presumably coming from the wetting layer. Measurements of island area and height over time indicated that an increase in height was accompanied by a sudden (within 2-3 minutes) increase in volume and decrease in area. Some islands grew by adding a ring of higher height around the edge before filling in the center. These rings, on average, would fill in less than 5 minutes. Generally, the islands started in a random shape, and gradually became more like a regular hexagon over time. These observations are very unusual because they do not fit the classical expectations based on Ostwald ripening and they show the role of Quantum Size Effects upon the coarsening.

***Numerical Simulations of Electric and Magnetic Fields for the Pulse Line Ion Accelerator.** SAMUEL PEREZ (*Contra Costa College, San Pablo, CA 94806*) ENRIQUE HENESTROZA (*Lawrence Berkeley National Laboratory, Berkeley, CA 94720*). The Pulse Line Ion Accelerator (PLIA) is a (slow-wave) helical structure whose purpose is to accelerate charged particles. It uses a voltage pulse to generate a traveling electric field along its length. In order to efficiently produce a working PLIA and know how to use it, a simulation of the PLIA was created and the electric and magnetic fields it produces were plotted using the Electromagnetic Field Solver "CST Microwave Studio". In addition to the plots offered by Microwave Studio, more specialized plots were created using the particle code WARP. The geometry is simple: a helix embedded in dielectric material inside a conducting box with a cylindrical vacuum through its center. The voltage pulse is applied on a loop around one end of the helix, thus coupling inductively to the helix. A coarse mesh was used at first so that adjustments could be made quickly. Once the simulation correctly produces a traveling wave, the helix was changed to its final dimensions and a finer mesh was used to generate sufficient data. The plots created by CST Microwave Studio show that the electric field travels the length of the PLIA at about 1/60 the speed of light, the expected value given the permittivity of the dielectric material, the helix dimensions, and the beam pipe radius. The field does not begin to move until after the voltage pulse ended. There are actually two fields, a positive and a negative field, which move with the negative field ahead of the positive field. The field is also defocusing in the transverse direction so that positive charges will be sent outward into the walls of the PLIA. In order to successfully use the PLIA, the beam will have to enter the structure so that it only interacts with the positive field. It is also necessary to have powerful solenoids around the PLIA to focus the beam. Continued work on the PLIA could prove it as an inexpensive slow-wave accelerator for use in Fusion research.

Optimization of Shield Mass for a Low Power, Fast-Spectrum Liquid-Metal Cooled Surface Reactor System. ROBERT FORESMAN (*Pomona College, Claremont, CA 91711*) DAVID I. POSTON (*Los Alamos National Laboratory, Los Alamos, NM 87545*). Extending our presence further into space furnishes opportunities for research science, potential human colonization beyond Earth, and a more mature understanding of the cosmos. One of the foremost challenges in this effort is the identification of a low-cost power source that will accommodate scientific instrumentation and mission necessities for long periods of time. Low power nuclear reactors that utilize well-tested materials and concepts such as stainless steel and water shields can operate in the 25 kW electrical range. By short-circuiting exotic designs, these reactors reduce the cost and time of development in the face of a strict U.S. budget. Gamma radiation dose to the Stirling alternator power conversion system and total astronaut dose can be kept to their nominal minimums of 20 MRad and 5 Rem/yr by burying the reactor in lunar surface material (regolith) on Moon missions.¹ An alternative option is to install a permanent water shield on the reactor. Minimization of additional shield mass for such a system is an interesting engineering problem that is ideally suited to a radiation transport software program called MCNPX (Monte Carlo Neutral Particle). MCNPX output files contain criticality statistics to ensure a stable reaction and allow direct determination of dosages. Shield thickness, placement of interstitial, high-Z shield elements, and boron concentration in shield water will be treated as variables for system optimization. Initial simulations show that roughly 93% of the gamma dose to astronauts at 800 meters from the reactor core is due to radiative capture in the water shield. A borated water shield that meets astronaut dosage requirements and has a total mass of roughly 5,000 kg can be constructed utilizing interstitial stainless-steel layers of

varied thickness. This total shield mass of 5000 kg must be compared to the total mass of a buried system configuration including burying equipment. Further investigations include the addition of different shielding materials such as depleted uranium throughout the shield as well as moving the reactor core off-center within the water shield.
¹Marclite, T. F., Dixon, D. D., Fischer, G. A., Doherty, S. P., Poston, D. I., and Kapernick, R. J. Design Of a Low Power, Fast-Spectrum, Liquid-Metal Cooled Surface Reactor System. Nuclear Systems Design Group, Los Alamos National Laboratory, Los Alamos, NM 87544., pp 1-3.

Particle Physics in the High School Classroom. CANDICE HUMPHERYS (*Brigham Young University-Idaho, Rexburg, ID 83460*) HELIO TAKAI (*Brookhaven National Laboratory, Upton, NY 11973*). The main goal of the Mixed Apparatus for Radar Investigation of Atmospheric Cosmic rays of High Ionization (MARIACHI) project is to explore the detection of ultra high energy cosmic rays via radio signals. To confirm that the data received using radio is legitimate, scintillator detectors (a known way to detect cosmic rays) have also been set up to collect data and have been placed in high school classrooms on Long Island. MARIACHI is involving students as participants in the project and faces two main problems: (a) the world of modern physics is absent from the high school physics curriculum and (b) techniques for data analysis need to be introduced. To bridge the gap between a cosmic ray shower being recorded by the scintillator setup and the actual physics phenomena, we have developed two low-cost experiments. First, the existence of atoms can be shown by the phenomenon of Brownian motion (particles in a fluid move randomly). Software was tried out successfully to test the practicality of tracking a particular particle to plot its position and show its randomness. The second experimental apparatus is a novel cloud chamber with a strong magnetic field. With this cloud chamber in the classroom, tracks from cosmic ray particles (as well as particles from other sources of radiation) can be visualized and students can get a grasp on what the scintillators are detecting. This particular cloud chamber exposes students to a wide range of modern physics from the existence of elementary particles to the relation between energy and matter through electron-positron production events. To introduce the first steps of data analysis, tutorials were developed to allow students and teachers alike to analyze the scintillator data to look for any possible problems with the detectors or interesting correlations with external parameters such as barometric pressure. The tutorials were tested by two high school students and their feedback was used to improve them.

Properties of Light Vector mesons in Dense Nuclei. SCARLET NORBERG (*Kent State University, Kent, OH 44243*) DENNIS WEYGAND (*Thomas Jefferson National Accelerator Facility, Newport News, VA 23606*). The strong force is a fundamental force, which describes the forces in the nucleus, and is expressed by Quantum Chromodynamics (QCD). In dense and hot matter, masses may change while the underlying symmetries remain intact. In addition, coupling constants may change. Thus properties of vector mesons, such as their masses and widths, may change in dense or hot matter. These modifications are related to the partial restoration of chiral symmetry at high density and/or temperature. The g7 experiment was performed using the Large Acceptance Spectrometer (CLAS) at Jefferson Lab using a tagged photon beam of energies up to 4 GeV on various nuclear targets. Because the photon can penetrate the nuclear volume, the interaction occurs approximately uniformly throughout the nuclear medium. The properties of the lightest vector mesons, rho, omega, and phi are investigated through their rare leptonic decay to e⁺e⁻. This decay channel is preferred over hadronic modes in order to eliminate the final state interactions of the decay products in the nuclear matter. The goal of this study is to examine any changes in the mass and/or width of rho, omega and phi produced in the nuclear medium. In this study, the mass and width of the rho meson have been measured in both a light nuclear target, deuterium, an intermediate target, carbon, and a heavy target, iron. The spectral function of the rho meson was compared to the correct resonance form, a Breit-Wigner function modified by an electromagnetic propagator (1/m³) required by the e⁺e⁻ decay. It was found that the mass and width of the rho meson does not change in carbon nor deuterium. In iron, while the mass of the meson is stable, there is an indication that the width changes by about 2 sigma, consistent with collisional broadening effects. Implications of the results of g7 will have a major impact on the interpretation of experiments of the low mass e⁺e⁻ pairs currently being performed in high-energy heavy ion collisions at the Relativistic Heavy Ion Collider (RHIC) at Brookhaven.

Quark Propagation and Hadronization in the Nuclear Medium. GRANT LARSEN (*University of Chicago, Chicago, IL 60637*) KAWTAR HAFIDI (*Argonne National Laboratory, Argonne, IL 60439*). Hadrons are color neutral combinations of quarks. The theory of the strong, or color, force is not yet entirely clear on how quarks break free of gluons

(the particles that hold hadrons together), and form new hadrons, a process known as hadronization. Because of confinement, an exotic effect of the strong force, no color charged particle (such as a quark) can exist in solitude. Therefore, to measure such particles, an indirect process is required. Firing electrons at targets in the right energy range can strike a quark hard enough to make this process of hadronization occur, but slowly enough that this process occurs within the small space of the target's nucleus. This was done with a 5.014 GeV beam in Thomas Jefferson National Accelerator Facility in Newport News, Virginia, on targets of deuterium, carbon, iron, and lead. The number of pions emitted from the heavier target compared to the number emitted from deuterium (normalized by the total number of events recorded in each case) was measured for the carbon, iron, and lead targets. This multiplicity ratio was compared between the different atoms and for pions that had different energies available, took different fractions of that energy, and that lost different amounts of that energy to gluon radiation. Also measured were quantities directly related to the energy loss of quarks propagating in the nuclear medium and the distance they do so before becoming hadrons. Using these data, relationships between the momentum and energy the electron imparts to the quark, the energy lost radiating gluons, the distance the quark goes before hadronizing, the fraction of the energy available that the hadron ends up with, and the likelihood that the nucleus reabsorbs the hadron can all be inferred. These results confirm the expectations of theorists as well as back up the results of related experiments, expanding the results to different kinematical ranges. These data also give theorists more information to work with to understand these processes. Still more interesting kinematical ranges, details of the effects of nuclear size, and the dependence of these processes on the flavor of the struck quark, are all yet to be investigated. All of these goals can be met using the forthcoming 11 GeV upgrade to Jefferson Lab.

Sensitivity Study of the Relative Fraction of Top/Anti-Top Events Produced via Gluon-fusion. *KELLY GREENLAND (Lock Haven University of Pennsylvania, Lock Haven, PA 17745) DR. RICARDO EUSEBI (Fermi National Accelerator Laboratory, Batavia, IL 60510).* In high-energy experimental particle physics, a primary goal is to study particles that the scientists create, and by studying those particles physicists results aid in confirming the validity of the standard model of particles. To date, the standard model is the best representative model of basic particles, and confirming the model helps to reassure physicists the model is indeed on the right path. At the Fermi National Accelerator Laboratory a circular particle accelerator, called the Tevatron, accelerates protons and anti-protons to approximately 0.999 times the speed of light before colliding with each other. The proton's constituents, gluons and quarks, may interact with enough energy to create particles not initially present. If a quark and anti-quark interact they will annihilate and may produce a top/anti-top quark pair. Also, a gluon may fuse with another gluon to produce a top/anti-top pair. This study focuses on finding the accuracy with which scientists can measure the ratio of top/anti-top pairs created by quark/anti-quark annihilation to that created by gluon-fusion. The degree of accuracy of measuring the relative fractions was determined via computer simulation. Initially gluon-fusion and quark-annihilation top/anti-top events were generated by Monte-Carlo simulations. Next, matrix element probabilities were determined for each event. Using these probabilities, a set of templates were created. Finally, in preparation to analyze the data, a likelihood was constructed based on the templates. The likelihood was never run on data, but only on Monte-Carlo simulations to obtain the degree of accuracy, or sensitivity, that this method can provide. Past studies claim an accuracy measurement of 22%. This study shows a strong improvement of the ratio to approximately 15%. While this is clearly an improvement, the expected degree of accuracy cannot yet ensure that the ratios predicted by the standard model, regarding production top/anti-top events, are indeed correct.

Simulation of a Very Long Baseline Neutrino Beam. *JORDAN HEIM (Purdue University, West Lafayette, IN 47906) MARY BISHAI (Brookhaven National Laboratory, Upton, NY 11973).* Observations indicating that the number of solar neutrinos incident upon Earth is fewer than predicted by the Standard Solar Model have led to the theory that the neutrinos are experiencing a phenomenon known as oscillation, where one flavor of neutrino becomes another. The confirmation of this theory is crucial to understanding the behavior of neutrinos. By employing a man-made neutrino beam, the energies and types of neutrinos can be carefully controlled and the expected numbers of neutrinos, taking into account oscillation, thus known. Computer simulations of the particle interactions throughout the beamline's many components were carried out with various pieces of software including MARS, GEANT, and Fluka05. This data was then analyzed

using packages such as GloBeS, and ROOT to create histograms of the physical phenomena. Repeating these exercises, while varying simulation parameters such as target properties, beam energy, and the length of the decay pipe, allowed the optimal characteristics to be found. With a predetermined far-detector distance of 1300Km, it was found that as the target length and density is increased, more particle interactions can be observed, as expected. Also, using a beam energy of forty to sixty GeV and using a shorter, but wider decay tunnel provides the best balance between reducing the unwanted high energy contribution while maintaining a reasonable flux rate at the far detector. These results provide guidelines for building a successful project which will yield an answer for the value of the mixing parameter which dictates the oscillating behavior of the particles and will reveal CP (charge parity) violation.

Simulation of Radioactive Ions for the Tevatron. *JOSEPH BOUIE III (Southern University, Baton Rouge, LA 70813) TERRENCE REESE (Fermi National Accelerator Laboratory, Batavia, IL 60510).* To generate a very pure and intense neutrino beam for Neutrino Physics experiments, it has been proposed to use the beta-decay of radioactive ions stored in a high energy decay ring. The original proposal was to use parts of the existing CERN infrastructure, namely the Proton Synchrotron (PS) and the Super Proton Synchrotron (SPS), to accelerate the ions to 100GeV, but recent work has shown that it would be advantageous to go to even higher energies. The Tevatron, located at Fermi National Accelerated Laboratory, will be retired from Collider Physics in a few years, and could be used for this purpose. However, the decay products from the ions will present a significant heat load to the superconducting magnets, which will limit the number of ions that can be accelerated. To understand where the limit is, a simulation of heat deposition from the decay products is needed.

Simulation of the BaBar Drift Chamber. *RACHEL ANDERSON (University of Wisconsin-Eau Claire, Eau Claire, WI 54701) JOCHEN DINGFELDER (Stanford Linear Accelerator Center, Stanford, CA 94025).* The BaBar drift chamber (DCH) is used to measure the properties of charged particles created from e^+e^- collisions in the PEP-II asymmetric-energy storage rings by making precise measurements of position, momentum and ionization energy loss (dE/dx). In October of 2005, the PEP-II storage rings operated with a luminosity of $10 \times 10^{33} \text{ cm}^{-2} \text{ s}^{-1}$; the goal for 2007 is a luminosity of $20 \times 10^{33} \text{ cm}^{-2} \text{ s}^{-1}$, which will increase the readout dead time, causing uncertainty in drift chamber measurements to become more significant in physics results. The research described in this paper aims to reduce position and dE/dx uncertainties by improving our understanding of the BaBar drift chamber performance. A simulation program—called GARFIELD—is used to model the behavior of the drift chamber with adjustable parameters such as gas mixture, wire diameter, voltage, and magnetic field. By exploring the simulation options offered in GARFIELD, we successfully produced a simulation model of the BaBar drift chamber. We compared the time-to-distance calibration from BaBar to that calculated by GARFIELD to validate our model as well as check for discrepancies between the simulated and calibrated time-to-distance functions, and found that for a 0° entrance angle there is a very good match between calibrations, but at an entrance angle of 90° the calibration breaks down. Using this model, we also systematically varied the gas mixture to find one that would optimize chamber operation, which showed that the gas mixture of 80:20 Helium:isobutane is a good operating point, though more calculations need to be done to confirm that it is the optimal mixture.

Simulations of the ILC Electron Gun and Electron Bunching System. *CHRISTIAN HAAKONSEN (McGill University, Montreal, QC H3A 2B7) AXEL BRACHMANN (Stanford Linear Accelerator Center, Stanford, CA 94025).* The International Linear Collider (ILC) is a proposed electron-positron collider, expected to provide insight into important questions in particle physics. A part of the global R&D effort for the ILC is the design of its electron gun and electron bunching system. The present design of the bunching system has two sub-harmonic bunchers, one operating at 108 MHz and one at 433MHz, and two 5-cell 1.3 GHz (L-band) bunchers. This bunching system has previously been simulated using the Phase and Radial Motion in Electron Linear Accelerators (PARMELA) software, and those simulations indicated that the design provides sufficient bunching and acceleration. Due to the complicated dynamics governing the electrons in the bunching system we decided to verify and expand the PARMELA results using the more recent and independent simulation software General Particle Tracer (GPT). GPT tracks the motion and interactions of a set of macro particles, each of which represent a number of electrons, and provides a variety of analysis capabilities. To provide initial conditions for the macro particles, a method was

developed for deriving the initial conditions from detailed simulations of particle trajectories in the electron gun. These simulations were performed using the Egun software. For realistic simulation of the L-band bunching cavities, their electric and magnetic fields were calculated using the Superfish software and imported into GPT. The GPT simulations arrived at similar results to the PARMELA simulations for sub-harmonic bunching. However, using GPT it was impossible to achieve an efficient bunching performance of the first L-band bunching cavity. To correct this, the first L-band buncher cell was decoupled from the remaining 4 cells and driven as an independent cavity. Using this modification we attained results similar to the PARMELA simulations. Although the modified bunching system design performed as required, the modifications are technically challenging to implement. Further work is needed to optimize the L-Band buncher design.

Single and Double GEM X-Ray Based Detectors. ERIC HUEY (Southern University A&M, Baton Rouge, LA 70811) DR. DAVID PETER SIDMONS (Brookhaven National Laboratory, Upton, NY 11973). The purpose of this research is to present results obtained from testing of a single and double GEM X-ray gaseous detectors. The detectors have been designed, assembled, and tested at NSLS controls and detector's group at BNL. The single and the double GEM detectors are intended to provide a noise and discharge free amplification to be used for Extended X-ray Absorption Fine Structure (EXAFS) procedure. A voltage of 450 volts across the single GEM provided a maximum gain of 900. A voltage of 350 volts across each of the double GEM provided a gain of 9000 without stressing the GEM and creating the possibility of discharges.

Software for The Perfect PID. KURTIS GEERLINGS (Michigan State University, East Lansing, MI 48825) HOLGER MEYER (Fermi National Accelerator Laboratory, Batavia, IL 60510). The Main Injector Particle Production Experiment (MIPP, FNAL E-907) promises to shed light on many aspects of the particle physics world, from proton radiography to nuclear physics and from neutrino flux measurements to non-perturbative QCD. MIPP uses several detectors in order to obtain nearly 100 percent acceptance for charged particles over a vast momentum range, yielding nearly perfect particle identification. The detectors include two beam cerenkovs, a time projection chamber (TPC), a threshold cerenkov, a ring imaging cerenkov (RICH), a time-of-flight system and an electromagnetic/hadronic calorimeter. While the detectors are very important, without software to analyze the data, no physics can be discovered. The MIPP software, written mainly in C++, includes packages to reconstruct tracks of charged particles in the TPC and packages to fit rings to the cerenkov radiation in the RICH. Equally important is the monte carlo package, which allows one to compare simulations with data. To most effectively test the analysis software with the simulation, the monte carlo must output its data in the same format as the experimental data. This process is often called digitization. In the case of the threshold cerenkov, it represents converting exact timing information from the simulation into a time to digital converter (TDC) signal, and the number of photoelectrons detected into an analog to digital converter (ADC) signal. This way, the monte carlo information resembles the data coming from detectors. Another important aspect to consider is testing and debugging of existing code. Since many people have contributed to the MIPP software, it is important to debug and test code written by other people. This helps to ensure that the software does what it is supposed to, and results are not based on false analysis.

Speeding up the Raster Scanning Methods used in the X-Ray Fluorescence Imaging of the Ancient Greek Text of Archimedes. MANISHA TURNER (Norfolk State University, Norfolk, VA 23504) DR. UWE BERGMANN (Stanford Linear Accelerator Center, Menlo Park, CA 94025). Progress has been made at the Stanford Linear Accelerator Center (SLAC) toward deciphering the remaining 10-20% of ancient Greek text contained in the Archimedes palimpsest. The text is known to contain valuable works by the mathematician, including the Method of Mechanical Theorems, the Equilibrium of Planes, On Floating Bodies, and several diagrams as well. The only surviving copy of the text was recycled into a prayer book in the Middle Ages. The ink used to write on the goat skin parchment is partly composed of iron, which is visible by x-ray radiation. To image the palimpsest pages, the parchment is framed and placed in a stage that moves according to the raster method. When an x-ray beam strikes the parchment, the iron in the ink is detected by a germanium detector. The resulting signal is converted to a gray-scale image on the imaging program, Rasplot. It is extremely important that each line of data is perfectly aligned with the line that came before it because the image is scanned in two directions. The objectives of this experiment were to determine the best parameters for producing well-aligned images and to reduce the scanning time. Imaging half a page of parchment during previous beam time for

this project was achieved in thirty hours. Equations were produced to evaluate count time, shutter time, and the number of pixels in this experiment. On Beamline 6-2 at the Stanford Synchrotron Radiation Laboratory (SSRL), actual scanning time was reduced by one fourth. The remaining pages were successfully imaged and sent to ancient Greek experts for translation.

Star Formation and Feedback in Adaptive Mesh Refinement Cosmological Simulations. SAM SKILLMAN (Harvey Mudd College, Claremont, CA 91711) BRIAN O'SHEA (Los Alamos National Laboratory, Los Alamos, NM 87545). Correctly simulating star formation within large-scale cosmological simulations is currently a problem of great interest. This is in part due to the recent explosion of observational data from projects such as the Sloan Digital Sky Survey, DEEP, and 2dF. Using ENZO, an adaptive mesh refinement (AMR) with N-body plus hydrodynamics cosmological code, I explore three star formation algorithms which lead to a range of star formation histories. Stellar feedback models are coupled to each of the star formation algorithms, and provide thermal, kinetic, and metal feedback in our simulations. Each star formation algorithm uses several parameters which I vary in order to gain an understanding of their effect on the star formation history of the universe.

Structural and Functional Studies of Multidrug Binding Protein, AcrR. DENAE CLAMPITT (Western Illinois University, Macomb, IL 61455) EDWARD YU (Ames Laboratory, Ames, IA 50011). This project addresses fundamental questions regarding the nature of multi-ligand recognition in transcriptional regulators. The primary target is the Escherichia coli AcrR repressor that regulates the multidrug transporter AcrB. The 215-residue AcrR consists of two domains, the C-terminal multi-ligand binding and the N-terminal DNA binding domains. Upon binding a wide variety of structurally diverse ligands in the C-terminal region, it triggers conformational change at the N-terminal domain, prohibiting the binding of AcrR to its target DNA. The sum result is the over-expression of the AcrB transporter, which, in turn, promotes efflux from the cell, thus protecting it from toxic substances. How can AcrR and other transcriptional repressors recognize a variety of toxic chemicals? To gain insight into the mechanism that AcrR uses to recognize multi-ligand, we crystallized the AcrR protein, and studied its function using circular dichroism and tryptophan fluorescence measurements. We also measured the binding affinities of rhodamine-6G, ciprofloxacin, and ethidium bromide with AcrR. As AcrR is capable of recognizing a variety of toxic chemicals, this research has the potential to contribute to the development of protein-based chemical sensors.

Study of the Effect of Larger Wire Diameter on Drift Chamber Performa. NATALIE HANSEN (Brigham Young University, Provo, UT 84606) MAC MESTAYER (Thomas Jefferson National Accelerator Facility, Newport News, VA 23606). A wire chamber is essentially a gas-filled box traversed by anode (sense) and cathode (field) wires held at a high electric potential difference that is used to detect charged particles. Electrons are freed as a particle ionizes gas atoms in its path. These electrons travel along field lines and register as a current when reaching the sense wires. The distance between wires, the gas composition and the voltage difference between wires all determine the detection efficiency. The drift chambers for the Continuous Electron Beam Accelerator Facility (CEBAF) Large Acceptance Spectrometer (CLAS) detector at Jefferson Lab use a 90% argon and 10% CO₂ gas mixture and sense wires of 20 μm diameter. Proposed changes for a planned upgrade include increasing the sense wire diameter to 30 μm, which, however, may lead to increased levels of noise. This project focused on assembling a prototype chamber to test the effect of changing the sense wire diameter. A previously built chamber was restrung with 30 μm wire, leaving one 20 μm wire for comparison. The associated electronic equipment and gas system were set up and the chamber is operational. The experimental results were plots of count rate versus voltage for different discriminator settings. Individual plots show a hint of a high voltage plateau around 1500–1525 V, despite the fact that much of the data were inconsistent, presumably due to bursts of external, electronic noise. When the hit rate was plotted versus gas gain rather than voltage, the individual graphs for different discriminator settings came very close to a universal curve. Any slight deviations from that curve may be due to the increased probability of spontaneous electron emission (noise) from the field wire. Increasing the sense wire radius and the voltage seems to yield only a modest increase of noise levels.

Suitability of a New Calorimeter for Identifying Exotic Meson Candidates. CRAIG BOOKWALTER (Florida State University, Tallahassee, FL 32306) PAUL EUGENIO (Thomas Jefferson National Accelerator Facility, Newport News, VA 23606). Exotic mesons, particles

that have quantum numbers that are inaccessible to conventional quark-model mesons, are predicted by quantum chromodynamics (QCD), but past experiments seeking to identify exotic candidates have produced controversial results. The HyCLAS experiment (E04005) at Thomas Jefferson National Accelerator Facility (TJNAF) proposes the use of the Continuous Electron Beam Accelerator Facility (CEBAF) Large Acceptance Spectrometer (CLAS) in Hall B to study the photoproduction of exotic mesons. However, the base detector package at CLAS is not ideal for observing and measuring neutral particles, particularly at forward angles. The Deeply Virtual Compton Scattering (DVCS) experiment at TJNAF has commissioned a new calorimeter for detecting small-angle photons, but studies must be performed to determine its suitability for a meson spectroscopy experiment. The $\eta\pi$ system has been under especial scrutiny in the community as a source for potential exotics, so the new calorimeter's ability at reconstructing these resonances must be evaluated. To achieve this, the invariant mass of showers in the calorimeter are reconstructed. Also, two electroproduction reaction channels analogous to photoproduction channels of interest to HyCLAS are examined in DVCS data. It is found that, while not ideal, the new calorimeter will allow access to additional reaction channels, and its inclusion in HyCLAS is warranted. Results in basic shower reconstruction show that the calorimeter has good efficiency in resolving π^0 decays, but its η reconstruction is not as strong. When examining $e\pi\alpha e\pi\eta$, preliminary reconstruction of the $\eta\pi^0$ system shows faint signals in the $a_0(980)$ region. In the $e\pi\alpha e\pi\eta$ channel, preliminary reconstruction of the $\eta\pi^+$ system gave good signals in the $a_0(980)$ and $a_2(1320)$ regions, but statistics were poor. While more analyses are necessary to improve statistics and remove background, these preliminary results support the claim that the DVCS calorimeter will be a valuable addition to CLAS for upcoming exotic meson searches in photoproduction.

Systematic Search for Lanthanum or Bismuth Oxide Scintillators.

ALEISHA BAKER (North Carolina A&T State University, Greensboro, NC 27411) STEPHEN DERENZO (Lawrence Berkeley National Laboratory, Berkeley, CA 94720). More than ever, there is need for new or improved scintillators to keep up with the advancements in radiation detection technology. Known scintillators decay slowly, have low light output, and can be difficult to manufacture. In efforts to discover new ideal scintillators, researchers must search, synthesize, and characterize compounds that exhibit luminescent traits. This research focused on 12 bismuth and lead compounds. Candidates were synthesized by means of a solid-state chemistry technique known as the ceramic method. The products were characterized using x-ray diffraction, fluorescence spectroscopy, and pulsed x-ray measurements. The compounds studied did not show attributes of a high scintillation. However, since several of the band gaps have band gaps greater than 3.5 eV, they may be modified to form semiconductor scintillators in the future.

***Systematic Studies of the Faraday Effect on Glass Interfaces.**

DANIEL CARRERO (Stony Brook University, Stony Brook, NY 11794) DR. CAROL SCARLETT (Brookhaven National Laboratory, Upton, NY 11973). The investigation into anomalous space-time curvature has shown strong signals of heavy consequence to this experiment. The understanding of said signals must be investigated in order to determine whether or not these signals are of consequence to anomalous space-time curvature due to photon interactions with an alternating magnetic field, or other effects including systematic anomalies. With respect to these systematic effects, the study of birefringence as a result of a possible Faraday Effect on glass windows used to encase a vacuum of 1×10^{-9} Torr was explored. A Relativistic Heavy Ion Collider (RHIC) quadra-pole magnet housing this vacuum will be ramped at a frequency of 80 mHz where residual magnetic field on the order of 200 gauss will represent a changing flux through the glass caps at the ends. Photon interactions propagating through the vacuum via an external laser will be subject to any birefringent effects of the glass. Such effects can cause deviations in our beam at the characteristic frequency of 80 mHz which when resolved on a photo receiver can mask any true, non systematic effects. In an effort to understand this, the development of an independent system isolating the glass windows was implemented. Using a motorized rotating stage, two permanent magnets each having a magnitude of .1 Tesla, was placed on the stage positioned 2cm from the window interface such that the overall magnetic field through the window was on the order of 200 gauss. A He-Ne laser beam with a wavelength of 514nm was then propagated through the window and magnetic field onto a photo receiver. The stage rotating at a frequency of 80 mHz generated a changing magnetic flux such that any birefringence effects will be resolved onto the photo receiver at the characteristic frequency of 80 mHz. Data was then collected from the

photo receiver in 5 minute intervals totaling 25 Hrs. This data, using Fortran code, was then Fourier analyzed such that any signals residing in a frequency range of 0 Hz-.1 Hz can be determined. Analyzing this data demonstrated that within the bounds of the sensitivity of the photo receiver and Fortran code, no signal was determined. The understanding of this effect helps rule out one systematic effect that can cause illegitimate results. These ramifications open other avenues for investigation, possibly minimizing systematic effects ultimately leaving true physical results.

The ChicaneTracker Module in the ORBIT Injection Upgrade.

DANIEL COUPLAND (Albion College, Albion, MI 49224) SARAH COUSINEAU (Oak Ridge National Laboratory, Oak Ridge, TN 37831). The accumulator ring in the Spallation Neutron Source (SNS) will accumulate up to 1014 protons at a time from a 1 GeV linear accelerator to produce neutrons by spallation. In order to satisfy radiation hazard requirements, no more than 0.02% of the beam in the SNS ring may be lost by collisions with the beam pipe. Since most accelerators lose 1–2% of their beam, the SNS must be far more effective in beam loss control than any previous high-intensity accelerator. This requires very precise understanding of the mechanisms which contribute to beam loss. One of the main sources of loss in the accelerator is in the injection area of the ring, where H^- particles are converted to protons by passing through a thin foil that strips off the electrons. Some of the H^- particles are not fully stripped, and live for a short time as H^0 particles in excited quantum states before decaying in the ring magnetic fields. If the magnetic fields are not optimized, particles that decay may be deflected from the paths intended for either H^- or protons and become lost in the accelerator. The SNS project will upgrade the beam power in the year 2010, and this will require a redesign of the injection region of the ring. Testing of new design schemes will be done primarily with the Objective Ring Beam Injection and Tracking Code (ORBIT), a modular simulation package designed at SNS specifically for modeling high intensity rings. In this project, the ORBIT code was upgraded to allow precise simulations of the injection region of the ring. This work included installing code that performs detailed tracking of all three relevant states of hydrogen through the dipole magnetic fields in the injection region, and determines on each step which neutral particles decay into protons. The physical configuration of the chicane is customizable, allowing particle positions to be compared to the real location of the beam pipe and losses to be determined. The code is configured to allow parallel runs on multiple machines to accommodate computationally intensive tests. Results from this code were benchmarked with previous studies of excited-state decay done by Danilov and Galambos *et al.*, and showed excellent agreement. Future modifications to the ORBIT injection region code may include a foil heating routine and propagation through higher-order magnetic fields. The updated ORBIT code will provide an important tool for optimizing the new injection region design.

The Effect of the Earth's Atmosphere on LSST Photometry.

ALEXANDRA RAHLIN (Massachusetts Institute of Technology, Cambridge, MA 02139) DAVID L. BURKE (Stanford Linear Accelerator Center, Stanford, CA 94025). The Large Synoptic Survey Telescope (LSST), a ground-based telescope currently under development, will allow a thorough study of dark energy by measuring, more completely and accurately than previously, the rate of expansion of the universe and the large-scale structure of the matter in it. The telescope utilizes a broadband photometric system of six wavelength bands to measure the redshifts of distant objects. The earth's atmosphere makes it difficult to acquire accurate data, since some of the light passing through the atmosphere is scattered or absorbed due to Rayleigh scattering, molecular absorption, and aerosol scattering. Changes in the atmospheric extinction distribution due to each of these three processes were simulated by altering the parameters of a sample atmospheric distribution. Spectral energy distributions of standard stars were used to simulate data acquired by the telescope. The effects of changes in the atmospheric parameters on the photon flux measurements through each wavelength band were observed in order to determine which atmospheric conditions must be monitored most closely to achieve the desired 1% uncertainty on flux values. It was found that changes in the Rayleigh scattering parameter produced the most significant variations in the data; therefore, the molecular volume density (pressure) must be measured with at most 8% uncertainty. The molecular absorption parameters produced less significant variations and could be measured with at most 62% uncertainty. The aerosol scattering parameters produced almost negligible variations in the data and could be measured with >100% uncertainty. These atmospheric effects were found to be almost independent of the redshift of the light source. The

results of this study will aid the design of the atmospheric monitoring systems for the LSST.

The Efficiency of Stripe Removal from a Galactic Map. CAROLYN MELDGIN (*Harvey Mudd College, Claremont, CA 91711*) GEORGE SMOOT (*Lawrence Berkeley National Laboratory, Berkeley, CA 94720*). The Galactic Emissions Mapping project (GEM) aims to isolate the radiation emitted by the Milky Way and other galaxies from the cosmic microwave background radiation. Two dimensional scans of the sky at different frequencies allow separation of the cosmic microwave background from the galactic signals. Signals are most informative in the microwave spectrum, where the frequency of the light is in the 0.5 to 5 GHz range, because the intensity of the galactic signal relative to the cosmic microwave background changes most rapidly. In recent years, widely available technology such as cell phones and microwave ovens have increased terrestrial noise, making the galactic signal extremely difficult to analyze. GEM uses data taken in 1999, when terrestrial sources of microwaves were less common. These scans were taken at 2.3 GHz in Cachoeira Paulista, Brazil. The scans have striped flaws caused by microwaves from a nearby radio station diffracting over the top of the shielding around the antenna. This paper describes the use of filtering techniques involving Fourier transforms to reduce or remove the striped flaws. It also describes a metric, based on the Principle of Maximum Entropy, to determine the efficiency of different stripe-removal filters.

***The Occasional Appearance of Carbon in Type Ia Supernovae.** JEROD PARRENT (*University of Oklahoma, Norman, OK 73071*) R. C. THOMAS (*Lawrence Berkeley National Laboratory, Berkeley, CA 94720*). Recent observations made by the Nearby Supernova Factory reveal C II absorption features below 14,000 km/s in the early photospheric spectra of the Type Ia Supernova (SN Ia) 2006D. The largest of these features is attributed to C II $\lambda 6580$, which dissipates before maximum brightness. Only a handful of SNe Ia have been observed to contain the C II $\lambda 6580$ feature. This is the largest observed carbon feature in SN Ia thus far and is additional evidence that carbon, and hence unburned material, can be detected at early times in SN Ia spectra. Presently, certain 3D hydro-dynamical SN Ia deflagration models contain unburned carbon and oxygen below the W7 (1D deflagration model) cutoff of 14,000 km/s. These observations support explosion models that contain unburned material at low velocities, such as 3D deflagrations and certain delayed-detonations. The sporadic nature of observed carbon features in SN Ia and its implications for explosion models will be discussed. We also emphasize the importance of obtaining spectropolarimetry data in order to test for asymmetries in the supernova.

***The Systematic Study of the Faraday Effect on Glass.** JOSEPH HEARD (*Community College of Philadelphia, Philadelphia, PA 19150*) DR. CAROL SCARLETT (*Brookhaven National Laboratory, Upton, NY 11973*). Systematic Studies of the Faraday effect on glass. In the midst of ongoing experiments to detect axion interactions a question arose concerning the systematic effects on the experiment. Specifically, whether laser beam deviation through a vacuum can cause skewed data. This was a concern due to the birefringence effects caused by electromagnetic fields radiating away from the glass interface enclosed in a vacuum. A separate experiment dedicated to determining if such an effect exists was needed. The experiment used a Newport motorized rotating stage on which two permanent magnets were mounted. Each magnet had a magnitude of .1 tesla. The stage was placed 2 cm. from a glass window interface. The magnetic field generated was measured at 200 gauss. A laser beam of wavelength 514 nm was directed through the glass and magnetic field on to a photo receiver. The rotation device was set into motion at an 80 mHz frequency. The photo receiver collected data every 0.1 seconds for 25 hours. Data collection occurred in five minute cycles. The 300 data periods were then averaged together to eliminate random fluctuations. The data was analyzed using Fast Fourier Transforms (FFT). The data analysis involved taking the FFT of the raw data to produce plots of amplitude versus frequency. FFT'd "white noise" produces a $1/f$ curve. The derivative of this curve is then taken. This technique eliminates the drift of the laser, which flattens out the $1/f$ curve. Any random fluctuations are reduced significantly, improving the resolution of any true signal. After analyzing the results of the experiment it is apparent that, if any Faraday effect is present, it does not deviate the laser beam's path enough to create any influence on the overall experiment data. Thus axion interaction experiments that employ this technique do not suffer from any corrupted data.

The Target View Screen and Related Imaging Systems at the Spallation Neutron Source. KATHLEEN GOETZ (*Middlebury College, Middlebury, VT 05753*) THOMAS J. SHEA (*Oak Ridge National*

Laboratory, Oak Ridge, TN 37831). The most intuitive method for monitoring a beam is to create a dynamic image at the location of interest. At this point in time, the Target View Screen System (TVS) is being employed to monitor the proton beam immediately before the spallation target. The Target View Screen system has produced very useful data during the commissioning of SNS but will soon succumb to radiation damage. As a result another similar radiation resistant system is being designed for permanent installation. Other proposed systems that use similar imaging technology include a view screen for the ring to target beam transport (RTBT) line, a pepper pot emittance meter for the linear accelerator front end and a neutron beam imager for neutron beam line six. A large portion of time is also being devoted to running the Target View Screen system in its last days of operation and analyzing the data being produced. Approximately one terabyte of data has been acquired.

Thermal Analysis of the ILC Superconducting Magnets. IAN ROSS (*Rose-Hulman Institute of Technology, Terre Haute, IN 47803*) JOHN WEISEND (*Stanford Linear Accelerator Center, Stanford, CA 94025*). Critical to a particle accelerator's functioning, superconducting magnets serve to focus and aim the particle beam. The Stanford Linear Accelerator Center (SLAC) has received a prototype superconducting quadrupole designed and built by the Centro de Investigaciones Energéticas, Medioambientales y Tecnológicas (CIEMAT) to be evaluated for the International Linear Collider (ILC) project. To ensure proper functioning of the magnet, the device must be maintained at cryogenic temperatures by use of a cooling system containing liquid nitrogen and liquid helium. The cool down period of a low temperature cryostat is critical to the success of an experiment, especially a prototype setup such as this one. The magnet and the dewar each contain unique heat leaks and material properties. These differences can lead to tremendous thermal stresses. The system was analyzed mathematically, leading to ideal liquid helium and liquid nitrogen flow rates during the magnet's cool-down to 4.2 K, along with a reasonable estimate of how long this cool-down will take. With a flow rate of ten gaseous liters of liquid nitrogen per minute, the nitrogen shield will take approximately five hours to cool down to 77 K. With a gaseous helium flow rate of sixty liters per minute, the magnet will take at least nineteen hours to cool down to a temperature of 4.2 K.

Time Synchronization Between Data Acquisition Boards Using GPS Signals. JOSEPH WYCKOFF (*Eastern Illinois University, Charleston, IL 61920*) THOMAS JORDAN (*Fermi National Accelerator Laboratory, Batavia, IL 60510*). Since Cosmic Rays move at an incredible speed, timing is an important part in the components in the detectors used to measure them. QuarkNet has many sites surrounding the country running cosmic ray shower studies. It uses Data Acquisition (DAQ) boards to convert the timing signals from Photo Multiplier Tubes (PMT) to an ANSI format that is readable using a terminal emulator program on a computer. The sites upload their data to a central server so users can run analysis, using data from all over the nation. Therefore timing is important so that students using data from different GPS sources can sort the data and see if an event happened at the same time in two different areas. An experiment was completed using 2 different GPS antennae to test the timing difference between two DAQ boards that received signals at identical times. A pulse generator set at 10 Hz to mimic a signal was used. The experiment was run for two periods of thirty minutes where the GPS antennae were switched between the two DAQ boards after the first period. The results of the tests showed that the detectors had a difference in timing of 121 nanoseconds with one of the detectors having a bias of 12 nanoseconds. The experiment showed that while using the QuarkNet detectors a user could only confidently say which detector fired first if there is more than a 100 ns difference in the signals. These results are in agreement with previous calculations of the timing difference between detectors using separate GPS antennae. More tests should be done to examine whether the timing difference between two DAQ boards could be reduced or if the timing difference will cause a problem to research that is being conducted.

Upgrading the Digital Electronics of the Bunch Current Monitors at the Stanford Linear Accelerator Center. JOSH KLINE (*Sacramento State University, Sacramento, CA 95813*) ALAN FISHER (*Stanford Linear Accelerator Center, Stanford, CA 94025*). The testing of the upgrade prototype for the bunch current monitors (BCMs) in the PEP-II storage rings at the Stanford Linear Accelerator Center (SLAC) is the topic of this paper. Bunch current monitors are used to measure the charge in the electron/positron bunches traveling in particle storage rings. The BCMs in the PEP-II storage rings need to be upgraded because components of the current system have failed and are known to be failure prone with age, and several of the integrated chips are

no longer produced making repairs difficult if not impossible. The main upgrade is replacing twelve old (1995) field programmable gate arrays (FPGAs) with a single Virtex II FPGA. The prototype was tested using computer synthesis tools, a commercial signal generator, and a fast pulse generator.

Using Boosted Decision Trees to Separate Signal and Background in $B \rightarrow Xs\gamma$ Decays. JAMES BARBER (*University of Massachusetts, Amherst, Amherst, MA 01003*) PHILIP BECHTLE (*Stanford Linear Accelerator Center, Stanford, CA 94025*). The measurement of the branching fraction of the flavor changing neutral current $B \rightarrow Xs\gamma$ transition can be used to expose physics outside the Standard Model. In order to make a precise measurement of this inclusive branching fraction, it is necessary to be able to effectively separate signal and background in the data. In order to achieve better separation, an algorithm based on Boosted Decision Trees (BDTs) is implemented. Using Monte Carlo simulated events, 'forests' of trees were trained and tested with different sets of parameters. This parameter space was studied with the goal of maximizing the figure of merit, Q , the measure of separation quality used in this analysis. It is found that the use of 1000 trees, with 100 values tested for each variable at each node, and 50 events required for a node to continue separating give the highest figure of merit, $Q = 18.37$.

Using LabVIEW for Complete Systems Control of an ECR Thin Film Deposition System. BRANDON BENTZLEY (*The College of New Jersey, Ewing, NJ 08628*) ANDREW POST-ZWICKER (*Princeton Plasma Physics Laboratory, Princeton, NJ 8543*). Interest in studying an electron cyclotron resonance (ECR) deposition system is fueled by ECR's better deposition rates and precision relative to traditional deposition systems; however, the ECR deposition system is extremely complex and requires that its gas flow control, magnets, 2.45 GHz source, and other components all work in concert. Operating the system requires an experienced user to constantly compensate for the dynamics of the system, such as argon gas pressure and magnetic field strength. A method of computer automation, such as LabVIEW, permits the system to operate itself, allowing for less experienced operators, reproducible conditions, and a safer working environment. LabVIEW, in conjunction with National Instruments hardware, sends and receives voltage signals and serial commands in order to control microwave power, magnet current, target bias voltage, vacuum and compressed-gas valve position, chamber pressure, and robotics commands. The VI takes many factors into account simultaneously, such as chamber pressure, ion current and spectroscopic data, in order to make decisions about the system state. LabVIEW was found to produce easy to manage, consistent, and reproducible conditions by simplifying complex procedures, such as system startup routines and robotics commands, to a click of a button, by compensating both accurately and quickly for changes in plasma conditions, and by checking the state of the system in order to prevent system malfunction.

Using Math Cad to generate a polynomial for comutation of beam position from Main Injector Extra-Wide Aperture Beam Position Monitor Electrode Signals. MILTON SMITH (*Southern University, Baton Rouge, LA 70807*) ROBERT WEBBER (*Fermi National Accelerator Laboratory, Batavia, IL 60510*). As far as mankind's knowledge of mathematical procedures, how it has influenced our lives by describing multiple scientific procedures. The research that was conducted sole purpose was to generate a polynomial that will compute beam positions based off measurements from two amplitude signal electrodes. Hence, the information from the BPM was compiled into data files which were separated into "horizontal" and "vertical" files. These files were received and dissected with the usage of an extraordinary mathematical computer software Math-Cad. Math-Cad gave the ability to manipulate the data files in order to generate such a polynomial that will compute beam position when only receiving signal amplitude measurements from two electrode plates. Hence, calculations of computed data, actual "on-axis" data, and plots expressed results where the best computed beam position should lie far within the allotted 50mm barriers of the BPM test stand. In conclusion, the polynomial successfully displayed computed beam position from receiving signal amplitudes from two electrode measurements. If you reduce the human and/or mechanical involvement it may decrease the error within the BPM test stand measurements.

Science Policy

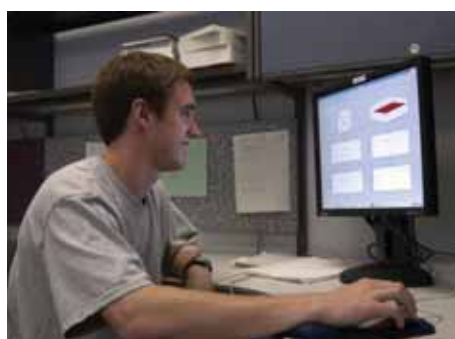
Policy Analysis: Rapid Response Vaccine Development for Emerging and Emergent Infectious Diseases. CATHERINE COLAIANNI (*Duke University, Durham, NC 27708*) THOMAS BATES (*Lawrence Livermore National Laboratory, Livermore, CA 94550*).

Despite billions of dollars spent in research and development, the U.S. is alarmingly under-prepared to defend against biological warfare. This is most notable when considering the availability of biodefense vaccines. Vaccine production facilities are disappearing, and the production methodology employed in most cases is slow, expensive and outdated. Additionally, there is no comprehensive capability or even a strategy to develop and produce vaccines rapidly as part of an emergency response to a new or emerging pathogen. To explore the current state of vaccine production and to consider possible new directions to enhance our national posture, we undertook a policy analysis starting with an in-depth review of the historical vaccine development cycle for *Bacillus anthracis*, including the time requirements and government funding. Next, we made simple projections for a similar path to develop vaccines for other NIAID Category A Priority pathogens. Finally, options were explored for new research and development directions (5 to 10 year timeline) to support a rapid vaccine development process amenable to emergency use. The long-term solution was assessed to be an end-to-end "pipeline approach" whereby either synthetic subunit or attenuated vaccines could be rapidly produced 'on-demand'; however, considerable research is still required for methods to rapidly identify virulence factors and antigenic regions.

The Economics of Sanctions — Iran. PETER NEWMAN (*Brigham Young University, Provo, UT 84604*) GARIANN GELSTON, BARBARA REICHMUTH (*Pacific Northwest National Laboratory, Richland, WA 99352*). Iran is currently pursuing an aggressive nuclear program with a declared goal of achieving long-term energy independence. While this is a worthwhile and generally accepted national planning objective, there is evidence to indicate that Iran's nuclear program may be driven by the desire to produce weapons. Talks are currently underway between the United Nations (UN) and Iran, in accordance with the Nuclear Nonproliferation Treaty, to halt Iran's uranium enrichment program; a precursor to nuclear weapons production. In the event UN-Iran talks fail, the United States Government is evaluating a sanctions package to levy against Iran to encourage their compliance. Gasoline is one commodity being considered for restriction. It is estimated Iran will consume 467,000 barrels per day (b/d) of gasoline in 2006, and import 182,000 b/d (nearly 40%) of that total; thus, making Iran vulnerable to sanctions against this commodity. In order to effectively sanction gasoline imports current and potential suppliers must be identified. Utilizing national and international statistical bureaus along with some information gathered from private firms a partial portrayal of gasoline imports into Iran can be illuminated. Measurement (unit) differences, accounting discrepancies, incomplete or omitted information, and the general lag in data accumulation pose a real problem in assembling an accurate and timely depiction of gasoline trade. While accounting discrepancies between statistical databases are non-reconcilable, determining trade quantities in spite of unit differences is possible. Adjusting for various units of measure is accomplished using specific gravities (density). Upon converting and compiling all data from various sources for years 2003–2005, approximately 50–75% of gasoline purchased by Iran can be characterized. Although these results will be useful in evaluating sanctions, they may be insufficient to create the desired economic impact. Further research is warranted to build upon these findings.

Uncertainty and Scale Issues in Linking Climate Change to the Watershed Scale: Ideas in Landscape Classification and Use of NASA Remote-Sensing Data. KANG CHANG (*University of Illinois at Urbana Champaign, Urbana-Champaign, IL 61820*) KAREN L. STEINMAUS (*Pacific Northwest National Laboratory, Richland, WA 99352*). This paper will identify various aspects of uncertainty in the water resource management decision making process in the face of future predicted climate changes. The focus of many current efforts is to understand global change at the watershed scale. However, methods for studying the watersheds are spatially smaller than the current methods of studying the impacts of climate change (GCMs 400km) yet the former methods are still at a larger scale than the study of the topographical intricacies that help to determine streamflow (landscape classification). The drive to elucidate other potential local environmental reactions stems from the fundamental and often forgotten truth that, we as living creatures depend on the services our ecosystems provide to us. Climate change is anticipated to impact a decidedly significant ecosystem service: water. There is projected to be an increase in the temperature of the Pacific Northwest (United States) which could mean increased winter streamflow and decreased spring streamflow in the Cascade Mountain Range (containing the Yakima river basin). The future supply complications are likely to stem from the smaller headwaters of the Yakima and apply to times of drought or flood. Future

AMES LABORATORY Ames, Iowa



Scientists at the Department of Energy Office of Science's Ames Laboratory seek solutions to energy-related problems through the exploration of chemical, engineering, materials and mathematical sciences, and physics.

Established in the 1940s with the successful development of the most efficient process to produce high-purity uranium metal for atomic energy, Ames Lab now pursues much broader priorities than the materials research that has given the Lab international credibility.

Responding to issues of national concern, Lab scientists are actively involved in innovative research, science education programs, the development of applied technologies, and the quick transfer of such technologies to industry. Uniquely integrated within a university environment, the Lab stimulates creative thought and encourages scientific discovery, providing solutions to complex problems and educating tomorrow's scientific talent.

Ames Laboratory is located in Ames, Iowa, on the campus of Iowa State University. Iowa State's 2,000-acre, park-like campus is home to more than 25,000 students. Ames is approximately 30 minutes north of Des Moines, Iowa's capital city.



ARGONNE NATIONAL LABORATORY Argonne, Illinois



Argonne National Laboratory descends from the University of Chicago's Metallurgical Laboratory, part of the World War Two Manhattan Project. The laboratory has about 2,900 employees, including about 1,000 scientists and engineers. Argonne occupies 1,500 wooded acres in DuPage County, Illinois, about 25 miles southwest of Chicago's Loop. Argonne research falls into broad categories:

- Basic science seeks solutions to a wide variety of scientific challenges. This includes experimental and theoretical work in biology, chemistry, high energy and nuclear physics, materials science, and mathematics and computer science.
- Scientific facilities help advance America's scientific leadership and prepare the nation for the future. These facilities are used by scientists thousands of scientists and students from the U.S. and abroad. The laboratory is also home to the Advanced Photon Source, the Center for Nanoscale Materials, the Intense Pulsed Neutron Source, and the Argonne Tandem Linear Accelerator System.
- Energy resources programs help insure a reliable supply of efficient and clean energy for the future. Argonne scientists and engineers are developing advanced batteries and fuel cells, as well as advanced electric power generation and storage systems.
- Environmental management includes work on managing and solving the nation's environmental problems and promoting environmental stewardship.
- National Security has increased in significance in recent years for the nation and for Argonne research. Argonne capabilities developed over the years for other purposes are helping to counter the threats of terrorism.

Argonne's Division of Educational Programs provides workforce development for faculty and students from universities to regional K-12 schools.



BROOKHAVEN NATIONAL LABORATORY Upton, New York

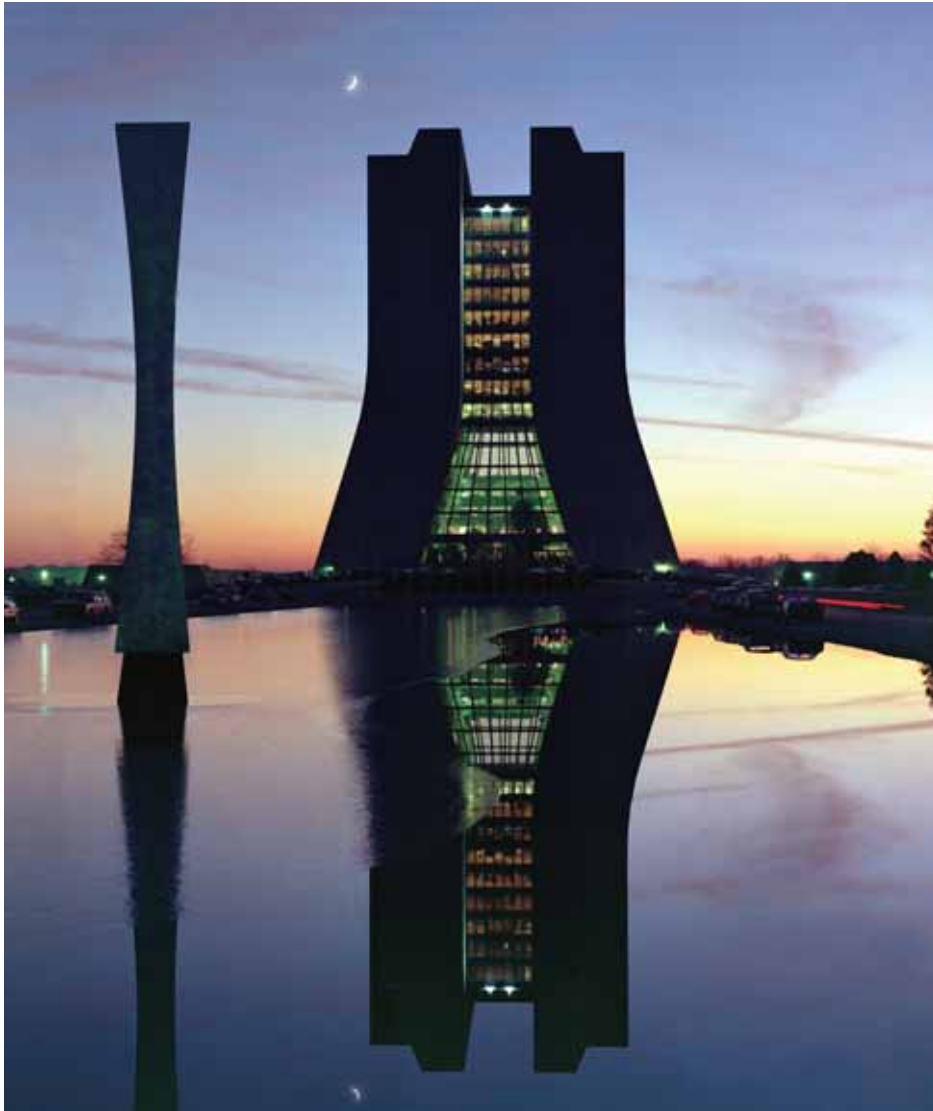


Established in 1947, Brookhaven National Laboratory is a Department of Energy, Office of Science multidisciplinary laboratory managed by Brookhaven Science Associates, a company founded by Battelle and Stony Brook University. Home to six Nobel Prizes, Brookhaven conducts research in the physical, biomedical, and environmental sciences, as well as in energy technologies and national security.

Located on a 5,300-acre site on eastern Long Island, New York, Brookhaven builds and operates major scientific facilities available to university, industry and government researchers. Among those facilities are the world's newest accelerator for nuclear physics research, the Relativistic Heavy Ion Collider (RHIC), and the National Synchrotron Light Source (pictured here) where approximately 2,500 researchers use beams of light, from x-rays to ultraviolet and infrared, to study materials as diverse as computer chips and proteins. In the near future, the Center for Functional Nanomaterials will be built at Brookhaven, one of five Department of Energy centers where researchers will study materials on the scale of a billionth of a meter, or only a few atoms.

A wide variety of both basic and applied research is conducted at Brookhaven. For instance, scientists are investigating the building blocks of matter using RHIC, the roots of drug addiction and brain metabolism using positron emission tomography, the effects of space radiation on astronauts using the newly built NASA Space Radiation Laboratory, and the effects of increased carbon dioxide in ecosystems. Brookhaven researchers also develop new technologies as varied as detectors for national security and oil burners with improved efficiency.

FERMI NATIONAL ACCELERATOR LABORATORY Batavia, Illinois

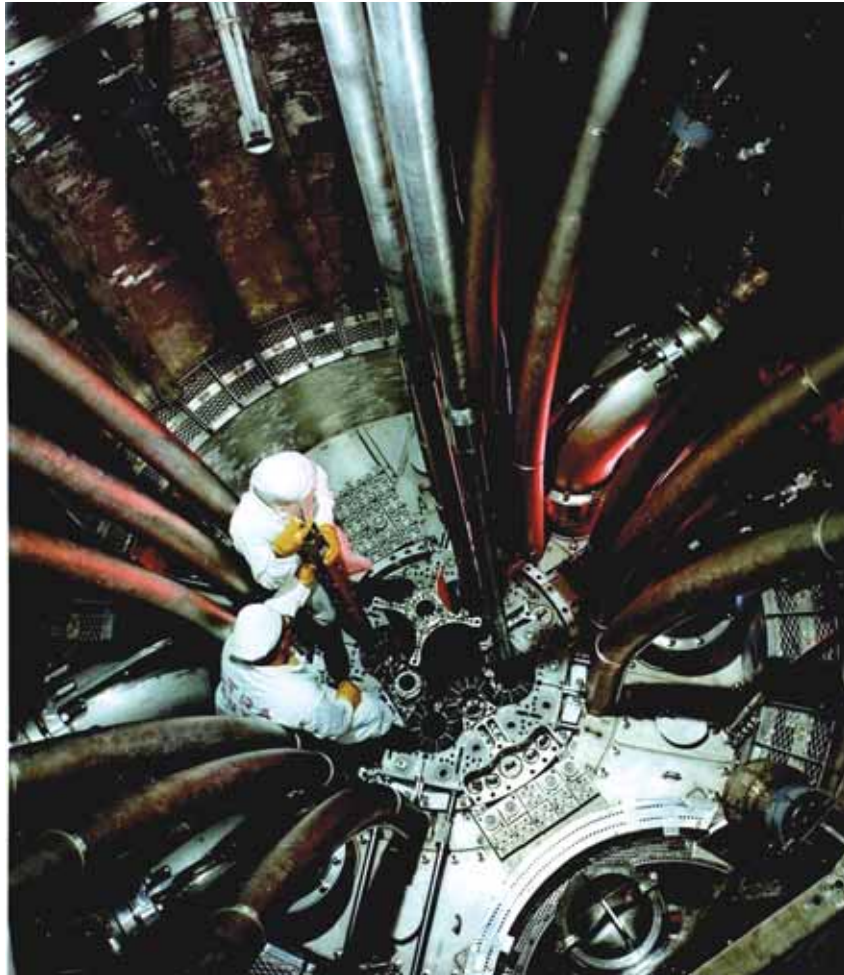


Fermilab is one of the world's foremost laboratories dedicated to high-energy physics research. It is operated for the Department of Energy Office of Science by a consortium of 90 research-oriented universities. More than 3,000 scientists from around the world use Fermilab for their experiments.

Fermilab is located on a 6,800-acre site about 35 miles west of Chicago, Illinois. The laboratory is home to the Tevatron Collider, the world's highest-energy particle accelerator. Two large detectors analyze the Tevatron's proton-antiproton collisions to unveil the fundamental forces and particles of the universe. Scientists at Fermilab discovered the bottom quark and the top quark, and first observed the tau neutrino.

Fermilab operates the world's most powerful proton beam for creating neutrinos. The Center for Particle Astrophysics at Fermilab includes groups studying cosmic rays, supernovae, dark energy and other phenomena.

IDAHO NATIONAL LABORATORY Idaho Falls, Idaho



In operation since 1949, The Idaho National Laboratory (INL) is a science-based, applied engineering National Laboratory dedicated to supporting the U.S. Department of Energy's missions in nuclear and energy research, science, and national defense.

INL stands out as a unique national and international resource. Notably, the Lab has been formally designated as the nation's command center for advanced civilian nuclear technology research and development, and is home to the unparalleled Critical Infrastructure Test Range, with assets as diverse as an isolable electric grid and wireless test bed. Leveraging these and numerous other distinguishing features, the Lab and its more than 3,300 scientists, engineers and support personnel build on the potential and promise of the theoretical for the benefit of the real world.

Located in southeast Idaho, INL covers 890 square miles of the Snake River Plain between Idaho Falls and Arco, Idaho. Offices and laboratories are also in the city of Idaho Falls (population 50,000), located about two hours from Grand Teton and Yellowstone national parks and other areas offering prime recreational opportunities.



LAWRENCE BERKELEY NATIONAL LABORATORY Berkeley, California



Lawrence Berkeley National Laboratory's research and development includes new energy technologies and environmental solutions with a focus on energy efficiency, electric reliability, carbon management and global climate change, and fusion. Frontier research experiences exist in nanoscience, genomics and cancer research, advanced computing, and observing matter and energy at the most fundamental level in the universe.

Ernest Orlando Lawrence founded the Berkeley Lab in 1931. Lawrence is most commonly known for his invention of the cyclotron, which led to a Golden Age of particle physics—the foundation of modern nuclear science—and revolutionary discoveries about the nature of the universe. Berkeley Lab's Advanced Light Source is its premier national user facility centrally located on the lab site overlooking the San Francisco Bay.



LAWRENCE LIVERMORE NATIONAL LABORATORY Livermore, California



Lawrence Livermore National Laboratory (LLNL) is a premier applied science laboratory that is part of the National Nuclear Security Administration (NNSA) within the Department of Energy. With more than 8,000 employees, LLNL is located on a one-square-mile site in Livermore, California. A larger (10 square miles) remote explosives testing site (Site 300) is situated 18 miles to the east.

LLNL is managed by the University of California (UC) for the National Nuclear Security Administration. Being part of the University helps foster intellectual innovation and scientific excellence. This University connection allows LLNL to recruit and retain a diverse world-class workforce and partner with the UC's extensive research and academic community. These factors are essential to sustaining the laboratory's scientific and technical excellence.

Lawrence Livermore National Laboratory is a national security laboratory with responsibility for ensuring that the nation's nuclear weapons remain safe, secure, and reliable. LLNL also applies its special expertise and multidisciplinary capabilities to prevent the spread and use of nuclear and other weapons of mass destruction and strengthen homeland security.

The Lab has pioneered the application of many technologies, from high-performance computers to advanced lasers, to meet national security needs. Today, the special capabilities developed for our stockpile stewardship and nonproliferation activities enable us to also meet enduring national needs in conventional defense, energy, environment, biosciences, and basic science. Research programs in these areas enhance the competencies needed for the Laboratory's national security mission.



LOS ALAMOS NATIONAL LABORATORY Los Alamos, New Mexico



The Los Alamos National Laboratory (LANL), located in the Jemez Mountains of northern New Mexico, offers the opportunity for students to work at a multi-disciplinary, world-class research facility while enjoying a truly unique environment. Long known for its artistic community, northern New Mexico also offers a variety of exciting outdoor recreational opportunities, including rock climbing and hiking in the adjacent mountains and canyons, proximity to the Rocky Mountains, and exceptional skiing opportunities at many nearby locations.

We offer a diverse research experience for undergraduate and graduate students as a means of assuring the continued vibrancy of the science, engineering, and technology at the laboratory. Serve your internship with us and you will have the opportunity to work in a team environment with some of the world's top scientists and engineers on critical issues involving our national security, environment, infrastructure, and security. We offer internship opportunities in areas that include: Biology, Chemistry, Computer Science, Physics, Mathematics, Materials Science, Environmental Science, and Engineering: Chemical, Civil, Computer, Electrical, Mechanical, Nuclear, and Software.

If you are a problem solver and independent thinker, a team player, a good communicator, like a hands-on approach, and are self-motivated, we offer you the challenge of an internship at Los Alamos National Laboratory.

NATIONAL RENEWABLE ENERGY LABORATORY Golden, Colorado



The National Renewable Energy Laboratory (NREL) is the Department of Energy's primary National Laboratory for renewable energy and energy efficiency research and development. From harvesting energy from the sun and wind, to advancing automotive systems, to developing biodegradable plastics from corn stalks, NREL develops renewable energy and energy efficiency technologies and practices, advances related science and engineering, and transfers knowledge and innovations to address the nation's energy and environmental goals. NREL is home to three national centers of excellence: the National Center for Photovoltaics, the National Bioenergy Center and the National Wind Technology Center.

NREL research has been recognized with 39 R&D 100 Awards, ranking first among National Laboratories per researcher, as well as numerous honors from *R&D*, *Discover*, and *Popular Science* magazines and leading scientific organizations.

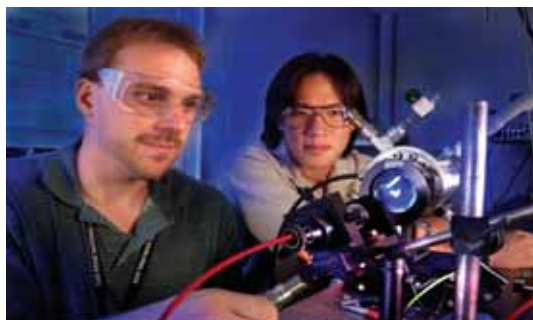
Innovative, challenging and dynamic—that's our culture. If you are interested in a research internship with an institution that believes creativity and individual uniqueness are at the core of our success, then explore your options at: www.nrel.gov. We value intern talent that adds to the rich pool of research findings produced by NREL each year. Intern accomplishments include:

- More than 24 students have been selected by the Office of Science to present major NREL research at the AAAS.
- More than 50 past student interns have been hired on to join the NREL family.
- Teacher researchers have produced over 50 renewable energy lessons for the classroom.
- NREL's Office of Education partners with over 75 universities throughout the nation.



NREL's main 327-acre site is in Golden, Colorado, just west of Denver. The Laboratory also operates the National Wind Technology Center on 307 acres about 20 miles north of Golden, adjacent to the Department of Energy's Rocky Flats Environmental Test Site. We are an equal opportunity employer committed to diversity.

OAK RIDGE NATIONAL LABORATORY Oak Ridge, Tennessee



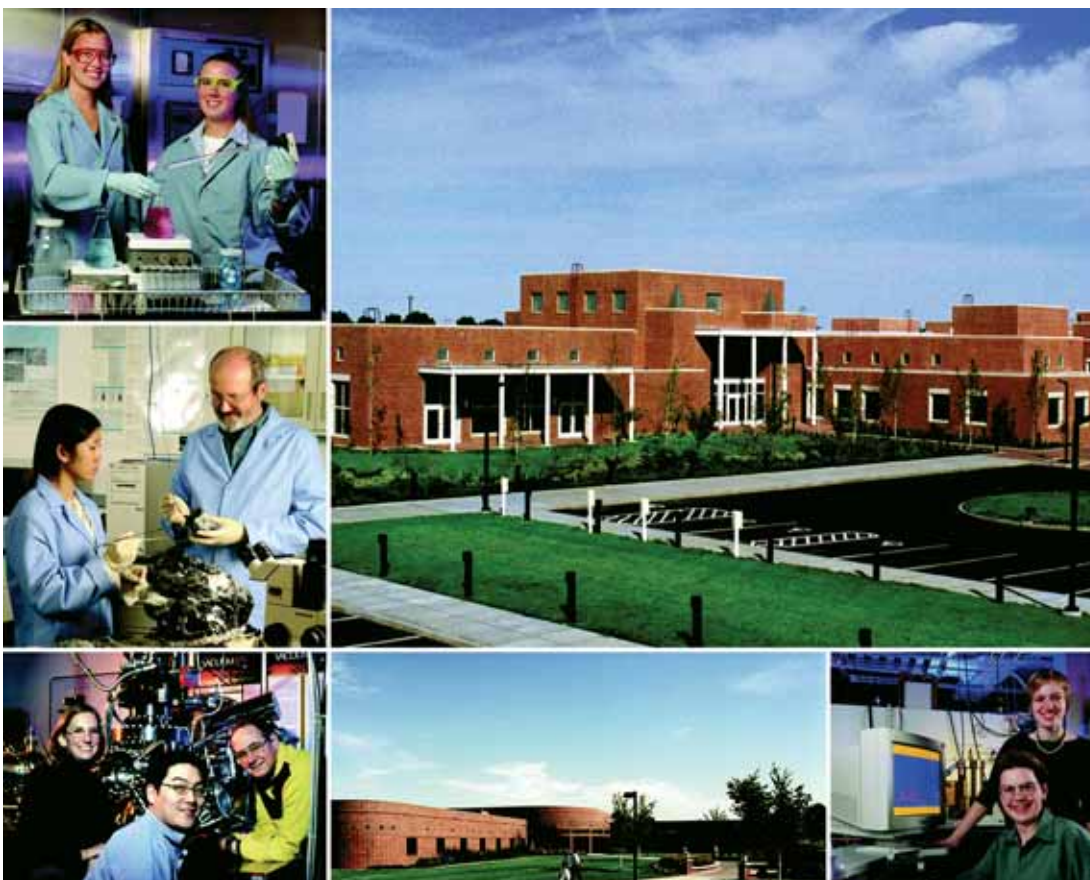
Oak Ridge National Laboratory is the Department of Energy's largest science and energy laboratory. Managed since April 2000 by a partnership of the University of Tennessee (UT) and Battelle, ORNL was established in 1943 as a part of the secret Manhattan Project to pioneer a method for producing and separating plutonium. More than 60 years later, ORNL's mission is to conduct basic and applied research that provides innovative solutions to complex problems.

ORNL, with funding that exceeds \$1 billion, has a staff of more than 4,000 and approximately 3,000 guest researchers who spend two weeks or longer each year in Oak Ridge. The Laboratory's six major scientific competencies, in support of DOE's Office of Science, include neutron science, energy, high performance computing, complex biological systems, advanced materials and national security.

ORNL is in the final stages of a \$300 million project to provide a modern campus for the next generation of great science. A unique combination of federal, state and private funds is building 13 new facilities. Included in these new facilities will be the Functional Genomics Center, the Center for Nanophase Materials Science, the Advanced Microscopy Laboratory, and the joint institutes for Computational Science, Biological Science and Neutron Science. ORNL is the site of the Office of Science's National Leadership Computing Facility for unclassified high-performance computing. On budget and on schedule 2006, the \$1.4 billion Spallation Neutron Source makes Oak Ridge the world's foremost center for neutron science research.

UT-Battelle has provided more than \$6 million in support of math and science education, economic development and other projects in the greater Oak Ridge region.

PACIFIC NORTHWEST NATIONAL LABORATORY Richland, Washington



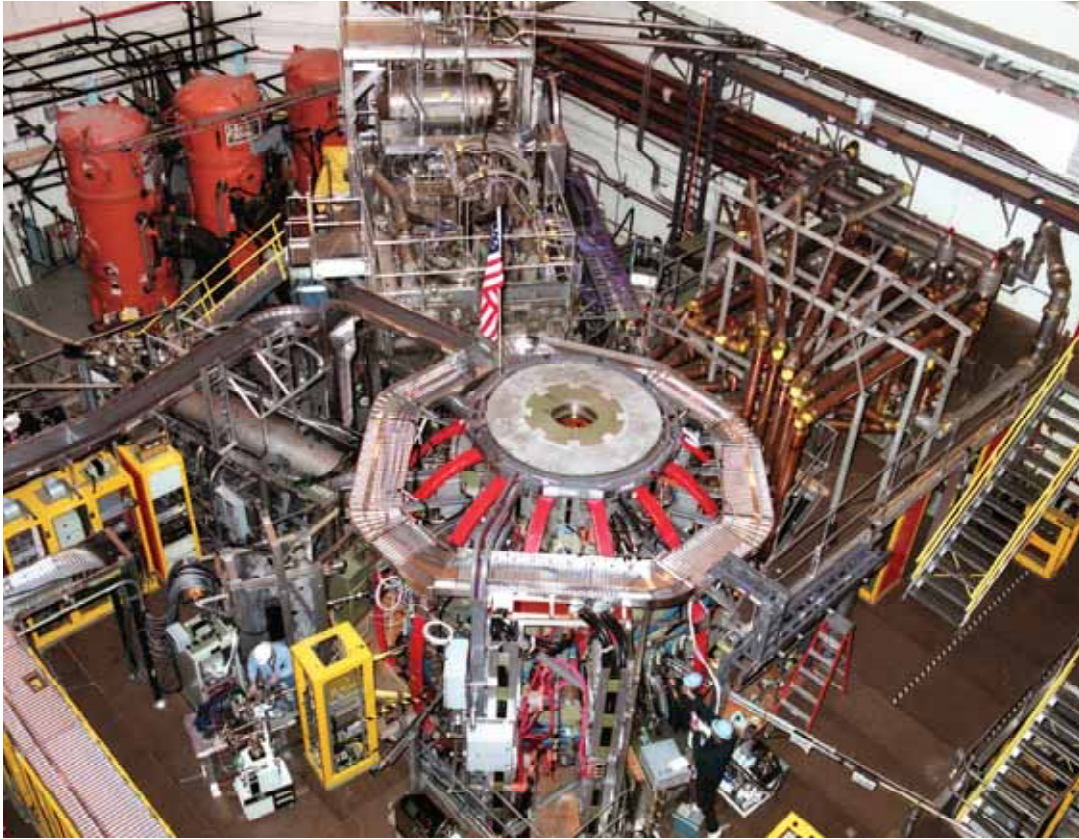
Pacific Northwest National Laboratory (PNNL) is a multi-purpose National Laboratory dedicated to delivering innovative science-based solutions to some of the nation's most pressing problems. PNNL conducts fundamental and applied research to address important issues including securing our homeland, reducing our dependence on foreign oil, transforming the energy system, making information access easier, and protecting our natural resources.

PNNL's facilities form a world-class campus, including many laboratories recognized as best-in-class for many research areas. With an international reputation for studies in chemistry, biology, computer sciences, and a wide range of other fields, award-winning PNNL researchers rapidly translate theory into concrete solutions. Many of the Laboratory's technologies have been developed into common consumer and industrial products, including the compact disc (CD).

The Laboratory consistently attracts some of the world's leading scientific talents shaping the future of science through a variety of on-site educational programs. As mentors and research partners, the Laboratory's staff trains young scientists and engineers to become tomorrow's inventors. Student research opportunities at PNNL include appointments in atmospheric science and global change, computational sciences, experimental chemistry, marine sciences, molecular biology, environmental studies, remediation, environmental microbiology, wildlife and fisheries biology, materials research, process science and engineering, economics and political science.

Located in southeastern Washington near the base of the Blue Mountains and the confluence of the Columbia, Snake and Yakima rivers, PNNL staff enjoy year around recreation, locally-produced fine wines, and the community's commitment to the arts.

PRINCETON PLASMA PHYSICS LABORATORY Princeton, New Jersey

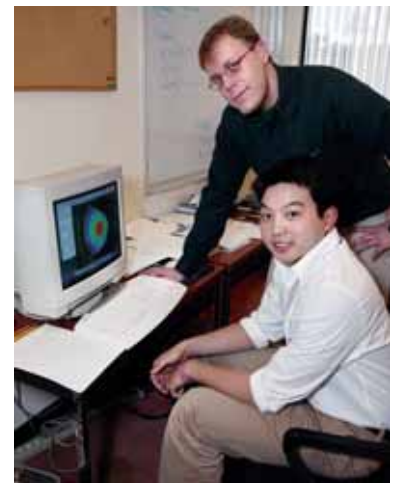


The world's reliance on fossil fuels is imperiling our environment. Fusion, the energy source of the sun and the stars, offers an inexhaustible alternative. A fusion-powered electric generator would not produce hydrocarbon emissions, greenhouse gases, or long-lived radioactive waste; nor would it emit chemicals that cause acid rain. Consequently, the U.S. Department of Energy (DOE) Office of Science has made the development of commercial fusion power one of its highest priorities.

DOE's Princeton Plasma Physics Laboratory (PPPL) is one of the world's leading facilities for fusion R&D.

Currently the PPPL is operating the National Spherical Torus Experiment (pictured above) and is building the National Compact Stellarator Experiment, both use magnetic fields to confine hot ionized gas (plasma) that serves as the fusion fuel. PPPL's theoretical physicists are developing computational physics models that can predict how various plasma configurations will perform, saving time and money.

PPPL experimental physicists collaborate with their colleagues worldwide in a free, mutually beneficial, exchange of information. Princeton researchers and engineers are using knowledge and skills gained in fusion research to solve other problems, including the development of plasma-based propulsion systems for space vehicles, studies of plasma phenomena that occur in the sun's corona and the earth's magnetosphere, and research on plasma sterilization of plastic food and beverage containers. PPPL is located about three miles from Princeton University's main campus in Princeton, NJ.



STANFORD LINEAR ACCELERATOR CENTER Menlo Park, California



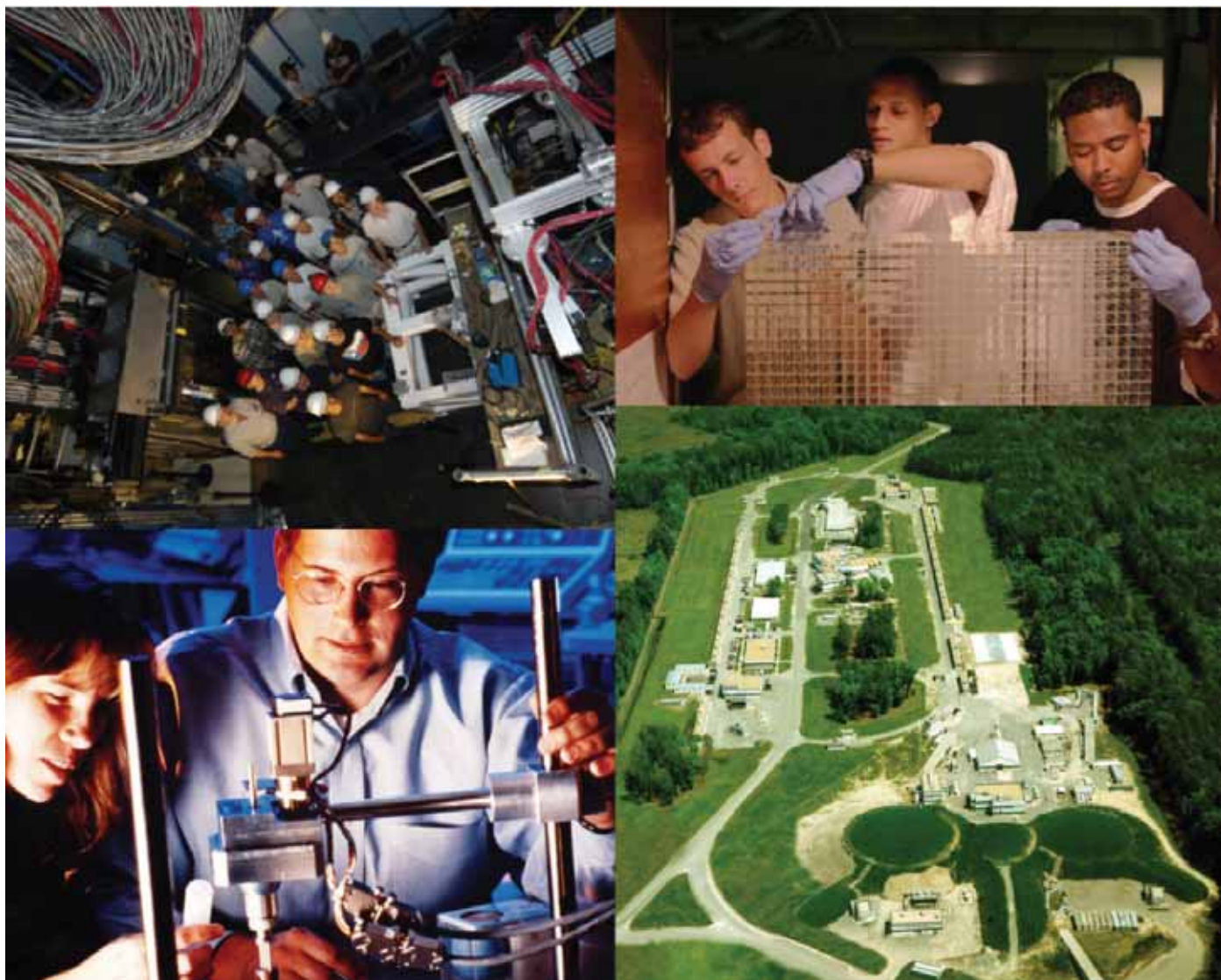
The Stanford Linear Accelerator Center (SLAC) is one of the world's leading laboratories for research in high-energy physics (HEP), particle astrophysics and cosmology, and synchrotron radiation research.

SLAC's HEP program seeks answers to fundamental questions about the ultimate structure of matter and the forces between these fundamental particles. The BABAR experiment investigates matter/anti-matter asymmetry and is the current focus of the HEP program. In addition, a vigorous R&D program is focused on realizing the next generation electron collider — the International Linear Collider, as part of a world-wide effort.

The Kavli Institute at SLAC for Particle Astrophysics and Cosmology bridges theoretical and experimental physics communities, and brings their combined strengths to bear on some of the most challenging and fascinating problems in particle astrophysics and cosmology to help us understand the birth and evolution of the universe.

The Stanford Synchrotron Radiation Laboratory (SSRL) at SLAC, provides high intensity x-ray beams for molecular and atomic scale studies in physics, biology, chemistry, medicine, and environmental science. The Linac Coherent Light Source (LCLS), a facility to provide even more intense x-ray capability is now under construction. Pioneering experiments at LCLS will advance our understanding of everything from the hidden physics inside planets, to how proteins function as the engines of life, to building nanotechnology devices for the backbone of future industry and technology.

THOMAS JEFFERSON NATIONAL ACCELERATOR FACILITY Newport News, Virginia



The Thomas Jefferson National Acceleration Facility, or Jefferson Lab, is a nuclear physics research laboratory located in Newport News, Virginia. Nuclear physics research scientists who use Jefferson Lab are on a journey of discovery into the nucleus of the atom. Their goal is to develop a roadmap of matter that helps unlock the secrets of how the universe is put together. Nuclear physics funding from the Department of Energy provides Jefferson Lab with leading-edge instrumentation, world-class facilities and training and support for the people involved in these pursuits. Forefront nuclear physics research conducted at Jefferson Lab provides solid foundations for other fields. The accumulation of new results and the intellectual training of new generations of scientists foster important advances in medicine, chemistry and other sciences.

Scientists at Jefferson Lab use the Continuous Electron Beam Accelerator Facility — the first large-scale application of superconducting radiofrequency technology — to conduct physics experiments. Using accelerated electron beams, experimenters probe the sub-nuclear realm. Using this same technology, Jefferson Lab has built the world's brightest high average power Free Electron Laser that offers unique capabilities for defense, industry, basic research and medicine.

Index of Authors

A

Abdullah, Fida 172
Abkemeier, Erik 180
Ackerman, Tom 197
Adesanya, Yemi 163
Aguiar, Jeffery 190
Alexander, Lizabeth 185
Allain, Jean-Paul 206
Allison, Elias 218
Allred, Shawn 182
Amadio, Brian 212
Andersen, Gary 147
Andersen, Matthew 211
Anderson, Erik 202
Anderson, Rachel 223
Anheier, Norm 219
Apte, Michael 183, 196
Arias, Tersi 212
Armstead-Williams, Cassandra 139
Arriaga, James 159
Attwood, David 202, 216
Avakian, Harut 210
Awuah, Kobbina 174
Azcona, Wendolie 196

B

Baba, Justin 167
Babnigg, Gyorgy 136
Backes, Rachel 167
Baker, Aleisha 225
Baker, David 199
Baker, Gary A. 157
Baker, Jeffrey 158
Baker, Scott 138
Balachandran, U. 204
Ball, Deborah Yarsike 198
Ballenger, Shawn 219
Barber, James 227
Barkhudarov, Philip 203
Barnes, Benjamin 170
Barnes, Tenisha 160
Barnett, Michael 212
Bates, Thomas 227
Baum, Sarah 198
Baumgartel, Lukas 213
Beach, Leila 144
Beatty, Cassandra 210
Bechtle, Philip 227
Becker, James 194
Belew, Brandon 213
Benjegerdes, Troy 163
Bennett, Patrick 202

Bennett, Rob 160
Bennett, Robert 136, 155
Bennett, Robert E. 162
Bentzley, Brandon 227
Benveniste, Helene 206, 208
Bergmann, Uwe 224
Berkel, Gary J. Van 153
Bhatt, Vatsal 188, 192
Bhattacharyya, Maryka 140, 141
Bi, Wenyi 140
Bishai, Mary 223
Biskie, Brian 171
Bjornstad, Kathleen 136
Blackburn, Shannon 194
Blakely, Eleanor 136
Bland, Les 220
Bland, Leslie 214
Blanton, Michael 196
Blattel, Arran 187
Bloom, Ira 177
Boardman, Sharla 197
Boggs, Bryan 202
Bonnesen, Peter 157
Bookwalter, Craig 224
Bouie, Joseph 223
Bowen, Amy 168
Bowling, Aaron 143
Brachmann, Axel 223
Bradley, Craig 175, 178
Brajuskovic, Branislav 170
Brearcliffe, Dale K. 198
Broadwater, Ombreyan 202
Brown, Chris 154
Brown, Kara 197
Brown, Kyndall 159
Brungard, Jamie 184
Budworth, Helen 139
Buell, Justin 170
Bullock, R. Morris 154
Bunn, Amoret 173, 195
Bunn, Jeffrey 202
Burch, Jay 183
Burke, David L. 225
Butcher, Thomas 179, 181
Byrum, Karen 218

C

Cameron, Rob 221
Campbell, Chelsea 192
Campbell, James A. 152
Cannon, William R 138
Capetillo, Abigail 147
Capetillo, Carmen 152

Capps, Charles 212
Capps, Gary 168, 173, 174
Cardo, Taisia 159
Carlson, Sarah 213
Carmichael, Justin 212
Carr, John 169
Carrado, Kathleen 149, 157
Carreiro, Eli 180
Carreras, Ben 199
Carrero, Daniel 225
Carrion, Joseph 208
Carson, Jennifer 212
Carter, Dave 204
Carter, J. David 199
Carter, Ken 218
Cassano, Michael 164
Cassella, Victor 190
Castano, Alejandra 149
Castillo, Vincent 169
Cavendor, Andrew 175
Cerio, Ben 219
Cesar, Scott 193
Chagnon, Timothy 160
Chang, Eric 176
Chang, Jonathan 163
Chang, Kang 227
Chen, Fanqing Frank 143
Chen, Liaohai (Leo) 144
Chen, Yu-Shen 205
Chesler, Elissa 163
Cheung, Teddy 219
Cho, Kelly 188, 196
Chou, Yeong-Shyung 171
Christen, David 201, 203
Christian, Kelly 167
Christophersen, Jon 182
Chu, Tsong-Lun 164
Chyall, Lawrence 143
Clampitt, Denae 224
Classen, Aimee 187, 192
Clemons, Dawn 162
Coates, Cameron 210
Coddling, Jennifer 149
Coffman, Catherine 141
Colaianni, Catherine 227
Collins, Jeff T. 178
Connolly, Mary 198
Convery, Mark 220
Cook, April 216
Cooper, Lauren 178
Copeland, Christopher 211
Cornejo, Anabey 138
Cotrell, Jason 170
Coupland, Daniel 225
Cousineau, Sarah 225
Craig, Paul 141, 158
Crosson, Kenya 192

Crowley, Raja 177
Culiat, Cymbeline 137
Curtis, Calvin 153
Cyran, Jenee 157

D

D'azzo-Caisser, Edward 164
Dai, Sheng 151
Dallas Jr., Monroe 176
Dalling, Ryan 211
Danaher, David 217
Daugherty, Stephen 219
Davis, Mark 137
Davis, Shurrita 183
Deatrick, Christopher 212
Degen, Cassandra 205
Deibler, Lisa 206
Delgadillo-Lariz, Mario 194
Delmau, Laetitia 149
Depouli, Laura 159
Derbakova, Anna 220
Derenzo, Stephen 225
Deru, Michael 177
Desmond, Hugh 213
Detert, Douglas 206
Dewey, Stephen 207
Diaz, Julian 169
Diercks, Lindsay 175
Dillon, Heather 175
Dilmanian, Avraham 209
Dimond, John 164
Dingfelder, Jochen 223
Dingus, Brenda 213
Dixon, Christopher 172
Doctor, Richard 178, 190
Donohoo, Pearl 177
Donohue, Erin 201
Downs, Janelle 189
Doyle, Brandi 178
Driemeyer, Patrick 170
Dringenberg, Emily 182
Du, Congwu 207
Duarte, Jeff 184
Duitsman, Michael 203
Dunn, John J. 141
Dunstan, Prishantha 169
Dwyer, Daniel 151
Dzubey Jr., Clarence 166

E

Eastland, Adrienne 150
Efstration, Emily 184
Eipeldauer, Mary D. 211
Elder, Andrew 171
Elgass, Laura Jane 199
Englehart, Jessica 187

Escalona, Averi 177
Estrada, Juan 213
Eugenio, Paul 224
Eusebi, Ricardo 223
Evans, Danielle 162
Exarhos, Greg 202

F

Fain, John 154
Fazio, Gina 166
Feigerle, Charles S. 153
Fenske, Kathryn 204
Ferguson, Sasheen 209
Fernandez, Matilda 218
Fernandez, Ramon 194
Ferrada, Juan 209
Ferrandon, Magali 166
Ferrell, Alishia 221
Figuereo, Suneidy Lemos 200, 216
Finkelstein, Nitai 163
Finn, Wendy 193
Fischer, Diane 211
Fisher, Alan 226
Fleckenstein, Aaron 162
Foley, Jill 220
Fonnesbeck, Jacqueline 154
Foresman, Robert 222
Forseth, Ry 188
Fowler, Joanna 152
Fox, Emily 139
Frank, James S. 215
Freeman, Clarissa 208
Freimuth, Erika 137
Frey, Merideth 215
Frumberg, David 208
Fuhrmann, Mark 157, 184
Fujita, Yoshiko 187
Fulton, George 197
Funsten, Herbert 221
Furan, Miguel 168
Fuss, Jill O. 138

G

Gabriel, Reginald 138
Gaddis, Jennifer 205
Gadgil, Ashok 185, 189, 194
Garcia, Guillermo 172
Garcia, Luis 189
Gardner, Steven 217
Garland, Shaun 185
Garrett, Latasha 158
Garza, Shirabrandy 144
Gates, Jennifer 180
Geerlings, Kurtis 224
Geisz, John 202
Gelston, Gariann 227

George, Easo P. 201
Gershon, Talia 205
Gibbs, Jacqueline 147
Giglio, Jeff 151
Gill, Gary 150
Ginley, David 175
Girard, Candace 152
Glagolenko, Irina 207
Glamm, Ryan 200
Goel, Kushboo 143
Goetz, Kathleen 226
Goheen, Steven C. 145
Goldberg, Margaret 150
Goldman, Liran 198
Goldschmidt, Azriel 215
Goldstein, Rita 206
Good, Morris 174
Goodnack, David 173
Goodpaster, Jason 156
Graf, Norman 215
Grant, Glenn 205
Gray, Leonard J. 165
Grayson, David 209
Green, Jim 168
Green, Meagan 206
Green, Renee 204
Green, Tim 136, 183, 184, 186, 196
Green, Timothy 193, 196
Greene, Virgil 202
Greenland, Kelly 223
Griffin, Jeffrey 176
Guillotte, Kenny 157
Gullikson, Erik 200
Gundel, Lara 171, 184
Gunderson, Carla 195
Gunter, Lee 185
Gutleber, Kathryn 136

H

Haakonsen, Christian 223
Hafidi, Kawtar 214, 222
Hahn, Marlene 187
Hahn, Richard 155
Hamedani, Matthew 204
Hammons, Joshua 205
Hannemann, Christopher 172
Hansen, Natalie 224
Hanson, Aaron 210
Hanson, Brett 141
Harp, Brianna 137
Harris, Daniel 142
Harrison, Sarah 214
Hart, Daniel 215
Hartmann, Janessa 156
Haskell, Daniel 190, 197
Hatcher, Jasmine 149

Hazen, Terry C. 185, 186
Head, Jeff 148
Heard, Joseph 226
Hebert, Jonathan 201
Heidfeld, Daniel 139
Heim, Jordan 223
Heiser, John 188, 191, 194
Hendricks-Holtz, Jacob 201
Henestroza, Enrique 222
Hice, James 161
Hickey, Eva 210
Higinbotham, Douglas W. 219
Hoch, Megan 141
Hoffmann, Christina 169
Hofherr, Leslie 207
Hoppe, Eric 152
Horton, Duane 189
Hovland, Paul 159
Howley, Ian 210
Hrma, Pavel 155
Hsu, Justin 182
Hu, Pat 181
Huang, Zhenyu 178
Huang, Zhuo 183, 196
Hubbard, Camden 202
Hubbard, Susan 197
Hubble, David 166
Huerta, Alejandra 150
Huesemann, Michael 192
Huestis, Edwin 174
Huey, Eric 224
Hulbert, Steve 172
Hulbert, Steven 200
Humpherys, Candice 222
Huntley, Laura 220
Huskey, Arlinda 178
Hussain, Zahid 176

I

Ice, Gene 202
Ilavsky, Jan 178, 179, 205
Impellitteri, Nick 140
Ince, Sarita 140
Irizarry, Melvin 217
Isang, Emmanuel 145

J

Jack, Neal 186
Jackson, Kevin 167
Jacobson, Jacob 211
Jager, Henriette 145
James, Surria 156
Janssens, Robert V. F. 209
Janzen, Paul 221
Jensen, Mark 203
Ji, Hantao 219

Joachimiak, Andrzej 146, 161
Jody, Bassam 151
Johnson, Christopher 180, 201
Johnson, Dabney K. 144, 147
Johnson, Jay 183
Johnson, Katie 190
Johnson, Ken 171
Johnson, Martha 145
Johnson, Nicholas 167
Johnston, Sereres 214
Jones, Ashley 145
Jones, Deanna 156
Jones, Donald 172
Jordan, Thomas 226
Jordan, Tiffany 140
Joseph, Jessica 173
Jostlein, Hans 214

K

Kaminsky, Terri 144
Kane, Stephen 157
Kapoor, Yuvraaj 143
Katz, David 161
Kaur, Simarjit 174
Kean, Nina 184
Kelez, Nicholas 176
Keller, Rachel 161
Kenney, Susan 147
Kerr, John 175
Kerr, Kijana 156
Kesete, Tigisti 155
Ketchum, Christina 221
Khericha, Soli 211
Khoo, Teng Lek 209
Kim, Chang Yub 145
King, Michael 154
Kinney, Teena 189
Kirby, Robert 204
Kirchstetter, Thomas W. 152, 171, 190
Klann, Raymond 209
Klapp, Caleb 163
Klett, James 199
Kline, Josh 226
Kneafsey, Tim 199
Kohut, Danny 141
Kotovskiy, Jack 176
Kowolik, Kristin 194
Kozemczak, Jason 209
Kreiner, Paul 179
Kridis, Dorra 184
Krishna, C. R. 187
Kronenberg, Amy 143
Krumdick, Gregory 167, 199
Kruse, Kara 139
Kumar, Abhik 214
Kunerth, Dennis C. 217

Kutscher, Chuck 172
Kyrpides, Nikos 159

L

Labissoniere, David 159
Lagory, Kirk 195
Laible, Phil 140, 143
Lamb, Michael 159
Lambert, Joseph 163
Lamone, Daniel 180
Lansey, Eli 215
Lara, Lesley 143
Larock, Richard C. 158
Larosee, Marsha 199
Larsen, Grant 222
Larsen, Matthew 139
Lascurain, Mary 174
Last, George 190
Lauro, Alessandro 213
Leahy, Chauncey 191
Lee, Kwok Wing 167
Lee, Richard W. 218
Lee, Sharon 154
Lee, Yin-Nan 188
Lehew, Jeffrey 160
Lehmann, Christopher 179
Lei, Kin Man 192
Leitner, Daniela 209
Leitner, Mattheus 172
Lelie, Daniel Van Der 137
Leonard, Sharon 155
Levander, Alejandro 202
Lewis, Christopher 163
Lewis, Matthew 167
Lewis, Michele A. 174
Lewis, Walter 162
Li, Huilin 139
Li, Zhian 165
Liang, Yue 136
Lichty, Peter 146
Lin, Kevin 176
Linares, Xioranny 176
Lindenbereg, Aaron 217
Ling, Bingjie 195
Link, Hal 167
Lipfert, Dana 153
Lipton, Ronald 215
Liu, Guodong 155
Liu, Jun 173
Liu, Leah 137
Liu, Yuan 216
Livesay, Eric 144
Lograsso, Barbara K. 200
Londono, Natalia 207
Loots, Gabriela G. 144
Lopez, Miguel 194

Louie, Michelle 142
Lowe, Michael 159
Lowe, Tim 163
Lucero, Brice 161
Lukasik, Tanya 206
Lumetta, Gregg 156
Luning, Jan 216
Lytle, Christian 220

M

Mabanta, Jennifer 219
MacDonell, Margaret 186, 187, 189, 194
Macnair, David 175, 178
Madejski, Grzegorz 214
Magedanz, Jeffrey 209
Mahajan, Devinder 148, 172, 177, 180, 181
Majewski, Jaroslaw 203
Majewski, Michael 151
Majewski, Stan 208
Malitsky, Yuri 164
Mallapragada, Surya 156
Malette, Megan 168
Mallo, Michael 168
Malone, Michelle 156
Maloney, Patrick 220
Mangel, Walter F. 136, 142
Manjarrez, Dianna 151
Manjasetty, Babu 138
Marks, Steve 182
Maroni, Victor 203
Marshall, Christopher 167
Martin, Elijah 217
Martin, Jeremy 214
Martin, Phillip 160
Martinez, Jose 165
Martinez, Lianne 221
Mason, Marcus 179
Massimini, Joseph 168
Mateo, Maria 160
Mattler, Jennifer 189
Mawdsley, Jennifer 170
Mayer, Marie 206
McCaffrey, Caitie 163
McClester, Natissa 176, 220
McConnell, Steven 209
McCorkle, Sean 138, 140, 162
McDermott, Amanda 153
McGill, Sandra 139, 142
McGugin, Mike 158
McIntyre, Gavin 169
McLaughlin, Scott 189
McLean, Jeff 186
McMahan, Peggy 210
McMurtry, Karl 219
Mehta, Apurva 214, 216, 217
Mejia, Evelyn 179

Meldgin, Carolyn 226
Melton, Lakeisha 207
Menard, Jonathan 214
Mentinova, Marija 153
Merino, Enrique 217, 218
Mestayer, Mac 224
Meyer, Holger 224
Michaels, Robert 172
Michaud III, Edward J. 139, 142
Middleton, Christine 214
Mielenz, Jonathan 146
Milczarek, Kylee 186
Miley, Terri 190
Millard, David 164
Miller, Ben 185
Miller, Christopher 220
Miller, Lisa 147
Milov, Alexander 215
Minjares, Maria 171
Mitchell, Evan 156
Mitchell, Troy 209
Mitchum, Samuel 160
Moderhack, Jamie 195
Mohon, Sara 171
Moline, Julia 181
Montag, Christoph 213
Montalvo, Diana Ortiz 152
Montaño, Gabriel 200
Montgomery, Sara 151
Moradmand, Ali 203
Morang, Melinda 218
Moriarty, Patrick 179
Morrell-Falvey, Jennifer 141
Morris, Amy 189
Mtingwa, Sekazi 168
Mueller, Jennifer 199
Mueller, Robert P. 185
Mukherji, Swapna 197
Musculus, Mark P. B. 174
Mussar, Kristin 146
Mylenski, Michael 139

N

Neil, Ashley 185
Nelson, Andy 220
Nelson, Brent 205
Nelson, Pamila 161
Nemesure, Seth 161
Newcombe, Caroline 173
Newman, Peter 227
Nguyen, Binh 142
Nilsson, Anders 206
Nolan, Martin 179
Norberg, Scarlet 222
Norby, Richard J 197
Norris, Boyana 164

North, Andrea 177
Nunez, Anita 185
Nutaro, James 181
Nutter Jr., Forrest W. 139

O

O'Brien, William 178
O'Connor, Paul 220
O'Dunikan, Kehinde 146
O'Neil, James P. 154, 174
O'Neill, Hugh 143, 158
O'Shea, Brian 224
Ogero, Frank 191
Okyere-Asiedu, Saka 200
Ottavio, Dan 164
Owens II, Allen 168
Owens, Erich 217
Owens, Lindsay 211
Owens, Robert 168

P

Pachikara, Jacob 148
Padilla, Mariano 216
Pai, Jessica 207
Paisley, Dennis 219
Panisko, Ellen 191
Paranthaman, Mariappan Parans 201
Park, Young Soo 182
Parker, Jack 193
Parrent, Jerod 226
Pasquarelli, Robert 153
Patananan, Alexander 145
Pate, Nicholas 171
Pelton, Mitch 162
Pena, Louis A. 207
Pena, Rodrigo 180
Perez, Ernie 185
Perez, Samuel 222
Perez, Shawn 214
Perkins, Neville 181
Perrine, Ken 160
Peters, Ben 177
Peters, Brittany 158
Peterson, Stephanie 137
Piccolo, Tasha 188
Pickett, Chris 175, 177
Piette, Mary Ann 187
Pink, Christopher 169
Pint, Cary 209
Plate, Randall 166
Pointer, W.d. 182
Policastro, Jessica 141
Pontillo, Frankie 182
Porter-Chapman, Yetta 148, 216
Portmann, Gregory J. 166
Post-Zwicker, Andrew 217, 218, 227

Poston, David I. 222
Potok, Thomas E. 160
Powell, Danny 177
Powers, Alicia 149
Pradhan, Zarrea 193
Pranger, Leah 149
Prestemon, Soren 168
Prettyman, Emily 218
Price, Joshua 169
Prinzen, Mia 196
Purpura, Melissa 152
Pye, Charles 221

Q

Quemada, Maria Melissa 185
Quock, Debby 162

R

Rahill, Daniel 186
Rahimi, Salim 136
Rahlin, Alexandra 227
Rajendran, Pradeep 150
Ramos, Natalia 186
Randolph, Priscilla 183
Ranganath, Sryan 171
Raphael, Alan 176
Ravet, Jeannene 191
Ray, Cody 178
Rearden, Bradley T. 162
Reese, Terrence 223
Rehm, Ernst 213
Reichmuth, Barbara 227
Reider, James 190
Resseguie, David 161
Rey, Christopher 168
Reynolds, Fedrick 179
Rice, Jonny 202
Riechers, Shawn 155
Rinker, Torri 138
Rivera, Melixa 144
Roberts, Joey 197
Robeson, Rachel 157
Robichaud, Robi 170
Roche, Kenneth 159
Roco, Constance 200
Roden, Dylan 147
Rodriguez, Dianna 196
Roe, Natalie 216
Rogers, Alistair 195
Rogers, Chanda 204
Rogers, Timothy 179
Roha, Rebecca 192
Rohatgi, Upendra S. 167
Rohay, Alan 198
Roney, Timothy 221
Rosa, Michelle 144

Ross, Ian 226
Rossier, Laura 193
Rowe, Nathan 175
Roy, Nimisha Ghosh 197
Roybal, Jonathan 146
Ruesch, Jeremiah 221
Rumbles, Garry 204
Rumore, Matthew 213
Russo, Thomas 180
Rutovytsky, Yevhen 197
Ryan, Kevin 165
Ryu, Jung Min 162

S

Sackschewsky, Michael 140
Sadler, Nicole 207
Sakara, Brooke 147
Salmeron, Miquel 203
Salvato, Carissa 192
Sanders, Jennifer 204
Sanfilippo, Antonio 160
Santiago, Angel 174
Sato, Linda 164
Saucedo, Alejandro 178
Savard, Guy 217
Savich, Theodore 165
Sawyer, Georgia 184
Scali, Anthony 158
Scarлата, Chris 156
Scarlett, Carol 225, 226
Schadt, Christopher 188, 196
Schiffer, Wynne 208
Schlueter, John 204
Schneider, Dieter 165
Schultheiss, Carl 166
Schultheiss, Kira 145
Schultz, Christine 190
Schultz, Irvin 190, 194, 197
Schweickert, Gerald 198
Scott, Daniel 205
Seifert, Gary 197
Selvey, Robert 191, 193
Seweryniak, Dariusz 212
Shaban, Elhag 179
Shah, Harsh 136
Shah, Naomi 209
Shaheen, Sean 205
Sharova, Natalia 154
Sharper, Allen 212
Shaw, Robert W. 153, 203
Shea, Thomas J. 226
Sherman, Steven 180
Shi, Liang 144
Shi, Xiae 148
Shin, Peter 155
Siddons, David Peter 224

Siddons, Peter 179
 Siebers, Anna 137
 Sikora, Ben 151
 Simmons-Willis, Tracey 155
 Simon, Matthew 175
 Singh, Michael 211
 Sisterson, Rachel 159
 Sit, Stefany 198
 Sivertz, Michael 219
 Skaritka, John 174
 Skeete, Dereck 191
 Skillman, Sam 224
 Skinner, Nathaniel 158
 Skow, Dane 160
 Slatest, Len 141, 158
 Slone, Tera 155
 Smith, Brandy 165
 Smith, Brennan 166
 Smith, Jillian 150
 Smith, Michael 170
 Smith, Milton 227
 Smith, Rakeya 161
 Smith, Ryan 198
 Smoot, George 226
 Snyder, Sarah 194
 Snyder, Seth 151, 153
 Snyderstrup, Louis 169
 Sonnenschein, Andrew 212
 Sosonkina, Masha 160
 Sovik, Nina 195
 Sparks, Rachel 219
 Springmann, Alessondra 219
 Sprouse, Mary 182
 Stampf, Dave 159, 163, 164
 Steinmaus, Karen L. 227
 Stepanyan, Stepan 218
 Stone, Jessica 145
 Storm, Amanda 155
 Stormberg, Angelica 139
 Strasberg, Matthew 216
 Stringfellow, William 145
 Stucker, Valerie 154
 Stutzman, Marcy 216
 Sullivan, Terry 192
 Swaminathan, S. 140, 147
 Swanson, Douglas 214
 Sweet, Desiree 187
 Szanyi, Janus 154

T

Taasevigen, Danny 138
 Tagler, David 174
 Takai, Helio 212, 214, 221, 222
 Tallerico, Tom 166
 Tanko, Zachariah 165
 Tawfik, Julian 181

Taylor, Benjamin 201
 Teachey, Christopher 188
 Temprosa, Aj 170
 Teodoro-Dier, Adriana 202
 Thakkar, Bharat 178
 Thanos, Peter K. 207
 Thelen, Michael P. 137
 Thiyagarajan, P. 150
 Thomas, R.C. 226
 Thomas, Shayla 153
 Thomassen, Kaitlin 187
 Tiede, David 150
 Tievsky, Dana 183
 Tinoco, Tomas 181
 Tiquia, Sonia 188, 196
 Titus, Valorie 191, 194
 Todd, Damon S. 210
 Tormos, Kathryn 140
 Torn, Margaret 189, 198
 Torok, Tamas 145
 Torres, Melissa 191
 Tran, Stephanie 173
 Tringides, Michael 221
 Tripathi, Anjali 215
 Troyer, Lyndsay 157
 Tsutakawa, Susan 146
 Tucker, Brian 206
 Tuesta, Alfredo 176
 Tully, Melissa 207
 Turner, John 148, 153, 167
 Turner, Manisha 224
 Tyagi Jr., Mangal 170
 Tyler, Abby 149, 200
 Tyner, Marlene 187

U

Um, Wooyong 157
 Undewood, Bakari 165
 Urena, Joel 208
 Urena, Katherine 152

V

Valdez, Maribel 178
 Valdez, Maryn 141
 Vallett, Paul 148
 Venkateswaran, Dharshini 147
 Verboom, Charlie 159, 161, 165
 Verkade, John 151
 Vetter, Jeffrey 163
 Vilayvong, Steven 216
 Vondrasek, Richard 169
 Vreeland, Amanda 207

W

Wade, David C 179
 Walker, Elyse 175

Walton, Rod 185, 187
Wanamaker, Laura 151
Wang, Jun 146
Wang, Richard 160
Wang, Wei 149, 193
Wang, Xiaoping 156
Warner, Marvin 149, 200
Watson, Bruce 220
Webber, Robert 227
Weil, Gabriel 216
Weisend, John 226
Weldy, Chad 192
Wellman, Dawn 151, 156
Welton, Robert F. 212
Westfall, Corey 205
Westin, Charlie 141
Weygand, Dennis 222
Whitaker, Sarah 146
Whitlock, Derrick 151
Whitlow, Kristin 216
Whittle, Ed 145
Wiggins, Latoria 148
Williams, Jaimee 211
Williams, Megan 186, 194
Williams, Ted 165, 179
Williamson, Jessica 216
Williamson, Rebecca 198
Wilson, Brent 210
Wilson, Leslie L. 153
Wishart, James 149, 152, 156
Wisnewski, Christy 136
Woicik, Patricia 206
Wolf, James 197
Wong, Daryl 148
Wong, Stanislaus S. 148
Woodruff, Dana 193
Woody, Craig 213
Wreschnig, Daniel 195
Wright, Brian 150
Wright, Kyal 203
Wright, Paul 171
Wu, Andy 171
Wu, Gordon 199
Wyckoff, Joseph 226

X

Xu, Nan 210

Y

Yamada, Masaaki 217
Yan, Yiton 219
Yannone, Steven M. 137, 141
Young, Jonathan 207
Yu, Edward 224
Yu, Minmin 142

Z

Zahra, Paul 161
Zakhour, Kamil 220
Zaltash, Abdolreza 173
Zellarchaffers, Priscilla 190
Zellner, Phillip 180
Zhang, Angela 144
Zhang, Weiqun 213
Zhang, Xiaohai 146
Zhang, Xiaoqian 215
Zholi, Alma 188
Zhou, Jizhong 142
Zhu, Weisha 138
Zrazhevskiy, Roman 159

Index of Schools

A

Acadia University 172
Albertson College of Idaho 205
Albion College 142, 161, 195, 217, 225
Alfred State College 158, 161
Allegheny College 157
Andrews University 214
Arizona State University 173
Auburn University 185
Austin College 214

B

Baker University 154
Baylor University 168
Benedict College 204
Benedictine University 140
Bergen Community College 155, 160, 162
Big Bend Community College 159, 161, 162, 165
Binghamton University 192
Birmingham-Southern College 185
Brigham Young University 197, 203, 211, 224, 227
Brigham Young University–Idaho 139, 156, 211, 217, 222
Bronx Community College 169, 194, 196
Brown University 201
Bucknell University 163

C

Cabrillo Community College 194
California State Polytechnic University–Pomona 147
California State University–Chico 221
California State University–Fresno 145, 198
Carleton College 220
Carnegie Mellon University 160, 176, 212
Cedarville University 166
Central Missouri State University 157
Central State University 155
Cheyney University of Pennsylvania 138, 140, 162
Chicago State University 150
Christopher Newport University 144, 147
City College of San Francisco 139
Clayton State University 139, 142
Clemson University 160
Colgate University 219
College of DuPage 199, 204
Colorado School of Mines 151, 153, 167, 175, 178
Columbia Basin College 189
Columbia Basin Community College 194
Columbia University 169
Community College of Philadelphia 226
Community College of Rhode Island 178, 191
Connecticut College 136

Contra Costa College 138, 142, 143, 154, 174, 222
Cornell University 137, 138, 163, 164, 208, 210, 215
CUNY–Bronx Community College 166

D

Del Mar College 137, 141
DePaul University 218
DePauw University 213
Diablo Valley College 181
Duke University 227

E

Earlham College 143, 157, 165
Eastern Illinois University 189, 205, 226
East Stroudsburg University 150
East Tennessee State University 145, 159
Elizabeth City State University 140, 147

F

FAMU-FSU College of Engineering 214
Farmingdale State University 177, 181
Fayetteville State University 180, 201
Fisk University 145
Florence-Darlington Technical College 176, 219, 220
Florida A&M University 212, 221
Florida State University 224
Franklin & Marshall College 220
Franklin W. Olin College of Engineering 177
Fullerton College 216

G

Georgia College & State University 156
Georgia Institute of Technology 149
Georgia Tech University 175, 178
Gettysburg College 192
Gonzaga University 171
Governors State University 161, 165
Greenville College 209
Gustavus Adolphus College 147

H

Hampton University 208
Hartnell Community College 150
Hartwick College 161
Harvey Mudd College 224, 226
Heritage University 152

I

Illinois Institute of Technology 178, 190
Illinois State University 195
Iowa State University 167

J

Jackson State University 145, 159
Jamestown Community College 158
Johns Hopkins University 195
Johnson City 159

K

Kansas State University 182
Katholieke Universiteit Leuven 213
Kent State University 222
Knox College 146

L

Lane Community College 140
La Salle University 206
Lawrence University 153, 198, 202
Lesley University 198
Lewis and Clark College 221
Lock Haven University of Pennsylvania 190, 223
Long Beach City Community College 196
Loyola University 187

M

Marist College 188
Maryville College 177
Massachusetts Institute of Technology 147, 205, 214, 215, 225
McGill University 223
McMurry University 149
Medgar Evers College 191
Merced College 210
Metropolitan State College of Denver 137
Michigan State University 173, 224
Michigan Technological University 139
Middlebury College 226
Middle Tennessee State University 146, 151, 197
Milwaukee School of Engineering 160
Minnesota State University 210
Monmouth College 217
Montana State University 138
Montgomery College 170
Morehouse College 211

N

Nassau Community College 136, 159, 180
New Mexico State University 152, 163
Newport News 147
New York University 141, 207
Norfolk State University 160, 202, 203, 224
North Carolina A&T State University 168, 183, 184, 216, 225
North Carolina State University 217
Northern Illinois University 171
Northern New Mexico Community College 218
Northwestern University 216

O

Oak Ridge National Laboratory 181
Occidental College 219
Ohio State University 200
Old Dominion University 219
Onondaga Community College 186
Oregon State University 138, 178, 209
Our Lady of the Lake University 171

P

Pacific Lutheran University 151
Pennsylvania State University 137, 158, 173, 186, 191, 202
Pensacola Christian College 174
Pomona College 222
Portland State University 170
Prairie State College 170
Purdue University 168, 182, 223
Purdue University–Calumet 162

Q

Queensborough Community College 149, 152, 156

R

Ramapo College of New Jersey 217, 218
Rensselaer Polytechnic Institute 169, 180, 212, 213
Rhodes College 149
Roane State Community College 209
Rochester Institute of Technology 141, 151, 153, 158
Rose-Hulman Institute of Technology 226

S

Sacramento City Community College 154
Sacramento State University 183, 196, 226
San Francisco State University 212
Santa Monica College 194
Shasta Community College 155
South Carolina State University 202
South Dakota School of Mines and Technology 205
Southern Adventist University 211
Southern University 215, 223, 227
Southern University–Baton Rouge 179
Southern University A&M 224
Southern University A&M of Baton Rouge 173
Springfield Technical Community College 152
St. Joseph's College 164, 190, 219
Stanford University 144, 150, 179, 187
State University of New York at Albany 139, 165
State University of New York at Binghamton 174
State University of New York at Buffalo 208
State University of New York at Farmingdale 172
State University of New York at Geneseo 151, 187
State University of New York at Stony Brook 148, 191, 192, 207, 214

State University of New York College of Environmental Science and Forestry 156
Stony Brook University 145, 167, 181, 188, 193, 206, 207, 209, 220, 225
Suffolk County Community College 157, 159, 163, 164, 196

T

Tennessee State University 165, 179
Tennessee Technological University 171, 201
Texas A&M University 179
Texas Southern University 151, 153, 155, 207
Texas Tech University 178, 179, 205
The City College of New York 179, 208
The College of New Jersey 227
The College of William and Mary 171, 210
The Cooper Union for the Advancement of Sciences and Art 184
The George Washington University 142
The Ohio State University 180
The University of the Virgin Islands 156
Three Rivers Community College 197

U

Unity College 194
University California–Santa Barbara 190, 197
University of Alabama in Huntsville 216
University of Arizona 148
University of California–Berkeley 136, 143, 146, 148, 154, 163, 171, 172, 176, 182, 185, 189, 199, 202, 210
University of California–Davis 136, 174, 184, 185, 207
University of California–Los Angeles 145
University of California–San Diego 137, 197, 198, 209
University of California–Santa Barbara 197
University of Chicago 213, 218, 222
University of Colorado at Denver 167
University of Delaware 172, 184, 200
University of Evansville 203
University of Florida 189, 218
University of Illinois 143, 159, 164, 185
University of Illinois at Chicago 136, 167, 169, 177
University of Illinois at Urbana Champaign 156, 166, 170, 199, 204, 205, 206, 209, 227
University of Iowa 175
University of Kansas 221
University of Maine 187
University of Maryland 141
University of Massachusetts 227
University of Massachusetts–Amherst 174
University of Michigan 187, 188, 199
University of Michigan–Dearborne 196
University of Missouri–Rolla 170, 183
University of Nevada–Las Vegas 221
University of New Hampshire 154
University of New Mexico 213
University of New Orleans 186, 194

University of North Carolina–Chapel Hill 220
University of Northern Iowa 209
University of Notre Dame 174, 176, 186
University of Oklahoma 168, 226
University of Oregon 164
University of Pittsburgh 151, 204
University of Puerto Rico 152, 186, 200, 216, 217
University of Puerto Rico at Mayaguez 144, 185
University of Rhode Island 193
University of Rochester 183
University of South Alabama 201, 203
University of South Carolina 193
University of Southern California 172
University of St. Thomas 220
University of Tennessee 158, 166, 167, 175, 177
University of Tennessee at Martin 202
University of Tennessee Chattanooga 141
University of Texas at Arlington 166
University of Texas at Austin 187
University of the Pacific 146, 190
University of Vermont 148
University of Virginia 153, 195, 198, 200
University of Washington 144, 146, 175, 197
University of Wisconsin–Madison 188, 206
University of Wisconsin–Eau Claire 223
University of Wyoming 182
Utah State University 149, 200
Utrecht University 203
UW Stevens Point 140

V

Valparaiso University 168
Vanderbilt University 189, 219
Virginia Polytechnic Institute and State University 180, 199

W

Wake Technical Community College 160
Walla Walla Community College 191
Washington State University 144, 155, 190, 206
Washington University School of Medicine 139
Wellesley College 215, 219
Wesleyan University 214
Western Illinois University 224
Western Kentucky University 192
Western Michigan University 162, 193, 212
Western Washington University 192
Westminster College 163, 204
Whitman College 157
Worcester Polytechnic Institute 212, 213

Y

Yale University 214
Yeshiva University 215



U.S. Department of Energy
Office of Science

